University of Southampton

Faculty of Engineering and Physical Sciences

Chemistry

Development of Broad-Spectrum Antimicrobials Using Modified Antisense Oligonucleotides

by

Hassan Gneid

Thesis for the degree of Doctor of Philosophy

September 2019

(رب زدني علما) طه :114

(O My lord increase my knowledge) Taha:114

حبيبتي, انما الاهداء لك وحدك. يا ملاكي من حبك تستمد روحي طاقتها و برضاك عني يوفقني ربي. امي حبيبتي

اللهم اغفر لابي و ارحمه و اجعله في جنان الخلد في اعلى عليين. كم نفتقدك يا ابي. 3/2/1990

University of Southampton

Abstract

Faculty of Engineering and Physical Sciences

Chemistry

Thesis for the degree of Doctor of Philosophy

Development of Broad-Spectrum Antimicrobials Using Modified Antisense Oligonucleotides

by

Hassan Gneid

Antibiotics have formed a corner stone of modern medicine. However, bacteria can develop resistance against antibacterial drugs and new antibiotics have to be created at all times to compete with this resistance. One way of potentially generating new antibiotics is by using antisense oligonucleotides (ASOs) that can recruit enzymes to cleave the mRNA of essential genes.

In chapter 2, we thus designed and synthesized a number of PNA-based ASOs targeting essential, reporter and virulence genes of *E. coli*. The cell penetrating peptide KFFKFFKFFK was covalently attached to the PNAs in order to facilitate the uptake of the oligonucleotides into the bacterial cells. Using a variety of antibacterial assays, we were able to show that PNAs functioning by sterically blocking the ribosome binding site are able to silence the activity of the *ftsZ* and *katG* gene. Unfortunately, PNAs that function by recruiting RNase P via the external guide sequence did not seem to have any gene silencing ability. *In vitro* studies suggested that this is because the PNA backbone cannot be recognized by the RNase P ribozyme.

In chapter 3 we therefore tried to recruit a different enzyme, RNase H. A number of LNA-DNA-LNA gapmers targeting the *ftsZ* gene in *E. coli* were designed and synthesized. The standard RNase H recruitment assay showed that these oligonucleotides are able to induce cleavage of the target mRNA by the enzyme. Microscopy studies confirmed that the gapmers are also able to induce gene silencing in bacteria, presumably through the recruitment of RNase H.

In Chapter 4, we systemically designed and screened libraries of chemically modified oligonucleotides containing the external guide sequence for their ability to recruit RNase P *in vitro*. We had a number of successful hits, mainly hybrids of DNA, LNA and to a lesser extent OMe. Due to the high DNA content of the hits, the potential dual recruiting of RNase P and RNase H was explored. A number of chemically modified oligonucleotides were identified that can induce *in*

vitro cleavage of their target mRNA by both enzymes. Such compounds are expected to have superior gene silencing ability. Microscopy studies confirmed the *in vitro* findings, as we were able to detect elongated *E. coli* cells (indicative of successful *ftsZ* gene silencing) for those compounds that showed potential dual recruitment activity.

The work presented in this thesis has shown a promising technology for the use of chemically modified antisense oligonucleotides as antibiotics, especially when their gene silencing could be enhanced by the recruitment of RNase P, RNase H or both. However, the biggest challenge for the development of any oligonucleotide based therapeutic remains their problematic delivery into the target cells or bacteria. Future efforts will thus have to focus on identifying more efficient ways of delivering oligonucleotides into bacterial cells.

Table of Contents

Table of Tables

Table of Figures

Table of Figures

Research Thesis: Declaration of Authorship

Print name:	Hassan Gneid
Title of thesis:	Development of Broad-Spectrum Antimicrobials Using Modified Antisense Oligonucleotides

I declare that this thesis and the work presented in it are my own and has been generated by me as the result of my own original research.

I confirm that:

1. This work was done wholly or mainly while in candidature for a research degree at this University;
2. Where any part of this thesis has previously been submitted for a degree or any other qualification at this University or any other institution, this has been clearly stated;
3. Where I have consulted the published work of others, this is always clearly attributed;
4. Where I have quoted from the work of others, the source is always given. With the exception of such quotations, this thesis is entirely my own work;
5. I have acknowledged all main sources of help;
6. Where the thesis is based on work done by myself jointly with others, I have made clear exactly what was done by others and what I have contributed myself;
7. None of this work has been published before submission

Signature: Date:

Acknowledgements

A few years back, when I decided to go back into education and increase my knowledge and skills, it sounded as an unreachable dream due to the commitments I had in life. Although I was surrounded by a mix of doubtful and supportive people, and had doubts myself, I still made up my mind and after that anything else was not going to be good enough. When I set myself a target, I fully commit myself to reach it. This did mean without any doubt a lot of sacrifices, as during a changing time in life you lose some and win some. To all those without whom these words would not have ever been written, to all those who came in at different stages during this project and helped me one way or another, it would not been possible for me to achieve what I set myself to achieve and my dream would have stayed as dream. Therefore, to all of you, there would never be enough words to thank you for your contributions and your help, but please do accept my grateful words in an achievement you all took part in as much as I did.

I would like to start by thanking my supervisor Dr. Jonathan K. Watts and my co-supervisor Dr. Phillip Ireland for giving me the opportunity to work on this project and helping me achieving my PhD. I would also like to thank the Watts group, both the current and previous members, for their help and support. Special thanks go to Pranathi Meda for her help in synthesizing the many oligonucleotides in Chapter 4, Dr. Min Wook Shin for helping me troubleshoot the microscope, and Julia Rembetsy-Brown for being supportive and helpful during the writing up. I would also like to thank DSTL for funding parts of this thesis, and Dr. Phillip Ireland (DSTL) for teaching me the bacterial assays. I would also like to express my gratitude for Dr. Liam Good who sent me the *E. coli* strains ATCC 25922 and AS19, which have been essential throughout my PhD. I would also like to thank all the people at the University of Massachusetts, RNA therapeutics Institute who helped make the transition from the UK to the USA easier, especially Mary Beth. I would like also to thank Dr. Eugen Stulz for allowing me to synthesis the first few PNAs using the expedite synthesiser owned by his group, Prof. Peter Roach and his group for teaching me essential biochemistry techniques, and Dr. Craig Mello and his group for the great collaboration we had at some point. At this point of achievement, I express my sincere gratefulness for my university in Syria (University of Damascus) and my tutors there, for teaching me the love of knowledge and the determination for high achievements.

Acknowledgements

I would like to thank my friends (Emma Britts, Hafeez Ahmad, Mohsen Deib, Abd Alrahman Hamdan, Mazen Hariri, Michael Moazami and Juahdi Monbo) whose contributions on a personal level were more than essential in reaching my target.

I would like to thank my Brother Yousif for his continuous love and support, my sister Hanan for her support and help, and my sister's family who always were there for me (her husband Simon, the two young men Adam and Colin, and the young princess Areej).

I would like to thank the love of my life, and the best thing that has ever happened to me, my beautiful wife Dr. Nathalie Busschaert, for all the help and the support on both personal and professional levels. I am also grateful to my family-in-law for their help and support, and for accepting me into their family. Towards the end of my PhD, I also gained the most precious gift in life: my beautiful son *Eden Rayan Gneid*. You gave me the inspiration and courage to keep going when things were tough, and I will try to make up for not always being there for you in the first year of your life. Just remember that this was all for you, my dearest son.

Finally, I have to end with thanking my inspiration and the source of the endless love and care in my life and who always believed in my capability and supported me when things were tougher: my mother.

Definitions and Abbreviations

°C	degrees centigrade
(Fmoc-Lys(Boc)-OH	N_α-Fmoc-N_ε-Boc-L-lysine
µL	microlitre
µm	micrometer
µmol	micromole
2-amino A	2-amino-2-deoxyadenosine
2'-F-ANA	2'-fluoro-DNA
2'-F-RNA	2'-fluoro-RNA
4'-S-RNA	4'-sulfur-RNA
A	adenine
Å	Ångstrom
A. baumannii	*Acinetobacter baumannii*
A. lwoffii	*Acinetobacter lwoffii*
Ac_2O	acetic anhydride
ACN	acetonitrile
ASO	Antisense oligonucleotides
B	β-alanine
B. anthracis	*Bacillus anthracis*
B. suis	*Brucella suis*
B. subtilis	*Bacillus subtilis*
Bhoc	benzhydryloxycarbonyl
BLAST	basic local alignment search tool
BNA	bridged nucleic acids
Boc	tert-butoxycarbonyl (protecting group for amines)

bp	basepair
Bu	butyl
Bz	benzoyl
C	cytosine
C. difficile	*Clostridium difficile*
C. elegans	*Caenorhabditis elegans*
calcd	calculated
Cas	CRISPR-associated protein
cDNA	complementary DNA
CeNA	cyclohexene nucleic acid
cfu/mL	colony-forming units per milliliter
CPG	controlled pore glass
CPG	controlled pore glass (solid support)
CPP	cell penetrating peptide
CRISPR	clustered regularly interspaced short palindromic repeats
crRNA	CRISPR RNA
DCC	*N*,*N*'-dicyclohexylcarbodiimide
DCM	dichloromethane
DDTT	3-(dimethylaminomethylidene)amino-3H-1,2,4-dithiazole-3-thione
DIC	*N,N*'-diisopropylcarbodiimide
DIPEA	*N,N*-diisopropylethylamine
DMF	*N,N*-dimethylformamide
DMPG	dimyristoyl phosphatidylglycerol
DNA	deoxyribonucleic acid
DNA-A	deoxy adenosine (n-bz) CED phosphoramidite
DNA-C	deoxy cytidine (n-acetyl) CED phosphoramidite
DNA-G	deoxy guanosine (*N,N*-DMF) CED phosphoramidite
DNA-T	thymidine CED phosphoramidite

DPPC	1,2-dipalmitoyl-*sn*-glycero-3-phosphocholine
dsDNA	double strand DNA
DSPC	1,2-distearoyl-*sn*-glycero-3-phosphocholine
E. coli	*Escherichia coli*
E. faecalis	*Enterococcus faecalis*
EGS	external guide sequences
enoyl-ACP	Enoyl-acyl carrier protein
eq	equivalents
ESI	electrospray ionisation
EtOAc	ethyl acetate
EtOH	ethanol
EU	european union
EYPC	egg yolk phosphatidylcholine
F	phenylanine [amino acid]
F. tularensis	*Francisella tularensis*
FACS	fluorescence-activated cell sorting
FAM	6-fluorescein
FDA	Food and drug administration
Fmoc	fluorenylmethyloxycarbonyl
Fmoc-AEEA-OH	[2-(2-(Fmoc-amino)ethoxy)ethoxy]acetic acid
Fmoc-Phe-OH	*N*-(9-Fluorenylmethoxycarbonyl)-L-phenylalanine
Fmoc-PNA-A(Bhoc)-OH	*N*-((*N6*-(Benhydryloxycarbonyl)aden-9-yl)acetyl)-*N*-(2-Fmoc-aminoethyl)glycine
Fmoc-PNA-C(Bhoc)-OH	*N*-((*N4*-Benzhydryloxycarbonyl)cytosine-1-yl)acetyl)-*N*-(2-Fmoc-aminoethyl)glycine
Fmoc-PNA-G(Bhoc)-OH	*N*-((*N2*-(Benhydryloxycarbonyl)guan-9-yl)acetyl)-*N*-(2-Fmoc-aminoethyl)glycine
Fmoc-PNA-T-OH	*N*-(Thymin-1-ylacetyl)-*N*-(2-Fmoc-aminoethyl)glycine
g	gram

G	guanine
GalNac	*N*-acetylgalactosamine
h	hour(s)
HATU	(1-bis(dimethylamino)methylene]-1H-1,2,3-triazolo[4,5-b]pyridinium 3-oxid hexa-fluorophosphate)
HOBt	hydroxybenzotriazole
HPLC	high performance liquid chromatography
iBu	isobutyryl
IC_{50}	half maximal inhibitory concentration
IPTG	isopropyl β-D-1-thiogalactopyranoside
IVT	*in vitro* transcription
K	lysine [amino acid]
K. pneumonia	*Klebsiella pneumoniae*
kbp	kilobasepair
L	litre
L. monocytogenes	*Listeria monocytogenes*
LB Broth	Luria Bertani Broth
LBA	Luria Bertani Agar
LNA	locked nucleic acid
M	molar (moles per litre)
M. smegnatis	*Mycobacterium smegmatis*
m/z	mass to charge ratio
Me	methyl
MeOH	methanol
mers	oligomers
MH Broth	Mueller Hinton Broth
MHA	Muller Hinton Agar
min	minute(s)

miRNA	microRNA
mL	millilitre
mM	millimolar
mmol	millimole(s)
MOE	2'-*O*-(2-methoxyethyl)
mol	mole(s)
mRNA	messenger RNA
MS	mass spectrometry
nm	nanometer
NMP	1-methyl-2-pyrrolidinone
NMR	nuclear magnetic resonance
NP	N3' phosphoramidate
nt	nucleotide
O	[2-(2-(amino)-ethoxy)ethoxy]acetyl
OD	optical density
OMe	2'-O-methyl
O-spacer monomer	[2-(2-(Fmoc-amino)ethoxy)ethoxy]acetic acid
P. aeruginosa	*Pseudomonas aeruginosa*
PACE	phosphonoacetate
PB	boranophosphate
PBP	Penicillin binding protein
PCR	polymerase chain reaction
PDB	protein database
PEG_{2000}-DSPE	1,2-distearoyl-*sn*-glycero-3-phosphoethanolamine-*N*-[methoxy(polyethylene glycol)-2000]
PEI	polyethyleneimine
PMO	phosphordiamidate morpholino oligomers
PMT	photomultiplier tube

PNA	peptide nucleic acids
PO	phosphorodiester
PPMO	peptide-phosphorodiamidate morpholino oligonucleotide
PS	phosphorothioate
PTFE	polytetrafluoroethylene
ptRNA	precursor tRNA
R	Arginine [amino acid]
RNA	ribonucleic acid
RNA-A	2’-tBDSilyl adenosine (n-bz) CED phosphoramidite
RNA-C	2’-tBDSilyl cytidine (n-acetyl) CED phosphoramidite
RNA-G	2’-tBDSilyl guanosine (n-ibu) CED phosphoramidite
RNAi	RNA interference
RNA-U	2’-tBDSilyl uridine CED phosphoramidite
RT	room temperature
S. aureus	*Staphylococcus aureus*
S. enetrica	*Salmonella enterica*
S. flexneri	*Shigella flexneri*
S. pseudintermedius	*Staphylococcus pseudintermedius*
S. pyogenes	*Streptococcus pyogenes*
S. typhimurium	*Salmonella typhimurium*
sgRNA	single guide RNA
siRNA	short interfering RNA
ssDNA	single strand DNA
T	thymine
T. maritima	*Thermotoga maritima*
tBDsilyl	*tert*-butyldimethylsilyl ethers
TEA	triethylamine
TFA	trifluoroacetic acid

TIS	triisopropylsilane
T_m	melting temperature
tRNA	transfer RNA
UNA	unlocked nucleic acid
UTR	untranslated region
UV	ultraviolet [light]
Vis	visible [light]
Y. pestis	*Yersinia pestis*
λ_{em}	fluorescence emission maximum

Chapter 1 Introduction

Ever since the discovery of penicillin in 1928[1] by Alexander Fleming led to the production of the first broad spectrum antibacterial drugs during the early 1940s,[2] antibiotics have formed a cornerstone of modern medicine. Before this time people died from simple infectious diseases like pneumonia or from blood poisoning resulting from a small cut to the skin. However, it soon became clear that bacteria can develop resistance against antibiotic drugs and that new antibiotics would constantly need to be created to compete with this resistance. Unfortunately, few new antibiotics have been developed since the 1970s and as a consequence antibiotic resistance has become an increasingly serious threat to society. A recent study by the European Centre for Disease Prevention and Control (ECDC) found > 650,000 cases of infections with drug-resistant bacteria in the European Union (EU) and European Economic Area (EEA) in 2015, resulting in 33,110 attributable deaths (53,000 cases and 2,100 deaths in the United Kingdom alone).[3] This corresponds to a 2.5-fold increase in antibiotic-resistant infections since 2007 (see **Figure 1**). It is thus clear that new antibacterial agents, especially drugs that are slow to develop resistance, are highly desirable.

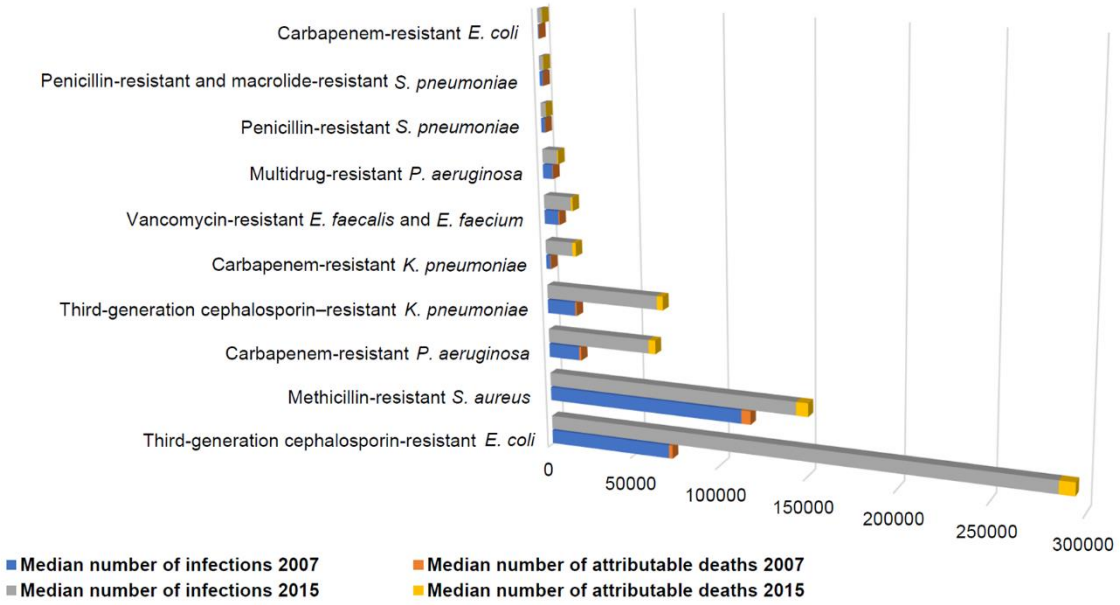

Figure 1. Increase in the number of infections and attributable deaths in the EU and EEA resulting from certain antibiotic resistant bacteria between 2007 and 2015. Graph generated from data obtained by ECDC.[3]

1.1 History of antibiotic development and resistance

Although the discovery of penicillin (**Figure 2**) in 1928 is generally regarded as the start of antibiotic development, researchers had already started developing drugs against bacterial infections prior to this date. As early as 1909 Ehrlich and Hata synthesised and screened derivatives of Atoxyl (**Figure 2**) - then a proposed treatment for trypanosomiasis - in the search for a treatment for syphilis, which is caused by the spirochete *Treponema pallidium.*[4] Their research led to the production of a drug called Salvarsan (**Figure 2**). A similar screening approach by Klarer and Fritz led in 1932 to the discovery of sulfonamidochrysoidine (Prontosil, **Figure 2**) as an antibacterial drug, which was quickly followed by the mass production of other sulphonamide analogues (often called "sulfa drugs") as antibiotics. As mentioned earlier, Fleming reported that penicillin exhibits antibacterial properties in 1928, but it was not until 12 years later when Florey and Chain reported an efficient method to purify penicillin for clinical trials that the antibiotic could be mass produced and distributed. Prior to this, the first hospital use of an antibacterial agent is believed to be the use of extracts of *Pseudomonas aeruginosa* in 1889 by Emmerich and Löw (which they called pyocyanase)[5].Although pyocyanase turned out to be inconsistent and too toxic for humans, further studies found that a number of compounds with antimicrobial activity can be extracted from *Pseudomonas aeruginosa.*[6] These compounds were later understood to be quorum sensing molecules, such as 2-alkyl-4-quinolones[7], *N*-(3-oxododecanoyl) homoserine lactone and 3-(1-hydroxydecylidene)-5-(2-hydroxyethyl)pyrrolidine-2,4-dione[8]. The discovery of the aforementioned antibiotics led to the golden era of antibiotic development between the 1940s and 1970s, which saw the emergence of many of the most common antibiotics used today (see **Figure 3**, top half). However, the last 50 years has seen a marked decline in the discovery of new antibiotics. In fact, no new class of antibiotics has been developed in recent years and the main approach has been limited to modifications of known antibiotics[9].

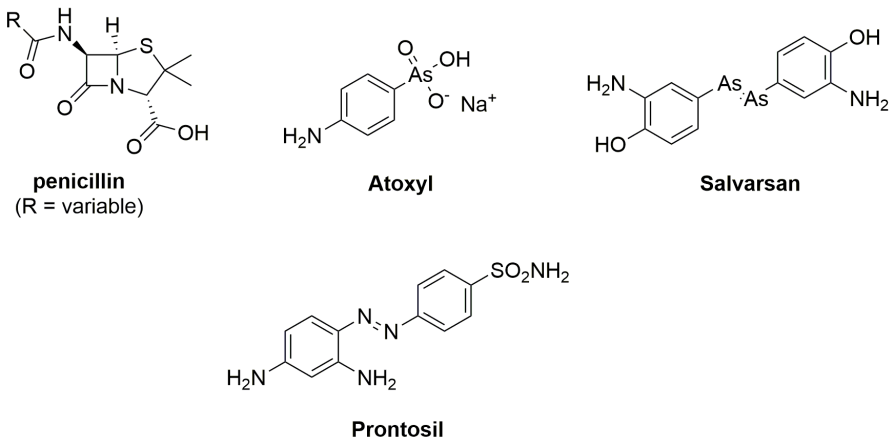

Figure 2. Structures of some of the earliest reported antibiotics.

The lack of novel antibiotics is particularly worrying in light of the resistance that pathogenic bacteria have developed against classic antibiotics such as penicillin. In the early days of antibiotic discovery, with the production and consumption of sulphonamide analogues in the 1930s and 1940s, sulfa drug resistance started to spread rapidly.[5] Fleming already warned about the possibility of the penicillin resistance occurring in certain conditions.[5] While *Treponema pallidium* did not develop any penicillin resistance,[10] other pathogenic bacteria managed to become immune to penicillin by enzymatic degradation. These resistances were already observed in a few cases in the early days of using penicillin.[11] Furthermore, other bacteria like *Enterobacteriaceae* developed resistance to penicillin and other β-lactam antibiotics such as cephalosporins and carbapenems.[12] Now it has become clear that bacteria have developed resistance against nearly all known antibiotics (see **Figure 3**, bottom half).

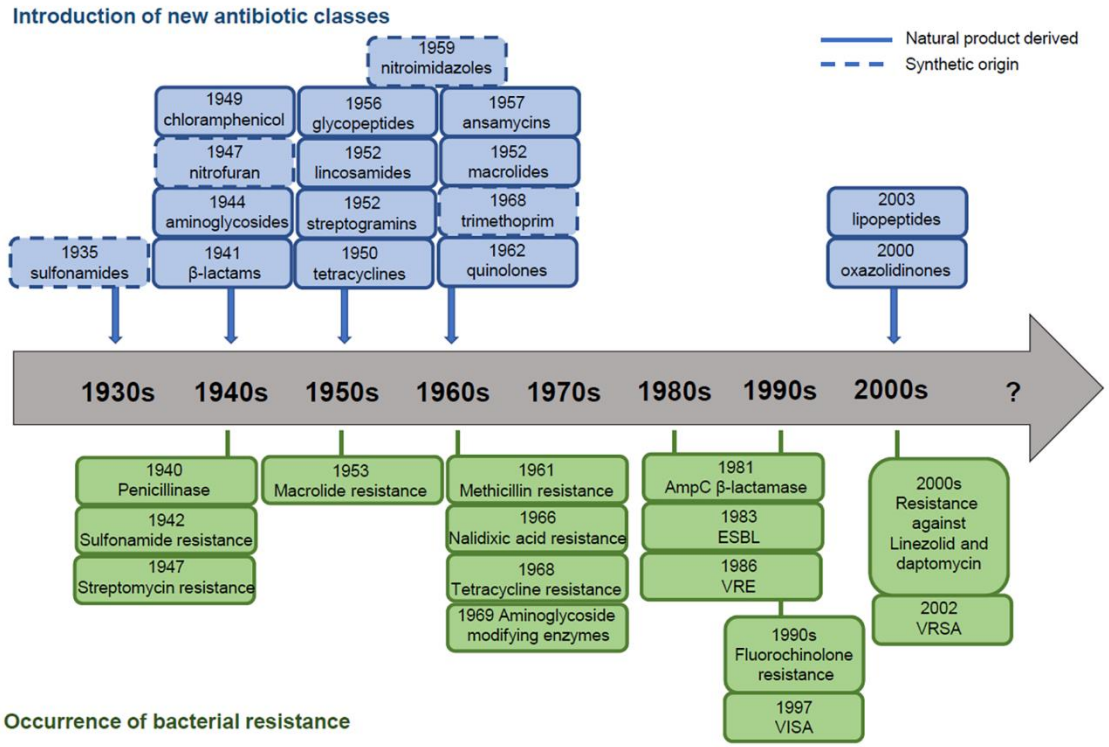

Figure 3. Antibiotic discovery and resistance time line. Source: World Health Organisation (Fact Sheet N˚194 Updates May 2013). ESBL: extended-spectrum beta lactamase, VRE: Vancomycin-resistant *Enterococcus*, VISA: Vancomycin-intermediate *Staphylococcus aureus.* VRSA: Vancomycin-resistant *Staphylococcus aureus.*[13]

Antibiotic resistance in bacteria is understood to be either intrinsic or acquired.[14] Intrinsic resistance means that an antibiotic has no activity against a certain type of bacteria due to the inherent structural or biochemical features of that bacterial strain (e.g. membrane composition or the absence of the target protein). The different composition in the cytoplasmic membrane between gram-positive and gram-negative bacteria is a good example of intrinsic resistance

against common antibiotics such as daptomycin: gram-negative bacteria contain a lower proportion of anionic phospholipids in their cytoplasmic membrane than gram-positive bacteria, which lowers the ability of Ca^{2+} to mediate the penetration of daptomycin into the cytoplasmic membrane.[15] Acquired resistance implies that the resistance is the result of genetic modifications in the bacterial genome or gene transfer between bacteria. There are several mechanisms by which bacteria can develop resistance against certain drugs (see **Figure 4**). One mechanism includes blocking or minimising antibiotic penetration into the bacterium or actively pumping the antibiotic drug out of the bacterium using an efflux pump, which results in a lower presence of the antibiotic in the intracellular environment. A second mechanism involves changes in the target of the antimicrobial drug (usually an enzyme) through genetic modifications or post-translational modifications. Alternatively, bacteria can also acquire resistance by developing a mechanism to change the chemical structure of the antibiotic drug, thereby rendering it inactive.[14]

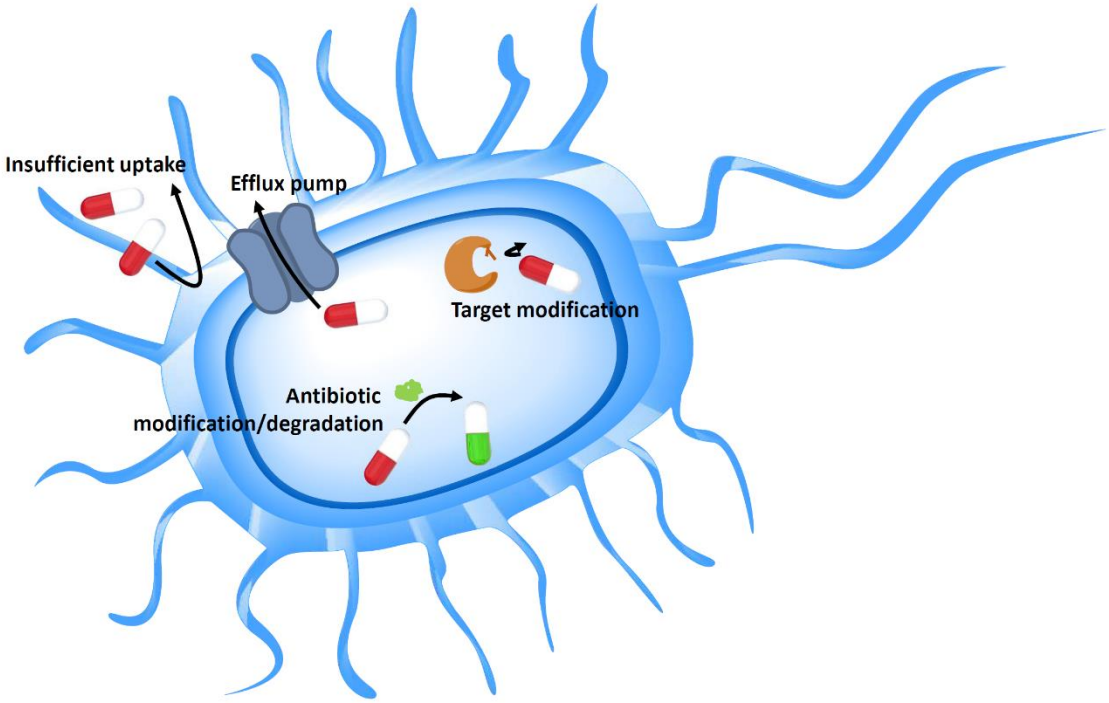

Figure 4. Mechanisms of antibiotics resistance: insufficient uptake due to changes in the outer membrane, removal of the antibiotic by an efflux pump, chemical modifications of the target so that it cannot be recognized by the antibiotic, enzymatic modification or degradation of the antibiotic to render it inactive.

Due to the worldwide problem with antibiotic resistance, there is a pressing need for new antibacterial agents. However, only very few novel antibiotics have been developed in the last few decades. Attempts to develop new antibiotics have therefore included approaches that go beyond the classical screening of compound libraries and chemical modifications of known

antibiotics towards new alternatives. One of these newer approaches to develop non-classical antibiotics is the use of oligonucleotide-based technologies.

1.2 Structure of DNA, RNA and oligonucleotides

The monomeric building blocks of DNA and RNA are nucleotides, which consist of a ribose or deoxyribose sugar, in RNA and DNA respectively, appended with a phosphate group at C5' and a nucleobase at C1' (**Figure 5**).[16, 17] The nucleobases in DNA are adenine (A), thymine (T), cytosine (C) and guanine (G), while the nucleobases in RNA are adenine (A), uracil (U), cytosine (C) and guanine (G). Nucleotides can be linked together to form oligonucleotides or longer DNA or RNA strands. The sequence of nucleobases in these polymeric strands corresponds to the primary structure. In naturally occurring DNA and RNA, the sugar moieties are joined via phosphodiester linkages between the 3'-hydroxyl group of one sugar and the 5'-hydroxyl group of a neighbouring sugar (**Figure 5**). In a regular primary DNA or RNA structure there are no 5'-5' or 3'-3' linkages, but they can be present in synthetic oligonucleotides.[18]

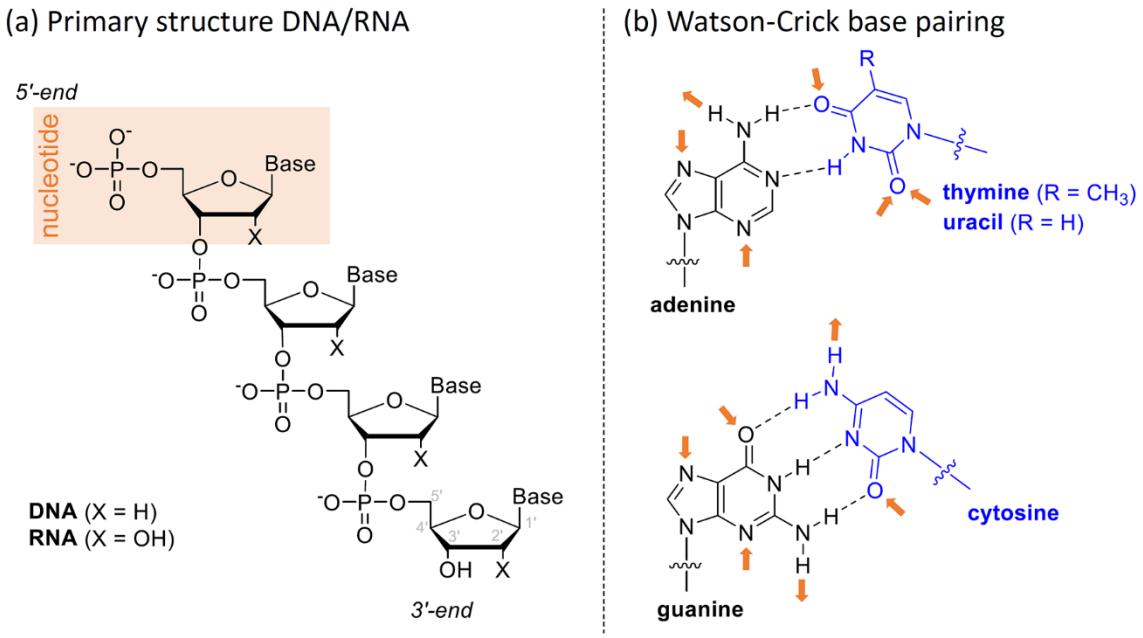

Figure 5. (a) Primary structure of DNA and RNA. The monomeric unit (nucleotide) is highlighted in orange. Labelling of the carbon atoms in the sugar ring is shown in grey on the bottom sugar residue. (b) Watson-Crick base pairing between adenine and thymine/uracil, and between guanine and cytosine. Unoccupied hydrogen bond donor and acceptor sites are indicated with an orange arrow.

The nucleobases contain many hydrogen bond donor and acceptor sites and can therefore interact with each other and other molecules. The most common interaction is the Watson-Crick base pairing between A and T/U, and between G and C (**Figure 5**).[16, 17] This interaction gives rise to the secondary structure of DNA and RNA, of which the antiparallel double helix is the most prevalent.[16, 17] The exact 3D structure of the double helix depends on the conditions in which it is formed and on the nature of the strands. RNA differs from DNA by the 2'-hydroxyl group on the sugar, and as a result the sugar prefers a different conformation in RNA (C3' endo) than in DNA (C2' endo), which has a profound effect on the type of helix formed.

Under standard conditions (low ionic strength), the dominant structure of double stranded DNA (dsDNA) is the B-form (**Figure 6**). This is a right-handed helix where the sugars adopt a C2' endo conformation and the base pairs sit directly on the helical axis and are nearly perpendicular. On the other hand, RNA helices adopt the A- form in low ionic strength (**Figure 6**). This form corresponds to the sugar in the C3`-endo conformation. The A-form is also a right-handed helix, but the base pairs in this form are displaced off-axis. As a result, the A-form has a wider diameter than the B-form and has more nucleotides per turn. Under certain conditions (low humidity and high salt concentrations), dsDNA can also adopt the A-form where the sugar conformation is C3'-endo. In general, most double helices adopt variations of the A- or B-forms (e.g., DNA-RNA heteroduplexes take on the A-form (**Figure 6**)).[19] Only on rare occasions have other types of helices been observed. For example, a left-handed double helix (Z-form DNA) was found to be adopted by a synthetic model of alternated G and C residues d(CGCGCGCGCGCG)$_2$ (**Figure 6**).[20]

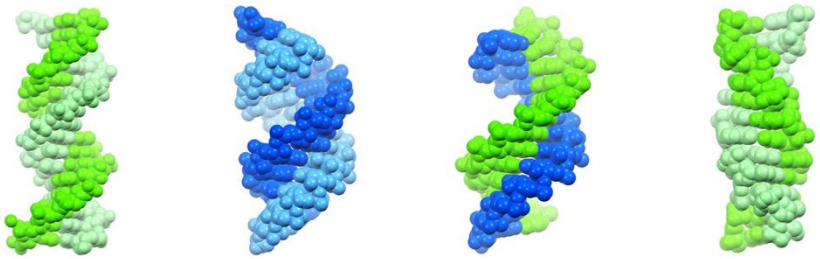

	B-form (dsDNA)	A-form (dsRNA)	A-form (DNA:RNA)	Z-form (dsDNA)
Helix handedness	right-handed	right-handed	right-handed	left-handed
Pitch (Å)	33.2	24.6	24.6	45.6
Residues per turn	10	11	11	12
Inclination of bp from horizontal	-1.2°	+19°	+19°	-9°
Sugar conformation	C2'-endo	C3'-endo	C3'-endo	C3' endo
Diameter of helix (nm)	2.0	2.3	2.3	1.8

Figure 6. Overview of the most common double helix forms of DNA and RNA, as well as some of their characteristics. DNA strands are shown in green, while RNA strands are shown in blue. The PDB files used to generate the figures are: 3bse (B-form dsDNA),[21] 3nd4 (A-form dsRNA),[22] 1efs (A-form DNA:RNA)[23] and 4ocb (Z-form dsDNA)[20].

It must be noted that the base pairs formed through standard Watson-Crick hydrogen bonding still have unused hydrogen bond donors and acceptors (**Figure 5**). It is also possible to form other types of hydrogen-bonded base pairs (called Hoogsteen base pairs). These characteristics make it possible for DNA or RNA to adopt secondary structures other than double helices, such as triple helices and G-quadruplexes.[24] Another important thing to note is that DNA double helices usually consist of two separate strands with interstrand base pairing. In contrast, RNA usually exists as a single-stranded species and can easily form intrastrand double helices through the formation of hairpin loops, bulges and junctions. As a result, RNAs are folded into compact and defined tertiary structures.[25] The ability of RNA to form tertiary structures is exemplified by transfer RNA (tRNA, **Figure 7**), the ribosome and other ribozymes, which are tightly folded RNA species with catalytic activity. It also implies that targeting RNA with oligonucleotides that can base pair to a section of the RNA requires careful design, as only regions that are available for base pairing can be targeted (e.g. loops and bulges).

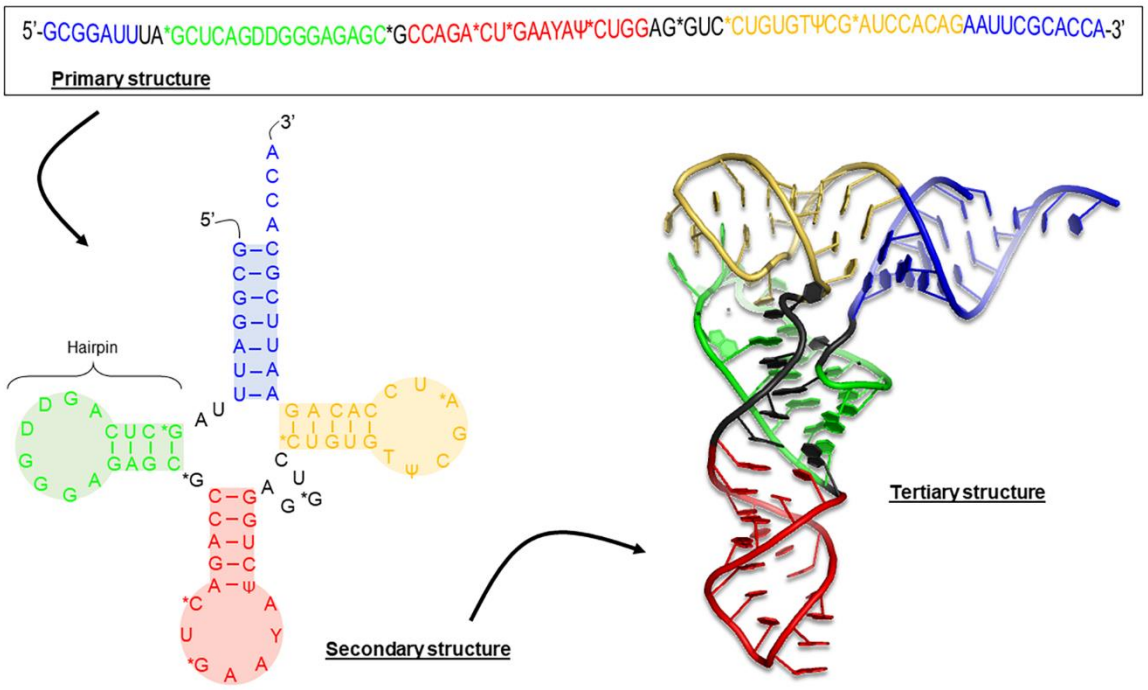

Figure 7. Overview of the primary, secondary and tertiary structure of yeast tRNA-Phe (PDB: 4tna).[26]

1.3 Antisense oligonucleotide technology

The central dogma of molecular biology states that genetic information is stored on DNA, and can be transcribed to RNA (by polymerases), which can be translated into proteins (by the ribosomes) (see **Figure 8**).[27, 28] As this process is central to all life on earth, it comes as no surprise that

traditional antibiotics target the machinery involved in this process as a means to kill bacteria (see **Figure 8**).[29] For example, quinolones target bacterial DNA gyrase or topoisomerase[30] and rifampin targets bacterial RNA polymerase,[31] which are all enzymes involved in the transcription of DNA into RNA. Other classes of antibiotics, such as tetracyclines[32] and macrolides[33], target bacterial ribosomes as a way of inhibiting translation of RNA into proteins. There are also antibiotics that have no effect on transcription or translation, but rather target the enzymes involved in cell wall synthesis (e.g. penicillins)[34], or disrupt bacterial membranes (e.g. lipopeptides)[35]. All these traditional antibacterial agents have in common that they are small-molecule based ligands that function as protein inhibitors, and as a consequence their development is difficult and time-consuming. Therefore, a potential way to develop new antimicrobials is by employing the facile design and synthesis of oligonucleotides.

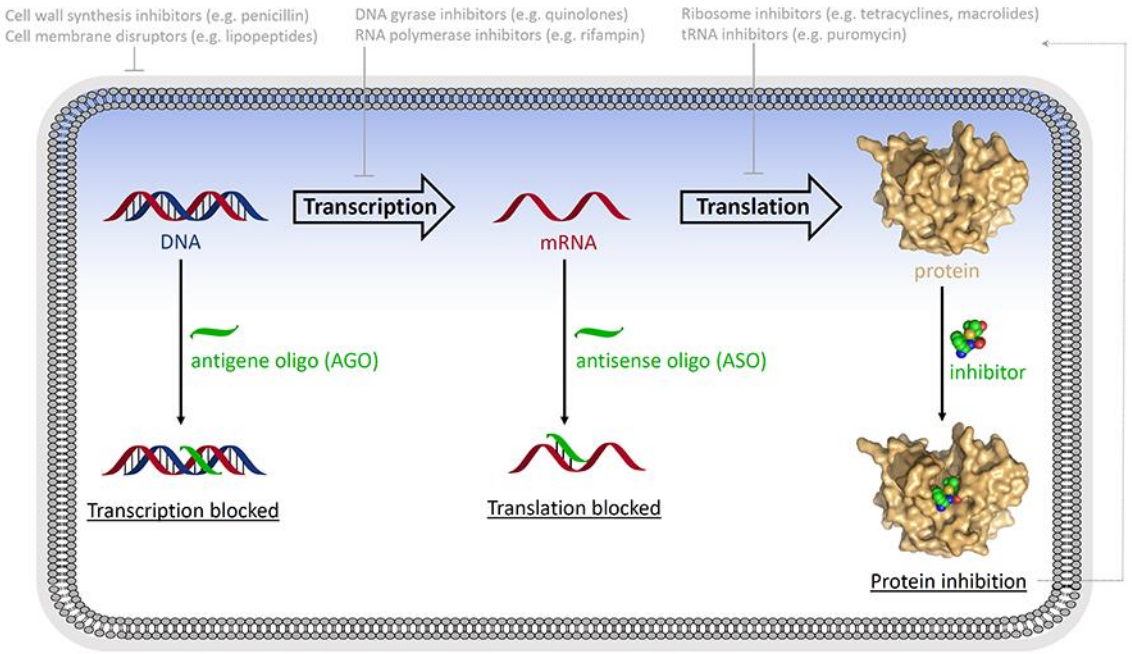

Figure 8. Overview of the targets of traditional antibiotics (top, light grey) and the mode of action of antigene and antisense oligonucleotides.

In principle, all stages of the central dogma can be targeted by oligonucleotides (see **Figure 8**). Protein inhibition could be achieved by aptamers (oligonucleotides that adopt a specific conformation able to bind to a given target) targeting essential proteins.[36] However, the selection and optimization of aptamers is still a long process, and a more viable approach could be to use oligonucleotides to bind to either DNA or mRNA. Oligonucleotides that bind to DNA and thereby inhibit transcription are called 'antigene oligonucleotides (AGOs)' (see **Figure 8**).[37, 38] Usually, these antigene oligonucleotides bind to double-stranded DNA via the formation of a triple helix via Hoogsteen or reversed Hoogsteen hydrogen bonding interactions. On the other hand,

oligonucleotides that bind to mRNA and thereby inhibit translation are called 'antisense oligonucleotides (ASOs)' (see **Figure 8**).[38] As antisense oligonucleotides bind to single stranded mRNA through the formation of a double helix via traditional Watson-Crick base-pairing interactions, their design is relatively easy. Consequently, this thesis will focus on the development of antisense oligonucleotides as antibacterial agents.

Antisense oligonucleotide (ASO) technologies aim to restrict the translation of a target mRNA into its corresponding protein using synthetic oligonucleotides that bind to and block (or 'silence') the function of the targeted mRNA (see **Figure 8**). The first application of gene targeting using synthetic DNA analogues was reported in 1978 by Zamecnik *et al.*, who used antisense oligonucleotides for the inhibition of Rous sarcoma virus replication and cell transformation.[39] Later on, in 1981, antisense oligonucleotides were investigated for the first time as antibacterial agents, by targeting protein synthesis with non-ionic methylphosphonate oligonucleotides complementary to the 3' end of 16S rRNA in *Escherichia coli*, but the investigators only achieved inhibition *in vitro*.[40] However, it was not until 1998 that Fomivirsen was approved by the American Food and Drug Administration (FDA) as the first antisense drug (see **Table 1**)[41].

In comparison to antibiotics based on small molecules or natural products, the development of new antibiotic using the ASO approach should require less time and provide a wider range of possible targets (any known gene in any bacterium). This is mainly due to the fact that an ASO-based antibiotic requires the design of a short oligonucleotide sequence that is complementary to a target bacterial gene (which is straightforward when the genome sequence of the bacteria is known), while classic antibiotics usually target specific proteins and therefore need more complicated design strategies and optimization steps.[42, 43] In addition, the toxicity and pharmacokinetic properties of ASOs is independent of their sequences, and in theory optimization steps are therefore not always required.[44] The hope is that the fast development of ASO antibiotics can keep up with emerging antibiotic resistance. However, the use of antisense oligonucleotides as an effective class of therapeutics has been hindered by challenges such as the *in vivo* instability of the oligonucleotides due to rapid degradation by exo- and endonucleases, the poor uptake of the antisense oligonucleotides into cells, and potential off-target effects of the oligonucleotides including inhibition of mismatched sequences or induction of immune responses.[45] The same problems have hindered the development of other oligonucleotide-based therapies, such as aptamers (short oligonucleotide sequences with a defined secondary structure that can bind to a specific [protein] target with high specificity)[46] and gene therapy (introduction of a full-length gene to the cell).[47]

Table 1. List of all FDA approved nucleic acid therapeutics drugs (2019), along with their chemical modification, mechanism of action and targeted disease.

Drug	FDA approval	Modification	Type of ON drug	Mechanism	Target
Fomivirsen (Vitravene)[41]	1998	DNA (PS)	ASO	Steric blocking and/or RNase H mediation	Cytomegalovirus retinitis
Pegaptanib (Macugen)[48]	2004	2'-OMe, 2'-F (PS)	Aptamer	Protein binding	Macular degeneration
Mipomersen (Kynamro)[49]	2013	DNA, 2'-MOE (PS)	ASO	RNase H mediation	Hypercholest-erolemia
Eteplirsen (Exondys 51)[50]	2016	PMO	Splice-switch ASO	Base pair with exon 51	Duchenne muscular dystrophy
Defibrotide (Defitelio)[51]	2016	Mix of oligonucleotides extracted from pig gut	Aptamer	Protein binding	VOD in HSCT[a]
Nusinersen (Spinraza)[52]	2017	2'-MOE (PS)	Splice-switch ASO	Promotes exon 7 inclusion	Spinal muscular atrophy
Luxturna[53]	2017	-	Adeno-associated virus vector-based gene therapy	Gene therapy	Retinal dystrophy
Patisiran (Onpattro)[54]	2018	RNA, 2'-OMe with 2 DNA overhangs (PS)	siRNA (lipid nanoparticle)	Ago mediation	Transthyretin amyloidosis
Inotersen (Tegsedi)[55]	2018	DNA, 2'-MOE (PS)	ASO	RNase H mediation	Transthyretin amyloidosis
Zolgensma[53]	2019	-	Adeno-associated virus vector-based gene therapy	Gene therapy	Spinal muscular atrophy

[a] VOD Veno-occlusive disease, HSCT Human stem cell transplantation

To overcome these challenges, researchers have developed a number of chemically modified DNA and RNA analogues with improved pharmacological properties, employed various strategies to increase the efficacy of the ASOs, and explored a plethora of different delivery methods (see sections below). As a result of these effort, the last five years has seen a sudden increase in the number of FDA-approved nucleic acid therapeutics (see **Table 1**). Many more oligonucleotides are in the late stages of clinical trials and could be approved by the FDA in the near future.[56] However, note that none of the FDA approved ASOs are used for the treatment of bacterial infections, suggesting that the challenges involved in the development of successful oligonucleotide-based antibiotics are even more complex.

1.3.1 Chemical modifications

Antisense oligonucleotides (ASOs) are based on short synthetic nucleic acids. These analogues are normally chemically modified to increase their stability and potency for gene silencing.[57] The chemical modifications can be categorised depending on the location of the modification: (1) modifications on the internucleotide linkage, (2) sugar modifications and (3) nucleobase modifications.

1.3.1.1 Internucleotide linkage modifications

One of the earliest modifications reported was the introduction of a phosphorothioate (PS) in the backbone in place of a phosphorodiester (PO) bond (see **Figure 9**). This modification has been shown to improve the stability of the oligonucleotides by increasing their nuclease resistance.[58] They are also known for their ability to improve the pharmacokinetic properties of oligonucleotide drugs by their ability to bind to serum proteins, thus increasing the *in vivo* circulation time.[59] However, PS modifications have the disadvantage of reducing the binding affinity for a complementary strand.[60] Nevertheless, nearly all of the FDA approved ASOs utilized the advantages of the PS backbone (see **Table 1**).

Other chemical modifications that can improve the stability of antisense oligonucleotides are *N3'* phosphoramidate (NP) linkages,[61] boranophosphate (PB) internucleotide linkages,[62] and phosphonoacetate (PACE) linkages[63, 64] (**Figure 9**). NP linkages adopt a north sugar conformation, and therefore mimic the dominant conformation in RNA rather than DNA.[61] NP modifications have also been shown to present good binding affinity and high nuclease resistance.[61] PACE oligonucleotides adopt A-form duplexes when bound to RNA targets and are therefore also RNA mimics.[63, 64] They show reduced binding affinity for RNA complementary strands,[64] but increased stability against nucleases.[63, 64] One major advantage of PACE ONs is that they can be taken up unassisted by the cells when the acetate groups are converted to neutral esters, which will be hydrolysed back to the anionic ONs inside the cells with the assistance of cellular esterases (an approach comparable to classic small-molecule prodrugs).[64, 65]

Researchers have also tried to replace the negatively charged backbone in DNA with neutral mimetics. Canonical examples are the peptide nucleic acids (PNA), where the bases are linked by amide bonds,[66, 67] and the phosphorodiamidate morpholino oligomers (PMOs), where substituted morpholine rings are linked by phosphorodiamidate linkages[68, 69] (see **Figure 9**). As a result of their highly modified nature, they are resistant to most nucleases and proteases.[70, 71] The PMO backbone is present in the FDA-approved drug Eteplirsen (see **Table 1**). The PNA modification

significantly increases the binding affinity with target RNA, presumably due to the lack of electrostatic repulsion with the negatively charged mRNA target strand.[69, 72-74] These modifications also have the advantage that they can be easily appended with peptides that can facilitate their cellular uptake.[75, 76]

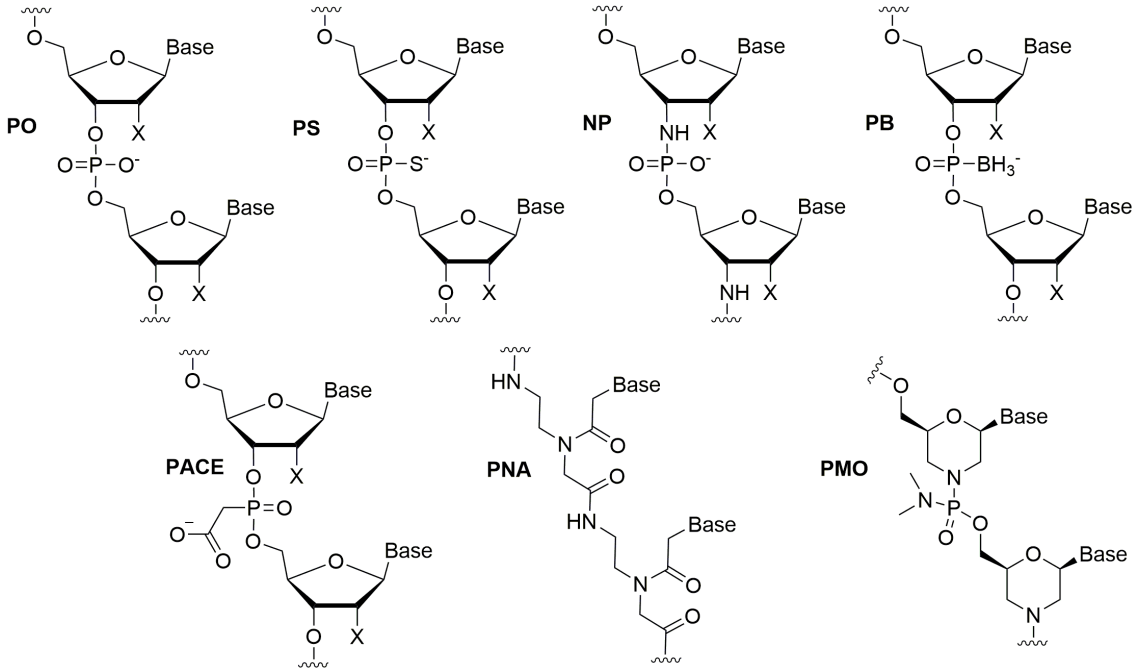

Figure 9. Commonly used oligonucleotides with chemically modified internucleotide linkages. The minor changes on the backbone of DNA and RNA introduce significant improvements to the oligonucleotides with regard the nuclease resistance, biological activity, binding affinity and cellular uptake. The chemical modifications in both PMO and PNA oligonucleotides results in neutral structure. X=H (DNA) or OH (RNA).

1.3.1.2 Sugar modifications

The improvement of binding and potency has also been achieved through a number of modifications that occur on the sugar ring. These chemically modified sugars offer control over nucleotide sugar puckering (**Figure 10**), which is closely related to the oligonucleotides' binding affinity to complementary strands, duplex conformation and level of enzyme interactions. B-form dsDNA sugars adopt the South puckering (C2' endo), whereas A-form dsRNA sugars prefer the North conformation (C3'-endo) (see also section 1.2).[45] As it is known that RNA-RNA duplexes are usually stronger than DNA-DNA or DNA-RNA duplexes[77], modifications that mimic or stabilize the North conformation are therefore expected to display the highest affinity towards their target mRNA.

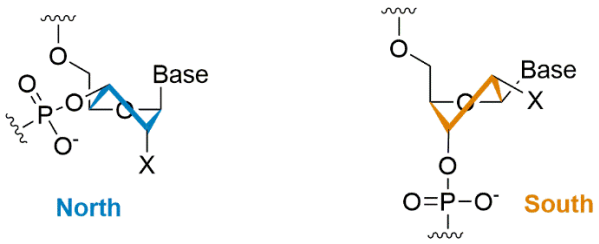

Figure 10. North and South nucleotide sugar puckering conformation.

One of the most commonly used modification on the sugar ring is 2'-*O*-methyl (2'-OMe) (see **Figure 11**).[78] 2'-OMe sugars have a North sugar conformation,[79, 80] mimicking RNA and tending to assemble into A-form duplexes.[80] In comparison to DNA, the introduction of 2'-OMe units increases the binding affinity toward complementary RNA,[81] and also increases the nuclease stability.[82] 2'-OMe modifications have been used widely in gapmers (see also Chapter 3). ASOs containing 2'-OMe have also made it to clinical trials[83] and are even present in the first FDA-approved aptamer (Macugen) and FDA-approved siRNA therapy (Onpattro) (see **Table 1**).[48] Other substitutions of the RNA 2'-OH are also widespread and have similar properties. The most common one is 2'-*O*-(2-methoxyethyl) (2'-MOE) (**Figure 11**),[84] which increases target binding affinity,[85, 86] improves nuclease stability[85] and adopts a North sugar confirmation suitable for RNA binding. As a consequence, 2'-MOE has found widespread use in ASO technologies and is present in most of the FDA approved antisense drugs (see **Table 1**).

2'-Fluoro-RNA (2'-F-RNA) (**Figure 11**),[87-89] is another sugar modification mimicking RNA by adopting a North conformation. The preference for the North conformation is influenced by the gauche effect exerted by the 2'-fluorine.[90] 2'-F-RNA increases the binding affinity for target RNA strands.[86, 88, 91] While some of this stabilization is the result of the preference for the North conformation, the main contribution towards the increased binding affinity comes from increased base-pairing and stacking interactions arising from the electronegative fluorine, through mechanisms that are not fully understood.[92] 2'-F-RNA modifications do not substantially increase exonuclease resistance.[85] This modification is also present in the FDA-approved aptamer, Macugen (**Table 1**).[48] An isomer of this modification, 2'-F-ANA (**Figure 11**), has also been reported. 2'-F-ANA is a DNA rather than RNA mimic, adopting a South/East sugar pucker (corresponding to the furanose form of arabinose rather than ribose, hence the name ANA).[90, 93, 94] 2'-F-ANA modifications increase binding to complementary RNA strands,[95, 96] and show enhanced nuclease stability.[97, 98]

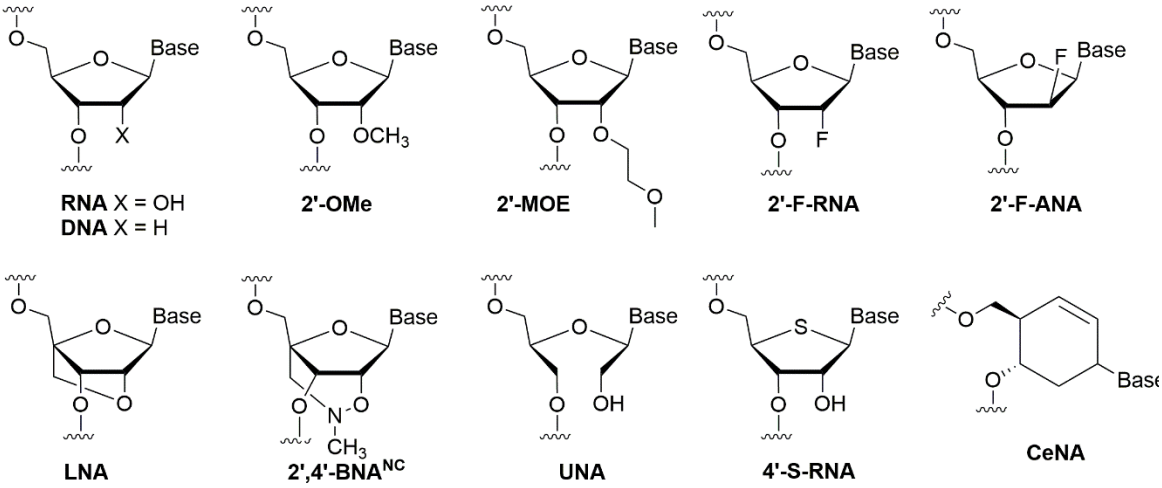

Figure 11. Commonly used oligonucleotides with chemically modified sugar units. Most modifications involve the 2' position of RNA. Other modifications include the replacement of the ring oxygen with sulphur (4'-S-RNA), bridges between C2' and C4' positions (LNA, BNA) and ring expansion (CeNA).

Locked nucleic acid (LNA) is an RNA analogue where a methylene bridges the 2'-OH and the C4' (see **Figure 11**).[99] Due to this cyclisation, the furanose conformation in LNA is restricted to the North conformation,[100, 101] which closely mimics the A-form of RNA and thus preorganizes LNA for RNA-binding.[99-101] The resulting duplexes possess some of the highest thermal stabilities known,[100] and also display improved nuclease resistance.[102] LNA is the best known member of a larger family of bicyclic or bridged nucleic acids (BNAs), which have different types of bridges to restrict the sugar conformation. Many types of BNA enhance the thermal stability of duplexes.[103, 104] For example, a recent BNA modification called 2`,4`-BNA^{NC} (**Figure 11**) exhibits higher binding affinity to cRNA and excellent single-mismatch discriminating ability.[105] In contrast to the highly restricted conformations of LNA and BNAs, unlocked nucleic acid (UNA) is missing a covalent bond between the C2'and C3' atoms of a ribose sugar and hence has a high degree of flexibility (see **Figure 11**). UNA modifications have been shown to lower duplex T_m.[106]

From the above discussion, it is clear that substitutions on the C2' atom are the most common modification of the sugar ring, although other types of alterations can also be beneficial. For example, 4'-S-RNA where the central oxygen is replaced by a sulfur atom (**Figure 11**), has been shown to enhance nuclease stability.[107, 108] Cyclohexene nucleic acid (CeNA) (see **Figure 11**) is an example of an expansion on the sugar ring.[109, 110] CeNA binds RNA with higher affinity than DNA, and shows increased serum stability.[109]

1.3.1.3 Nucleobase modifications

Not only modifications to the backbone of DNA and RNA can influence the affinity towards the target mRNA of an antisense oligonucleotide, changes to the bases themselves will also affect the binding strength. Some of the most common modifications involving the nucleobases involve the positions 4 and 5 for the pyrimidines and 2, 6 and 7 for purines. Modifications in these positions do not affect the geometry of the double helix, but can affect the stability of the duplex.[111] Methylation of cytosine at the 5-position (**Figure 12**), for example, was found to enhance the binding affinity of DNA/RNA heteroduplexes.[84] Furthermore, unmodified ssDNA can trigger TLR9 elimination (a type of innate immune response),[112, 113] while the presence of a 5-methyl group in cytosine has been shown to reduce TLR9 recognition and thus results in lower immune-mediated toxicity of the ASO.[114]

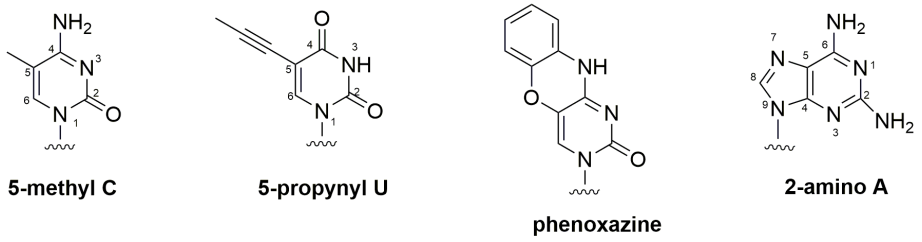

Figure 12. Selected nucleobase modifications that increase binding affinity with complementary nucleic acids.

Another example of a nucleobase modification is 5-propynyl-modified uracil (see **Figure 12**). This analogue enhances duplex stability by increasing π-π stacking interactions.[115-117] Similarly, the tricyclic cytosine analogue phenoxazine (**Figure 12**) pairs with guanosine with increased binding affinity due to stronger stacking interactions.[118] Rather than increasing the stacking between bases, it is also possible to enhance base pairing by promoting additional hydrogen bonding. For example, the 2-aminoadenosine (2-amino A) modification (see **Figure 12**) provides an extra hydrogen bond with thymine and thereby enhances duplex stability compared to unsubstituted adenosine.[119] Of course, it is also possible to combine modified nucleobases with modified backbones in order to optimize the properties of the oligonucleotide. The investigation of any new antisense oligonucleotide will thus have to include careful consideration (and possible screening) of the types of modifications that are most suited for its specific application.

1.3.2 Approaches to inhibit protein translation by targeting mRNA

The compatibility between the chemically modified oligonucleotides and DNA/RNA is one of the principles of gene silencing. However, after duplex formation between the ASO and the target mRNA, there are a number of mechanisms by which the ASO can inhibit protein translation. Steric blocking is conceptually the easiest mechanism. It is based on the principle that by binding to complementary mRNA, the ASO blocks ribosome assembly (see **Figure 13**).[120] Disadvantages of steric blocker ASOs include the difficulty of detecting their translational inhibition[91] and the requirement for high doses.[111] Newer technologies have emerged over the years that elicit cleavage of the target RNA by the recruitment of endogenous endonucleases. Because the target mRNA is degraded by this process, the ASO becomes catalytic and dosage can thus be reduced, which has facilitated the development of ASOs as therapeutics.[45, 111] A number of different enzymes can be recruited for the cleavage of target mRNA, the most relevant of which are RNase P and RNase H (they will be covered in more detail in Chapter 2 and Chapter 3 respectively) (see **Figure 13**).[45]

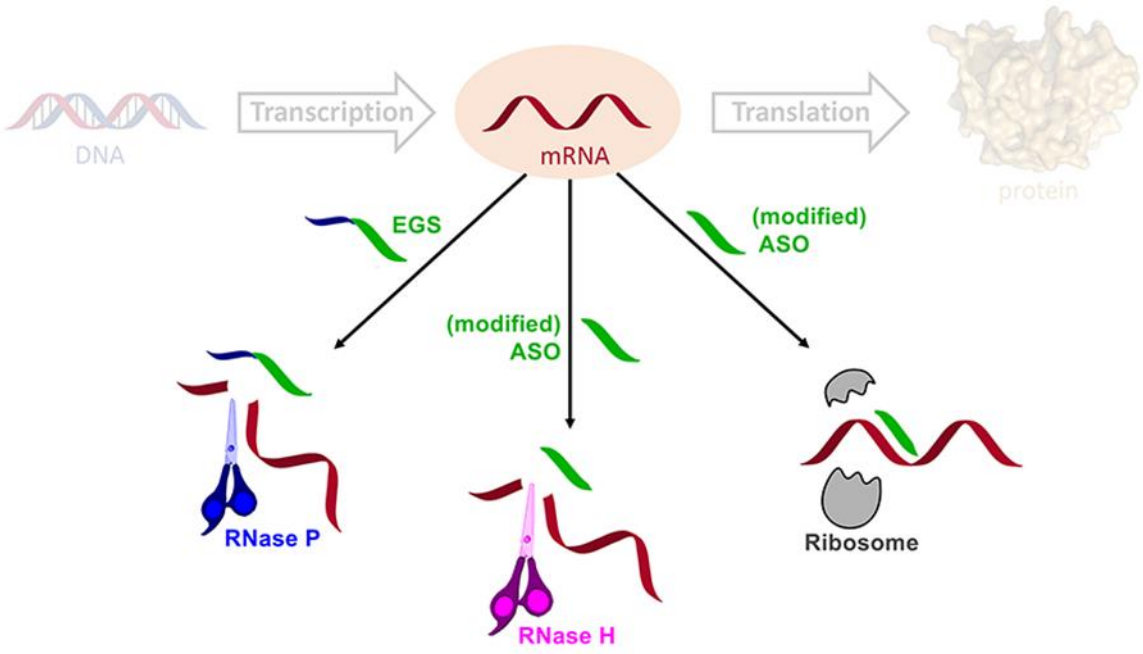

Figure 13. Antisense oligonucleotides applied to inhibit mRNA translation by steric blocking of the ribosomal binding site, or by the recruitment of nucleases such as RNase P or RNase H.

RNase H is the most common enzyme to be recruited by ASOs to cleave their target mRNA, especially in eukaryotic cells (see also FDA approved drugs in **Table 1**).[121] RNase H is also present in bacteria and the recruitment of this enzyme by ASOs is therefore a possible strategy for antibiotic development (see Chapter 3). The natural substrate of RNase H is a DNA/RNA duplex,

where it catalyses the cleavage of the RNA strand.[91, 122-124] This implies that, for the ASOs to be a successful RNase H recruiter, it needs to display a DNA-like structure.[125-127] This limits the applications of many chemically modified ASOs, which usually display a more RNA-like structure (see discussion above). This problem has been largely overcome by the introduction of 'gapmers', which are oligo-nucleotides that contains modified nucleotides at the 3' and 5' ends for increased affinity and nuclease stability, and a central stretch of DNA that is capable of recruiting RNAse H.[45, 57, 128, 129] Gapmer technology will explained in more detail in Chapter 3.

RNase P is a ubiquitous endonuclease found in all three domains of life: bacteria, eukarya and archaea.[130] The natural substrate for RNase P is a precursor tRNA and the design of ASOs able to recruit this enzyme is therefore not straightforward. Altman and co-workers were the first to develop a mechanism to recruit RNase P for the cleavage of a target mRNA in 1990.[131] They coined this technology 'external guide sequence' (EGS). This EGS approach towards the development of antisense oligonucleotides as antibiotics will be explained in more detail in Chapter 2 and Chapter 4.

There have also been other approaches developed that can result in gene silencing by recruiting different nucleases, such as approaches based on microRNAs (miRNA) and small interfering RNAs (siRNA).[45] However, these technologies are tailored toward mammalian cells and are not being used in bacterial cells. Covering these topics would thus be beyond the scope of this report given that this project focusses on antisense oligonucleotides in bacteria.

1.3.3 Clustered regularly interspaced short palindromic repeats (CRISPR)

Beside the recruitment by antisense oligonucleotides of RNase H or RNase P for the degradation of target mRNA, there are other possible oligonucleotide-based technologies that could lead to the development of new antibiotics. A potential candidate is the use of CRISPR (clustered regularly interspaced short palindromic repeats), which has boomed in the last few years. During this PhD, I was privileged to collaborate with Professor Craig Mello and his research group on a project involving the use of chemical modifications of the DNA template to improve the efficiency of CRISPR in eukaryotic cells (data not included in this thesis).[132]

CRISPR is a gene editing mechanism used naturally by bacteria as a type of adaptive immunity against invading viruses (**Figure 14**).[133] As a bacterium overcomes a viral infection, the bacterium can store a fragment of the viral genome into its own DNA to provide immunity against a future infection. This is achieved by inserting the fragment of viral DNA into short snippets of replicated

DNA sequences located in the CRISPR locus of the bacterium.[134, 135] This modified DNA is subsequently transcribed into RNA, and the transcribed CRISPR RNA (crRNA) functions as a guide for the CRISPR-associated protein (Cas) to find and cleave viral DNA should the virus invade the bacterium again, through complementarity between the crRNA and the viral DNA.[136]

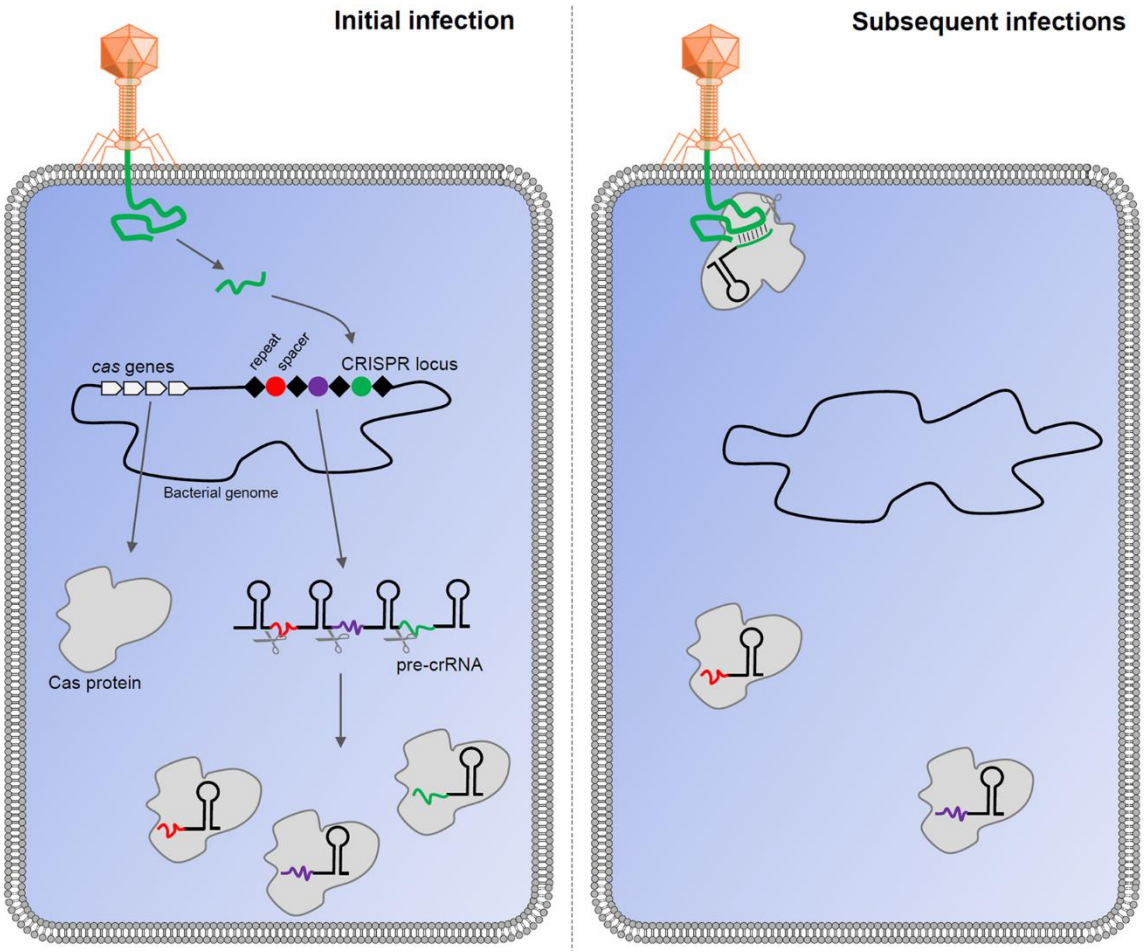

Figure 14. CRISPR adaptive immune system in bacteria. During an initial infection by a virus, the bacteria can incorporate some of the viral DNA into its own genome in the CRISPR locus. This region can get transcribed to pre-crRNA, which is cleaved to mature crRNAs that form complexes with the appropriate Cas protein. If a subsequent infection occurs, the viral DNA is recognized and cleaved by the crRNA/Cas complex.

The gene *cas* is not universal, and many different Cas proteins are known.[137] CRISPR/Cas systems are thus divided into two main classes (class 1 and class 2).[138-140] The difference between them is that class 1 CRISPR/Cas systems consist of multi-protein effector complexes, whereas class 2 systems utilize a single effector protein.[141] The most commonly used CRISPR/Cas system employs *Streptococcus pyogenes* Cas9 (*Sp*Cas9). In this system, the complex formed from CRISPR RNA (crRNA) and DNA endonuclease enzyme Cas9 is able to induce cleavage of both strands of a target dsDNA.[142, 143] This CRISPR/Cas9 system has been manipulated to allow precise genetic engineering in various organisms.[144, 145] In this case, crRNA is replaced with a synthetic single guide RNA

(sgRNA), which has a region complementary to the target DNA and a region that allows complex formation with Cas9.[146] When this system induces cleavage of the target dsDNA at the desired position, it opens the door for precise gene deletions, point mutations, gene insertions or other genetic techniques. As a result, the interest in CRISPR technology has been growing rapidly in the last 5 years.[147] However, the focus has been largely on the use of CRISPR in eukaryotic cells, which is beyond the scope of this thesis.

We mentioned above that the CRISPR/Cas system is naturally present in bacteria as a defence mechanism against viruses. It should thus be possible to highjack the natural system and design CRISPR technology where the bacteria will cleave its own DNA, resulting in antibacterial activity. Researchers have shown that reprogramming of the CRISPR system toward self-targeting and cleaving of the bacterial genome generally leads to cell death.[148, 149] Both endogenous and exogenous Cas proteins have been used to this extent. For example, Gomaa *et al.* showed that transformation of *E. coli* cells with a plasmid encoding an engineered CRISPR1 array targeting genomic DNA, leads to the removal of these cells from the culture.[150] Citorik, Mimee and Lu engineered bacteriophages delivering a genetic construct encoding for Cas9 and sgRNAs against various virulence and antibiotic-resistance genes in *E. coli*.[151] They were able to demonstrate the antibacterial activity of their constructs in both cultures and *Galleria mellonella* moth animal infection models. Bikard *et al*. used the same approach to selectively kill virulent, but not avirulent, strains of *S. aureus* through phagemid-mediated delivery of a CRISPR/Cas9 system targeting virulence genes of *S. aureus*.[152] This was further corroborated by the effectiveness of their CRISPR/Cas9 system to kill *S. aureus* in a mouse skin infection model. We expect that this field will continue to grow and that more CRISPR-based antimicrobials will start to emerge, especially when the challenges regarding the delivery of these systems can be overcome.[148, 149, 153]

1.3.4 Approaches for the delivery of ASOs into cells

The largest problem hindering the use of ASOs as antibacterial agents is the delivery of these oligonucleotides into bacteria.[42] For an antisense oligonucleotide to have any therapeutic value, it has to be able to reach its target DNA or RNA strand and therefore it has to be able to cross the cell membrane to reach the cytoplasm and/or nucleus. However, the physiochemical properties of ASOs are not stacking in their favour as a potential drug. Antisense oligonucleotides fail Lipinski's rule of five on all accounts (Clog*P* ≤ 5, molecular weight ≤ 500 g/mol, ≤ 5 hydrogen bond donors and ≤ 10 hydrogen bond acceptors).[154] The high molecular weight and the length of ASOs (8-50 nucleotides) hinder diffusion across the lipid bilayer of the host cells.[154] These factors cause

difficulties in absorbing ASOs in the blood stream and therefore limit the oral administration of ASOs. As a result, most FDA approved oligonucleotide-based drugs are administered through injection (intravenous, intravitreal or intrathecal depending on targeted organ), and many have targets located in the liver where ASOs tend to accumulate.[42, 155, 156]

The delivery of oligonucleotides to prokaryotic cells is even more challenging than for eukaryotic cells. Unlike eukaryotic membranes, bacterial cell membranes contain large amounts of negatively charged lipids such as cardiolipin and phosphatidylglycerol, and therefore carry a net negative charge.[157] As most oligonucleotides are highly hydrophilic and carry a negative charge themselves (except PNA and PMO), diffusion across bacterial membranes is very unfavourable. In addition, bacteria are surrounded by a thick cell wall consisting of cross-linked peptidoglycan (Gram-positive bacteria), or by a thinner cell wall surrounded by a second lipid bilayer (Gram-negative bacteria), which provide additional barriers for ASOs to reach their target (**Figure 15**).[158, 159] It is important to note that small-molecule based antibiotics penetrate the outer membrane of Gram-negative bacteria mostly through porins (narrow ß-barrel proteins with a channel lined with charged amino acids), but this route is not available to oligonucleotides.[160] To overcome these barriers, many strategies have been developed to aid the delivery of ASOs into bacteria, mainly by reducing the charge repulsion between the bacterial membrane and the ASOs.[42]

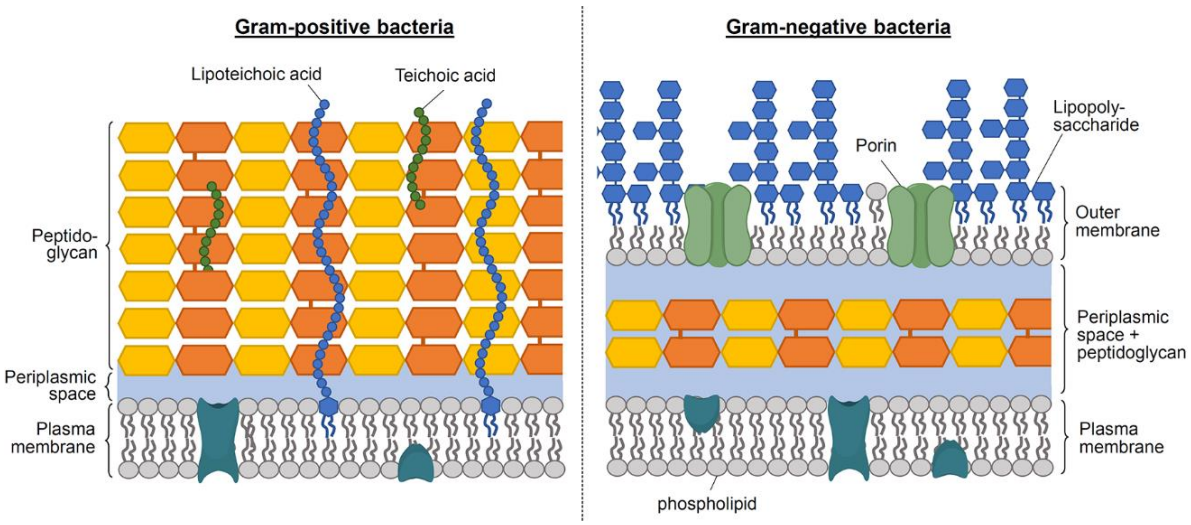

Figure 15. Comparison between the cell membrane and cell wall of Gram-positive and Gram-negative bacteria.

1.3.4.1 Non-peptidic delivery methods

One way to deliver oligonucleotides into cells is the use of physical transformation techniques. These involve the formation of transient pores in the cell membrane by means of strong physical forces, such as electric currents or ultrasound, through which DNA can enter the cell.[161] The most

commonly used method in bacteria is electroporation, in which the cells are exposed to a brief electric pulse to generate transient nanometer-sized pores in the cell membrane through which DNA (usually plasmids) can pass.[161, 162] In addition to these physical methods, DNA can be inserted into bacteria when using chemically competent cells. To create competent cells, the bacterial growth medium is adjusted to allow more efficient uptake of DNA (often the presence of high concentrations of divalent cations such as Ca^{2+} and Mg^{2+} is needed, as well as a heat-shock).[163] While these methods have been used to deliver plasmids encoding for ASOs into bacterial cells (most ASOs using the external guide sequence technology have been tested this way, see Chapter 2: introduction), it must be noted that these methods are only useful for *in vitro* proof-of-concept studies and are not suitable for clinical use of ASOs as antibiotics.

As viruses are essentially DNA (or RNA) packaged into a protein capsule capable of inserting its genetic material into host cells, it comes as no surprise that viruses have been employed for the delivery of oligonucleotides and longer gene constructs.[164, 165] In fact, both FDA-approved gene therapies, Luxturna and Zolgensma, employ engineered viruses for efficient cellular delivery (see **Table 1**). Bacteriophages are viruses that selectively target certain bacteria, and could therefore be utilized for the delivery of ASOs to bacteria. However, viral DNA is longer than the 8-50 nucleotide long ASOs and viral vector-based delivery of ASOs is therefore not common. In addition, bacteriophages can have a very narrow host range, implying that new viruses need to be engineered for each type of target bacteria.[148, 149, 153] The use of bacteriophages for the delivery of oligonucleotide-based antibiotics has therefore been limited to the proof-of-principle studies of the CRISPR systems discussed in section 1.3.3.

Cationic polymers,[166, 167] as well as lipid nanoparticles constituting of cationic, anionic or neutral lipids (**Figure 16**) have proven very efficient delivery vehicles for ASOs in mammalian cells.[168-171] However, when used for the delivery of ASOs to bacterial cells, it was found that these classic delivery systems showed less efficient oligonucleotide uptake and higher cytotoxicity in bacterial cells than in mammalian cells.[172] Nevertheless, some researchers have achieved good oligonucleotide uptake in bacteria using various liposome or lipid-polymer formulations.

Lagacé and co-workers used anionic liposomes constituting of 10:1 DPPC:DMPG (**Figure 16**) for the delivery of an ASO targeting the *lacZ* gene in *E. coli*.[173] They were able to show measurable uptake of the oligonucleotides into the cell and a 42% reduction in β-galactosidase activity after delivery of the liposome-encapsulated anti-*lacZ* ASO (compared to 6% for the free ASO). Meng *et al.* were able to restore susceptibility to fluoroquinolone-resistant *E. coli* by delivering an ASO targeting *acrB* mRNA using a liposome made from the EYPC, PEG_{2000}—DSPE and DMPG encapsulating a complex of the ASO with polyethyleneimine (PEI) (**Figure 16**).[174] More recently,

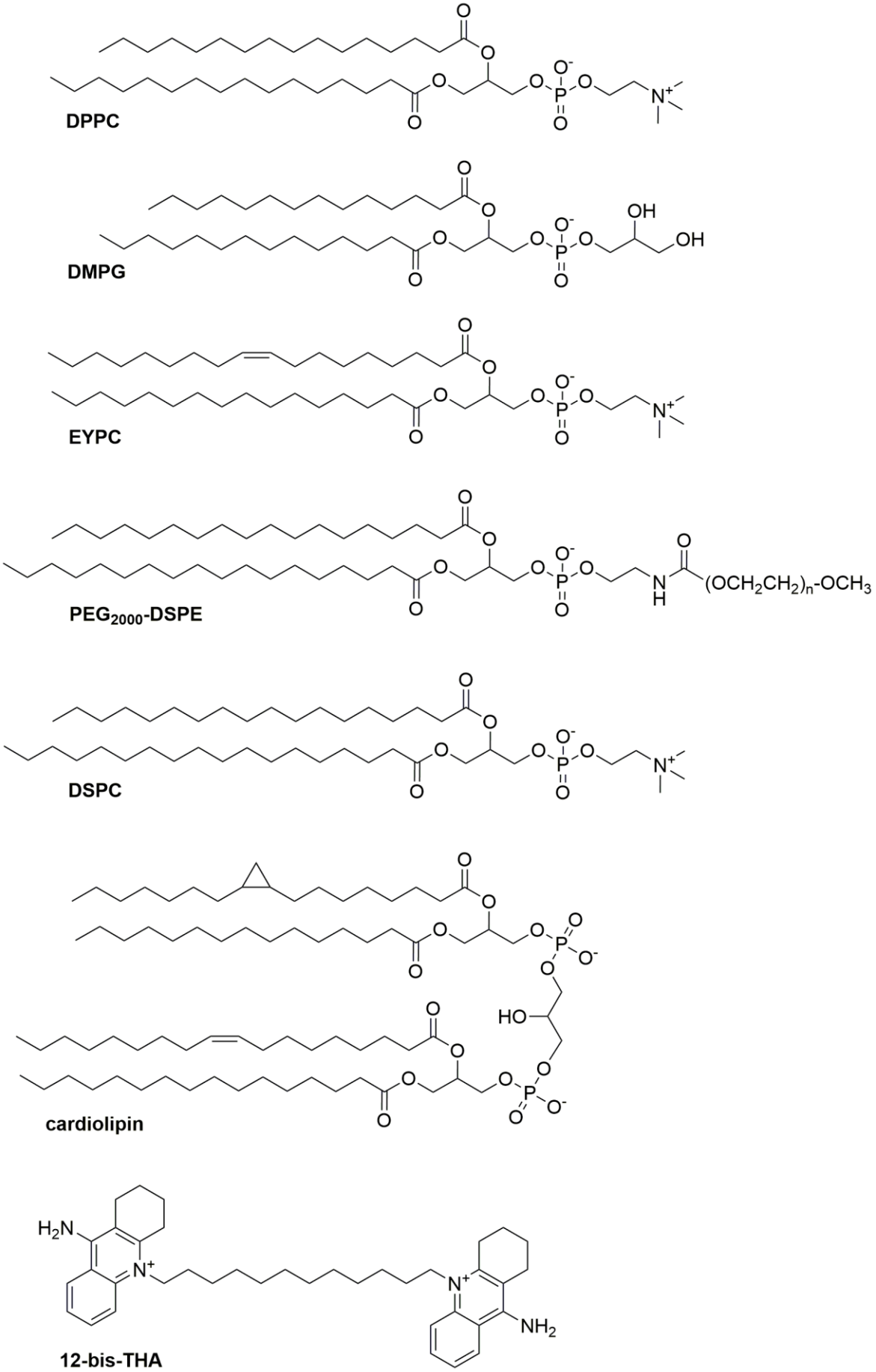

Figure 16. Structures of some of the lipids used for the delivery of ASOs in bacterial cells.

Malinge and colleagues showed that various nucleic acids (11 nt ssDNA, 15 bp and 95 bp dsDNA, 9 kbp DNA plasmid, 1000 nt RNA and 11 nt ASO) could be efficiently internalized by *E. coli* and *P. aeruginosa* when first condensed with the cationic polymer PEI, followed by encapsulation into anionic DSPC/cardiolipin liposomes (**Figure 16**).[175] Additionally, they showed that the application of their system for the delivery of an anti-*acpP* ASO leads to significant growth inhibition in both bacteria species.

Bolaamphiphiles are amphiphilic molecules with two hydrophilic headgroups (usually cationic) connected by a hydrophobic chain, and as such have also been used for oligonucleotide delivery. Marín-Menéndez *et al.* used the cationic bolaamphiphile 12-bis-THA (**Figure 16**) to form self-assembled nanoplexes with transcription factor decoy (TFD) oligonucleotides and showed that these nanoplexes could deliver the oligonucleotides to *E. coli* and *C. difficile*.[176] Similarly, Stewart and co-workers employed the same cationic bolaamphiphile for the delivery of ASOs against various essential genes in *C. difficile*.[177]

Another strategy commonly employed for the delivery of oligonucleotides to mammalian cells, is the covalent attachment of a ligand recognized by native membrane receptors.[155] The most famous example is the use of GalNAc to increase the uptake of oligonucleotides into liver cells through binding to the asialoglycoprotein receptor which is expressed in the hepatocytes.[178, 179] Trylska and colleagues have tried to develop a similar strategy for the delivery of ASOs into bacterial cells, based on the observation that many bacteria need vitamin B12 for growth but cannot make the vitamin themselves and therefore express membrane proteins for its uptake.[180, 181] They covalently linked vitamin B12 to a PNA ASO targeting the mRNA encoding Red Fluorescent Protein (RFP), and were able to show effective delivery of these constructs into *E. coli* and *S. typhimurium*.[182]

1.3.4.2 Cell penetrating peptides

Cell penetrating peptides (CPPs) are widely used as drug delivery vehicles and have become the most promising strategy for the delivery of ASOs into bacteria.[183] CPPs are short peptides that usually carry a high cationic charge due to numerous lysine and/or arginine residues, and that have been shown to mediate the uptake of various drugs into cells. Most CPPs are derived from natural sources, such as the HIV Tat protein[184] and derivatives of antennapedia transcription protein (*Drosophila*).[185] The earliest attempt of using cationic peptides to deliver drugs across biological membrane goes back to 1978, when Ryser and Shen were able to deliver an anticancer drug in drug resistant cells *in vitro* and in mouse models using a poly-L-lysine conjugate.[186] Later

on, in 1995, a CPP was used for the first time to deliver an antisense oligonucleotide aimed at reducing the expression of the amyloid precursor protein into cells.[187] While many studies have used CPPs for ON delivery since then, their mechanism of action is still not fully understood.[183] It is likely that the mechanism depends on the exact nature of the CPP, the nature of the target cell and the experimental procedure. The cationic charge of these peptides seems to play a major role in their mechanism. This charge allows the peptide to interact with the proteoglycans outside the cell membrane, or with the phospholipids of the cell membrane. Upon this interaction, the CPPs are internalized through endocytotic pathways[188] or via direct membrane translocation.[189] Direct membrane translocation might be more relevant for bacterial studies, as this resembles the mechanism of action of antimicrobial peptides.[190] The mechanism of direct translocation is not fully understood and suggestions involve the formation of (transient) toroidal or barrel pores, carpet models or spontaneous (or gradient-mediated) translocation without membrane disruption (see **Figure 17**). [183, 189, 190]

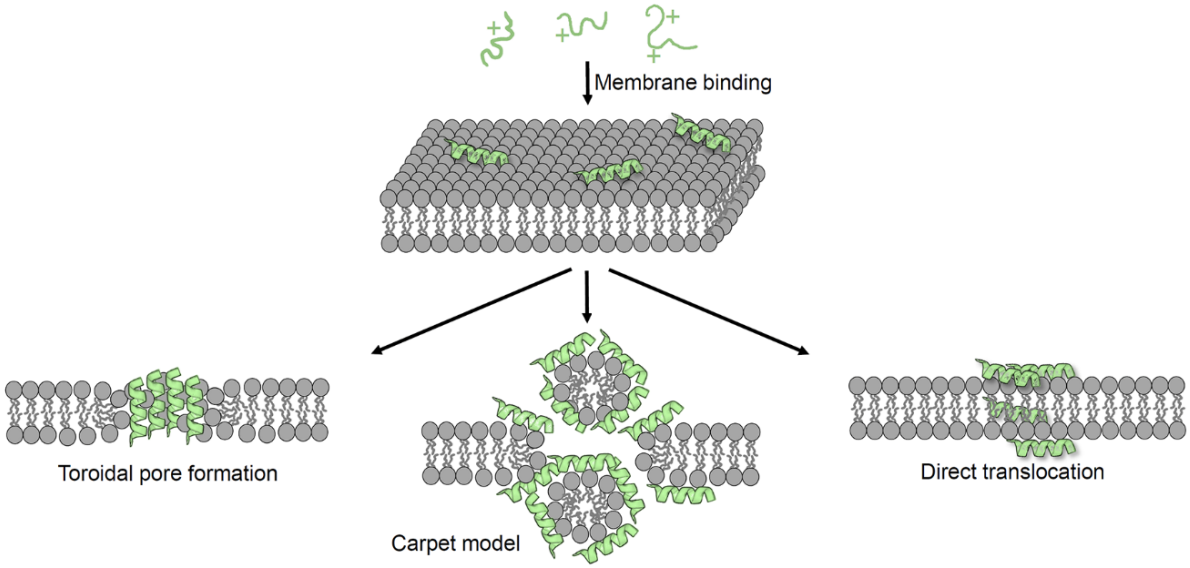

Figure 17. Proposed mechanisms for the direct translocation of CPPs through cell membranes. Upon interaction of the CPP with the membrane, either transient pores are formed, or the membrane becomes 'carpeted' with the peptide, leading to destabilization. Spontaneous translocation (sometimes driven by membrane potential) across the membrane has also been suggested. The peptide is shown as an α-helix for clarity (not all CPPS are helices).

For CPPs to function as delivery vehicles for ASOs, the peptide can either be covalently conjugated to the oligonucleotide, or non-covalent CPP/ASO nanocomplexes can be formed between negatively charged ASOs and positively charged CPPs.[183] While the latter has been used successfully for the delivery of oligonucleotides to mammalian cells,[191-193] it has not been used for the delivery to bacterial cells. Covalent attachment of the peptide to the ASO is a more common strategy. However, it is difficult to conjugate negatively charged oligonucleotides to CPPs because

of the aggregation or precipitation that will occur as a result of the complementary charges.[194] Nonetheless, researchers have reported some success in conjugating negatively charged oligonucleotides to CPPs using thiol-maleimide reactions[195] or 'click' chemistry between and azide and alkyne (see **Figure 18**).[196] An easier way to overcome the synthetic problems of covalent conjugation, is the use of a neutral backbone such as PNA and PMO (see **Figure 9**) for the ASO. Because the PNA backbone involves peptide linkages itself, a CPP can be easily assembled at the C- or N-terminus of the PNA during solid-phase synthesis, without the need for a separate conjugation step. This is not possible for the PMO backbone, for which a separate conjugation step is required. This can be done either through a linker, or via a direct amide coupling between the secondary amine of PMO and the carboxylic acid of the peptide C-terminus (see **Figure 18**).

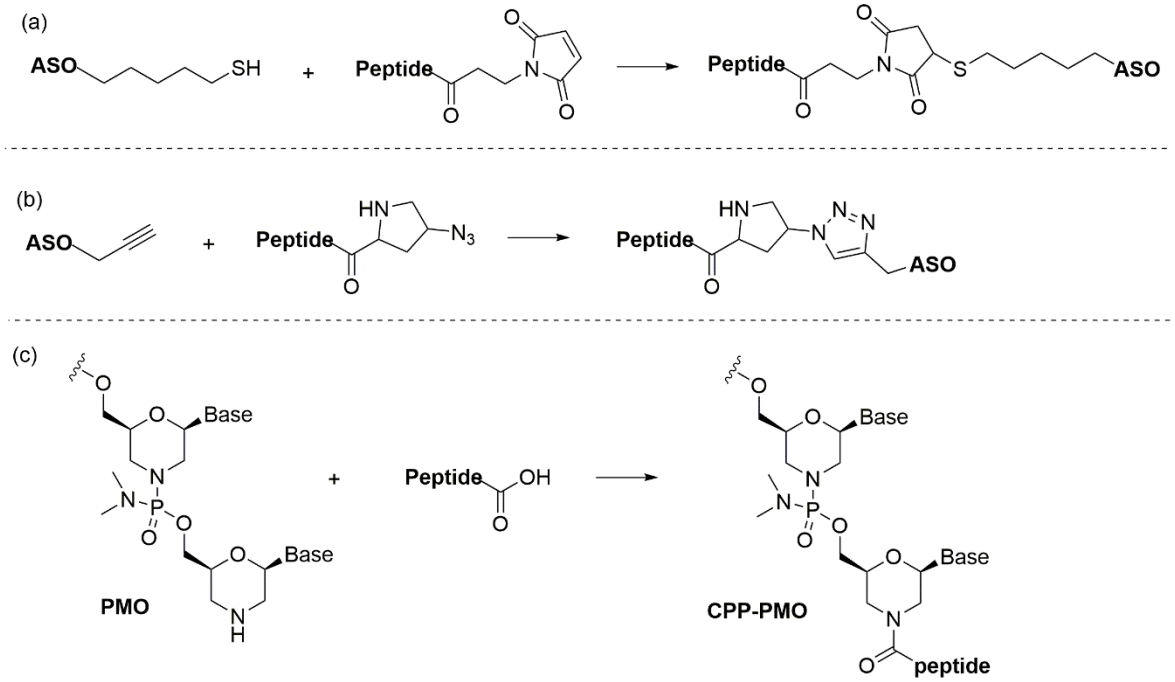

Figure 18. Conjugation strategies for linking CPPs to oligonucleotides: (a) thiol-maleimide reaction; (b) click reaction; (c) direct amide coupling between PMO and a CPP.

Good and co-workers were the first to use CPPs conjugated to PNA as a potential antisense antibacterial agent.[197] They attached the membrane active peptide KFFKFFKFFK to an antisense PNA targeting the *lacZ* and *acpP* genes, and showed that this conjugation significantly increased the potency of the PNA. Many researchers have followed in their footsteps and the most commonly used CPPs for increasing the uptake of PNA and PMO into bacterial cells are now KFFKFFKFFK and RXRRXRRXRRXRXRXB (X is 6-aminohexanoic acid, and B is ß-alanine).[42] These two peptides sequences have shown high efficiency in delivering PNA and PMO into a variety of Gram-positive and Gram-negative bacteria.[42] For example, the KFFKFFKFFK peptide has been used to

deliver ASOs into *E. coli,*[197-200] *S. typhimurium,*[201] *L. monocytogenes,*[202, 203] *S. aureus,*[204, 205] *S. pyogenes,*[206] *B. suis*,[207] *S. pseudintermedius,*[204] *K. pneumonia,*[208] and *M. smegmatis;*[209];while the RXRRXRRXRRXRXRXB peptide has been employed for delivery into *E. coli,*[201, 210, 211] *S. aureus,*[212, 213] *P. aeruginosa,*[214, 215], *A. lwoffii,*[194],*A. baumannii,*[105, 194, 211] *K. pneumonia,*[211] *S. enterica*[211] and *S. flexneri.*[211] Franzyk and co-workers tested a variety of 16 different antimicrobial peptides for their ability to improve the uptake of antisense PNAs into *E. coli.*[216] They found eight peptides that were able to increase the delivery of PNA (buforin 2-A, drosocin, oncocin 10, Pep-1-K, KLW-9,13-a, (P59→W59)-Tat48− 60, BF-2A-RXR and drosocin-RXR). Antisense oligonucleotides conjugated to ASOs have also been shown to be effective against intracellular infection, which requires additional uptake of the ASO by the infected host cell before it can reach the bacteria. Abushahba *et al.* synthesized conjugates of a PNA targeting the *rpoA* genes with different CPPs and showed that they had antimicrobial activity against the intracellular pathogen *L. monocytogenes* in bacterial cultures and in a *Caenorhabditis elegans* (*C. elegans*) infection model.[217] Similarly, Boyle and co-workers developed PNA-CPP conjugates that can inhibit the growth of *B. suis* in bacterial cultures and in infected murine macrophages.[207] In light of these successes, the use of CPPs is arguably the most promising strategy in the development of antisense antibacterial agents with clinical relevance.

1.4 Antisense oligonucleotides as antibacterial agents in animals

As mentioned earlier, the first use of antisense oligonucleotides as antibacterial agents was in 1981, when protein synthesis and growth were targeted with non-ionic oligonucleotides complementary to the 3' end of 16S rRNA in *Escherichia coli*.[40] The research on using antisense oligonucleotides ASOs as an efficient antibiotic has progressed significantly since it started over three decades ago. This has been mainly due to the identification of essential genes and the number of sequenced genomes (allowing more facile target identification), but also due the developments on chemical modifications (see section 1.3.1) and the ability to recruit nucleases such as RNase P (see section 1.3.2). Finally, the penetration through cell walls in bacteria using cell-penetration peptides (CPPs) conjugated to the ASO has had a major impact on the potential of using ASOs as antibacterial drugs (see section 1.3.4).[121] These advances have inspired a variety of studies demonstrating the antibacterial properties of antisense oligonucleotides in bacterial cultures.[42, 218] Some of these studies have already been discussed throughout this introduction, and more examples will be given in Chapter 2 and Chapter 3. However, the number of reports that have demonstrated the potential for treating bacterial infections by ASOs in animal models is still limited.[121]

In 2005, Geller *et al.* were the first to report the targeting of an essential gene (*acpP)* in *E. coli* in a mouse model of infection. The report showed a reduction in bacterial growth in both cultures and in mice using a PMO antisense oligonucleotide, but the strongest effects were seen using a membrane-permeable mutant *E. coli* strain (AS19).[219] Later studies indicated that tethering of a cell penetrating peptide (CPP) can significantly improve the effectiveness of the PMO to treat mice infected with *E. coli*.[220] The same group have also reported the *in vitro* and *in vivo* (mice models) antibacterial activity of CPP-conjugated PMOs targeting the *acpP* gene in *A. lwoffii* and *A. baumannii,*[194] as well as *B. anthracis*.[221] Similarly, Tan *et al.* used a PNA-CPP conjugate to target the *acpP* gene in *E. coli* and showed that it was effective in rescuing infected mice.[200] More recent studies have also shown success in targeting other essential genes in bacteria *in vivo*. Sawyer and colleagues demonstrated efficient targeting of *gyrA* (a gene required for replication) in *S. aureus* by applying a CPP-PMO in a skin wound model of infection.[222] Additionally, the same group reported successful targeting of *ftsZ* (a gene involved in cell division) in *S. aureus* in a mouse model using CPP-LNA. They reported a 60% increase in survival rate of the mice after a single treatment dose of 3 mg/kg.[223] More recently, Howard *et al.* showed that CPP-PMO conjugates targeting the essential genes *acpP*, *lpxC*, or *rpsJ* of *P. aeruginosa* can inhibit biofilm formation and can reduce infection in mouse models of pneumonia.[224]

A recent trend in the field has been the targeting of virulence genes in bacteria. Targeting virulence genes can make pathogenic bacteria less aggressive when causing infections. It is believed that targeting virulence genes rather than essential genes may reduce the chance of bacterial resistance (antibiotic resistance), as there is weaker evolutionary pressure to develop resistance. Oh, Zang and Jeon targeted various regions of the *cmeABC* operon, which is responsible for the multidrug efflux pump in *Campylobacter jejuni.* They found two regions that, when targeted by PNAs, resulted in increased sensitivity to ciprofloxacin and erythromycin.[225] Goh *et al.* also used PNAs to target *mecA* and *ftsZ* and they found an increased sensitivity to oxacillin and a decrease in the targeted mRNA levels in *S. aureus* and *S. pseudintermedius.*[121] Meng *et al.* targeted the same gene (*mecA)* in *S. aureus* using phosphorothioate DNA and using anionic liposomes as carriers. They reported an increased survival rate of 30-50% in a mouse model of sepsis, when the mice were treated with a mixture of the ASO and oxacillin.[226]

Despite these success stories, it must be noted that most work on ASOs as antibiotics has been achieved using steric blockers. The recruitment of enzymes to cleave the target mRNA and thus reduce the dosage of the ASO, is rarer and largely limited to the recruitment of RNase P. However, RNase P recruitment has been mainly achieved using RNA-based oligonucleotides and very few modified ASOs have been investigated (see Chapter 2). There is therefore still a need to develop ASOs that can be used as powerful antibacterial agents.

1.5 Aim of the thesis

The aim of this thesis is to combine the benefits of modified nucleotides (higher RNA affinity, higher nuclease stability and improved pharmacokinetics) with the benefits of recruiting RNases (lower dosage of the ASO), and thereby increase the potential of antisense oligonucleotides as antibacterial agents.

Chapter 2 External Guide Sequence (EGS) technology using PNAs

2.1 Introduction and Aim

EGS, or external guide sequence, is the name given to an oligonucleotide technology first developed by Altman and co-workers as a means to recruit RNase P to cleave an mRNA strand.[227] In order to understand the full potential of this technology, it is necessary to first look at the fundamental properties of the nuclease.

2.1.1 RNase P

Ribonuclease P (RNase P) is a ribozyme and an endonuclease that processes the 5'-end in tRNA. RNase P is conserved among the three kingdoms of life (archaea, prokaryotes and eukaryotes). The components of RNase P in all kingdoms consist of a chain of RNA and a number of proteins, varying from one protein in bacteria to five proteins in archaea and ten in humans.[228, 229] A study has shown that the RNA component can display catalytic activity *in vitro* in the absence of the protein subunit, however with a reduced efficiency compared to the full RNase P complex.[230]

In prokaryotes, the RNA subunit is called M1 RNA and the protein subunit is called C5. M1 RNA and C5 protein are encoded by the *rnpB* and *rnpA* genes, respectively.[229] RNase P cleaves a variety of substrates in cells (see **Figure 19**) including a role in the maturation of tRNAs. Indeed, a precursor to amber-suppressing $tRNA^{Tyr}$ from *E. coli* was the first substrate analysed for RNase P cleavage.[231] More studies of the tRNA precursor substrates in *E. coli* and their models have shown that the sequence at the cleavage sites always consists of the junction between the single stranded region and double stranded region. However, these cleavage regions are not identical and they do not all share the typical structure of tRNA (stems and loops) (see **Figure 19**).[227, 232-234] Rieter *et al.* suggested a universal mechanism in which the RNase P functions in bacteria. In this mechanism, the C5 protein binds on top of M1 RNA and helps direct the complex to the precursor tRNA by interacting with the leader part of the precursor tRNA. This interaction allows the M1

RNA domains C and S to make multiple interactions with the TΨC and D loop regions in tRNA, respectively (see **Figure 20**).[235]

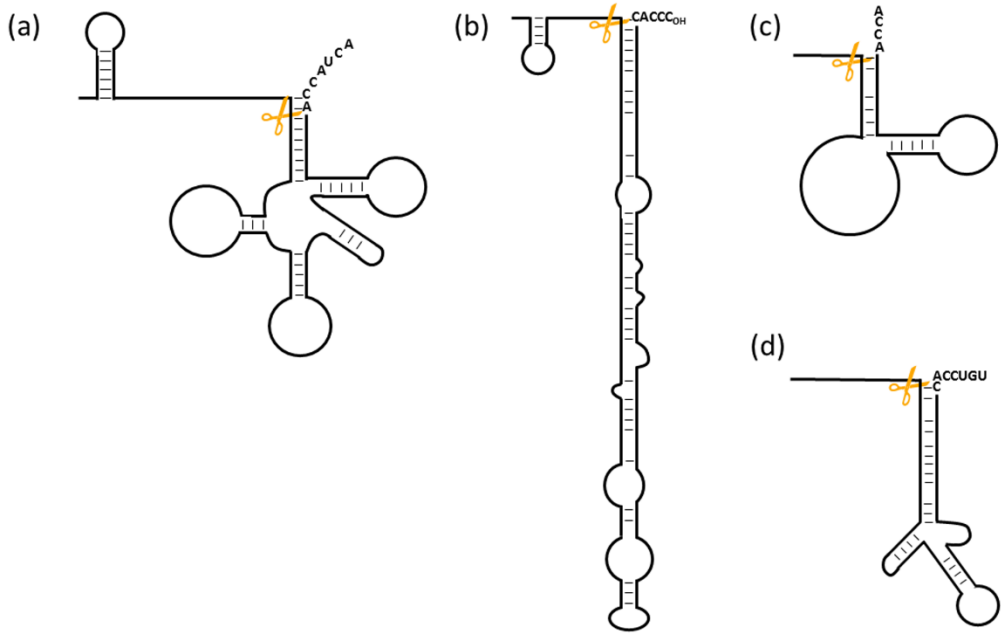

Figure 19. Different substrates for RNase P from *E. coli*. (a) Precursor to a tRNA. (b) Precursor to 4.5S RNA. (c) Precursor to tmRNA. (d) Precursor to a phage RNA. The orange scissors denote the RNase P cleavage site.[130]

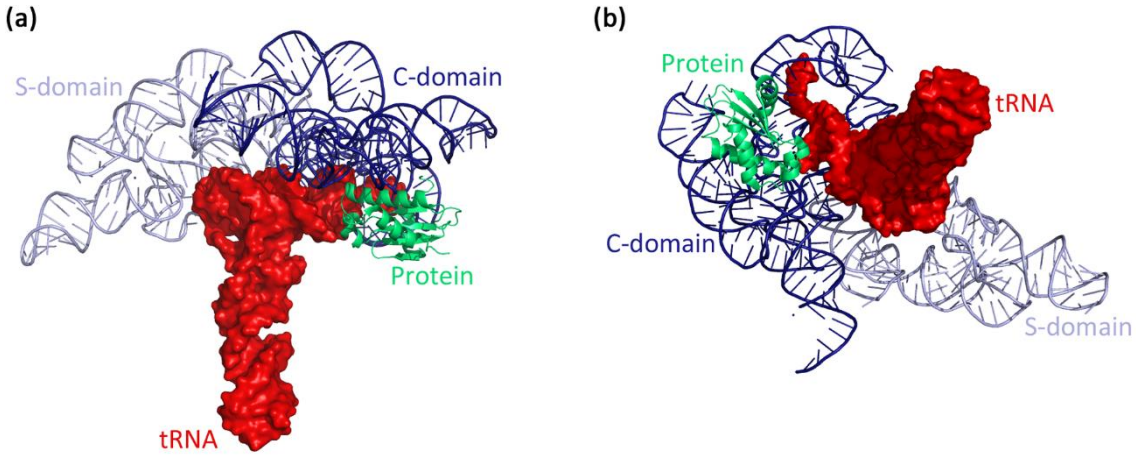

Figure 20. Two views of the crystal structure of the *T. maritima* RNase P holoenzyme, composed of a large RNA subunit (338 nucleotides, 110 kDa) and a small protein component (117 amino acids, 14.3 kDa), in complex with tRNA (76 nucleotides, 26 kDa). The RNA component serves as the primary biocatalyst in the reaction and contains two domains, termed the catalytic (C, blue) and specificity (S, light blue) domains. The RNase P protein (cyan) binds the 59 leader region of the pre-tRNA substrate and assists in product release. Transfer RNA (tRNAPhe) (red) makes multiple interactions with the active fold of the RNA component of RNase P. PDB ID: 3Q1Q.[235]

In 1990, Forster and Altman published a paper reporting the ability to recruit RNase P for the cleavage of RNA substrates that lack the conserved features of the usual substrates of RNase P,

but is made possible in the presence of an additional small RNA. RNase P is naturally guided by the single stranded sequence at the 3' end of precursor tRNA (ptRNA), so that it can cleave this RNA at the 5' end (see **Figure 21a**). Altman and co-workers suggested that to recruit RNase P for the cleavage of any mRNA by an antisense oligonucleotide, the ASO has to form a stem duplex with the targeted mRNA and must have an extra non-complementary strand sequence RCCA-3', with R any base, to recruit RNase P (see **Figure 21b**). They coined this technology External Guide Sequence (EGS).[131] Soon after the first publication, various research groups started to investigate the applications of EGS in both prokaryotic cells and eukaryotic cells targeting a wide spectrum of genes.

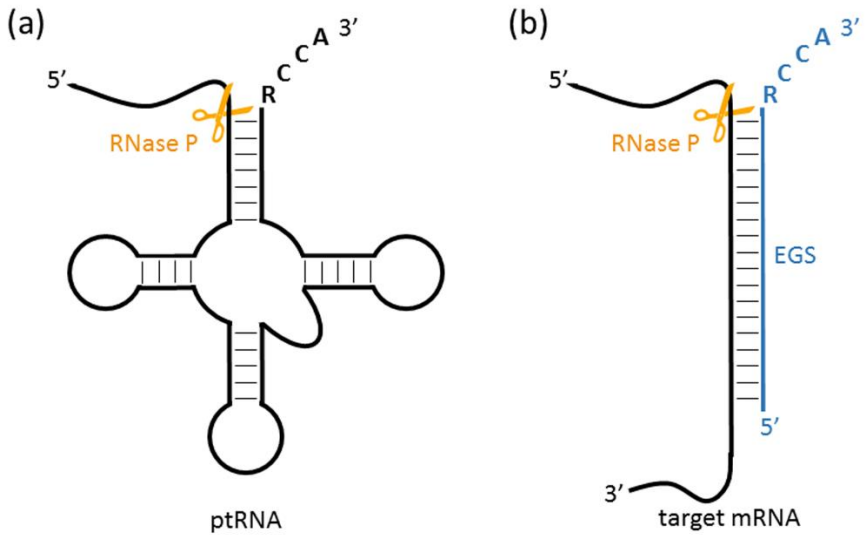

Figure 21. Summary of the EGS scheme. (a) A precursor tRNA. (b) Reduced structure of mRNA (black), complexed to an antisense oligonucleotide employing EGS technology (blue). The orange scissors denote the RNase P cleavage sites.[236]

2.1.2 EGS in Bacteria

In 1995, Takada *et al*. reported the first example of EGS-mediated gene regulation in *Escherichia coli*. They observed a 50% reduction on the induction of β-galactosidase (*lacZ*) and alkalinephosphatase (*phoA*) activity by a plasmid encoding an RNA-based EGS (**Table 2**).[237] A few years later, Altman and colleagues also tested their EGS technology against bacteria. They reported a reduction in the level of microbial viability to less than 10% by reducing the level of expression of the essential protein gyrase A (*gyrA*) – a protein known to exist in about 1,500 copies per *Escherichia coli* (**Table 2**).[238] In another study, Jeffery *et al.* used external guide sequence technology to disrupt the type III secretion system in *Salmonella enterica serovar Typhimurium*. These secreted proteins impose a number of effects to help the pathogen survive

and escape an immune response, and are thus involved in assaults on host cells. EGSs complementary to *invB* or *invC* mRNA were designed and shown to be responsible for the single site cleavage on these mRNAs by endogenous RNase P, leading to a decrease in type III secretion and interference with host invasion (**Table 2**).[239]

Tolmasky and co-workers managed to block resistance to the antibiotic amikacin in *Escherichia coli* by designing various EGSs complementary to *aac (6`)-Ib* mRNA in different locations (**Table 2**). They identified accessible regions in the *aac (6`)-Ib* mRNA for binding antisense oligonucleotides *in vitro*. Binding experiments showed significant changes in the binding affinity due to small changes in the targeted location, but no correlation between binding affinity and *in vitro* RNase P-mediated cleavage was observed, as EGSs with different binding affinities mediated high levels of mRNA cleavage. Nevertheless, under the more stringent conditions of *in vivo* experiments, only the two EGS oligonucleotides with the highest affinities showed significant inhibition. EGSs with lower binding affinity did not have any considerable impact on reversing bacterial resistance. The group thus concluded that *in vitro* binding affinity of an EGS can be predictive of the EGS's ability to inhibit gene expression *in vivo*.[240] The level of *aac (6`)-Ib* mRNA was observed to be lowered by approximately 50% in the presence of the highest affinity EGS compound[240]. Subsequently, Tolmasky *et al.* tried to find nuclease-resistance analogues that can function as EGSs against *aac (6`)-Ib* mRNA. In this study they reported various modifications on the backbone of the oligonucleotides and investigated the effect of the modification on RNase P recruitment. They designed a series of oligonucleotides containing 2 regions: a 5'-13-nucleotide segment antisense to the target mRNA (AS region), followed by an ACCA sequence at the 3'-end responsible for EGS activity by interacting with a UGG sequence within RNase P (ACCA region). The group found that fully PS, 2'-O-methyl and PMO modified oligonucleotides were unable to recruit RNase P *in vitro* (see Chapter 1 for the structures of these modifications). They also performed a detailed study of DNA-based EGS where some of the nucleotides were modified with LNA. When all nucleotides in the ACCA region are DNA, the constructs failed to induce cleavage of the targeted mRNA *aac (6')-Ib,* regardless of the modification of the AS region (DNA or LNA). However, substitution of the two middle Cs in the ACCA region from DNA to LNA did induce cleavage of the targeted mRNA, and replacing all three terminal CCA nucleotides at the 3'-end by LNA (e.g. LNA2, **Table 2**) did not increase the observed cleavage activity more than that observed in the case of the 2 middle Cs being LNA. On the other hand, the cleavage activity was maximised when the three inner residues in the ACCA region were substituted to LNA. The replacement of only the adenine residues in the ACCA region to LNA did not induce any cleavage.[241] These observations confirmed an earlier claim made by Altman *et al.,* pointing to the importance of 2'-OH at the C residue located nearer to the 5' end of the ACCA region for a full EGS activity[242].

In a more recent study, the Tolmasky group used EGS technology to target *aac (6`)-Ib* mRNA in *Acinetobacter baumannii*.[243] In a previous report they had shown that this gene could be successfully silenced in *Acinetobacter baumannii* by simple steric blocking of translation initiation.[105] For the EGS oligonucleotides, they used a hybrid oligomer composed of the LNA analogue 2',4'-bridged nucleic acid-NC (BNA^{NC}) and DNA conjugated to a permeabilizing peptide (e.g., BDA2, **Table 2**). They compared the activity of the BNA^{NC} containing oligomers, to analogues containing the more common 'bridged' nucleic acid LNA (e.g., LDA2, **Table 2**). While the BNA^{NC} containing EGSs showed some RNase P recruiting activity *in vitro*, their activity was significantly lower than the LNA/DNA hybrid analogues (see Chapter 1 for the structure of BNA^{NC}).

EGS technology has also been applied to target virulence genes from *Yersinia pestis in vitro* and *in vivo* expressed in *Escherichia coli* (**Table 2**). Successful inhibition of the targeted genes *yscN* and *yscS* was shown *in vitro* and a clear reduction was observed when those genes were expressed in *E. coli*. The ubiquitous expression and high conservation of RNase P means the EGS technology should work in *Y. pestis* as well.[244]

Table 2. Sequences of published ASOs using EGS technology against bacteria.

Name	Sequence	Target (+ Organism)	Backbone	Ref.
AP-EGS, DS1-EGS	not reported	*phoA and lacZ (E. coli)*	RNA	[237]
gyr241	GACCGCCGAGUCACCACCAG	*gyrA (E. coli)*	RNA	[238]
gyr241	CACUGCGGAAUCGCCACCAG	*gyrA (S. Typhimurium)*	RNA	[238]
invB 108 EGS	AAUGCAAAUAAAUCCACCA	*invB (S. Typhimurium)*	RNA	[239]
invC 98 EGS	GGCGUGAUUUCACAAACCA	*invC (S. Typhimurium)*	RNA	[239]
InvC 293 EGS	ACGAUUUUCCCUGUCACCA	*invC (S. Typhimurium)*	RNA	[239]
EGS A2	CGATCTCATATCGACCA	*aac(6')-Ib (E. coli)*	RNA	[240]
EGS C3	AGGAACAGTACTTGACCA	*aac(6')-Ib (E. coli)*	RNA	[240]
LNA2	CAAGTACTGTTCCACCA	*aac(6')-Ib (E. coli)*	LNA/DNA	[241]
LDA2	CGATATGAGATCGACCA	*aac(6`)-Ib (A. baumannii)*	LNA/DNA	[243]
BDA2	CGATATGAGATCGACCA	*aac(6`)-Ib (A. baumannii)*	BNA^{CN}/DNA	[243]
EGS-N1, EGS-N2 and EGS-S1	not reported	*yscN and yscS (E. coli)*	RNA	[244]
rEGSe, rEGSx	libraries not reported	*vjbR and yscN (E. coli)*	RNA	[245]
EGS73	GAGTATCAACTAAAACACCAG	*mglB (E. coli)*	RNA	[246]
EGS155	GGTATTGCTTGAGGAGACCAG	*mglB (E. coli)*	RNA	[246]
PPMO-EGSs	Library	*gyrA (E. coli, S. aureus, P. aeruginosa, B. subtilis and E. faecalis)*	PPMO	[247]
EGSb1	CCGUUUCGAACUCACCA	*ftsZ (E. coli)*	RNA	[248]

Xiao and colleagues developed a method that rapidly selects the accessible and cleavable sites in mRNA by *E. coli* RNase P and random external guide sequences.[245] Later, the group applied this method in the screening of rEGS and identified two EGSs, EGS73 and EGS155, that inhibited the virulence regulator MgIB of *Francisella tularensis in vitro* and in *E. coli* (**Table 2**). EGS148 induced *F. tularensis* mgIB mRNA cleavage *in vitro*.[246]

Altman *et al.* showed inhibition for the expression of the *gyrA* and *rnpA* genes from various different bacteria and of the *cat* gene, which determines the resistance to the antibiotic chloramphenicol in *Escherichia coli*, by EGSs made up of a peptide-phosphorodiamidate morpholino oligonucleotide (PPMO) rather than RNA (**Table 2**).[247] However, Altman and colleagues did notice a change in the cleavage site of the target mRNA for the PPMO-based EGSs compared to RNA-based EGSs. They also observed that PPMO-EGSs could enter various species of Gram positive and Gram negative bacteria.[247]

Tolmasky and co-workers studied EGS technology in supressing the cell division gene *ftsZ* in *E. coli*. The study showed significant binding ability and RNase P-mediated degradation of *ftsZ* mRNA *in vitro* (**Table 2**). The group also noted filamentation (cell elongation without division) when testing *in vivo*.[248]

A number of other studies have shown applications for the EGS technology in recruiting RNase P to mediate targeted mRNA cleavage even in species of other kingdoms, such as fungi (e.g. *saccharomyces*[249]) and *archaea.*[250] All the above examples suggest that EGS technology might provide a useful means for silencing the gene expression of disease-relevant targets. However, it must be noted that the majority of the research has been performed on RNA-based oligonucleotides. While RNA is the natural substrate for RNase P, it is unstable and prone to cleavage by nucleases and therefore it is not the ideal scaffold for antisense technologies. The use of chemically modified oligonucleotides in the EGS approach has been limited to LNA or PPMO backbones, and less successfully to BNA^{NC} modifications (see **Table 2**).[251] There are thus many other DNA/RNA-analogues that have not yet been tested but may be useful to optimize and broaden the applications of EGS technology.

2.1.3 Aim of this chapter

The aim of this chapter is to investigate whether PNA-based oligonucleotides are compatible with EGS technology and can be used to silence bacterial genes by recruiting RNase P.

2.2 Results and discussion

2.2.1 Design and synthesis

As mentioned in the introduction, the aim is to recruit Ribonuclease P (RNase P) by using an External Guide Sequence (EGS) that employs a complementary oligonucleotide that mimics the structural features of precursor tRNA.[252] For this project, the backbone of the oligonucleotides was chosen to be Peptide Nucleic Acid (PNA), which is an analogue of DNA where the negatively charged phosphate backbone is replaced with an uncharged peptide backbone made from *N*-(2-aminoethyl)-glycine units linked by amide bonds, while the A, C, G and T nucleobases are attached to the backbone by methylene carbonyl linkages (see **Figure 22**). The high affinity of PNA for RNA is partly due to the absence of negative charges on the backbone, circumventing electrostatic repulsion. The peptidic scaffold of PNA has the added advantage that it can be easily attached to cell penetrating peptides (CPP), which have been shown to improve the delivery of oligonucleotide analogues into bacterial cells (see Chapter 1).[253] In order to investigate the generality of the approach, we designed and synthesized PNAs containing the EGS tail against a variety of different gene classes, i.e. essential genes (*ftsZ*), reporter genes (*lacZ*) and virulence genes (*katG*).

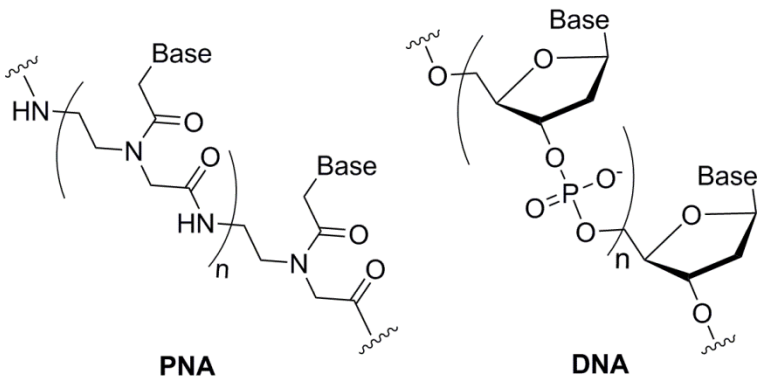

Figure 22. Comparison of the structure of the neutral backbone of PNA and the negatively charged backbone of DNA.

2.2.1.1 Design and synthesis of PNAs targeting *ftsZ* mRNA

Good and colleagues have previously revealed that the genes *ftsZ* and *acpP* are essential genes in *Escherichia coli*, and that silencing of those genes using antisense peptide nucleic acids (PNA) and expressed antisense RNA results in a 50% reduction in growth rate. The antisense PNAs specific for *acpP* (Ec108) and *ftsZ* (Ec326) were designed with the following sequences, $(KFF)_3K$-O-

tcaaacatag for Ec108, and $(KFF)_3K$-O-tcaaacatag for Ec326, where O is [2-(2-(amino)-ethoxy)ethoxy]acetyl linking the peptide $(KFF)_3K$ to the PNA oligo strand.[254] The cell-penetrating peptide $(KFF)_3K$ improves gene silencing over unconjugated PNA, presumably due to more efficient delivery of the PNAs into the bacterial cells.[197]

We decided to use Good's anti-*ftsZ* PNA (Ec326) as a starting point for our technology development. The originally reported anti-*ftsZ* PNA works through steric blocking of the start codon region and is unable to recruit a nuclease such as RNase H or RNase P. Previous studies by Good and co-workers had shown that the start codon region is the most effective region to target by PNA-based ASOs.[255] This region includes parts of the conserved Shine-Dalgarno motif that corresponds to the ribosome binding site and is located in the 5' untranslated region (5'-UTR). Therefore, binding of antisense PNAs to this region leads to the inability of the ribosome to bind to the mRNA and as a result translation is inhibited. We therefore wanted to see if the efficiency of these antisense PNAs could be improved by the addition of the external guide sequence (ACCA), to generate PNA-Ec326-EGS. The synthesis of PNA oligonucleotides was performed using an Expedite 8900 solid-phase synthesizer, purified using reversed-phase HPLC and characterized by reverse phase liquid chromatography connected to mass spectrometry (see Chapter 6 for experimental details). The PNAs were obtained at a purity of at least 90% (see Appendix A for HPLC chromatograms). **Table 3** gives an overview of the sequences, experimental masses and purities of the synthesised anti-*ftsZ* PNAs.

Table 3. Sequence, expected *m/z*, found *m/z* and purity for synthesised anti-*ftsZ* PNAs.

PNA	Sequence	Expected *m/z*	Found *m/z*	Purity (%)
PNA-Ec326	$(KFF)_3K$-O-tcaaacatag	4260.51	4259.96	96.6
PNA-Ec326-EGS	$(KFF)_3K$-O-tcaaacatagacca	5313.53	5313.39	>90.0

2.2.1.2 Design and synthesis of PNAs targeting *lacZ* mRNA

In an earlier study, Good *et al.* have developed PNAs that can target the reporter gene *lacZ*. They showed a high efficiency for PNA-1900 (sequence $(KFF)_3K$-O-catagctgtttc) at low concentration, causing a 50% reduction in β-galactosidase (*lacZ*) activity.[197] Once again, we decided to use this PNA (PNA-1900) as a starting point and compare its activity to an EGS analogue (PNA-1900-EGS). Synthesis was performed in a similar manner to the anti-*ftsZ* PNAs (see section 2.2.1.1). The PNAs were obtained at a purity of at least 90% (see Appendix A for HPLC chromatograms). **Table 4** gives an overview of the sequences and obtained masses of the synthesized anti-*lacZ* PNAs.

Table 4. Sequence, expected *m/z*, found *m/z* and purity for synthesised anti-*lacZ* PNAs.

PNA	Sequence	Expected *m/z*	Found *m/z*	Purity (%)
PNA-1900	$(KFF)_3$K-O-catagctgtttc	4775.98	4775.13	>90.0
PNA-1900-EGS	$(KFF)_3$K-O-catagctgtttcacca	5828.99	5828.56	>92.3

2.2.1.3 Design and synthesis of PNAs targeting *katG* mRNA

PNA-based oligonucleotides capable of silencing the virulent *katG* gene have not been reported and had to be designed from scratch. To find suitable 11- or 12-mer target sequences, we studied a number of sequences that overlapped the translational start site. The choice for the translational start site, or ribosome binding site, was guided by the fact that Good's PNAs against *ftsZ* and *lacZ* (see previous sections) function by steric blocking of this site. Additionally, by targeting the translational start site a good comparison between pure steric blocking and RNase P recruitment by EGS sequences can be obtained.

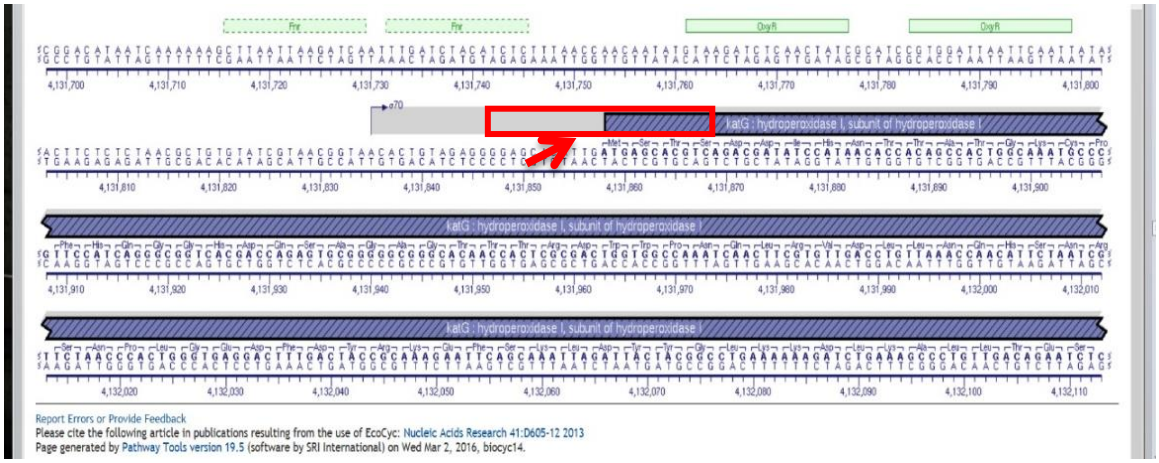

Figure 23. A screenshot of the *katG* sequence as shown in the genome browser at ecocyc.org. The red box shows the region spanning the translational initiation site, where we searched for suitable 12-mer antisense sequences.

To find suitable 11- or 12-mer antisense oligonucleotides against the *katG* gene, we examined various sequences that overlapped the translational start site (see **Figure 23**). First, the EcoCyc[256] website was used to determine the mRNA sequence of the *KatG* gene in *E. coli* strain MG1655. We considered a target window that contains 11 nucleotides from the 5'-untranslated region (UTR) and 11 nucleotides from the beginning of the translated region. To design our antisense oligonucleotides, we then choose all 12-mers that are complementary to a section of this 22-nucleotide target region. A BLAST search was subsequently performed on all 12-mers to identify which oligonucleotides might cause interference due to binding to other targets besides *katG* (see **Table 5**). Two sequences were identified as potential antisense PNAs (PNA-katG1 and PNA-katG2),

and they were synthesized on an Expedite 8900 solid-phase synthesizer. The EGS analogues for these two sequences were also synthesised and given the names PNA-katG1-EGS and PNA-katG2-EGS respectively. In all cases, the same cell penetrating peptide used by Good and co-workers, $(KFF)_3K$, was linked to the anti-*katG* PNAs during the solid–phase synthesis. The PNAs were obtained at a purity of at least 80% (see Appendix A for HPLC chromatograms). **Table 6** gives an overview of the sequences and obtained masses of the synthesised anti-*katG* PNAs.

Table 5. BLAST results of antisense sequences against *kat*G and their potential matching genes. The vertical line in the sequences indicates the separation between the untranslated region and the translation start site of *katG*. Sequences bolded and underlined are the final synthesized oligonucleotides. nc = non coding region.

Sequence	Number of Matches	Suitable?
CCTCGTGTAAC | T	4 (four 11-mers including 2 nc)	no
CTCGTGTAAC | TA	7 (one 12-mer, six 11-mers including 3 nc)	no
TCGTGTAAC | TAC	9 (two 12-mers including 1 nc, seven 11-mers including 1 nc)	no
CGTGTAAC | TACT	11 (one 12-mer, ten 11-mers including 3 nc)	no
GTGTAAC | TACTC	10 (one 12-mer, nine 11-mers including 2 nc)	no
TGTAAC | TACTCG	8 (one 12-mer, seven 11-mers)	no
GTAAC | TACTCGT	11 (three 12-mers, eight 11-mers including 1 nc)	no
TAAC | TACTCGTG	9 (nine 11-mers including 1 nc)	no
AAC | TACTCGTGC	5 (one 12-mer, four 11-mers)	yes
AC | TACTCGTGCA	6 (one 12-mer, five 11-mers)	no
C | TACTCGTGCAG	2 (two 11-mers)	yes

Table 6. Sequence, expected *m/z*, found *m/z* and purity for the synthesised anti-*katG* PNAs.

PNA	Sequence	Expected *m/z*	Found *m/z*	Purity (%)
PNA-KatG1	$(KFF)_3K$-O-O-aactactcgtgc	4915.13	4914.23	>88.7
PNA-KatG1-EGS	$(KFF)_3K$-O-O-aactactcgtgcacca	5968.15	5967.66	>87.3
PNA-KatG2	$(KFF)_3K$-O-O-ctactcgtgcag	4931.13	4931.22	>80.0
PNA-KatG2-EGS	$(KFF)_3K$-O-O-ctactcgtgcagacca	5984.15	5983.64	>80.0

2.2.1.4 Design and synthesis of control PNAs

In order to check if any potential activity is due to selective gene silencing or due to general PNA toxicity, we synthesized a number of control PNAs that should not match any mRNA sequence in *E. coli*. Several negative controls (1176UNRLTD, SP183, SP181, 111UNRLTD, 1901Mis1900 and Bas1) have been previously reported by Liam Good *et al*.[197] As done for the anti-*katG* sequences above, we computationally checked for off-target effects in *E. coli* using BLAST, in an attempt to maximize our likelihood of synthesizing clean, non-toxic control sequences (see **Table 7**). The sequences with the least chance of off-target effects were then synthesized, purified and characterized by mass spectrometry in order to be tested as negative controls. **Table 8** gives an

overview of the sequences and obtained masses of the synthesized control PNAs (see Appendix A for HPLC chromatograms).

Table 7. BLAST results of potential negative control sequences. Sequences bolded and underlined are the final synthesized oligonucleotides. nc = non coding region.

Name of sequence	Sequence	Number of BLAST matches
Bas1	CTAACATGTCG	2 (two 10-mers)
111UNRLTD	CCCCTATTGTCC	1 (one 11-mer)
1176UNRLTD	GCAAGCGACTGTGGA	10 (one 12-mer, 9 11-mers incl 1 nc)
SP183 SC1873	GTGACTCGATGTCTT	5 (three 12-mers inc 2 nc, two 11-mers incl 1 nc)
1901MIS1900	CAATGTCGTTTC	3 (three 11-mers)
SP181 SCSP4	TCACTATCTC	0

Table 8. Sequence, expected *m/z*, found *m/z* and purity for the synthesised control PNAs.

PNA	Sequence	Expected *m/z*	Found *m/z*	Purity (%)
PNA-111UNRLTD	$(KFF)_3$K-O-O-cccctattgtcc	4842.07	4841.19	>79.0
PNA-1901	$(KFF)_3$K-O-caatgtcgtttc	4775.97	4775.14	>65.0
PNA-Bas1	$(KFF)_3$K-O-ctaacatgtcg	4518.78	4518.05	>88.8
PNA-SP181	$(KFF)_3$K-O-O-tcactatctc	4321.00	4320.99	>90.0

2.2.2 Antibacterial activity

The ability of the PNAs containing the EGS sequence to recruit RNase P can be investigated by comparing their gene silencing ability to that of PNAs without the EGS sequence (i.e. PNAs that function by steric blocking of the ribosome binding site). Ideally, the EGS-PNAs should display a higher efficiency in gene silencing compared to the steric blockers due to their ability to recruit RNase P. This recruitment leads to cleavage of the bound mRNA and so only catalytic amounts of the PNA should be needed for gene silencing, compared to stoichiometric amounts for steric blockers. We decided to start with the PNA sequence used by Good *et al.* to silence the *ftsZ* gene by steric blocking (PNA-Ec326)[257] and compare it to the analogous PNA containing the EGS sequence (PNA-Ec326-EGS). *ftsZ* is an essential gene involved in cell division[258] and silencing can be easily detected by elongation of the bacteria cells. Furthermore, the degree of inhibition of *ftsZ* can be quantified by measuring the optical density (OD_{620nm}) of the growing cultures, as *ftsZ* silencing stops the bacteria from growing. The protocol for antimicrobial susceptibility testing recommended by the Clinical and Laboratory Standards Institute (CLSI) was used to test the antibacterial activity of the PNAs.[259] This protocol uses a starting bacterial concentration of 10^5 colony forming units per millilitre of bacterial suspension (10^5 cfu/mL). All assays were performed

using two strains of *E. coli*, namely wild type strain ATCC25922 and the membrane permeable strain AS19 that should allow more efficient uptake of the PNAs.[254]

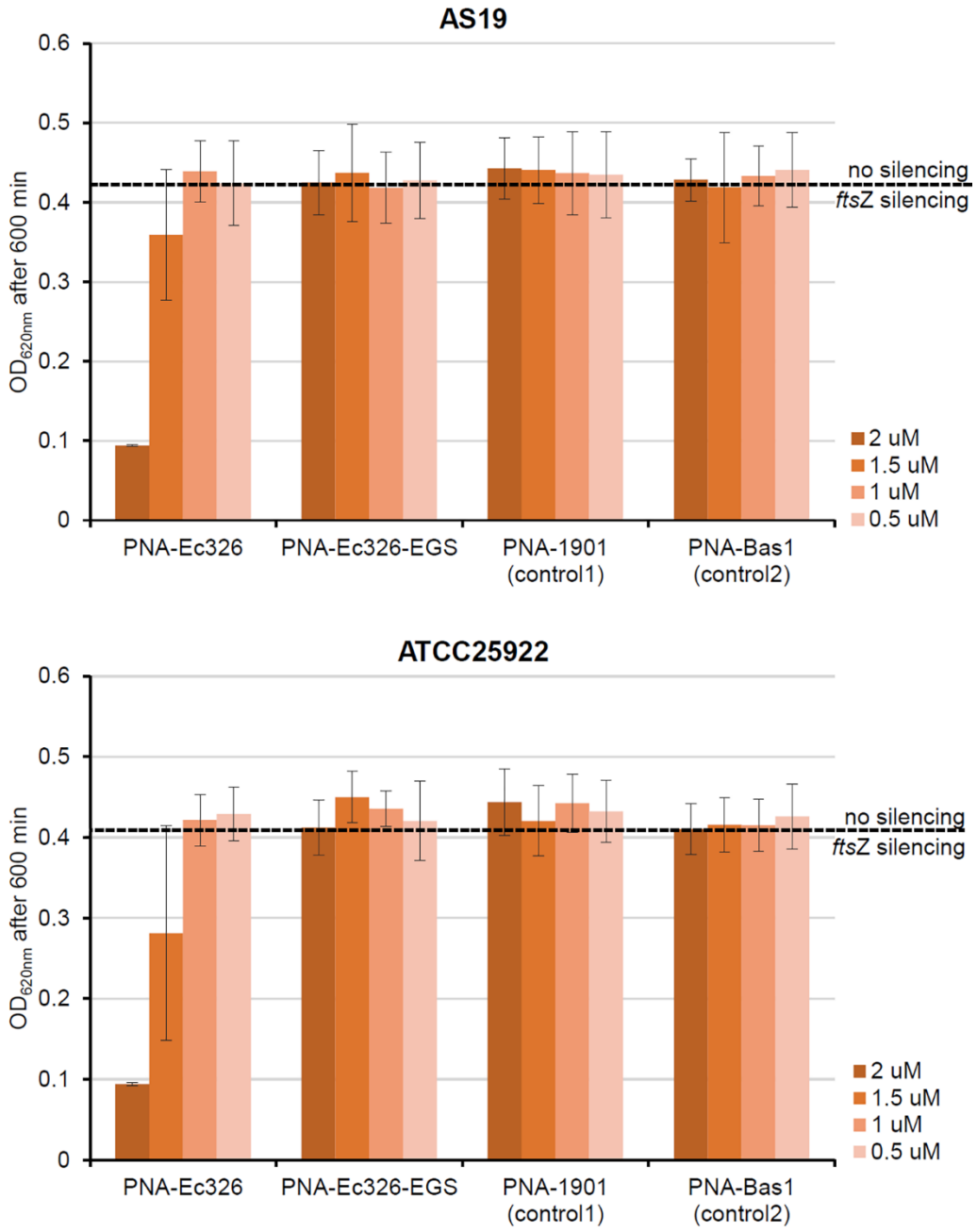

Figure 24. Potential *ftsZ* silencing by PNA analogues. 10 µL PNA at 10x the desired concentration was added to 90 µL *E. coli* cultures at 10^5 cfu/mL in a 96 well plate, and the OD_{620nm} was measured after 600 min at 37 ˚C using a FC MultiSkan device. *E. coli* strains AS19 (top) and ATCC25922 (bottom) were used. All results are the average of minimum 2 biological and 2 technical repeats, with error bars indicating standard deviations.

In an initial study, the PNAs were added to *E. coli* cultures at 10^5 cfu/mL in a 96 well plate and the OD_{620nm} was measured for 1230 min at 37 ˚C using a FC MultiSkan device. Whether or not *ftsZ* silencing has occurred can be seen from the OD_{620nm} values at 600 min (**Figure 24**, full growth

curves can be found in Appendix A). After 600 min the bacterial cultures without PNAs or with control PNAs have reached their stationary phase (maximum OD_{620nm}), while the bacterial cultures with PNAs that induce *ftsZ* silencing display lower OD_{620nm} values due to a delay in growth. As can be seen from **Figure 24**, only the steric blocker PNA-Ec326 is able to induce gene silencing at a concentration of 2 µM (but not at lower concentrations). Microscopy images of the bacteria treated with PNA-Ec326 confirmed *ftsZ* silencing by this sequence, as shown by the elongation of the bacterial cells (see **Figure 25**). On the other hand, EGS analogue PNA-Ec326-EGS appeared to be completely inactive under the conditions of the assay and showed similar growth curves to the control PNAs (**Figure 24**).

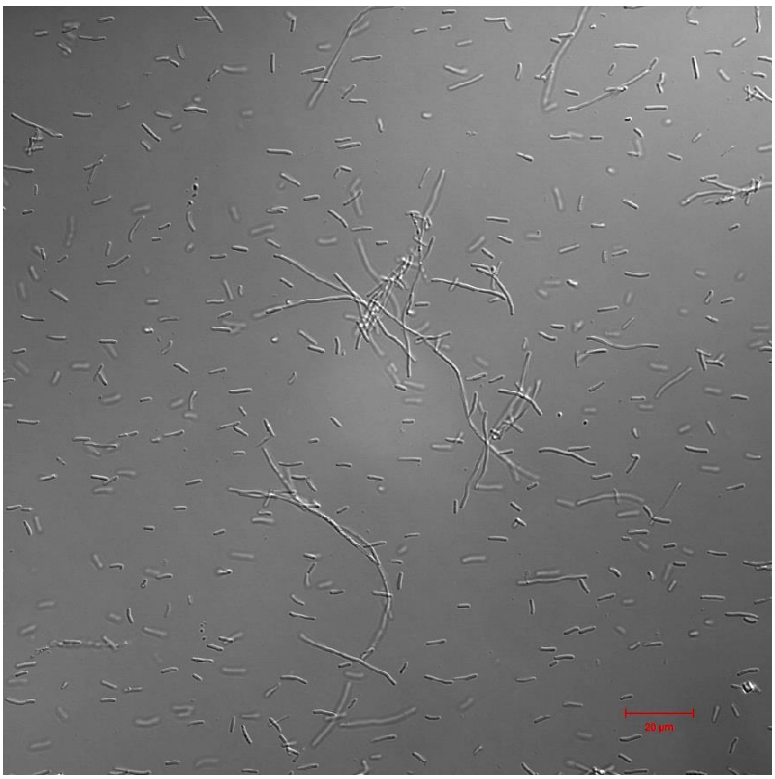

Figure 25. Microscopy image showing the elongation phenotype in *E. coli* AS19 caused by *ftsZ* gene inhibition. 1.5 µM PNA-Ec326 was incubated with *E. coli* cultures at 10^5 cfu/mL for 1230 min at 37 ˚C. The image was taken by a confocal microscope (laser microscope, ZEI 55, LSM710, HAL100). The red scale bar represents 20 µm.

The inactivity of the EGS-PNA is surprising, given that it has the same sequence as PNA-Ec236 but with just 4 additional bases attached (the EGS sequence). It was therefore expected that PNA-Ec326-EGS would display similar activity to PNA-Ec326 (in case RNase P is not recruited and only steric blocking occurs), or show higher activity to PNA-Ec326 (in case RNase P is recruited). In order to test whether PNA-Ec326-EGS has any gene silencing ability, the experiment was repeated at higher concentrations of the PNA (2, 4 and 6 µM), as shown in **Figure 26**. At the lowest PNA concentrations of 2 µM and 4 µM, the maximum OD_{620nm} is still reached within 600 min and no

ftsZ silencing is observed. Upon the addition of 6 µM PNA-Ec326-EGS to the *E. coli* strains, a decrease in bacterial growth is observed (**Figure 26**, full growth curves can be found in Appendix A). However, a similar decrease is also observed for the control PNAs, PNA-1901 and PNA-Bas1, which are unable to bind to *ftsZ* mRNA due to sequence mismatch. The observed inhibition of bacterial growth may therefore be a consequence of general PNA toxicity and not due to *ftsZ* silencing.[260]

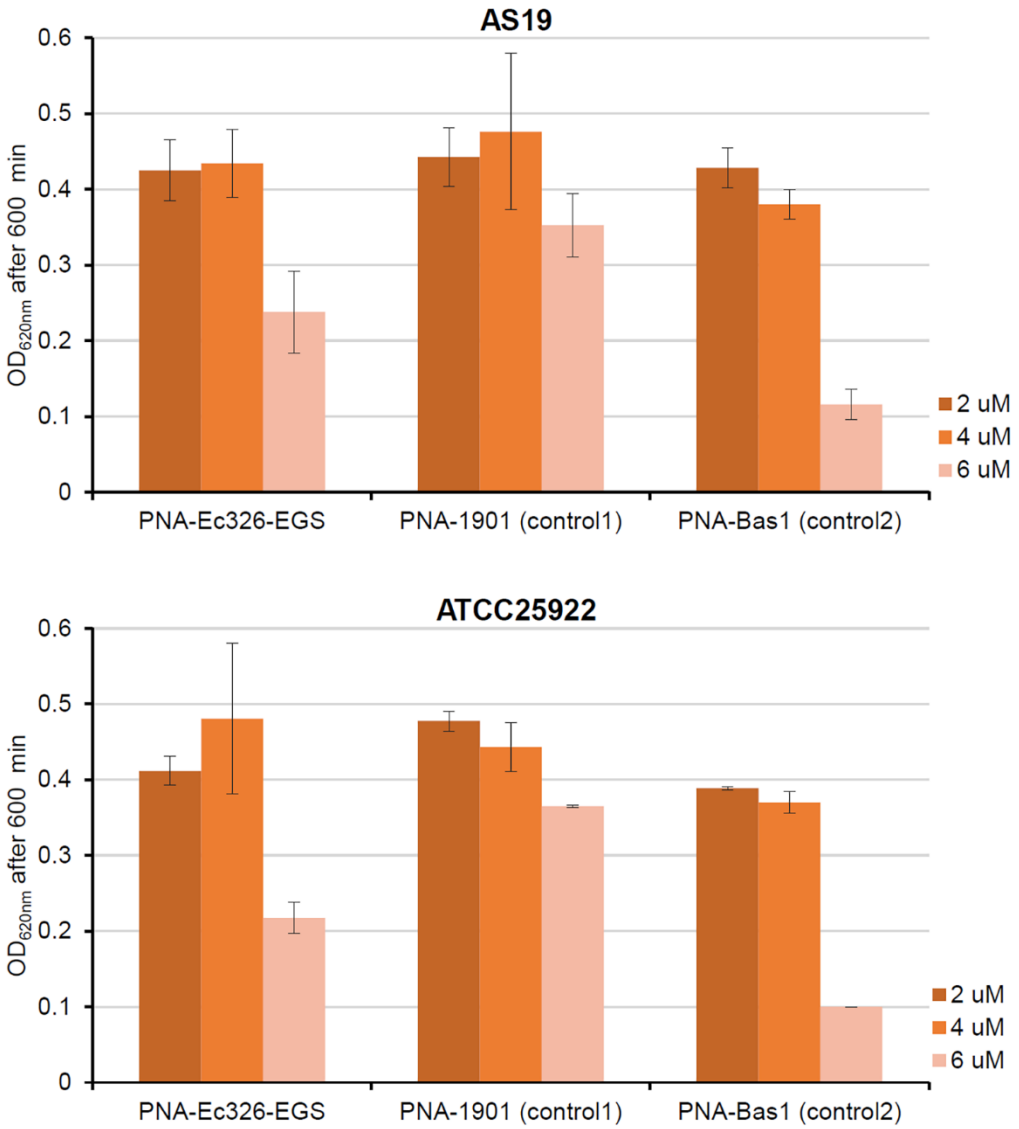

Figure 26. Potential *ftsZ* silencing by high concentrations of PNA-Ec236-EGS. 10 µL PNA in 10x the desired concentration was added to 90 µL *E. coli* cultures at 10^5 cfu/mL in a 96 well plate, and the OD_{620nm} was measured after 600 min at 37 ˚C using a FC MultiSkan device. *E. coli* strains AS19 (top) and ATCC25922 (bottom) were used. All results are the average of minimum 2 biological and 2 technical repeats, with error bars indicating standard deviations.

We then sought to find out whether only PNA-Ec326-EGS is inactive, or whether all EGS-PNAs are unable to induce gene silencing. One of the other EGS-PNAs investigated, was an antisense PNA

against the reporter gene *lacZ*. This gene expresses the protein β-galactosidase, which is responsible for the digestion of lactose. When cells are treated with X-gal (a lactose derivative), β-galactosidase mediated digestion produces a blue colour.[261] This blue colour is commonly used as an indicator for the presence and activity of β-galactosidase. Conversely, the absence of the blue colour can be used as an indicator for successful inhibition of β-galactosidase expression or *lacZ* silencing. Under standard bacterial growth conditions, expression of β-galactosidase is inhibited by the lac repressor.[261] However, in the case of insufficient glucose and in the presence of lactose, the repressor of the lac operon is temporarily removed allowing the transcription of the *lacZ* gene and other genes[261]. Thus, in order to investigate *lacZ* silencing by antisense technology, the experiments have to be performed under conditions of *lacZ* transcription (i.e. low glucose and high lactose concentrations). Usually, lactose is replaced by IPTG as an inducer that is not digestible and therefore can maintain a constant concentration, thus keeping the transcription of *lacZ* at a constant level throughout the experiment.[261]

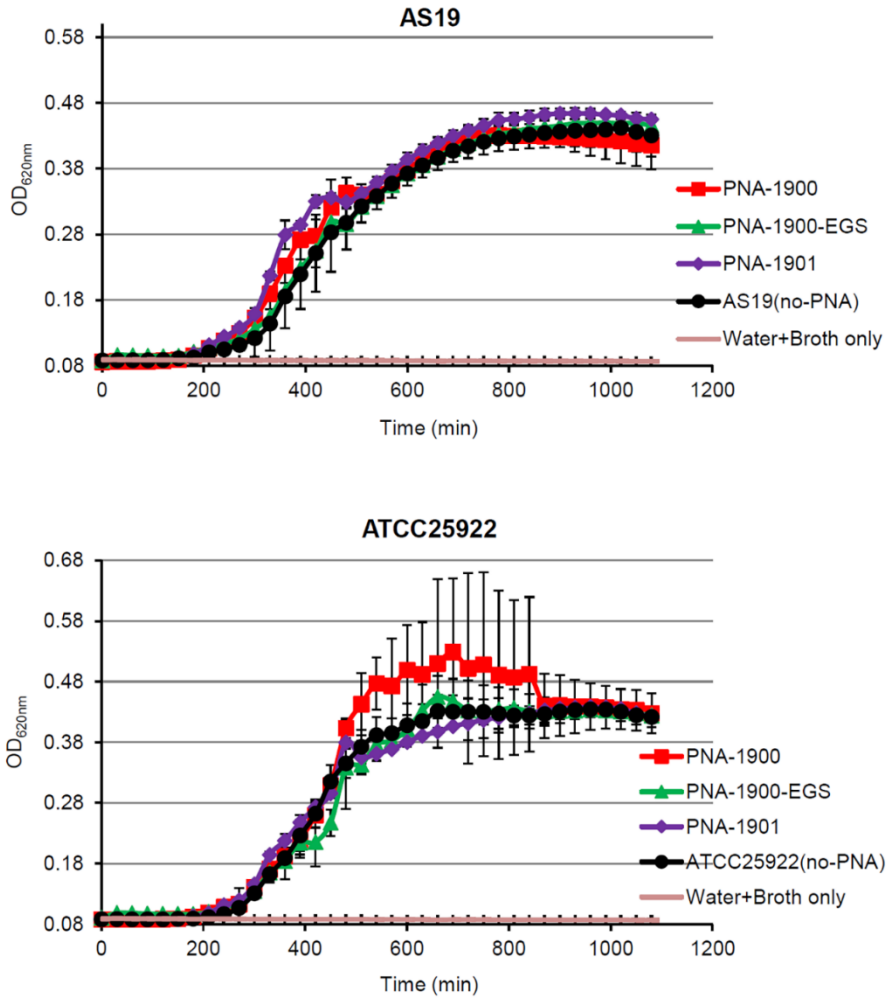

Figure 27. Potential toxicity effect by anti-*lacZ* PNAs in *E. coli* AS19 (top) and ATCC25922 (bottom). The optical density at 620 nm (OD_{620nm}) was measured at 37 °C for 1200 min after the addition of the PNAs to the *E. coli* cultures (final concentration of 4 µM). The *E. coli* strains were grown in MH broth and used in the experiment at 10^5 cfu/mL. The results are the average of at least 1 biological and 2 technical repeats, with error bars representing standard deviations.

A steric blocking PNA sequence suitable for inhibiting *lacZ* expression was reported by Good and co-workers (PNA-1900).[197] We thus wanted to explore its *lacZ* silencing ability along with that of an EGS analogue (PNA-1900-EGS). Given the general PNA toxicity discussed above, we first looked at the bacterial toxicity of these PNAs. The *lacZ* gene is not essential for bacterial survival and silencing of this gene should not affect growth. As shown in **Figure 27**, the addition of 4 µM of the anti-*lacZ* PNAs does not the change the growth curves of both membrane permeable AS19 and wild type ATCC25922 *E. coli* strains. Therefore, we can study *lacZ* silencing at PNA concentrations at or below 4 µM without worrying about confounding effects from PNA-induced toxicity.

To test lacZ silencing by the PNAs, PNA (final concentration 2 µM) and a mixture of IPTG and X-gal (final concentration 0.1 mM IPTG and 0.2 mg/mL X-gal) were added to *E. coli* cultures at 10^5 cfu/mL in a 96-well plate and subsequently incubated at 37 ˚C using the FC MultiSkan. Pictures were taken of the growing cultures at regular intervals using a flatbed scanner (**Figure 28**). The blue colour indicative of β-galactosidase started to appear after 16 h incubation with the PNAs. As shown in **Figure 28**, there are no significant differences in blueness generated by the various PNAs. It appears that the largely qualitative visual assessment of the blue colour is not sensitive enough to pick up differences between the gene silencing ability of the steric blocking PNA and the EGS-PNA. We therefore shifted our focus towards the silencing of a different gene that can be measured quantitatively.

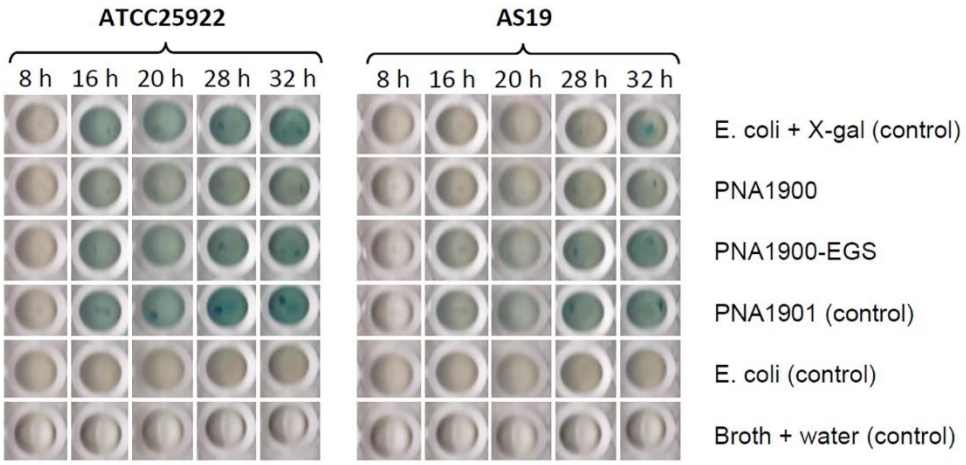

Figure 28. Potential silencing of *lacZ* by 2 µM PNAs in *E. coli* strains ATCC25922 (left) and AS19 (right). The plate was shaken and incubated at 37 °C using a FC multiSkan. Pictures were taken using a flatbed scanner after 8, 16, 20, 28 and 32 h incubation. The *E. coli* strains were grown in MH broth and used in the experiment at 10^5 cfu/mL. One replicate is shown, the second replicate gave comparable results and is given in Appendix A.

To be able to draw a conclusion on the decreased potency of the PNA-EGS analogues compared to the steric blockers, we chose *katG* as a third targeted gene. This gene is a virulence gene under

the positive control of the protein OxyR, which is induced when bacteria are exposed to high concentrations of hydrogen peroxide (H_2O_2). The *katG* gene encodes for the catalase HPI, which upon induction scavenges the hydrogen peroxide[262]. Silencing of *katG* can therefore be deduced from the ability of bacterial cells to withstand hydrogen peroxide poisoning. When *katG* mRNA is translated (no silencing), bacterial cells will be able to grow in the presence of H_2O_2. However, when *katG* translation is blocked (gene silencing), the bacterial cells will be killed by H_2O_2 and growth is delayed. A measurement of bacterial growth using the optical density at 620 nm in the presence of hydrogen peroxide will thus allow quantification of *katG* silencing. Prior to testing gene silencing ability, it was necessary to find the optimal concentrations of hydrogen peroxide, i.e. the H_2O_2 concentrations that can be tolerated by bacteria expressing *katG* but not by bacteria that lack *katG*. An IC_{50} study of H_2O_2 tolerance was run on two *E. coli* strains, namely the wild type BW25113/7636 and genetically modified JW3914-1/10827 (*katG* knock-out). These experiments indicated that the optimal condition for testing *katG* silencing should include around 50-70 µg/mL hydrogen peroxide, as this concentration is toxic for the *katG* knock-out strain but not for wild type *E. coli* (see Appendix A). Further optimization of the experimental conditions revealed that the bacteria and PNAs should be pre-mixed for 2 h prior to the addition of H_2O_2 (see Appendix A). We also checked whether the anti-*katG* PNAs displayed any off-target effects. When 10 µM of the studied PNAs were added to 10^5 cfu/mL *E. coli* BW25113 in the absence of hydrogen peroxide, the PNAs did not influence bacterial growth (see **Figure 29**). This result indicates that these PNAs are not toxic to the *E. coli* strain BW25113 when *katG* mRNA is not present in the cells (no off-target effects).

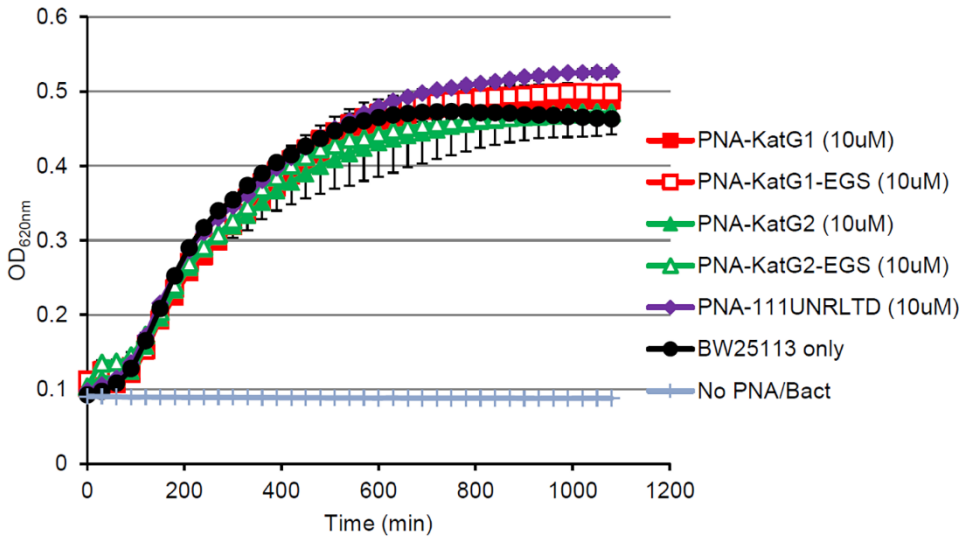

Figure 29. Potential toxicity of PNAs targeting *katG* mRNA against wild-type *E. coli* strain BW25113. The optical density at 620 nm (OD_{620nm}) was measured at 37 °C for 1200 min after the addition of the PNAs to the *E. coli* cultures (final concentration of 10 µM). The *E. coli* strain was grown in MH broth and used in the experiment at 10^5 cfu/mL. The results are the average of at least 1 biological and 2 technical repeats, with error bars representing standard deviations.

In order to test the *katG* silencing abilities of the PNAs, we pre-mixed 2 µM PNA with *E. coli* BW25113 cultures at 10^5 cfu/mL in a 96-well plate at 37 °C for 2 h. After 2 h, H_2O_2 was added at various concentrations and the optical density at 620 nm (OD_{620nm}) was measured for 1200 min at 37 °C. The OD_{620nm} value measured 600 min after the addition of hydrogen peroxide can give a good indication of the silencing ability. The results are shown in **Figure 30**. The study confirmed that the PNAs have no off-target toxicity at 2 µM in the absence of H_2O_2 (high OD_{620nm} values). In contrast, the low OD_{620nm} values observed in the presence 65 µg/mL H_2O_2 and above indicate that these hydrogen peroxide concentrations are too toxic for the cells and cannot be used to draw conclusion regarding gene silencing (see **Figure 30**). The optimal concentration of the hydrogen peroxide is therefore 55 µg/mL. At this concentration, *katG* silencing is observed only in the case of the steric blocker PNA-katG1, while no gene inhibition is seen for its EGS analogue PNA-katG1-EGS, or the PNAs targeting the second region (PNA-katG2 and PNA-katG2-EGS) (see **Figure 30**).

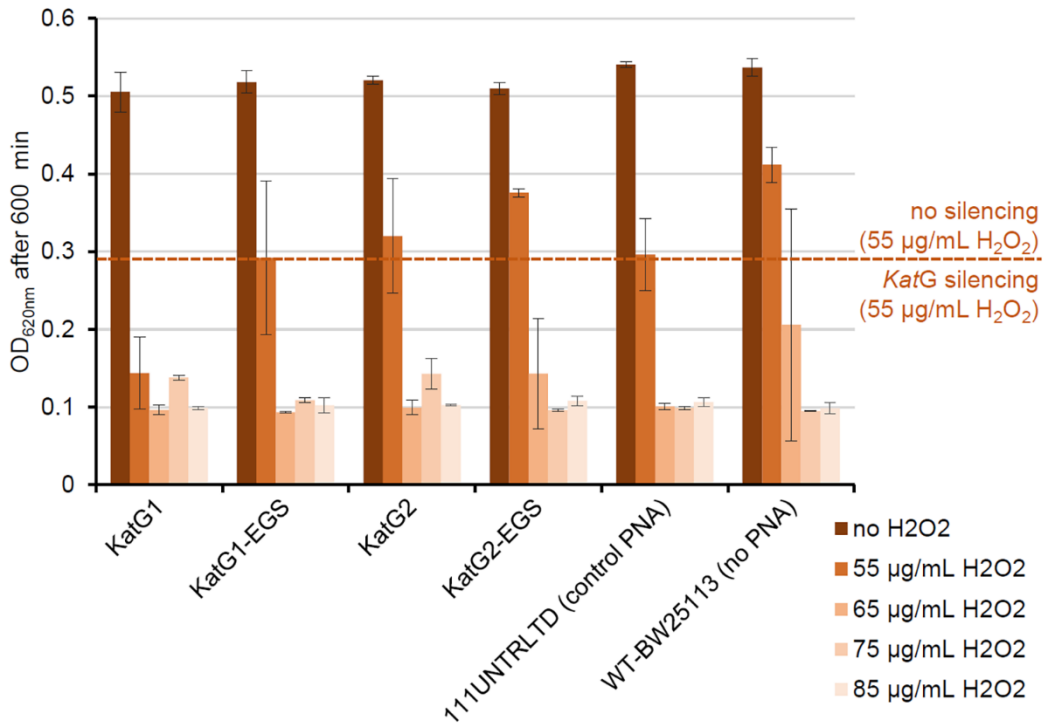

Figure 30. Potential silencing of *katG* by 2 µM PNAs in *E. coli* strain BW25113 in the presence of various concentrations of hydrogen peroxide. 2 µM PNA was pre-mixed with *E. coli* BW25113 cultures at 10^5 cfu/mL in a 96-well plate at 37 °C for 2 h. After 2 h, H_2O_2 was added at various concentrations and the optical density at 620 nm (OD_{620nm}) was measured after 600 min at 37 °C. The *E. coli* strain was grown in MH broth. The results are the average of at least 1 biological and 2 technical repeats, with error bars representing standard deviations.

These results are consistent with the observations for *ftsZ* silencing by PNAs (see above). In both cases the steric blocker PNAs were able to silence their target gene, while the analogous PNA containing the EGS sequence showed no gene silencing ability at all. This is surprising because

these EGS-PNAs were designed to recruit RNase P and expected to be equally potent or better gene silencers than the steric blocking PNAs. There could be a number of reasons why the EGS-PNAs are not as potent as expected: (1) the EGS-PNAs fail to recruit RNase P, (2) the 4 additional nucleobases that make up the EGS sequence interfere with binding to the correct mRNA sequence (off-target effects), and/or (3) the extra bases make these PNAs too long for efficient uptake by the bacteria. We therefore decided to investigate these possibilities in more detail, starting with *in vitro* studies to determine the ability of the various PNA oligonucleotides to recruit RNase P.

2.2.3 *In vitro* recruitment of RNase P

PNA is a highly modified oligonucleotide backbone that bears little resemblance to the original DNA/RNA structure. It is therefore quite possible that RNase P is not able to recognize and bind to a PNA/mRNA duplex, preventing the use of PNA for EGS technology. To investigate this possibility, we performed *in vitro* mRNA cleavage experiments using purified RNase P. Even though several *in vitro* experiments with RNase P have been reported in the past,[241, 248] we were unable to reproduce these results (see below). It was thus necessary to first develop our own method for detecting the *in vitro* cleavage.

2.2.3.1 Optimising the *in vitro* assay

Tolmasky and co-workers have previously reported the RNase P mediated cleavage of *ftsZ* mRNA.[248] Based on theoretical predictions of accessibility, they decided to target the *ftsZ* region 1041-1053 using oligonucleotide EGSb1 (CCGUUUCGAACUCACCA). RNase P recruitment was detected by observing the *in vitro* cleavage of the target mRNA labelled with the radioactive ^{32}P. As this *ftsZ* region has been successfully targeted using EGS-technology in the past, we decided to perform all *in vitro* RNase P recruitment assays with this region. However, in the absence of a phosphorimager, we had to employ a fluorescently labelled RNA target in order to detect cleavage of the target mRNA by RNase P.

As such, we synthesised a 40 nucleotide long stretch of the targeted mRNA-ftsZ1041 and labelled it with 6-fluorescein (6-FAM) at the 5' end. The full length of the *fts*Z mRNA is shown in Appendix A with the targeted region highlighted. The aim is to achieve cleavage of this mRNA-ftsZ1041 into two parts: a FAM labelled 24-mer and an unlabelled 16-mer (see **Figure 31**). To help with detection, we also synthesised a 6-FAM labelled control 24-mer that corresponds to the expected cleaved part. This control can function as a 'ladder' in gels to identify if the target mRNA is cleaved

or not. Finally, we synthesised EGSb1 (now called RNA-ftsZ1041-EGS) and its analogue RNA-ftsZ1041 without the EGS tail (see **Table 9**). All RNAs were synthesized on solid phase using an ABI 394 oligonucleotide synthesizer (protocols can be found in Chapter 6), purified using HPLC and characterized using mass spectrometry (**Table 9**). HPLC chromatograms are given in Appendix A.

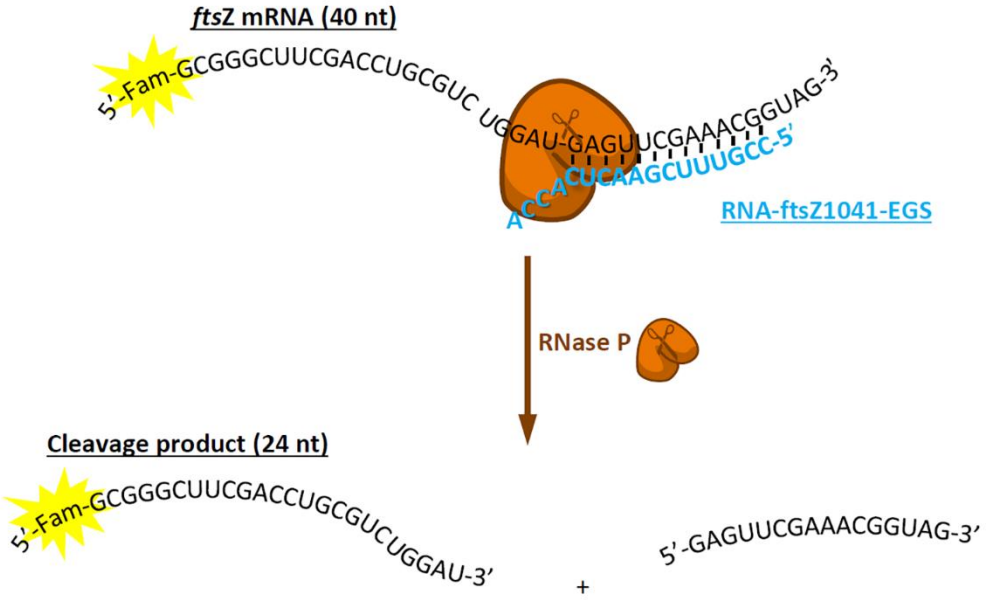

Figure 31. Recruitment of RNase P (shown as brown shape) by RNA-ftsZ1041-EGS (light blue) bound to target FAM-labelled mRNA-ftsZ1041 (black) The expected cleavage site is denoted by the brown scissors, and the expected cleaved products are shown at the bottom of the figure (a FAM-labelled 24-mer and an unlabelled 16-mer).

Table 9. Sequences, expected *m/z* and found *m/z* for synthesised ftsZ1041 RNAs.

RNA	Sequence	Expected *m/z*	Found *m/z*	Purity (%)
*fts*Z RNA (40nt)	FAM-*GCGGGCUUCGACCUGCGUC-UGGAUGAGUUCGAAACGGUAG*	13460.15	13460.71	>85.0
Cleavage product (24nt)	FAM-*GCGGGCUUCGACCUGCGUCUGGAU*	8214.03	8213.32	>85.0
RNA-ftsZ1041-EGS	*CCGUUUCGAACUCACCA*	5306.20	5305.75	>90.0
RNA-ftsZ1041	*CCGUUUCGAACUC*	4037.43	4036.57	>93.0

As mentioned in the introduction, bacterial RNase P consists of C5 protein and M1 RNA. The C5 protein was purchased from *GenScript* and used as provided by the supplier. M1 RNA is the RNA component of RNase P and is coded by the *rnp*B gene (see Appendix A for the full sequence).[230] The double stranded DNA template for this RNA was purchased from *Integrated DNA Technologies* (*IDT*) and amplified using PCR (PCR protocol and purification is described in Chapter 6). The M1 RNA was prepared from this DNA template using the *Thermo Scientific* TranscriptAid

T7 High Yield Transcription Kit #K0441 *in vitro* transcription (IVT) kit (protocol is given in Chapter 6).

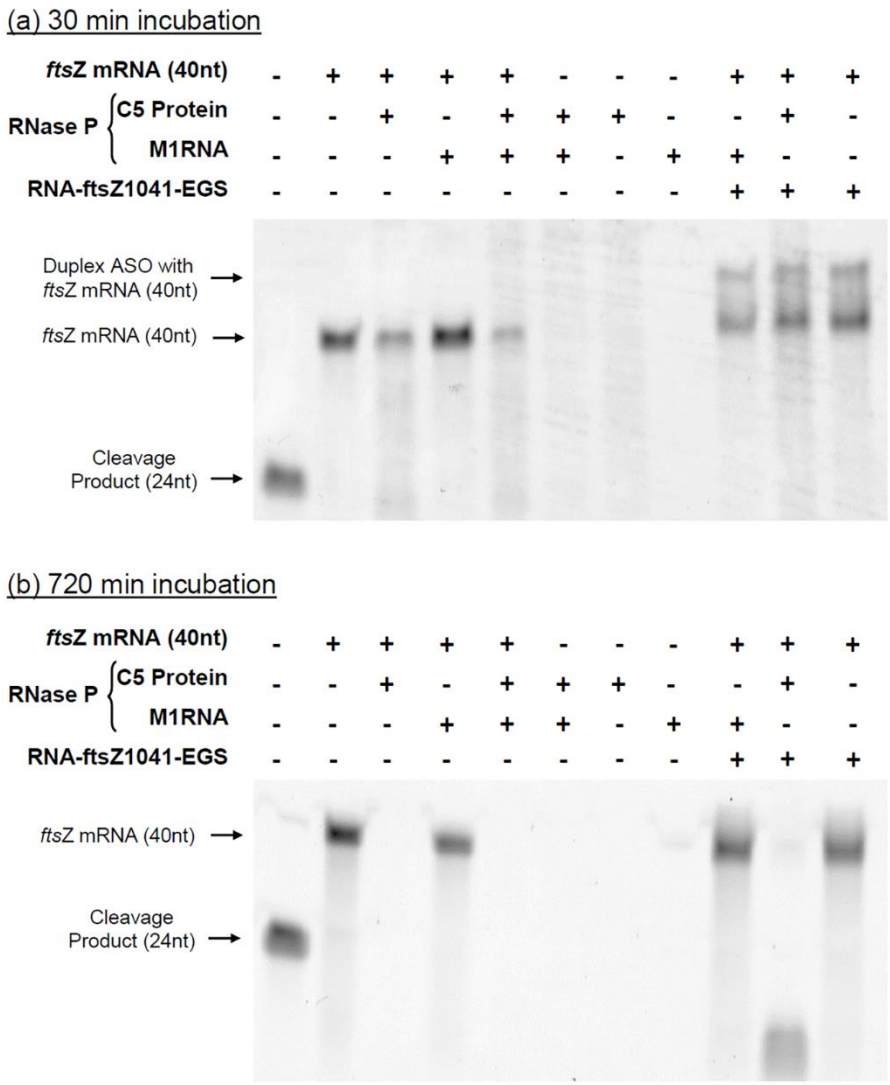

Figure 32. *In vitro* RNase P recruitment by Tolmasky's RNA-ftsZ1041-EGS. A mixture of the FAM labelled ftsZ RNA (40nt) target (1 pmol) and RNA-ftsZ1041-EGS (50 pmol) were preincubated at 25 °C for 2 h. M1 RNA (5 pmol) and C5 protein (70 pmol) were preincubated at 37 °C for 15 mins, and then added to the preincubated target/ASO mixture. The reaction was run at 37 °C for 30 min (a) or 720 min (b), and stopped by adding gel loading buffer (95% formamide, 1 mM EDTA, 0.01% Bromophenol Blue). The samples were analysed by 15% denaturing urea polyacrylamide gel. The gels were visualized using a Typhoon FLA 7000 biomolecular imager equipped with a FAM filter. The location and size of the initial target and the expected cleavage product are shown on the left. The first well contains a synthesised FAM labelled 24-mer that is used as a ladder.

We initially used the protocol described by Tolmasky and co-workers for studying the *in vitro* recruitment of RNase P.[248] In this assay, target mRNA, ASO-EGS, M1 RNA and the C5 protein are mixed in a ratio of 1:50:5:70 respectively and incubated at 37 °C. At various time points, the reaction was stopped by the addition of gel loading buffer (95% formamide, 1 mM EDTA, pH 8,

0.01% Bromophenol blue). The amount of cleavage was investigated by running a 15% denaturing urea polyacrylamide gel (urea-PAGE). For the oligonucleotides described in this chapter, cleavage could be visualized through the FAM labelled oligonucleotides using a GE Typhoon FLA 7000 biomolecular imager. Selective cleavage of *fts*Z mRNA (40nt) by RNase P recruited with the help of RNA-ftsZ1041-EGS should produce a FAM-labelled 24 nucleotide long fragment. However, no 24-mer was observed after 30 min for the conditions where RNA-ftsZ1041-EGS and RNase P were added to the target *fts*Z mRNA (40nt) (see **Figure 32a**). We then increased the reaction time to 90, 180, 360 and 720 min, but a 24-nucleotide fragment was never observed, even after 720 min (see **Figure 32b,** and Appendix A for time points 90, 180 and 360 min). In contrast, the addition of C5 protein alone (well 3) or RNase P alone (well 5) showed cleavage of the original *fts*Z mRNA (40nt) even in the absence of any antisense oligonucleotide (see **Figure 32**). Furthermore, this cleavage appears to be non-specific, as complete disappearance of the target *fts*Z RNA (40nt) is observed, without the appearance of a FAM-labelled 24-mer. Interestingly, when the C5 protein is not present and only M1 RNA is added to the target (well 4), no cleavage of the *fts*Z RNA (40nt) is observed. As the C5 protein alone is not supposed to have any catalytic activity, these results suggest that the commercial C5 protein was contaminated with non-specific RNases. To investigate the activity of the M1 RNA part of RNase P, we excluded the protein component C5, doubled the amount of M1 RNA in the assay and extended the incubation time to 2 and 3 days. However, no cleavage of the *fts*Z mRNA (40nt) was observed under these conditions either (**Figure 33**), suggesting that there is another factor at play.

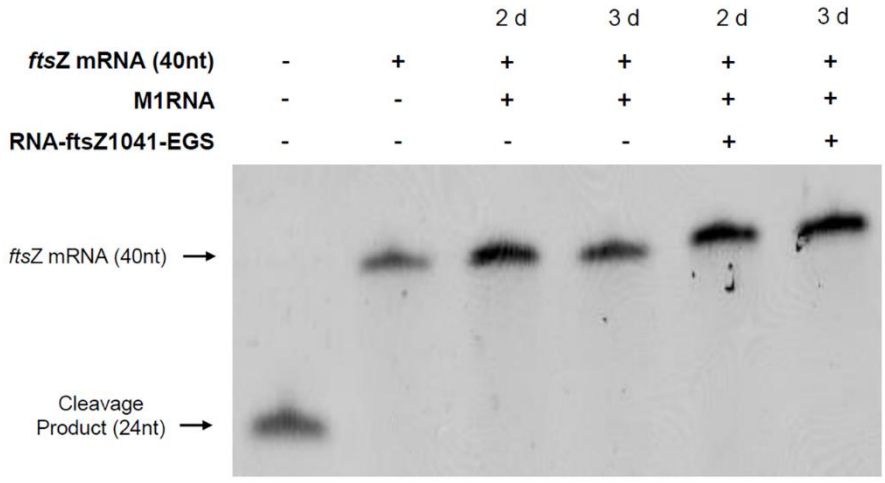

Figure 33. *In vitro* M1 RNA recruitment by Tolmasky's RNA-ftsZ1041-EGS. A mixture of FAM labelled ftsZ RNA (40nt) target (1 pmol) and RNA-ftsZ1041-EGS (50 pmol) were preincubated at 25 °C for 2 h, followed by the addition of M1 RNA (10 pmol). The reaction was run at 37 °C for 2days (2 d) and 3 days (3 d), and stopped by adding gel loading buffer (95% formamide, 1 mM EDTA, 0.01% Bromophenol Blue). The samples were analysed by 15% denaturing urea polyacrylamide gel. The gels were visualized using A Typhoon FLA 7000 biomolecular imager equipped with a FAM filter. The location and size of the initial target and the expected cleavage product are shown on the left. The first well contains a synthesised FAM labelled 24-mer that is used as a ladder.

A possible reason for the failure of the previous approach is base pairing between the external guide sequence tail and the mRNA targeted region. The first "A" of the ACCA tail could base pair with a "U" in the target RNA, and the second "C" of the ACCA tail could base pair with a "G" in the target (**Figure 34**). This was not expected to be a hindering reason, because the same region was targeted for RNase P recruitment by Tolmasky,[248] but we realised that this could be interfering with RNase P mediated cleavage. However, it is also possible that RNase P recruitment did not occur because we attached FAM labels to the mRNA and/or because we did not use the full length of the targeted mRNA *fts*Z, but a 40 nucleotide section of the target mRNA (which might adopt a different secondary structure). Nevertheless, the presence of the recruiter RNA-ftsZ104-EGS showed a band higher than the band corresponding to the target *fts*Z mRNA (40nt) (see **Figure 32**), suggesting strong duplex formation between the target RNA and the recruiter RNA-ftsZ1041-EGS. Therefore, we decided to shift the target region away from the original region, as shown in **Figure 34**. The three proposed RNase P recruiters (RNA-ftsz1041-EGS1, RNA-ftsz1041-EGS2, and RNA-ftsz1041-EGS3) were synthesised on solid phase using an ABI 394 oligonucleotide synthesizer (protocols can be found in Chapter 6), purified using HPLC and characterized using mass spectrometry (see **Table 10** and Appendix A for the HPLC chromatograms).

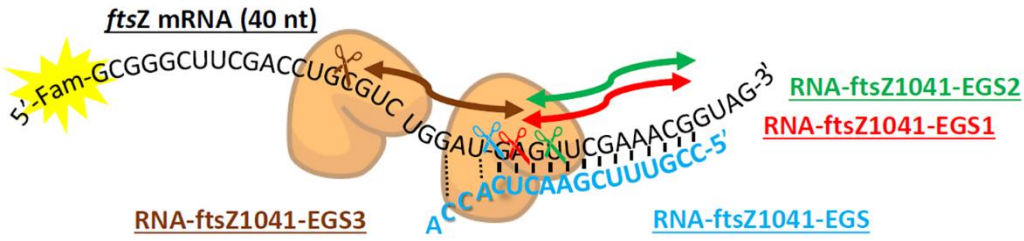

Figure 34. Recruitment of RNase P (brown shape) to the FAM-labelled mRNA-ftsZ1041 (black sequence) by various RNA-ftsZ104-EGSs. The original region targeted by RNA-ftsZ1041-EGS is shown in blue, with the undesired base pairing between the EGS tail and the target region indicated with dotted lines. The figure also shows the new EGS sequences generated by shifting the target region one base towards the 3' end in the case of RNA-ftsZ1041-EGS1 (red), two bases toward the 3'-end in the case of RNA-ftsZ1041-EGS2 (green), and nine bases towards the 5'-end of the target mRNA in the case of RNA-ftsZ1041-EGS3 (brown). The expected cleavage sites are denoted by scissors.

Table 10. Sequence, expected *m/z*, found *m/z* and purity of the synthesised RNA-ftsZ1041-EGSs.

RNA	Sequence	Expected *m/z*	Found *m/z*	Purity (%)
RNA-ftsZ1041-EGS1	*ACCGUUUCGAACUACCA*	5330.23	5329.7	>90.0
RNA-ftsZ1041-EGS2	*UACCGUUUCGAACACCA*	5330.23	5329.8	>90.0
RNA-ftsZ1041-EGS3	*CUCAUCCAGACGCUCCA*	5305.22	5304.9	>90.0

We explored the efficiency of the new RNase P recruiters RNA-ftsZ104-EGS1, RNA-ftsZ104-EGS2 and RNA-ftsZ104-EGS3 at time points of 1.5, 3, 6 and 24 h. We also tried to explore the effectiveness of the newly targeted regions by lowering the excess of RNase P and antisense oligonucleotides to a ratio of 1:1.1:4.4 for the target mRNA, the EGS sequences and the M1 RNA respectively (as compared to the previous ratio of 1:50:5 with a 70-fold excess of protein). The C5 protein was omitted from this assay, as it appeared to be contaminated with unselective RNases (see above) coupled with the fact that the M1 RNA is the catalytic portion of RNase P and the protein is not required for activity *in vitro*[235]. The results are shown in **Figure 35**. In the case of RNA-ftsZ1041-EGS1 and RNA-ftsZ1041-EGS2 cleavage is only observed after 6 h, and the cleavage does not seem to be efficient. In contrast, cleavage was apparent in the case of RNA-ftsZ1041-EGS3 as early as the first time point of 1.5 h and the cleavage increased with increasing incubation time. Given these results, we decided to use the region targeted by RNA-ftsZ1041-EGS3 to investigate the ability of PNA to recruit RNase P using EGS technology.

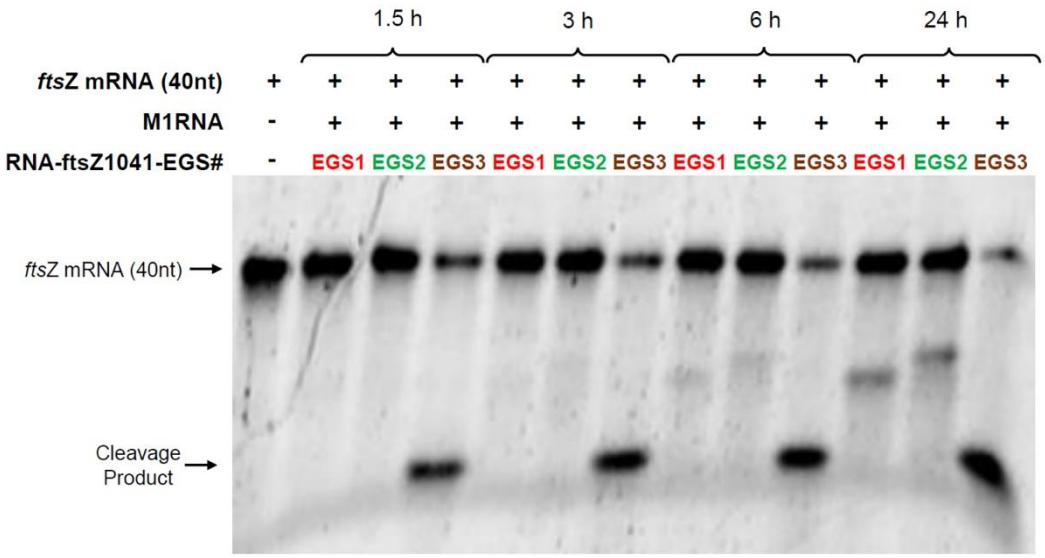

Figure 35 Exploring RNase P recruitment by the newly designed ASOs targeting new regions (RNA-ftsZ1041-EGS1, RNA-ftsZ1041-EGS2 and RNA-ftsZ1041-EGS3). A mixture of the FAM labelled ftsZ RNA (40nt) target (2 pmol) and RNA-ftsZ1041-EGS# (2.2 pmol) were preincubated at 25 °C for 15 min, followed by the addition of M1 RNA (8.8 pmol). The reaction was run at 37 °C for 1.5, 3, 6 and 24 h, and stopped by adding gel loading buffer (95% formamide, 1 mM EDTA, 0.01% Bromophenol Blue). The samples were analysed by 15% denaturing urea polyacrylamide gel. The gels were visualized using a Typhoon FLA 7000 biomolecular imager equipped with a FAM filter. The location and size of the initial target and the expected cleavage product are shown on the left.

2.2.3.2 Testing for *in vitro* recruitment of RNase P by PNA

After optimising the conditions of the *in vitro* assay in the previous section, we studied the effectiveness of the PNA-based oligonucleotides in recruiting the M1 RNA component *in vitro*. For

this, the PNA analogue of the most effective recruiter was synthesized (PNA-ftsZ1041-EGS3), as well as its analogue appended with the uptake peptide $(KFF)_3K$ (Pep-PNA-ftsZ1041-EGS3). We were specifically interested in the latter, as we have used PNA analogues conjugated with this cell penetrating peptide for the bacterial studies (section 2.2.2). **Table 11** gives an overview of the newly synthesized PNAs (see Chapter 6 for experimental details of the synthesis, and Appendix A for HPLC chromatograms). As a negative control, we purchased the RNA analogue without the EGS tail (RNA-ftsZ1041) from *ChemGenes*.

Table 11. Sequences, expected *m/z*, found *m/z* and purity for the synthesised PNAs.

PNA	Sequence	Expected *m/z*	Found *m/z*	Purity (%)
PNA-ftsZ1041-EGS3	K-O-O-cucauccagacgcucca	4928.73	4927.05	>90.0
Pep-PNA-ftsZ1041-EGS3	$(KFF)_3$K-O-O-cucauccagacgcucca	6195.40	6194.82	>90.0

The results for the *in vitro* assay with the PNAs are shown in **Figure 36**. The PNA analogues did not recruit RNase P after 1.5 h (no cleavage band is observed). Even after 24 h there was no cleavage in the case of the PNA-ftsZ1041-EGS3, and non-selective cleavage of the mRNA with peptide conjugated to the PNA (Pep-PNA-ftsZ1041-EGS3). Instead, strong duplex formation between the target mRNA and the PNAs is observed (high bands). This can be explained by the higher affinity for mRNA in the case of neutral PNA oligonucleotides compared to negatively charged RNA oligonucleotides. It is likely that the large structural and electrostatic difference between PNA and the normal substrate for RNase P (RNA) is the reason for its inactivity.

While it is clear that PNAs are not able to recruit RNase P, it is also unlikely that the recruitment of RNase P is the only problem for the EGS-modified PNAs, as gene silencing to the same extent as the steric blocking PNAs would be expected. The most probable reason for the *complete* inactivity of the EGS-PNAs in the bacterial assays is insufficient uptake into the bacterial cells. Good *et al.* had already noted that a longer 15-mer analogue of PNA-1900 is significantly less active at silencing *lacZ* than the original 12-mer PNA; even though the 15-mer is fully matched to the target mRNA and therefore will show higher binding affinity.[197] The authors speculated that this decreased silencing ability is probably due to limited delivery of the longer PNA into the cells. As all EGS-PNAs reported in this chapter are in the range of 14 to 16 bases long, compared to 10 to 12 bases for the steric blocking PNAs, it is likely that their uptake is problematic.

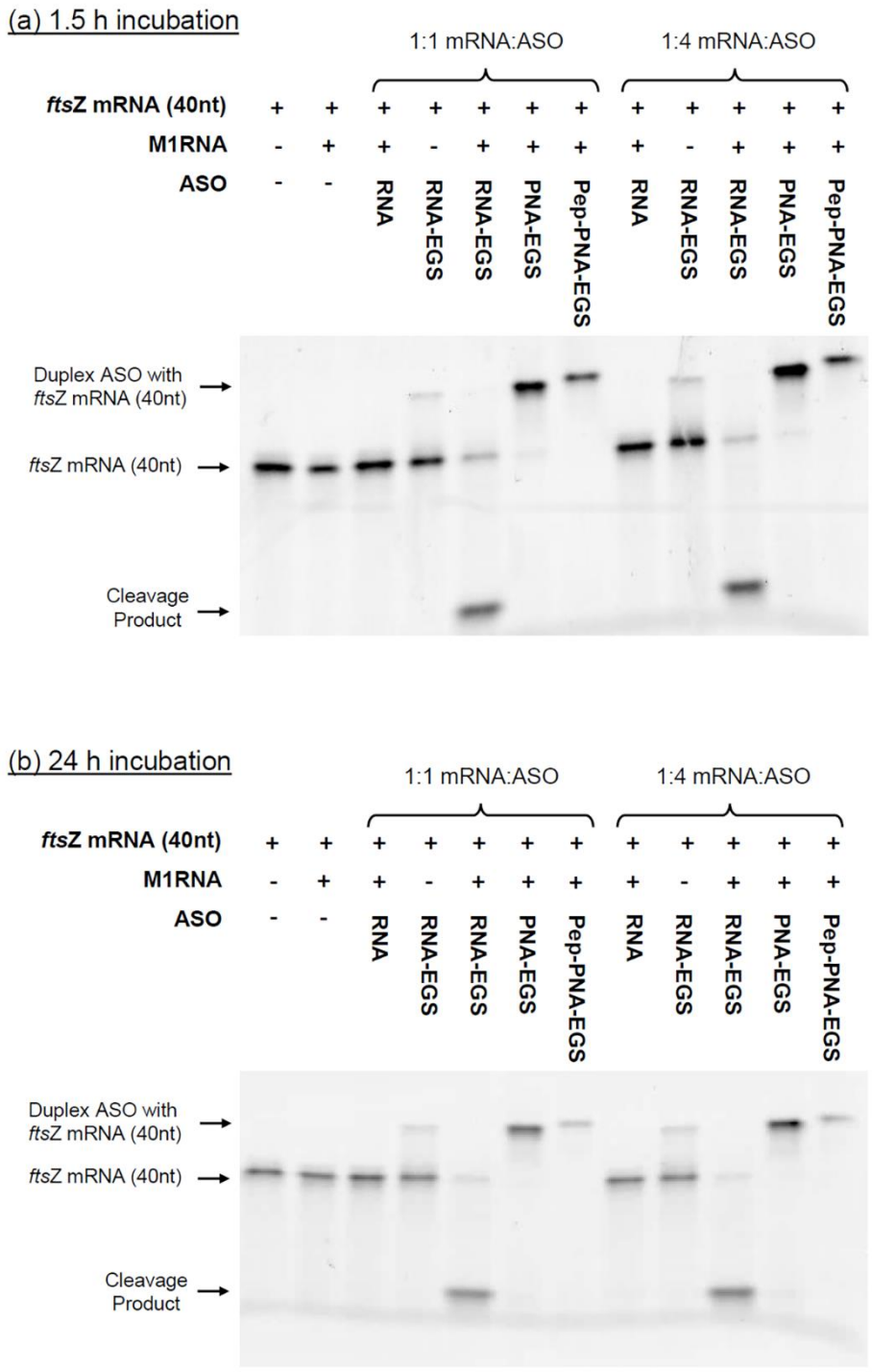

Figure 36. Potential *in vitro* recruitment of RNase P by PNAs. A mixture of the FAM labelled ftsZ mRNA (40nt) target (2 pmol) and ASO (2.2 pmol or 8.8 pmol) were preincubated at 25 °C for 15 min, followed by the addition of M1 RNA (8.8 pmol). The reaction was run at 37 °C for 1.5 and 24 h, and stopped by adding gel loading buffer (95% formamide, 1 mM EDTA, 0.01% Bromophenol Blue). The samples were analysed by 15% denaturing urea polyacrylamide gel. The gels were visualized using a Typhoon FLA 7000 biomolecular imager equipped with a FAM filter. The location and size of the initial target and the expected cleavage product are shown on the left. The ASOs used were RNA-ftsZ104 (RNA), RNA-ftsZ1041-EGS3 (RNA-EGS), PNA-ftsZ1041-EGS3 (PNA-EGS) and Pep-PNA-ftsZ1041-EGS3 (Pep-PNA-EGS).

2.3 Conclusions

In this chapter we have successfully designed and synthesized a number of PNAs targeting essential, reporter and virulence genes of *E. coli*. The cell penetrating peptide KFFKFFKFFK was covalently attached to the PNAs in order to facilitate the uptake of the oligonucleotides into the bacterial cells. Using a variety of antibacterial assays, we were able to show that the PNAs that function by sterically blocking the ribosome binding site are able to silence the activity of the *ftsZ* and *katG* genes. Unfortunately, the PNAs that function by recruiting RNase P via the external guide sequence (EGS-PNAs) did not seem to have any gene silencing ability. We have identified two reasons for this inactivity: (1) *in vitro* studies indicated that the PNA backbone cannot be recognized by RNase P and (2) the PNA-EGS are likely too long for efficient uptake into the bacterial cells compared to the shorter steric blocking PNAs.

While PNA is not able to recruit RNase P, other modified oligonucleotides might still show RNase P recruiting activity. As only a limited number of chemically modified oligonucleotides have been tested using EGS technology, it might be instructional to see if other types of chemically modifications are still able to recruit RNase P (e.g., MOE, OMe, DNA, 2'-F-RNA, LNA and PS). This investigation will be discussed in detail in Chapter 4.

Chapter 3 LNA-DNA gapmers as antibiotics

3.1 Introduction

The compatibility between the chemically modified oligonucleotides and DNA/RNA is one of the principles of gene silencing. Steric blockers were the earliest antisense oligonucleotides (ASOs); they function by binding to their complementary mRNA target and thereby block the ribosomes from binding to the mRNA and initiating translation.[120] In chapter 2 we showed that steric blocker PNAs possess gene silencing ability and we tried to improve this silencing ability by recruiting the enzyme RNase P using EGS technology in *E. coli*. Unfortunately, this RNase P recruiting strategy did not show an encouraging potency and we therefore decided to investigate the recruitment of another enzyme (RNase H).

3.1.1 RNase H

Ribonuclease H (RNase H) is an enzyme that specifically hydrolyses the phosphodiester bonds of an RNA strand hybridized to DNA. Hydrolysis occurs resulting in breakage of the P-O3' bond. There are various types of RNase H, classified into RNase HI, HII and HIII based on differences in their amino acid sequences. RNase HI represent type1 RNase H while RNases HII and HIII represent type 2 RNase H.[263, 264] Crystal structures of RNases H from both types 1 and 2 have shown that these proteins share a number of common features, such as a conserved main chain fold (coined the RNase H-fold), and a conserved steric configuration of four acidic residues that make up the active site. Based on these similarities in structure, it has been suggested that all RNases H (type 1 and 2) share an identical catalytic mechanism.[129] A number of crystal structure studies observed the presence of two metal ions (Mg^{2+}) coordinated by the acidic active site residues, the scissile phosphate group of the substrate and water molecules. It has also been observed that the distance between the two metal ions is different when RNase H is bound to either an RNA/DNA substrate, an intermediate transition state mimic or a cleaved product mimic[265-267]. Based on these findings a catalysis mechanism has been suggested for RNase H.

In the suggested mechanism, metal ion A helps in the formation of the substrate nucleophile (OH^-), while metal ion B probably destabilizes the enzyme-substrate complex and therefore lowers the energy barrier of the phosphoryl transfer reaction.[8] After binding the DNA/RNA substrate, the metal ions move closer to each other so that the OH^- nucleophile can attack the phosphorus atom and form a pentavalent transition state, where the additional negative charge is potentially stabilized by the close distance of the two metal ions, followed by conversion to the 5'-phosphate and 3'-OH products (See **Figure 37**) [129, 265-267]

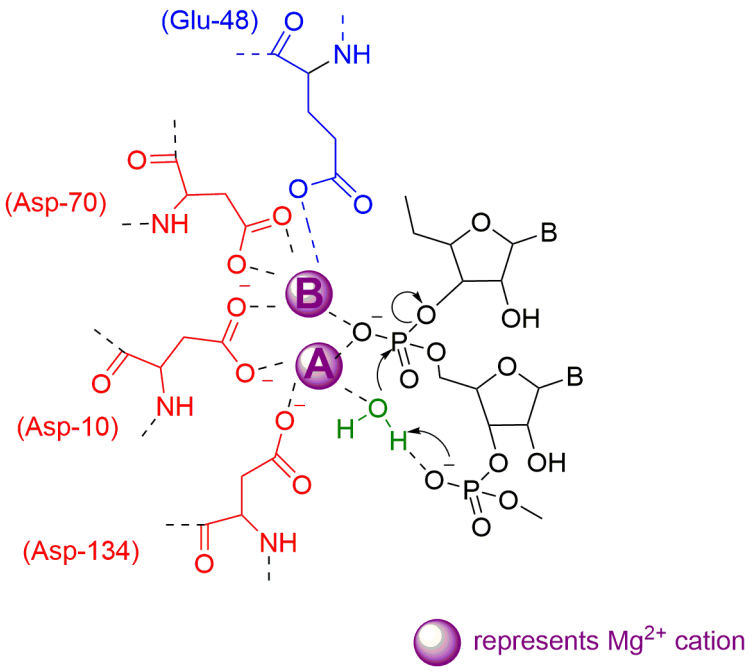

Figure 37. Proposed mechanism of the cleavage of RNA by RNase H and the role of the two metal ions in the catalysis. Residues Asp10, Glu48, Asp70 and Asp134 form the active site (metal biding site) of RNase HI in *E. coli.* Metal ion A helps in the formation of the substrate nucleophile and the product release, while metal ion B destabilizes the enzyme-substrate complex and therefore encourages the phosphoryl transfer reaction.

While the *E. coli* RNase HI crystal structure with substrate has not yet been reported, a high similarity was reported for the crystal structure of human RNase HI in complex with a RNA/DNA substrate and Mg^{2+} and the crystal structure of *E. coli* RNase HI free from the substrate. It can thus be assumed that the substrate recognition mechanism of human RNase HI and *E. coli* RNase HI is highly comparable. The co-crystal of human RNase HI with substrate and Mg^{2+} shows that the RNA/DNA hybrid binds to RNase HI with the DNA backbone fitting into one groove, and the RNA backbone fitting into a second groove containing the active site separated from the first groove by a ridge (see **Figure 38**). In the RNA-binding groove the 2'-OH groups of four adjacent ribonucleotides (two on both side of the cleavage site) contact the side chain of Glu48 (in the case of *E. coli* RNase HI) and the backbone atoms of Cys13, Gly15, Asn16 and Gln72. The DNA-binding

groove consists of two DNA-binding sites. The first site is the major phosphate-binding pocket formed by residues Arg41, Thr43 and Asn100 for *E. coli* RNase HI, and helps fix the B-form of DNA. The second site is a channel formed of Trp81, Trp85 and Ala93 in *E. coli* RNase HI. It is this DNA-binding groove, with its two sites, that provides RNase H with its high specificity for RNA/DNA hybrids, as an RNA strand cannot fit in the DNA-binding groove due to steric hindrance caused by the 2'-OH group of RNA with the indole ring of Trp221.[268]

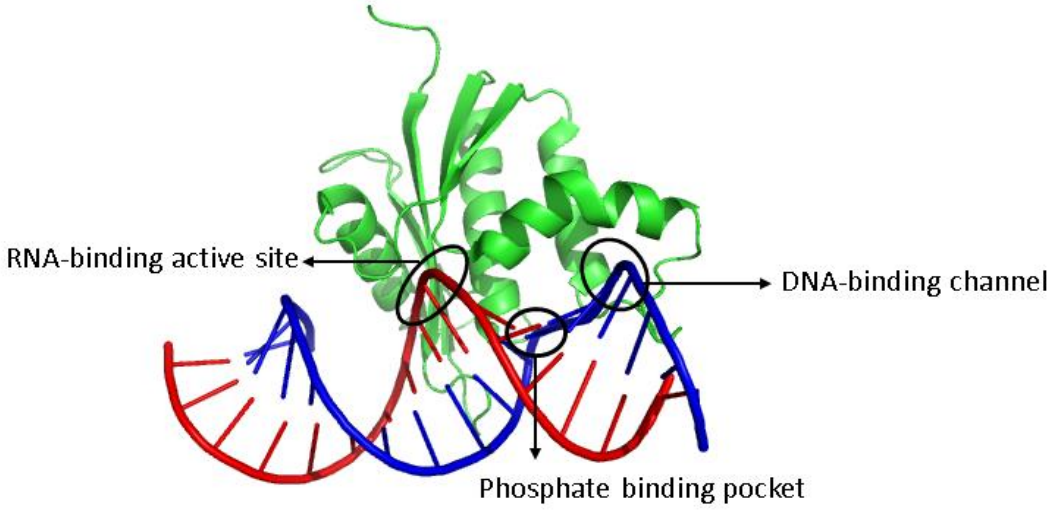

Figure 38. The crystal structure of human RNase HI C-domain complexed with a RNA/DNA hybrid (PBD code 2QK9). The structure of human RNase HI C domain is shown in green, DNA in blue and RNA in red. The regions comprising the binding sites for DNA and RNA with the protein are indicated.

Due to its ability to specifically cleave the RNA strand in RNA/DNA hybrids, RNase H has been employed as a means to increase the efficiency of antisense technologies in eukaryotic cells.[57] In this respect, RNase H is recruited to cleave the target mRNA strand bound by DNA-based antisense oligonucleotides. It was already mentioned in Chapter 1 that the use of ASOs can be hindered by nucleic acids instability *in vivo*, problematic uptake of the ASO into the targeted cells or off-target effects. Many of these problems can be overcome by the use of chemically modified oligonucleotides (see also Chapter 1). However, while some modifications can still be recognized by RNase H, it is important to note that many chemically modified oligonucleotides are incompatible with RNase H recruitment. For example, changing one of the non-bridging oxygens in the sugar-phosphate backbone of DNA from oxygen to sulfur (PS-DNA), is known to increase the resistance to nuclease degradation,[269-271] and exhibits good compatibility with RNase H-mediated mRNA cleavage.[272] In contrast, the sugar modification locked nucleic acid (LNA), which greatly increases the binding affinity towards RNA strands,[100] is not compatible with RNase H activity[273]. In this analogue the modified sugar features a methylene bridge joining the 2'-O to C4',

and as a consequence the sugar is locked in a restricted north conformation mimicking A-form RNA.[99-101] As we mentioned earlier, recruiting RNase H requires a DNA/RNA hybrid and as LNA is a mimic of RNA (and thus forms a RNA/RNA-like duplex), it will not be able to be recognized by RNase H. In order to overcome this problem and combine the advantages of recruiting RNase H with the advantage of using modified oligonucleotides such as LNA, 'gapmer' technology has been introduced.

3.1.2 Gapmers as optimized RNase H recruiting oligonucleotides

Gapmers are oligonucleotides containing a hybrid-forming region surrounded by 5'- and 3'-flanking regions containing high affinity chemical modifications[274] (see **Figure 39**). This 'gapmer' design benefits from the high nuclease stability and a higher binding affinity of the oligonucleotide strand provided by the wings of the gapmer (through chemical modifications), while the middle of the gapmer (normally DNA or DNA analogues) helps to recruit RNase H which in turn catalyses the cleavage of bound mRNA. Gapmers designed according to this strategy are the dominant antisense technology in clinical development for gene silencing in patients.[57]

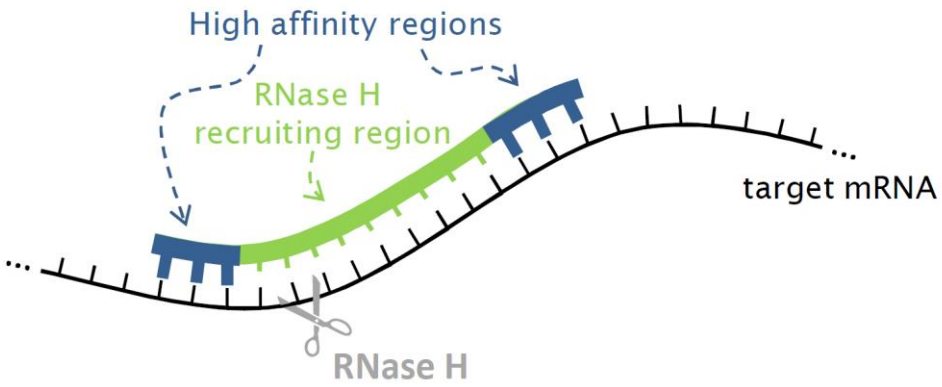

Figure 39. Figure explaining the gapmer design strategy. The central region of the ASO (green) functions as an RNase H recruiter, while the flanking regions (blue) increase the binding affinity between the gapmer and the target mRNA. The cleavage is thought to happen nearer to the 5'-end of the mRNA (2-3 bases).

Some of the most common modifications used for the flanking regions are 2'-*O*-methoxyethyl RNA (MOE) and locked nucleic acid (LNA)[275]. Gapmers are also generally designed with a phosphorothioate (PS) backbone, as this modification is able to recruit RNase H (as PS-DNA)[276], provides increased nuclease resistance and has improved pharmacokinetic properties compared to a PO backbone (e.g. better cellular uptake and increased binding to plasma proteins)[59] LNA

gapmers show the highest potency in many tissues in vivo due to a combination of several properties[277]. LNA is known to induce the highest increase in binding affinity of any modified oligonucleotide towards complementary RNA or DNA strands (an increase in T_m of about 4-8°C per modification)[100, 278]. One consequence of this exceptionally high affinity appears to be that LNA-based ASOs still have high gene silencing ability when they are relatively short sequences (12- to16-mers). Koch and co-workers, for example, have shown that short LNA-based gapmers (12- to 13-mers) display improved potency against apolipoprotein B mRNA *in vitro* and *in vivo* in mice and monkeys compared to longer gapmers (14- to 20-mers).[279] The authors speculated that this could be partly due to more efficient cellular uptake of the short LNAs.

While there are number of other studies showing that gapmers (LNA-based or other) can be used for gene silencing in eukaryotic systems,[280] to the best of our knowledge there are no examples of the use of gapmers for the recruitment of RNase H in prokaryotes. While there have been reports on the use of gapmers to induce gene silencing in bacteria,[105, 177] they have not been shown to function by recruitment of RNase H. This is somewhat surprising for a number of reasons. Many studies in eukaryotic systems employ the commercially available *E. coli* RNase H for *in vitro* investigations of the RNase H recruiting ability of different ASOs gapmers.[281, 282] This indicates that gapmers should be able to recruit RNase H in bacteria as well. Additionally, as mentioned above, LNA-based gapmers can be made quite short, which makes them particularly well adapted to bacteria – both because shorter oligonucleotides seem to be taken up better (see also Chapter 2), and because bacterial genomes are less complex and thus short oligomers do not have as many concerns about specificity in bacteria as they do in eukaryotic cells. Finally, LNA-modified oligonucleotides have already been used in steric blocking or EGS-based gene silencing in bacteria[121], and LNA-based gapmers should therefore be well tolerated by prokaryotic systems. We thus decided to explore gene silencing in bacteria through LNA gapmer-mediated RNase H recruitment.

3.1.3 Aim of this chapter

The aim of this chapter is to investigate whether short LNA-based gapmers are able to recruit RNase H and induce gene silencing in bacteria.

3.2 Results and discussion

3.2.1 Design and synthesis

Chapter 2 showed that silencing of the *ftsZ* gene can be easily quantified by monitoring bacterial growth using the optical density at 600 nm. We therefore decided to keep *ftsZ* as the target gene. As the KFFKFFKFFK peptide showed promising delivery ability for the short steric blocking PNAs in Chapter 2, we also decided to use the same cell penetrating peptide for the delivery of the gapmers presented in this chapter.

A typical gapmer design for high affinity modifications like LNA is to include 2-4 nucleotides of LNA per wing, flanking 8-10 nucleotides of DNA in the central gap. (At least 7 bases of DNA are required for potent recruitment of RNase H, and gaps of 8 or more bases are considered preferable).[102, 280] For example, 3-9-3 gapmers (i.e. gapmers consisting of 9 nucleotides in the central DNA region responsible for RNase H recruitment flanked by 3 nucleotides on each side that provide stronger binding to mRNA) have previously been shown to be one of the most potent gapmer designs for gene silencing[279, 283].In light of the problematic delivery of longer oligonucleotides discussed in Chapter 2, we decided to focus our designs on the shorter end of this spectrum, including 3-9-2 and 3-8-2 gapmers targeting *ftsZ* (see **Figure 40**). For the central gap we chose PS-DNA because this chemical modification is still able to recruit RNase H, but has higher nuclease resistance compared to natural DNA. Locked nucleic acid (LNA) was chosen for the two flanking regions as it displays one of the highest binding affinities to mRNA. A series of 14-mer gapmers with the following general structure were thus designed: 5'- [3-nt PS-LNA] – [8/9-nt PS-DNA] – [2-nt PS-LNA] -3' (see **Figure 40**).

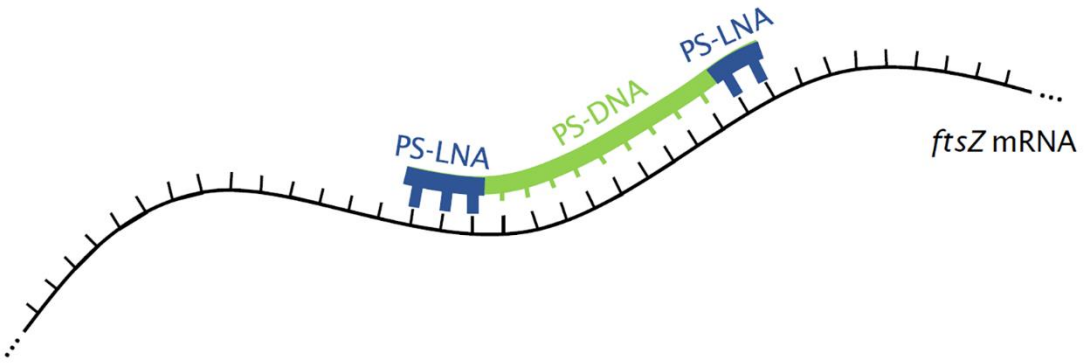

Figure 40. General scheme of a typical 3-9-2 LNA gapmer used in this chapter to silence the *ftsZ* gene. The central 9-mer (green) is made of PS-DNA for facile recruitment of RNase H, while the 3-mer and 2-mer flanking regions (blue) are made from a PS-LNA backbone.

3.2.1.1 Design and synthesis of LNA gapmers targeting *ftsZ*

Because mRNA can adopt many secondary structures in which double stranded regions are unsuitable targets for ASOs due to competition, we synthesised six oligonucleotides with gapmer configuration that are antisense to different regions of the *ftsZ* gene. The first three gapmers target the same regions as the various anti-*ftsZ* PNAs discussed in Chapter 2. The first gapmer (Gap-1) corresponds to the sequence suggested by Liam Good and co-workers (Ec326)[254] and targets the *fts*Z untranslated region (UTR). Because the antisense region reported by Good is only 10 nucleotides long, this sequence was designed as a 2-6-2 LNA-DNA-LNA gapmer in spite of the fact that this gap length is expected to be marginal in its ability to recruit RNase H.[102, 280] The second gapmer (Gap-2) corresponds to the original sequence published by Tolmasky and colleagues targeting *ftsZ*-1041.[248] We also included our suggested sequence from Chapter 2, where the antisense region used by Tolmasky was shifted 9 bases towards the 5' end (Gap-3). As the antisense region of these sequences corresponds to a 13-mer, Gap-2 and Gap-3 were designed as 3-8-2 LNA-DNA-LNA gapmers. All three gapmers based on previous oligonucleotides targeting *ftsZ* were synthesized on a ABI 394 DNA synthesizer, purified using ion exchange HPLC and characterized by mass spectrometry (see **Table 1** and Appendix B for HPLC chromatograms).

Table 12. Name, target region, sequence, expected *m/z* and found *m/z* for synthesised anti-*ftsZ* gapmers. Underlined and bolded regions represent DNA, not underlined or bolded represent LNA. All sequences have a PS backbone.

Name	Target region	Sequence	Expected *m/z*	Found *m/z*
Gap-1	ftsZ-Ec326UTR	TC**AAACAT**AG	3276.36	3276.3
Gap-2	ftsZ-1041	CCG**TTTCGAAC**TC	4217.54	4217.4
Gap-3	ftsZ-1032	CTC**ATCCAGAC**GC	4211.54	4211.4
Gap-4	ftsZ-475	ATA**GTGATCAGA**GA	4684.77	4684.47
Gap-5	ftsZ-902	CAG**CTCGTCATT**CA	4575.73	4575.44
Gap-6	ftsZ-904	GCT**CGTCATTCA**TA	4576.71	4576.43

In addition to these three gapmers, we also designed three ASOs that target unexplored regions of the *ftsZ* gene. This was done to identify the best *ftsZ* region for the development of antisense-based antibiotics. In order to select suitable regions within the *ftsZ* gene for silencing by gapmers, it was necessary to calculate the possible secondary structures adopted by this gene. First, the EcoCyc[256] website was used to determine the mRNA sequence of the *ftsZ* gene in *E. coli* strain BW25113. The mRNA sequence was subsequently investigated using Mfold[284] to determine the single stranded sites (using the ss-count). This allowed us to identify three regions of at least 14 nucleotides long that have a high single-strand character (ss-count of 20 or higher for all residues), and complementary ASOs were designed to bind to the chosen regions (see **Figure 41**).

To minimize possible off-target effects resulting from partial complementarity to other *E. coli* genes, the chosen single strands were analysed further using a standard nucleotide BLAST against *E. coli* strain BW25113 (taxonomy ID=679895). Finally, the five regions showing minimal off-target effects during the BLAST search were investigated using IDT's online "OligoAnalyzer" software,[285] which confirmed that there are no overly strong hairpin or self-dimerizing structures present in the gapmers. Three target regions were identified in this manner: ftsZ-475, ftsZ-902 and ftsZ-904. The corresponding antisense sequences (Gap-4, Gap-5 and Gap-6 respectively) were synthesized as 3-9-2 LNA-DNA-LNA gapmers on an ABI 394 DNA synthesizer, purified using ion exchange HPLC and characterized by mass spectrometry (see **Table 1** and Appendix B for HPLC chromatograms).

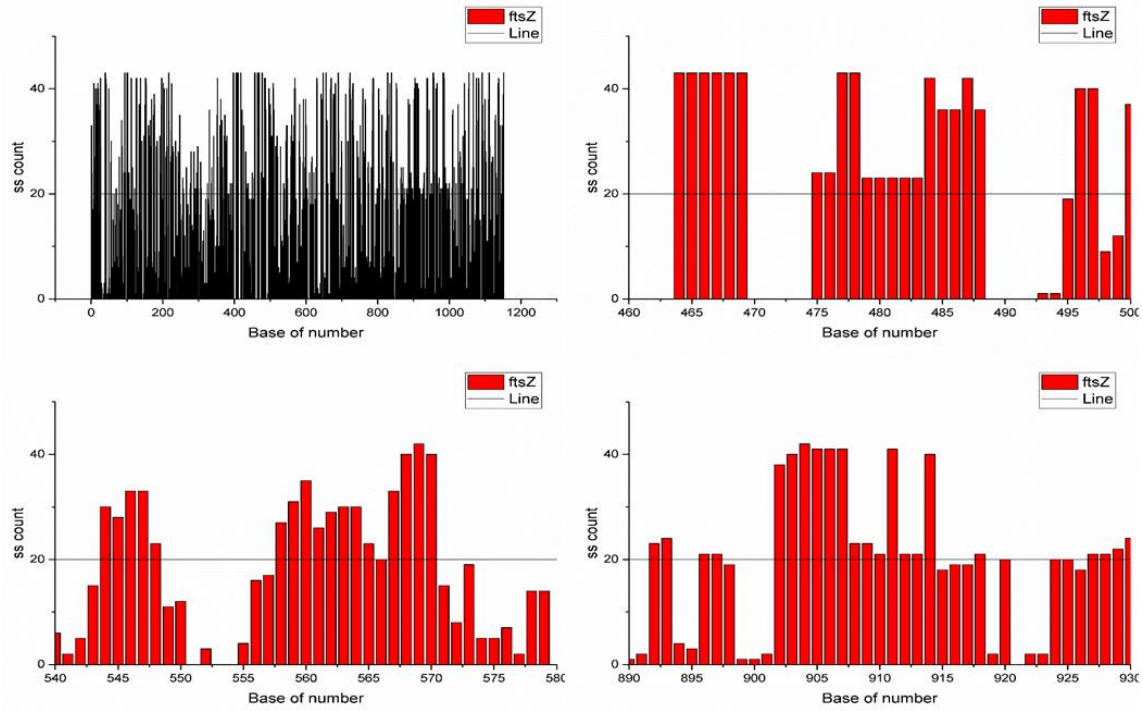

Figure 41. Ss-count for the *ftsZ* mRNA calculated using Mfold, Top left is the full length of the mRNA, and the rest are regions with at least 12 consecutive nucleotides with ss-count above 20. Based on the selected regions above we designed three antisense oligonucleotides targeting sections in these regions.

3.2.1.2 Synthesis and functionalisation of cell penetrating peptide $(KFF)_3K$

Cell penetrating peptides (CPPs) have been increasingly used to enhance the uptake of synthetic oligonucleotides into cells.[286] There are two main strategies that utilise CPPs for the uptake of oligos into cells.[183] One strategy is to covalently attach the peptide to the nucleotide, which has been mainly applied for the delivery of uncharged analogues such as PNA (see also Chapter 2). Alternatively, non-covalent complexation between the positively charged peptides and the negatively charged oligonucleotides has found great utility in the delivery of siRNA. The $(KFF)_3K$

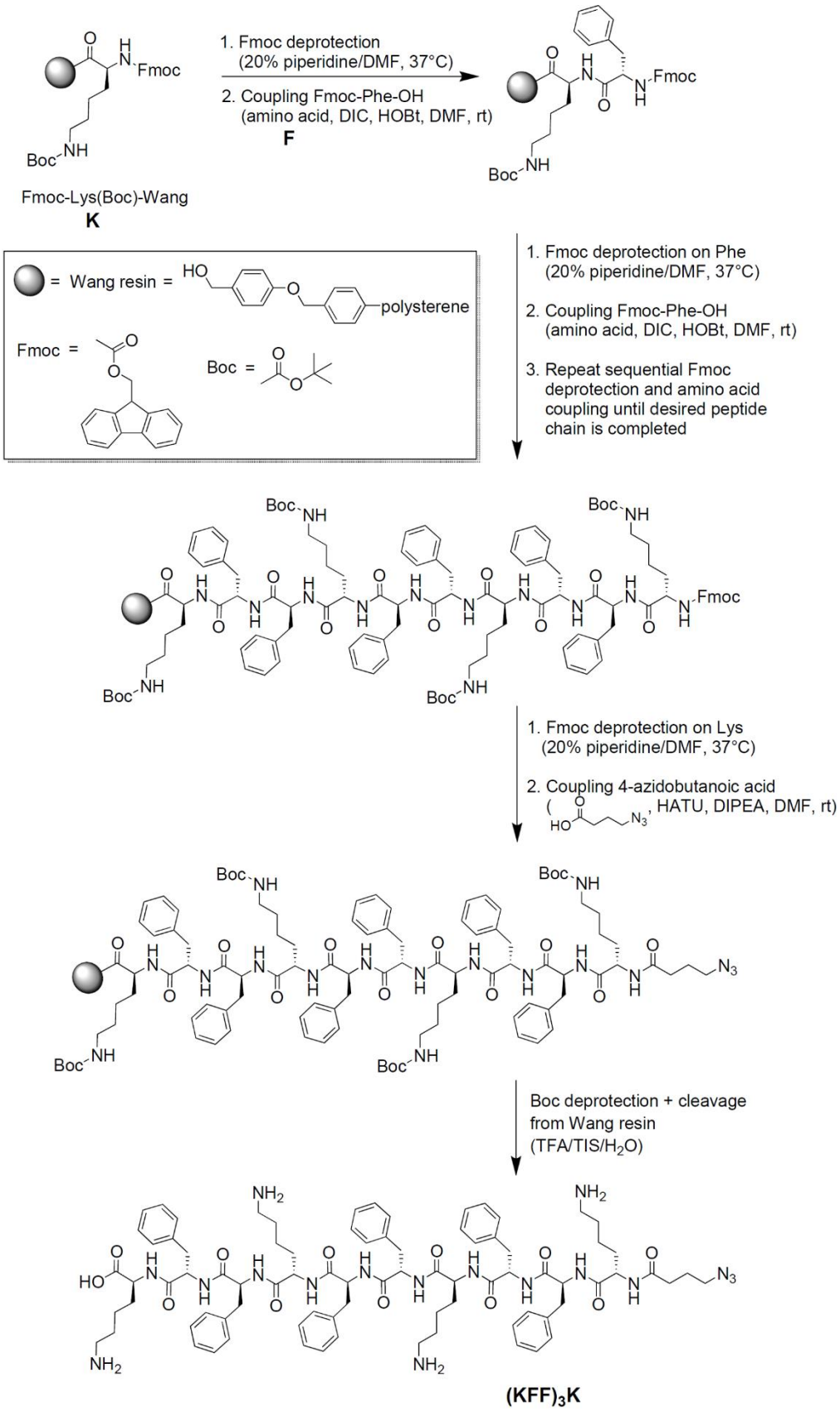

Scheme 1. Manual synthesis on Wang resin of the azido-modified $(KFF)_3K$ cell penetrating peptide. Synthesis was performed by sequential Fmoc deprotections (using 20% piperidine in DMF at 37°C) and peptide coupling reactions (using DIC/HOBt for the first 3 couplings, and HATU/DIPEA for all other coupling reactions).

peptide has been reported as a potent CPP vector, especially when it is covalently conjugated with PNAs and also with a number of other oligonucleotides analogues (see also Chapter 2).[197, 286, 287] Therefore, the $(KFF)_3K$ peptide was synthesised manually on Wang-resin using a series of sequential Fmoc deprotections and peptide coupling reactions (**Scheme 1**, see Chapter 6 for experimental details). Prior to cleavage from the resin, the peptide was functionalised with an azido group through a coupling reaction with freshly synthesized 4-azidobutanoic acid (**Scheme 1**, see Chapter 6 for experimental details). After cleavage from the resin and Boc deprotection of the lysine side chains, the peptide was purified using reversed-phase HPLC and characterized using mass spectrometry (**Table 13**). Initially, the $(KFF)_3K$ peptide will be used to facilitate cellular uptake through non-covalent complexation with the anti-*ftsZ* LNA gapmers. If necessary, however, the addition of the azide functionality allows covalent attachment of the peptide to the gapmers using click reactions with alkyne-containing oligonucleotides.

Table 13. Sequence, expected *m/z* and found *m/z* for the synthesised CPP.

CPP	Sequence (N to C terminus)	Expected *m/z*	Found *m/z*
$(KFF)_3K$	KFFKFFKFFK-butanoate-N_3	1524.88	1524.84

3.2.2 *In vitro* recruitment of RNase H

In Chapter 2, we used an *in vitro* assay to gain a better understanding of the failed recruitment of RNase P. Here in Chapter 3, our strategy is to inspect the RNase H recruitment ability of the gapmers first *in vitro*, in order to eliminate any unsuccessful gapmers before moving to bacterial studies. To be able to visualize the cleavage of the target mRNA upon recruitment of RNase H, it was necessary to first synthesize 40-nucleotide fragments of the *ftsZ* mRNA labelled with fluorescein (FAM). **Table 14** gives an overview of the FAM-labelled *ftsZ* regions and the gapmers that target them. All sequences were synthesized on an ABI 394 DNA synthesizer, purified using ion exchange HPLC and characterized by mass spectrometry (see **Table 14** and Appendix B for HPLC chromatograms).

Table 14. Name, sequence, expected *m/z* and found *m/z* for synthesised FAM-labelled *ftsZ* mRNA regions. All sequences are RNA with PO backbone. The gapmers that target each region are also indicated.

Name	Sequence	Targeted by …	Expected *m/z*	Found *m/z*
ftsZ-UTR RNA	FAM-*ACAAAUCGGAGAGAAACUAUGUUUGAACCAAUGGAACUUA*	Gap-1	13447.79	13449
ftsZ-1041 RNA	FAM-*GCGGGCUUCGACCUGCGUCUGGAUGAGUUCGAAACGGUAG*	Gap-2/3	13460.15	13460.71
ftsZ-458 RNA	FAM-*UGUCCAAGCAUGUGGACUCUCUGAUCACUAUCCCGAACGA*	Gap-4	13280.57	13282.8
ftsZ-885 RNA	FAM-*UACUUCUCUUGACCCGGAUAUGAAUGACGAGCUGCGCGUA*	Gap-5/6	13337.59	13339

The *in vitro* activity of the gapmers was investigated using RNase H kit EN0201, purchased from Thermo Fisher Scientific. In 30 µL reaction were mixed 4 x 10^{-3} units of RNase H, 2 pmol target mRNA, 8.8 pmol gapmer and 10x reaction buffer. The reaction was run at 37 °C for 24 h. At two different time points (1.5 h and 24 h), a 7 µL sample was withdrawn from the reaction, and 7 µL formamide was added to stop the reaction. The samples were subsequently loaded onto a denaturing 15% urea polyacrylamide gel, separated using electrophoresis and visualized on a GE Typhoon FLA 7000 biomolecular imager with the FAM channel. The experiment was performed in duplicate. The result for one of the repeats after 1.5 h incubation is shown in **Figure 42**; the results for the other repeats and the 24 h incubation repeats are given in Appendix B and gave comparable results. All six gapmers appear to be able to recruit RNase H and induce cleavage of their target mRNA. The weakest cleavage band is seen for Gap-1, while the other gapmers show clearer and intense cleavage bands (see **Figure 42**). We therefore decide to study the antibacterial properties of all six gapmers.

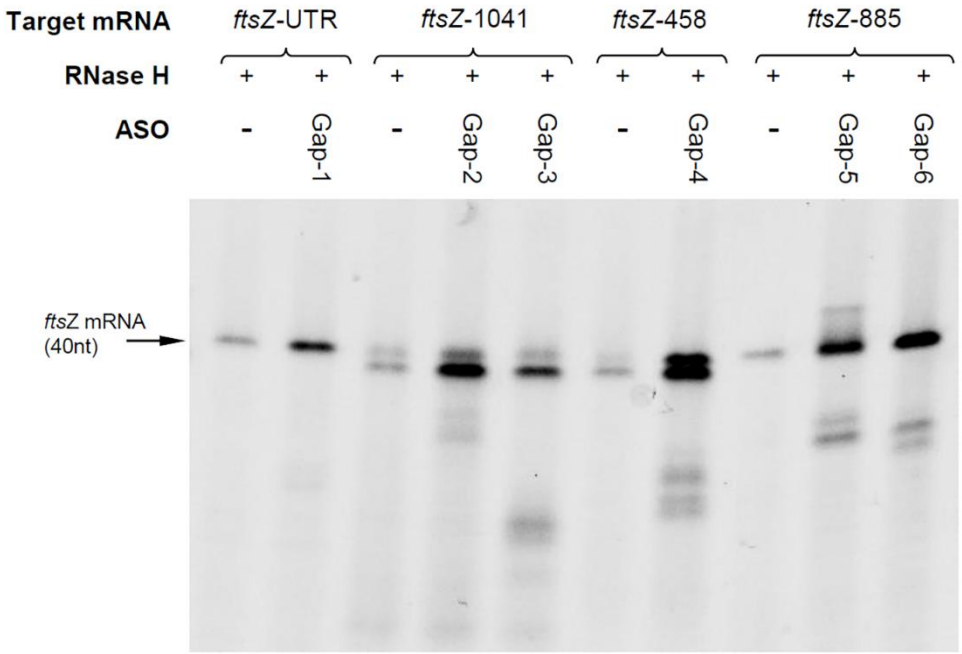

Figure 42. *In vitro* recruitment of RNase H by the LNA-DNA-LNA gapmers. A mixture of RNase H (4 x 10^{-3} units), the FAM labelled target mRNA (2 pmol) and ASO (8.8 pmol) were incubated at at 37 °C for 1.5 h and stopped by adding formamide. The samples were analysed by 15% urea-PAGE and visualized using a Typhoon FLA 7000 biomolecular imager equipped with a FAM filter. The location and size of the initial target is shown on the left, bands below the target band are presumably due to RNase H mediated cleavage of the target mRNA.

3.2.3 Bacterial assays

3.2.3.1 Optical density measurement of bacterial growth inhibition

After the promising *in vitro* results discussed above, we wanted to investigate whether LNA-based gapmers can be used as antibiotics by targeting the essential *ftsZ* gene in *E. coli*. The influence of the anti-*ftsZ* gapmers on the bacterial growth of *E. coli* strains was therefore investigated by following the optical density at 620 nm (experiments are comparable to those described in Chapter 2). The experiments were conducted on both wild type *E. coli* (ATCC 25922) and *E. coli* AS19. The latter strain has a more permeable membrane[257] and should therefore allow more efficient uptake of the gapmers.

We initially tried to achieve LNA-DNA gapmer uptake by pre-mixing the $(KFF)_3K$ peptide and the LNA gapmers, rather than by covalently attaching the peptide to the gapmers. While covalent conjugation is often more efficient for the delivery of oligonucleotides,[223] pre-mixing is experimentally easier and allows a wider and more facile screening of potential antisense oligonucleotides. Additionally, covalent conjugation holds the risk that the construct folds upon itself due to the charge complementarity of the peptide and the oligonucleotide, rendering it unsuitable for binding to the target mRNA. However, many cell penetrating peptides have antimicrobial properties themselves[190, 260] and it was therefore necessary to find the highest concentration of the $(KFF)_3K$ that is non-toxic to *E. coli* and suitable for gene silencing experiments. The bacterial growth in the presence of various concentrations of the $(KFF)_3K$ peptide was thus monitored via the optical density at 620 nm (OD_{620nm}). The results are shown in **Figure 43**.

For the membrane-permeable AS19 strain, the $(KFF)_3K$ peptide caused complete killing of the bacteria at concentrations of 6.25 µM and above (**Figure 43**). These concentrations are clearly too toxic for the cells and cannot be used for the gapmer-induced *ftsZ* silencing investigations. More interesting was the effect of the peptide at 3.125 µM, which led to a small delay in bacterial growth without fully wiping out the cultures (**Figure 43**). We speculated that this could be due to the interaction of the cationic peptides with the bacterial membrane;[288, 289] this might destabilize the bacterial cells enough to cause the observed delay in growth, but not enough to kill the bacteria. If this is true, this peptide concentration should be ideal for gene silencing experiments. At lower concentrations (1.625 µM), the peptide did not have any effect on the growth curve of *E. coli* AS19 (**Figure 43**). For wild type *E. coli*, the results indicate that $(KFF)_3K$ is toxic for the cells at concentrations of 20 µM and above, while concentrations up to 10 µM are non-toxic and can be used for LNA-DNA gapmer delivery (**Figure 43**). It is notable that the peptide is significantly more toxic to the membrane-permeable AS19 *E. coli* strain than to wild type *E. coli.* This is

however not surprising because CPPs function by interaction with the membrane.[288, 289] Given the fact that the AS19 strain is already more permeable than wild type *E. coli*,[257] it is expected that this strain will be more sensitive toward the effects of cell penetrating peptides such as $(KFF)_3K$.

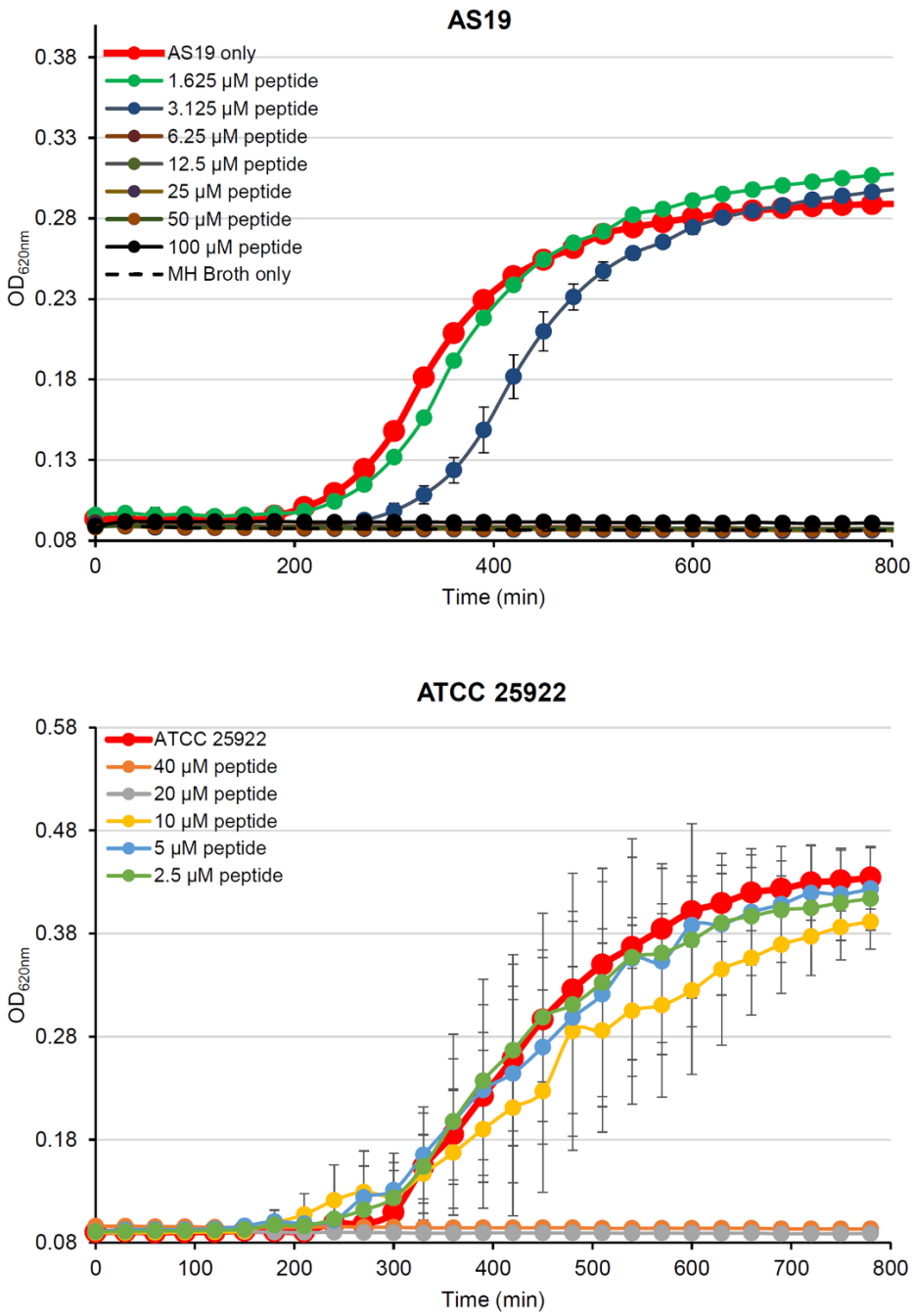

Figure 43. Toxicity of the $(KFF)_3K$ peptide against *E. coli* AS19 (top) and wild type *E. coli* ATCC 25922 (bottom). The *E.coli* strains at 10^5 cfu/mL were added to a solution of the peptide and the OD_{620nm} value was measured for 800 min at 37 °C. The results are the average of at least 1 biological and 2 technical repeats, with error bars representing standard deviations.

Based on these results, we decided to work with two concentrations of the $(KFF)_3K$ peptide (1.5 µM and 3 µM) for the *ftsZ* silencing experiments in *E. coli* AS19, and one concentration (10 µM) for the gene silencing experiments in wild type *E. coli.* Because the AS19 strain is more permeable, we postulated that the gapmers are more likely to function in this strain than in wild type *E. coli.* The studies with wild type *E. coli* were therefore limited to the gapmers that showed the best results in the *in vitro* RNase H recruitment assay (Gap-4, Gap-5 and Gap-6). The next step requires optimization of the peptide/oligonucleotide ratio. The $(KFF)_3K$ peptide used in this chapter has 4 nominal positive charges due to the presence of four lysine amino acids, while the LNA-DNA gapmers have 9 to 13 nominal negative charges originating from the phosphorothioate linkages. Due to the inherent toxicity of the peptide, achieving excess positive charges allows only low concentrations of the gapmers and is therefore unlikely to lead to gene silencing. Instead, we tested three different gapmer:peptide ratios (2:1, 1:1, 1:2). This way we screen a range of conditions that involve either excess gapmer, excess peptide or equimolar concentrations of gapmer and peptide. Thus, the initial *ftsZ* gene silencing experiment consisted of mixing the gapmers with the $(KFF)_3K$ peptide at the desired ratio and final concentration. *E. coli* strains at 10^5 cfu/mL were subsequently added to the pre-mixed gapmer/peptide solution and the bacterial growth was monitored for 800 min using the FC-accuSkan plate reader. The obtained growth curves are given in **Figure 44** - **Figure 46**.

In the case of 1.5 µM peptide as the oligonucleotide delivery vehicle for AS19 cells, none of the gamer/peptide mixtures caused observable inhibition of bacterial growth (see **Figure 44**). On the other hand, in the case of 3 µM peptide as the oligonucleotide delivery vehicle for AS19 cells, we observed the opposed trend from what was expected. The addition of 3 µM peptide alone resulted in a small delay in bacterial growth without completely killing the bacteria, as discussed above. When both peptide and gapmer were added to AS19 *E.coli*, this delay was no longer observed and the growth curves became comparable to the growth curve of AS19 alone (without the addition of peptide or gapmer) (see **Figure 45**). Similar results were seen for the measurements in wild type *E.coli* (ATCC 25922) (see **Figure 46**). If the gapmer/peptide mixture induced *ftsZ* gene silencing, a longer delay in bacterial growth would be expected, or even complete killing of the bacterial culture. The fact that a reduction in the toxicity of the peptide is seen instead, is probably due to the coulombic interaction between the negatively charged gapmers and the positively charged peptide. As the positive charge is essential for the function of cell penetrating peptides, this interaction likely reduces the effectiveness of the $(KFF)_3K$ peptide as a delivery vehicle. As a result, none of the tested gapmer/peptide combinations led to the desired delay in bacterial growth due to silencing of the *ftsZ* gene. The reduction in peptide toxicity was most pronounced for a gapmer:peptide ratio of 2:1, and could also be observed at 1:1 ratios (but

not for 1:2 gapmer:peptide ratios). This would be expected for the proposed mechanism of charge-charge interactions between the gapmer and peptide. At lower gapmer concentrations the shielding of the positive charges of the peptide is less efficient and the peptide can therefore still cause a delay in bacterial growth at the lowest gapmer:peptide ratio.

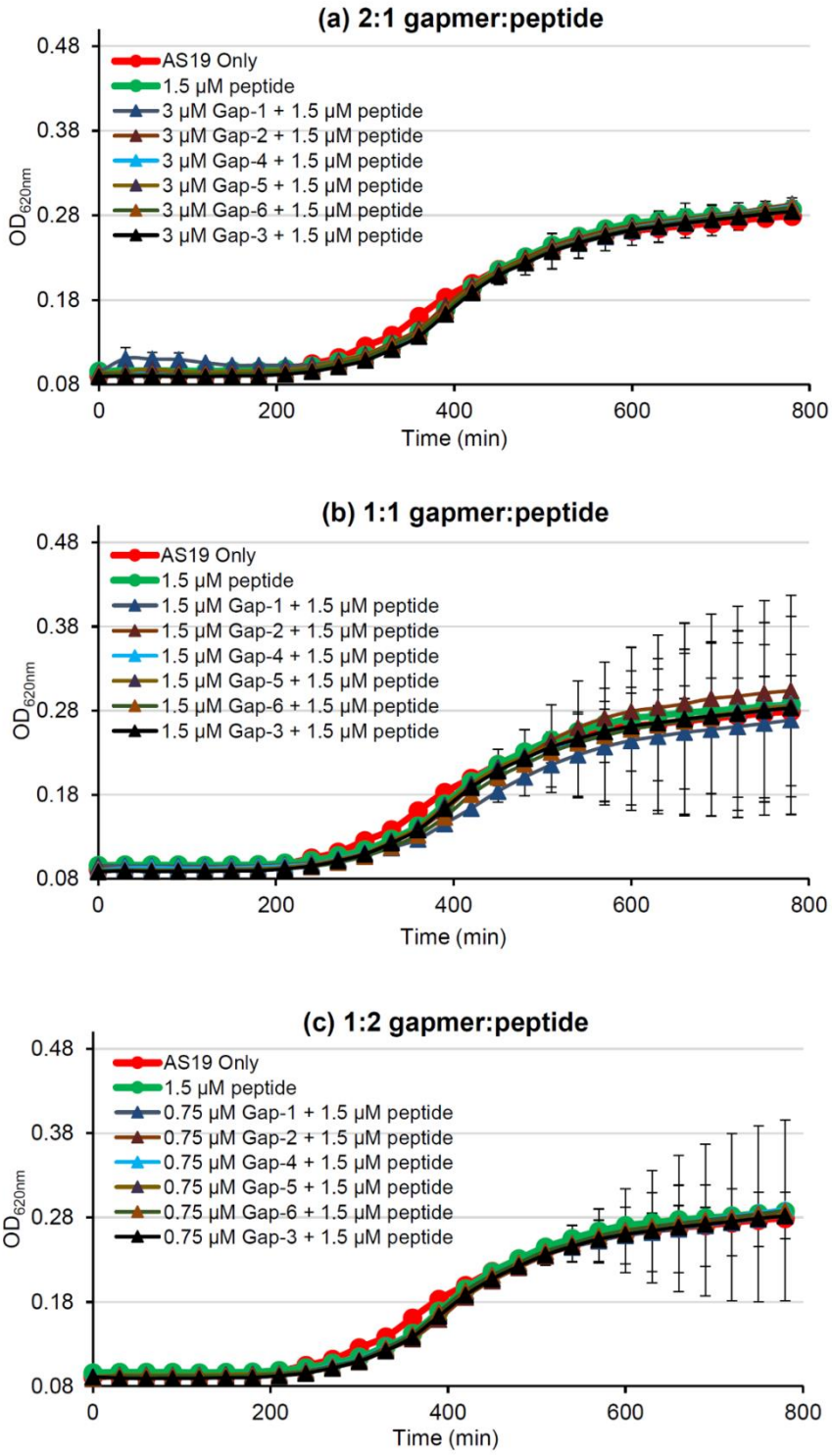

Figure 44. Attempted growth arrest by *ftsZ* gene inhibition by the DNA-LNA gapmers delivered by 1.5 µM $(KFF)_3K$ peptide to *E. coli* AS19. *E.coli* strain AS19 at 10^5 cfu/mL was added to a pre-mixed solution of the gapmer and the peptide, and the OD_{620nm} value was measured for 800 min at 37°C. The results are the average of at least 1 biological and 2 technical repeats, with error bars representing standard deviations.

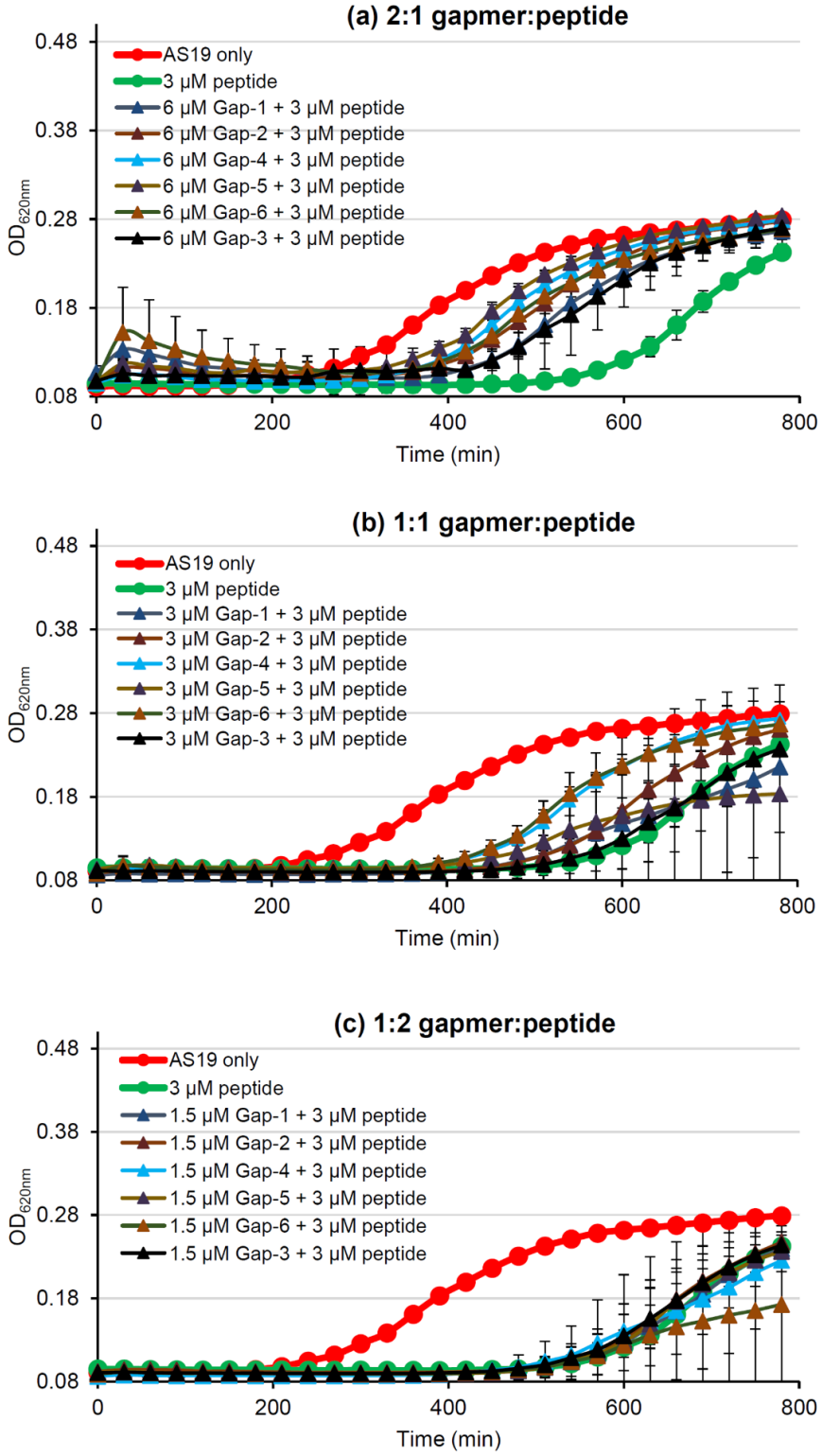

Figure 45. Attempted growth arrest by *ftsZ* gene inhibition by the DNA-LNA gapmers delivered by 3 μM $(KFF)_3K$ peptide to *E. coli* AS19. *E.coli* strain AS19 at 10^5 cfu/mL was added to a pre-mixed solution of the gapmer and the peptide, and the OD_{620nm} value was measured for 800 min at 37°C. The results are the average of at least 1 biological and 2 technical repeats, with error bars representing standard deviations.

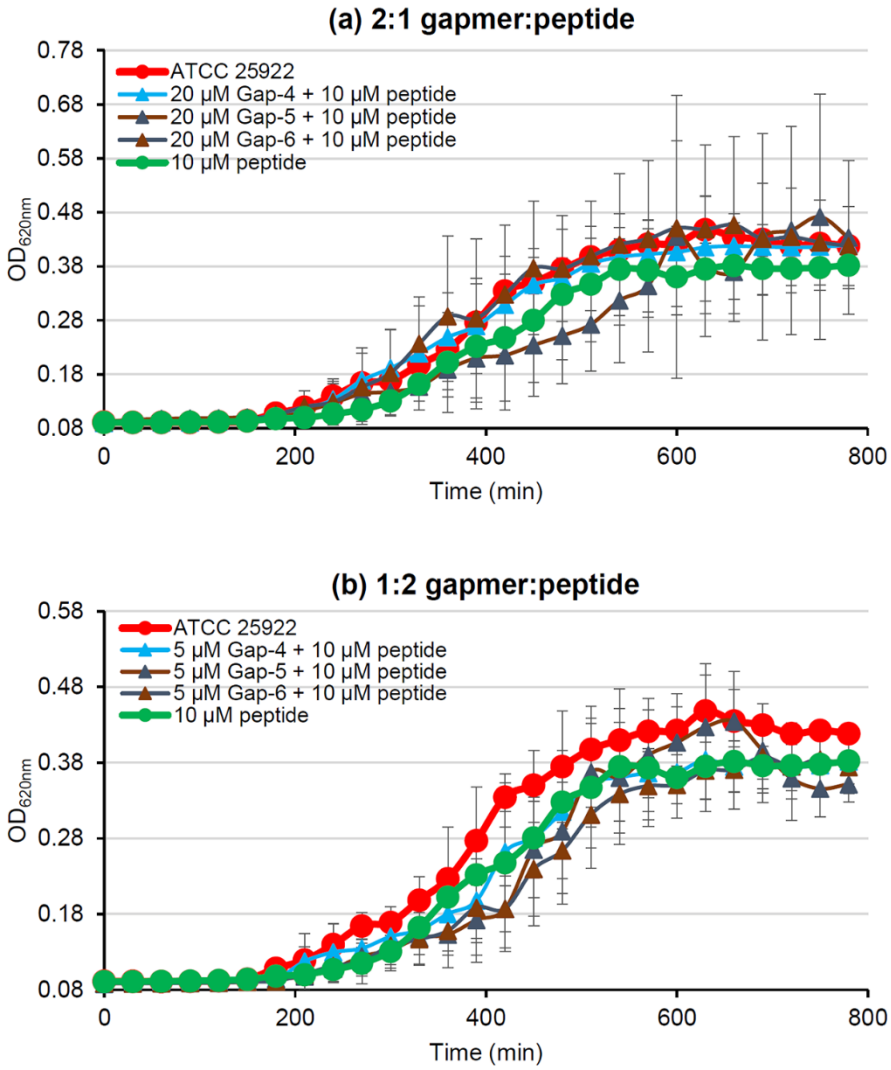

Figure 46. Attempted growth arrest by *ftsZ* gene inhibition by the DNA-LNA gapmers delivered by 10 µM $(KFF)_3K$ peptide to *E.coli* ATCC25922. *E. coli* strain ATCC25922 at 10^5 cfu/mL was added to a pre-mixed solution of the gapmer and the peptide, and the OD_{620nm} value was measured for 800 min at 37°C. The results are the average of at least 1 biological and 2 technical repeats, with error bars representing standard deviations.

Because the coulombic interaction between the gapmers and the cell penetrating peptide was problematic when they were mixed together, we assumed that this would form an even larger problem when the oligonucleotide and peptide would be covalently attached. We therefore decided not to pursue this avenue, and instead wanted to see if some of the LNA-DNA-LNA gapmers can be taken up by *E. coli* cells without the aid of the $(KFF)_3K$ peptide. To increase the chance of a positive result, the gapmers where tested at high concentration. Thus, *E. coli* strains at 10^5 cfu/mL were added to a gapmer solution to achieve a final concentration of 100 µM ASO, and the bacterial growth was monitored for 800 min using the FC-accuSkan plate reader. The results are shown in **Figure 47**. Even this high concentration of oligonucleotides did not show an obvious delay in bacterial growth. However, we noticed that the growth curves of *E. coli* AS19 became

very erratic in the presence of the gapmers. A second biological repeat was thus conducted for this experiment, and similarly noisy curves were obtained (see Appendix B).

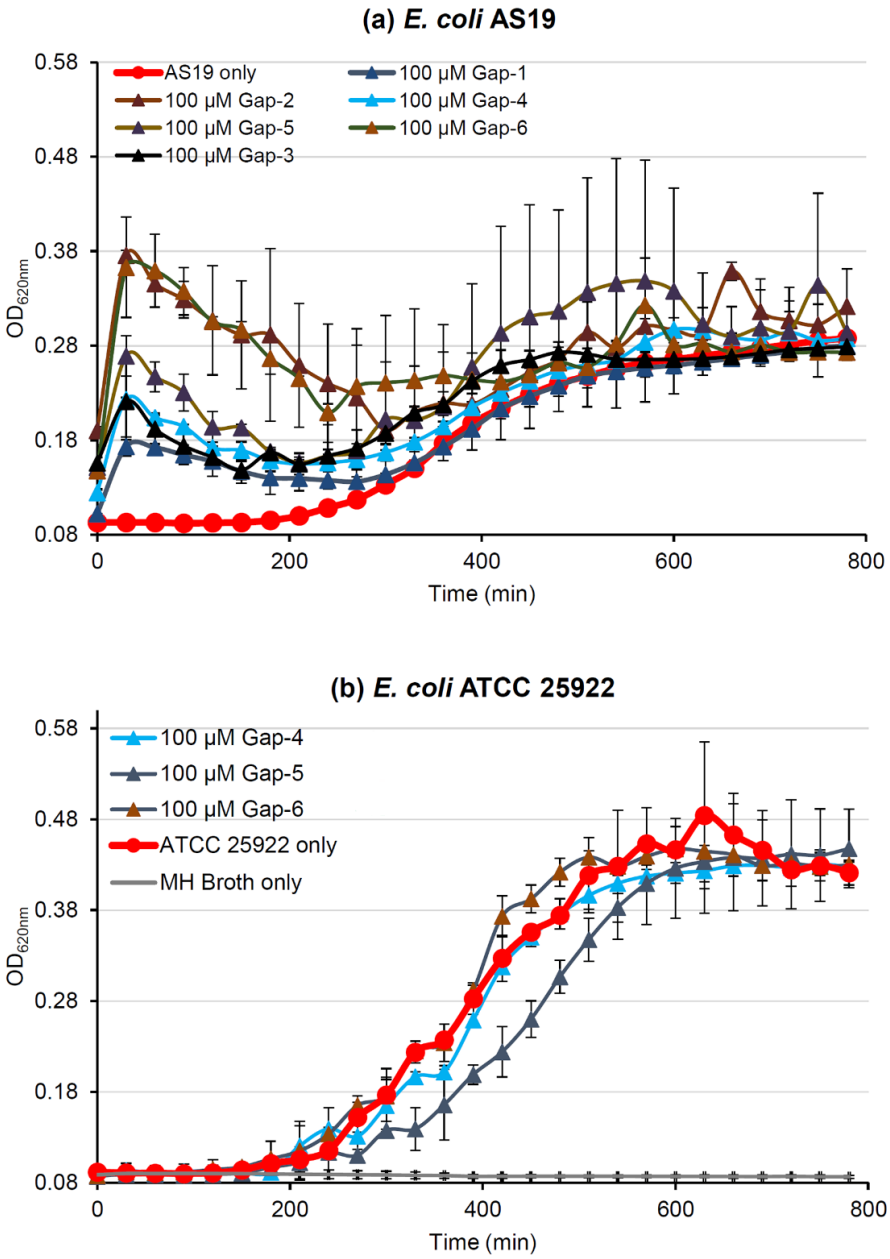

Figure 47. Potential silencing of *ftsZ* by high concentrations of LNA-DNA-LNA gapmers in (a) *E. coli* AS19, and (b) wild type *E. coli* ATCC 25922. The *E. coli* strains at 10^5 cfu/mL were added to the gapmer (final concentration 100 µM), and the OD_{620nm} value was measured for 800 min at 37°C. The results are the average of at least 1 biological and 2 technical repeats, with error bars representing standard deviations.

We speculated that this might be the result of successful silencing of the *ftsZ* gene by the ASOs. Indeed, when the activity of the *ftsZ* gene is blocked, extremely elongated bacterial cells are observed (see also Chapter 2). While this inhibition normally also results in lower OD_{620} as previously discused, it is possible that these elongated cells result in significant scattering of light,

and thus could lead to the noisy growth curves observed for *E. coli* AS19 (**Figure 47a**). To test this hypothesis, we wanted to see if we could detect the elongated cells more directly using microscopy.

3.2.3.2 Microscopy studies for the detection of *ftsZ* silencing

The optical density measurements hinted at possible *ftsZ* silencing by high concentrations of gapmer, but the indirect measurement of ftsZ silencing using OD620 might be unsuitable if highly elongated cells are causing significant scattering. Thus, we tried to detect *fts*Z gene silencing more directly by looking for the indicative elongation phenotype using microscopy techniques. Gapmers were added to 100 µL of *E. coli* AS19 cultures at 10^5 cfu/mL to achieve a final concentration of 100 µM. The mixture was subsequently incubated at 37 °C whilst shaking. At various time points, 10 µL of the bacterial culture was transferred onto an adhesive microscope slide, flame-dried and rinsed carefully with 100 µL sterile ultra-pure water. After drying, the samples were visualized in brightfield mode on a Leica DMi8 inverted microscope with 20x and 40x objectives. The contrast of the images was digitally enhanced using *ImageJ*.[290] Full experimental details are given in Chapter 6.

We started by determining the optimal incubation time for phenotype detection. Brightfield microscopy images were taken after 200 min, 400 min and 600 min incubation times; which corresponds to the beginning, the middle and end of the log phase of *E. coli* AS19 (see for example the growth curve of AS19 alone in **Figure 47**). This experiment was performed with Gap-2 only, because other classes of oligonucleotides complementary to the Gap-2 binding site had previously been shown to be active at silencing ftsZ.[248] As a control, we used *E. coli* AS19 in the absence of gapmer (termed "Blank"). The results are given in **Figure 48** (using a 20x objective; additional images obtained using a 40x objective are shown in Appendix B). The elongation phenotype can be easily detected after 200 min incubation of *E. coli* AS19 with Gap-2, and is a clear indication of successful *ftsZ* silencing through the recruitment of RNase H (**Figure 48**). While the typical elongated bacterial cells are still detectable after 400 min incubation, an increase of the healthy population without the elongation phenotype is also observed (**Figure 48**). After 600 min incubation time, it became challenging to detect any elongated cells among the overwhelming healthy population (**Figure 48**).

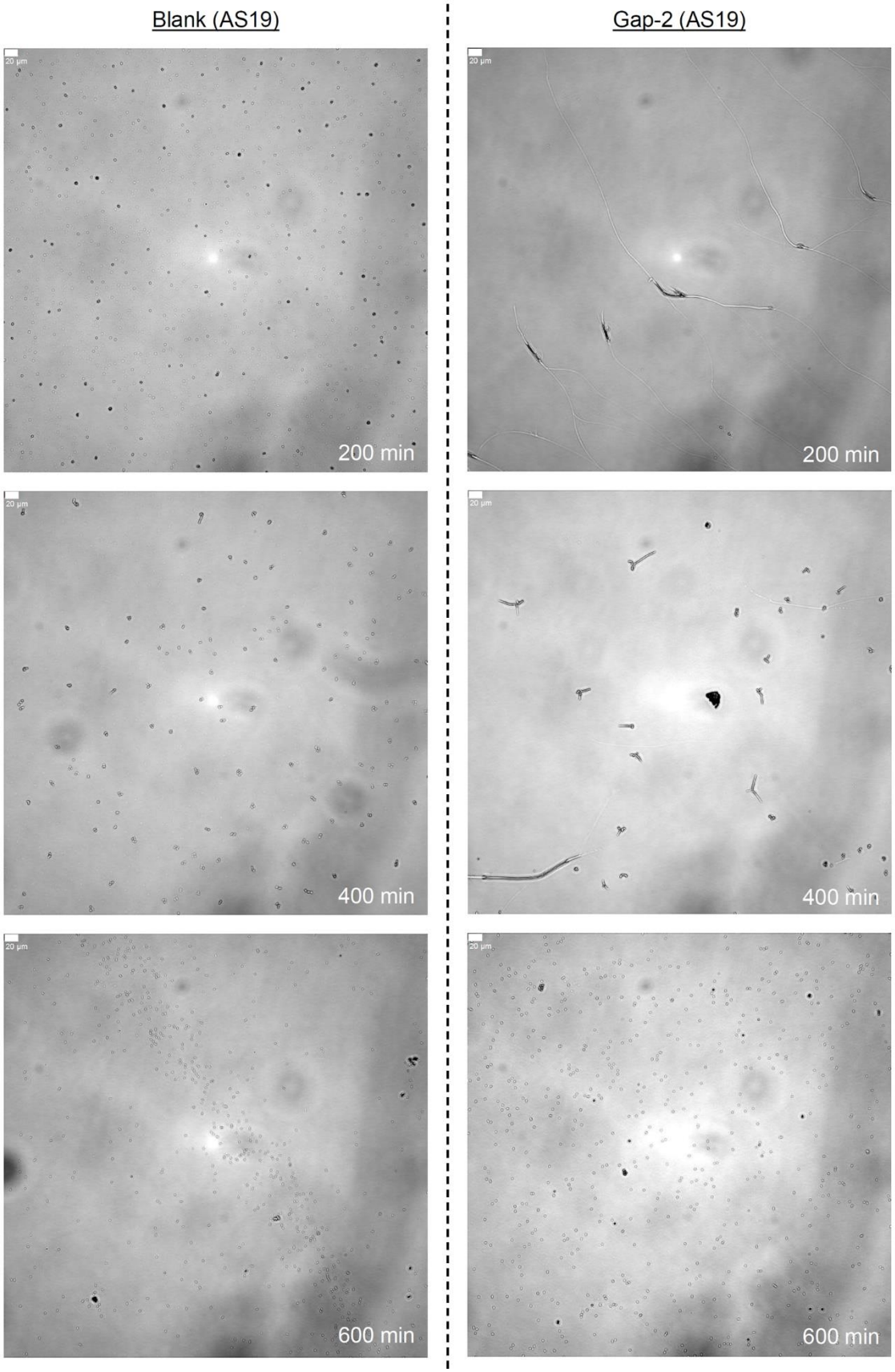

Figure 48. Brightfield images (20x objective) of *E. coli* AS19 incubated for 200 min, 400 min and 600 min at 37 °C in the absence or presence of 100 µM Gap-2. The experiment was performed as described in the main text. The scale bar represents 20 µm. The images on the left are obtained for *E. coli* AS19 without gapmer (blank), and the images on the left are obtained for *E. coli* AS19 incubated with 100 µM Gap-2.

These observations provide a better understanding of the optical density measurements. After short incubation times (200 min), the cfu/mL is low because the bacteria are still in the lag phase and the presence of elongated cells is not expected to cause major changes in the optical density values (except for possible erratic spikes due to scattering). After longer incubation times that normally correspond to the log phase (400 min or more), the healthy population will have continued to grow, resulting in an increase in OD_{620nm}. We therefore think that not all bacterial cells in the culture have successfully taken up the gapmer. In those cells that were affected by the ASO, the *ftsZ* gene is successfully silenced (as seen from the elongation phenotype), and they will not divide anymore (another consequence of *ftsZ* silencing). However, those cells that were not affected, continue to grow throughout the experiment and eventually make up most of the sample. This is why only healthy cells are seen in the microscopy studies after 600 min incubation, and why the bacterial growth curve looks like that of untreated *E. coli* AS19.

While the initial experiment suggests that there are still problems with the efficient uptake of the gapmers into the bacterial cells, it did show that silencing of the *ftsZ* gene can readily be detected at 200 min incubation time. We therefore studied all six gapmers synthesized in this chapter using the microscopy assay discussed above. Extremely elongated *E. coli* cells are observed for all tested gapmers (see **Figure 49**, and Appendix B for images obtained using a 40x objective). The elongation phenotype is the dominant phenotype in the case of Gap-2, Gap-3, Gap-5 and Gap-6; while a larger number of healthy bacteria are seen for Gap-1 and Gap-4. However, microscopy techniques only provide qualitative assessments of the gene silencing ability of ASOs and we can therefore not determine which gapmer preforms better than the other gapmers. Nevertheless, the observation of the elongation phenotype is proof that the LNA-DNA-LNA gapmers designed in this chapter are able to induce silencing of the *ftsZ* gene in *E. coli* AS19 cells. Because these gapmers do not target the ribosome binding site, silencing is most likely a consequence of the recruitment of RNase H.

3.3 Conclusions

In this chapter we successfully designed and synthesized six LNA-DNA-LNA gapmers against the *ftsZ* gene in *E. coli*. Initial *in vitro* studies showed effective recruitment of RNase H by all investigated gapmers. We tried to observe *ftsZ* gene silencing in bacteria by measuring optical density but encountered a number of problems. First, a cell penetrating peptide (KFFKFFKFFK) was manually prepared to facilitate uptake of the gapmers into the bacterial cells. However, the strong coulombic interaction between the negatively charged gapmers and the positively charged

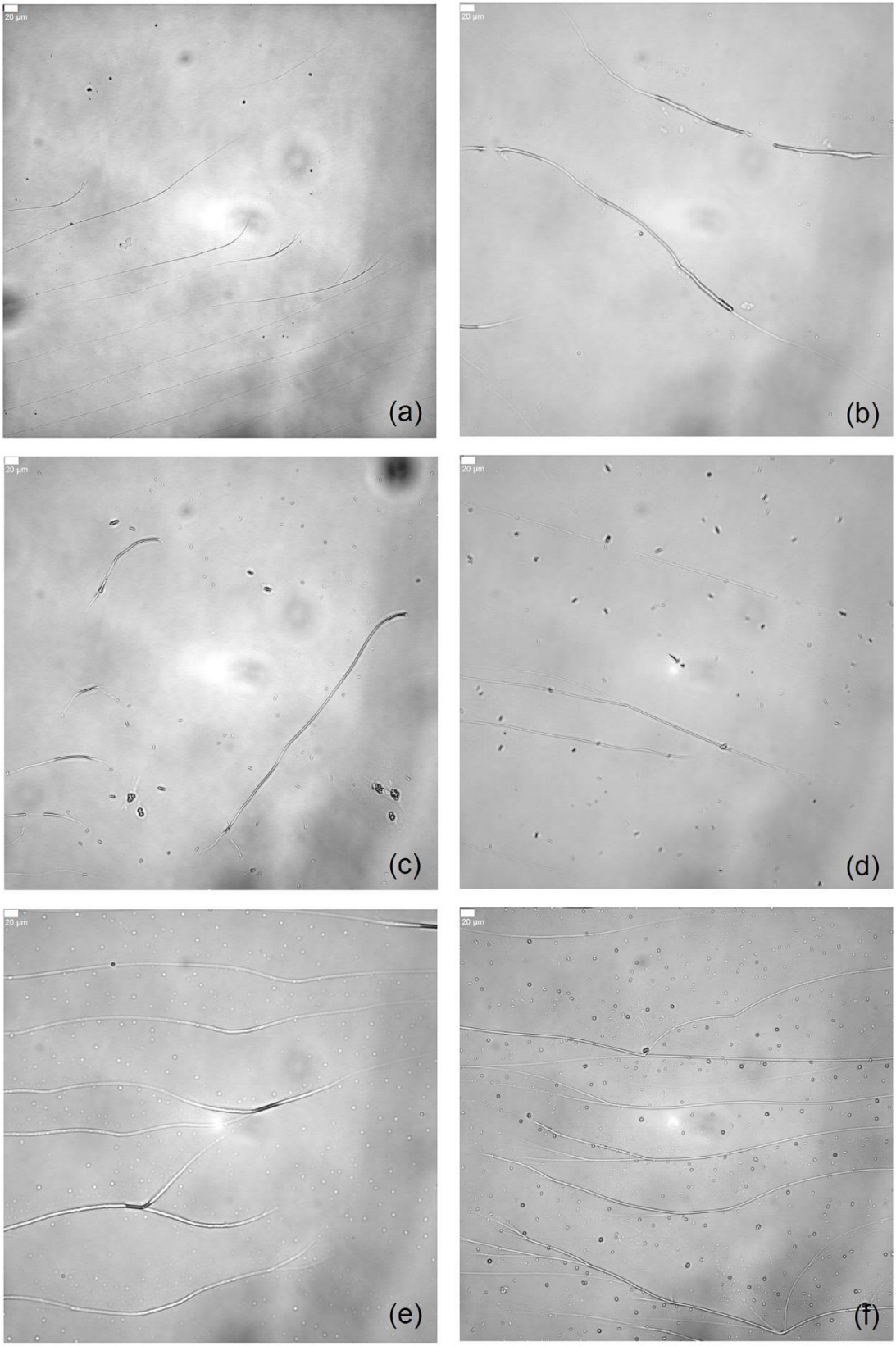

Figure 49. Brightfield images (20x objective) of *E. coli* AS19 incubated for 200 min at 37 °C in the presence of 100 µM gapmers. The experiment was performed as described in the main text. The scale bar represents 20 µm. (a) Gap-1; (b) Gap-2; (c) Gap-3; (d) Gap-4; (e) Gap-5; and (f) Gap-6.

peptide rendered this approach ineffective. Instead, we wanted to see if high concentrations of the ASOs could lead to silencing of the *ftsZ* gene, but the growth curves obtained through optical density measurements were too erratic for interpretation. On the other hand, microscopy studies revealed the presence of elongated cells after 200 min incubation with any of the gapmers. This elongation phenotype is proof of successful silencing of the *ftsZ* gene by the ASOs, presumably through the recruitment of RNase H. However, when the incubation time was prolonged to 400 or 600 min, the elongated cells were overwhelmed by a large number of healthy bacterial cells. These observations teach us that: (1) not all *E. coli* cells were able to take up the gapmer and therefore continued to grow, and (2) optical density measurements are not suitable to detect effective *ftsZ* silencing in *E. coli.*

While we were able to show that the LNA-DNA-LNA gapmers can recruit RNase H and silence the *ftsZ* gene in *E. coli* cells, there remains future work to be done. The successful experiments were performed on AS19 cells, which are more permeable than wild type *E. coli* cells, and even in this case there is evidence for insufficient uptake of the ASOs into the bacteria. It might therefore be instructive to try various delivery methods (e.g. liposomes, and cationic polymers) to increase the effectiveness of the gapmers. In addition, *ftsZ* silencing could only be detected using microscopy studies. In order to obtain quantitative data about the efficiency of gene silencing by RNase H recruiting gapmers in bacteria, we are in the process of measuring *ftsZ* mRNA levels directly and quantitatively by RT-qPCR. Alternatively, future studies could target different genes for which optical density measurements might correlate more directly with gene silencing (e.g. targeting *aac(6')-Ib,* which encodes amikacin resistance, or *katG,* which enhances hydrogen peroxide resistance (Chapter 2)).

Finally, the fact that a strong phenotype appears at 200 min incubation but that healthy cells take over the culture at longer timepoints suggests the existence of an escape mechanism which would need to be addressed before these approaches could be useful for antibiotic approaches. Further studies should address the nature of this escape mechanism.

Chapter 4 Optimizing oligonucleotides for dual recruitment of RNase P and RNase H

4.1 Introduction and aim

In Chapter 2 we tried to enhance the gene silencing ability of antisense oligo-nucleotides by recruiting RNase P using the External Guide Sequence (EGS) technology. For this purpose, we used the chemically modified oligonucleotide PNA, which has been used extensively in gene silencing in bacteria (see Chapter 1).[197] Unfortunately, our *in vitro* studies with purified RNase P showed that the PNA backbone cannot be recognized by this enzyme. In Chapter 3, we thus decided to try to recruit a different enzyme, namely RNase H, using DNA-LNA gapmers. In this case, the *in vitro* assays with purified RNase H did show that our gapmers are able to recruit the enzyme to cleave the target mRNA. We were also able to show that these gapmers have gene silencing ability in bacteria. This is not surprising, as it is well established which types of chemical modifications are tolerated by RNase H and which positions of the antisense oligonucleotide can be replaced by chemically modified nucleotides (see also Chapter 3 introduction).[281] This is not the case for RNase P, for which few chemically modified oligonucleotides have been investigated (see Chapter 2: introduction). Moreover, for many applications of oligonucleotide technologies, partial modification is not enough to provide suitable stability for therapeutic use – rather, modification of every nucleotide is required.[291] The aim of this chapter is therefore threefold:

- Aim 1: Determine which types of chemical modifications are tolerated by RNase P, as well as which positions of the antisense EGS-sequence are amenable to modifications.
- Aim 2: Develop oligonucleotides that are able to recruit both RNase P and RNase H to cleave the target mRNA (dual recruitment).
- Aim 3: Determine if the chemically modified EGS oligonucleotides (including dual recruiters), which are expected to have higher stability than DNA or RNA, also display potent antibacterial activity.

4.2 Results and discussion

4.2.1 *In vitro* recruitment of RNase P

4.2.1.1 Library 1: chimeras of RNA and one type of chemical modification

As was the case in Chapters 2 and 3, we decided to target the *ftsZ* gene in *E. coli* because it is an essential gene for this type of bacteria. Silencing of this gene can therefore easily be observed through either inhibition of bacterial growth or observation of the elongation phenotype.[292, 293] In Chapter 2 we found that the optimal region to target was ftsZ1032 (this region was shifted 9 nucleotides towards the 5' end compared to the *ftsZ* target region reported by Tolmasky and co-workers)[248]. The successful *in vitro* studies with RNase P in Chapter 2 were performed using an RNA oligonucleotide named RNA-ftsZ1041-EGS3, which corresponds to the sequence CUCAUCCAGACGCUCCA. In this chapter we modified various parts of the optimal recruiter sequence to explore the impact of these modifications on recruiting the RNase P active component M1 RNA. Initially (Library 1), we maintained the RNA chemistry and PO backbone and only introduced one modification at a time to one region. The chemical modifications include DNA (Set 1), OMe (Set 2), MOE (Set 3), 2'-F (Set 4), LNA (Set 5) and PS (Set 6) (see Chapter 1 for the structures of these modifications). The regions where these modifications were introduced into the oligonucleotide are illustrated in **Figure 50**.

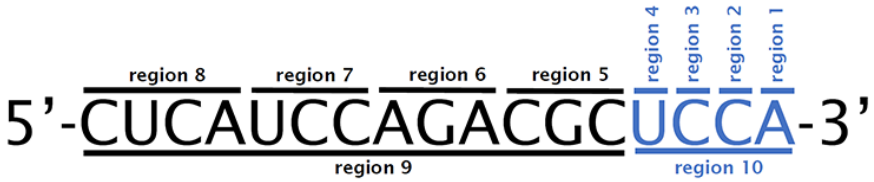

Figure 50. Schematic overview of the regions of the antisense oligonucelotide that are systematically replaced with chemically modified nucleotides (DNA, OMe, MOE, 2'-F, LNA or PS). The EGS tail is shown in blue, while the main body of the antisense oligonucleotide is shown in black. For library 1, the number of the modified region corresponds to the sequence number.

In these designs, we investigated both modifications in the EGS tail and in the main body of the oligonucleotide. Because the EGS tail is essential for the recruitment of RNase P, we presumed that the tail would be more sensitive towards chemical modifications than the main body. Thus, each nucleotide of the tail was modified individually (sequences 1-4). An analogue where the entire tail was modified was also investigated (sequence 10). The body of the antisense oligonucleotide was divided into four regions for which tolerance towards chemical modification

was explored. Sequence 8 contains four modified nucleotides, while sequences 7, 6 and 5 contain three modified nucleotides from the 5' end respectively. In addition, complete modification of the body was investigated (sequence 9).

The oligonucleotides explored in this library are listed in the table below (**Table 15**). The various oligonucleotides are all named L#S#S#, which refers to the library number, set number and sequence number. All oligonucleotides in Library 1 were purchased from *ChemGenes* and used as provided by the supplier.

Table 15. Sequence and naming of the oligonucleotides of Library 1. Bold and underlined regions of the sequences represent the presence of the indicated modification, while the regions that are not bold nor underlined represent RNA.

#	Sequence	Modification					
		DNA[a]	OMe	MOE[a]	2'-F	LNA[a]	PS
seq1	*CUCAUCCAGACGCUCC**A***	L1S1S1	L1S2S1	L1S3S1	L1S4S1	L1S5S1	L1S6S1
seq2	*CUCAUCCAGACGCUC**C**A*	L1S1S2	L1S2S2	L1S3S2	L1S4S2	L1S5S2	L1S6S2
seq3	*CUCAUCCAGACGCU**C**CA*	L1S1S3	L1S2S3	L1S3S3	L1S4S3	L1S5S3	L1S6S3
seq4	*CUCAUCCAGACGC**U**CCA*	L1S1S4	L1S2S4	L1S3S4	L1S4S4	L1S5S4	L1S6S4
seq5	*CUCAUCCAGA**CGC**UCCA*	L1S1S5	L1S2S5	L1S3S5	L1S4S5	L1S5S5	L1S6S5
seq6	*CUCAUCC**AGA**CGCUCCA*	L1S1S6	L1S2S6	L1S3S6	L1S4S6	L1S5S6	L1S6S6
seq7	*CUCA**UCC**AGACGCUCCA*	L1S1S7	L1S2S7	L1S3S7	L1S4S7	L1S5S7	L1S6S7
seq8	***CUCA**UCCAGACGCUCCA*	L1S1S8	L1S2S8	L1S3S8	L1S4S8	L1S5S8	L1S6S8
seq9	***CUCAUCCAGACGC**UCCA*	L1S1S9	L1S2S9	-[b]	L1S4S9	-[b]	L1S6S9
seq10	*CUCAUCCAGACGC**UCCA***	L1S1S10	L1S2S10	L1S3S10	L1S4S10	L1S5S10	L1S6S10

[a] For DNA, MOE and LNA, uracil (U) residues are replaced by thymine (T). [b] Due to the high price of MOE and the known difficulties with oligonucleotides containing a high amount of LNA[294], these sequences were not synthesized.

To determine the ability of the chemically modified oligonucleotides to recruit RNase P, we performed the same *in vitro* assay optimized in Chapter 2 (see also Chapter 6 for experimental details). For this assay, we used only the catalytic M1 RNA part of RNase P, without the C5 protein. In order to visualize and quantify cleavage, a 40-nucleotide region of the targeted mRNA was synthesised and labelled with FAM at the 5' end (*ftsZ* mRNA (40nt)), as described in Chapter 2. Successful recruitment of RNase P would result in selective cleavage of this mRNA fragment, producing a 14-mer labelled with 6-fluorescein at its 5' end and an unlabelled 25-mer. The *in vitro* experiments were performed using 2 pmol target RNA (*ftsZ* mRNA (40nt)), 8.8 pmol recruiter EGS oligonucleotide and 8.8 pmol M1 RNA. After 1.5 h and 24 h a 15% denaturing urea polyacrylamide gel (urea PAGE) was run on the samples to determine the amount of target RNA cleavage at both time points. The gels were visualized using a Typhoon FLA 7000 biomolecular imager with FAM filter. For each gel, 17 nt and 40 nt FAM-labelled oligonucleotides were included as a guidance for

the position of the expected bands due to the cleaved product (15 nt) and the full-length RNA target (40 nt) respectively. In addition, every set included control experiments where the recruiter oligonucleotide was either an unmodified RNA strand without EGS tail (*RNA*, no cleavage expected), or an unmodified RNA strand with EGS tail (*RNA-EGS*, high cleavage rate expected). Each experiment was performed in triplicate. The results for one repeat after 1.5 h incubation are given in **Figure 51**. All other repeats and the 24 h incubation repeats can be found in Appendix C.

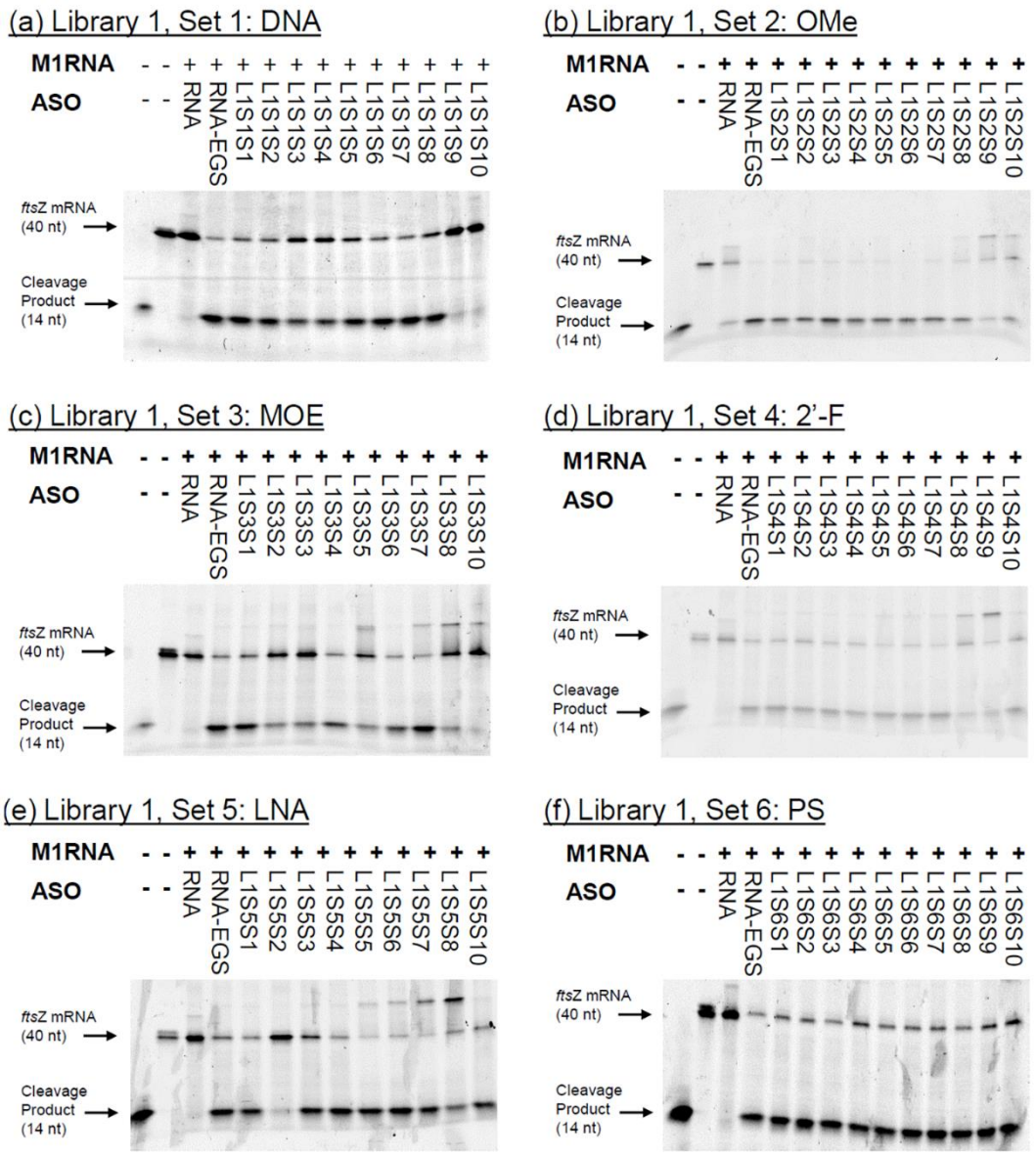

Figure 51. *In vitro* recruitment of RNase P by the oligonucleotides in Library 1, set 1 (a), set 2 (b), set 3 (c), set 4 (d), set 5 (e) and set 6 (f). A mixture of the FAM labelled target mRNA (2 pmol) and ASO (8.8 pmol) were preincubated at 37 °C for 15 min, followed by the addition of M1 RNA (8.8 pmol). The reaction was run at 37 °C for 1.5 h, and stopped by adding gel loading buffer. The samples were analysed by 15% urea PAGE, visualized using a Typhoon FLA 7000 biomolecular imager equipped with a FAM filter. The location and size of the initial target and the expected cleavage product are shown on the left. The first well contains a synthesised FAM-labelled 17-mer and the second well contains FAM-labelled target *ftsZ* mRNA (40nt) only; they are intended as a ladder.

The intensity of the bands corresponding to the cleaved product and the uncleaved target mRNA were determined by densitometry using *ImageJ*.[290] This allowed for the determination of the percent of target mRNA that was cleaved by M1 RNA after recruitment by the EGS antisense oligonucleotides. In some cases, such as LNA and MOE sequences, an additional third band was observed above the uncleaved target mRNA band (see **Figure 51**). This band was attributed to stable duplex formation between the (uncleaved) target mRNA with the antisense oligonucleotide. This band was counted as uncleaved target when calculating the percent cleavage:

$$\%\ cleavage = \frac{intensity\ cleaved\ product}{intensity\ (cleaved\ product + target\ mRNA + ASO\_mRNA\ complex)} \cdot 100\%$$

For reproducibility reasons (e.g., using different batches of M1 RNA), the data was further converted to relative cleavage compared to the unmodified RNA-EGS control that was run alongside each batch:

$$relative\ cleavage = \frac{\%\ cleavage\ by\ modified\ ASO}{\%\ cleavage\ by\ unmodified\ RNA - EGS}$$

The data was subsequently averaged for all 3 repeats at both time points (1.5 h and 24 h incubation of the target mRNA with the ASO and M1 RNA). The results of this data work-up is shown in **Figure 52**. A relative cleavage value > 1 indicates that the chemically modified RNA is better at recruiting M1 RNA than unmodified RNA, while a value close to 0 indicates that the modified ASO displays low RNase P recruiting activity. Most values are between 0 and 1, showing that the majority of the modified ASOs are able to recruit RNase P to some extent, but not as good as unmodified RNA. Furthermore, nearly all sequences induced complete cleavage of the target mRNA after 24 h (see **Figure 52b**), indicating that chemical modifications can be widely included in EGS technology. Note that the error bars in **Figure 52** are relatively small, suggesting that 'relative cleavage' is a reliable method to present the data.

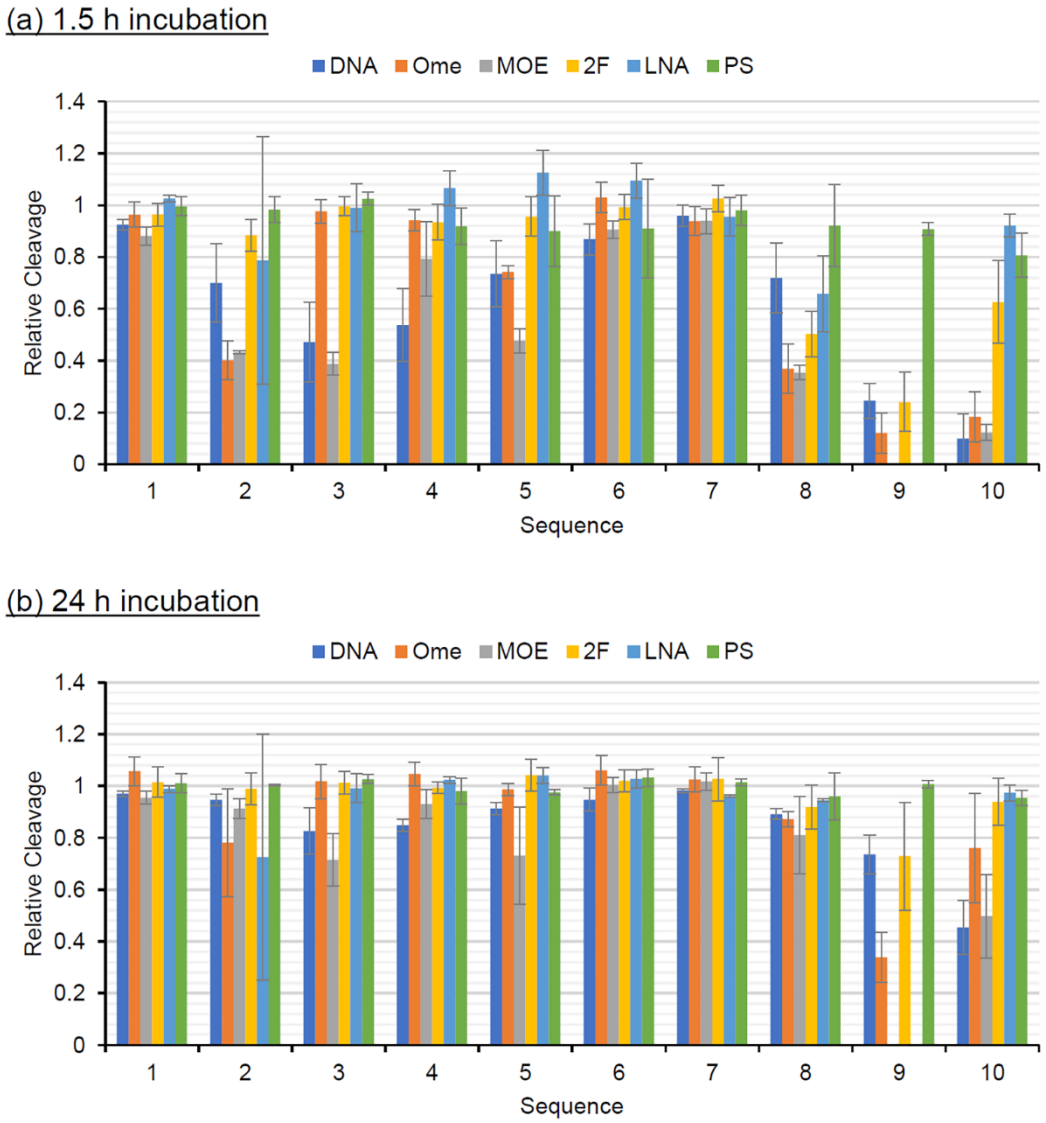

Figure 52. Relative cleavage of target mRNA by RNase P recruited by the oligonucleotides in Library 1, after 1.5 h incubation (a) or 24 h incubation (b). The values were calculated as described in the main text. Each value is the average of three independent repeats and the error bars represent standard deviations.

To facilitate interpretation of the data, we also plotted the relative cleavage values as a heat map in OriginPro 2017 (**Figure 53**). We only produced the heat map for 1.5 h incubation time, as this allows better differentiation between the various sequences and modifications (after 24 h most relative cleavage values were close to 1, see **Figure 52b**). Relative cleavage values of > 0.66 are shown in shades of green (high activity), values between 0.33 and 0.66 are shown in light green/amber (medium activity), and values < 0.33 are shown in shades of red (low activity).

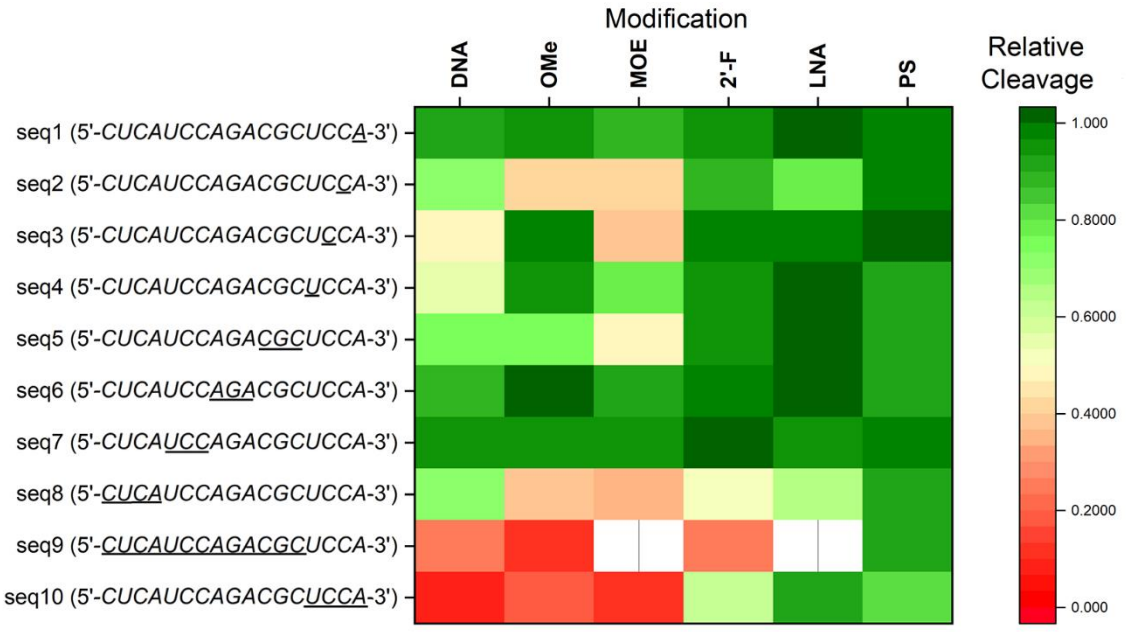

Figure 53. Heat map of the relative cleavage values for the *in vitro* recruitment of RNase P by the oligonucleotides in Library 1 after 1.5 h incubation. The values were calculated as described in the main text and are the average of three independent repeats.

There are a number of trends that can be easily concluded from the heat map shown in **Figure 53**. Firstly, the PS modification and LNA analogues are well tolerated across all positions in the antisense oligonucleotide. The 2'-F modification also appears well tolerated, except where the modification involves the 5' end (sequences 8 and 9). The other modifications follow the trend OMe > DNA > MOE, with the MOE modification being the worst.

It is also clear that changes in the nucleotides of the EGS tail are not equally tolerated. Chemical modifications of the first nucleotide from the 3' end (sequence 1) seem to be generally accepted by RNase P. The second nucleotide from the 3' end (sequence 2) is less tolerant towards modifications, with diminished activity seen for LNA, 2'-F and DNA, and no activity in the case of OMe and MOE. Similarly, the third nucleotide from the 3' end (sequence 3) also does not tolerate every modification – only OMe, 2'-F, and LNA have shown RNase P recruitment activity. The final position in the EGS tail (sequence 4), on the other hand, has shown great tolerance for all modifications except DNA. When the entire EGS tail was modified (sequence 10), efficient cleavage was only observed for LNA and 2'-F. This agrees with the data obtained for the modifications of the individual nucleotides of the tail: LNA and 2'-F were tolerated in every position, while OMe and MOE were not tolerated in position 2 and DNA was not tolerated in position 3.

Modifications in the body of the antisense oligonucleotide also have shown various degrees of RNase P recruitment. Not unexpectedly, the middle of the antisense region (sequences 6 and 7)

accepted all modifications tested. In contrast, the region closer to the EGS tail (sequence 5) was less tolerant towards chemical alterations. This region has a high activity for 2'-F and LNA, less activity for DNA and OMe, and minimal activity for MOE. The 5' end region (sequence 8) appeared to be the least tolerant region toward modifications, with diminished activity observed for DNA, LNA and 2'-F, and no activity seen for OMe and MOE. In agreement with this, when we applied the modifications DNA, OMe, 2'-F and PS to the full length body (sequence 9), only PS showed an acceptable activity. MOE and LNA modifications were not included in this study (sequence 9), due to the high price of MOE and the aggregative tendency of fully-modified LNA sequences.

Results from testing of this first library make it clear which types of modifications are tolerated in which positions of EGS oligonucleotides; this can provide guidance in developing the optimal EGS sequence. Since we only studied one modification in Library 1, it was logical to expand our study to combine two types of modifications in the sequences in Library 2.

4.2.1.2 Library 2: chimeras of two types of chemical modifications

In order to obtain EGS oligonucleotides with higher stability than the natural substrate RNA, we investigated the RNase P recruiting ability of fully modified oligonucleotides that contain two different types of chemical modifications (Library 2). The results from testing of Library 1 were used as a guide in the design of Library 2. As stated above, the 5' end of the EGS-ASOs was the least tolerant towards modifications, with significant RNase P activity only observed for LNA and DNA. Therefore, two types of chimera oligonucleotides were synthesized — oligos that contained LNA at the 5' end (sets 1-4) or olignucleotides that contained DNA at the 5' end (sets 5-8). In addition, Library 1 results indicated that the PS backbone is well tolerated by RNase P at any position in the sequence. All oligonucleotides in Library 2 were thus synthesized with a PS backbone, due to the better pharmacokinetic properties of PS backbones compared to PO backbones[295] (note: the PS backbone is not counted as one of the two modifications). The oligonucleotides in Library 2 were synthesised by Pranathi Meda.

4.2.1.2.1 Chimeras with LNA at the 5' end

The oligonucleotides in sets 1-4 were designed as gapmer-like designs, containing LNA at the 5' and 3' ends and another chemical modification in the middle – either OMe (set 1), MOE (set 2), 2'-F (set 3) or DNA (set 4). LNA was also used at the 3' end because it showed the highest RNase P

recruiting activity at this position in Library 1, and because we rationalised that the gapmer configuration would provide the best stability against exonucleases.[296]

We explored four types of gapmer configurations. The LNA region at the 5' end was either 4 or 7 nucleotides long, while the LNA region at the 3' end was either 1 or 2 nucleotides long. **Table 16** gives an overview of the oligonucleotides in sets 1-4. For the OMe modification, the uracil in region 4 was also replaced with an LNA residue (thymine), because LNA showed higher RNase P recruiting ability at this position. Similarly, from Library 1 it was clear that the MOE modification is not well tolerated just before the EGS-tail, and the cytosine residue before the tail was therefore replaced with an LNA residue (set 2). Because DNA performed better than LNA at the 5' end in Library 1, but was not well tolerated in some of the residues of the tail, set 4 was extended with sequences that contain only two LNA residues at the 5' end, one residue at the 3' end and various positions in the body and tail of the oligonucleotides (L2S4S5, L2S4S6 and L2S4S7).

Table 16. Sequence and naming of the oligonucleotides of Library 2, sets 1-4. Normal text represents LNA, bolded and italic regions represent OMe, bolded regions represent MOE, underlined regions represent 2'-F and bolded and underlined region represent DNA.

Name	Sequence
Library 2, Set 1: LNA/OMe chimeras, all PS	
L2S1S1	CTCA***UCCAGACGC***T***CC***A
L2S1S2	CTCA***UCCAGACGC***T***C***CA
L2S1S3	CTCATCC***AGACGC***T***CC***A
L2S1S4	CTCATCC***AGACGC***T***C***CA
Library 2, Set 2: LNA/MOE chimeras, all PS	
L2S2S1	CTCA**TCCAGACG**C**TCC**A
L2S2S2	CTCA**TCCAGACG**C**TC**CA
L2S2S3	CTCATCC**AGACG**C**TCC**A
L2S2S4	CTCATCC**AGACG**C**TC**CA
Library 2, Set 3: LNA/2'-F chimeras, all PS	
L2S3S1	CTCAUCCAGACGCUCCA
L2S3S2	CTCAUCCAGACGCUCCA
L2S3S3	CTCATCCAGACGCUCCA
L2S3S4	CTCATCCAGACGCUCCA
Library 2, Set 4: LNA/DNA chimeras, all PS	
L2S4S1	CTCA**TCCAGACGCTCC**A
L2S4S2	CTCA**TCCAGACGCTC**CA
L2S4S3	CTCATCC**AGACGCTCC**A
L2S4S4	CTCATCC**AGACGCTC**CA
L2S4S5	CT**CATCCAGAC**GCTC**C**A
L2S4S6	CT**CATCCAGACG**CTC**C**A
L2S4S7	CT**CAT**C**CAG**A**CG**CTC**C**A

All of the oligonucleotides in sets 1-4 of Library 2 were subjected to the same *in vitro* RNase P recruitment assay as described for Library 1, and the data was worked up as detailed above. The results are shown in **Figure 54** and **Figure 55** (the gels of the second 1.5 h repeat and 24 h repeats are given in Appendix C). None of the modified oligonucleotides in these sets yielded more than 33% relative cleavage compared to unmodified natural RNA. Instead, duplex formation between the EGSs and the target mRNA is seen (bands higher than the original mRNA target), even though the gels are run under denaturing conditions. It is possible that this strong duplex formation is the reason for the inability of the compounds in these sets to recruit RNase P. Therefore, the chimeras with LNA at the 5' end were not investigated any further.

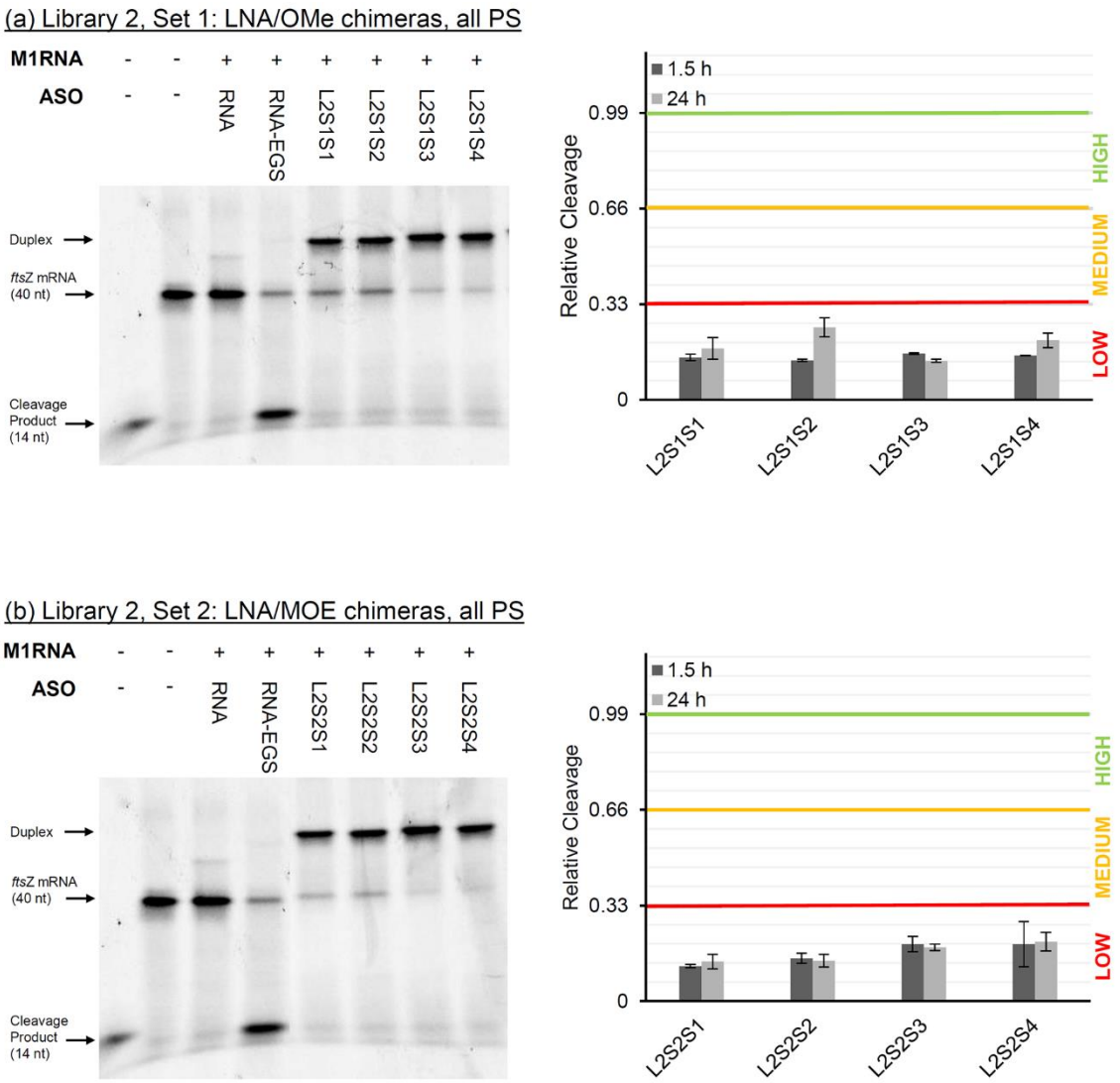

Figure 54. *In vitro* recruitment of RNase P by the oligonucleotides in Library 2, Set 1 (a) and Set 2 (b). A mixture of the FAM labelled target mRNA (2 pmol) and ASO (8.8 pmol) were preincubated at 25 °C for 15 min, followed by the addition of M1 RNA (8.8 pmol). The reaction was run at 37 °C for 1.5 and 24 h, and stopped by adding gel loading buffer. The samples were analysed by urea PAGE and visualized using a Typhoon FLA 7000 biomolecular imager. Gels obtained after 1.5 h incubation are shown on the left. The first well contains a FAM labelled 17-mer and the second well contains target mRNA only; they are intended as a ladder. The calculated relative cleavage (average of two repeats) is shown in the bar graphs on the right.

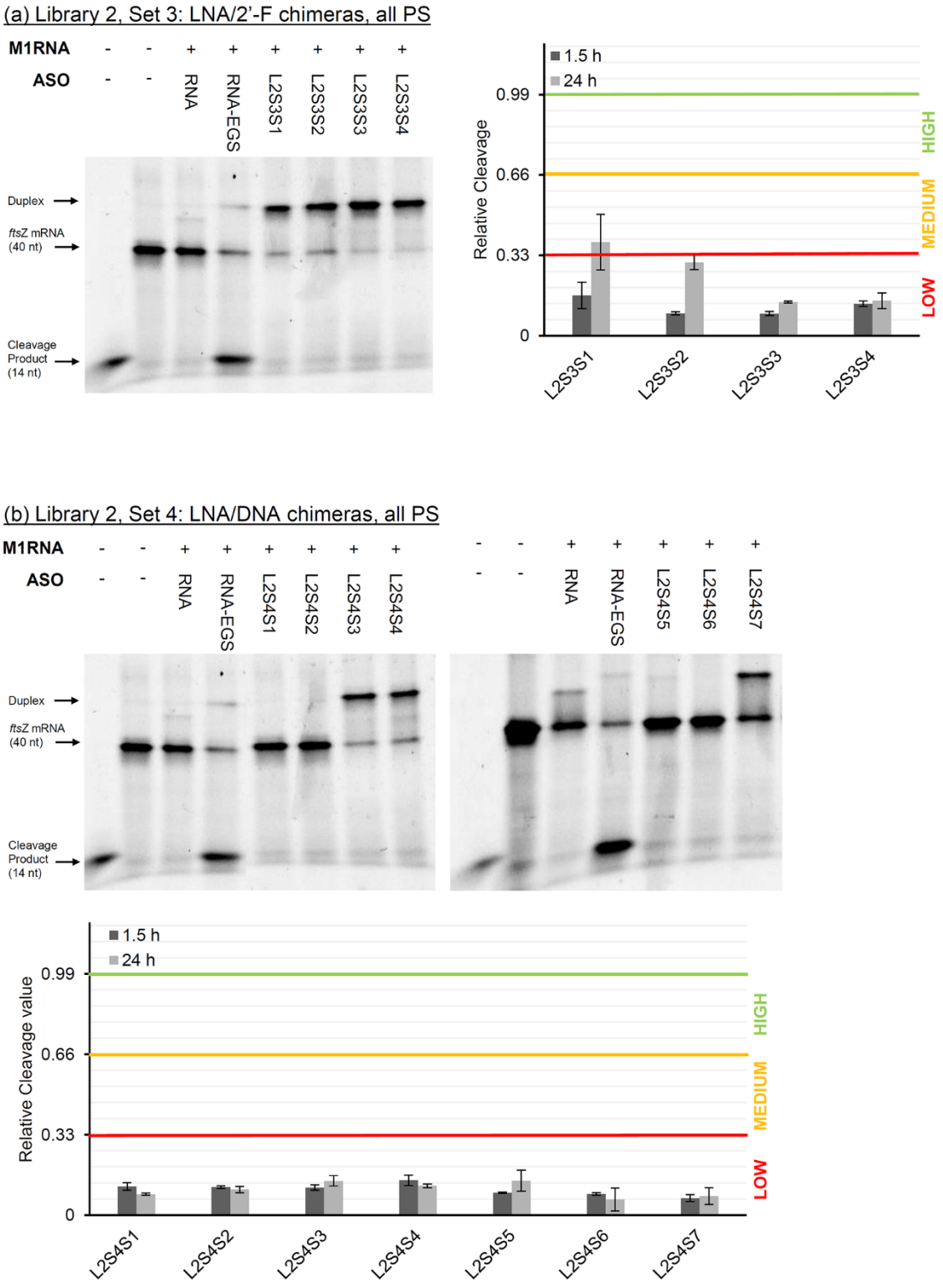

Figure 55. *In vitro* recruitment of RNase P by the oligonucleotides in Library 2, Set 3 (a) and Set 4 (b). A mixture of the FAM labelled target mRNA (2 pmol) and ASO (8.8 pmol) were preincubated at 25 °C for 15 min, followed by the addition of M1 RNA (8.8 pmol). The reaction was run at 37 °C for 1.5 and 24 h, and stopped by adding gel loading buffer. The samples were analysed by urea PAGE and visualized using a Typhoon FLA 7000 biomolecular imager. Gels obtained after 1.5 h incubation are shown on the left. The first well contains a FAM labelled 17-mer and the second well contains target mRNA only; they are intended as a ladder. The calculated relative cleavage (average of two repeats) is shown in the bar graphs on the right.

4.2.1.2.2 Chimeras with DNA at the 5' end

As mentioned earlier, for sets 5-8 the 5' end was chosen to be DNA because it is one of the few modifications tolerated at this position. The oligonucleotides in these sets were designed as chimeras with designs mirroring those of sets 1-4 discussed above. The oligonucleotides consisted of either 4 or 7 DNA residues at the 5' end and 1 or 2 DNA bases at the 3' end, with other chemical modifications in the middle – either OMe (set 5), MOE (set 6), 2'-F (set 7) or LNA (set 8). As was the case for the LNA/OMe and LNA/MOE chimeras, the DNA/OMe (set 5) and DNA/MOE (set 6) chimeras also contained an extra DNA residue in the tail or body of the oligonucleotide in order to increase the chance of high rates of RNase P mediated cleavage. An overview of the oligonucleotides in sets 5-8 is given in **Table 17**.

Table 17. Sequence and naming of the oligonucleotides of Library 2, sets 5-8. Bold and underlined regions of the sequences represent DNA, bolded and italic regions represent OMe, bolded regions represent MOE, underlined regions represent 2'-F and normal text represents LNA.

Name	Sequence
Library 2, Set 5: DNA/OMe chimeras, all PS	
L2S5S1	**CTCA*UCCAGACGCTCCA***
L2S5S2	**CTCA*UCCAGACGCTCCA***
L2S5S3	**CTCATCC*AGACGCTCCA***
L2S5S4	**CTCATCC*AGACGCTCCA***
Library 2, Set 6: DNA/MOE chimeras, all PS	
L2S6S1	**CTCATCCAGACGCTCCA**
L2S6S2	**CTCATCCAGACGCTCCA**
L2S6S3	**CTCATCCAGACGCTCCA**
L2S6S4	**CTCATCCAGACGCTCCA**
Library 2, Set 7: DNA/2'-F chimeras, all PS	
L2S7S1	**CTCA**UCCAGACGCUCC**A**
L2S7S2	**CTCA**UCCAGACGCUC**CA**
L2S7S3	**CTCATCC**AGACGCUCC**A**
L2S3S4	**CTCATCC**AGACGCUC**CA**
Library 2, Set 8: DNA/LNA chimeras, all PS	
L2S8S1	**CTCA**TCCAGACGCTCC**A**
L2S8S2	**CTCAT**CCAGACGCTC**CA**
L2S8S3	**CTCATCC**AGACGCTCC**A**
L2S8S4	**CTCATCC**AGACGCTC**CA**

The *in vitro* RNase P recruitment activity of the compounds in sets 5-8 were tested as described for Library 1. The results are shown in **Figure 56** and **Figure 57** (the gels of the second 1.5 h repeat and 24 h repeats are given in Appendix C). None of the DNA/OMe (set 5), DNA/MOE (set 6) or DNA/2'-F (set 7) chimeras induced significant cleavage or duplex formation and these chimeras were therefore not studied any further. However, two of the four DNA/LNA chimeras in set 8 did

show medium to high cleavage (L2S8S1 and L2S8S3, see **Figure 57b**). Both chimeras contain only one DNA residue at the 3' end, while the two inactive oligonucleotides in the same set (L2S8S2 and L2S8S4) contain two DNA residues at the 3' end. It is therefore clear that the optimal DNA/LNA chimera can only accommodate one DNA residue in the EGS tail, while the remainder of the tail should remain LNA. Due to these promising results, we decided to further optimize the structure of the DNA/LNA chimeras.

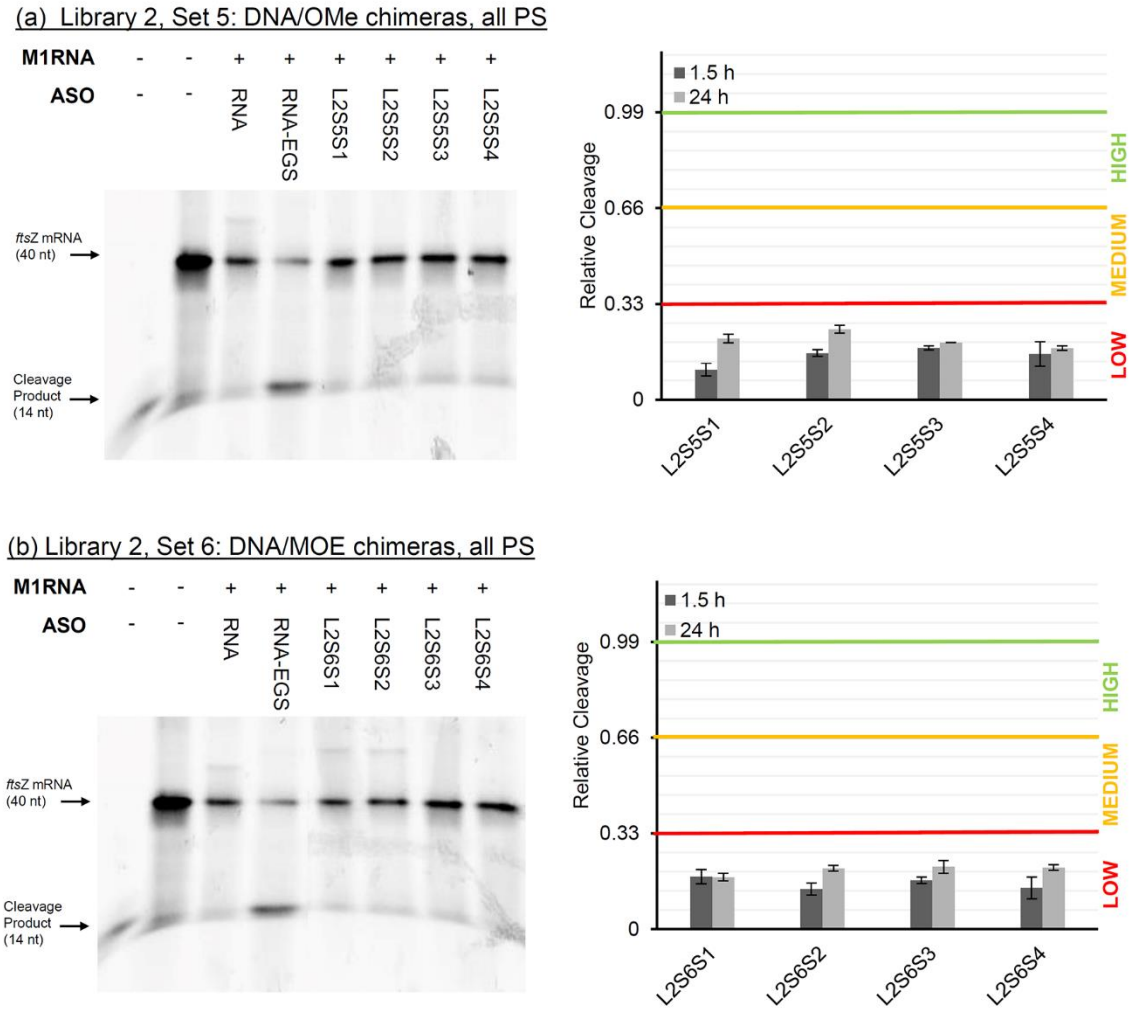

Figure 56. *In vitro* recruitment of RNase P by the oligonucleotides in Library 2, set 5 (a) and set 6 (b). A mixture of the FAM labelled target mRNA (2 pmol) and ASO (8.8 pmol) were preincubated at 25 °C for 15 min, followed by the addition of M1 RNA (8.8 pmol). The reaction was run at 37 °C for 1.5 h and 24 h, and stopped by adding gel loading buffer. The samples were analysed by urea PAGE and visualized using a Typhoon FLA 7000 biomolecular imager. Gels obtained after 1.5 h incubation are shown on the left. The first well contains a FAM labelled 17-mer and the second well contains target mRNA only; they are intended as a ladder. The calculated relative cleavage (average of two repeats) is shown in the bar graphs on the right.

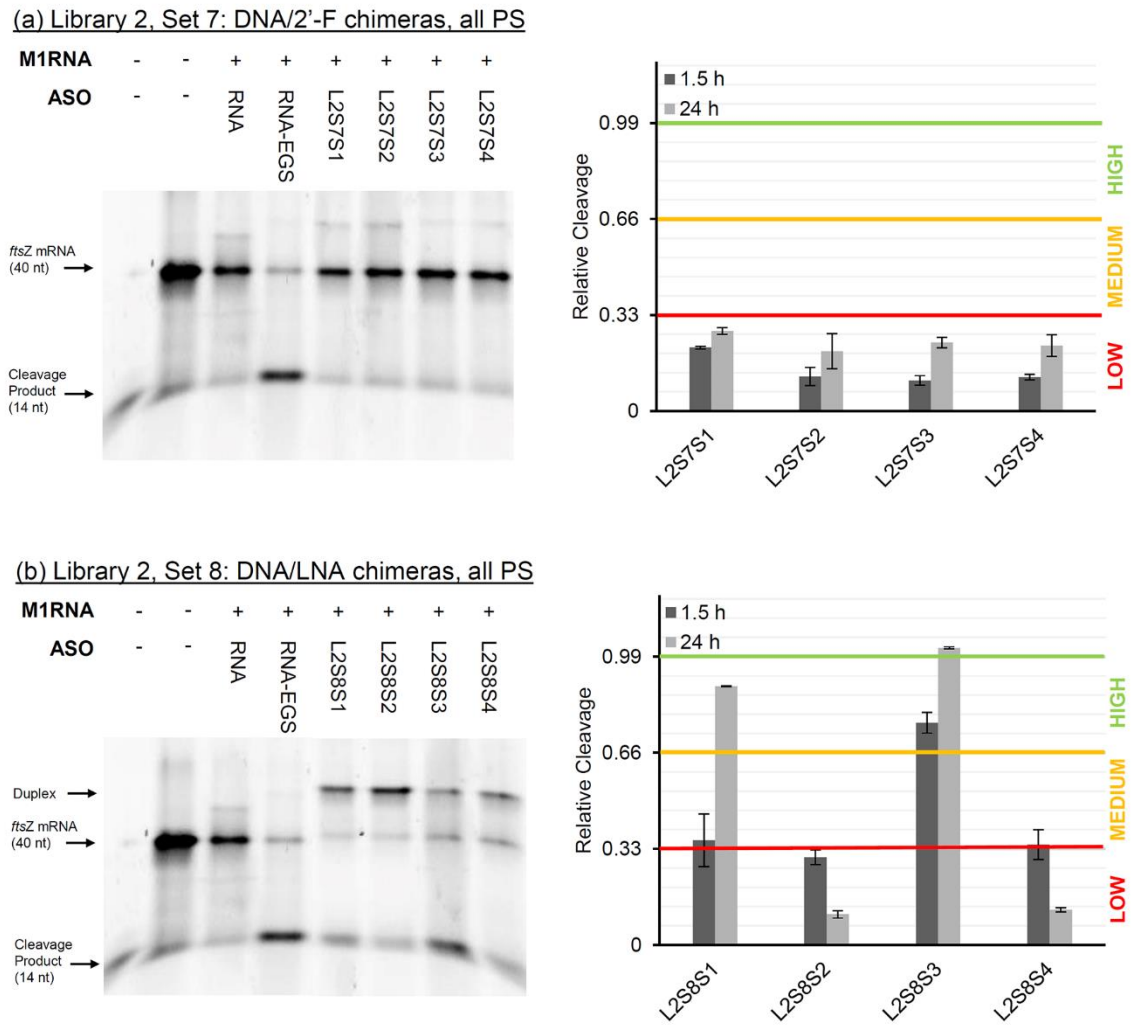

Figure 57. *In vitro* recruitment of RNase P by the oligonucleotides in Library 2, set 7 (a) and set 8 (b). A mixture of the FAM-labelled target RNA (2 pmol) and ASO (8.8 pmol) were preincubated at 25 °C for 15 min, followed by the addition of M1 RNA (8.8 pmol). The reaction was run at 37 °C for 1.5 and 24 h, and stopped by adding gel loading buffer. The samples were analysed by urea PAGE and visualized using a Typhoon FLA 7000 biomolecular imager. Gels obtained after 1.5 h incubation are shown on the left. The first well contains a FAM labelled 17-mer and the second well contains target RNA only; they are intended as a ladder. The calculated relative cleavage (average of two repeats) is shown in the bar graphs on the right.

4.2.1.2.3 Optimization of the DNA/LNA chimeras

From the previous set (set 8), it was clear that DNA/LNA chimeras with one DNA residue at the 3' end, and four or seven DNA residues at the 5' end induce cleavage of the target mRNA by RNase P. However, the oligonucleotide with seven DNA residues at the 5' end (L2S8S3) displayed significantly better RNase P recruiting activity than the one with four DNA residues (L2S8S1). A new set of DNA/LNA chimeras was therefore designed in order to determine the optimal length for the DNA stretch at the 5' end. In set 9 the DNA component at the 5' end was gradually increased from four to ten nucleotides. A sequence where the entire mRNA binding region (13 nucleotides) consists of DNA residues was also included. In addition, we wanted to see if the DNA

residue at the 3' end is necessary for optimal RNase P recruitment. Set 10 was therefore designed as an analogue to set 9, but replacing the 3' end residue from DNA to LNA. **Table 18** gives an overview of all sequences in Library 2 sets 9-10.

Table 18. Sequence and naming of the oligonucleotides of Library 2, sets 9-10. Bold and underlined regions of the sequences represent DNA, not bolded or underlined represents LNA.

Name	Sequence
Library 2, Set 9: DNA/LNA chimeras with 3'-DNA, all PS	
L2S8S1[a]	**CTCA**UCCAGACGCUCC**A**
L2S9S1	**CTCAT**CCAGACGCTCC**A**
L2S9S2	**CTCATC**CAGACGCTCC**A**
L2S8S3[a]	**CTCATCC**AGACGCUCC**A**
L2S9S3	**CTCATCCA**GACGCTCC**A**
L2S9S4	**CTCATCCAG**ACGCTCC**A**
L2S9S5	**CTCATCCAGA**CGCTCC**A**
L2S9S6	**CTCAUCCAGACGC**TCC**A**
Library 2, Set 10: DNA/LNA chimeras with 3'-LNA, all PS	
L2S10S1	**CTCA**TCCAGACGCTCCA
L2S10S2	**CTCAT**CCAGACGCTCCA
L2S10S3	**CTCATC**CAGACGCTCCA
L2S10S4	**CTCATCC**AGACGCTCCA
L2S10S5	**CTCATCCA**GACGCTCCA
L2S10S6	**CTCATCCAG**ACGCTCCA
L2S10S7	**CTCAUCCAGA**CGCTCCA
L2S10S8	**CTCAUCCAGACGC**TCCA

[a] These sequences were originally tested in Library 2, set 8.

The EGS-sequences in sets 9 and 10 were subjected to the *in vitro* RNase P recruitment assay described above, and the results are given in **Figure 58** and **Figure 59** (the gels of the second 1.5 h repeat and 24 h repeats are given in Appendix C). In general, the RNase P recruitment is higher for the compounds containing a 3'-DNA (set 9) than for the analogous compounds without the DNA residue at the 3' end (set 10). For both sets, the optimal length for the continuous DNA stretch at the 5' end appears to be 6, 7 or 8 residues long (L2S9S2, L2S8S3 and L2S9S3 for set 9; L2S10S3, L2S10S4 and L2S10S5 for set 10). Shorter or longer stretches of DNA result in lower relative cleavage values, as shown in **Figure 58** and **Figure 59**. These results can be easily rationalized. DNA is not the natural substrate for RNase P and when the DNA stretch becomes too long, the ribozyme can no longer be recruited by the ASO. On the other hand, LNA is more RNA-like and could thus potentially be recognized by RNase P. However, LNA is also known to significantly increase the stability of the duplex between target mRNA and antisense oligonucleotide.[297] This is also clear from the results presented here – the sequences with a short DNA stretch and long LNA stretch (e.g., L2S8S1, L2S9S1 and L2S9S2) show a band above the target mRNA band, indicative of

the formation of a strong duplex with the ASOs (**Figure 58** and **Figure 59**). As these sequences also have reduced RNase P recruiting activity, it appears that this strong binding induced by a high LNA content is detrimental for activity. Optimal RNase P recruitment is therefore achieved for the intermediate situation, with 6-8 DNA residues at the 5' end and the rest of the sequence LNA. These results corresponds with previous observations by Tolmasky and co-workers, who found that both the position and the amount of LNA residues in DNA/LNA chimeras affect their RNase P recruitment ability (although their EGS compounds had different conformations, and did not have the PS backbone).[298]

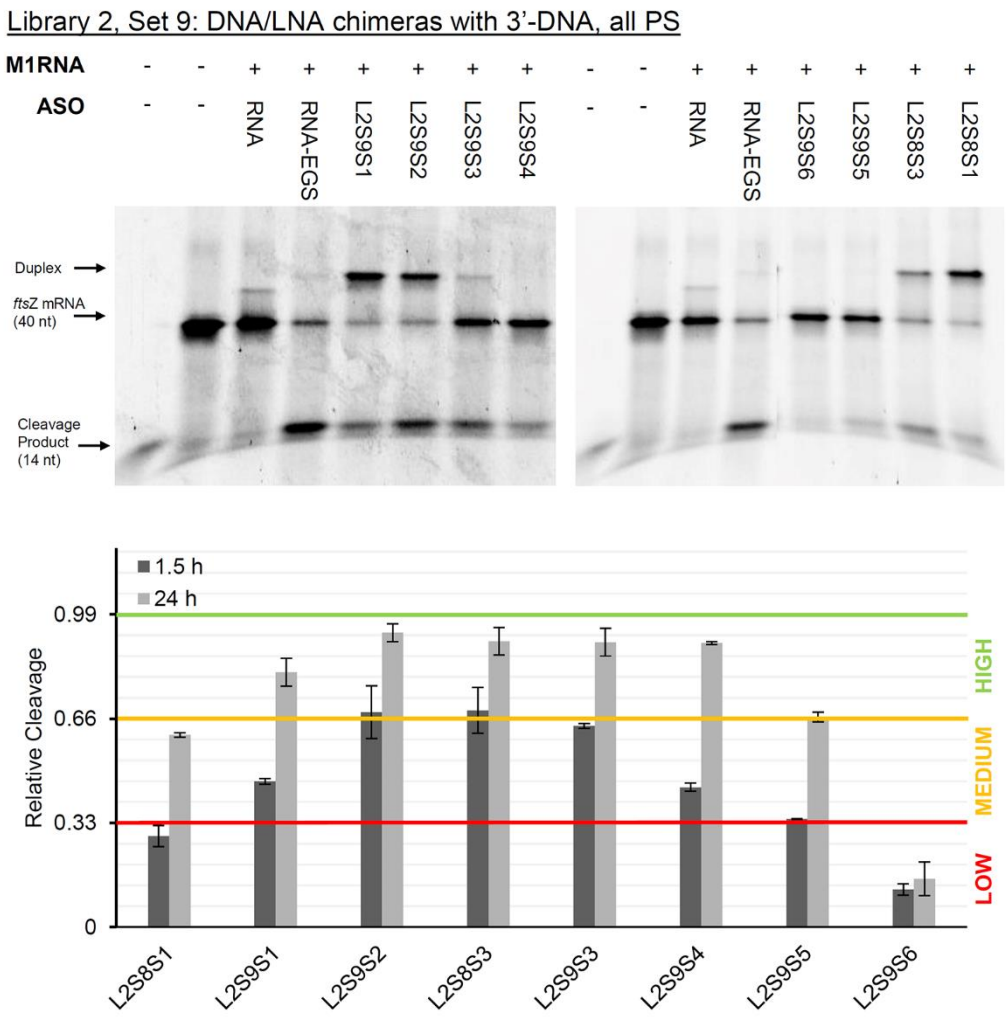

Figure 58. *In vitro* recruitment of RNase P by the oligonucleotides in Library 2, set 9. A mixture of the FAM-labelled target RNA (2 pmol) and ASO (8.8 pmol) were preincubated at 25 °C for 15 min, followed by the addition of M1 RNA (8.8 pmol). The reaction was run at 37 °C for 1.5 h or 24 h, and stopped by adding gel loading buffer. The samples were analysed by urea PAGE and visualized using a Typhoon FLA 7000 biomolecular imager. The gels obtained after 1.5 h incubation are shown at the top. The first well contains a FAM-labelled 17-mer and the second well contains target RNA only; they are intended as a ladder. The calculated relative cleavage (average of two repeats) is shown in the bar graphs at the bottom.

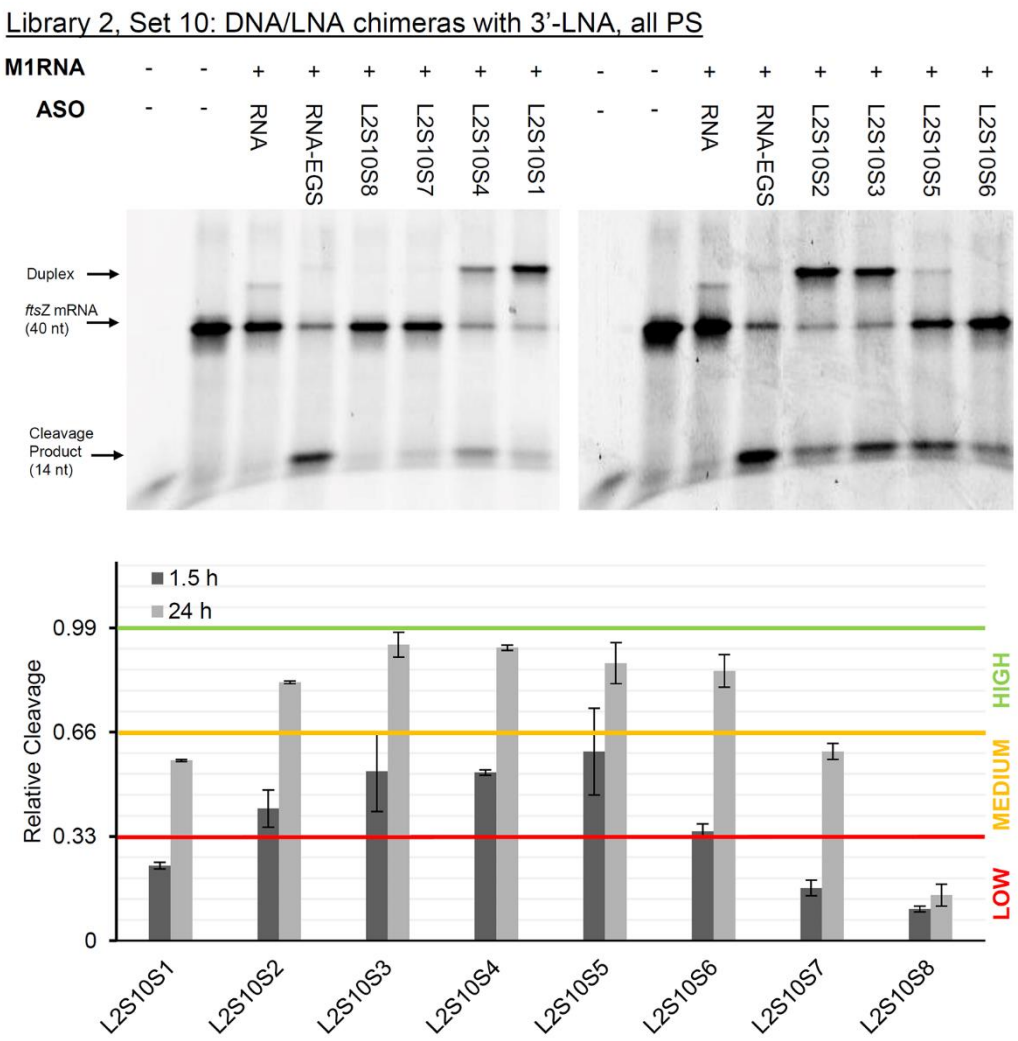

Figure 59. *In vitro* recruitment of RNase P by the oligonucleotides in Library 2, set 10. A mixture of the FAM-labelled target RNA (2 pmol) and ASO (8.8 pmol) were preincubated at 25 °C for 15 min, followed by the addition of M1 RNA (8.8 pmol). The reaction was run at 37 °C for 1.5 h or 24 h, and stopped by adding gel loading buffer. The samples were analysed by urea PAGE and visualized using a Typhoon FLA 7000 biomolecular imager. The gels obtained after 1.5 h incubation are shown at the top. The first well contains a FAM-labelled 17-mer and the second well contains target mRNA only; they are intended as a ladder. The calculated relative cleavage (average of two repeats) is shown in the bar graphs at the bottom.

4.2.1.3 Library 3: chimeras of three types of chemical modifications

In an effort to obtain the optimal antisense oligonucleotide, we were interested to determine if EGSs can be designed that contain 3 different types of chemical modifications. We used the results from Library 1 and Library 2 as a guide to help us designing the new library (Library 3). In the previous section, we discovered that DNA/LNA chimeras have good RNase P recruitment activity. Two of the three modifications would thus be LNA and DNA. For the third modification, we chose OMe rather than MOE or 2'-F. The MOE modification showed inferior activity at various positions in Library 1, while 2'-F is costly and has been shown to only provide minimal resistance against nucleases.[299] As was the case for Library 2, all oligonucleotides in Library 3 have a PS

backbone because it appeared well tolerated in Library 1 (the PS backbone is not counted as one of the three modifications). The oligonucleotides in Library 3 were synthesised by Pranathi Meda.

Two approaches were chosen to design the oligonucleotides in Library 3: (a) maintain the EGS tail as fully LNA-modified and modify the antisense region of the oligonucleotides with various combinations of LNA, DNA and OMe, and (b) maintain the body as DNA/LNA and investigate variable LNA/DNA/OMe combinations in the tail. In addition, as RNA is the natural substrate for RNase P, we also investigated if chimeras of RNA, DNA and LNA can be suitable for RNase P recruitment.

4.2.1.3.1 Variable antisense region with a fixed LNA tail

For the first set, we kept the EGS tail as LNA, since this is the only modification that is well tolerated at every position in the tail (see sequence 10 in Library 1). The main body, which is the antisense region that binds to the target mRNA, consisted of various combinations of LNA, DNA and OMe. However, rather than testing every possible combination, we rationally selected the modification in each position based on the results obtained in Library 1. A schematic of the design of the oligonucleotides in Library 3 set 1 is shown in **Figure 60** (note that the 'regions' denoted on the figure refer to the regions identified in **Figure 50** when designing Library 1).

The 12 oligonucleotides from L3S1S1 to L3S1S10 follow a clear logic based on the results from Library 1 (see **Figure 60**). As mentioned, the tail was fixed to LNA. The region just before the tail (region 5) was also maintained as LNA, because LNA showed much better activity at this position than either DNA or OMe (relative cleavage of 1.12 for LNA versus 0.73 and 0.74 for DNA and OMe respectively in Library 1). For region 6, LNA or OMe modifications were used, because they both showed relative cleavage values > 1 in Library 1 (versus 0.87 for DNA). For region 7, all 3 modifications showed comparable activity in Library 1 (relative cleavage ~0.95), and so all 3 modifications were explored here. Finally, for region 8 we chose DNA or LNA because OMe was not tolerated at this position in Library 1 (relative cleavage of 0.35). Note that some of the designs yielded DNA/LNA chimeras that were already tested in Library 2 (see **Figure 60**).

In addition to these 12 compounds, we investigated 3 additional oligonucleotides that have a high number of OMe modifications in their core (L3S1S11, L3S1S12 and L3S1S13). They were included in the series because Library 1 had shown that OMe can be tolerated in the middle of the oligonucleotide (regions 5, 6 and 7), but not at the 5' end (region 8) or the 3' end (EGS tail). An overview of the sequences explored in this set is shown in **Table 19**.

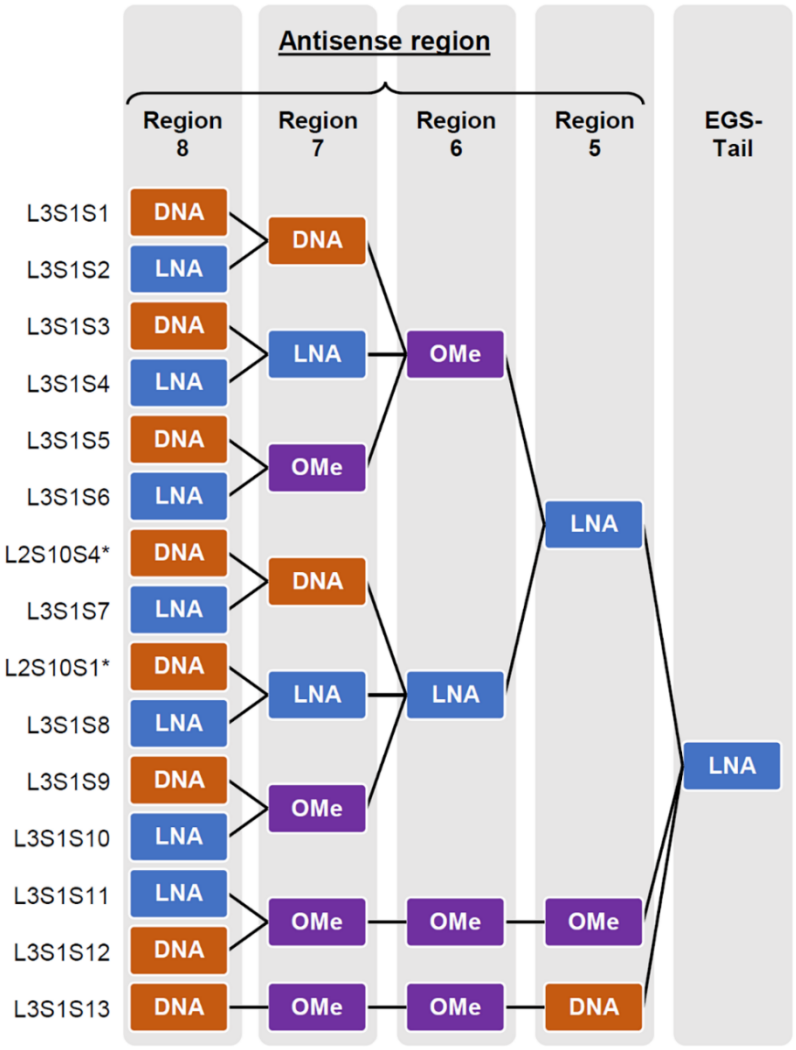

Figure 60. Schematic overview of the design of the oligonucleotides in Library 3, set 1 (tail kept as LNA, antisense region variable). Sequences denoted with * were originally tested in Library 2.

Table 19. Sequence and naming of the oligonucleotides of Library 3, sets 1. Normal text represents LNA, bold and underlined represents DNA, italic and bolded represents OMe.

Name	Sequence
L3S1S1	**CTCAUCC*AGA***CGCUCCA
L3S1S2	CTCA**UCC*AGA***CGCUCCA
L3S1S3	**CTCA**UCC***AGA***CGCUCCA
L3S1S4	CTCAUCC***AGA***CGCUCCA
L3S1S5	**CTCA*UCCAGA***CGCUCCA
L3S3S1	CTCA***UCCAGA***CGCUCCA
L2S10S4[a]	**CTCATCC**AGACGCTCCA
L3S1S7	CTCA**UCC**AGACGCUCCA
L2S10S1[a]	**CTCA**TCCAGACGCTCCA
L3S1S8	CTCAUCCAGACGCUCCA
L3S1S9	**CTCA*UCC***AGACGCUCCA
L3S1S10	CTCA***UCC***AGACGCUCCA
L3S1S11	CTCA***UCCAGACGC***UCCA
L3S1S12	**CTCA*UCCAGA*CGC**UCCA
L3S1S13	**CTCA*UCCAGACGC***UCCA

[a] These sequences were originally tested in Library 2, set 10.

The EGS-sequences in Library 3 set 1 were subjected to the *in vitro* RNase P recruitment assay as described above for Library 1, and the results are given in **Figure 61** (the gels of the second 1.5 h repeat and 24 h repeats are given in Appendix C). Only four compounds showed medium activity after 1.5 h incubation and medium to good activity after 24 h incubation (relative cleavage value > .33), namely L3S1S1, L3S1S5, L2S10S4 and L3S1S9. These compounds have the following configurations (region 8 – region 7 – region 6 – region 5 – tail, see **Figure 50** and **Figure 60**): DNA-DNA-OMe-LNA-LNA (L3S1S1), DNA-OMe-OMe-LNA-LNA (L3S1S5), DNA-DNA-LNA-LNA-LNA (L2S10S4) and DNA-OMe-LNA-LNA-LNA (L3S1S9).

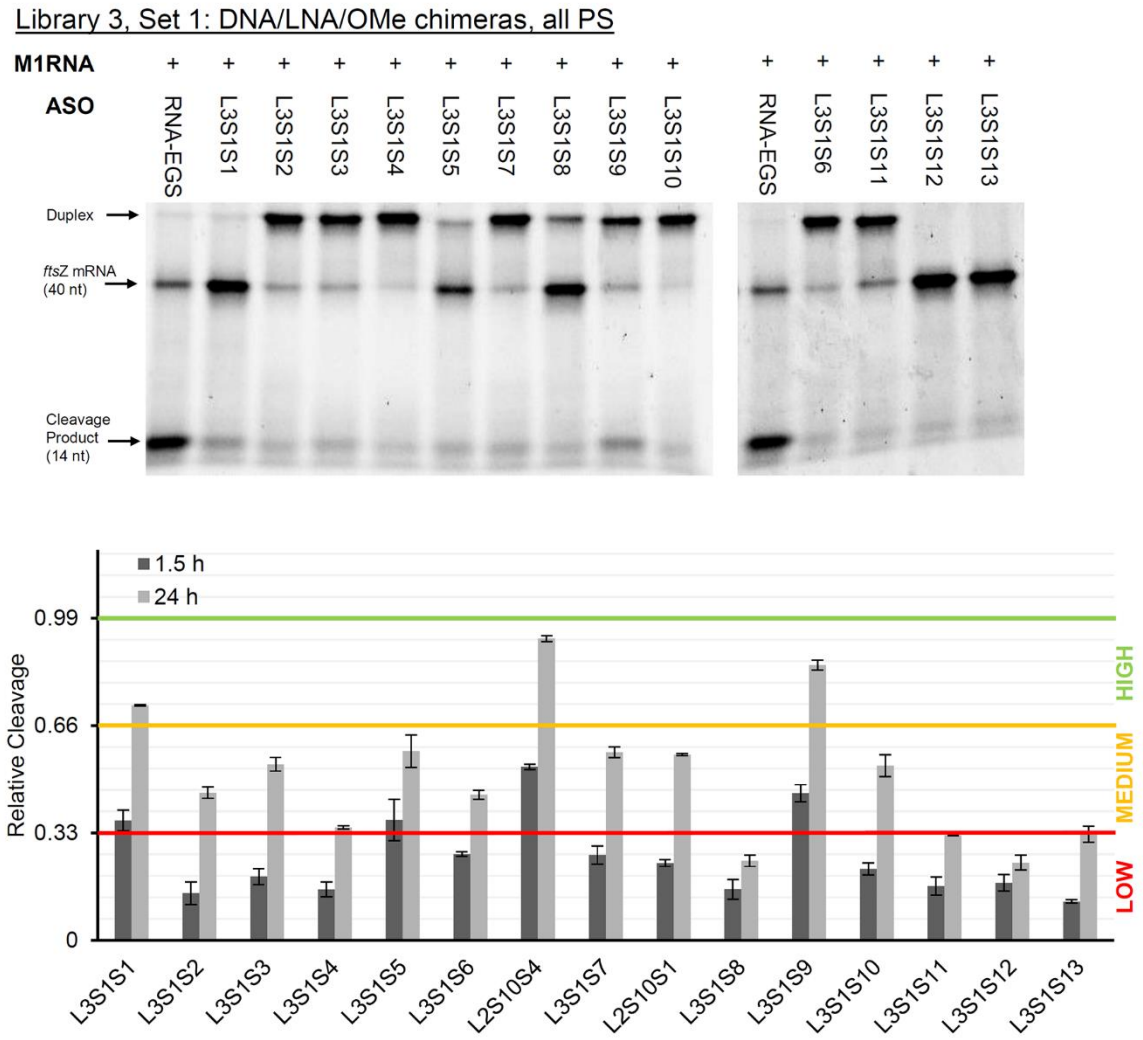

Figure 61. *In vitro* recruitment of RNase P by the oligonucleotides in Library 3, set 1. A mixture of the FAM-labelled target RNA (2 pmol) and ASO (8.8 pmol) were preincubated at 25 °C for 15 min, followed by the addition of M1 RNA (8.8 pmol). The reaction was run at 37 °C for 1.5 h or 24 h, and stopped by adding gel loading buffer. The samples were analysed by urea PAGE and visualized using a Typhoon FLA 7000 biomolecular imager. The gels obtained after 1.5 h incubation are shown at the top. The calculated relative cleavage (average of two repeats) is shown in the bar graphs at the bottom.

The four active oligonucleotides have in common that they all lack LNA at the 5' end (both region 8 and region 7), clearly indicating that LNA is not well tolerated at the 5' terminus. In contrast, the low activity seen for L3S1S11, L3S1S12 and L3S1S13 indicates that region 5 should be LNA and not DNA or OMe. In conclusion, to design an oligonucleotide with three different chemical modifications capable of efficient RNase P recruitment, region 8 should be DNA, region 7 can be DNA or OMe, region 6 can be OMe or LNA, and region 5 and the EGS tail should be LNA.

4.2.1.3.2 Fixed DNA/LNA antisense region with a variable tail

As the EGS tail is crucial for RNase P binding and recruiting, we designed a second set of oligonucleotides containing various combinations of DNA, LNA and OMe in this tail. For this set (set 2), the antisense region was fixed to the configuration that was found to be optimal in Library 2 (L2S8S3 and L2S10S4), namely 7 residues of DNA at the 5' end followed by 6 residues of LNA, and the tail consists of DNA/LNA/OMe combinations. The first nucleotide of the tail (region 4) was set to be OMe or LNA, because these two modifications displayed better activity at this position in Library 1 than DNA (relative cleavage of 0.54 for DNA versus .95 and 1.06 for OMe and LNA respectively). The same restriction was applied to the second nucleotide (region 3), for the same reason (relative cleavage in Library 1 was 0.47 for DNA, 0.97 for OMe and 0.99 for LNA). The third nucleotide (region 2) was fixed to LNA, because it was the only modification with high activity in Library 1 (relative cleavage >.75). The last nucleotide of the tail (region 1) was found to be tolerant towards all modifications in Library 1, and therefore all 3 modifications were included at this position. A schematic overview of the design of Library 3 set 2, as described above, is shown in **Figure 62**. The sequences corresponding to this library set are given in **Table 20**.

Table 20. Sequence and naming of the oligonucleotides of Library 3, sets 2. Bold and underlined represent DNA, not bolded or underlined represents LNA, italic and bolded represent OMe.

Name	Sequence
L3S2S1	**CTCAUCC**AGACGC***TC***C**A**
L3S2S2	**CTCAUCC**AGACGC***TC***CA
L3S2S3	**CTCAUCC**AGACGC***TC***C***A***
L3S2S4	**CTCAUCC**AGACGC***T***CC**A**
L3S2S5	**CTCAUCC**AGACGC***T***CCA
L3S2S6	**CTCAUCC**AGACGC***T***CC***A***
L3S2S7	**CTCAUCC**AGACGCT***C***C**A**
L3S2S8	**CTCAUCC**AGACGCT***C***CA
L3S2S9	**CTCAUCC**AGACGCT***C***C***A***
L2S8S3[a]	**CTCATCC**AGACGCUCC**A**
L2S10S4[a]	**CTCATCC**AGACGCTCCA
L3S2S10	**CTCAUCC**AGACGCTCC***A***

[a] These sequences were originally tested in Library 2.

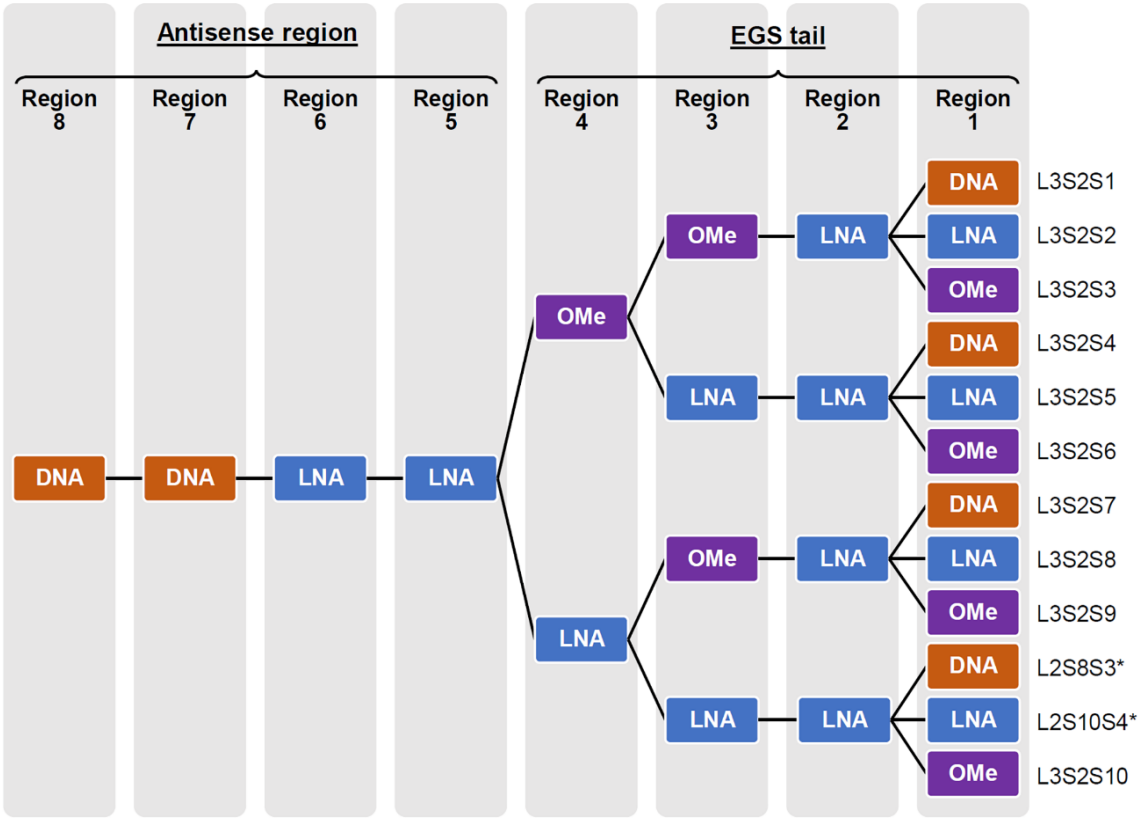

Figure 62. Schematic overview of the design of the oligonucleotides in Library 3, set 2 (antisense region fixed to DNA/LNA, EGS tail variable). Sequences denoted with * were originally tested in Library 2.

The EGS-sequences in Library 3 set 2 were subjected to the *in vitro* RNase P recruitment assay described for Library 1, and the results are given in **Figure 63** (the gels of the second 1.5 h repeat and 24 h repeats are given in Appendix C). Most of the oligonucleotides in this set showed medium to high activity after 1.5 h incubation and (very) high activity after 24 h incubation. The only exceptions are the first 3 compounds in the set (L32S1, L3S2S2 and L3S2S3), which have a tail configuration of OMe-OMe-LNA-X (where X is DNA, LNA or OMe). The lowest activity was seen for L3S2S3, with an OMe-OMe-LNA-OMe tail configuration. This data suggests that OMe can be tolerated in the EGS tail to some extent, but RNase P cannot be efficiently recruited anymore when the OMe content is too high.

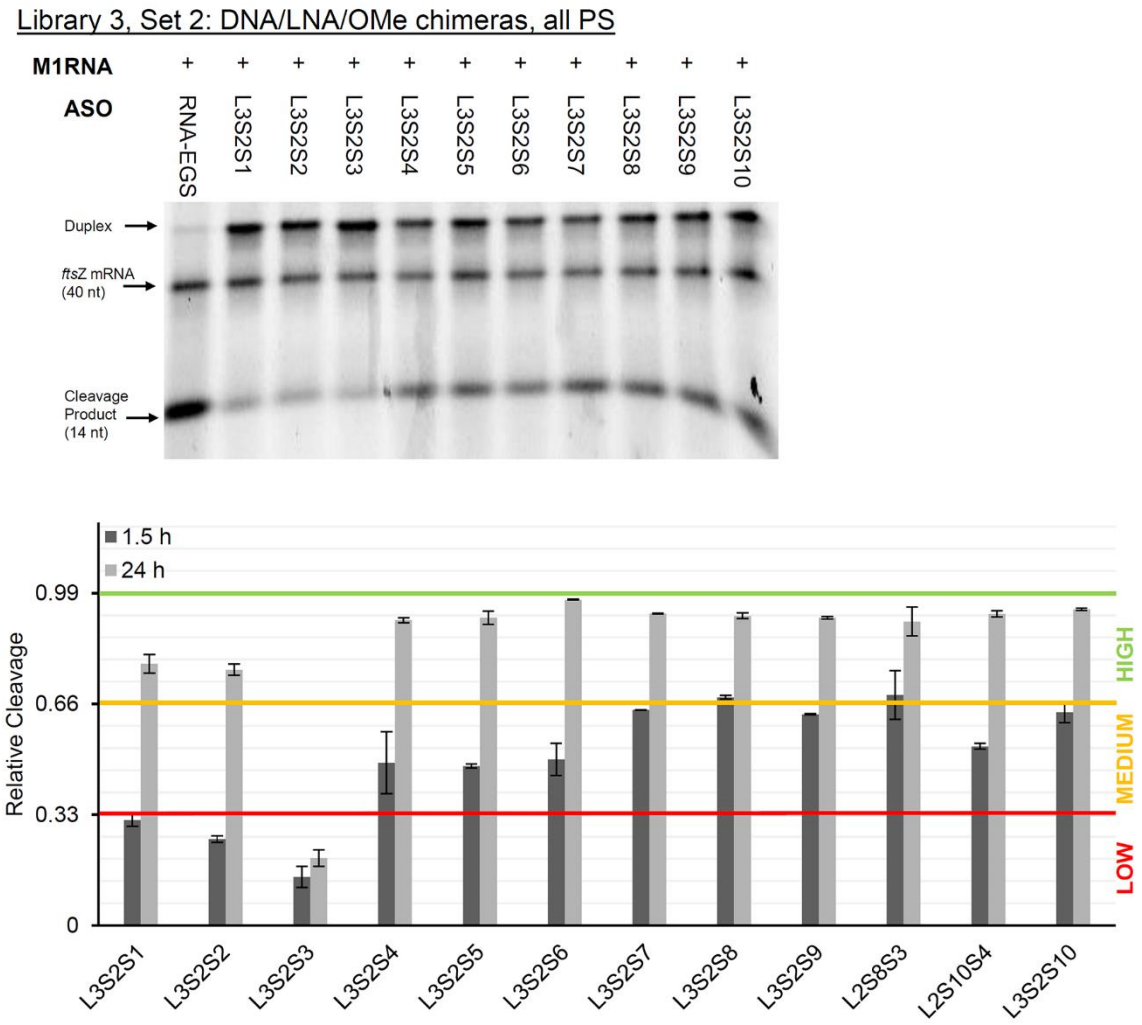

Figure 63. *In vitro* recruitment of RNase P by the oligonucleotides in Library 3, set 2. A mixture of the FAM labelled target mRNA (2 pmol) and ASO (8.8 pmol) were preincubated at 25 °C for 15 min, followed by the addition of M1 RNA (8.8 pmol). The reaction was run at 37 °C for 1.5 and 24 h, and stopped by adding gel loading buffer. The samples were analysed by urea PAGE and visualized using a Typhoon FLA 7000 biomolecular imager. The gel obtained after 1.5 h incubation is shown at the top. The calculated relative cleavage (average of two repeats) is shown in the bar graph at the bottom.

The highest RNase P recruiting activity after 1.5 h incubation was seen for the oligonucleotides with a tail configuration of LNA-OMe-LNA-X (where X is DNA, LNA or OMe), namely L3S2S7, L3S2S8 and L3S2S9. In Library 2 set 9 and set 10 we noticed that an optimal tail could match a variety of antisense region designs, with an optimal antisense region consisting of 6 to 8 DNA residues at the 5' end and the rest of the region LNA. To see if the same holds true for the EGS tails discovered in this library, we designed two more sets (Library 3 set 3 and Library 3 set 4) (**Table 21**). In these sets the tail was fixed to the optimal configuration in either L3S2S7 or L3S2S8, and the antisense region consisted of a range of DNA/LNA ratios. The DNA stretch at the 5' end was increased gradually from 5 nucleotides in the first compound in each set, to 9 nucleotides in the last compound of each set.

Table 21. Sequences and naming of the oligonucleotides of Library 3, sets 3-4. Bold and underlined represent DNA, not bolded or underlined are LNA, italic and bolded are OMe.

Name	Sequence
Library 3, Set 3: DNA/LNA/OMe chimeras, all PS, expanded from L3S2S7	
L3S3S1	**CTCAT**CCAGACGCT***C***C**A**
L3S3S2	**CTCATC**CAGACGCT***C***C**A**
L3S2S7[a]	**CTCATCC**AGACGCT***C***C**A**
L3S3S3	**CTCATCCA**GACGCT***C***C**A**
L3S3S4	**CTCATCCAG**ACGCT***C***C**A**
Library 3, Set 4: DNA/LNA/OMe chimeras, all PS, expanded from L3S2S8	
L3S4S1	**CTCAT**CCAGACGCT***C***CA
L3S4S2	**CTCATC**CAGACGCT***C***CA
L3S2S8[a]	**CTCATCC**AGACGCT***C***CA
L3S4S3	**CTCATCCA**GACGCT***C***CA
L3S4S4	**CTCATCCAG**ACGCT***C***CA

[a] These sequences were originally tested in Library 3, set 2.

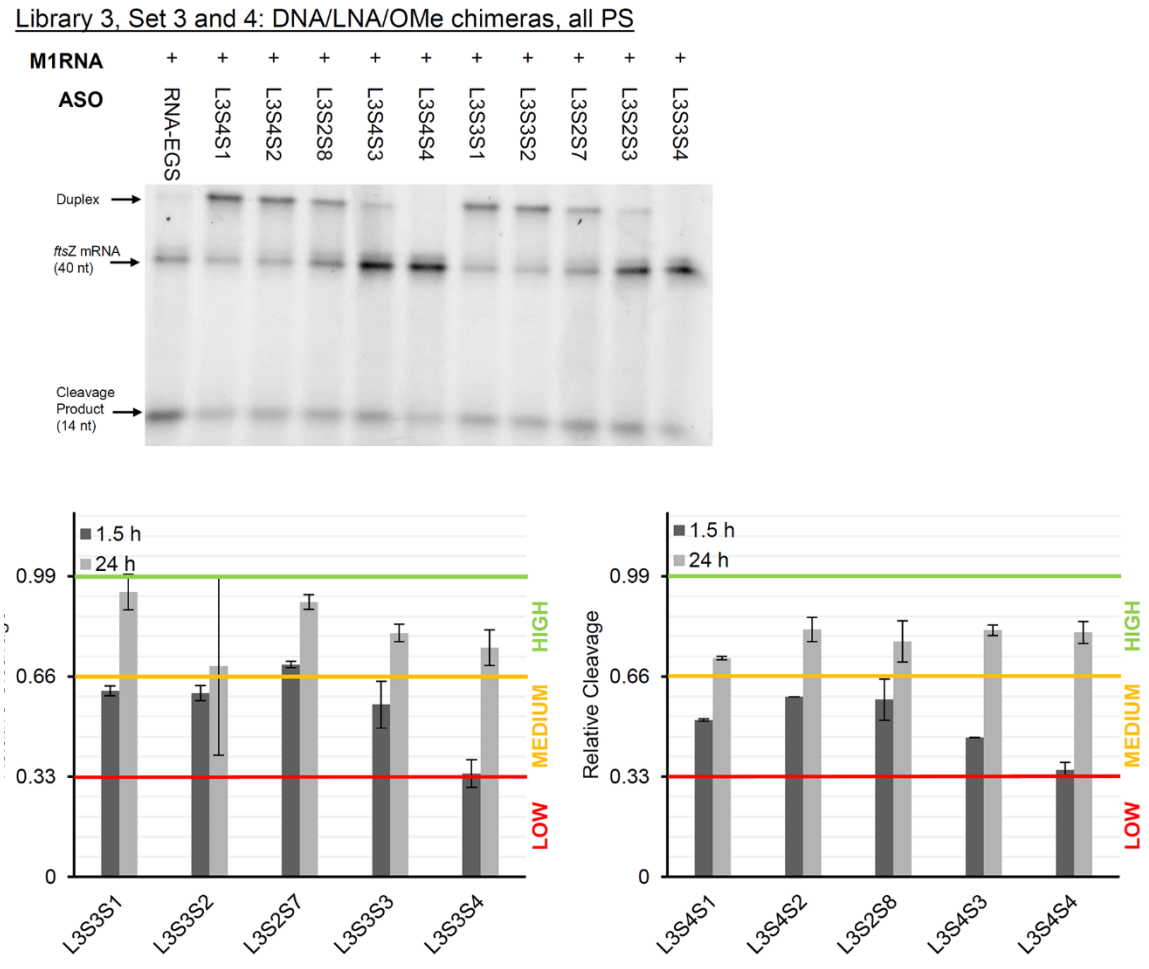

Figure 64. *In vitro* recruitment of RNase P by the oligonucleotides in Library 3, set 3 and set 4. A mixture of the FAM labelled target mRNA (2 pmol) and ASO (8.8 pmol) were preincubated at 25 °C for 15 min, followed by the addition of M1 RNA (8.8 pmol). The reaction was run at 37 °C for 1.5 and 24 h, and stopped by adding gel loading buffer. The samples were analysed by urea PAGE and visualized using a Typhoon FLA 7000 biomolecular imager. The gel obtained after 1.5 h incubation is shown at the top. The calculated relative cleavage (average of two repeats) is shown in the bar graphs at the bottom.

The results for the *in vitro* RNase P recruitment assay of sets 3 and 4 are shown in **Figure 64**. As was the case for Library 2 sets 9 and 10, there is a clear optimal length for the continuous DNA stretch at the 5' terminus in the oligonucleotides of Library 3 sets 3 and 4. Once again, the highest relative cleavage values are obtained for the compounds that have 6 or 7 DNA residues at the 5' end, with lower activity seen for oligonucleotides with a higher or lower DNA content. Thus, our earlier conclusion that the best configuration for the antisense region consists of 7 DNA residues at the 5' end followed by 6 LNA residues holds true irrespective of the configuration in the EGS tail.

4.2.1.3.3 RNA/DNA/LNA chimeras

As RNA is the natural substrate for RNase P, we also wanted to investigate if chimeras could be designed with three types of chemistries such as RNA, DNA and LNA. This would allow us to confirm the conclusions drawn in the previous sections and to investigate additional configurations. Two sequences were synthesized for this set. One sequence had RNA as its antisense region and had an EGS tail with LNA-LNA-DNA-LNA configuration (L3S5S1), because DNA was only a little bit less active than LNA in region 2 (relative cleavage value of 0.70 for DNA versus 0.79 for LNA in Library 1). For the second sequence we wanted to confirm the ideal antisense region modification and this oligonucleotide is thus made up of 7 DNA residues at the 5' end, followed by 6 LNA residues and 4 RNA residues in the EGS tail (L3S5S2). The table below shows the two oligonucleotides with the modifications as explained.

Table 22. Sequence and naming of the oligonucleotides of Library 3, set 5, and the relative cleavage values after 1.5 h and 24 h incubation with mRNA and RNase P. Bold and underlined represent DNA, not bolded or underlined represents LNA, italic represent RNA.

Name	Sequence	Relative cleavage after 1.5 h incubation	Relative cleavage after 24 h incubation
L3S5S1	*CUCAUCCAGACGC*TC**C**A	0.45 ± 0.02	0.77 ± 0.02
L3S5S2	**CTCATCC**AGACGC*UCCA*	0.75 ± 0.03	0.94 ± 0.02

Table 22 also shows the relative cleavage that was observed for these two compounds in the *in vitro* RNase P recruitment assay described above (the gels can be found in Appendix C). The first compound (L3S5S1) showed medium relative cleavage (> 0.33) after 1.5 h and high cleavage after 24 h (> 0.66). While this relative cleavage value is not bad, it is not optimal keeping in mind that this oligonucleotide consists mainly of the natural substrate RNA; recall that all rates are calculated as relative to the fully RNA EGS. We can therefore conclude that the LNA-LNA-DNA-LNA

tail configuration is not as good as any of the EGS tail configurations tested in Library 3 set 2, or that this tail is not compatible with RNA body. In contrast, the second oligonucleotide (L3S5S2) showed high RNase P recruitment activity after 1.5 and 24 h incubation (> 0.66). This confirmed our previous findings that a 7 nucleotide DNA and 6 nucleotide LNA chimera is a suitable configuration for the body (antisense region) of EGS oligonucleotides, in combination with multiple tail designs.

4.2.2 Dual recruitment of RNase P and RNase H

We realized that the oligonucleotides with the ability to successfully recruit RNase P in the previous libraries contained a high content of DNA. This inspired us to search for oligonucleotides that can recruit both RNase P and RNase H, as DNA is the natural substrate of RNase H (see Chapter 3). Such 'dual recruiters' might possess superior antibacterial activity than traditional EGS sequences (recruitment of RNase P alone) or gapmers (recruitment of RNase H alone). In order to see which EGSs are also able to recruit RNase H, we performed the *in vitro* RNase H assay described in Chapter 3. Briefly, 4 x10^{-3} units of RNase H (Thermo Scientific RNase H kit EN0201), 2 pmol target mRNA and 8.8 pmol EGS were mixed in a volume of 30 µL, and the reaction was run at 37 °C. A sample was withdrawn after 1.5 h and 24 h, formamide was added to stop the reaction and a 15% denaturing urea polyacrylamide gel (urea PAGE) was run on the samples. The gels were then visualized using the FAM channel of a GE Typhoon FLA 7000. The gels can be found in Appendix C. The absolute amount of cleavage by RNase H was calculated using *ImageJ*[290] by dividing the intensity of the band of the cleaved product, by the intensity of the uncleaved bands. We focused our attention towards those oligonucleotides that have a high percentage of DNA residues in their sequence: Library 2 set 9, Library 2 set 10, Library 3 set 2, Library 3 set 3 and Library 3 set 4.

4.2.2.1 Library 2 sets 9 and 10

Library 2 set 9 contained oligonucleotides with a number of DNA residues at the 5'-end, one single DNA residue at the 3' end, and the rest of sequence LNA (see **Table 18**). Library 2 set 10 is an analogous series to set 9, but with LNA at the 3' terminus (see **Table 18**). For both sets, the DNA stretch at the 5' end was gradually increased from 4 to 10 nucleotides, and an analogue where the full antisense region (13 nucleotides) was set to DNA was also included. **Figure 65** shows the relative cleavage by RNase P (bar graph) and the absolute cleavage by RNase H (lines) induced by

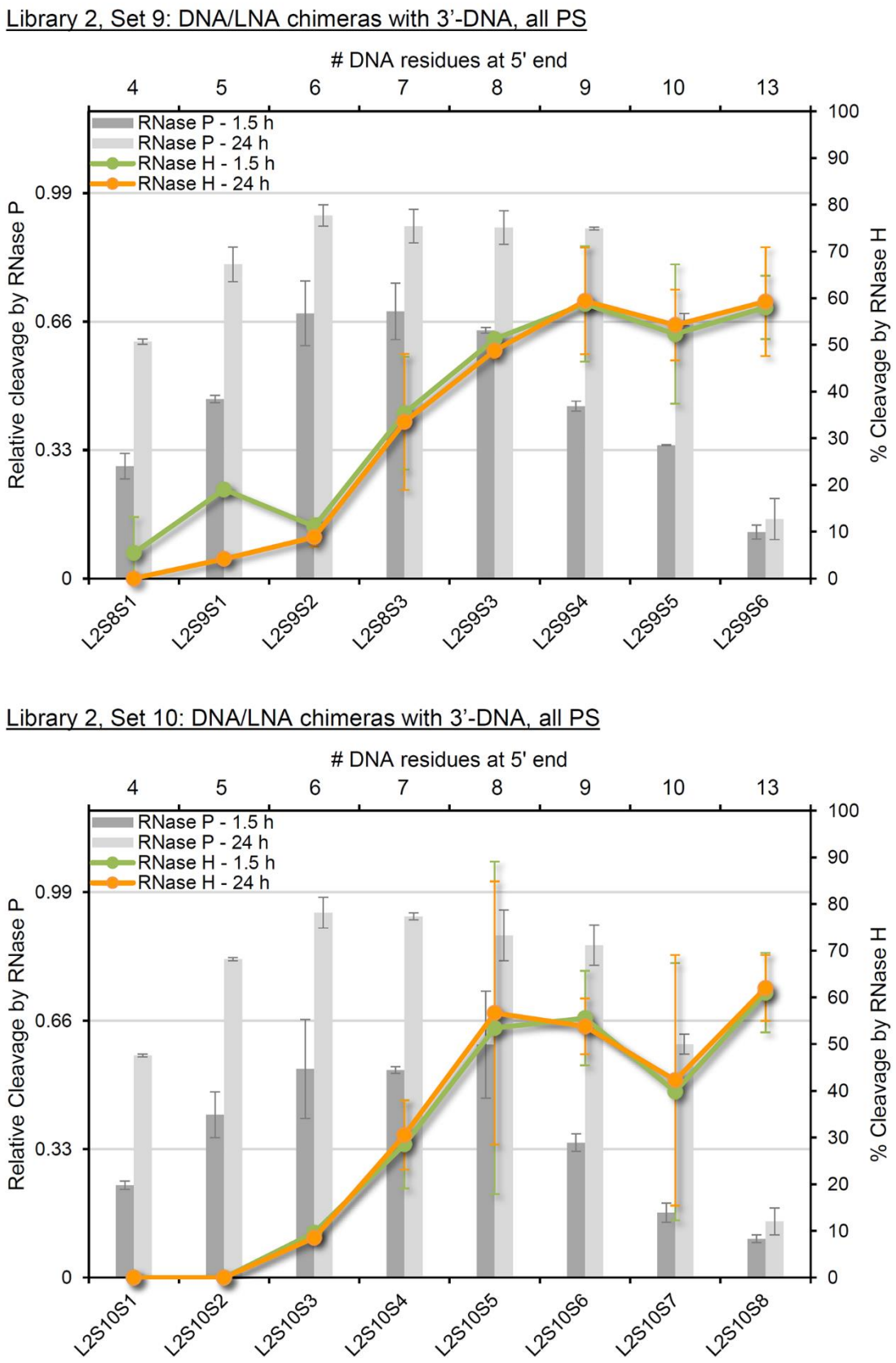

Figure 65. *In vitro* recruitment of RNase P (bars) and RNase H (lines) by the oligonucleotides in Library 2, set 9 (top) and Library 2, set 10 (bottom). Experiments were conducted as described in the main text. All data is the average of two repeats with error bars representing standard deviations.

the compounds in these two sets. As expected, the efficiency of RNase H increased as the DNA stretch at the 5' terminus gets longer, requiring at least 7 contiguous deoxynucleotides for robust RNase H recruitment, with even higher activity seen for DNA tracts of 8 and above. In contrast, the RNase P recruitment efficiency shows a more parabolic relationship with the length of the DNA stretch (as discussed in section 0). This implies that not all compounds can recruit both enzymes. Inspection of **Figure 65** indicates that the oligonucleotides with 7, 8 or 9 DNA residues at the 5' end (L2S8S3, L2S9S3 and L2S9S4 for set 9; and L2S10S4, L2S10S5 and L2S10S6 for set 10) are able to induce medium to high cleavage rates by both RNase P and RNase H and can thus be considered 'dual recruiters'.

4.2.2.2 Library 3 set 2

In Library 3 set 2 we explored oligonucleotides that had 7 DNA residues at its 5' end, followed by 6 LNA residues and EGS tails with various compositions (see **Figure 62** and **Table 20**). As the oligonucleotides with 7 DNA residues at the 5' end showed dual recruitment ability in the sets discussed above (Library 2 set 9 and 10), it was expected that these compounds would also be suitable dual recruiters for RNase P and RNase H. Our focus was on those sequences that had shown the highest RNase P recruitment activity in section 4.2.1.3 (L3S2S7, L3S2S8, L3S2S9 and L3S2S10). We also included L2S5S2, which had the same configuration of the antisense region (7 DNA residues and 6 LNA residues), but an EGS tail that was pure RNA. The results are summarized in **Figure 66** (the gels from the *in vitro* RNase H recruitment assay can be found in Appendix C).

The highest cleavage by RNase H was observed for L3S2S7, which contains one additional DNA nucleotide at the 3' end. It is not clear why this compound has higher activity than the other chimeras. Normally, it is expected that the length of the continuous stretch of DNA is important for RNase H recruitment ability, but this stretch is 7 nucleotides long for all oligonucleotides in this set. It is possible that the extra DNA residue at the 3' end aids in other aspects of RNase H mediated cleavage, such as product release. One other oligonucleotide also showed moderate cleavage by RNase H (L3S5S2, which has an all RNA EGS tail). Those two compounds can be considered dual recruiters. The other three oligonucleotides in this set have high RNase P recruitment activity, but the RNase H recruitment activity is lower.

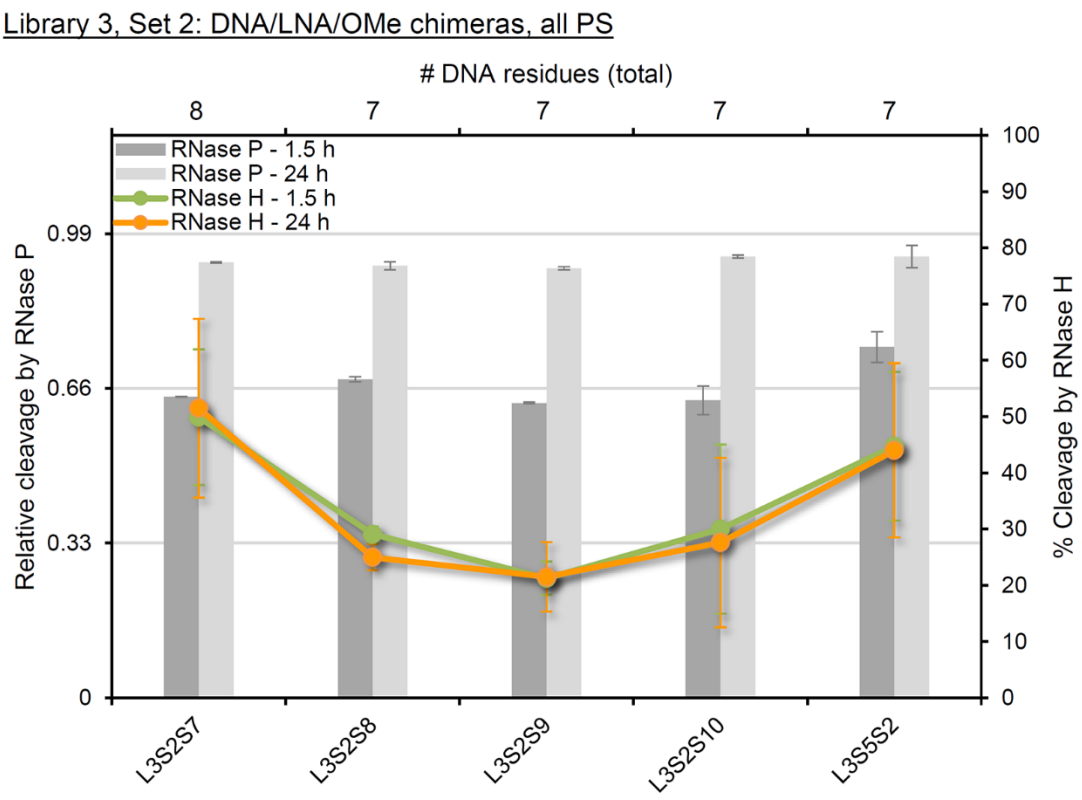

Figure 66. *In vitro* recruitment of RNase P and RNase H by the oligonucleotides in Library 3, set 2. Experiments were conducted as described in the main text. All data is the average of two repeats with error bars representing standard deviations.

4.2.2.3 Library 3-sets 3 and 4

Library 3 sets 3 and 4 are the expanded versions of L3S2S7 and L3S2S8. In these sets the tail was fixed to the optimal configuration in either L3S2S7 (LNA-OMe-LNA-DNA) or L3S2S8 (LNA-OMe-LNA-LNA), and the antisense region was gradually varied from 5 to 9 DNA residues at the 5' end (the rest of the sequence was LNA) (see **Table 21**). AS L3S2S7 showed dual recruitment activity as described above, we postulated that these compounds would also be good dual recruiters for RNase P and RNase H. In addition, these two sets are comparable to Library 2 sets 9 and 10, which also explored the effect of the length of the DNA stretch at 5' end.

The results are summarized in **Figure 67** (the gels from the *in vitro* RNase H recruitment assay can be found in Appendix C). All compounds in these sets showed modest to high cleavage by RNase H (> 33% cleavage). There is a small correlation between the amount of DNA at the 5' end and the ability to recruit RNase H, but the trend is less pronounced than in Library 2 sets 9 and 10 (see **Figure 65**). As all oligonucleotides in these sets were also able to induce medium to high cleavage by RNase P (relative cleavage > 0.35 after 1.5 h), all compounds in these two sets can be considered 'dual recruiters'.

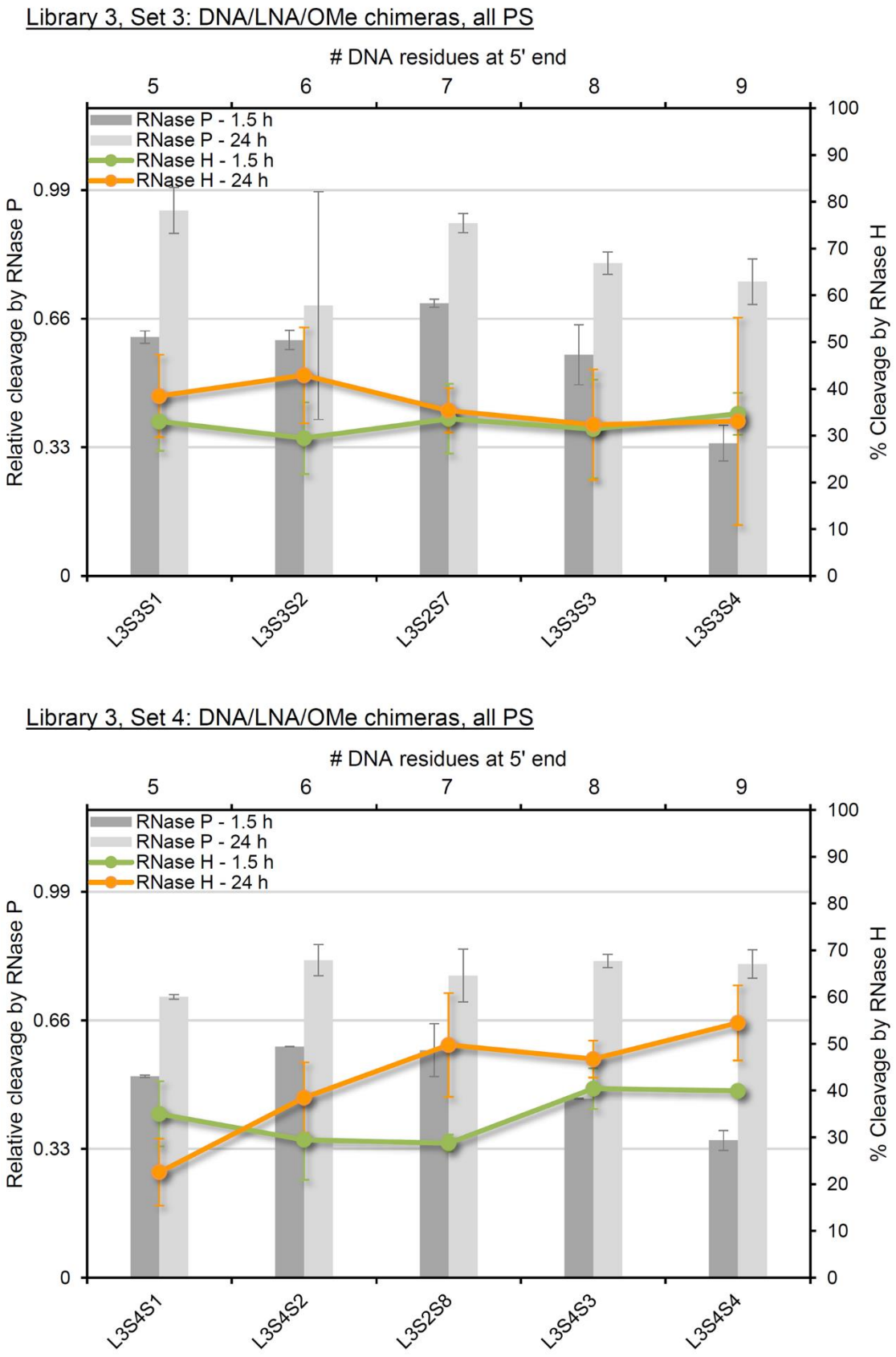

Figure 67. *In vitro* recruitment of RNase P and RNase H by the oligonucleotides in Library 3, set 3 (top) and Library 3, set 4 (bottom). Experiments were conducted as described in the main text. All data is the average of two repeats with error bars representing standard deviations.

4.2.3 Broadening the dual recruitment approach to other targets

All *in vitro* assays with chemically modified oligonucleotides discussed in the previous sections targeted the *ftsZ* region 1032-1044. Ideally, the nature of the target mRNA should not affect the ability of a particular chemical composition to recruit RNase P. However, for other classes of oligonucleotides, there can be sequence-specific interactions with particular chemical modifications.[300] Thus a successful design for one sequence may not be ideal for all sequences. Therefore, in this section we describe studies to test the ability of various oligonucleotides to induce RNase P mediated cleavage of target mRNAs using the chemically modified templates optimized in libraries 1-3. We also wanted to see whether the 'dual recruitment' approach is generally applicable to any bacterial mRNA target. We tested this using multiple target regions on both the *ftsZ* gene and the *lacZ* gene.

4.2.3.1 Identifying other target mRNA sequences

In Chapter 2 it became clear that not all regions of an mRNA strand can be successfully targeted by an EGS-ASO for the *in vitro* recruitment of RNase P. This could be due to either secondary structure formations in the mRNA, which prevents the EGS-ASO from binding to its target, or to duplex formation between the EGS tail and the mRNA, thereby preventing efficient recruitment of RNase P. It was therefore necessary to first identify potential target mRNAs that are suitable for the *in vitro* RNase P assay, by targeting them with EGSs that consist of the natural unmodified RNA substrate of this enzyme (Library 4). We explored different regions of the *ftsZ* gene (set 1), as well as different regions of the *lacZ* gene (sets 2, 3 and 4). The oligonucleotides in Library 4 were synthesised by Pranathi Meda.

4.2.3.1.1 Alternative regions of the ftsZ gene

In Library 4 set 1, we targeted the untranslated region (UTR) of *fts*Z mRNA. In particular, our design was based on the accessible region of the UTR that was successfully silenced by Good and co-workers using PNA (see Chapter 2).[254] However, because the antisense mRNA binding region of the EGSs studied in this chapter is longer than the steric blocking region of Good's PNA, we studied three putative accessible regions of the UTR (L4S1S2/L4S1S3, L4S1S5 and L4S1S7). **Figure 31** shows a schematic representation of the areas of the *ftsZ* UTR targeted by Library 4 set 1. L4S1S2 and L4S1S3 target the exact same region of the UTR, but differ in the first nucleotide of

the EGS tail (region 4). As both -ACCA and -UCCA have been reported as tails for EGSs, we wanted to see which tail is the most efficient for this particular target region.

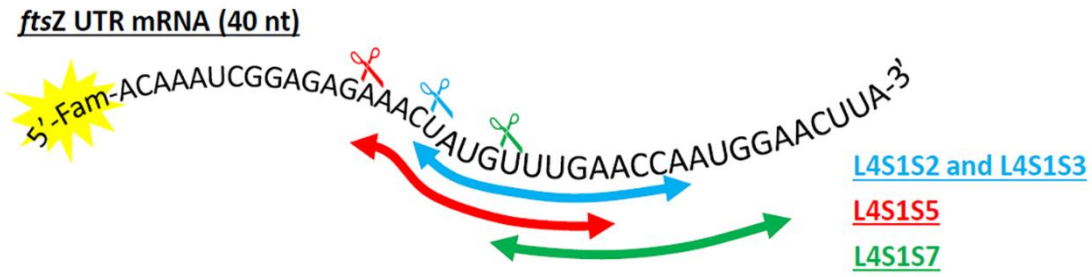

Figure 68. Areas of *ftsZ* untranslated region (UTR) mRNA targeted by the various oligonucleotides in Library 4 set 1 (L4S1S2, L4S1S3, L4S1S5 and L4S1S7) The expected cleavage site is denoted by the scissors (the colour of the scissors corresponds to the colour of the EGS oligonucleotide)

In order to be able to perform the *in vitro* RNase P recruitment assay, we also synthesized the 40 nt long FAM-labelled *ftsZ* UTR region (L4S1S8). Additionally, as successful cleavage of the target by the various EGS should generate FAM-labelled oligonucleotides of 13 to 20 nucleotides long (depending on the EGS), we also prepared a FAM-labelled 17-mer that can be used as a ladder (L4S1S9). Finally, ASO analogues without the EGS tail were synthesised for each target region as negative controls (L4S1S1, L4S1S4, and L4S1S6). **Table 23** provides an overview of all sequences in Library 4 set1, as well as the length of the cleavage product expected after successful recruitment of RNase P.

Table 23. Sequences and naming of the oligonucleotides of Library 4, set 1 (RNA, PO backbone). The expected length of the cleavage product is indicated.

Name	Sequence	Cleavage product
L4S1S1	*UGGUUCAAACAUA*	No cleavage
L4S1S2	*UGGUUCAAACAUAUCCA*	17-mer
L4S1S3	*UGGUUCAAACAUAACCA*	17-mer
L4S1S4	*UCAAACAUAGUUU*	No cleavage
L4S1S5	*UCAAACAUAGUUUACCA*	13-mer
L4S1S6	*CCAUUGGUUCAAA*	No cleavage
L4S1S7	*CCAUUGGUUCAAAACCA*	21-mer
L4S1S8	Fam-*ACAAAUCGGAGAGAAACUAUGUUUGAACCAAUGGAACUUA*	n/a (target)
L4S1S9	Fam-*ACAAAUCGGAGAGAAAC*	n/a (ladder)

The result of the *in vitro* RNase P recruitment assay (24 h incubation) is shown in **Figure 69**, the second repeat at 24 h incubation and the 1.5 h incubation repeats are shown in Appendix C. This

set shows weak but successful selective cleavage of the targeted *ftsZ* UTR (L4S2S8) for all four oligonucleotides (L4S1S2, L4S1S3, L4S1S5 and L4S1S7), with the strongest band intensity in the case of L4S1S3 (19% cleavage after 24 h incubation). Therefore, we will use this sequence to investigate the RNase P recruitment ability of the chemically modified oligonucleotides in Library 5 (see below).

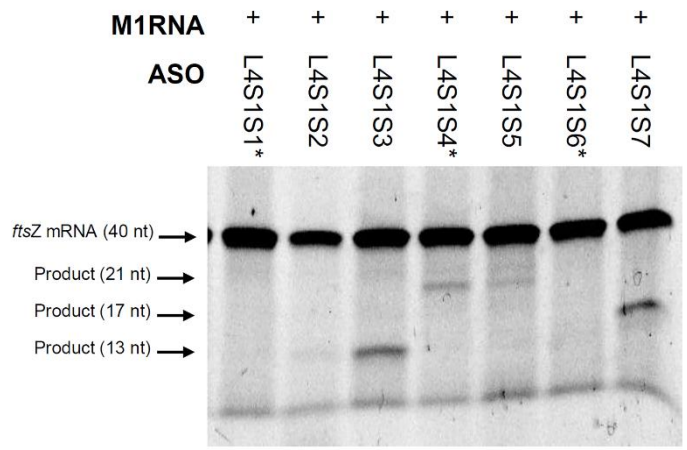

Figure 69. *In vitro* recruitment of RNase P by the oligonucleotides in Library 4, Set 1. A mixture of the FAM labelled target mRNA (2 pmol) and ASO (8.8 pmol) were preincubated at 25 °C for 15 min, followed by the addition of M1 RNA (8.8 pmol). The reaction was run at 37 °C for 24 h, and stopped by adding gel loading buffer. The samples were analysed by 15% denaturing urea polyacrylamide gel, visualized using a Typhoon FLA 7000 biomolecular imager equipped with a FAM filter. The location and size of the initial target and the expected cleavage product are shown on the left. Compounds indicated with * do not have the EGS tail (negative controls).

4.2.3.1.1 Identifying regions of the lacZ gene

We also wanted to develop EGSs against the reporter gene *LacZ*. We investigated 3 potential regions of the *lacZ* mRNA as target: the 5'-untranslated region (*lacZ*-UTR, targeted by set 2), the region around 360 (*lacZ*-360, targeted by set 3) and the region around 1729 (*lacZ*-1729, targeted by set 4). The 5'-UTR was chosen because it has been successfully silenced by PNAs by Good and co-workers (see Chapter 2).[254] However, because the antisense mRNA binding region of the EGSs studied in this chapter is longer than the steric blocking region of Good's PNA, we studied three putative accessible regions of the 5'-UTR (L4S2S2, L4S2S4/L4S2S5 and L4S1S7/L4S2S8). The regions around 360 and 1729 were chosen after calculating the ss-count using Mfold,[284] and identifying regions with continuous stretches of 12 or more nucleotides with an ss-count higher than 20 (see Appendix C). Thus, these two regions are predicted to not be involved in stable self-structure (secondary structure formation) and should therefore be available for the EGSs to bind. Two areas of *lacZ*-360 were explored as binding regions for EGSs (L4S3S2/L4S3S3, and L4S3S5/L4S3S6), whereas only one area of *lacZ*-1729 was investigated (L4S4S2/L4S4S3). **Figure 70**

provides a schematic overview of all the regions targeted by the EGSs in Library 4 sets 2, 3 and 4, and the sequences are given in **Table 24**.

We also wanted to determine which EGS tail (UCCA or ACCA) is best in recruiting RNase P toward each specific target. Therefore, two analogous oligonucleotides with different tails were synthesized for most of the targeted regions. In order to be able to perform the *in vitro* RNase P recruitment assay, we also synthesized the 40 nt long FAM-labelled mRNA target for each of the studied areas (L4S2S9 for *lacZ*-UTR, L4S3S7 for *lacZ*-360, and L4S4S4 for *lacZ*-1729). Additionally, we also prepared some shorter FAM-labelled oligonucleotides that can be used as a ladder to detect successful cleavage of the target mRNA. Finally, ASO analogues without the EGS tail were synthesised for each target region as negative controls. **Table 24** provides an overview of all sequences in Library 4 sets 2, 3 and 4, as well as the length of the cleavage product expected after successful recruitment of RNase P.

Table 24. Sequences and naming of the oligonucleotides of Library 4, set 2, 3 and 4 (RNA, PO backbone). The expected length of the cleavage product is indicated.

Name	Sequence	Cleavage product
Library 4, set 2: targeting *lacZ*-UTR		
L4S2S1	*UCAUAGCUGUUUC*	No cleavage
L4S2S2	*UCAUAGCUGUUUCACCA*	12-mer
L4S2S3	*CAUGGUCAUAGCU*	No cleavage
L4S2S4	*CAUGGUCAUAGCUUCCA*	17-mer
L4S2S5	*CAUGGUCAUAGCUACCA*	17-mer
L4S2S6	*AAUCAUGGUCAUA*	No cleavage
L4S2S7	*AAUCAUGGUCAUAUCCA*	20-mer
L4S2S8	*AAUCAUGGUCAUAACCA*	20-mer
L4S2S9	Fam-*AAUUUCACACAGGAAACAGCUAUGACCAUGAUUACGGAUU*	n/a (target)
L4S2S10	Fam-*AAUUUCACACAGGAAAC*	n/a (ladder)
Library 4: set 3: targeting *lacZ*-360		
L4S3S1	*AUUAAAUGUGAGC*	No cleavage
L4S3S2	*AUUAAAUGUGAGCUCCA*	15-mer
L4S3S3	*AUUAAAUGUGAGCACCA*	15-mer
L4S3S4	*ACAUUAAAUGUGA*	No cleavage
L4S3S5	*ACAUUAAAUGUGAUCCA*	17-mer
L4S3S6	*ACAUUAAAUGUGAACCA*	17-mer
L4S3S7	Fam-*GACGGGUUGUUACUCGCUCACAUUUAAUGUUGAUGAAAGC*	n/a (target)
L4S3S8	Fam-*GACGGGUUGUUACUCGC*	n/a (ladder)
L4S3S9	Fam-*GACGGGUUGUUACUC*	n/a (ladder
Library 4: set 4: targeting *lacZ*-1729		
L4S4S1	*CAUCAUAUUUAAU*	No cleavage
L4S4S2	*CAUCAUAUUUAAUUCCA*	17-mer
L4S4S3	*CAUCAUAUUUAAUACCA*	17-mer
L4S4S4	Fam-*GGGUGGAUCAGUCGCUGAUUAAAUAUGAUGAAAACGGCAA*	n/a (target)
L4S4S5	Fam-*GGGUGGAUCAGUCGCUG*	n/a (ladder)

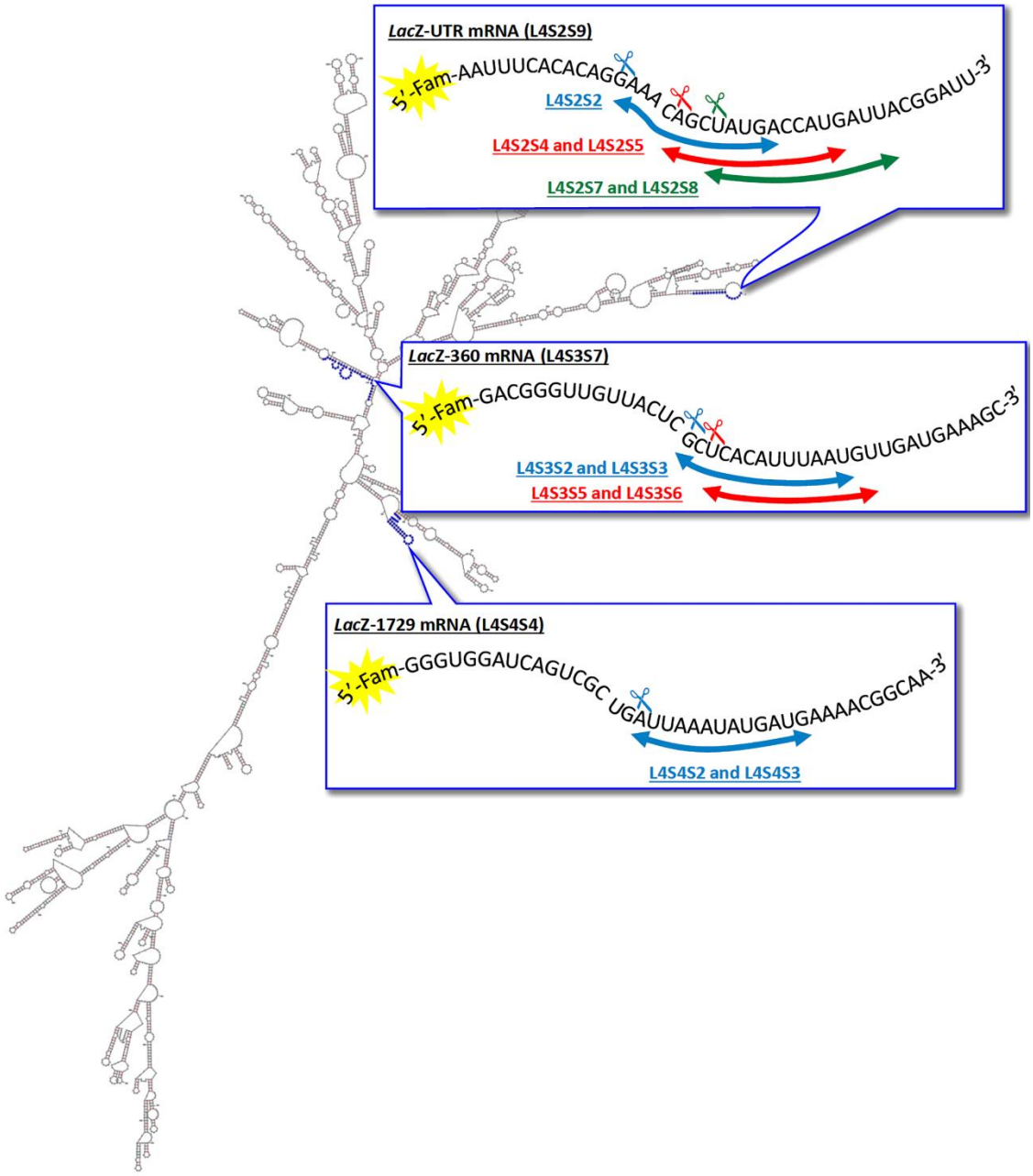

Figure 70. Calculated secondary structure for *lacZ* mRNA (Mfold). Areas targeted by the oligonucleotides in Library 4 sets 2, 3 and 4 are highlighted in blue. The boxes show the FAM-labelled 40-nt target mRNAs synthesized for each area, as well as the regions of these mRNAs that are targeted by the various EGSs. The expected cleavage site is denoted by the scissors (the colour of the scissors corresponds to the colour of the EGS oligonucleotide)

The result of the *in vitro* RNase P recruitment assay (24 h incubation) is shown in **Figure 71**, the second repeat at 24 h incubation and the 1.5 h incubation repeats are shown in Appendix C. As was the case for the *ftsZ* untranslated region, sets 2 (*lacZ*-UTR) and set 3 (*lacZ*-360) show weak but selective cleavage of the target mRNA by RNase P. The best cleavage was seen for L4S2S2 (20% cleavage after 24 h) and L4S3S3 (52% cleavage after 24 h). These two sequences will thus be used to investigate the RNase P recruitment ability of the chemically modified oligonucleotides in

Library 5 (see below). The oligonucleotides in set 4 (*lacZ*-1729) also show cleavage, but not at the expected position and we will therefore not use this target region any further.

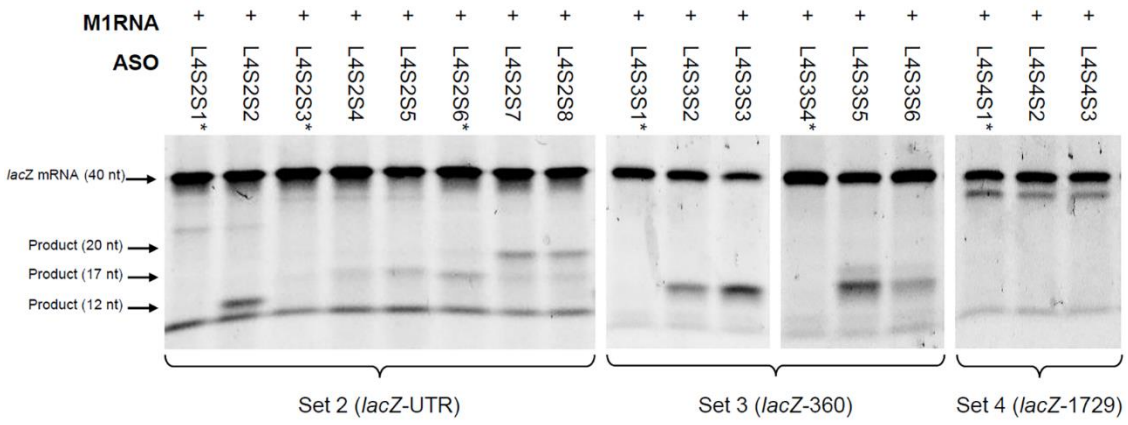

Figure 71. *In vitro* recruitment of RNase P by the oligonucleotides targeting regions of lacZ mRNA (Library 4, sets 2 , 3 and 4). A mixture of the FAM-labelled target RNA (2 pmol) and ASO (8.8 pmol) were preincubated at 25 °C for 15 min, followed by the addition of M1 RNA (8.8 pmol). The reaction was run at 37 °C for 24 h, and stopped by adding gel loading buffer. The samples were analysed by 15% denaturing urea polyacrylamide gel, visualized using a Typhoon FLA 7000 biomolecular imager equipped with a FAM filter. The location and size of the initial target and the expected cleavage product are shown on the left. Compounds indicated with * do not have the EGS tail (negative controls).

4.2.3.2 Chemically modified EGSs targeting *ftsZ* and *lacZ* regions

In Library 5, we applied the chemical modifications found to be suitable for dual recruitment of RNase P and RNase H (section 4.2.2) to the mRNA targets identified in the previous section. The best target region in the previous section (*lacZ*-360) was targeted by L4S3S3 (52% cleavage by RNase P after 24 h incubation). We therefore focused our investigation on this target area, with only a few additional chemically modified EGSs tested for the other two successful target regions (L4S1S3 *ftsZ*-UTR, and L4S2S2 *lacZ*-UTR).

4.2.3.2.1 Chemically modified EGSs targeting lacZ-360

Initially, we investigated the ability of chemically modified analogues of L4S3S3 tail to recruit RNase P to the *lacZ*-360 mRNA target, as this was found to be the best target region. We studied three sets of chemical modifications, corresponding to the most optimal chemical modifications found when targeting *ftsZ* 1032 in section 4.2.2. The first set contained DNA/LNA chimeras with the same configuration as Library 2 set 9 (i.e., a stretch of DNA on the 5'-end, and a single DNA nucleotide on the 3'-end). The second set consisted of DNA/LNA chimeras with the same configuration of the best oligonucleotides from Library 2 set 10 (LNA throughout the 3'-end),

while the third set consisted of DNA/LNA/OMe chimeras with the same composition as Library 3 set 4 (a single OMe nucleotide in the ACCA tail). **Table 25** provides an overview of the sequences in Library 5 sets 1-3.

Table 25. Sequences and naming of the oligonucleotides of Library 5, sets 1-3. Bold and underlined represent DNA, not bolded or underlined are LNA, italic and bolded are OMe.

Name	Sequence
Library 4, Set 1: DNA/LNA chimeras with 3'-end DNA, all PS (analogues of Library 2 set 9)	
L5S1S1	**ATTA**AATGTGAGCACC**A**
L5S1S2	**ATTAA**ATGTGAGCACC**A**
L5S1S3	**ATTAAA**TGTGAGCACC**A**
L5S1S4	**ATTAAAT**GTGAGCACC**A**
L5S1S5	**ATTAAATG**TGAGCACC**A**
L5S1S6	**ATTAAATGT**GAGCACC**A**
L5S1S7	**ATTAAATGTG**AGCACC**A**
L5S1S8	**ATTAAATGTGAGC**ACC**A**
Library 5, Set 2: DNA/LNA chimeras with 3'-end LNA, all PS (analogues of Library 2 set 10)	
L5S2S1	**ATTAAA**TGTGAGCACCA
L5S2S2	**ATTAAAT**GTGAGCACCA
L5S2S3	**ATTAAATG**TGAGCACCA
Library 5, set 3" DNA/LNA/OMe chimeras, all PS (analogues of Library 3 set 4)	
L5S3S1	**ATTAA**ATGTGAGCA***C***CA
L5S3S2	**ATTAAA**TGTGAGCA***C***CA
L5S3S3	**ATTAAAT**GTGAGCA***C***CA
L5S3S4	**ATTAAATG**TGAGCA***C***CA
L5S3S5	**ATTAAATGT**GAGCA***C***CA

All oligonucleotides in these sets were subjected to the same *in vitro* RNase P and RNase H recruitment assays as described above for the other EGSs. The results for Library 5 set 1 are shown in **Figure 72** (the second repeat of the RNase P gels, and the gels of the RNase H assay are provided in Appendix C). Very little cleavage is observed for all oligonucleotides in this set (including the unmodified RNA comparison) after 1.5 h incubation of the target mRNA with the EGSs and RNase P. This made the calculation of relative cleavage values for RNase P impossible at this time point. After 24 h incubation, the cleavage became more pronounced and it was possible to calculate relative cleavage values (albeit with large errors). These values are shown in the bar graph of **Figure 72**. While most of the oligonucleotides in this set are able to recruit RNase P to some extent, the recruiting ability appears to be much smaller than observed for the *ftsZ*-1032 target studied in the analogous Library 2 set 9. It is possible that the values in this set are less reliable due to the small amount of RNase P induced cleavage observed for the oligonucleotides, including the comparison RNA. In contrast to this, the RNase H recruiting ability of the compounds in this set displayed the expected relationship of increasing cleavage by RNase H upon

lengthening the DNA stretch at the 5' end (**Figure 72**). We can thus conclude that the chemically modified EGSs in this set are able to recruit both RNase P and RNase H towards this target mRNA (*lacZ*-360) as well, although the RNase P recruitment ability was lower than desired.

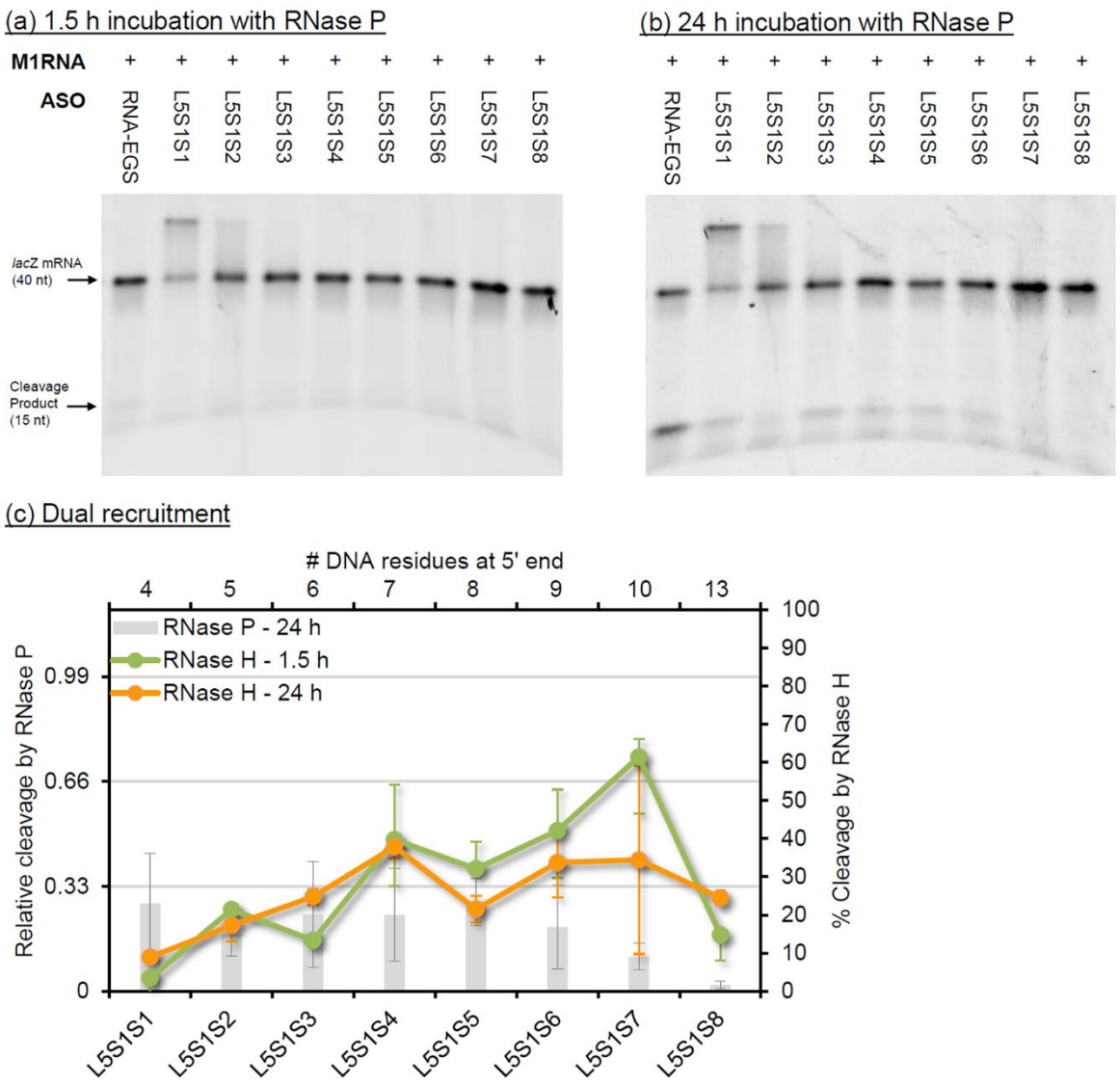

Figure 72. *In vitro* recruitment of RNase P and RNase H by the oligonucleotides in Library 5, set 1. Experiments were conducted as described in the main text. RNA-EGS refers to L4S3S3. (a) Urea PAGE gel after 1.5 h incubation of the target mRNA with ASO and M1 RNA. (b) Urea PAGE gel after 24 h incubation of the target mRNA with ASO and M1 RNA. (c) Plot of the relative cleavage by RNase P and % cleavage by RNase H recruited by the various oligonucleotides. All data is the average of two repeats with error bars representing standard deviations.

The results for Library 5 sets 2 and 3 are comparable to those of Library 5 set 1 and are given in **Figure 73**. Cleavage by RNase P is virtually undetectable after 1.5 h incubation, but can be observed after 24 h incubation. The RNase P recruitment ability is thus lower than expected, presumably because the original unmodified RNA-EGS also had relatively low RNase P recruitment activity. However, as these oligonucleotides all have a high DNA content, they are all able to

recruit RNase H. Their RNase H recruiting ability is comparable to that of the analogous compounds targeting *ftsZ* 1032 in Library 2 set 10 and Library 3 set 4.

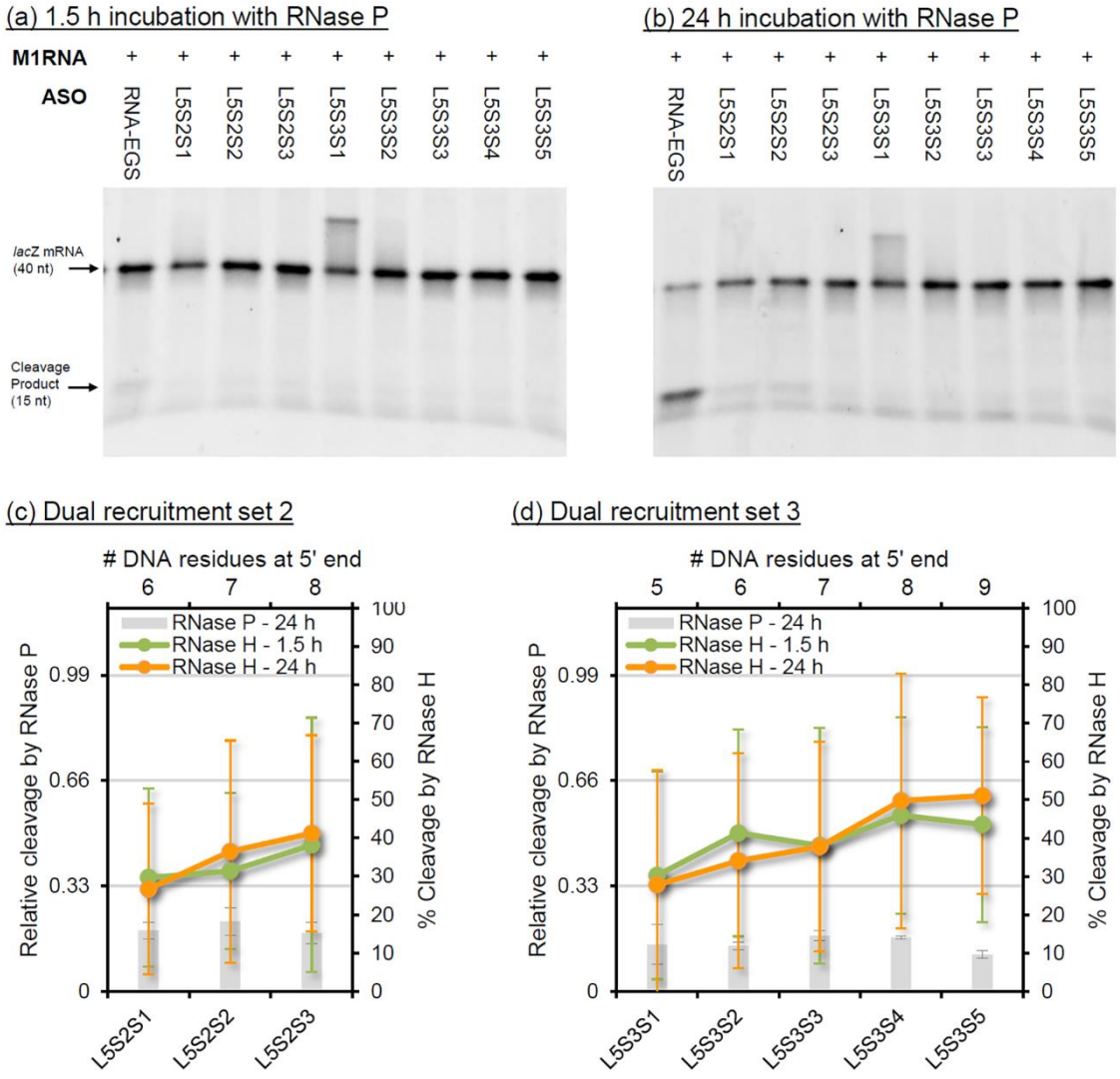

Figure 73. *In vitro* recruitment of RNase P and RNase H by the oligonucleotides in Library 5, set 2 and set 3. Experiments were conducted as described in the main text. RNA-EGS refers to L4S3S3. (a) Urea PAGE gel after 1.5 h incubation of the target mRNA with ASO and M1 RNA. (b) Urea PAGE gel after 24 h incubation of the target mRNA with ASO and M1 RNA. (c+d) Plot of the relative cleavage by RNase P and % cleavage by RNase H recruited by the various oligonucleotides. All data is the average of two repeats with error bars representing standard deviations.

4.2.3.2.1 Chemically modified EGSs targeting ftsZ-UTR and lacZ-UTR

From the previous section it was clear that the relatively low activity of the parent compound, *lacZ*-360, might make it hard to explore the activity of its chemically modified analogues, and thus the sequence generality of our approach. We therefore tried an additional set of chemically modified EGSs, but targeting the untranslated region of *ftsZ* and *lacZ*. This set is the chemically modified analogues of L4S1S3 (*ftsZ*-UTR) and L4S2S2 (*lacZ*-UTR), Although these two compounds

showed lower RNase P recruitment ability than L4S3S3 targeting *lacZ*-360, we still wanted to see whether they might be better suited for the introduction of chemical modifications. The oligonucleotides in this set have the configuration of the most promising DNA/LNA chimeras of Library 2 set 9. **Table 26** shows the names, sequences and targets of the oligonucleotides in this set.

Table 26. Sequences, naming and target region of the oligonucleotides of Library 5, set 4. Bold and underlined represent DNA, not bolded or underlined are LNA.

Name	Sequence	Target region
L5S4S1	**TGGTTCA**AACATAACC**A**	*ftsZ*-UTR
L5S4S2	**TGGTTCAA**ACATAACC**A**	*ftsZ*-UTR
L5S4S3	**TCATAGC**TGTTTCACC**A**	*lacZ*-UTR
L5S4S4	**TCATAGCT**GTTTCACC**A**	*lacZ*-UTR

The oligonucleotides in this set were subjected to the same *in vitro* RNase P and RNase H recruitment assays described above, and the results are shown in **Figure 74** (the second repeats are provided in Appendix C). None of the chemically modified EGSs showed measurable cleavage by RNase P. Even the unmodified RNA analogous displayed little cleavage (~4% after 1.5 h and ~20% after 24 h incubation). We can therefore not draw any conclusions regarding the RNase P recruitment ability of these chemical modifications. Due to the high DNA content of these sequences, the compounds in this set retained their ability to recruit RNase H (see **Figure 74**). In conclusion, the results obtained for Library 5 sets 1-3 indicated that the chemically modified EGS are able to recruit both RNase P and RNase H to different mRNA targets as well (*lacZ*-360). However, the low activity observed for these compounds, as well as the compounds in Library 5 set 4, demonstrate the difficulty in identifying a region of the targeted mRNA that is amenable towards robust RNA cleavage through EGS technology.

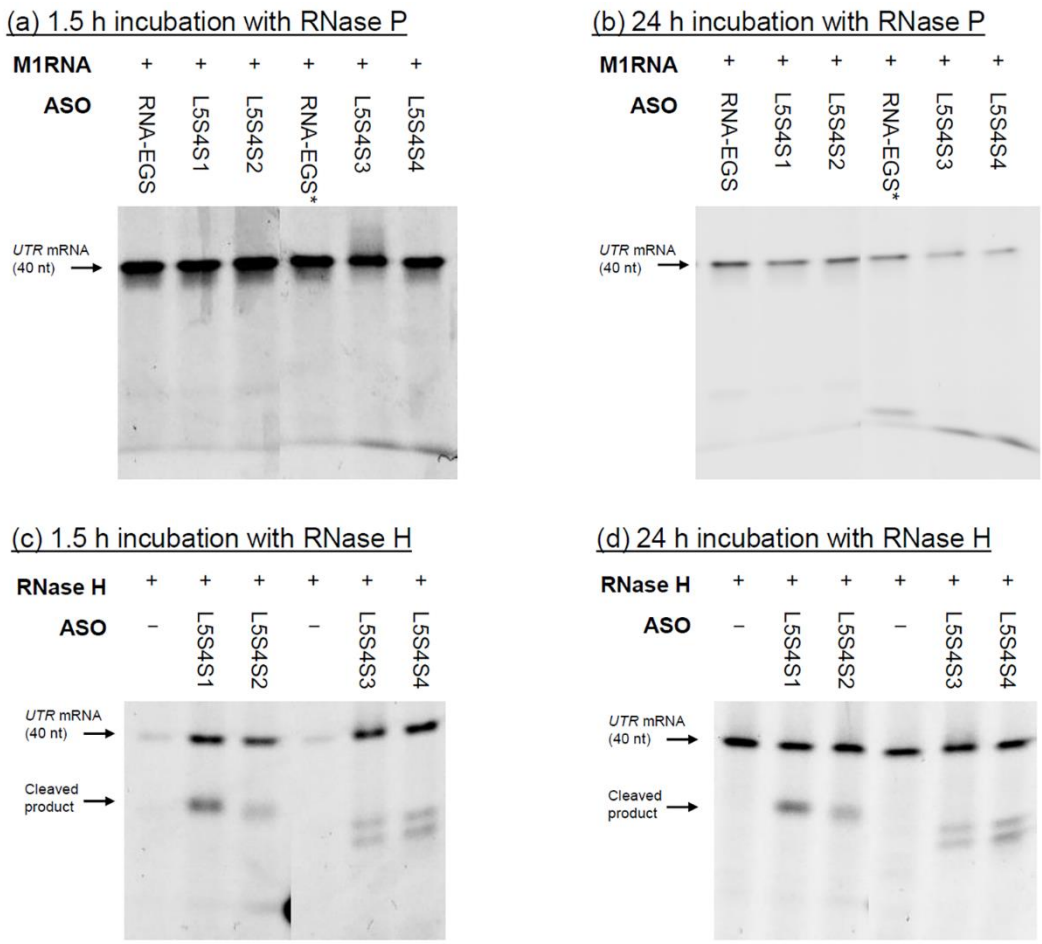

Figure 74. *In vitro* recruitment of RNase P and RNase H by the oligonucleotides in Library 5, set 4. Experiments were conducted as described in the main text. RNA-EGS refers to L4S1S3 and RNA-EGS* refers to L4S2S2. (a) Urea PAGE gel after 1.5 h incubation of the target mRNA with ASO and M1 RNA. (b) Urea PAGE gel after 24 h incubation of the target mRNA with ASO and M1 RNA. (c) Urea PAGE gel after 1.5 h incubation of the target mRNA with ASO and RNase H. (d) Urea PAGE gel after 24 h incubation of the target mRNA with ASO and RNase H.

4.2.4 Bacterial assays

Following the promising *in vitro* results, we decided to test the anti-*ftsZ* gene silencing ability of the best oligonucleotides in *E. coli* AS19. In Chapter 3 it became clear that the best way to do this is to look for the elongation phenotype indicative of *ftsZ* silencing using a microscope. Thus, *E. coli* AS19 cultures at 10^5 cfu/mL were prepared as a working solution. The oligonucleotides were added to 100 µL of the bacterial culture solution to achieve a final concentration of 100 µM concentration. The mixture was subsequently incubated at 37°C for 200 min whilst shaking. 10 µL of the bacterial culture was then transferred onto an adhesive microscope slide, flame-dried and rinsed carefully with 100 µL sterile ultra-pure water. After drying, the samples were visualized in brightfield mode on a Leica DMi8 inverted microscope with 20x and 40x objectives. The contrast

of the images was digitally enhanced using *ImageJ*.[290] The 200 min incubation time was chosen because our previous work (see Chapter 3) indicated that this is the best time point to see the elongation phenotype (at longer incubation times the *E. coli* cells that were not affected by the oligonucleotide start to outnumber the affected by the oligonucleotide elongated *E. coli* cells). Full experimental details are given in Chapter 6.

We tested 12 oligonucleotides in total, and also performed a blank experiment where no oligonucleotide was added. The results using a 20x objective are given in **Figure 75**-**Figure 78** (images obtained at 40x are shown in Appendix C). Two compounds were included as negative controls: L2S1S1 and L5S1S2. The first control, L2S1S1, is a LNA/OMe chimera that failed to induce significant cleavage of *ftsZ* mRNA in the *in vitro* RNase P assay (relative cleavage value of 0.15 after 1.5 h incubation). Furthermore, this sequence contains no DNA residues and will therefore be unable to recruit RNase H. The second control, L5S1S2, was originally designed to target the *lacZ* gene (see section 4.2.3.2.1) and should therefore not induce elongation of the bacteria. Comparison of **Figure 75b** (L2S1S1) and **Figure 75c** (L5S1S2) with the untreated *E. coli* AS19 cells (**Figure 75a**), indicates that these compounds behaved as expected. Only small, healthy *E. coli* cells were observed that did not show the elongation phenotype. In addition to these two negative controls, we also tested the *ftsZ* silencing ability of L5S4S1 in *E. coli* AS19. This sequence was designed to target *fts*Z mRNA at the UTR region (as opposed to region 1032-1041 for most other oligonucleotides). While L5S4S1 showed little RNase P recruiting activity *in vitro* (section 4.2.3.2.1), it did display RNase H recruiting ability and can also inhibit gene expression as a steric blocker (because it targets the translation initiation site). As shown in **Figure 75d**, this oligonucleotide was able to silence the *ftsZ* gene in bacteria, leading to the observed elongation phenotype.

For the active compounds, we focused on those sequences that had shown efficient dual recruitment activity for RNase P and RNase H in section 4.2.2. These include three DNA/LNA chimeras with 3'-DNA (L2S8S3, L2S9S3 and L2S9S4), three DNA/LNA chimeras with 3'-LNA (L2S10S4, L2S10S5 and L2S10S6), one DNA/LNA/RNA chimera (L3S5S2) and two DNA/LNA/OMe chimeras (L3S2S7 and L3S2S8). **Figure 76-Figure 78** show the elongation phenotype for most of the tested oligonucleotides. This extreme elongation is the typical result of successful cleavage of the mRNA strand of the division gene *fts*Z.[248, 292, 293] This implies that the sequences that functioned as dual recruiters *in vitro* were also able to successfully recruit at least one of the cleaving enzymes (RNase P and RNase H), if not both, in *E. coli* cells.

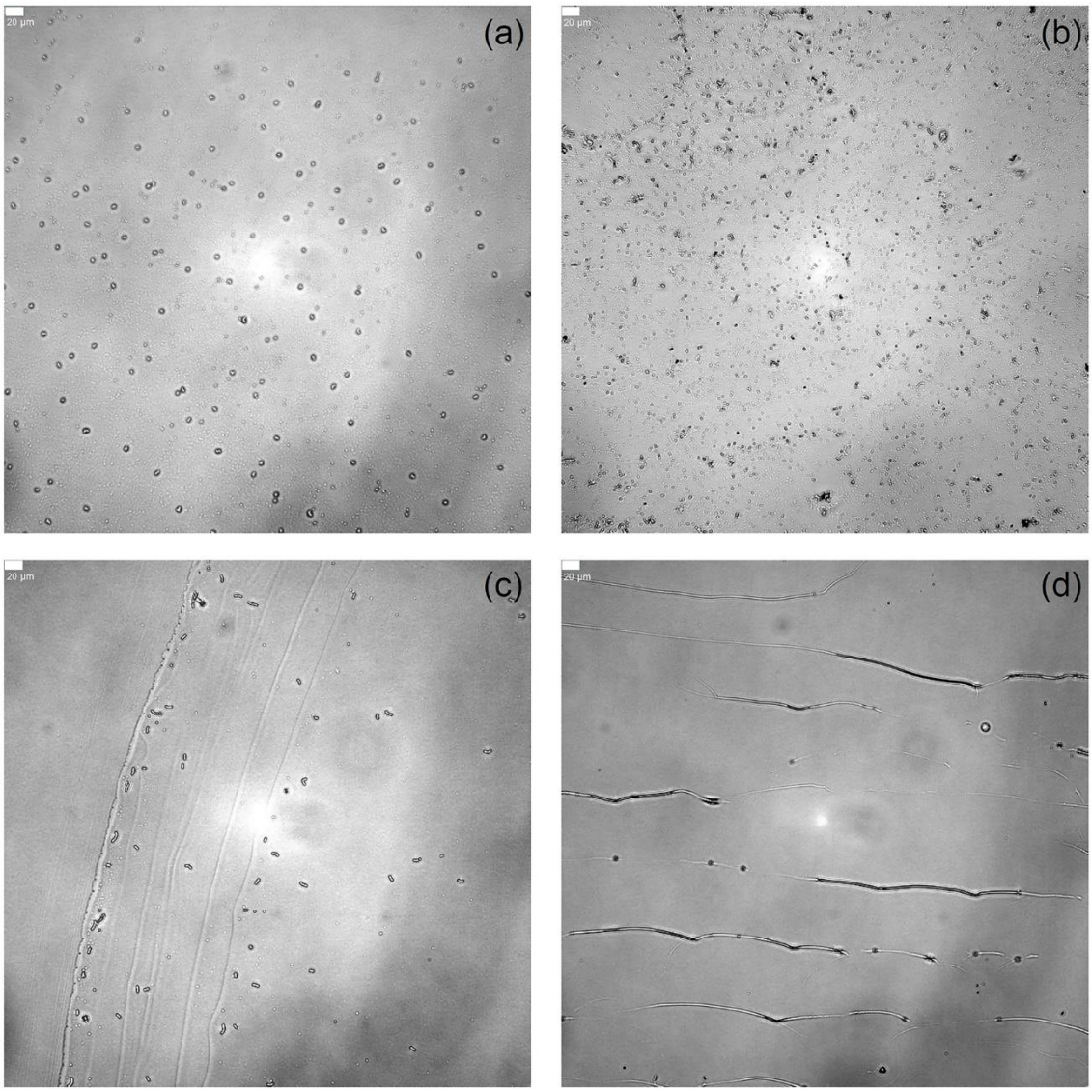

Figure 75. Brightfield images of *E. coli* AS19 incubated for 200 min at 37 °C in the presence of 100 µM oligonucleotides. The experiment was performed as described in the main text. The scale bar represents 20 µm. (a) untreated AS19; (b) low efficiency control L2S1S1; (c) mismatch control L5S1S2; (d) *ftsZ*-UTR targeting L55S4S1

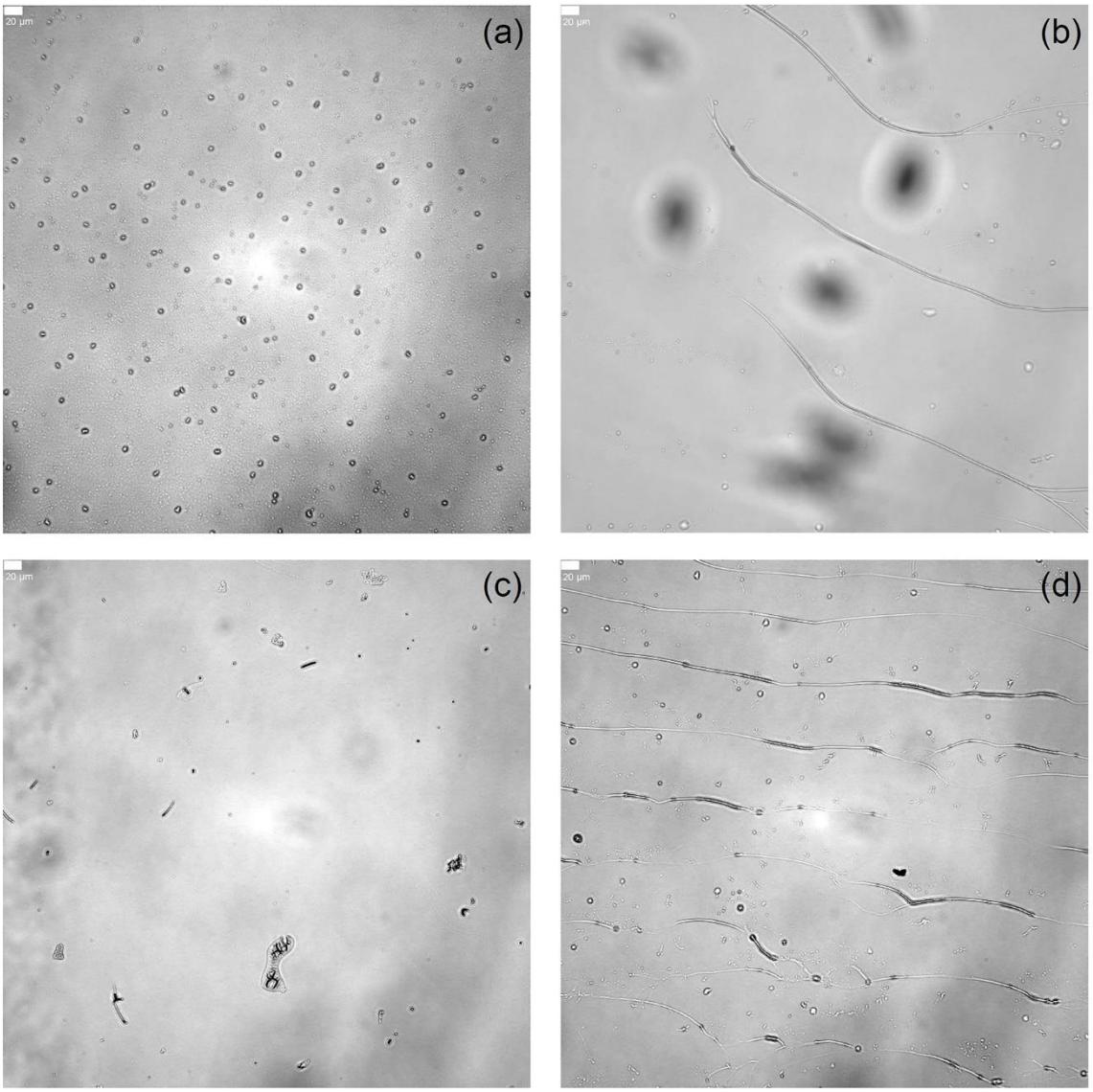

Figure 76. Brightfield images of *E. coli* AS19 incubated for 200 min at 37 °C in the presence of 100 µM oligonucleotides. The experiment was performed as described in the main text. The scale bar represents 20 µm. (a) Untreated AS19; (b) DNA/LNA chimera L2S8S3; (c) DNA/LNA chimera L2S9S3; (d) DNA/LNA chimera L2S9S4.

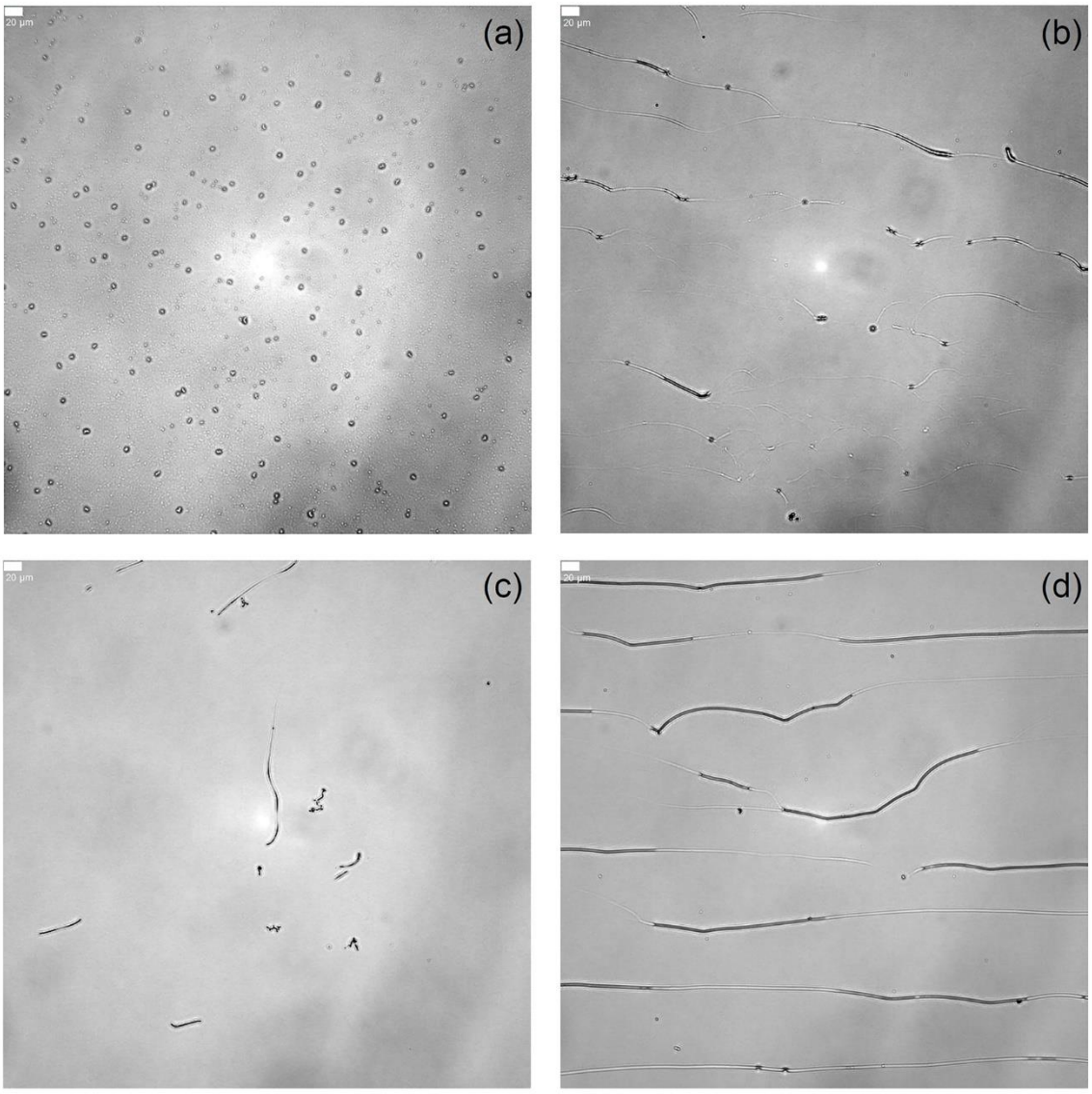

Figure 77. Brightfield images of *E. coli* AS19 incubated for 200 min at 37 °C in the presence of 100 µM oligonucleotides. The experiment was performed as described in the main text. The scale bar represents 20 µm. (a) Untreated AS19, (b) DNA/LNA chimera L2S10S4, (c) DNA/LNA chimera L2S10S5, (d) DNA/LNA chimera L2S10S6.

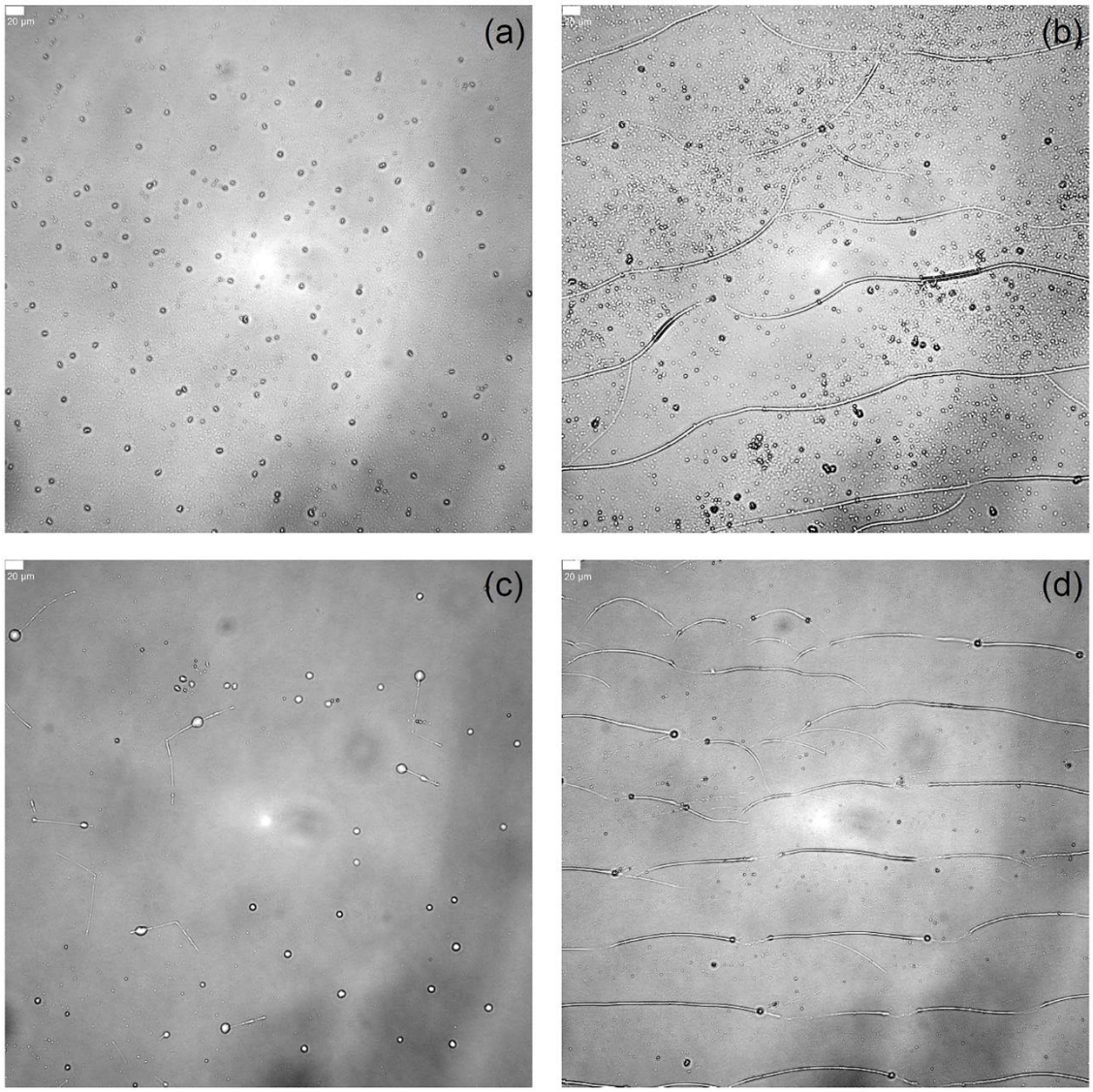

Figure 78. Brightfield images of *E. coli* AS19 incubated for 200 min at 37 °C in the presence of 100 µM oligonucleotides. The experiment was performed as described in the main text. The scale bar represents 20 µm. (a) Untreated AS19; (b) DNA/LNA/RNA chimera L3S5S2; (c) DNA/LNA/OMe chimera L3S2S7; (d) DNA/LNA/OMe chimera L3S2S8.

In conclusion, these bacterial studies have shown a good correlation with the *in vitro* RNase P and RNase H recruitment assays. Those sequences that showed potent activity *in vitro*, also induced the elongation phenotype in bacteria (indicative of successful *ftsZ* silencing). On the other hand, control compounds that did not show activity for RNase P or RNase H recruitment *in vitro*, did not lead to elongation of the bacteria. We can therefore expect that chemically modified oligonucleotides displaying promising results in vitro, particularly when fully chemically modified and thus nuclease-resistant, have the potential for gene silencing in bacteria.

4.3 Conclusions

In this chapter we successfully identified a number of chemical modifications that are compatible with external guide sequence (EGS) technology. This was achieved through an in-depth study of the *in vitro* RNase P recruiting ability of a large number of oligonucleotide libraries. We found that the PS backbone is widely accepted by the ribozyme, and EGS sequences can thus be fully modified with PS. All other modifications investigated (DNA, OMe, MOE, 2'-F and LNA) were only compatible with EGS technology when they are introduced at certain positions. The best results were obtained for various DNA/LNA chimeras. For these chimeras it was discovered that DNA is the most favourable modification at the 5' end, and LNA is the best modification for the rest of the sequence and the EGS tail. One or two LNA residues in the EGS tail can be replaced by OMe, with the best results obtained for OMe in region 3 of the tail. In addition, the residue at the 3' end (region 1 of the EGS tail) can also tolerate DNA.

As DNA appeared well accepted in the EGS sequences, we wanted to see if these compounds could also recruit RNase H. A number of oligonucleotides were identified possessing this dual recruitment ability for RNase P and RNase H, mainly DNA/LNA chimeras. These sequences were studied further for their ability to silence the *ftsZ* gene in bacteria. Microscopy studies showed clear elongation of *E. coli* cells that were incubated with these oligonucleotides, providing evidence that the 'dual recruiters' are also able to exert their gene silencing ability in bacteria. We also tried to expand the dual recruitment approach to other target regions (*ftsZ* untranslated region and various regions of the *lacZ* gene), with little success. This was largely the consequence of the low RNase P recruitment activity of the unmodified RNA-EGS, demonstrating the difficulty in identifying a suitable target region for RNase P recruitment. Testing the generality of the dual recruitment approach therefore remains future work, and will largely depend on the successful identification of a potent mRNA target region.

Chapter 5 Conclusions and Future Work

The overall aim of this thesis was to develop chemically modified antisense oligonucleotides that can function as antibiotics. To achieve this goal, we initially investigated PNA analogues as potential RNase P recruiters in bacteria. While PNAs that sterically block the untranslated region showed effective *ftsZ* and *katG* gene silencing ability in *E. coli*, the PNAs that were designed to recruit RNase P had no activity in bacteria. An *in vitro* assay to determine the RNase P recruitment ability under controlled conditions was therefore optimized. This assay indicated that the PNA backbone is most likely too different from the natural substrate of RNase P and cannot be recognized by this enzyme.

It was thus decided to try to recruit a different enzyme for the cleavage of the target mRNA of chemically modified antisense oligonucleotides, namely RNase H. A series of LNA-DNA-LNA gapmers targeting the *ftsZ* gene in *E. coli* were designed and synthesized and an *in vitro* RNase H recruitment assay showed effective recruitment of the desired enzyme by these ASOs. Microscopy studies confirmed that the gapmers are also able to induce *ftsZ* gene silencing in *E. coli* AS19.

Encouraged by the results with RNase H, we wanted to identify those chemically modified oligonucleotides that can be recognized by RNase P. A systematic screening of the *in vitro* RNase P recruiting ability of various libraries of chemically modified oligonucleotides was therefore performed. A number of oligonucleotides were shown to have RNase P recruiting ability, mainly hybrids of DNA, LNA and to a lesser extent OMe. Due to the high DNA content of the successful hits, the potential dual recruiting of RNase P and RNase H was explored. A number of chemically modified oligonucleotides were identified that can induce *in vitro* cleavage of their target mRNA by both enzymes. Such compounds are expected to have superior gene silencing ability. Microscopy studies confirmed the *in vitro* findings, as we were able to detect elongated *E. coli* cells (indicative of successful *ftsZ* gene silencing) for those compounds that showed potential dual recruitment activity.

The work presented in this thesis has shown a promising technology for the use of chemically modified antisense oligonucleotides as antibiotics, especially when their gene silencing could be enhanced by the recruitment of RNase P, RNase H or both. The chemical modifications can provide improved stability and pharmacokinetics to the ASOs, while the recruitment of the

RNases should increase the efficiency of the ASOs (and thus lower the concentration needed to function as an antibiotic). It must be noted that the work presented in this thesis was performed on *E. coli* strain AS19. This strain is more permeable and allows better uptake of the oligonucleotides into the bacterial cell. The biggest challenge for the development of any oligonucleotide-based therapeutic thus remains their problematic delivery into the target cells or bacteria. Future efforts will have to focus on identifying more efficient ways of delivering oligonucleotides into bacterial cells (e.g., liposome formulations, cationic polymers, different cell penetrating peptides,…).

This thesis focused on the recruitment of RNase P and RNase H. Recent years, however, have seen a boom in the use of CRISPR-Cas technology for gene editing purposes. While most of the research has focused on mammalian cells, the CRISPR system is derived from the immune system of bacteria. We therefore foresee that the CRISPR technology will be employed to battle the antibiotic crisis in the future.

Chapter 6 Materials and Methods

6.1 Synthesis

6.1.1 Materials

Monomers. PNA monomers were purchased from *Link Technologies Ltd*: *N*-(thymin-1-ylacetyl)-*N*-(2-Fmoc-aminoethyl)glycine (Fmoc-PNA-T-OH), *N*-((*N*6-(benhydryloxycarbonyl)aden-9-yl)acetyl)-*N*-(2-Fmoc-aminoethyl)glycine (Fmoc-PNA-A(Bhoc)-OH), *N*-((*N*4-benzhydryloxycarbonyl)cytosine-1-yl)acetyl)-*N*-(2-Fmoc-aminoethyl)glycine (Fmoc-PNA-C(Bhoc)-OH), *N*-((*N*2-(benhydryloxycarbonyl) guan-9-yl)acetyl)-*N*-(2-Fmoc-aminoethyl)glycine (Fmoc-PNA-G(Bhoc)-OH), O-spacer monomer [2-(2-(Fmoc-amino)ethoxy)ethoxy]acetic acid Fmoc-AEEA-OH. Amino acid monomers were obtained from *Sigma Aldrich*: N_{α}-Fmoc-N_{ε}-Boc-L-lysine (Fmoc-Lys(Boc)-OH, *N*-(9-fluorenylmethoxycarbonyl)-L-phenylalanine (Fmoc-Phe-OH). DNA and RNA monomers were purchased from *ChemGenes Corporation:* deoxy adenosine (n-bz) CED phosphoramidite (DNA-A), thymidine CED phosphoramidite (DNA-T), deoxy cytidine (n-acetyl) CED phosphoramidite (DNA-C), deoxy guanosine (N,N-DMF) CED phosphoramidite (DNA-G), 2'-tBDSilyl uridine CED phosphoramidite (RNA-U), 2'-tBDSilyl guanosine (n-ibu) CED phosphoramidite (RNA-G), 2'-tBDSilyl adenosine (n-bz) CED phosphoramidite (RNA-A), 2'-tBDSilyl cytidine (n-acetyl) CED phosphoramidite (RNA-C), LNA monomers were synthesised, purified and characterised by Dr. Vivek Sharma according to literature procedures.[100] All monomers were dried under argon for at least 30 minutes prior to use. The oligonucleotides in Chapter 4 were all synthesized by Pranathi Meda.

Solid supports. Fmoc-PAL-PEG-PS resin (loading 0.17 mmol/g) from *Fisher Scientific* was used during PNA synthesis (**Figure 79**). Fmoc-Lys(Boc)-Wang resin from *Sigma Aldrich* was used for manual peptide synthesis (**Figure 79**). The 1000 Å Unylinker Molecule LCAA CPG was used as the solid support for RNA and LNA-DNA gapmer synthesis (*ChemGenes Corporation*) (**Figure 79**). All solid supports were dried under argon for at least 30 minutes prior to use.

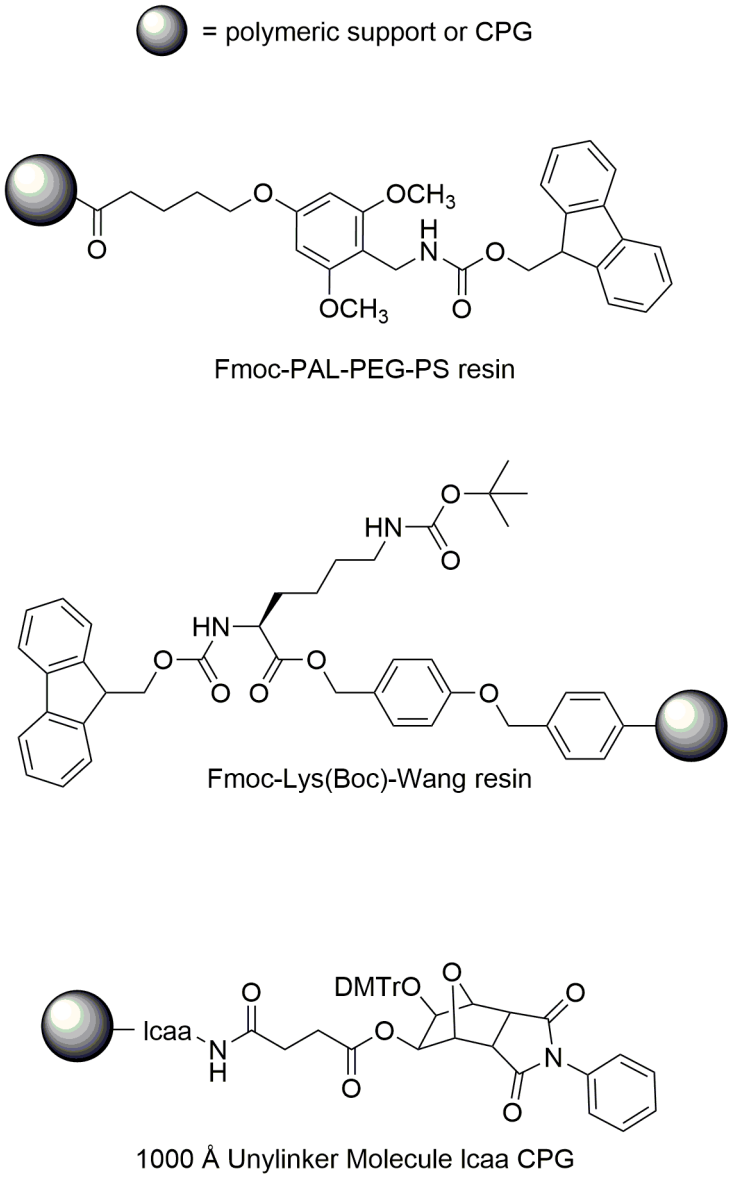

Figure 79. Structure of Fmoc-PAL-PEG-PS resin, Fmoc-Lys(Boc)-Wang resin and the 1000 Å Unylinker Molecule LCAA CPG.

Other Chemicals. DDTT solution (0.10 M), oxidation solution (0.02 M Iodine/Pyridine/H_2O/THF) and CAP B (16% *N*-methylimidazole in THF) were obtained from *ChemGenes Corporation*. CAP A (acetic anhydride/pyridine/THF 1:1:8) and activator solution (0.5 M ETT in acetonitrile) were purchased from *TEDIA High Purity Solvents*. All other reagents/solvents (HATU (1-bis(dimethylamino)methylene]-1H-1,2,3-triazolo[4,5-b]pyridinium 3-oxid hexa-fluorophosphate), DIPEA (*N,N*-diisopropylethyl amine), lutidine, NMP (1-methyl-2-pyrrolidinone), DMF (*N,N*-dimethylformamide), piperidine, Ac_2O (acetic anhydride), TFA (trifluoroacetic acid), *m*-cresol, ammonium hydroxide, ethyl 4-bromobutanoate, sodium azide, EtOAc (ethyl acetate), acetonitrile, $MgSO_4$, DCM (dichloromethane), Et_2O (diethyl ether), hexane, DIC (diisopropylcarbodiimid), HOBt

(hydroxybenzotriazole) and TIS (trisisopropylsilane)) were obtained from *Fisher Scientific*, *Sigma Aldrich*, *VWR* or *Fluorochem* and used without further purification unless stated otherwise. DMF moisture content was determined using a *Mettler Toledo* C20S Compact Coulometric KF Titrator.

Purification and analysis. Purification was performed using an *Agilent* 1260 Infinity HPLC. Purified PNA or DNA/LNA samples were concentrated using a *Savant* SPD111V SpeedVac Concentrator. Mass spectrometry (LC-MS) was performed using an *Agilent* 6530 Accurate Mass Q-TOF LC/MS and data was analysed using the supplied MassHunter Workstation software. Concentrations of stock solutions were determined using a *Thermo Scientific* NanoDrop One microvolume UV-Vis spectrophotometer.

6.1.2 Synthesis of PNAs

PNA monomers, amino acid monomers and the O-spacer were prepared at a concentration of 0.2 mol/L in anhydrous DMF. PNA monomers were activated and coupled using 0.19 M HATU in a mixture of DIPEA, lutidine and NMP in a percentage ratio 49:49:2. The Fmoc de-block solution consisted of 20% piperidine in anhydrous DMF. The capping solution was freshly prepared as a mixture of Ac_2O, DIPEA and DMF in a percentage ratio of 5:6:89 respectively.

12 mg PAL resin was loaded into the cartridge and the PNAs were synthesised on 1 µmol scale using an *Expedite 8900* according to the manufacturer's instructions (**Scheme 2**). At the end of the synthesis cycles, the resin in the columns was dried by flushing with argon for a minimum of 5 min. The PNAs were subsequently cleaved of the resin by vortexing the resin in 1 mL TFA:*m*-cresol (9:1), and then leaving the mixture to rest for 90 min (this step also results in deprotection of the nucleobase Bhoc groups). The resin was removed by filtering the PNA solution in TFA:*m*-cresol twice over 0.45 µm PTFE filters. The PNA solution was then left to dry overnight at room temperature. Dried pellets were observed and diluted in 1 mL milliQ water. Reverse-phase HPLC was performed for purification (Column: C_{18}, 3 µm, 120 Å, 10 mm x 30 mm; Eluent A: 0.1% TFA in milliQ water; Eluent B: 0.08% TFA in acetonitrile; gradients: 0% to 5% B over 3mins, 5% to 20% B over 15 mins, 20% to 95% B over 3 mins; Flow rate: 2 mL/min; Temperature: 60˚C; Detector: 260 nm; Injection volume: 500 µL/injection). The collected fractions were dried on a SpeedVac for 5 h and subsequently diluted in 1 mL milliQ water. PNAs were characterised using LC-MS ESI+ and the concentration of the final PNA solution was determined spectrophotometrically at 260 nm using a NanoDrop device (extinction coefficients were determined according to calculation sheet provided in personal contact from Dr. Richard T. Pon from the University of Calgary, University Core DNA Services; the extinction coefficient values were also confirmed by ATDBio Ltd

publications). Purity was determined by analytical HPLC (HPLC (Column: XSelect CSH C_{18}, 5 µm, 120 Å, 4.6 mm x 150 mm; Eluent A: 0.1% TFA in milliQ water; Eluent B: 0.08% TFA in acetonitrile; gradients: 0% to 5% B over 5mins, 5% to 35% B over 30 mins, 35% to 95% B over 3 mins; Flow rate: 2 mL/min; Temperature: 60˚C; Detector: 260 nm; Injection volume: 10 µL/injection) (see Appendices for HPLC chromatograms).

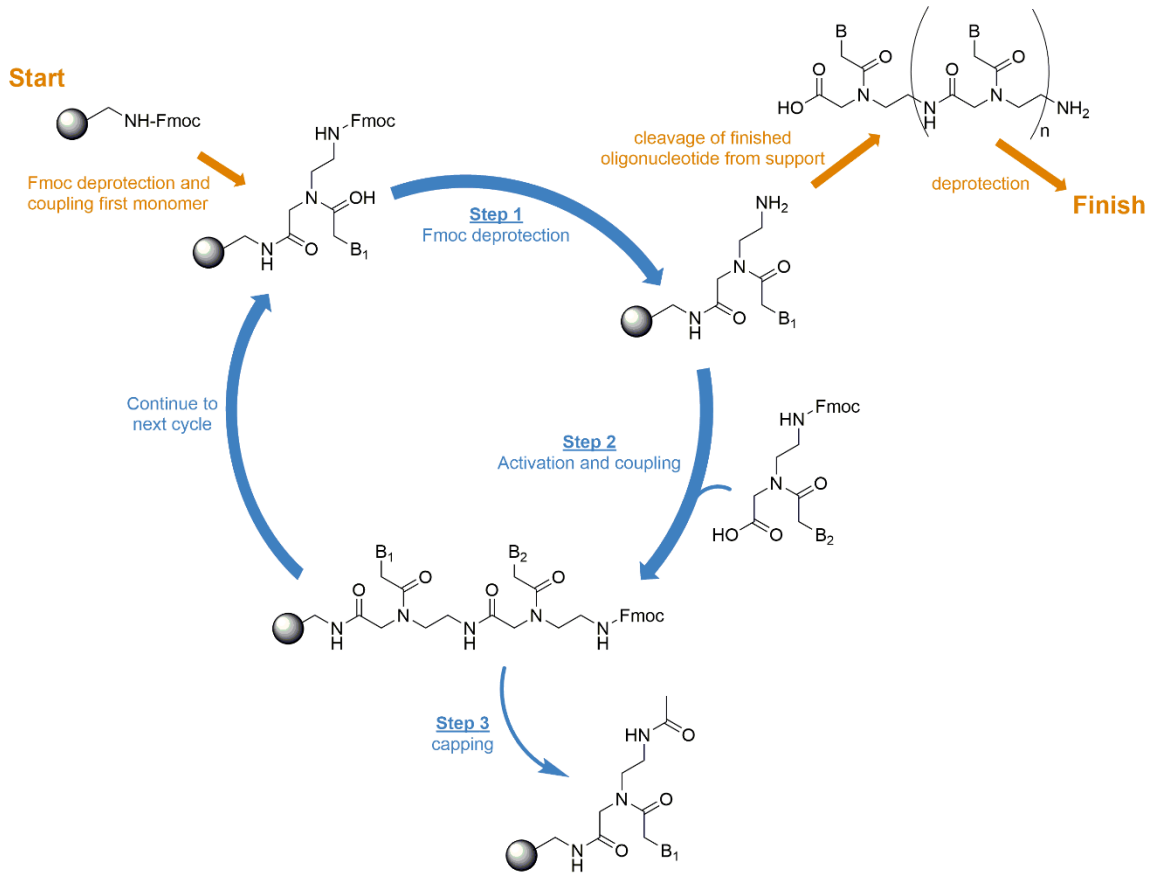

Scheme 2. Expedite PNA synthesis cycle (1 µM scale protocol). The Fmoc deprotection solution consisted of 20% piperidine in anhydrous DMF. PNA monomers were activated and coupled using 0.19 M HATU in a mixture of DIPEA, lutidine and NMP in a percentage ratio 49:49:2. The capping solution was prepared as a mixture of Ac_2O, DIPEA and DMF in a percentage ratio of 5:6:89 respectively

6.1.3 Synthesis of LNA-DNA gapmer and RNA targets

The oligonucleotides were synthesised according to the manufacturer's instructions on a 1 µmol scale using an ABI 394 DNA synthesizer with 1000 Å UnyLinker-functionalised LCAA CPG resin loaded (25 mg CPG per 1-µmol synthesis). Solutions of monomers were prepared at concentrations of 0.15 mol/L in DMF. Phosphoramidite oligonucleotide synthesis proceeds in the 3'- to 5'-direction and one nucleotide is added per synthesis cycle, as shown in **Scheme 3**. For the FAM-labelled target mRNAs, 6-FAM phosphoramidite (*ChemGenes Corporation*) was added as the

last step of the sequence. Detritylation was performed using 3% trichloroacetic acid in dichloromethane. The coupling step used 5-(ethylthio)-1H-tetrazole as activator (0.5 M in acetonitrile). Capping was achieved using a mixture of acetic anhydride, pyridine and THF in a 1:1:8 ratio (Cap A) and 16% *N*-methylimidazole in THF (Cap B). The oxidation step was carried out using either 0.02 M Iodine/Pyridine/H_2O/THF or 0.10 M dimethylamino-methylidene)amino)-3H-1,2,4-dithiazoline-3-thione (DDTT), giving the oligonucleotide phosphodiester or phosphorothioester respectively. At the end of the synthesis cycles, the CPG resin in the cartridge was dried by flushing it with argon for a minimum of 5 min. The oligonucleotides were subsequently cleaved from the CPG solid support and the Unylinker moiety and base protecting groups were removed by vortexing with concentrated ammonium hydroxide and leaving it to rest at room temperature for 48 h. The solid support was removed by centrifugation. The solution was then dried overnight using a SpeedVac at room temperature. The dried pellets were diluted in 1 mL milliQ water and purified using ion exchange HPLC (Column: C_{18}, 3 µm, 120 Å, 10 mm x 30 mm; Eluent A: 0.1% TFA in milliQ water; Eluent B: 0.08% TFA in acetonitrile; gradients: 0% to 5% B over 3mins, 5% to 20% B over 15 mins, 20% to 95% B over 3 mins; Flow rate: 2 mL/min; Temperature: 60˚C; Detector: 260 nm; Injection volume: 500 µL/injection). The collected fractions were dried on a SpeedVac for 5 h and subsequently diluted in 1 mL milliQ water.

The oligonucleotides were characterised using LC-MS (ESI- mode) and the concentration of the final solutions was determined spectrophotometrically at 260 nm using a NanoDrop device (extinction coefficients were determined according to calculation sheet provided in personal contact from Dr. Richard T. Pon from the University of Calgary, University Core DNA Services, which calculates the total extension coefficients for the oligonucleotides from the extinction coefficients of the monomers); the extinction coefficient values were also confirmed by ATDBio Ltd publications). Purity was determined by analytical HPLC (Column: XBridge C_{18}, 5 µm, 120 Å, 4.6 mm x 150 mm; Eluent A: 0.1M TEAA in milliQ water; Eluent B: 0.1 M TEAA in 20% acetonitrile/milliQ water; gradients: 0% to 30% B over 3mins, 30% to 80% B over 15 mins, 80% to 100% B over 3 mins; Flow rate: 2 mL/min; Temperature: 60˚C; Detector: 260 nm; Injection volume: 10 µL/injection) (see Appendices for HPLC chromatograms).

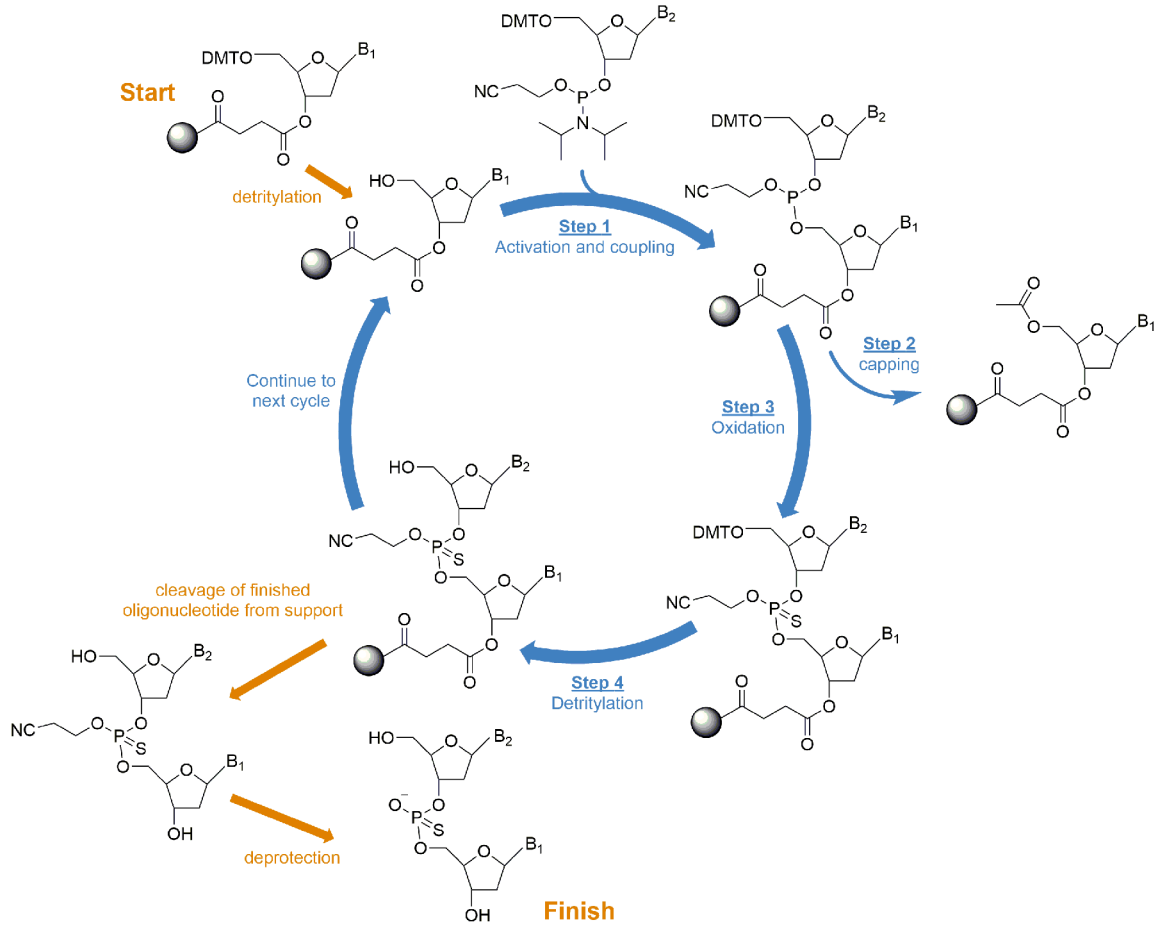

Scheme 3. The phosphoramidite oligonucleotide synthesis cycle, using PS-DNA as an example. Activation and coupling used a 5-(ethylthio)-1H-tetrazole solution, capping was performed using acetic anhydride and *N*-methylimidazole, oxidation using DDTT ((dimethylamino-methylidene)amino)-3H-1,2,4-dithiazoline-3-thione) and detrtiylation using trichloroacetic acid. Cleavage from the resin and nucleobase deprotection was achieved using ammonium hydroxide.

6.1.4 $(KFF)_3K$ peptide synthesis

4-Azidobutanoic acid synthesis. 4-Azidobutanoic acid was synthesized according to a literature procedure[301] (see **Scheme 4**). Ethyl 4-bromobutanoate (2.86 mL, 2 mmol, 1 eq) and sodium azide (650.1 mg, 10 mmol, 5 eq) were dissolved in DMF (10 mL) and the mixture was stirred at 77 ˚C for 30 h. The reaction mixture was subsequently diluted in 200 mL ethyl acetate and washed with DI water (2 x 100 mL) and brine (100 mL). The organic phase was dried with $MgSO_4$, filtered and concentrated to dryness. The obtained ethyl 4-azidobutanoate was then hydrolysed at room temperature using an aqueous solution of sodium hydroxide (1 M, 20 mL). The reaction was monitored by TLC (1:1, hexane:EtOAc, vanillin stain) until completion. The formed sodium 4-azidobutanoate was protonated using a solution of hydrochloric acid until the pH = 3. The formed 4-azidobutanoic acid was then extracted using DCM, after which the solvent was removed under reduced pressure. ^{1}H NMR was in agreement with the published spectra (**Figure 80**)[301]. ^{1}H NMR

(400 MHz, $CDCl_3$) δ ppm 1.92 (2H, quintet, *J* = 7 Hz), 2.48 (2H, t, *J* = 7 Hz), 3.38 (2H, t, *J* = 7 Hz), COOH proton was not visible.

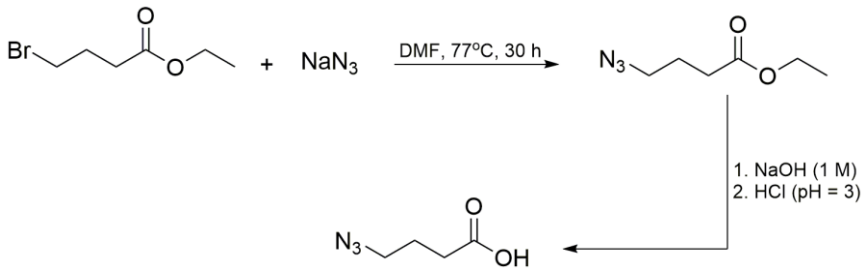

Scheme 4. 4-azido butanoic acid synthesis.

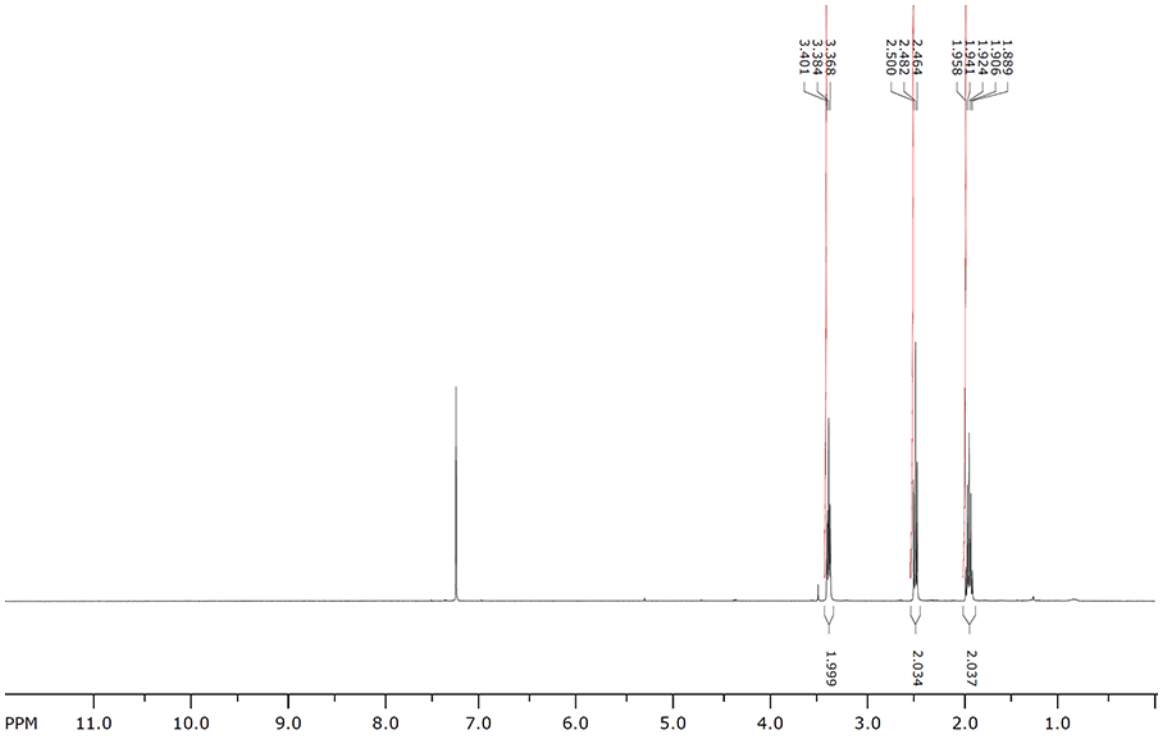

Figure 80. ^{1}H NMR of 4-azidobutanoic acid in $CDCl_3$ at 298 K.

Solid-phase peptide synthesis. Preparation of resin (resin-K): Fmoc-Lys(Boc)-Wang resin (100 mg, 0.4-0.6 mmol/g loading) (*Sigma-Aldrich* #856013) was inserted into a syringe, 1 mL DMF was added and the mixture was shaken using a plate shaker for 20 minutes to swell the resin. Deprotection of the Fmoc group was carried out on-resin by adding 1 mL of 20% piperidine/DMF and shaking the mixture for 30 minutes at 37˚C using a *Boekel Scientific* Incubator Shaker II. The reaction was monitored by subjecting a small amount of resin to a Kaiser test and when the blue

colour indicative of free amines was observed, the reaction was terminated. The resin was then washed 3 times with 3 mL of DMF, DCM and Et_2O respectively.

Kaiser test: The Kaiser test (Ninhydrin test) was prepared in-house using a standard protocol. Bottle A was prepared by mixing 49 mL of pyridine with 1 mL of a solution containing 16.5 mg of KCN in 25 mL distilled water. Bottle B contained 1 g of ninhydrin dissolved in 20 mL *n*-butanol, and bottle C contained 40 g of phenol dissolved in 20 mL of *n*-butanol. A small amount (10-12) of beads of the resin were removed from the reaction and taken to a test tube. A test tube without beads was always run in parallel as reference. A few (2-3) drops of reagents A, B and C were added respectively to the test tubes, and the tubes were heated at 110 °C for 5 minutes. For peptide coupling reactions, a colourless or faint blue colour of the beads and solution indicates complete coupling, a dark blue solution with colourless beads indicates a nearly complete coupling(and requires extending the coupling time or capping unreacted chains), a light blue solution with dark blue beads indicates incomplete coupling and recoupling is required, and a dark blue colour for both solution and beads indicates a failed coupling (which therefore requires that the amino acids and reagents need to be checked and the coupling should be repeated). For Fmoc deprotection reactions, a deep blue colour for both solution and beads is indicative of effective deprotection.

First and second coupling (resin-KF and resin-KFF): A solution of the phenylalanine coupling mixture was prepared by dissolving Fmoc-Phe-OH (116.232 mg, 0.3 mmol, 6 eq), DIC (0.0470 mL, 0.3 mmol, 6 eq) and HOBt (40.536 mg, 0.3 mmol, 6 eq) in 1.5 mL DMF. This mixture was subsequently added to the resin and shaken for 2 hours at room temperature. The reaction was monitored by subjecting a small amount of resin to a Kaiser test and when a yellowish colour indicative of successful coupling was observed, the reaction was terminated. The resin was then washed 3 times with 3 mL of DMF, DCM and Et_2O respectively. The Fmoc groups on the surface of the synthesised peptide were then deprotected using 20% piperidine/DMF until a deep blue colour was observed in the Kaiser test (as described above). The coupling of a second phenylalanine amino acid was performed by repeating the steps described above.

Third coupling (resin-KFFK): A solution of the lysine coupling mixture was prepared by dissolving Fmoc-Lys(Boc)-OH (140.565 mg, 0.3 mmol, 6 eq), DIC (0.0470 mL, 0.3 mmol, 6 eq) and HOBt (40.536 mg, 0.3 mmol, 6 eq) in 1.5 mL DMF. This mixture was added to the resin and shaken for at least 2 h at room temperature until a yellow colour was observed in the Kaiser test (as described above) and the resin was washed 3 times with 3 mL of DMF, DCM and Et_2O respectively. The Fmoc groups on the surface of the synthesised peptide were then deprotected using 20% piperidine/DMF as described above.

Fourth to tenth coupling (resin-KFFKFFKFFK): During the addition of the fourth amino acid, it was noted that the coupling was not as successful as the previous steps (based on the Kaiser test). The coupling reagents (DIC+HOBt) in all of the later coupling steps were therefore replaced by a solution of HATU (114.072 mg, 0.3 mmol, 6 eq) and DIPEA (52.26 µL, 0.3 mmol, 6 eq). Thus, for each coupling step a solution of the Fmoc-protected amino acid in DMF (0.3 mmol, 6 eq) and a solution of HATU and DIPEA in DMF (0.3 mmol, 6 eq) were added to the resin at a total volume of 1.5 mL DMF. The resin was subsequently shaken at room temperature until a yellow colour was observed in the Kaiser test (as described above). At the end of each coupling step, the resin was washed 3 times with 3 mL of DMF, DCM and Et_2O respectively. After each coupling step, the Fmoc groups on the surface of the synthesised peptide were deprotected using 20% piperidine/DMF until a deep blue colour was observed in the Kaiser test (as described above). When the full peptide was synthesized (resin-KFFKFFKFFK), the final Fmoc group was also removed according to the above methods.

Azide modification (resin-KFFKFFKFFK-N_3): A solution of the azide coupling mixture was prepared by dissolving 4-azidobutanoic acid (38.74 mg, 0.3 mmol, 6 eq), HATU (114.07 mg, 0.3 mmol, 6 eq) and DIPEA (52.26 µL, 0.3 mmol, 6 eq) in 1.5 mL DMF. This mixture was added to the resin and shaken for at least two hours at room temperature until a yellow colour was observed in the Kaiser test (as described above). The resin was then washed 3 times with 3 mL of DMF, DCM and Et_2O respectively.

Cleavage from the resin: The resin was swollen for three hours in 4 mL of TFA/TIS/H_2O in a ratio 9.5/0.25/0.25. The resin was subsequently dried by vacuum pump and washed with TFA (1x) and DCM (4x). The produced yellowish solution was concentrated on rotary vacuum, and washed using 3 mL DCM (3x), followed by 3 mL methanol (3x). Cold Et_2O (1 mL) was added and the mixture was centrifuged to collect the precipitate. The supernatant was removed and discarded, and the precipitate was washed further with Et_2O (2x). After drying on air, the precipitate was dissolved in water. Reverse-phase HPLC was performed for purification (Column: C_{18}, 3 µm, 120 Å, 10 mm x 30 mm; Eluent A: 0.1% TFA in milliQ water; Eluent B: 0.08% TFA in acetonitrile; gradients: 0% to 5% B over 3 mins, 5% to 20% B over 15 mins, 20% to 95% B over 3 mins; Flow rate: 2 mL/min; Temperature: 60 ˚C; Detector: 260 nm; Injection volume: 500 µL/injection). The collected fractions were dried on a SpeedVac for 5 hours and subsequently diluted in 1 mL milliQ water.

Characterization: The peptide was characterized by mass spectrometry on a LC-MS ESI+, expected *m/z* 1524.88 (found *m/z* = 1524.84). The concentration of the stock solution was determined by UV spectroscopy at 260 nm, using the extinction coefficient for phenylalanine is (195 cm^{-1} M^{-1})[302]so that for the peptide KFFKFFKFFK the extinction coefficient is 1170 cm^{-1} M^{-1}. Purity was

determined to be 83% by analytical HPLC (Column: XSelect CSH C_{18}, 5 µm, 120 Å, 4.6 mm x 150 mm; Eluent A: 0.1% TFA in milliQ water; Eluent B: 0.08% TFA in acetonitrile; gradients: 0% to 5% B over 5 mins, 5% to 35% B over 30 mins, 35% to 95% B over 3 mins; Flow rate: 2 mL/min; Temperature: 60˚C; Detector: 260 nm; Injection volume: 10 µL/injection)) (see Appendix B for HPLC chromatograms).

6.2 Bacterial studies

6.2.1 Materials

E. coli strains ATCC 25922 and AS19 were a kind gift from Dr. Liam Good[254]. *E. coli* strains BW25113 (CGSC#7636), JW1638-1 (CGSC#9395), JW3914-1 (CGSC#10827), SM101 (CGSC#7255) and SM105 (CGSC#7256) were purchased from the *E. coli* Genetic Stock Center at Yale University. All bacterial strains were converted to glycerol stocks and stored at -80˚C. The glycerol used for bacterial stocks was purchased from *Fisher Scientific* (catalogue #BP229-1) and passed through a PTFE membrane filter (pore size of 0.45 µm, and diameter of 25 mm) purchased from *Fisher Scientific* (catalogue #50-104-9907) prior to use. Bacterial cultures were grown in Luria Bertani Broth (LB) (powder purchased from *Sigma-Aldrich*, catalogue #L3522) or Mueller Hinton Broth (MH) (powder purchased from *Sigma-Aldrich*, catalogue #70192). Counting plates used freshly prepared Luria Bertani Agar (LBA) (powder purchased from *Sigma-Aldrich*, catalogue #L2897) or Muller Hinton Agar (MHA) (powder purchased from *Thermo Scientific,* catalogue #R454082). The agar plates were prepared in sterile disposable petri dishes, 100 x 15 mm, purchased from *Fisher Scientific*. 3% Hydrogen peroxide (H_2O_2) was purchased from *Fisher Scientific* and titrated before each use in order to establish the correct concentration. Bacterial assays were performed in sterile clear polystyrene flat bottom *Corning* Costar 96-well plates. During the assays, the 96-well plates were covered with a medical grade polyurethane BreatheEasy sealing membrane. Optical density was measured using a *Thermo Scientific* MultiSkan FC microplate photometer equipped with a 620 nm filter and incubator. Microscopy studies were performed on a *Leica* DMi8 inverted microscope with 20x and 40x objectives. Adhesive microscopy slides were used (*Thermo scientific* Polylisine precleaned microscope slides) with sterile cover plates (*Leica* Surgipath Premier Cover Glass).

6.2.2 LB and MH broth preparation

Luria Bertani (LB) broth was prepared as directed by the manufacturer. 25 g LB powder was dissolved in 1 L milliQ water, resulting in a solution containing 10 g/L tryptone, 10 g/L NaCl and 5 g/L yeast extract. The LB broth solution was dispensed in 30 mL glass vials capped with screw caps in aliquots of 9 mL. The glass vials were subsequently autoclaved using a wet cycle of 121 °C for 15 minutes. The broth solutions were allowed to cool to room temperature prior to use. Excess broth was stored at room temperature and used within 7 days of preparation.

Mueller Hinton (MH) broth was prepared as directed by the manufacturer. 21 g MH powder was dissolved in 1 L milliQ water, resulting in a solution containing 2 g/L beef infusion solids, 17.5 g/L casein hydrolysate and 1.5 g/L starch. The MH broth solution was dispensed in 30 mL glass vials capped with screw caps in aliquots of 9 mL. The glass vials were subsequently autoclaved using a wet cycle of 121 °C for 15 minutes. The broth solutions were allowed to cool to room temperature prior to use. Excess broth was stored at room temperature and used within 7 days of preparation.

6.2.3 LB and MH agar plate preparation

Luria Bertani Agar (LBA) was prepared as directed by the manufacturer. 35 g of LBA powder was dissolved in 1 L milliQ water, resulting in a mixture of 10 g/L tryptone, 5 g/L NaCl, 5 g/L yeast extract and 15 g/L agar. The medium was sterilized by autoclaving in a wet cycle of 121 °C for 15 minutes. After autoclaving, the LB agar solution was placed in a water bath set at 60 °C. When the agar cooled to a temperature in the range of 40-50 °C, it was plated aseptically in sterile 100 x 15 mm petri dishes at about 10 mL/plate. Sterile lids were placed onto the petri dishes and the agar was allowed to solidify. The plates were used after they cooled down to room temperature. Excess plates were stored in a fridge (4 °C) and used within 7 days of preparation. When agar plates from the fridge were used, they were allowed to equilibrate to room temperature prior to use.

Mueller Hinton Agar (MHA) was prepared as directed by the manufacturer. 38 g of MHA powder was dissolved in 1 L milliQ water, resulting in a mixture of 17.5 g/L acid digest of casein, 2 g/L beef extract, 1.5 g/L starch and 17 g/L agar. The medium was sterilized by autoclaving in a wet cycle of 121 °C for 15 minutes. After autoclaving, the MH agar solution was placed in a water bath set at 60 °C. When the agar cooled to a temperature in the range of 40-50 °C, it was plated aseptically in sterile 100 x 15 mm petri dishes at about 10 mL/plate. Sterile lids were placed onto the petri dishes and the agar was allowed to solidify. The plates were used after they cooled down to room

temperature. Excess plates were stored in a fridge (4 °C) and used within 7 days of preparation. When agar plates from the fridge were used, they were allowed to equilibrate to room temperature prior to use.

6.2.4 Bacterial glycerol stock preparation

Glycerol was diluted in milliQ water in a 1:1 ratio and passed through a PTFE filter with a pore size of 0.45 µm to sterilize the solution. Bacterial cultures were incubated overnight in Luria Bertani (LB) broth at 37 ˚C (except SM101 at 30˚C) using a *New Brunswick* Innova 44 incubator shaker with shaking at 200 rpm. The glycerol stocks were subsequently prepared by diluting 500 µL of the overnight bacterial culture with 500 µL of the sterile, diluted glycerol solution. All glycerol stocks were stored in -80 °C freezers and were kept on ice when removed from the freezer.

6.2.5 Bacterial culture preparation

E.coli strains AS19, ATCC 25922, BW25113, JW1638-1, JW3914-1 SM101 and SM105 were prepared as follows: 10 µL was taken from a glycerol stock using a combo 10/1 µL inoculation loop (*Fisher Scientific*, catalogue #22-170-201) and added to 10 mL LB broth in a 100 mm sterile polypropylene culture tube with dual position snap cap (*Fisher Scientific*, catalogue #22-010-078). The bacterial suspension was incubated overnight at 37 ˚C (except SM101 at 30˚C) using a *New Brunswick* Innova 44 incubator shaker with shaking at 200 rpm. 100 µL from the overnight culture was diluted into 9 mL of MH broth (MH broth has a lighter colour more suitable for measuring optical density) and incubated until OD_{620nm} = 0.1 (approximately 2.5 hours). A series of dilutions (10^{-1}-10^{-7} fold) were prepared in MH broth. Dilution 10^{-3} (corresponding to 10^5 cfu/mL) was taken as the working solution for the bacterial assays. Counting plates were taken from the dilutions 10^{-5} to 10^{-7} and plated on MH agar plates. Counting plates were left in an incubator at 37 ˚C (except SM101 at 30 ˚C) overnight and counted the following day to confirm the concentration of the working solution at 10^5 cfu/mL.

6.2.6 ftsZ silencing assays (optical density)

10 µL of the ASOs (at 10x the final concentration in nuclease-free water (*Ambion*)) were pipetted into a 96-well plate, and 90 µL of the *E. coli* cultures prepared as described above was added. A

breathable membrane was used to seal the 96-wells plate. Bacterial growth was monitored by measuring the optical density at 620 nm (OD_{620nm}) using a MultiSkan FC microplate photometer with incubator set to 37 ˚C. Measurements were taken in normal mode at 30 min intervals using a 620 nm filter, and background shaking was allowed at low speed.

6.2.7 katG silencing assays (optical density)

Hydrogen peroxide titration. Hydrogen peroxide (H_2O_2) was titrated before each use in order to establish the correct concentration. The H_2O_2 titration procedure was adopted from the method by Bakersfield College.[303] A $KMnO_4$ solution was prepared at 0.025 M. 1 mL of the hydrogen peroxide solution (approx. 3 mass%) was dispensed into an Erlenmeyer flask and weighed. 4 mL of 4 M sulfuric acid was added and the solution was titrated with $KMnO_4$ until the purple colour lasts for 15 seconds or more. Every titration was repeated twice. The concentration of H_2O_2 was calculated from the volume of 0.025 M $KMnO_4$ used in the titration and the knowledge that 5 moles of H_2O_2 are consumed per 2 moles of permanganate:

$$2\ \mathrm{MnO_4^-} + 5\ \mathrm{H_2O_2} + 6\ \mathrm{H^+} \rightarrow 2\ \mathrm{Mn^{2+}} + 5\ \mathrm{O_2} + 8\ \mathrm{H_2O}$$

Optical density measurements. 10 µL of the ASOs (at 10x the final concentration in nuclease-free water (*Ambion*)) was pipetted into a 96-well plate, and 80 µL of the *E. coli* cultures prepared as described above was added. A breathable membrane was used to seal the 96-wells plate. The plates were incubated for 2 hours using a MultiSkan FC microplate photometer with incubator set to 37 ˚C and with OD_{620nm} readings taken every 15 min. After 2 hours of premixing, 10 µL of hydrogen peroxide (at 10x the final concentration) was added and bacterial growth was monitored by measuring OD_{620nm} using a MultiSkan FC microplate photometer with incubator set to 37 ˚C. Measurements were taken in normal mode at 30 min intervals using a 620 nm filter, and background shaking was allowed at low speed.

6.2.8 lacZ silencing assays

10 µL of the ASOs (at 10x the final concentration in nuclease-free water (*Ambion*)), 5 µL of IPTG (at 20x the final concentration of 0.1 mM in nuclease-free water (*Ambion*)), 5 µL of X-gal (at 20x the final concentration of 0.2 mg/mL nuclease-free water (*Ambion*)), and 80 µL of the *E. coli* cultures prepared as described above were pipetted into a 96-well plate in that order. A breathable membrane was used to seal the 96-wells plate. The cultures were incubated using a

MultiSkan FC microplate photometer with incubator set to 37 ˚C, and background shaking at low speed. The plate was taken out of the incubator at regular intervals (8, 16, 20, 28 and 32 hours) and a picture was taken for visual inspection using a *CANON* CanoScan LiDE 220 colour image flatbed scanner.

6.2.9 Microscopy assays

E. coli AS19 cultures prepared as described above were transferred into a 96-well plate, and stock solutions of the ASOs were added to achieve a final concentration of 100 µM in a total volume of 100 µL. A breathable membrane was used to seal the 96-well plate. The bacteria were incubated at 37 ˚C using a MultiSkan FC microplate photometer with background shaking at low speed. After 200 minutes, 10 µL of the bacterial culture was transferred onto an adhesive microscope slide (*Thermo scientific* Polylisine precleaned microscope slides), flame-dried and rinsed carefully with 100 µL sterile ultra-pure water (*Ambion*). After drying, the samples were visualized in brightfield mode on a *Leica* DMi8 inverted microscope with 20x and 40x objectives. The contrast of the images was digitally enhanced using *ImageJ*.[290]

6.3 *In vitro* studies

6.3.1 M1 RNA synthesis

PCR. The RNase P components are the C5 protein and the M1 RNA. C5 protein was purchased from *GenScript* but was proven to be contaminated with other RNases. M1 RNA is the RNA component of RNase P and had to be synthesized for the *in vitro* RNase P assays. M1 RNA is encoded by the *rnp*B gene.[230] The sequence of this gene was determined using EcoCyc[256] and used to purchase the DNA template and PCR primers from *Integrated DNA Technologies (IDT)* (sequences of the DNA template and primers are shown in **Figure 81**). The DNA template was amplified using a polymerase chain reaction (PCR). PCR was run by mixing the Q5 Hot Start High-Fidelity Master Mix (M0494S, *New England BioLabs*), 10 µM of each primer and 5 ng DNA template in a total volume of 5 µL. The thermocycling PCR settings were determined using the online *New England BioLabs* T_m Calculator (see **Figure 81** for the recommended settings).[304] The reaction was performed using an *Applied Biosystems* SimpliAmp Thermal Cycler.

(a) Sequence *rnp*B gene and primers

>gnl|ECOLI|EG30069 rnpB "RNPB-RNA" (complement(3270592..3270216)) Escherichia coli K-12 substr. MG1655

GAAGCTGACCAGACAGTCGCCGCTTCGTCGTCGTCCTCTTCGGGGGAGACGGGCGGAG
GGGAGGAAAGTCCGGGCTCCATAGGGCAGGGTGCCAGGTAACGCCTGGGGGGGAAACC
CACGACCAGTGCAACAGAGAGCAAACCGCCGATGGCCCGCGCAAGCGGGATCAGGTAA
GGGTGAAAGGGTGCGGTAAGAGCGCACCGCGCGGCTGGTAACAGTCCGTGGCACGGTA
AACTCCACCCGGAGCAAGGCCAAATAGGGGTTCATAAGGTACGGCCCGTACTGAACCCG
GGTAGGCTGCTTGAGCCAGTGAGCGATTGCTGGCCTAGATGAATGACTGTCCACGACAG
AACCCGGCTTATCGGTCAGTTTCACCT

> Forward primer: 5`-TAATACGACCTCACTATAGGGAA-3`

> Reversed primer: 5`-AGGTGAAACTGACCGATAAG-3`

(b) Recommended PCR settings

Initial denaturation:	30 seconds at 98 °C
25-35 cycles:	step 1 = 5-10 seconds at 98 °C
	step 2 = 10-30 seconds at 45-72 °C
	step 3 = 15-30 seconds at 72 °C
Final extension:	5-10 minutes at 72 °C
Hold:	4-10 °C

(c) PCR result

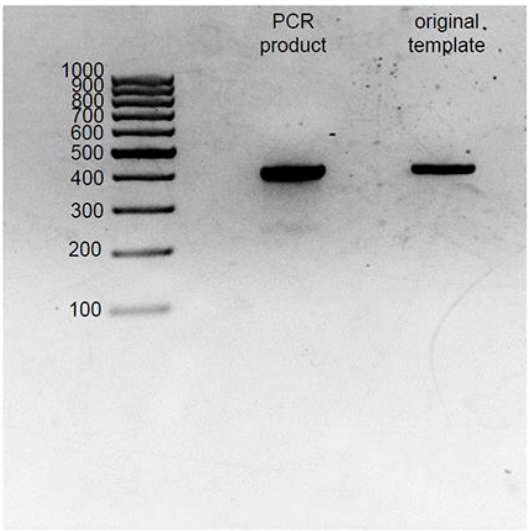

(d) IVT result

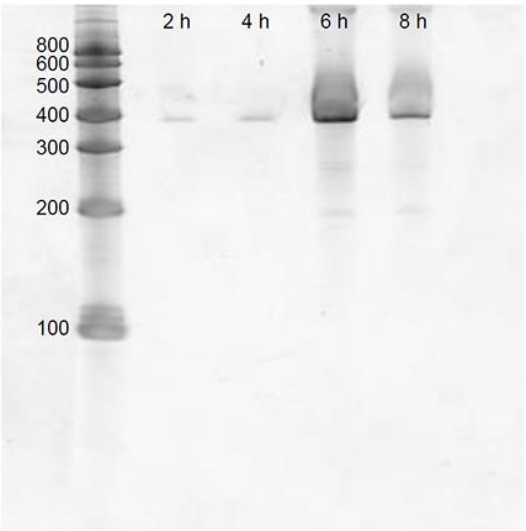

Figure 81. (a) The dsDNA template for M1 RNA as obtained from EcoCyc, as well as the primers used for PCR. (b) Recommended PCR settings calculated using *New England BioLabs* T_m Calculator. (c) 2% agarose gel for the dsDNA template for M1 RNA (SYPRO Orange staining). From left to right: GeneRuler 100 bp DNA Ladder #SM0241, dsDNA template for M1 RNA 50 ng PCR product, and 20 ng original DNA template purchased from IDT. (d) 6% TBE-urea gel for M1 RNA produced by IVT kit #K0441 (SYPRO Orange staining). From left to right: RiboLadder™ 100 bp RNA Standard, 2 h, 4 h, 6 h and 8 h IVT reaction times.

The concentration of the obtained DNA product was determined spectrophotometrically at 260 nm using a NanoDrop device. The purity of the final DNA product was determined by 2% agarose gel electrophoresis. The gel was prepared by dissolving 2 g agarose powder (*Invitrogen* UltraPure Agarose, *Thermo Fisher* catalogue #16500500) in 100 mL milliQ water. The agarose solution was then heated at full power by microwave for 1 minute, followed by heating for another minute whilst avoiding overboiling. 10 µL of a 10 mg/mL ethidium bromide solution (*Sigma-Aldrich*, catalogue #E1510) was added and the gel was casted using a *Thermo Scientific* Owl EasyCast B2 Mini Gel Electrophoresis Systems. 10 µL of the DNA product sample was combined with 2 µL of 6x TriTrack DNA Loading Dye (*Thermo Scientific* catalogue #R1161) and the obtained mixture was loaded into one of the wells of the freshly prepared agarose gel. 6 µL of GeneRuler 100 bp DNA Ladder (*Thermo Scientific* catalogue #SM0241) was loaded in a separate well as a reference. The gel was run at 90 V for 1.5 hours using a *Thermo Scientific* Owl EasyCast B2 Mini Gel Electrophoresis Systems and visualised using a GE ImageQuant LAS 4000 biomolecular imager.

IVT. The DNA template was subsequently converted to M1 RNA by *in vitro* transcription (IVT) using TranscriptAid T7 High Yield Transcription Kit #K0441, purchased from *Thermo Scientific*. The IVT reaction was performed according to the manufacturer instructions. All frozen reaction components were thawed, mixed by pipetting up and down and centrifuged briefly to collect all drops. The TranscriptAid Enzyme mix and the nucleotide mix were kept on ice, while the 5x TranscriptAid reaction buffer was kept room temperature. The reaction components were combined at room temperature in the following order: 4 µL 5x TranscriptAid reaction buffer, 8 µL ATP/CTP/GTP/UTP nucleotides mix, 1 µg DNA template, 2 µL TranscriptAid Enzyme mix and a calculated amount of DEPC-treated water to reach a total volume of 20 µL. The combined components were then mixed by pipetting up and down, centrifuged briefly to collect all drops and incubated at 37 °C for 6 hours using an *Applied Biosystems* SimpliAmp Thermal Cycler.

The obtained M1 RNA was purified from the template DNA after the IVT reaction according to the instructions and components of the *in vitro* transcription kit. 2 µL of DNase I (RNase-free) was added to the transcription reaction mixture, and the mixture was incubated for 15 minutes at 37 °C using an *Applied Biosystems* SimpliAmp Thermal Cycler. Subsequently, the DNase I was inactivated by the addition of 2 µL of 0.5 M EDTA (pH 8.0), followed by incubation for 10 minutes at 65 °C using an *Applied Biosystems* SimpliAmp Thermal Cycler. After DNase I digestion, M1 RNA was purified using the *Thermo Scientific* GeneJET RNA Purification Kit #K0731 according to the instructions from the manufacturer. The reaction volume was adjusted to 100 µL with nuclease-free water, 300 µL of Lysis buffer was added and the mixture was mixed by pipetting up and down. The mixture was then transferred to the GeneJET RNA purification column inserted in a

collection tube and centrifuged for 1 minutes at ≥ 12000xg. The collection tube was discarded and the GeneJET RNA purification column was placed into a new 2 mL collection tube. 700 µL of wash buffer 1 was added to the GeneJET RNA purification column and centrifuged for 1 minutes at ≥ 12000xg. The flow-through was discarded and the purification column was placed back into the collection tube. 600 µL of wash buffer 2 was added to the GeneJET RNA purification column and centrifuged for 1 minute at ≥ 12000xg. The flow-through was discarded again and the purification column was placed back into the collection tube. Then, 250 µL of wash buffer 2 was added to the GeneJET RNA purification column and centrifuged for 2 minutes at ≥ 12000xg. The collection tube containing the flow-through was discarded and the purification column was placed into a sterile 1.5 mL RNase-free microcentrifuge tube. 50 µL of nuclease-free water was added to the centre of the GeneJET RNA purification column membrane and centrifuged for 1 minute at ≥ 12000xg to elute the pure M1 RNA. The purification column was discarded, and the RNA was characterized and stored at -20 °C (if used within 24 hours) or -80 °C (for long-term storage). The IVT product (M1 RNA) was characterised by Novex TBE-Urea Gels, 6%, 10 well, run using a *Life Technology-Invitrogen* mini gel tank electrophoresis system. The gel was stained post-run using SYPRO orange by soaking the gel for 2 minutes in 100 mL TBE buffer (Tris-borate-EDTA) containing 10 µL of SYPRO orange dye (*Invitrogen* SYPRO Orange Stain (5,000x concentrate in DMSO)). The gel was washed by soaking in water for 1 minute and visualised using a GE LAS 4000 biomolecular imager with SYPRO gold filer. The concentration of the final M1 RNA product was determined spectrophotometrically at 260 nm using a NanoDrop device. **Figure 81** shows typical gels obtained after PCR (for DNA template amplification) and IVT reactions (to obtain final M1 RNA product).

6.3.2 *In vitro* RNase P assay

2 pmol FAM-labelled target mRNA, 8.8 pmol ASO and 8.8 pmol M1 RNA are mixed in 6 µL buffer (total volume 30 µL) and incubated at 37 °C using an *Applied Biosystems* SimpliAmp Thermal Cycler. At various time points, the reaction was stopped by the addition of gel loading buffer (95% formamide, 1 mM EDTA, pH 8, 0.01% bromophenol blue), which was added to the reaction sample in a 1:1 ratio. The amount of cleavage was investigated by running 14 µL of each reaction on a 15% denaturing urea polyacrylamide gel (*Fisher Scientific*/*Invitrogen*) using a *Life Technology-Invitrogen* mini gel tank electrophoresis system. The gels were visualized through the FAM labelled oligonucleotides using a GE Typhoon FLA 7000 biomolecular imager (FAM filter).

The intensity of the bands corresponding to the cleaved product, the uncleaved target mRNA and the complex of target mRNA and ASO, were determined using *ImageJ*.[290] The percent of target mRNA that was cleaved by M1 RNA was then calculated as follows:

$$\%cleavage = \frac{intensity\ cleaved\ product}{intensity\ (cleaved\ product + target\ mRNA + \ mRNA/EGS\ complex)} \cdot 100\%$$

For reproducibility reasons (e.g., using different batches of M1 RNA), the data was further converted to relative cleavage compared to an unmodified RNA-EGS control:

$$relative\ cleavage = \frac{\%cleavage\ by\ modified\ ASO}{\%cleavage\ by\ unmodified\ RNA - EGS}$$

6.3.3 *In vitro* RNase H assay

In vitro RNase H recruitment ability was investigated using RNase H kit EN0201, purchased from *Thermo Fisher Scientific*. 4 x 10^{-3} units of RNase H, 2 pmol target mRNA, 8.8 pmol oligonucleotide and 3 µL 10x reaction buffer (200 mM Tris-HCl (pH 7.8), 400 mM KCl, 80 mM $MgCl_2$, 10 mM DTT) were mixed and nuclease-free water was added to obtain a final volume of 30 µL. The reaction was run at 37 °C for 24 h. At two different time points (1.5 h and 24 h), a 7 µL sample was withdrawn from the reaction, and 7 µL formamide was added to stop the reaction. The samples were subsequently loaded onto a denaturing 15% urea polyacrylamide gel (*Fisher Scientific*/*Invitrogen*) and the gel was run using a *Life Technology-Invitrogen* mini gel tank electrophoresis system. The gels were visualized through the FAM labelled oligonucleotides using a GE Typhoon FLA 7000 biomolecular imager (FAM filter).

Appendix A Supporting Information for Chapter 2

A.1 HPLC chromatograms of synthesized oligonucleotides

This section provides the analytical HPLC chromatograms for all PNA and RNA oligonucleotides synthesized for Chapter 2 (**Figure A1** - **Figure A21**).

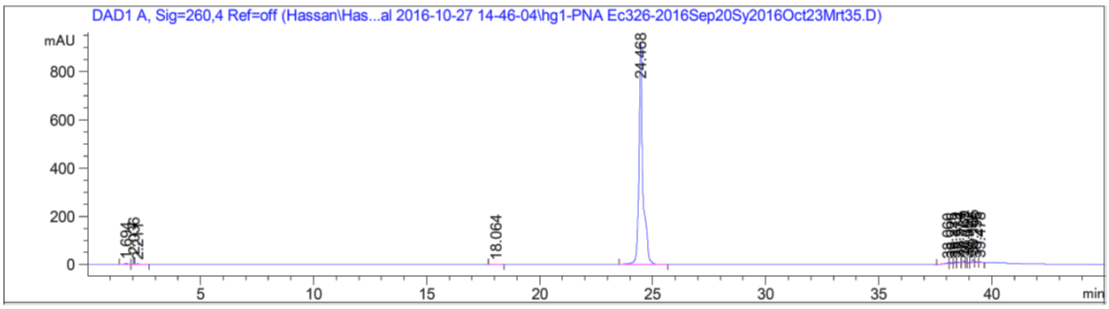

Figure A1. Analytical HPLC of purified PNA-Ec326 (reversed-phase C18, detector at 260 nm). Purity 96.6%.

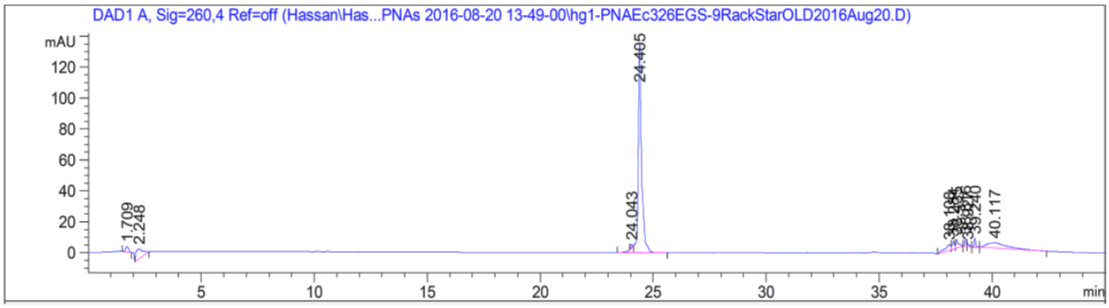

Figure A2. Analytical HPLC of purified PNA-Ec326-EGS (reversed-phase C18, detector at 260 nm). Purity > 90.0%

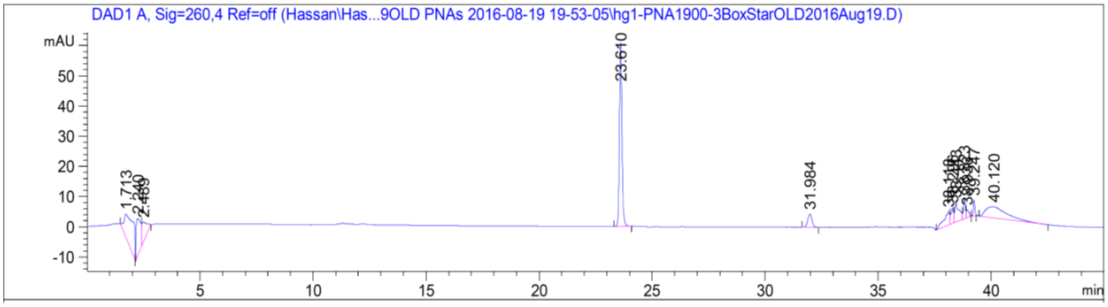

Figure A3. Analytical HPLC of purified PNA-1900 (reversed-phase C18, detector at 260 nm). Purity > 90.0%.

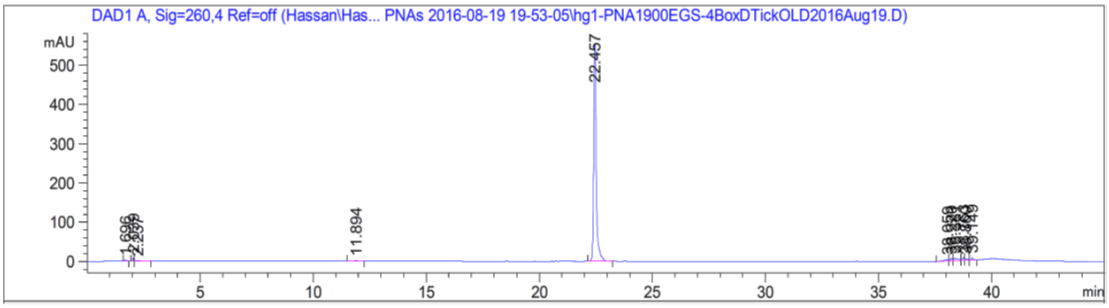

Figure A4. Analytical HPLC of purified PNA-1900-EGS (reversed-phase C18, detector at 260 nm). Purity > 92.3%.

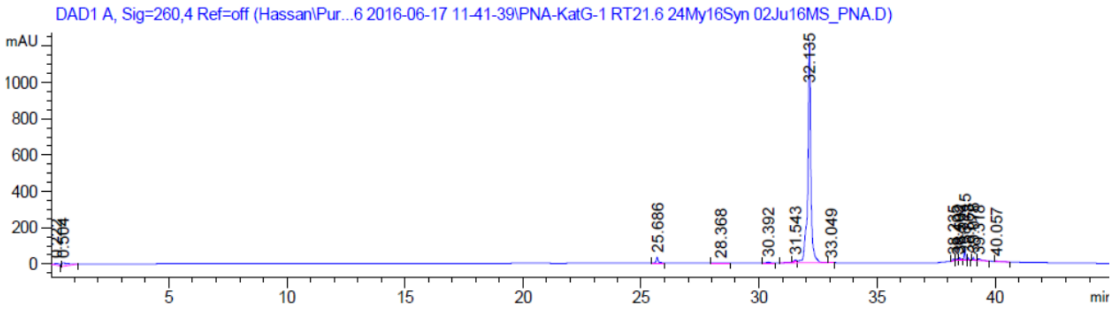

Figure A5. Analytical HPLC of purified PNA-katG1 (reversed-phase C18, detector at 260 nm). Purity > 88.7%.

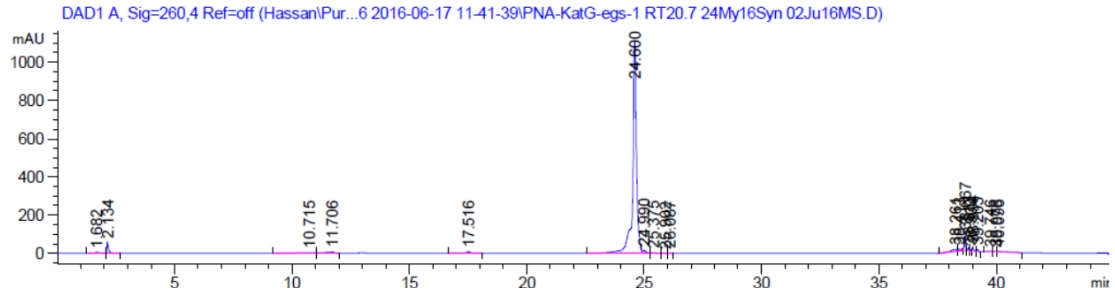

Figure A6. Analytical HPLC of purified PNA-katG1-EGS (reversed-phase C18, detector at 260 nm). Purity > 87.3%.

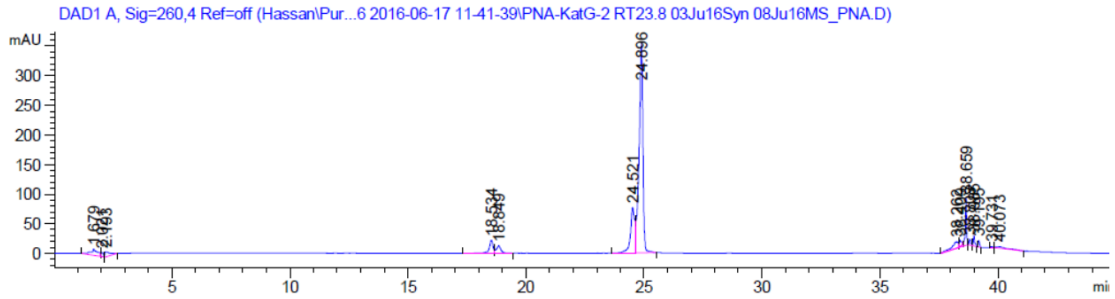

Figure A7. Analytical HPLC of purified PNA-katG2 (reversed-phase C18, detector at 260 nm). Purity > 80.0%.

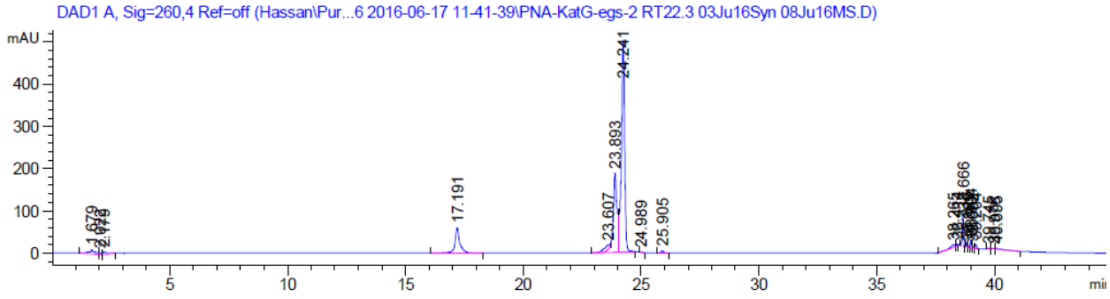

Figure A8. Analytical HPLC of purified PNA-katG2-EGS (reversed-phase C18, detector at 260 nm). Purity > 80.0%.

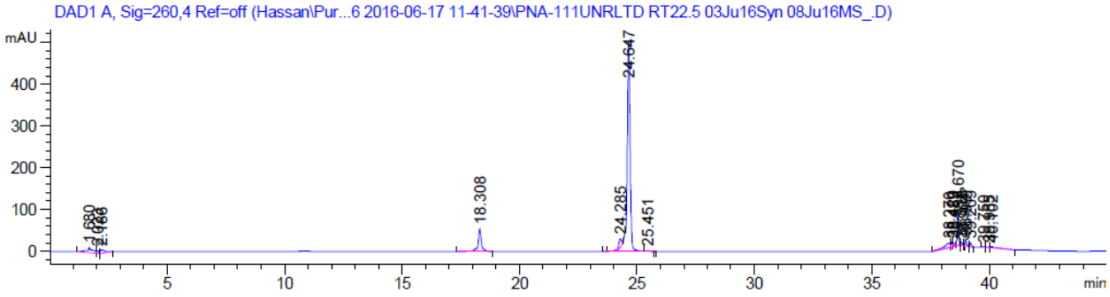

Figure A9. Analytical HPLC of purified PNA-111UNRLTD (reversed-phase C18, detector at 260 nm). Purity > 79.0%.

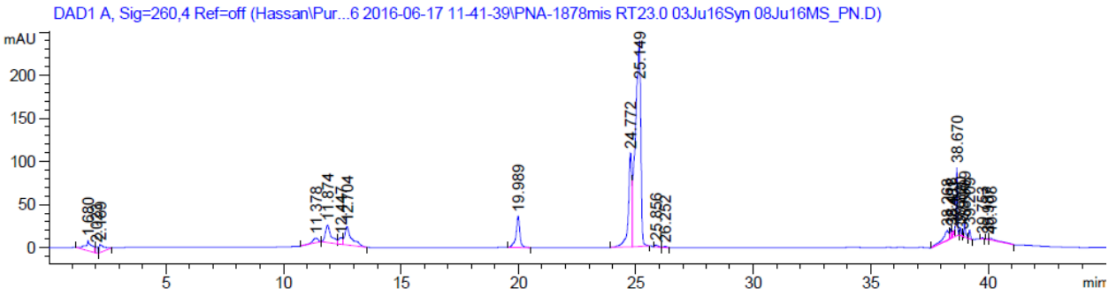

Figure A10. Analytical HPLC of purified PNA-1901 (reversed-phase C18, detector at 260 nm). Purity > 65.0%.

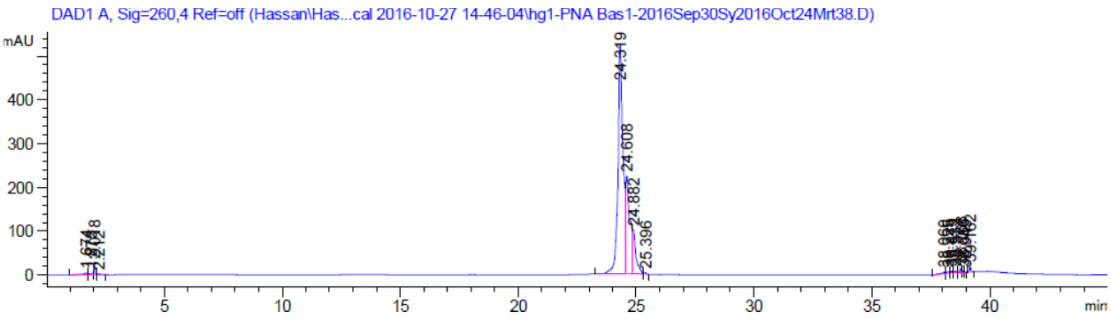

Figure A11. Analytical HPLC of purified PNA-Bas1 (reversed-phase C18, detector at 260 nm). Purity > 88.8%.

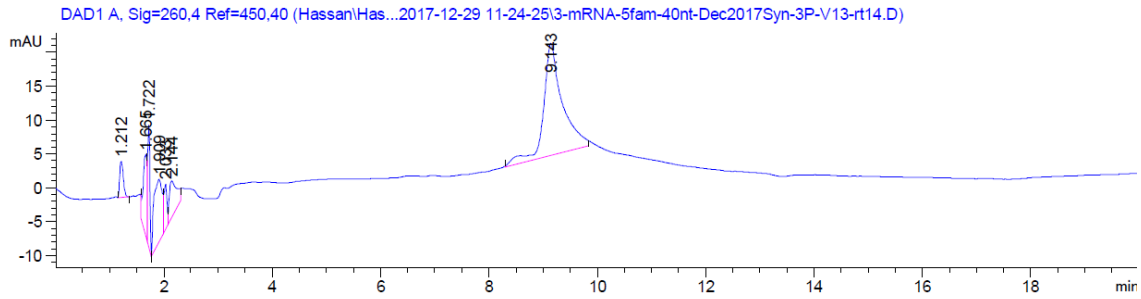

Figure A12. Analytical HPLC of purified ftsZ mRNA (40nt) (reversed-phase C18, detector at 260 nm). Purity 85.0%.

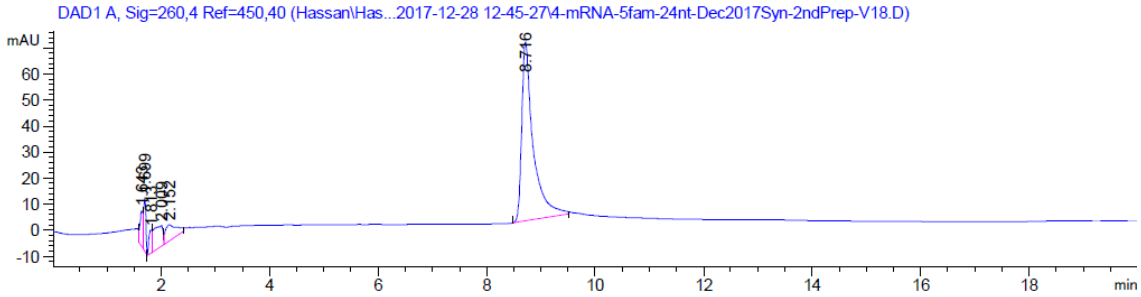

Figure A13. Analytical HPLC of purified cleavage product control (24nt) (reversed-phase C18, detector at 260 nm). Purity > 85.0%.

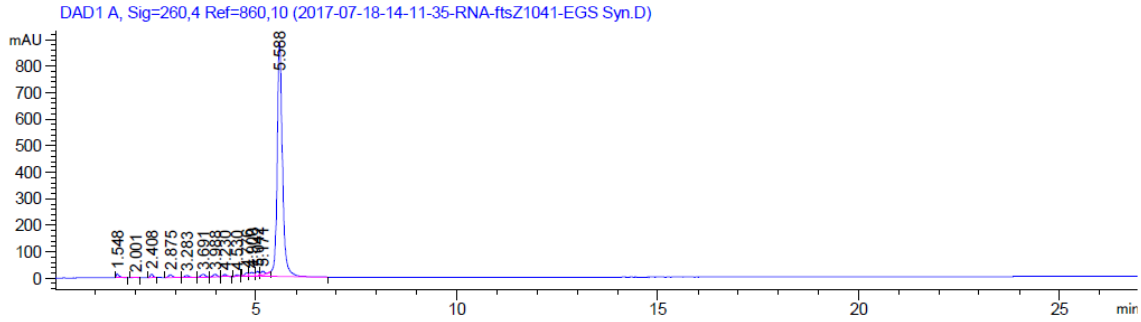

Figure A14. Analytical HPLC of purified RNA-ftsZ1041-EGS (reversed-phase C18, detector at 260 nm). Purity >90.0%.

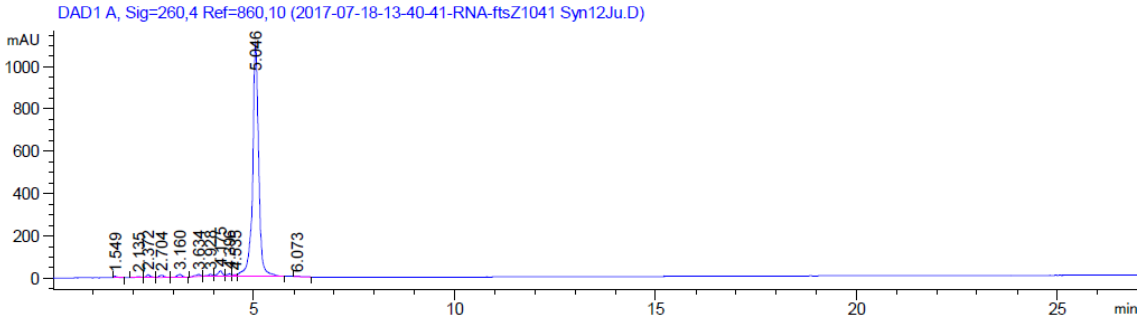

Figure A15. Analytical HPLC of purified RNA-ftsZ1041 (reversed-phase C18, detector at 260 nm). Purity > 93.0%.

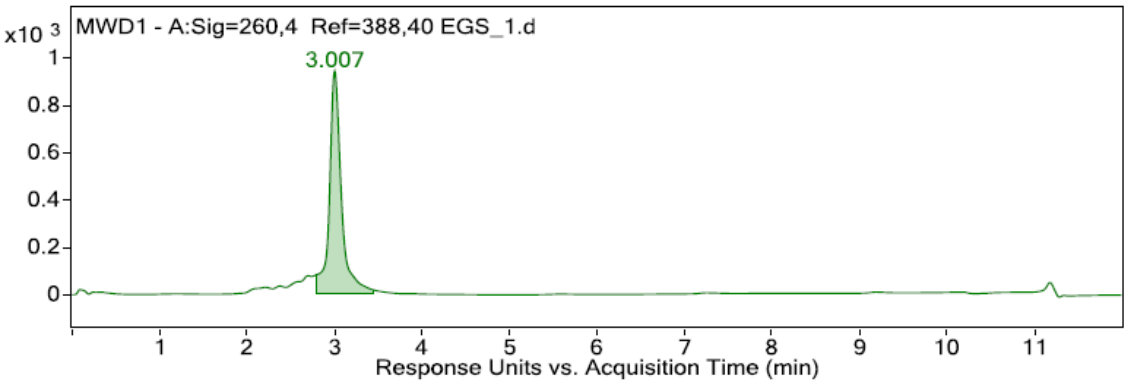

Figure A16. Analytical HPLC of purified RNA-ftsZ1041-EGS1 (reversed-phase C18, detector at 260 nm). Purity >90.0%.

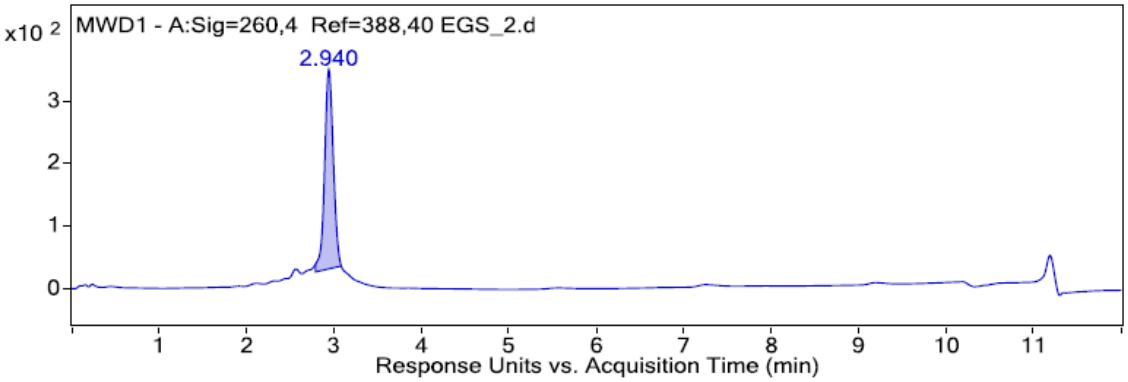

Figure A17. Analytical HPLC of purified RNA-ftsZ1041-EGS2 (reversed-phase C18, detector at 260 nm). Purity >90.0%.

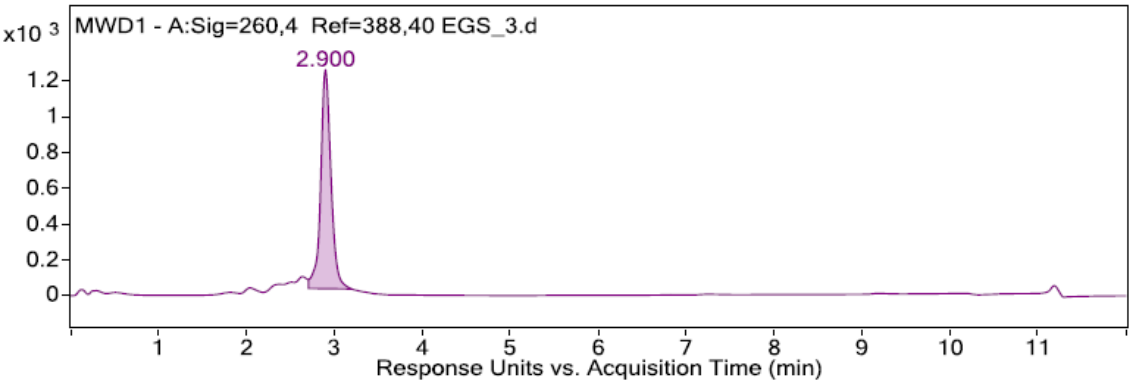

Figure A18. Analytical HPLC of purified RNA-ftsZ1041-EGS3 (reversed-phase C18, detector at 260 nm). Purity >90.0%.

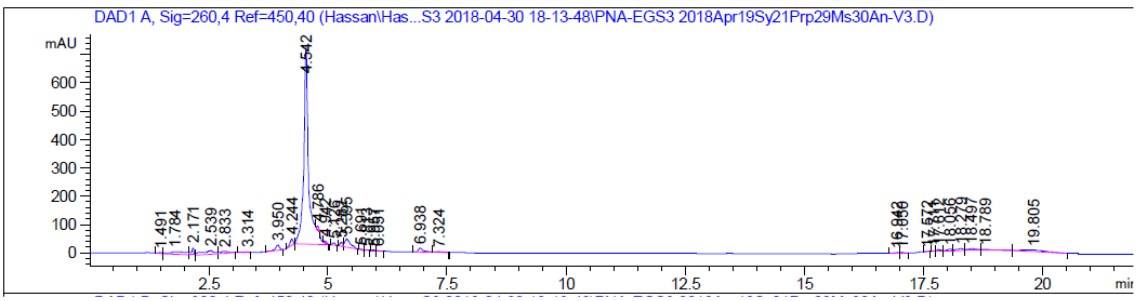

Figure A19. Analytical HPLC of purified PNA-ftsZ1041-EGS3 (reversed-phase C18, detector at 260 nm). Purity >90.0%.

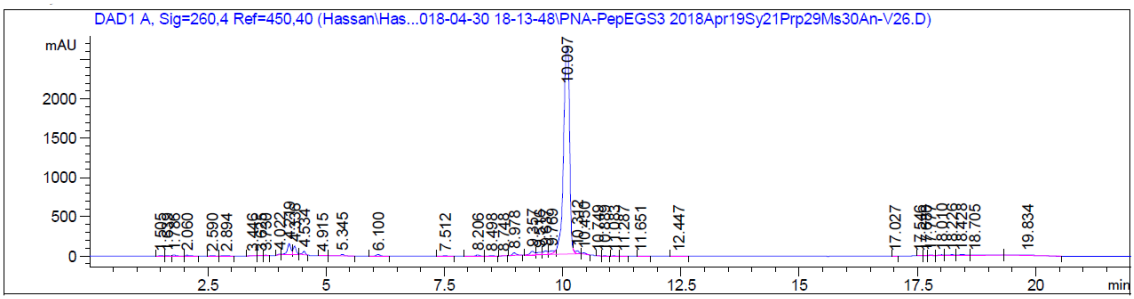

Figure A20. Analytical HPLC of purified Pep-PNA-ftsZ1041-EGS3 (reversed-phase C18, detector at 260 nm). Purity >90.0%.

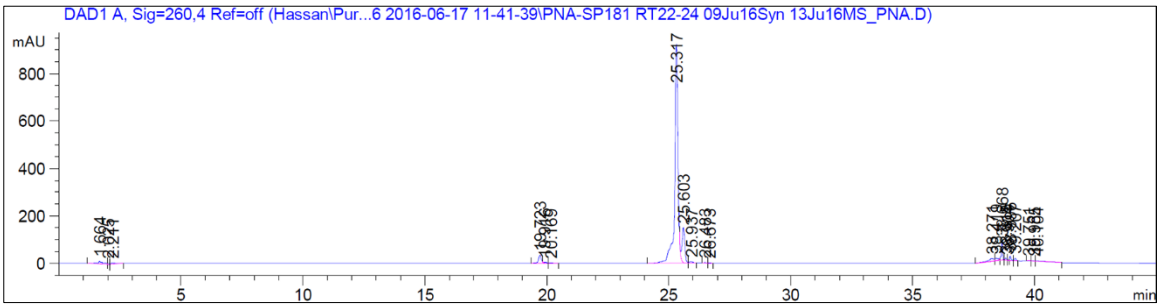

Figure A21. Analytical HPLC of purified SP181 (reversed-phase C18, detector at 260 nm). Purity >90.0%.

A.2 Full growth curves of *ftsZ* or *katG* silencing assays

In this section we will give the full growth curves of the graphs given in Chapter 2 where the full growth curve was not given in the main text (**Figure A22 – Figure 40**).

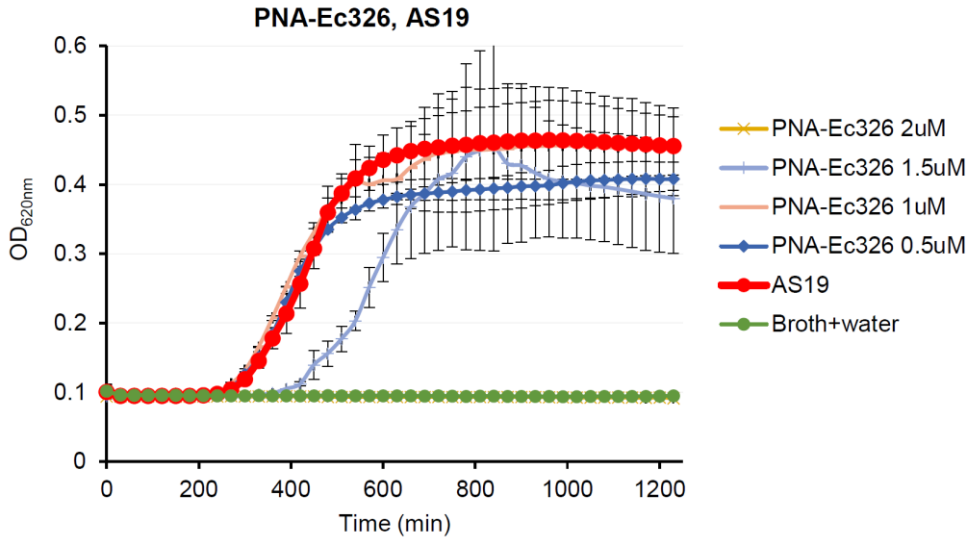

Figure A22. Potential *ftsZ* silencing in *E. coli* AS19 by PNA-Ec326 (steric blocker). 10 µL PNA in 10x the desired concentration was added to 90 µL *E. coli* cultures at 10^5 cfu/mL in a 96 well plate, and the OD_{620nm} was measured for 1200 minutes at 37˚C using a FC MultiSkan device. All results are the average of minimum 2 biological and 2 technical repeats, with error bars indicating standard deviations.

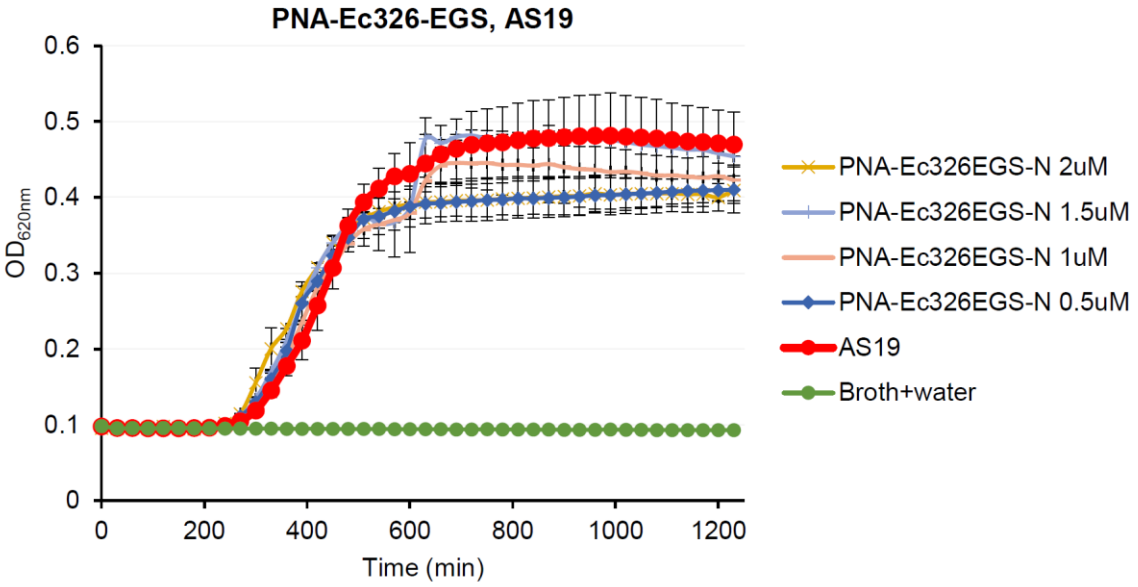

Figure A23. Potential *ftsZ* silencing in *E. coli* AS19 by PNA-Ec326-EGS (external guide sequence). 10 µL PNA in 10x the desired concentration was added to 90 µL *E. coli* cultures at 10^5 cfu/mL in a 96 well plate, and the OD_{620nm} was measured for 1200 minutes at 37˚C using a FC MultiSkan device. All results are the average of minimum 2 biological and 2 technical repeats, with error bars indicating standard deviations.

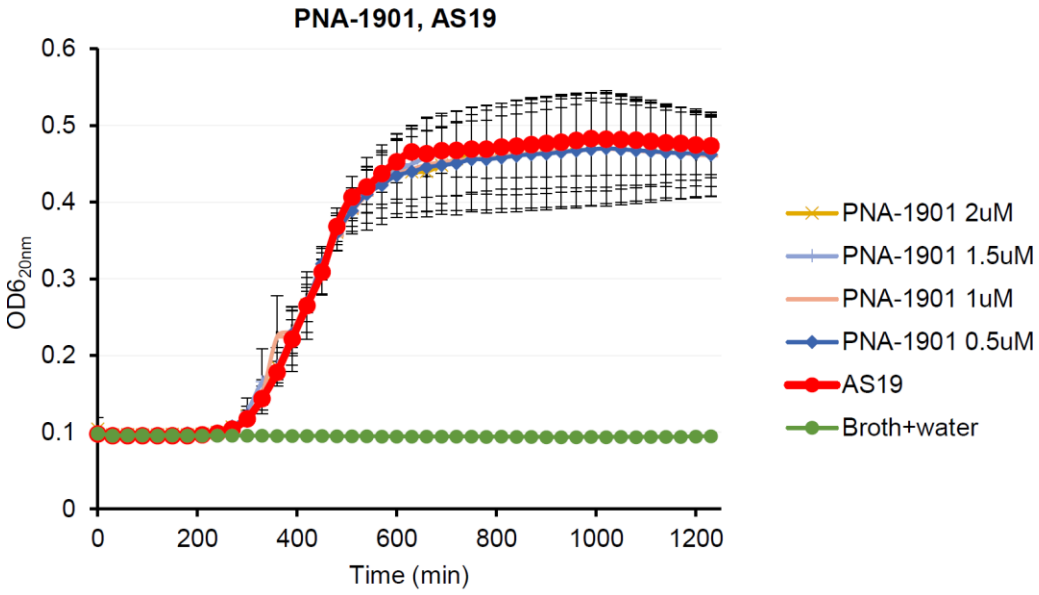

Figure A24. Potential *ftsZ* silencing in *E. coli* AS19 by PNA-1901 (negative control). 10 µL PNA in 10x the desired concentration was added to 90 µL *E. coli* cultures at 10^5 cfu/mL in a 96 well plate, and the OD_{620nm} was measured for 1200 minutes at 37˚C using a FC MultiSkan device. All results are the average of minimum 2 biological and 2 technical repeats, with error bars indicating standard deviations.

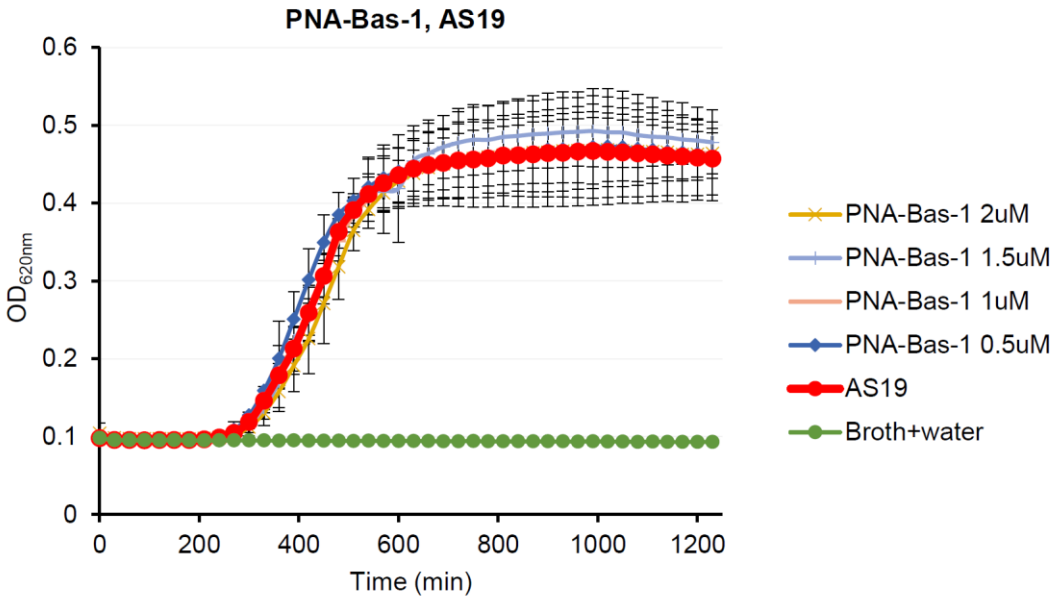

Figure A25. Potential *ftsZ* silencing in *E. coli* AS19 by PNA-Bas-1 (negative control). 10 µL PNA in 10x the desired concentration was added to 90 µL *E. coli* cultures at 10^5 cfu/mL in a 96 well plate, and the OD_{620nm} was measured for 1200 minutes at 37˚C using a FC MultiSkan device. All results are the average of minimum 2 biological and 2 technical repeats, with error bars indicating standard deviations.

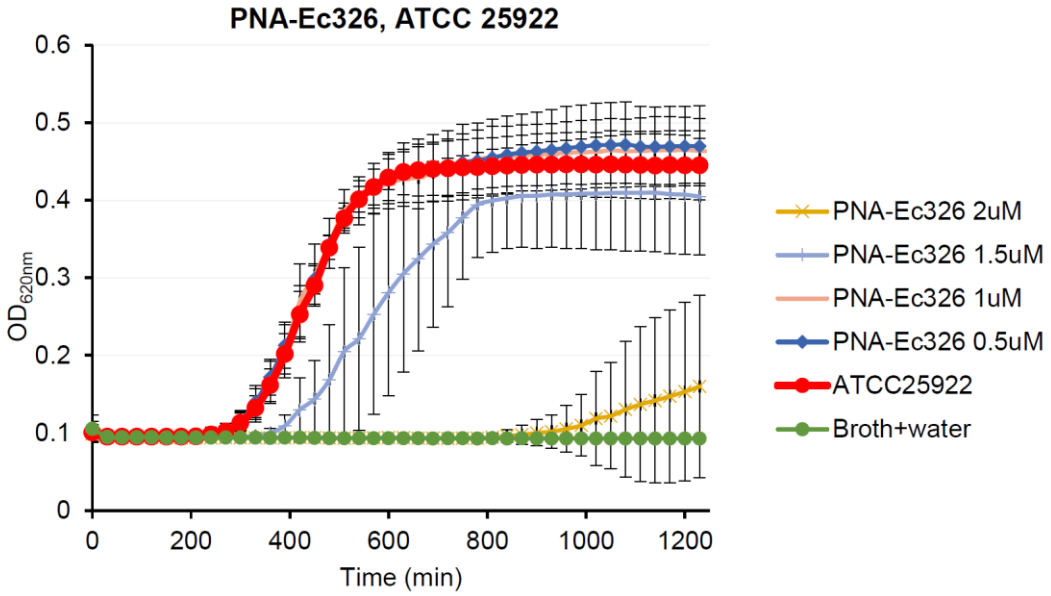

Figure A26. Potential *ftsZ* silencing in *E. coli* ATCC 25922 by PNA-Ec326 (steric blocker). 10 µL PNA in 10x the desired concentration was added to 90 µL *E. coli* cultures at 10^5 cfu/mL in a 96 well plate, and the OD_{620nm} was measured for 1200 minutes at 37˚C using a FC MultiSkan device. All results are the average of minimum 2 biological and 2 technical repeats, with error bars indicating standard deviations.

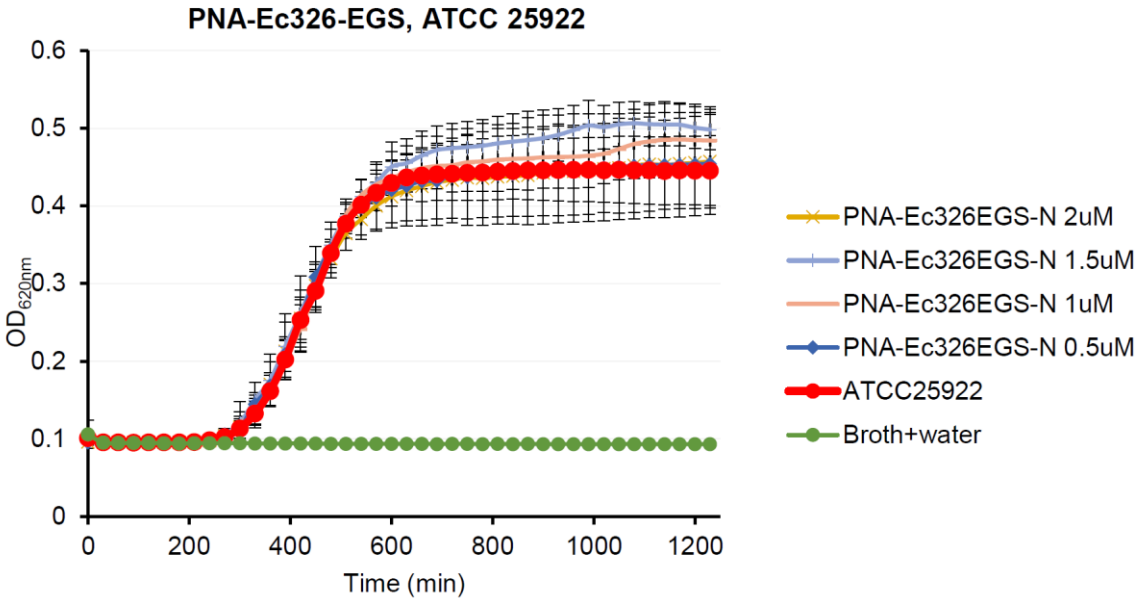

Figure A27. Potential *ftsZ* silencing in *E. coli* ATCC 25922 by PNA-Ec326-EGS (external guide sequence). 10 µL PNA in 10x the desired concentration was added to 90 µL *E. coli* cultures at 10^5 cfu/mL in a 96 well plate, and the OD_{620nm} was measured for 1200 minutes at 37˚C using a FC MultiSkan device. All results are the average of minimum 2 biological and 2 technical repeats, with error bars indicating standard deviations.

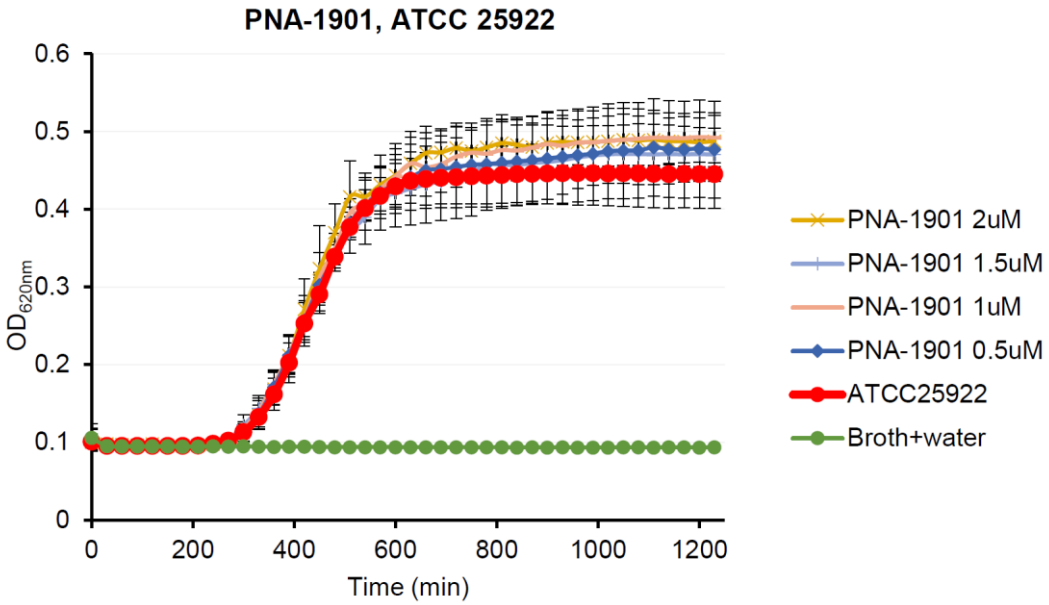

Figure A28. Potential *ftsZ* silencing in *E. coli* ATCC 25922 by PNA-1901 (negative control). 10 µL PNA in 10x the desired concentration was added to 90 µL *E. coli* cultures at 10^5 cfu/mL in a 96 well plate, and the OD_{620nm} was measured for 1200 minutes at 37˚C using a FC MultiSkan device. All results are the average of minimum 2 biological and 2 technical repeats, with error bars indicating standard deviations.

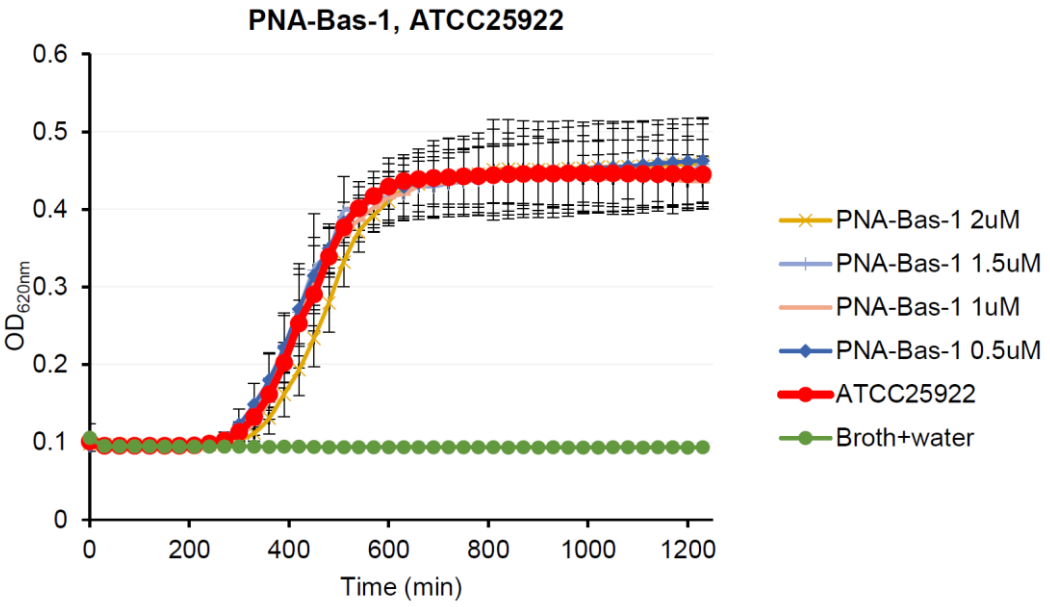

Figure A29. Potential *ftsZ* silencing in *E. coli* ATCC 25922 by PNA-Bas-1 (negative control). 10 µL PNA in 10x the desired concentration was added to 90 µL *E. coli* cultures at 10^5 cfu/mL in a 96 well plate, and the OD_{620nm} was measured for 1200 minutes at 37˚C using a FC MultiSkan device. All results are the average of minimum 2 biological and 2 technical repeats, with error bars indicating standard deviations.

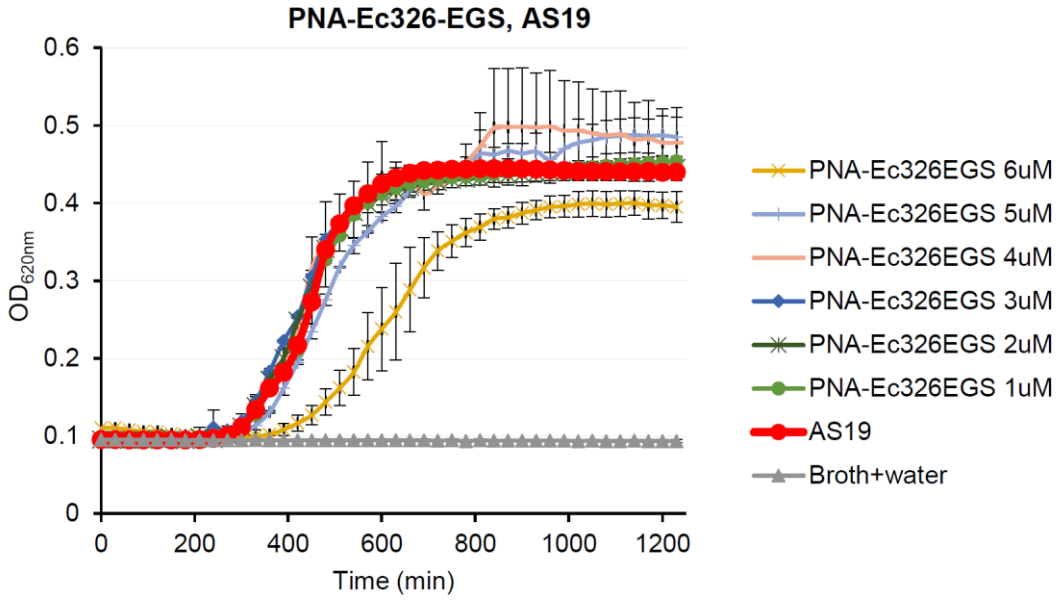

Figure A30. Potential *ftsZ* silencing in *E. coli* AS19 by high concentrations of PNA-Ec326-EGS (external guide sequence). 10 µL PNA in 10x the desired concentration was added to 90 µL *E. coli* cultures at 10^5 cfu/mL in a 96 well plate, and the OD_{620nm} was measured for 1200 minutes at 37˚C using a FC MultiSkan device. All results are the average of minimum 2 biological and 2 technical repeats, with error bars indicating standard deviations.

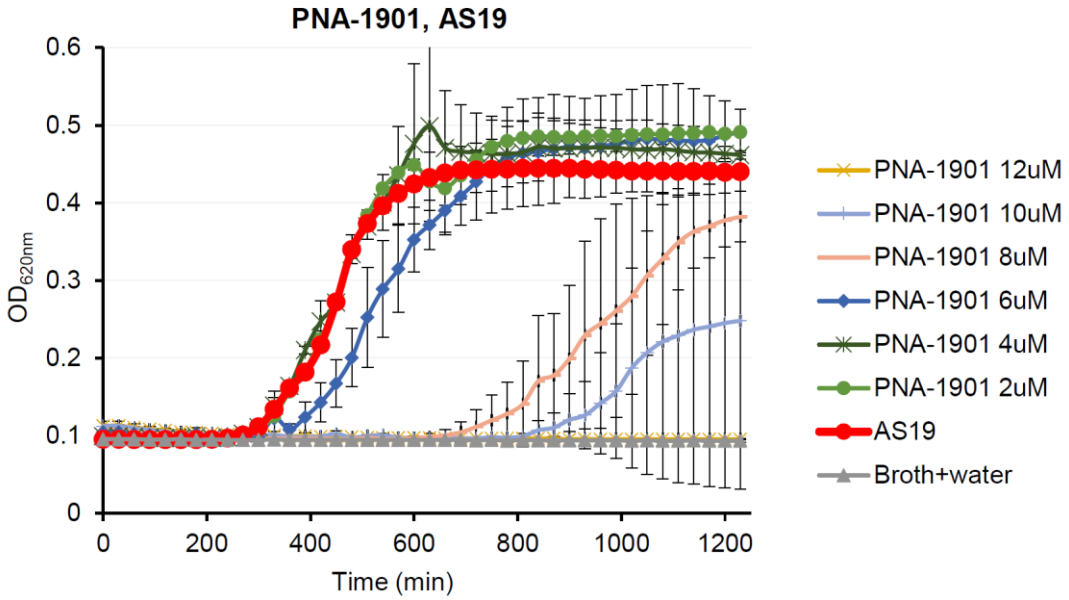

Figure A31. Potential *ftsZ* silencing in *E. coli* AS19 by high concentrations of PNA-1901 (negative control). 10 µL PNA in 10x the desired concentration was added to 90 µL *E. coli* cultures at 10^5 cfu/mL in a 96 well plate, and the OD_{620nm} was measured for 1200 minutes at 37˚C using a FC MultiSkan device. All results are the average of minimum 2 biological and 2 technical repeats, with error bars indicating standard deviations.

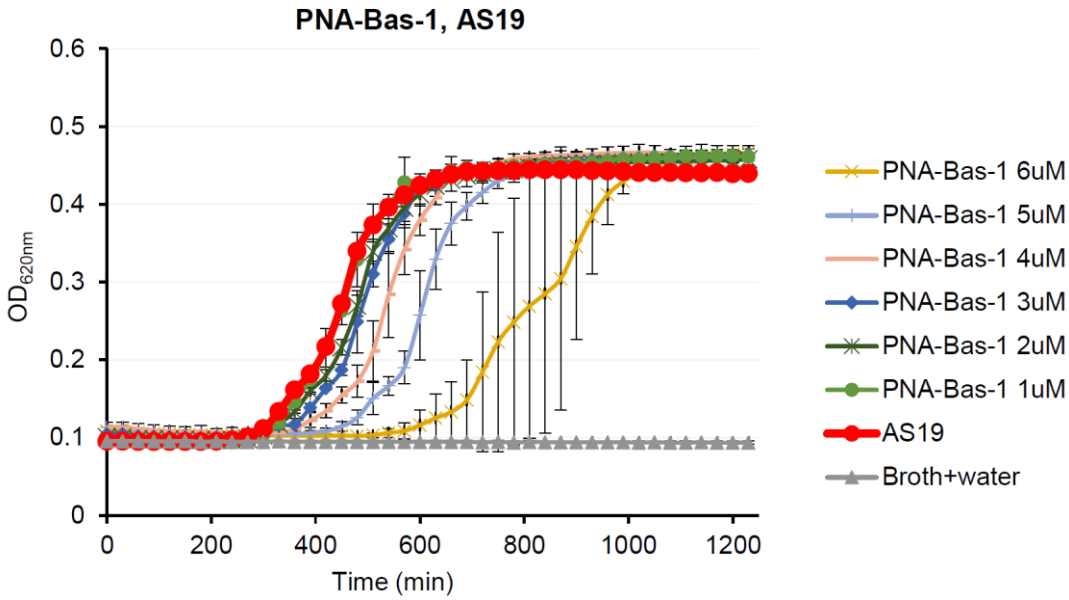

Figure A32. Potential *ftsZ* silencing in *E. coli* AS19 by high concentrations of PNA-Bas-1 (negative control). 10 µL PNA in 10x the desired concentration was added to 90 µL *E. coli* cultures at 10^5 cfu/mL in a 96 well plate, and the OD_{620nm} was measured for 1200 minutes at 37˚C using a FC MultiSkan device. All results are the average of minimum 2 biological and 2 technical repeats, with error bars indicating standard deviations.

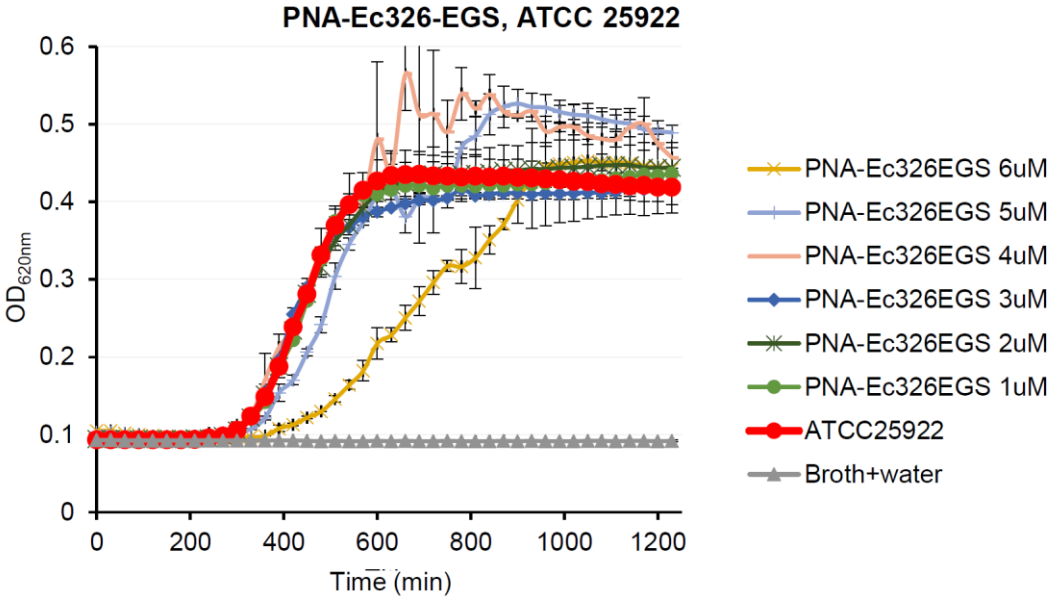

Figure A33. Potential *ftsZ* silencing in *E. coli* ATCC 25922 by high concentrations of PNA-Ec326-EGS (external guide sequence). 10 µL PNA in 10x the desired concentration was added to 90 µL *E. coli* cultures at 10^5 cfu/mL in a 96 well plate, and the OD_{620nm} was measured for 1200 minutes at 37˚C using a FC MultiSkan device. All results are the average of minimum 2 biological and 2 technical repeats, with error bars indicating standard deviations.

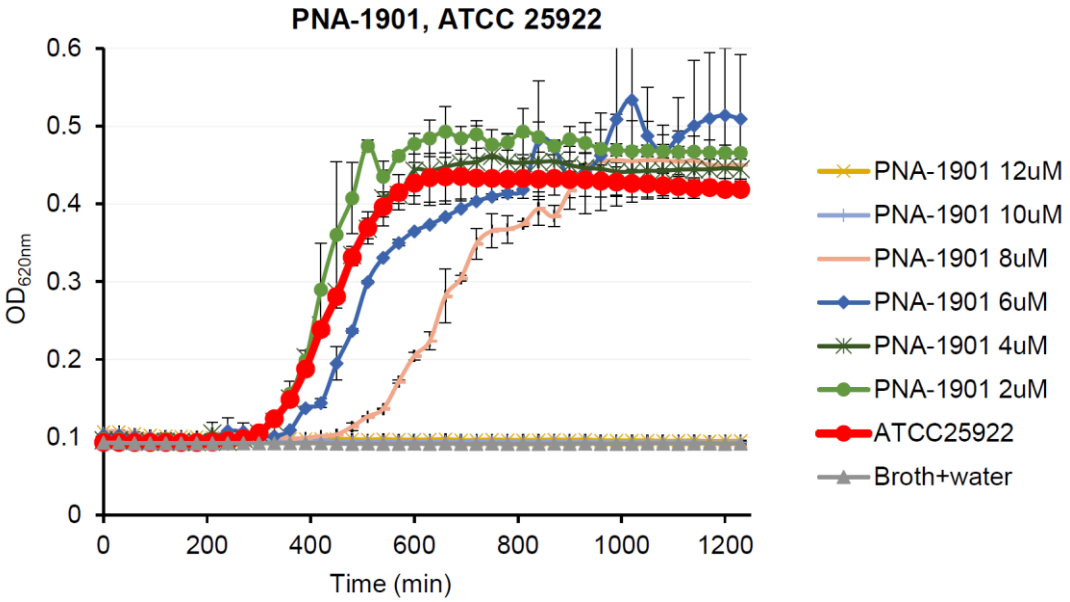

Figure A34. Potential *ftsZ* silencing in *E. coli* ATCC 25922 by high concentrations of PNA-1901 (negative control). 10 µL PNA in 10x the desired concentration was added to 90 µL *E. coli* cultures at 10^5 cfu/mL in a 96 well plate, and the OD_{620nm} was measured for 1200 minutes at 37˚C using a FC MultiSkan device. All results are the average of minimum 2 biological and 2 technical repeats, with error bars indicating standard deviations.

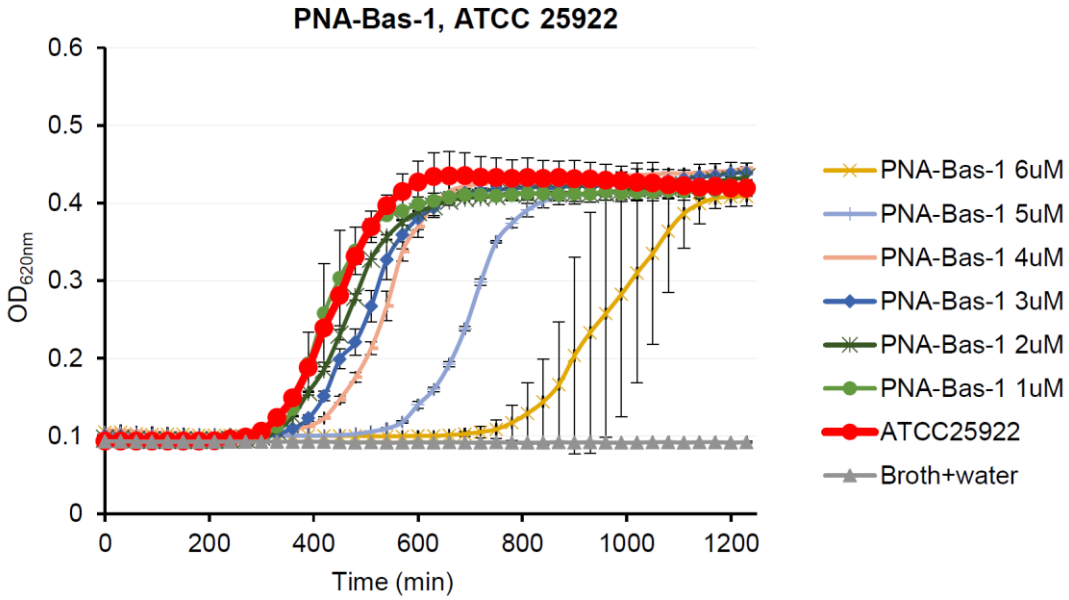

Figure A35. Potential *ftsZ* silencing in *E. coli* ATCC 25922 by high concentrations of PNA-Bas-1 (negative control). 10 µL PNA in 10x the desired concentration was added to 90 µL *E. coli* cultures at 10^5 cfu/mL in a 96 well plate, and the OD_{620nm} was measured for 1200 minutes at 37˚C using a FC MultiSkan device. All results are the average of minimum 2 biological and 2 technical repeats, with error bars indicating standard deviations.

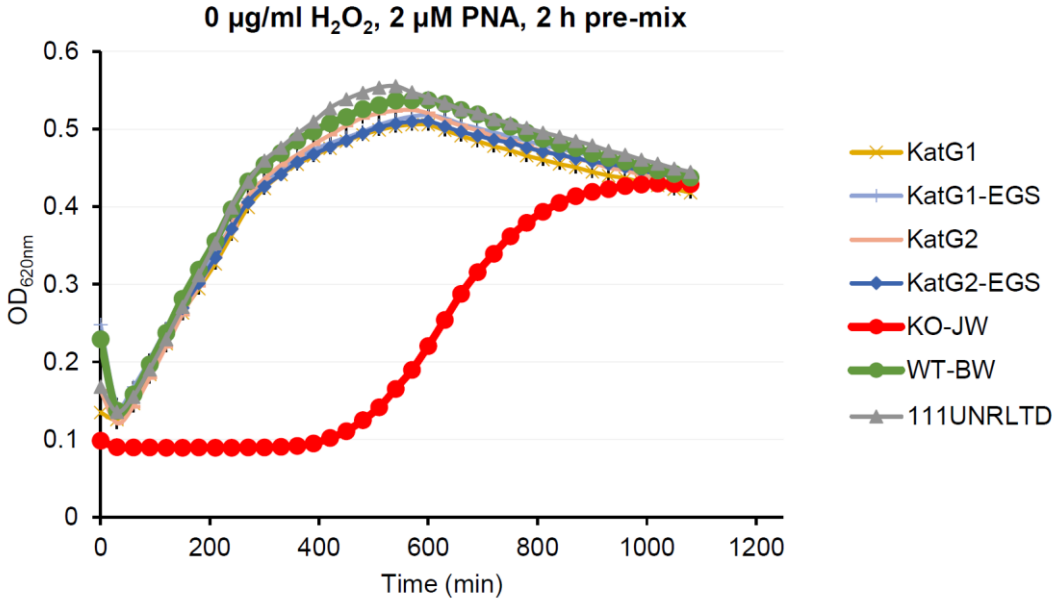

Figure A36. Potential silencing of *katG* by 2 µM PNAs in *E. coli* strain BW25113 in the presence 0 µg/mL hydrogen peroxide. 2 µM PNA was pre-mixed with *E. coli* BW25113 cultures at 10^5 cfu/mL in a 96-well plate at 37 °C for 2 hours. After 2 hours, H_2O_2 was added and the optical density at 620 nm (OD_{620nm}) was measured for 1200 min at 37 °C. The *E. coli* strain was grown in MH broth. The results are the average of at least 1 biological and 2 technical repeats, with error bars representing standard deviations.

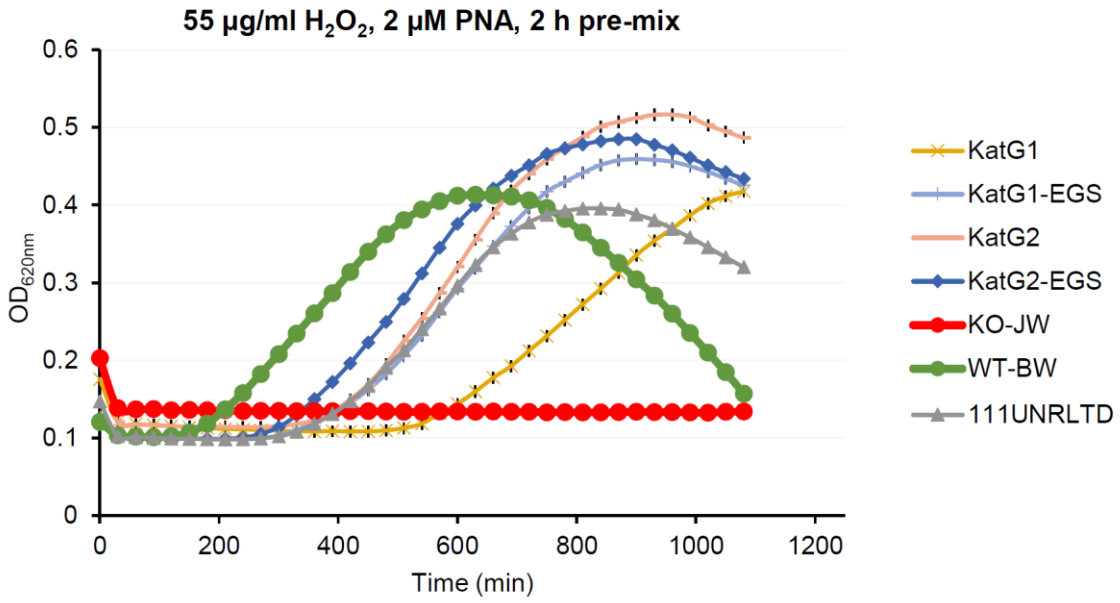

Figure A37. Potential silencing of *katG* by 2 µM PNAs in *E. coli* strain BW25113 in the presence 55 µg/mL hydrogen peroxide. 2 µM PNA was pre-mixed with *E. coli* BW25113 cultures at 10^5 cfu/mL in a 96-well plate at 37 °C for 2 hours. After 2 hours, H_2O_2 was added and the optical density at 620 nm (OD_{620nm}) was measured for 1200 min at 37 °C. The *E. coli* strain was grown in MH broth. The results are the average of at least 1 biological and 2 technical repeats, with error bars representing standard deviations.

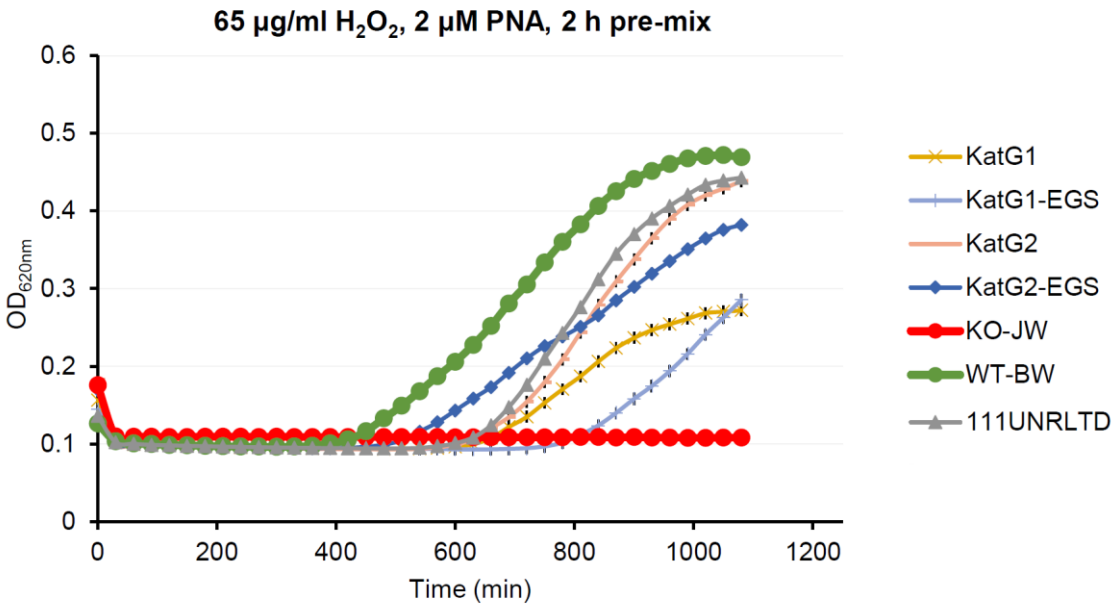

Figure A38. Potential silencing of *katG* by 2 µM PNAs in *E. coli* strain BW25113 in the presence 65 µg/mL hydrogen peroxide. 2 µM PNA was pre-mixed with *E. coli* BW25113 cultures at 10^5 cfu/mL in a 96-well plate at 37 °C for 2 hours. After 2 hours, H_2O_2 was added and the optical density at 620 nm (OD_{620nm}) was measured for 1200 min at 37 °C. The *E. coli* strain was grown in MH broth. The results are the average of at least 1 biological and 2 technical repeats, with error bars representing standard deviations.

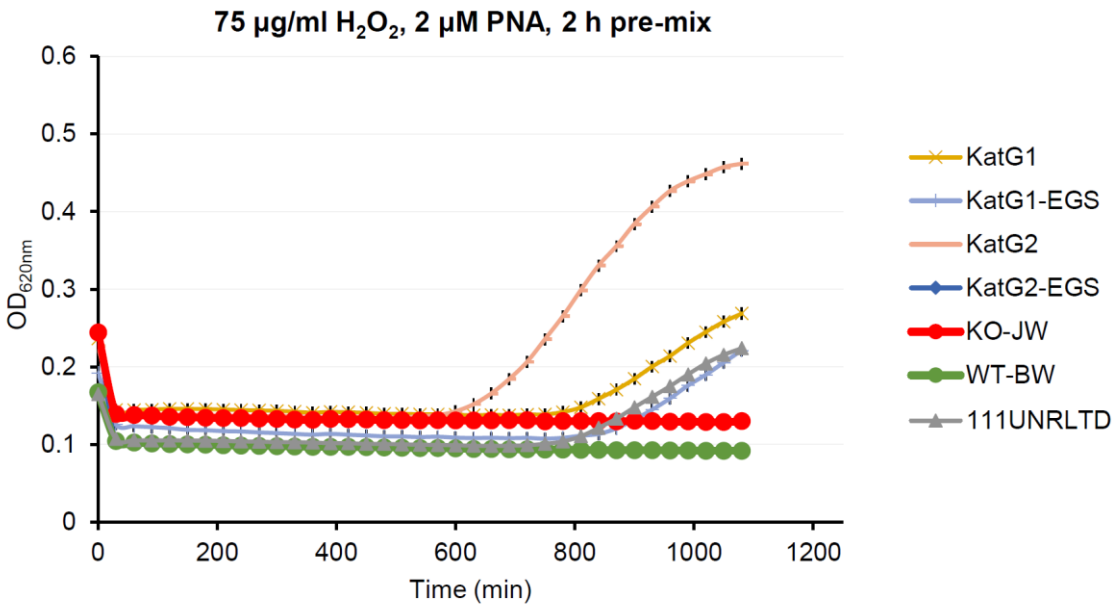

Figure A39. Potential silencing of *katG* by 2 µM PNAs in *E. coli* strain BW25113 in the presence 75 µg/mL hydrogen peroxide. 2 µM PNA was pre-mixed with *E. coli* BW25113 cultures at 10^5 cfu/mL in a 96-well plate at 37 °C for 2 hours. After 2 hours, H_2O_2 was added and the optical density at 620 nm (OD_{620nm}) was measured for 1200 min at 37 °C. The *E. coli* strain was grown in MH broth. The results are the average of at least 1 biological and 2 technical repeats, with error bars representing standard deviations.

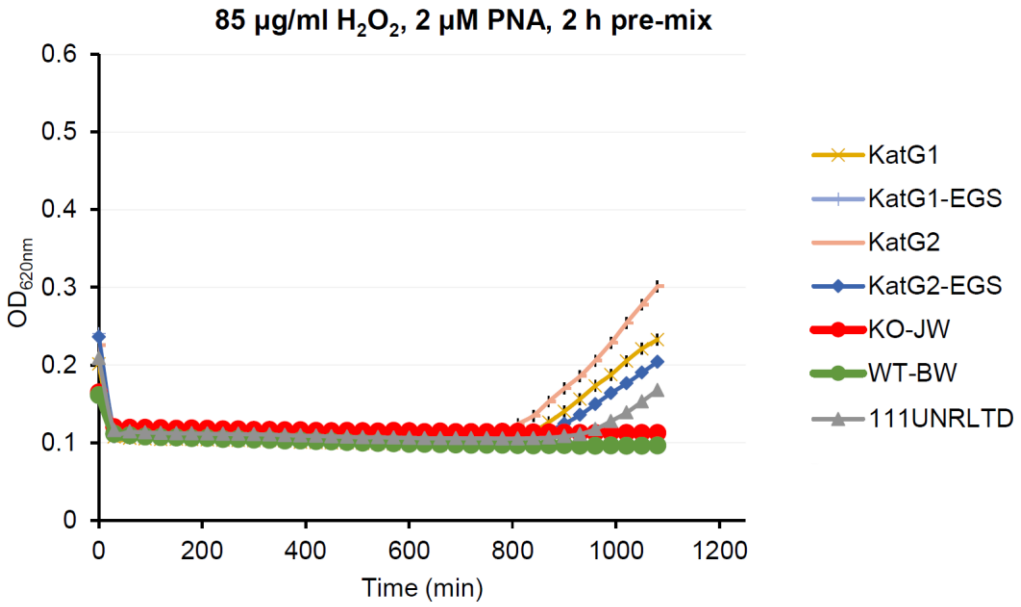

Figure A40. Potential silencing of *katG* by 2 µM PNAs in *E. coli* strain BW25113 in the presence 85 µg/mL hydrogen peroxide. 2 µM PNA was pre-mixed with *E. coli* BW25113 cultures at 10^5 cfu/mL in a 96-well plate at 37 °C for 2 hours. After 2 hours, H_2O_2 was added and the optical density at 620 nm (OD_{620nm}) was measured for 1200 min at 37 °C. The *E. coli* strain was grown in MH broth. The results are the average of at least 1 biological and 2 technical repeats, with error bars representing standard deviations.

A.3 Additional repeats of *lacZ* silencing assay

To test *lacZ* silencing by the PNAs, PNA (final concentration 2 µM), and a mixture of IPTG and X-gal (final concentration 0.1 mM IPTG and 0.2 mg/mL X-gal) were added to *E. coli* cultures at 10^5 cfu/mL in a 96-well plate and subsequently incubated at 37 ˚C using the FC MultiSkan. Pictures were taken of the growing cultures at regular intervals using a flatbed scanner. **Figure A41** shows the results of both technical repeats. The blue colour indicative of β-galactosidase started to appear after 16 h incubation with the PNAs.

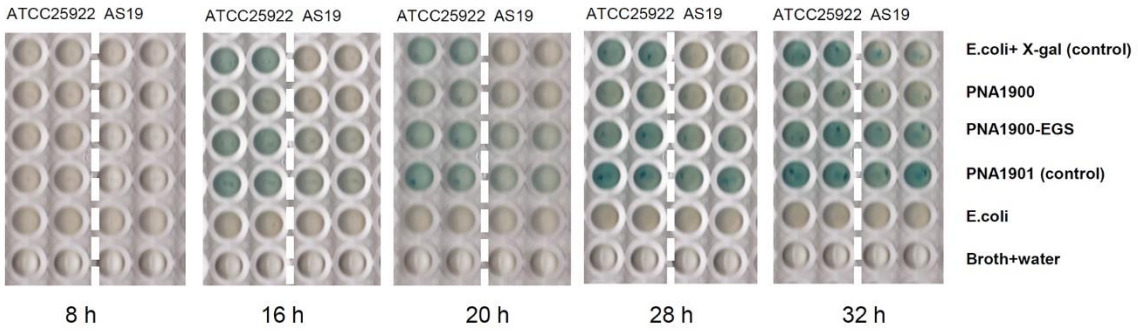

Figure A41. Potential silencing of *lacZ* by 2 µM PNAs in *E. coli* strains ATCC 25922 (left) and AS19 (right). The plate was shaken and incubated at 37 °C using a FC multiSkan. Pictures were taken using a flatbed scanner after 8, 16, 20, 28 and 32 h incubation. The *E. coli* strains were grown in MH broth and used in the experiment at 10^5 cfu/mL.

A.4 Optimization of the *katG* gene silencing assay

A.4.1 Hydrogen peroxide IC_{50} for three *E. coli* strains

The three *E. coli* strains investigated for the *katG* gene silencing assays are: wild type BW25113/ 7636, JW3914-1/10827 (genetically modified –*katG*), and JW1638-1/9395 (genetically modified –*sodC*). The effect on bacterial growth was measured for a range of H_2O_2 concentrations (0.1875 µg/mL – 192 µg/mL) in order to determine the IC_{50} value of H_2O_2 in each *E. coli* strain. The results show a significant difference in the H_2O_2 IC_{50} values for the wild type BW25113 and the knockout strains JW3914-1(-*kat*G) and JW1638-1 (-*sod*C) (see **Figure A42**). The IC_{50} value was 8.8 µg/mL for JW3914-1 and 30 µg/mL for JW1638-1 and approximately 79 µg/mL for wild type BW25113. The results also suggest that for this range of concentrations, H_2O_2 toxicity is unlikely to be seen for wild type *E. coli* cells, unless if the *katG* gene is silenced by the PNAs.

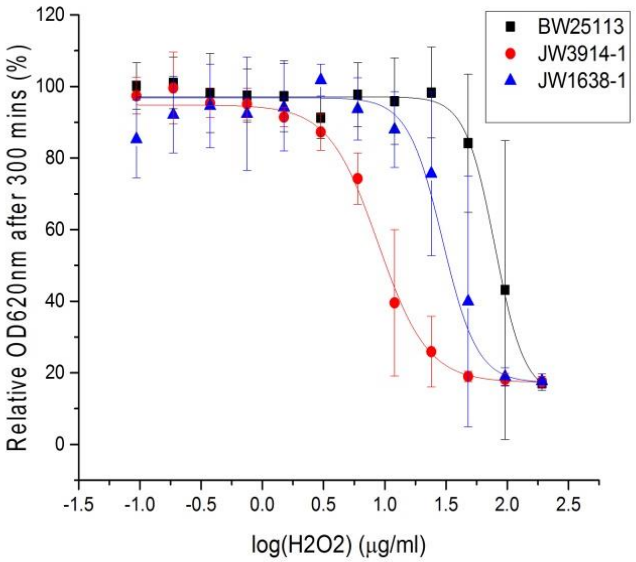

Model	DoseResp		
Equation	y = A1 + (A2-A1)/(1 + 10^((LOGx0-x)*p))		
Reduced Chi-Sqr	0.19892	0.16076	0.39828
Adj. R-Square	0.99615	0.99885	0.99177
		Value	Standard Error
Relative OD620nm after 300 mins	A1	13.7312	8.6599
	A2	97.12357	1.23018
	LOGx0	1.89886	0.11716
	p	-3.58646	2.03343
	span	83.39237	8.87377
	EC20	116.60823	52.45369
	EC50	79.22438	21.37157
	EC80	53.82555	10.66424
	A1	17.35213	0.51293
	A2	94.81797	0.84665
	LOGx0	0.9464	0.0302
	p	-2.14803	0.18435
	span	77.46584	1.07671
	EC20	16.85335	1.60439
	EC50	8.83897	0.61465
	EC80	4.63572	0.38071
	A1	17.24033	1.46636
	A2	96.87059	2.02941
	LOGx0	1.47158	0.08474
	p	-3.06476	0.85383
	span	79.63027	2.61561
	EC20	46.56147	10.03325
	EC50	29.6197	5.77958
	EC80	18.84233	4.67184

Figure A42. IC_{50} values for H_2O_2 toxicity against various *E. coli* strains. 10 µL H_2O_2 in 10 fold the desired concentration was added to 90 µL *E. coli* cultures at 10^5 cfu/mL in a 96 well plate, and the OD_{620nm} was measured after 300 min at 37 ˚C using a FC MultiSkan device. *E. coli* strains BW25113 (black), JW3914-1 (red) and JW1638-1 (blue) were used. All results are the average of minimum 1 biological and 2 technical repeats, with error bars indicating standard deviations. IC_{50} values after 300 min were determined as the following JW1638-1 (30 µg/mL), JW3914-1 (8.8 µg/mL), BW25113 did not not show complete inhibition in the range chosen for H_2O_2 (estimated IC_{50} is 79 µg/mL).

A.4.2 Optimizing working hydrogen peroxide concentrations

A range of hydrogen peroxide concentrations were chosen at the values 192, 48, 12, 3 and 0.75 µg/mL (see **Figure A43 - Figure A48**). In this range and in the presence of 2 µM PNA with 30 minutes of PNA/bacteria pre-mixing, an overwhelming bacteriocidal effect for the bacterium was observed at the high concentration of 192 µg/mL and no growth inhibition was observed at concentrations 48 µg/mL and below. These results indicated the necessity to work in a narrower range of hydrogen peroxide concentrations.

The next set of hydrogen peroxide concentrations we chose to work with were 160, 120, 80 and 40 µg/mL (see **Figure A49 – Figure A56**). In this set of experiments JW1638-1 was introduced as a knocked-out gene control (-*sodC*), and wild type BW25113 was introduced to this set of experiment as a positive control. It was observed that concentrations of hydrogen peroxide of 120 µg/mL and above still show a complete kill of the bacterial cultures. However, 80 µg/mL H_2O_2 seems to have delayed the growth for about 400 minutes, except for SP181 where 40 µg/mL also caused a complete kill. Nevertheless, this set of experiments gave an indication for the optimal working concentration range of hydrogen peroxide is between 48 µg/mL and 120 µg/mL, for a PNA/bacteria pre-mixing time of 30 minutes and a PNA concentration of 2 µM.

The third set of experiments was run with hydrogen peroxide concentrations of 90, 80, 70, 60 and 50 µg/mL, and a PNA/bacteria pre-mixing time of 30 minutes and a PNA concentration of 2 µM (see **Figure A57 – Figure A63**). For control compound SP181, a H_2O_2 concentration of 90 µg/mL still caused a complete kill. In addition, concentrations in the range 60-80 µg/mL seem to have delayed the growth and only a small delay in bacterial growth is seen for 50 µg/mL H_2O_2. These results suggest that the range 50-90 µg/mL hydrogen peroxide is the optimal range to work with in order to test the efficiency of the PNAs in silencing the gene *katG*. In addition, PNA sequences PNA-katG1, PNA-katG1-EGS and PNA-katG2 showed a complete kill at a H_2O_2 concentration of 80 µg/mL and above when compared to the negative PNA sequence SP181. This difference might be caused by the PNAs sequences specifically targeting the gene *katG*.

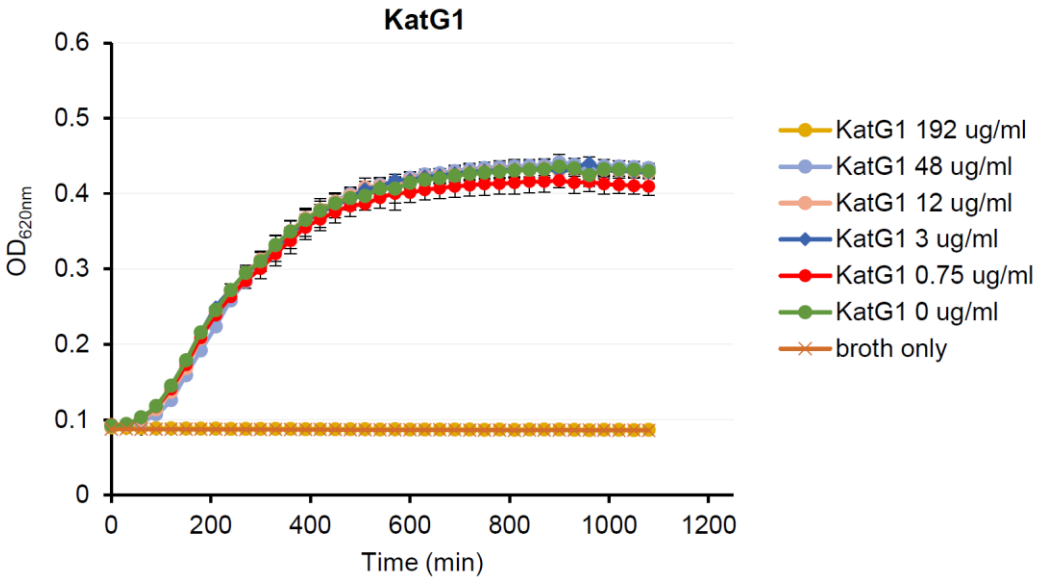

Figure A43. Optimizing the H_2O_2 concentration (range 0.75 – 192 µg/mL). PNA-KatG1 (2 µM) was pre-mixed with *E. coli* cultures at 10^5 cfu/mL in a 96-well plate at 37°C for 30 min. Then, H_2O_2 was added at various concentrations and the OD_{620nm} was measured for 1200 min at 37˚C using a FC MultiSkan device. *E. coli* strains BW25113 were used. All results are the average of minimum 1 biological and 2 technical repeats, with error bars indicating standard deviations.

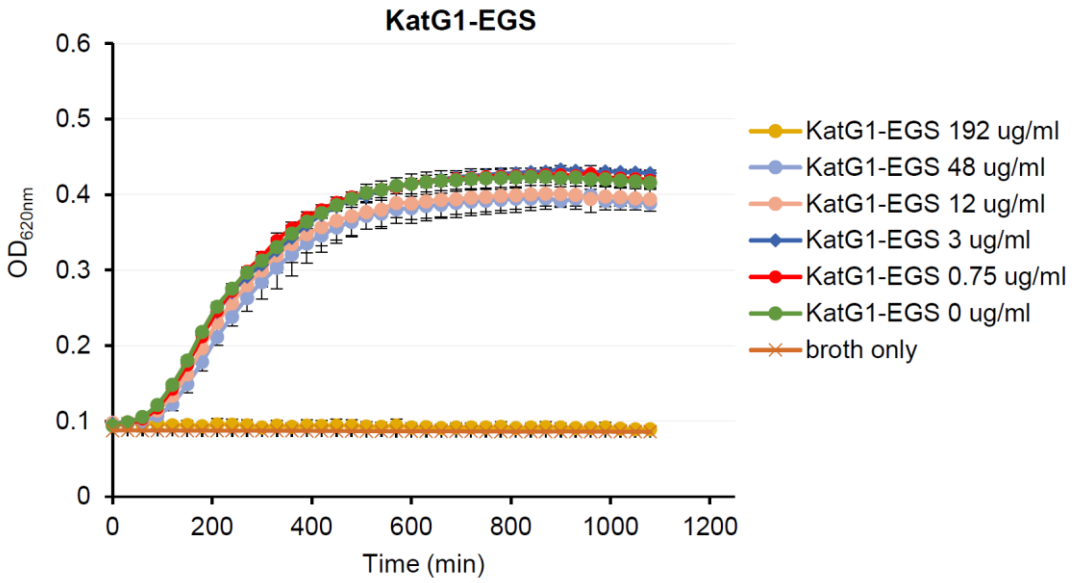

Figure A44. Optimizing the H_2O_2 concentration (range 0.75 – 192 µg/mL). PNA-KatG1-EGS (2 µM) was pre-mixed with *E. coli* cultures at 10^5 cfu/mL in a 96-well plate at 37°C for 30 min. Then, H_2O_2 was added at various concentrations and the OD_{620nm} was measured for 1200 min at 37˚C using a FC MultiSkan device. *E. coli* strains BW25113 were used. All results are the average of minimum 1 biological and 2 technical repeats, with error bars indicating standard deviations.

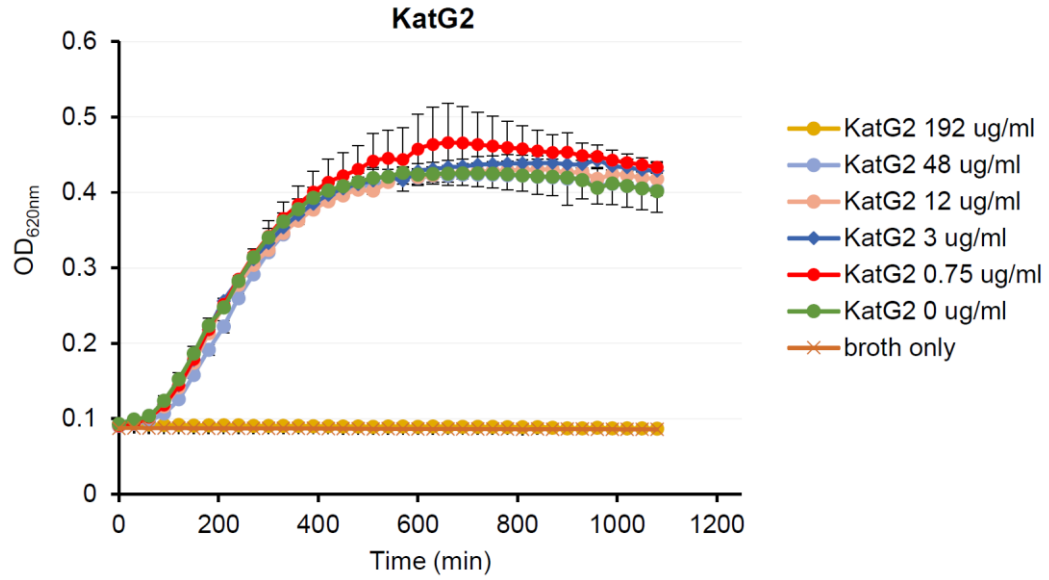

Figure A45. Optimizing the H_2O_2 concentration (range 0.75 – 192 µg/mL). PNA-KatG2 (2 µM) was pre-mixed with *E. coli* cultures at 10^5 cfu/mL in a 96-well plate at 37°C for 30 min. Then, H_2O_2 was added at various concentrations and the OD_{620nm} was measured for 1200 min at 37˚C using a FC MultiSkan device. *E. coli* strains BW25113 were used. All results are the average of minimum 1 biological and 2 technical repeats, with error bars indicating standard deviations.

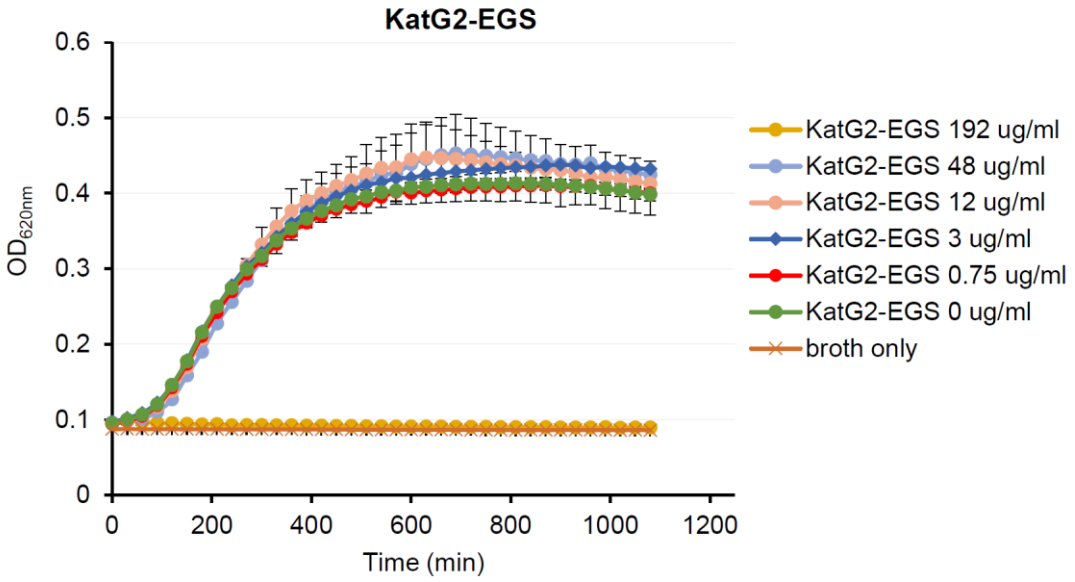

Figure A46. Optimizing the H_2O_2 concentration (range 0.75 – 192 µg/mL). PNA-KatG2-EGS (2 µM) was pre-mixed with *E. coli* cultures at 10^5 cfu/mL in a 96-well plate at 37°C for 30 min. Then, H_2O_2 was added at various concentrations and the OD_{620nm} was measured for 1200 min at 37˚C using a FC MultiSkan device. *E. coli* strains BW25113 were used. All results are the average of minimum 1 biological and 2 technical repeats, with error bars indicating standard deviations.

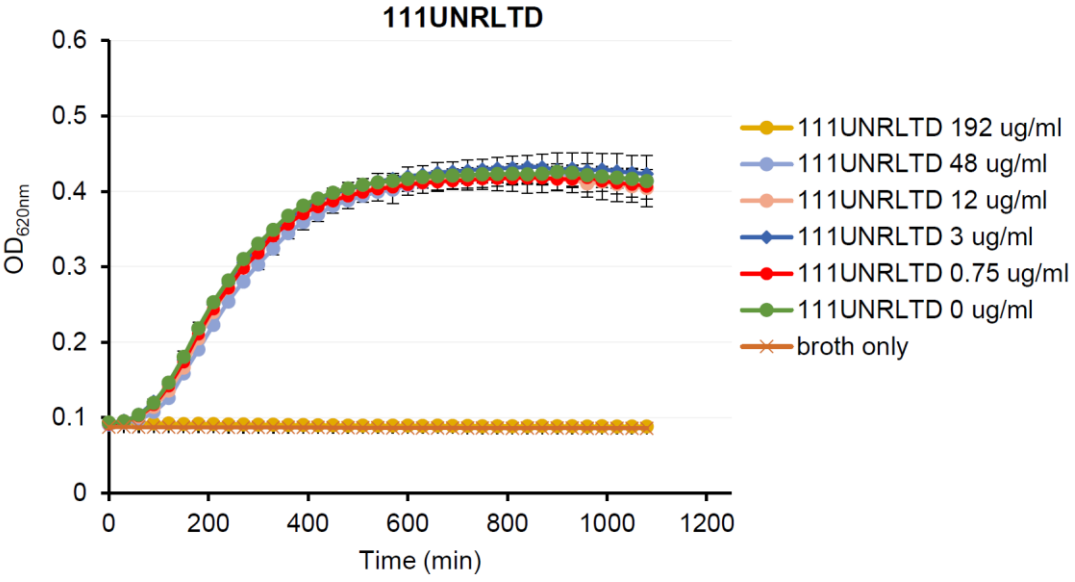

Figure A47. Optimizing the H_2O_2 concentration (range 0.75 – 192 µg/mL). 111UNRLTD (2 µM) was pre-mixed with *E. coli* cultures at 10^5 cfu/mL in a 96-well plate at 37°C for 30 min. Then, H_2O_2 was added at various concentrations and the OD_{620nm} was measured for 1200 min at 37˚C using a FC MultiSkan device. *E. coli* strains BW25113 were used. All results are the average of minimum 1 biological and 2 technical repeats, with error bars indicating standard deviations.

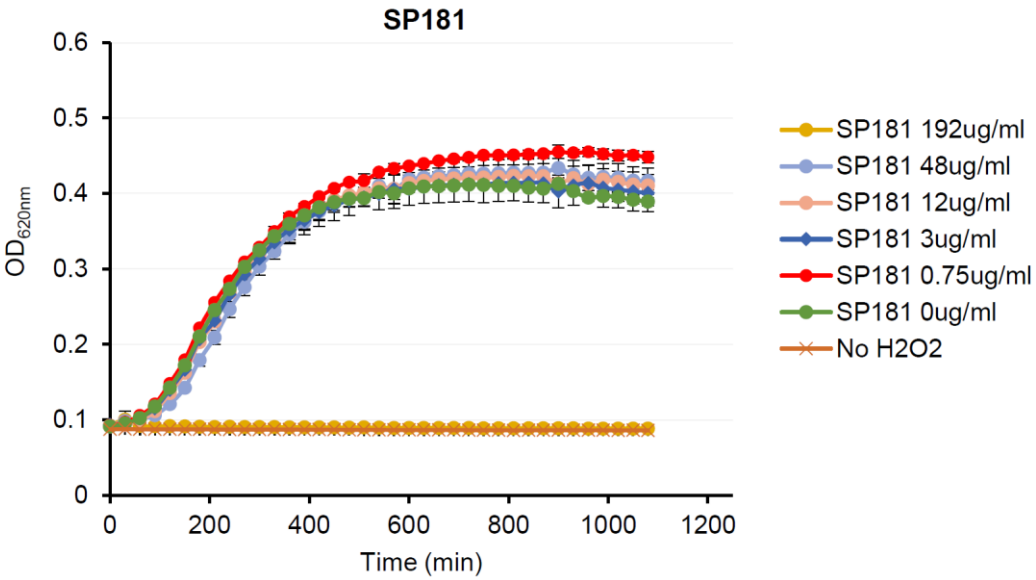

Figure A48. Optimizing the H_2O_2 concentration (range 0.75 – 192 µg/mL). SP181 (2 µM) was pre-mixed with *E. coli* cultures at 10^5 cfu/mL in a 96-well plate at 37°C for 30 min. Then, H_2O_2 was added at various concentrations and the OD_{620nm} was measured for 1200 min at 37˚C using a FC MultiSkan device. *E. coli* strains BW25113 were used. All results are the average of minimum 1 biological and 2 technical repeats, with error bars indicating standard deviations.

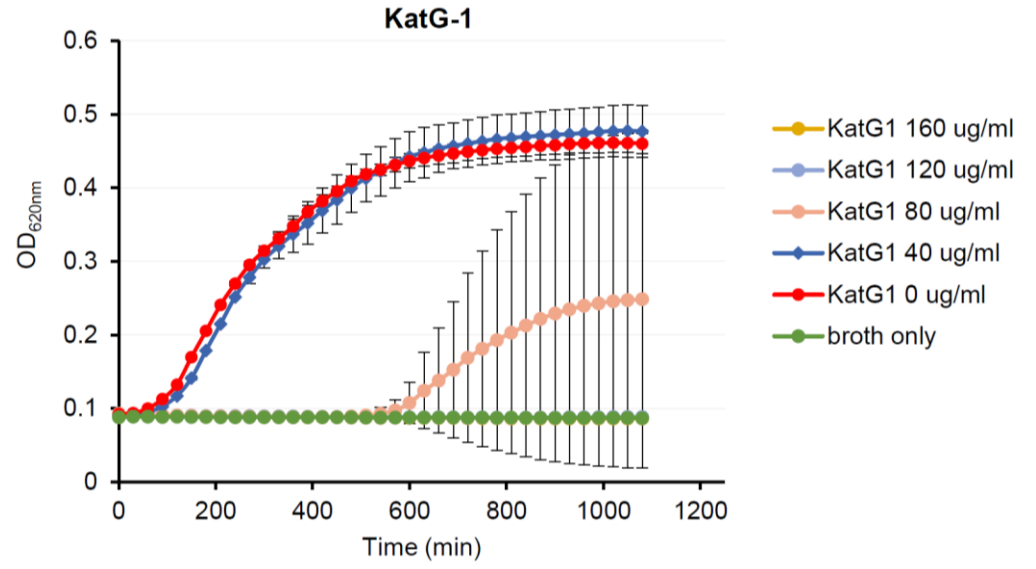

Figure A49. Optimizing the H_2O_2 concentration (range 40 – 160 µg/mL). 2 µM PNA-KatG1 was pre-mixed with *E. coli* cultures at 10^5 cfu/mL in a 96-well plate at 37°C for 30 min. Then, H_2O_2 was added at various concentrations and the OD_{620nm} was measured for 1200 min at 37˚C using a FC MultiSkan device. *E. coli* strains BW25113 was used. All results are the average of min. 1 biological and 2 technical repeats, error bars indicate standard deviations.

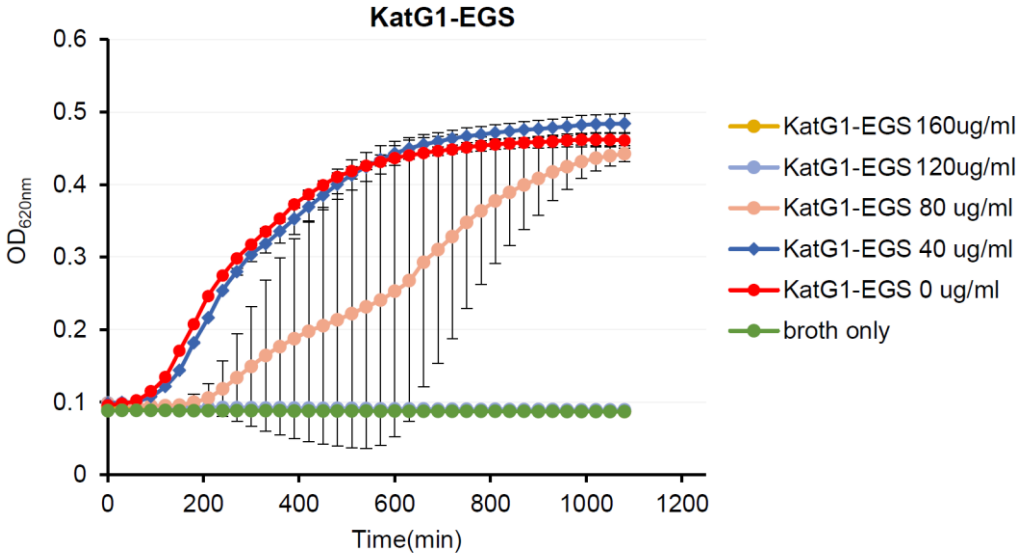

Figure A50. Optimizing the H_2O_2 concentration (range 40 – 160 µg/mL). 2 µM PNA-KatG1-EGS was pre-mixed with *E. coli* cultures at 10^5 cfu/mL in a 96-well plate at 37°C for 30 min. Then, H_2O_2 was added at various concentrations and the OD_{620nm} was measured for 1200 min at 37˚C using a FC MultiSkan device. *E. coli* strains BW25113 was used. All results are the average of min. 1 biological and 2 technical repeats, error bars indicate standard deviations.

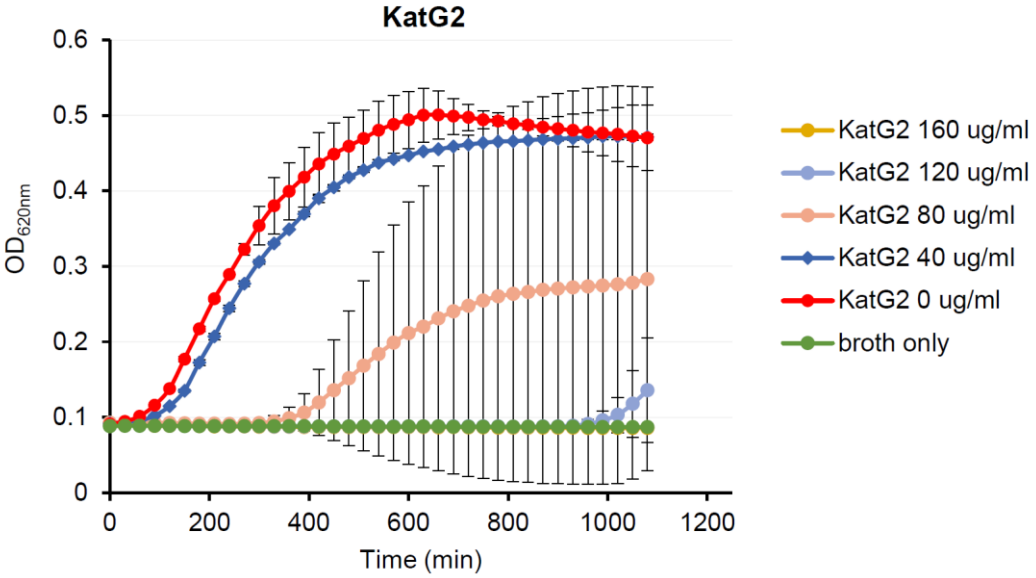

Figure A51. Optimizing the H_2O_2 concentration (range 40 – 160 µg/mL). 2 µM PNA-KatG2 was pre-mixed with *E. coli* cultures at 10^5 cfu/mL in a 96-well plate at 37°C for 30 min. Then, H_2O_2 was added at various concentrations and the OD_{620nm} was measured for 1200 min at 37˚C using a FC MultiSkan device. *E. coli* strains BW25113 was used. All results are the average of min. 1 biological and 2 technical repeats, error bars indicate standard deviations.

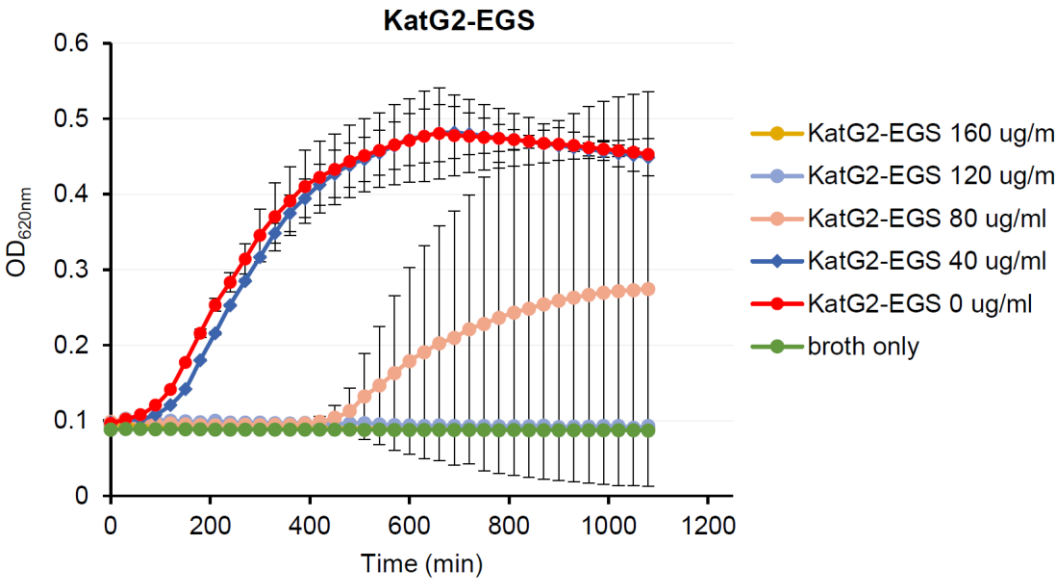

Figure A52. Optimizing the H_2O_2 concentration (range 40 – 160 µg/mL). 2 µM PNA-KatG2-EGS was pre-mixed with *E. coli* cultures at 10^5 cfu/mL in a 96-well plate at 37°C for 30 min. Then, H_2O_2 was added at various concentrations and the OD_{620nm} was measured for 1200 min at 37˚C using a FC MultiSkan device. *E. coli* strains BW25113 was used. All results are the average of min. 1 biological and 2 technical repeats, error bars indicate standard deviations.

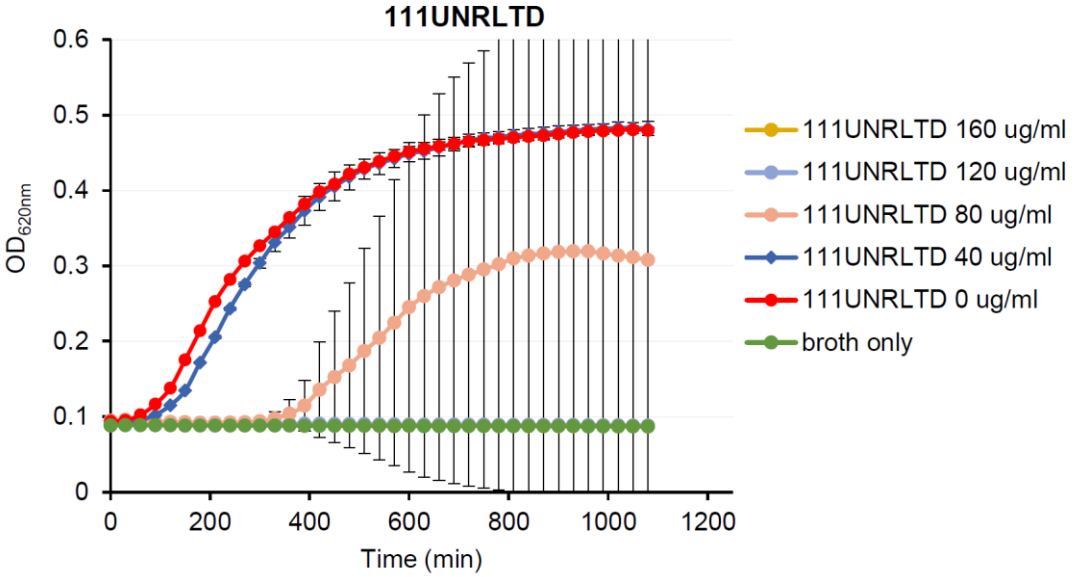

Figure A53. Optimizing the H_2O_2 concentration (range 40 – 160 µg/mL). 2 µM 111UNRLTD was pre-mixed with *E. coli* cultures at 10^5 cfu/mL in a 96-well plate at 37°C for 30 min. Then, H_2O_2 was added at various concentrations and the OD_{620nm} was measured for 1200 min at 37˚C using a FC MultiSkan device. *E. coli* strains BW25113 was used. All results are the average of min. 1 biological and 2 technical repeats, error bars indicate standard deviations.

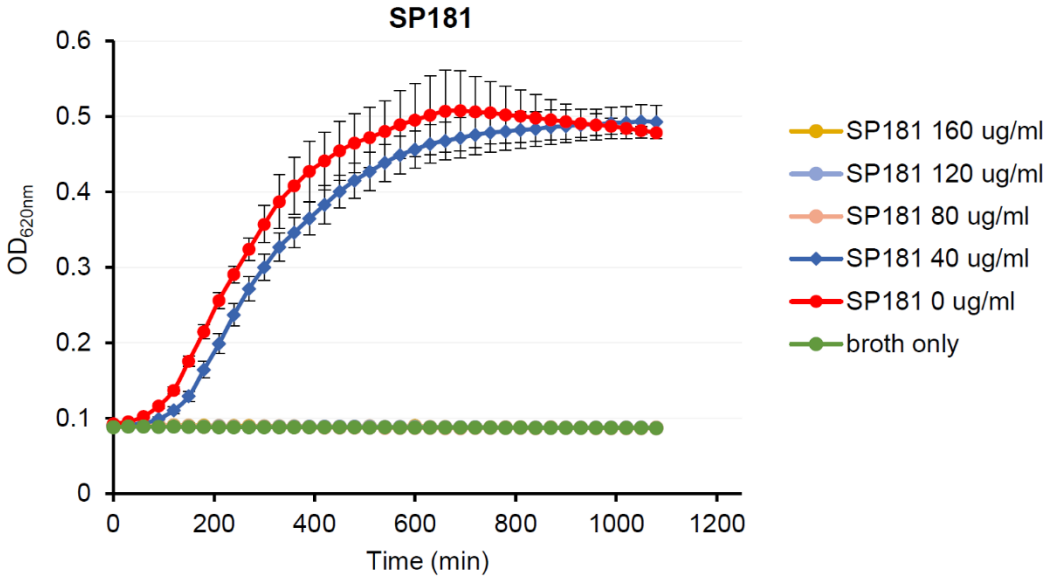

Figure A54. Optimizing the H_2O_2 concentration (range 40 – 160 µg/mL). 2 µM SP181 was pre-mixed with *E. coli* cultures at 10^5 cfu/mL in a 96-well plate at 37°C for 30 min. Then, H_2O_2 was added at various concentrations and the OD_{620nm} was measured for 1200 min at 37˚C using a FC MultiSkan device. *E. coli* strains BW25113 was used. All results are the average of min. 1 biological and 2 technical repeats, error bars indicate standard deviations.

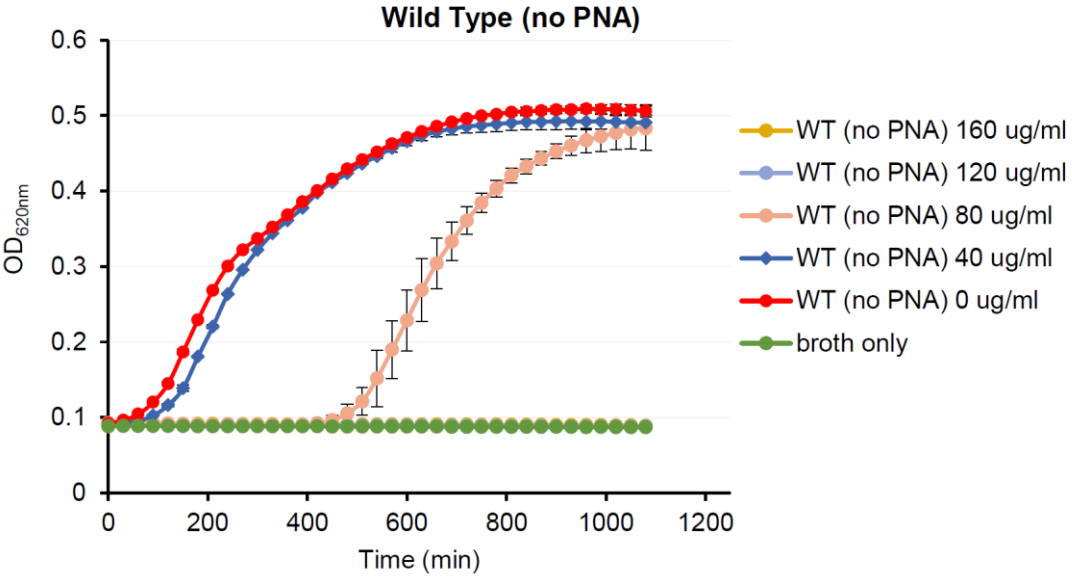

Figure A55. Optimizing the H_2O_2 concentration (range 40 – 160 µg/mL). *E. coli* cultures at 10^5 cfu/mL in a 96-well plate were incubated at 37°C for 30 min. Then, H_2O_2 was added at various concentrations and the OD_{620nm} was measured for 1200 min at 37˚C using a FC MultiSkan device. *E. coli* strains BW25113 was used. All results are the average of min. 1 biological and 2 technical repeats, error bars indicate standard deviations.

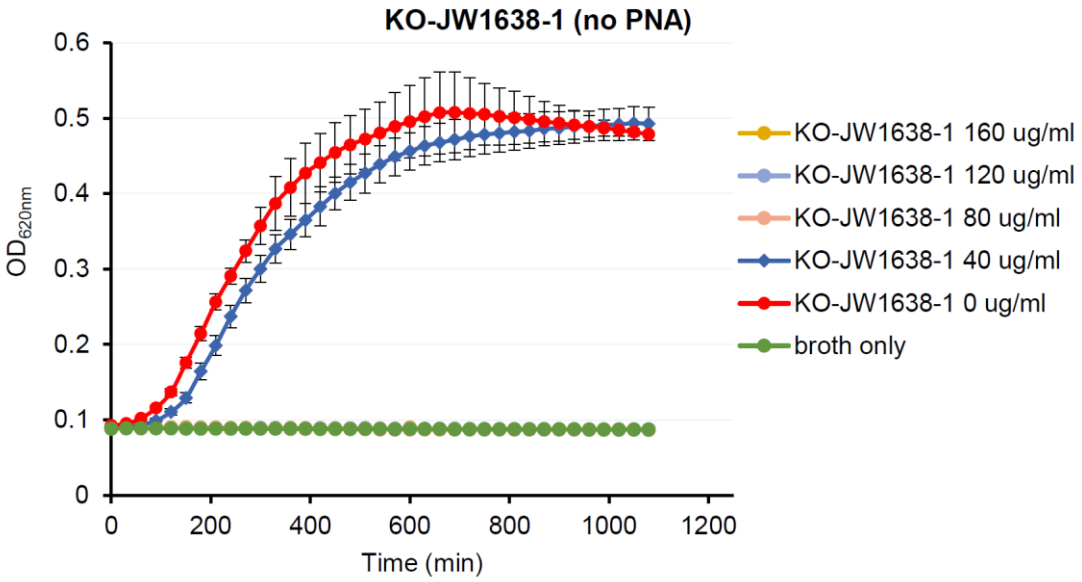

Figure A56. Optimizing the H_2O_2 concentration (range 40 – 160 µg/mL). *E. coli* cultures at 10^5 cfu/mL in a 96-well plate were incubated at 37°C for 30 min. Then, H_2O_2 was added at various concentrations and the OD_{620nm} was measured for 1200 min at 37˚C using a FC MultiSkan device. *E. coli* strains JW1638-1 was used. All results are the average of min. 1 biological and 2 technical repeats, error bars indicate standard deviations.

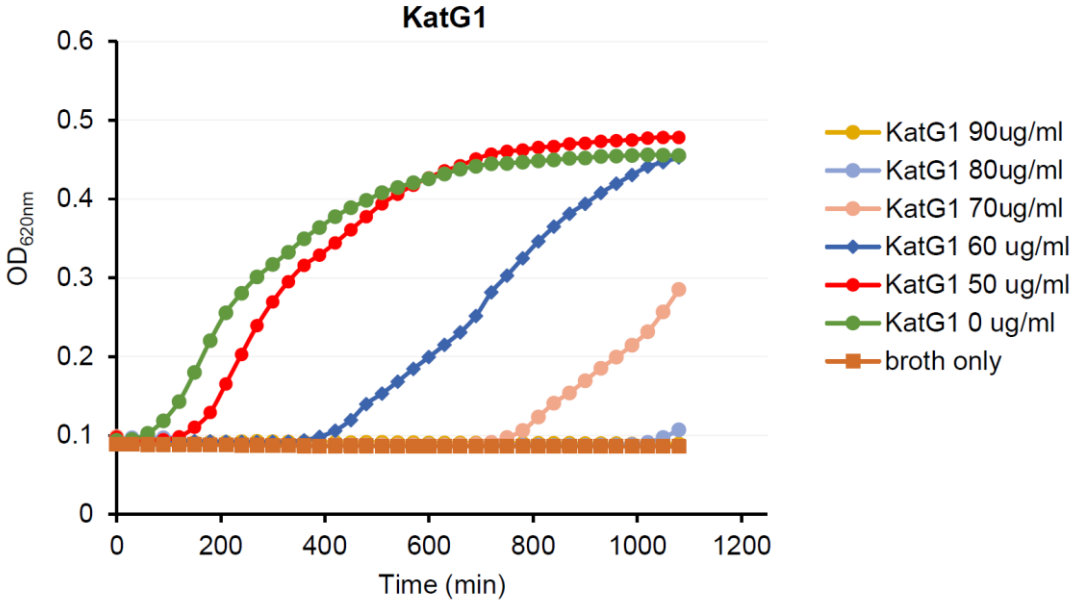

Figure A57. Optimizing the H_2O_2 concentration (range 50 – 90 µg/mL). 2 µM PNA-KatG1 was pre-mixed with *E. coli* cultures at 10^5 cfu/mL in a 96-well plate at 37°C for 30 min. Then, H_2O_2 was added at various concentrations and the OD_{620nm} was measured for 1200 min at 37˚C using a FC MultiSkan device. *E. coli* strains BW25113 was used. All results are the average of minimum 1 biological and 2 technical repeats, error bars indicate standard deviations.

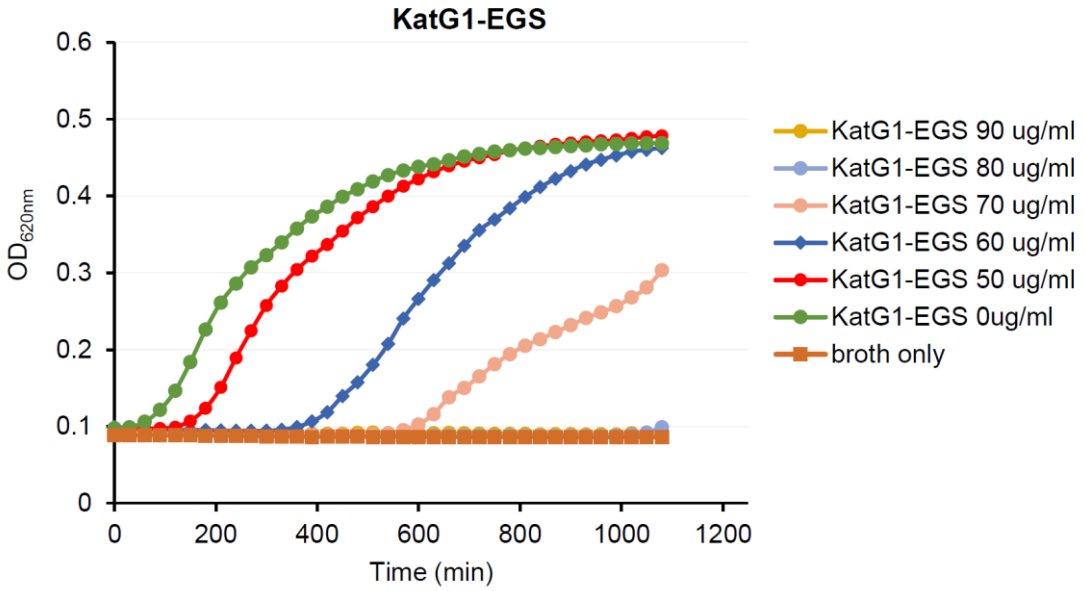

Figure A58. Optimizing the H_2O_2 concentration (range 50 – 90 µg/mL). 2 µM PNA-KatG1-EGS was pre-mixed with *E. coli* cultures at 10^5 cfu/mL in a 96-well plate at 37°C for 30 min. Then, H_2O_2 was added at various concentrations and the OD_{620nm} was measured for 1200 min at 37˚C using a FC MultiSkan device. *E. coli* strains BW25113 was used. All results are the average of minimum 1 biological and 2 technical repeats, error bars indicate standard deviations.

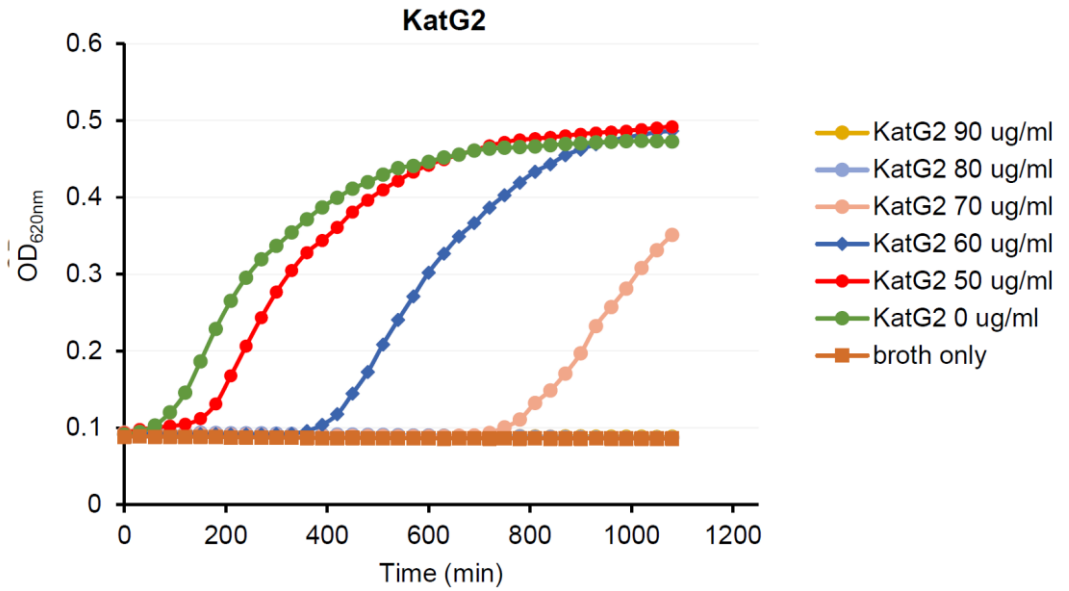

Figure A59. Optimizing the H_2O_2 concentration (range 50 – 90 µg/mL). 2 µM PNA-KatG2 was pre-mixed with *E. coli* cultures at 10^5 cfu/mL in a 96-well plate at 37°C for 30 min. Then, H_2O_2 was added at various concentrations and the OD_{620nm} was measured for 1200 min at 37˚C using a FC MultiSkan device. *E. coli* strains BW25113 was used. All results are the average of minimum 1 biological and 2 technical repeats, error bars indicatestandard deviations.

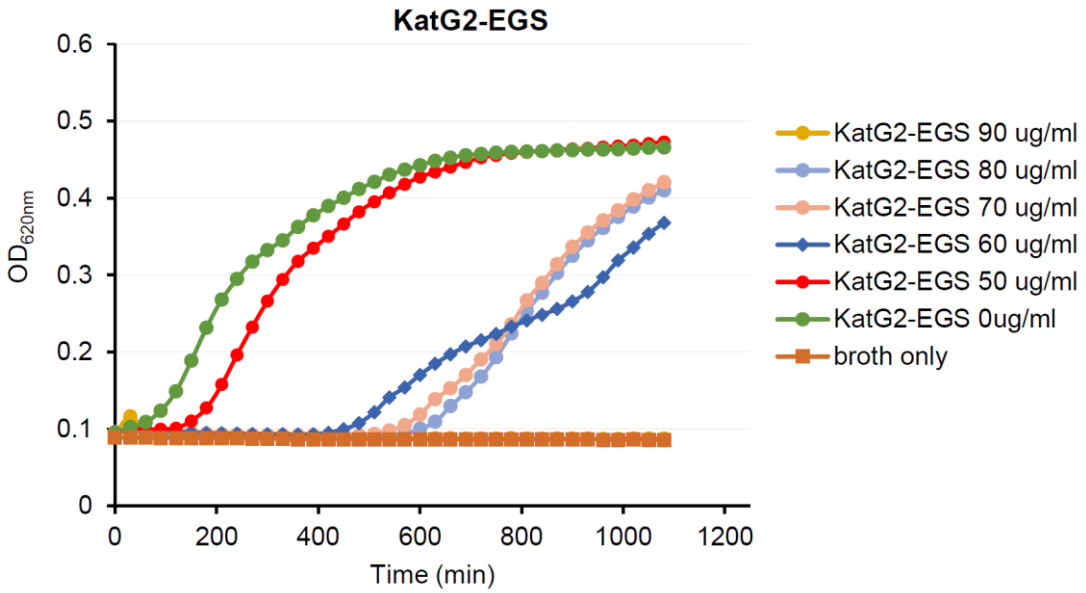

Figure A60. Optimizing the H_2O_2 concentration (range 50 – 90 µg/mL). 2 µM PNA-KatG2-EGS was pre-mixed with *E. coli* cultures at 10^5 cfu/mL in a 96-well plate at 37°C for 30 min. Then, H_2O_2 was added at various concentrations and the OD_{620nm} was measured for 1200 min at 37˚C using a FC MultiSkan device. *E. coli* strains BW25113 was used. All results are the average of minimum 1 biological and 2 technical repeats, error bars indicate standard deviations.

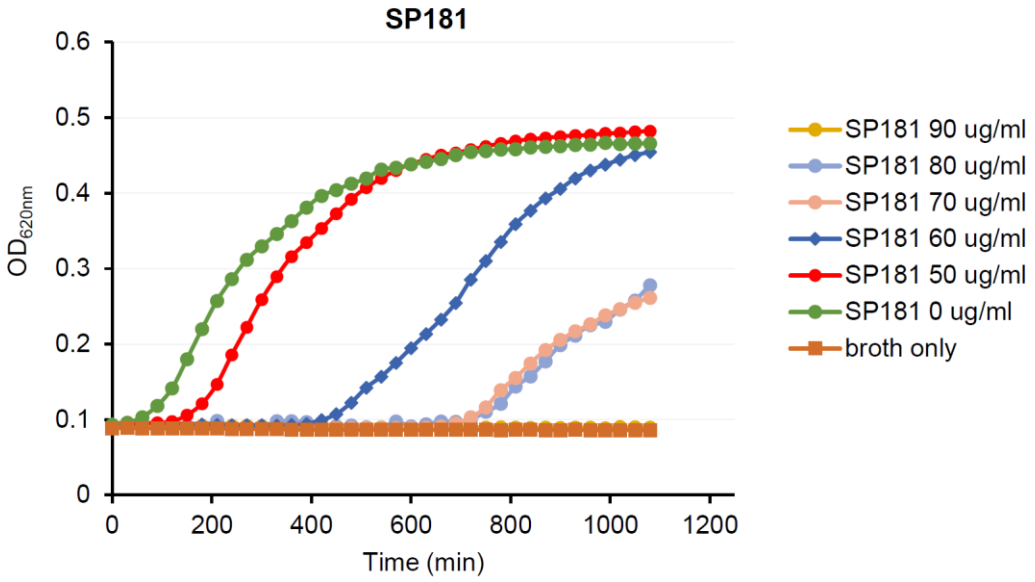

Figure A61. Optimizing the H_2O_2 concentration (range 50 – 90 µg/mL). 2 µM SP181 was pre-mixed with *E. coli* cultures at 10^5 cfu/mL in a 96-well plate at 37°C for 30 min. Then, H_2O_2 was added at various concentrations and the OD_{620nm} was measured for 1200 min at 37˚C using a FC MultiSkan device. *E. coli* strains BW25113 was used. All results are the average of minimum 1 biological and 2 technical repeats, error bars indicate standard deviations.

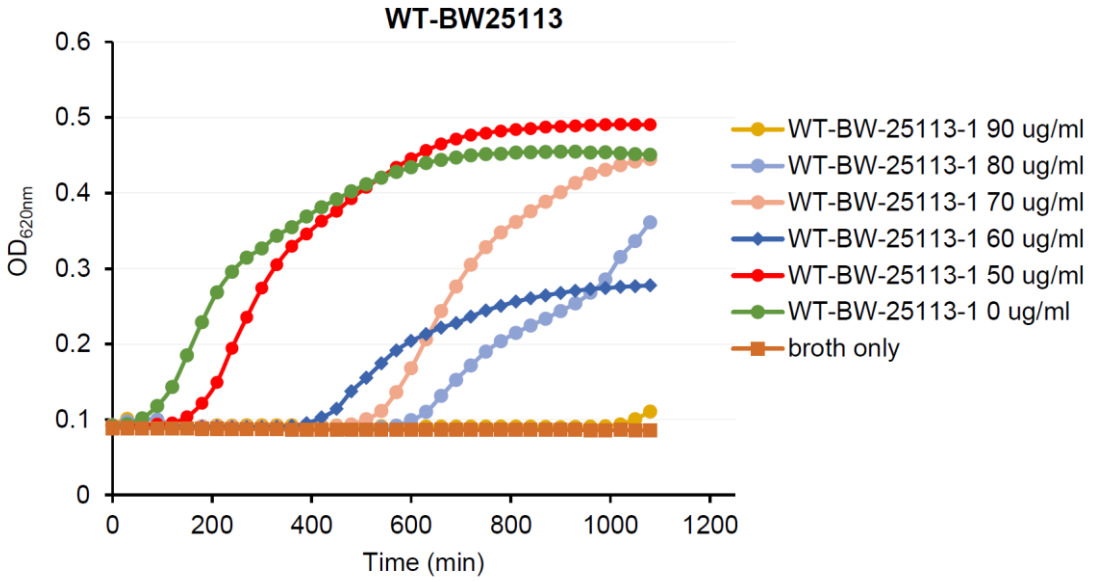

Figure A62. Optimizing the H_2O_2 concentration (range 50 – 90 µg/mL). *E. coli* cultures at 10^5 cfu/mL in a 96-well plate were incubated at 37°C for 30 min. Then, H_2O_2 was added at various concentrations and the OD_{620nm} was measured for 1200 min at 37˚C using a FC MultiSkan device. *E. coli* strains BW25113 was used. All results are the average of minimum 1 biological and 2 technical repeats, error bars indicate standard deviations.

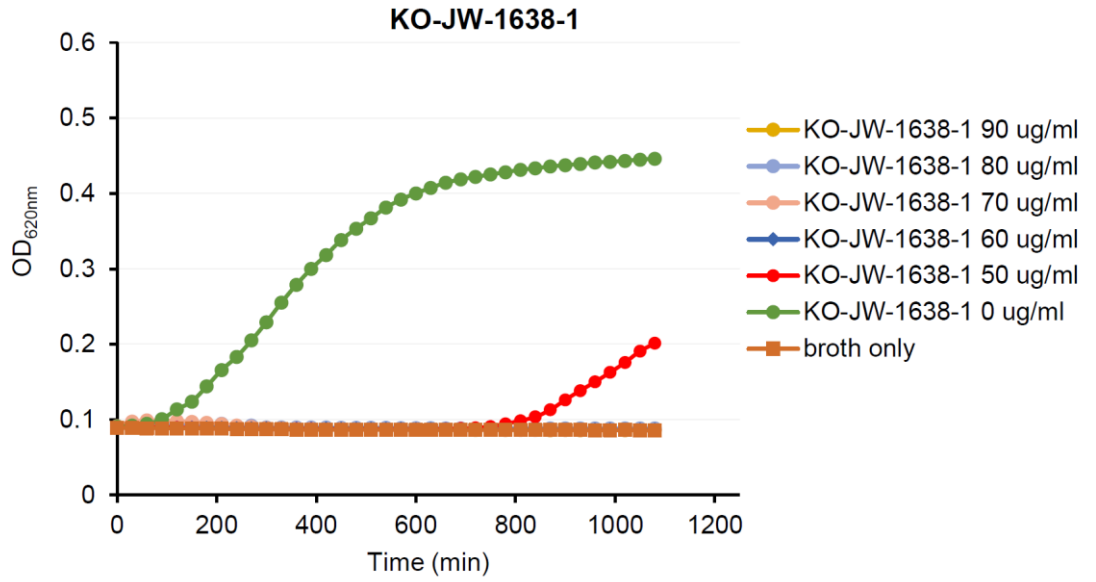

Figure A63. Optimizing the H_2O_2 concentration (range 50 – 90 µg/mL). *E. coli* cultures at 10^5 cfu/mL in a 96-well plate were incubated at 37°C for 30 min. Then, H_2O_2 was added at various concentrations and the OD_{620nm} was measured for 1200 min at 37˚C using a FC MultiSkan device. *E. coli* strains JW1638-1 was used. All results are the average of minimum 1 biological and 2 technical repeats, error bars indicate standard deviations.

A.4.3 Optimizing PNA/bacteria pre-mixing times for *katG* gene silencing assays

We wanted to see whether longer PNA/bacteria pre-mixing times of up to 2 hours are possible. It is necessary that the *E. coli* remains in the log phase in order to achieve an increase in PNA uptake, but still preventing the bacteria from overgrowing the initial PNA concentration. Monitoring the bacterial growth curves showed that the bacteria had a very slow growing rate during the 2 hours of pre-mixing the PNAs with the bacterial cultures (see **Figure A64**). For the final experiments (discussed in the main text) it was thus decided to use a 2 hours incubation time between the PNAs and the bacterial cultures, use H_2O_2 concentrations in the range 50-90 µg/mL (or 55-85 µg/mL), and to use PNA-111UNRLT as negative control.

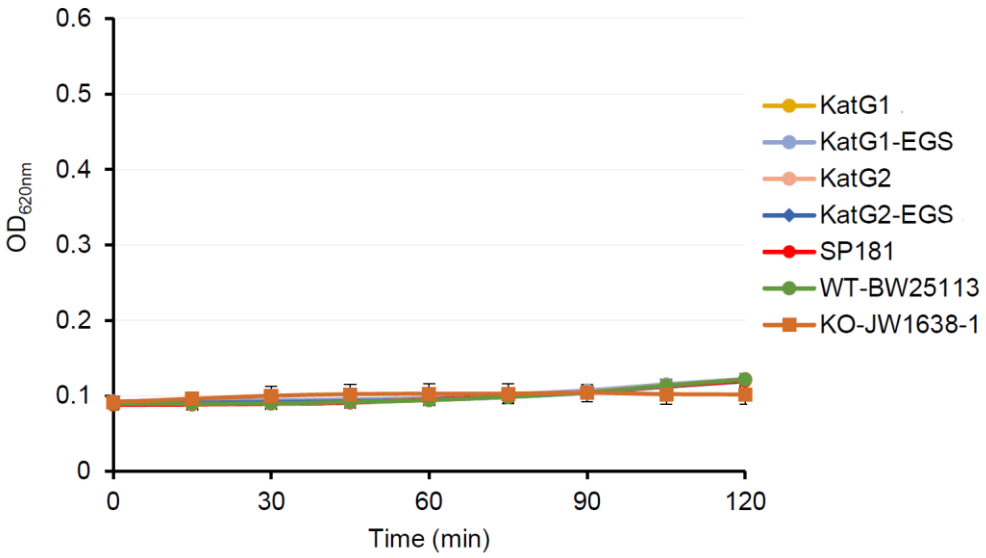

Figure A64. Growth curves for the bacterial cultures in the presence of 2 µM PNA. The hydrogen peroxide is not present at this stage (will be added after this pre-mixing step). 10 µL of PNA at 20 µM was added to 90 µL *E. coli* cultures at 10^5 cfu/mL in a 96 well plate, and the OD_{620nm} was measured for 120 min every 15 minutes at 37˚C using a FC MultiSkan device. *E. coli* strains BW25113 and JW1638-1 were used. All results are the average of minimum 1 biological and 2 technical repeats, with error bars indicating standard deviations. Vertical scale is the same as that of normal growth curves.

A.5 Full sequence of the *ftsZ* and *rnpB* genes

A.5.1 *ftsZ* sequence

The full-length sequence, obtained from EcoCyc, of the *E.coli ftsZ* gene is shown below. The area bolded and underlined corresponds to the 40 nucleotide region that was synthesized as a FAM-labelled target mRNA model for *in vitro* RNase P recruitment studies:

>gnl|ECOLI|EG10347 ftsZ "EG10347-MONOMER" 105305..106456 Escherichia coli K-12 substr. MG1655

atgTTTGAACCAATGGAACTTACCAATGACGCGGTGATTAAAGTCATCGGCGTCGGCGGCGGCGGCGGTAA
TGCTGTTGAACACATGGTGCGCGAGCGCATTGAAGGTGTTGAATTCTTCGCGGTAAATACCGATGCACAAG
CGCTGCGTAAAACAGCGGTTGGACAGACGATTCAAATCGGTAGCGGTATCACCAAAGGACTGGGCGCTGG
CGCTAATCCAGAAGTTGGCCGCAATGCGGCTGATGAGGATCGCGATGCATTGCGTGCGGCGCTGGAAGGT
GCAGACATGGTCTTTATTGCTGCGGGTATGGGTGGTGGTACCGGTACAGGTGCAGCACCAGTCGTCGCTG
AAGTGGCAAAAGATTTGGGTATCCTGACCGTTGCTGTCGTCACTAAGCCTTTCAACTTTGAAGGCAAGAAG
CGTATGGCATTCGCGGAGCAGGGGATCACTGAACTGTCCAAGCATGTGGACTCTCTGATCACTATCCCGAA
CGACAAACTGCTGAAAGTTCTGGGCCGCGGTATCTCCCTGCTGGATGCGTTTGGCGCAGCGAACGATGTAC
TGAAAGGCGCTGTGCAAGGTATCGCTGAACTGATTACTCGTCCGGGTTTGATGAACGTGGACTTTGCAGAC
GTACGCACCGTAATGTCTGAGATGGGCTACGCAATGATGGGTTCTGGCGTGGCGAGCGGTGAAGACCGTG
CGGAAGAAGCTGCTGAAATGGCTATCTCTTCTCCGCTGCTGGAAGATATCGACCTGTCTGGCGCGCGCGGC
GTGCTGGTTAACATCACG**GCGGGCTTCGACCTGCGTCTGGATGAGTTCGAAACGGTAG**GTAACACCATCC
GTGCATTTGCTTCCGACAACGCGACTGTGGTTATCGGTACTTCTCTTGACCCGGATATGAATGACGAGCTGC
GCGTAACCGTTGTTGCGACAGGTATCGGCATGGACAAACGTCCTGAAATCACTCTGGTGACCAATAAGCAG
GTTCAGCAGCCAGTGATGGATCGCTACCAGCAGCATGGGATGGCTCCGCTGACCCAGGAGCAGAAGCCGG
TTGCTAAAGTCGTGAATGACAATGCGCCGCAAACTGCGAAAGAGCCGGATTATCTGGATATCCCAGCATTC
CTGCGTAAGCAAGCTGATtaa-3`

A.5.2 *rnpB* sequence

The full-length sequence, obtained from EcoCyc, of the *E.coli rnpB* gene is shown below. This gene was used for the synthesis of M1RNA:

>gnl|ECOLI|EG30069 rnpB "RNPB-RNA" (complement(3270592..3270216)) Escherichia coli K-12 substr. MG1655

GAAGCTGACCAGACAGTCGCCGCTTCGTCGTCGTCCTCTTCGGGGGAGACGGGCGGAGGGGAGGAAAGT
CCGGGCTCCATAGGGCAGGGTGCCAGGTAACGCCTGGGGGGGAAACCCACGACCAGTGCAACAGAGAGC
AAACCGCCGATGGCCCGCGCAAGCGGGATCAGGTAAGGGTGAAAGGGTGCGGTAAGAGCGCACCGCGC
GGCTGGTAACAGTCCGTGGCACGGTAAACTCCACCCGGAGCAAGGCCAAATAGGGGTTCATAAGGTACGG

CCCGTACTGAACCCGGGTAGGCTGCTTGAGCCAGTGAGCGATTGCTGGCCTAGATGAATGACTGTCCACG
ACAGAACCCGGCTTATCGGTCAGTTTCACCT

A.6 Additional gels of the *in vitro* RNase P assay

To investigate the *in vitro* RNase P recruiting ability of PNAs, we used an optimized version of an assay published by Tolmasky. Additional optimization gels, as well as the full gel (uncropped) of the results shown in the main text are given in this section (**Figure A65 - Figure A73**).

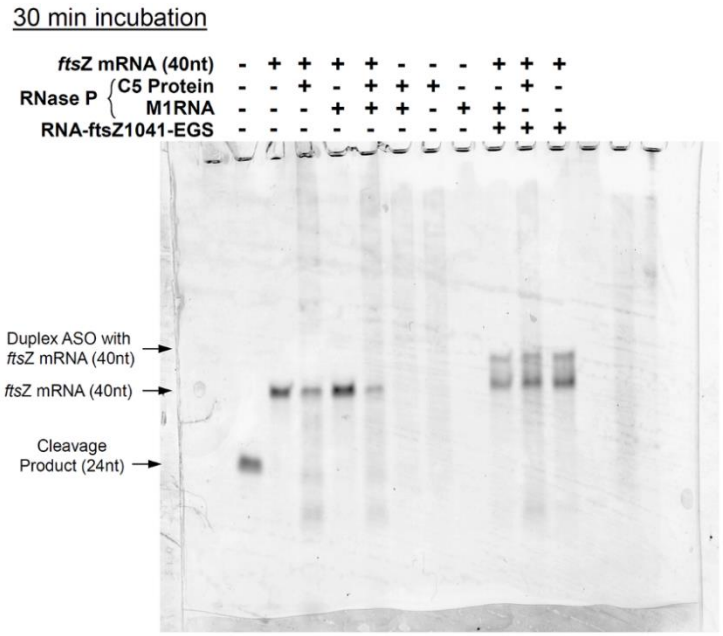

Figure A65. *In vitro* RNase P recruitment by Tolmasky's RNA-ftsZ1041-EGS. A mixture of the FAM labelled ftsZ mRNA (40nt) target (1 pmol) and RNA-ftsZ1041-EGS (50 pmol) were preincubated at 25 °C for 2 hours. M1RNA (5 pmol) and C5 (70 pmol) were preincubated at 37 °C for 15 mins, and then added to the preincubated target/ASO mixture. The reaction was run at 37 °C for 30 min and stopped by adding gel loading buffer (95% formamide, 1 mM EDTA, 0.01% Bromophenol Blue). The samples were analysed by 15% urea-PAGE and visualized using a GE Typhoon FLA 7000 biomolecular imager equipped with a FAM filter. The first well contains a synthesised FAM labelled 24-mer that is used as a ladder.

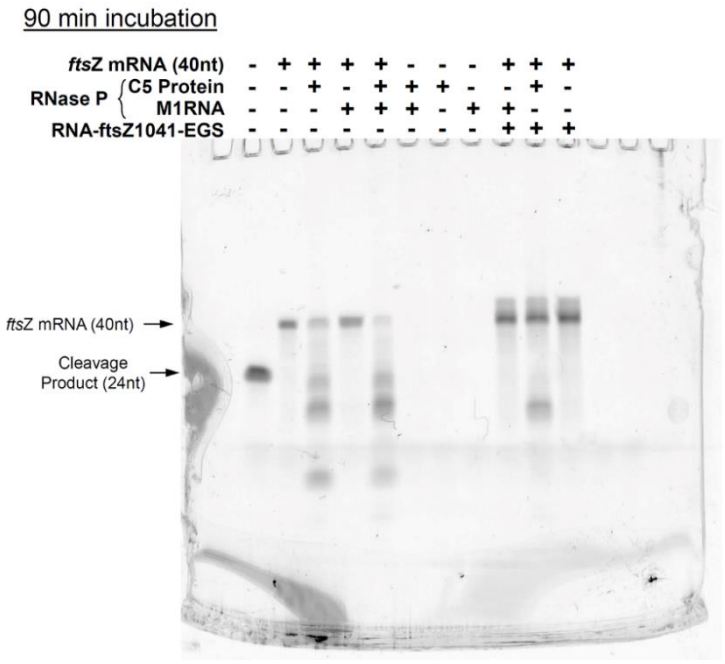

Figure A66. *In vitro* RNase P recruitment by Tolmasky's RNA-ftsZ1041-EGS. A mixture of the FAM labelled ftsZ mRNA (40nt) target (1 pmol) and RNA-ftsZ1041-EGS (50 pmol) were preincubated at 25 °C for 2 hours. M1RNA (5 pmol) and C5 (70 pmol) were preincubated at 37 °C for 15 mins, and then added to the preincubated target/ASO mixture. The reaction was run at 37 °C for 90 min and stopped by adding gel loading buffer (95% formamide, 1 mM EDTA, 0.01% Bromophenol Blue). The samples were analysed by 15% urea-PAGE and visualized using a GE Typhoon FLA 7000 biomolecular imager equipped with a FAM filter. The first well contains a synthesised FAM labelled 24-mer that is used as a ladder.

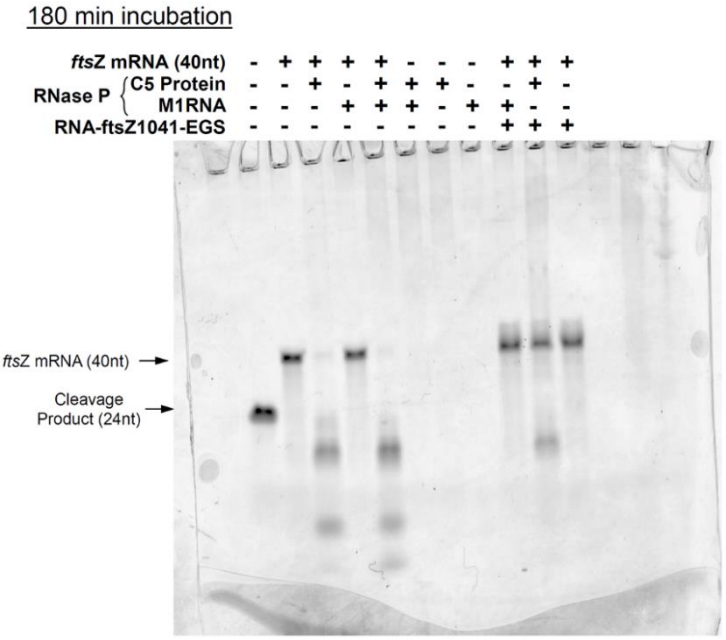

Figure A67. *In vitro* RNase P recruitment by Tolmasky's RNA-ftsZ1041-EGS. A mixture of the FAM labelled ftsZ mRNA (40nt) target (1 pmol) and RNA-ftsZ1041-EGS (50 pmol) were preincubated at 25 °C for 2 hours. M1RNA (5 pmol) and C5 (70 pmol) were preincubated at 37 °C for 15 mins, and then added to the preincubated target/ASO mixture. The reaction was run at 37 °C for 180 min and stopped by adding gel loading buffer (95% formamide, 1 mM EDTA, 0.01% Bromophenol Blue). The samples were analysed by 15% urea-PAGE and visualized using a GE Typhoon FLA 7000 biomolecular imager equipped with a FAM filter. The first well contains a synthesised FAM labelled 24-mer that is used as a ladder.

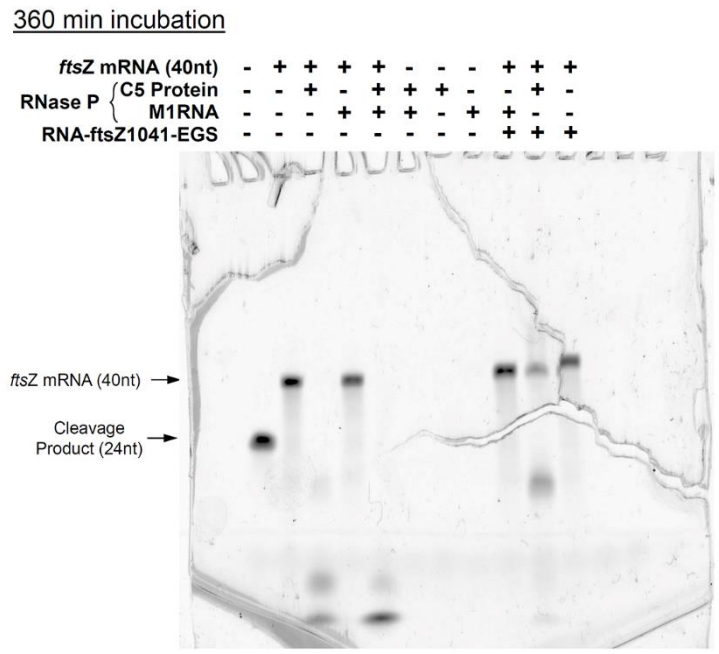

Figure A68. *In vitro* RNase P recruitment by Tolmasky's RNA-ftsZ1041-EGS. A mixture of the FAM labelled ftsZ mRNA (40nt) target (1 pmol) and RNA-ftsZ1041-EGS (50 pmol) were preincubated at 25 °C for 2 hours. M1RNA (5 pmol) and C5 (70 pmol) were preincubated at 37 °C for 15 mins, and then added to the preincubated target/ASO mixture. The reaction was run at 37 °C for 360 min and stopped by adding gel loading buffer (95% formamide, 1 mM EDTA, 0.01% Bromophenol Blue). The samples were analysed by 15% urea-PAGE and visualized using a GE Typhoon FLA 7000 biomolecular imager equipped with a FAM filter. The first well contains a synthesised FAM labelled 24-mer that is used as a ladder.

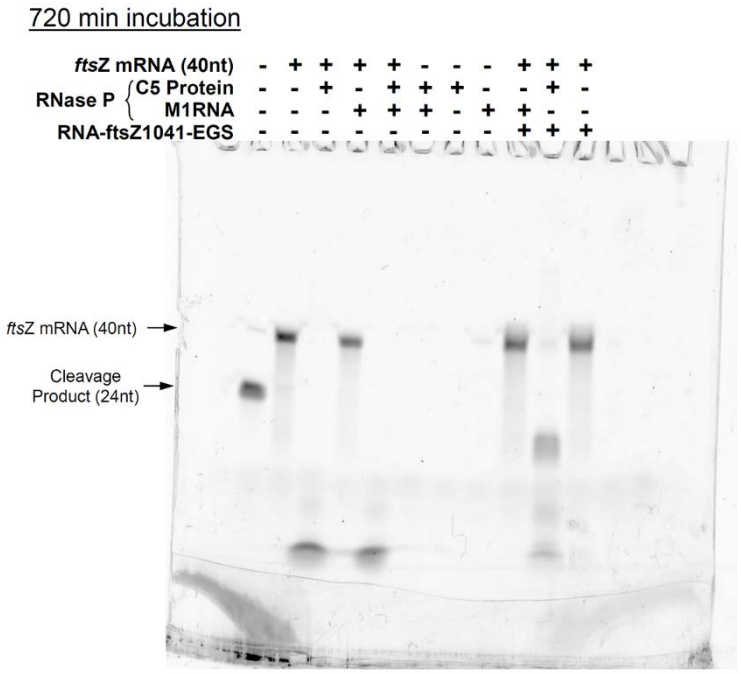

Figure A69. *In vitro* RNase P recruitment by Tolmasky's RNA-ftsZ1041-EGS. A mixture of the FAM labelled ftsZ mRNA (40nt) target (1 pmol) and RNA-ftsZ1041-EGS (50 pmol) were preincubated at 25 °C for 2 hours. M1RNA (5 pmol) and C5 (70 pmol) were preincubated at 37 °C for 15 mins, and then added to the preincubated target/ASO mixture. The reaction was run at 37 °C for 720 min and stopped by adding gel loading buffer (95% formamide, 1 mM EDTA, 0.01% Bromophenol Blue). The samples were analysed by 15% urea-PAGE and visualized using a GE Typhoon FLA 7000 biomolecular imager equipped with a FAM filter. The first well contains a synthesised FAM labelled 24-mer that is used as a ladder.

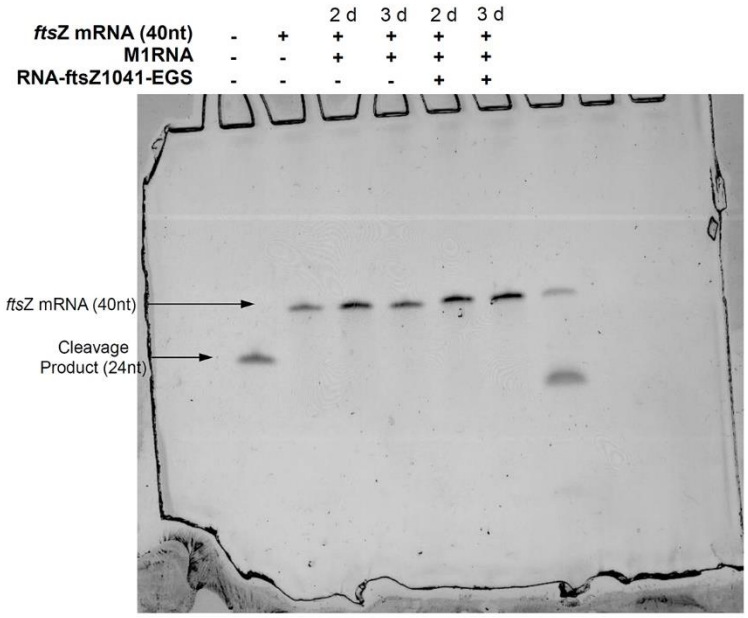

Figure A70. *In vitro* M1RNA recruitment by Tolmasky's RNA-ftsZ1041-EGS. A mixture of the FAM labelled *ftsZ* mRNA (40nt) target (1 pmol) and RNA-ftsZ1041-EGS (50 pmol) were preincubated at 25 °C for 2 hours, followed by the addition of M1RNA (10 pmol). The reaction was run at 37 °C for 2days (2 d) and 3 days (3 d), and stopped by adding gel loading buffer (95% formamide, 1 mM EDTA, 0.01% Bromophenol Blue). The samples were analysed by 15% urea-PAGE and visualized using a GE Typhoon FLA 7000 biomolecular imager equipped with a FAM filter. The first well contains a synthesised FAM labelled 24-mer that is used as a ladder.

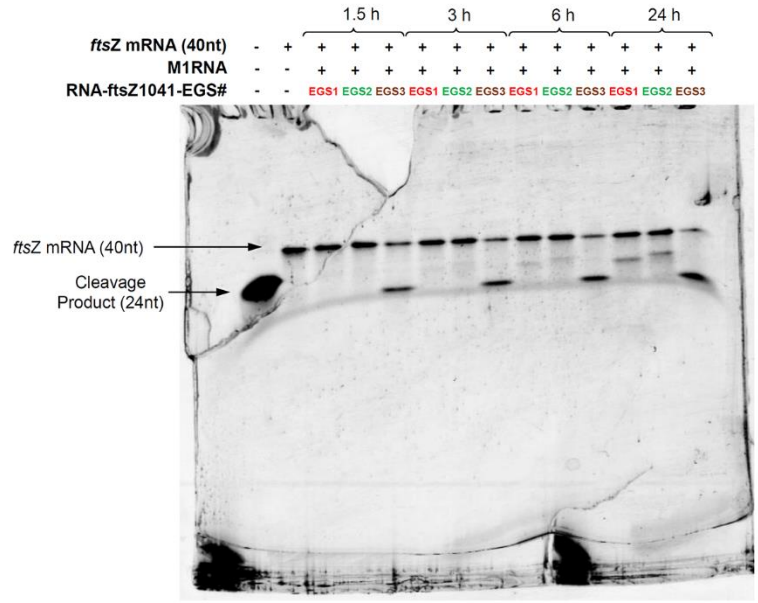

Figure A71. Exploring the RNase P recruitment by the newly designed ASOs targeting new regions (RNA-ftsZ1041-EGS1, RNA-ftsZ1041-EGS2 and RNA-ftsZ1041-EGS3). A mixture of the FAM labelled *ftsZ* mRNA (40nt) target (2 pmol) and RNA-ftsZ1041-EGS# (2.2 pmol) were preincubated at 25 °C for 15 min, followed by the addition of M1RNA (8.8 pmol). The reaction was run at 37 °C for 1.5, 3, 6 and 24 hours, and stopped by adding gel loading buffer (95% formamide, 1 mM EDTA, 0.01% Bromophenol Blue). The samples were analysed by 15% urea-PAGE and visualized using a GE Typhoon FLA 7000 biomolecular imager equipped with a FAM filter.

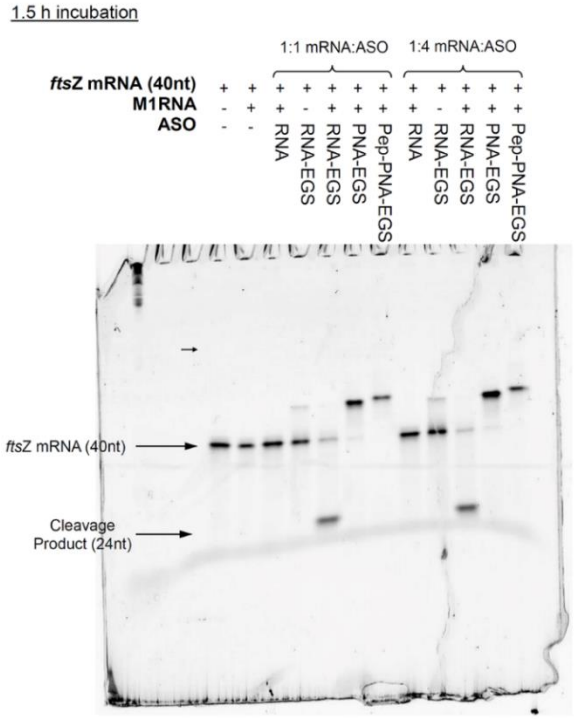

Figure A72. Potential *in vitro* recruitment of RNase P by PNAs. A mixture of the FAM labelled *ftsZ* mRNA (40nt) target (2 pmol) and ASO (2.2 pmol or 8.8 pmol) were preincubated at 25 °C for 15 min, followed by the addition of M1RNA (8.8 pmol). The reaction was run at 37 °C for 1.5 hours, and stopped by adding gel loading buffer (95% formamide, 1 mM EDTA, 0.01% Bromophenol Blue). The samples were analysed by 15% urea-PAGE and visualized using a GE Typhoon FLA 7000 biomolecular imager equipped with a FAM filter.

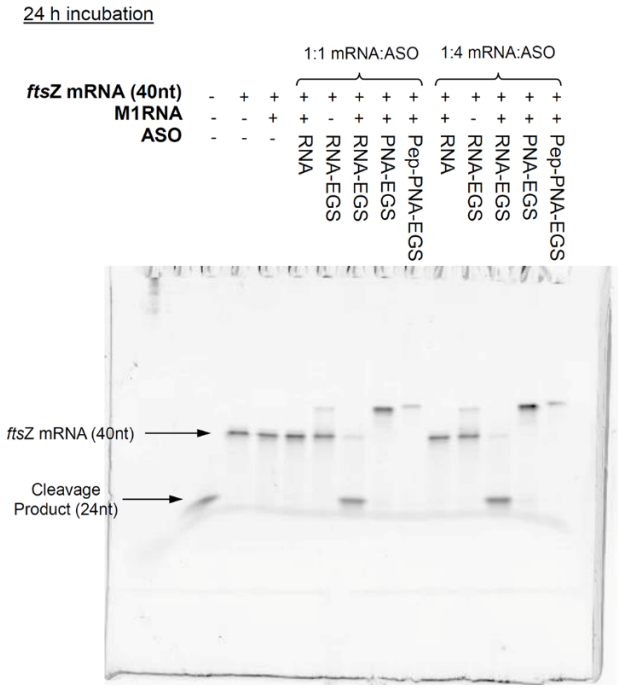

Figure A73. Potential *in vitro* recruitment of RNase P by PNAs. A mixture of the FAM labelled *ftsZ* mRNA (40nt) target (2 pmol) and ASO (2.2 pmol or 8.8 pmol) were preincubated at 25 °C for 15 min, followed by the addition of M1RNA (8.8 pmol). The reaction was run at 37 °C for 24 hours, and stopped by adding gel loading buffer (95% formamide, 1 mM EDTA, 0.01% Bromophenol Blue). The samples were analysed by 15% urea-PAGE and visualized using a GE Typhoon FLA 7000 biomolecular imager equipped with a FAM filter.

Appendix B Supporting Information for Chapter 3

B.1 HPLC chromatograms of synthesized oligonucleotides

This section provides the analytical HPLC chromatograms for all LNA-DNA gapmers, peptides and target mRNA oligonucleotides synthesized for Chapter 3 (**Figure B1** - **Figure B11**).

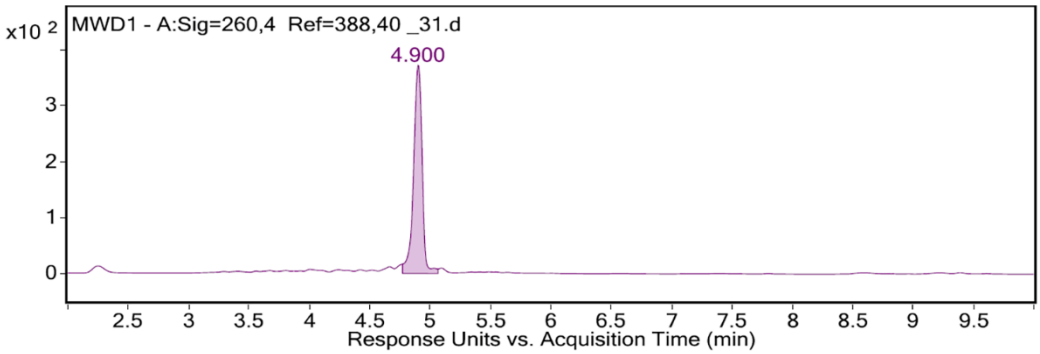

Figure B1. Analytical HPLC of purified Gap-1 (reverse-phase C18 column, detector 260 nm). Purity > 90%.

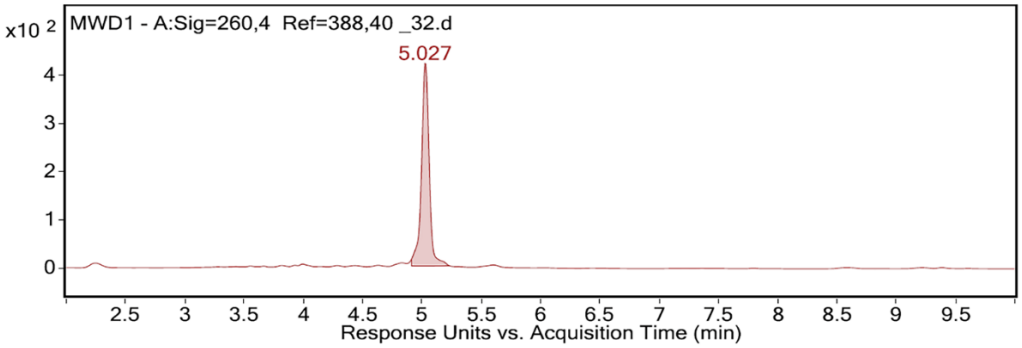

Figure B2. Analytical HPLC of purified Gap-2 (reverse-phase C18 column, detector 260 nm). Purity > 90%.

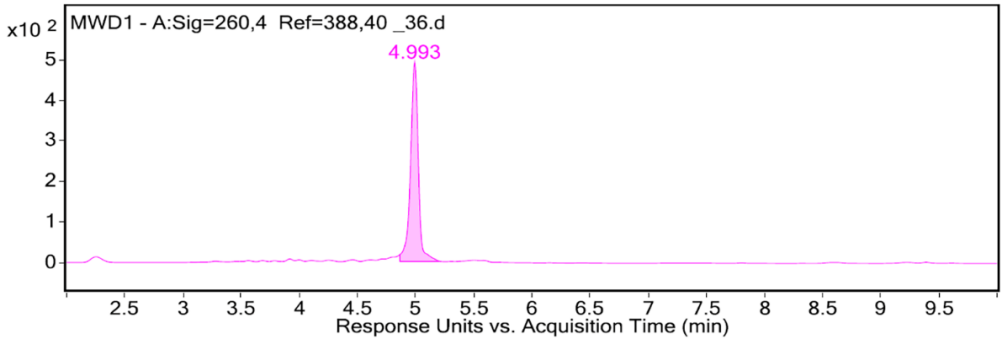

Figure B3. Analytical HPLC of purified Gap-3 (reverse-phase C18 column, detector 260 nm). Purity > 90%.

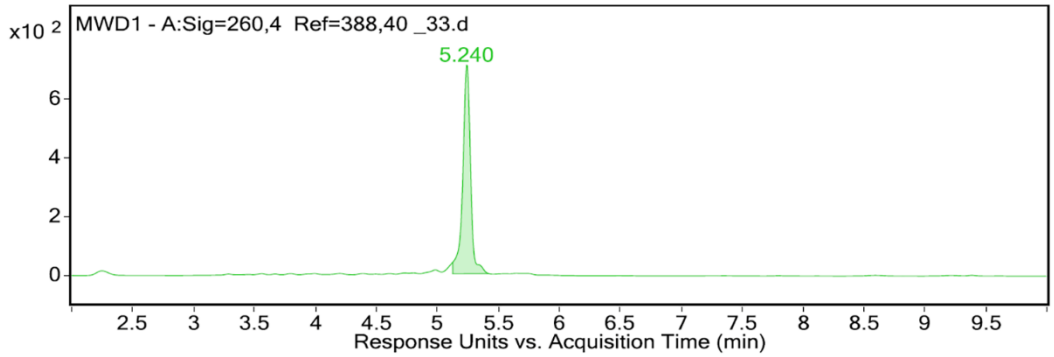

Figure B4. Analytical HPLC of purified Gap-4 (reverse-phase C18 column, detector 260 nm). Purity > 90%.

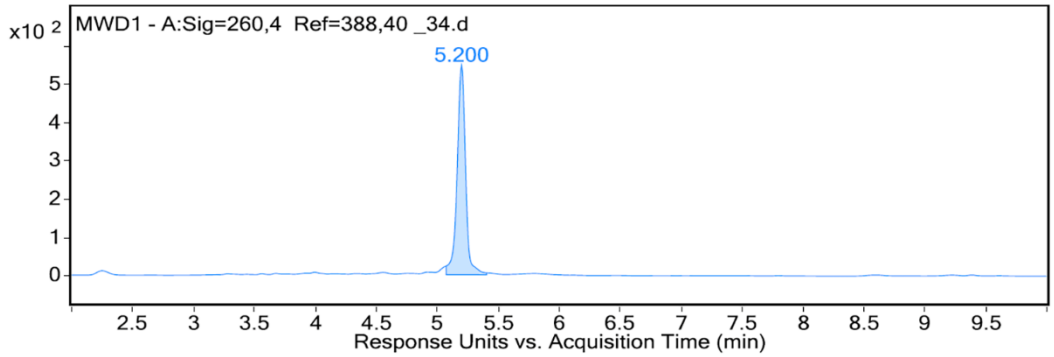

Figure B5. Analytical HPLC of purified Gap-5 (reverse-phase C18 column, detector 260 nm). Purity > 90%.

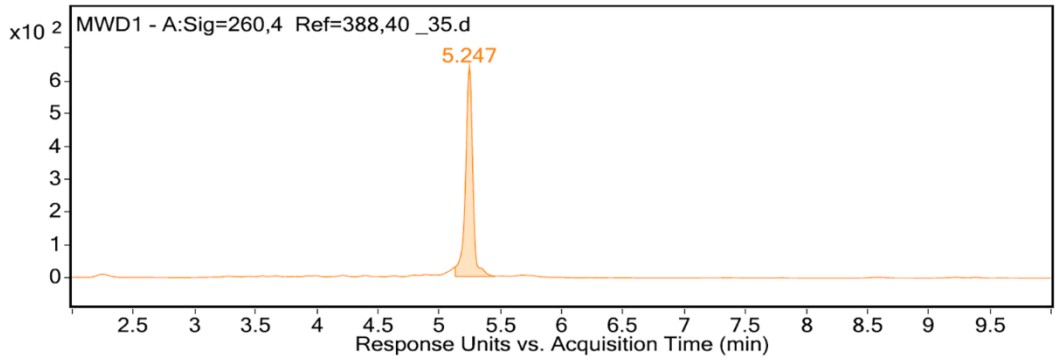

Figure B6. Analytical HPLC of purified Gap-6 (reverse-phase C18 column, detector 260 nm). Purity > 90%.

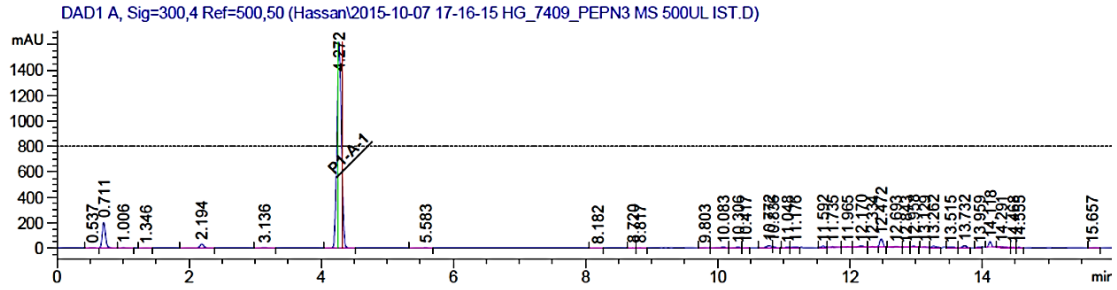

Figure B7. Analytical HPLC of the purified cell penetrating peptide $(KFF)_3K$ (reverse-phase C18 column, detector at 300 nm). Purity > 79.5%.

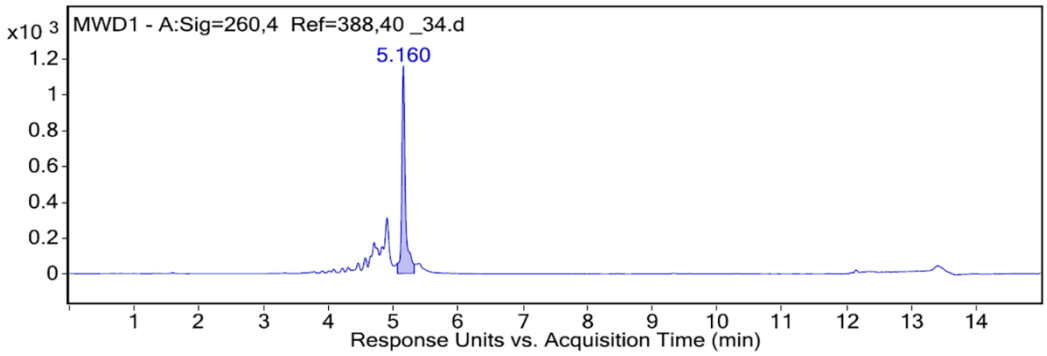

Figure B8. Analytical HPLC of purified ftsZ-UTR-mRNA (reverse-phase C18 column, detector 260 nm). Purity > 75%.

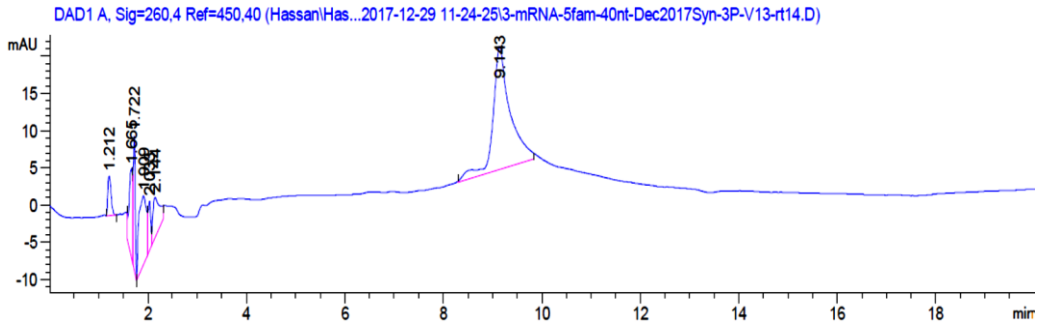

Figure B9. Analytical HPLC of purified ftsZ-1041-mRNA (reverse-phase C18 column, detector 260 nm). Purity 85.0%.

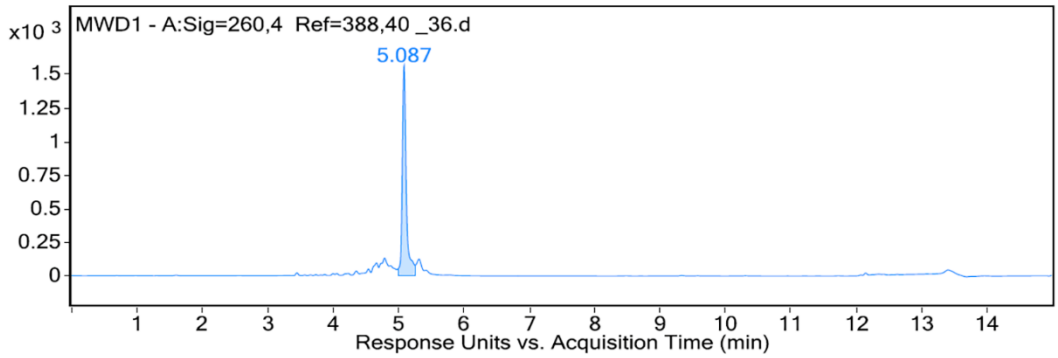

Figure B10. Analytical HPLC of purified ftsZ-458-mRNA (reverse-phase C18 column, detector 260 nm). Purity > 90%.

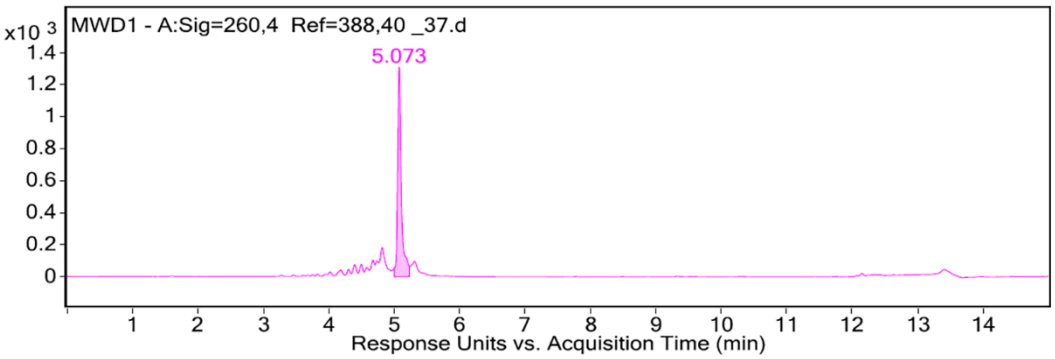

Figure B11. Analytical HPLC of purified ftsZ-885-mRNA (reverse-phase C18 column, detector 260 nm). Purity > 90%.

B.2 Additional gels of the *in vitro* RNase H assay

The *in vitro* activity of the gapmers was investigated using RNase H kit EN0201, purchased from Thermo Fisher Scientific. In 30 µL reaction were mixed 4 x 10^{-3} units of RNase H, 2 pmol target mRNA, 8.8 pmol gapmer and 10x reaction buffer. The reaction was run at 37 °C for 24 hours. At two different time points (1.5 h and 24 h), a 7 µL sample was withdrawn from the reaction, and 7 µL formamide was added to stop the reaction. The samples were subsequently loaded onto a denaturing 15% urea polyacrylamide gel, run using electrophoresis and visualized on a GE Typhoon FLA 7000 biomolecular with the FAM channel at 700 pmt. The results are shown in **Figure B12-Figure B13.**

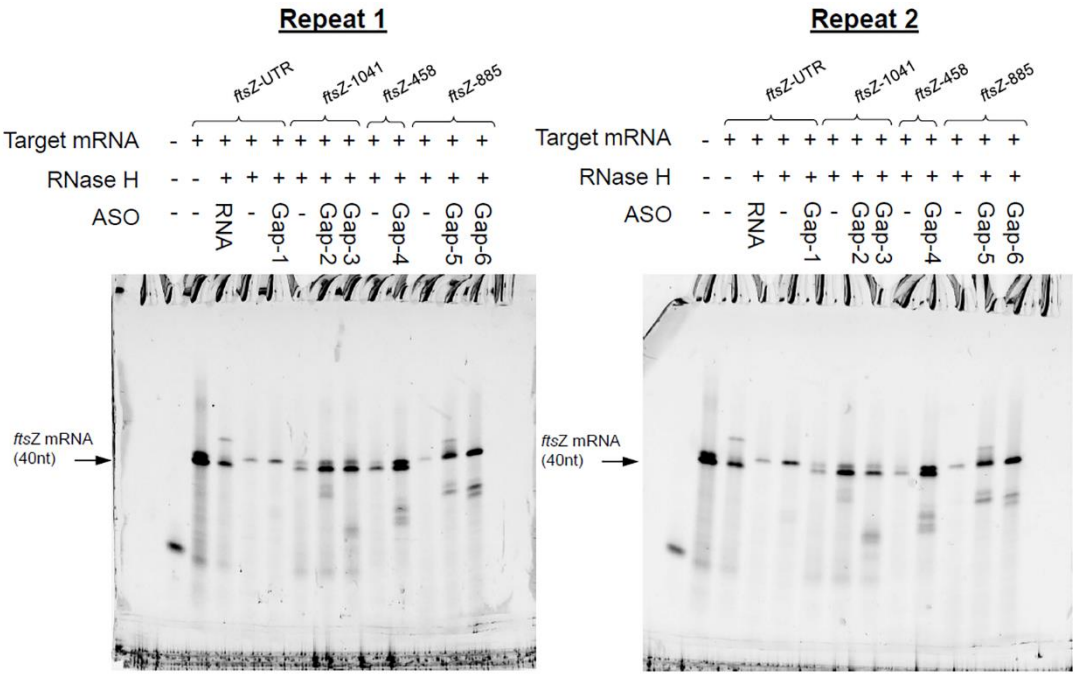

Figure B12. *In vitro* recruitment of RNase H by the LNA-DNA-LNA gapmers. A mixture of RNase H (4 x 10^{-3} units), the FAM labelled target mRNA (2 pmol) and ASO (8.8 pmol) were incubated at at 37 °C for 1.5 hour and stopped by adding formamide. The samples were analysed by 15% urea-PAGE and visualized using a Typhoon FLA 7000 biomolecular imager equipped with a FAM filter. The location and size of the initial target is shown on the left, bands below the target band are presumably due to RNase H mediated cleavage of the target mRNA. The first well contains a FAM-labelled 17-mer that is used as a ladder. The compound labelled 'RNA' is an unmodified RNA analogue of the gapmers.

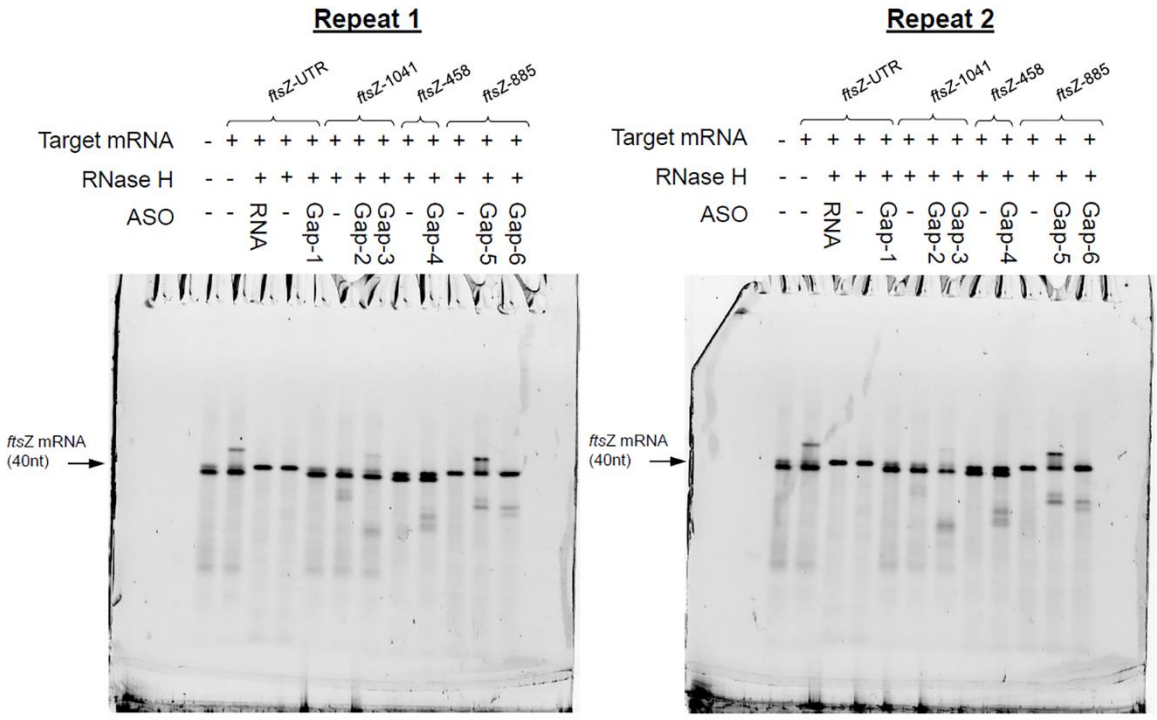

Figure B13. *In vitro* recruitment of RNase H by the LNA-DNA-LNA gapmers. A mixture of RNase H (4 x 10^{-3} units), the FAM labelled target mRNA (2 pmol) and ASO (8.8 pmol) were incubated at at 37 °C for 24 hours and stopped by adding formamide. The samples were analysed by 15% urea-PAGE and visualized using a Typhoon FLA 7000 biomolecular imager equipped with a FAM filter. The location and size of the initial target is shown on the left, bands below the target band are presumably due to RNase H mediated cleavage of the target mRNA. The first well contains a FAM-labelled 17-mer that is used as a ladder. The compound labelled 'RNA' is an unmodified RNA analogue of the gapmers.

B.3 Additional growth curves

We wanted to see if some of the LNA-DNA-LNA gapmers can be taken up by *E. coli* cells without the aid of the $(KFF)_3K$ peptide. To increase the chance of a positive result, the gapmers where tested at high concentration. However, we noticed that the growth curves of *E. coli* AS19 became very erratic in the presence of the gapmers (see main text). A second biological repeat was thus conducted for this experiment, and similarly noisy curves were obtained (**Figure B14**). The AS19 cells grew slower in this experiment and the results were therefore not averaged with the first growth curves (AS19 is a 'weaker', more permeable strain and often grows very slowly).

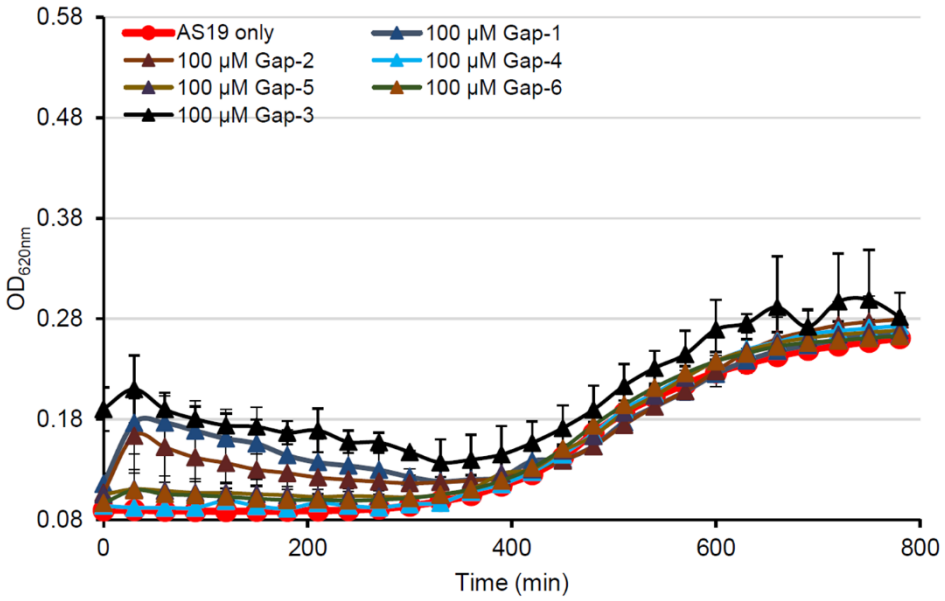

Figure B14. Potential silencing of *ftsZ* by high concentrations of LNA-DNA-LNA gapmers in *E. coli* AS19. The *E. coli* strains at 10^5 cfu/mL were added to the gapmer (final concentration 100 µM), and the OD_{620nm} value was measured for 800 minutes at 37°C. The results are the average of at least 1 biological and 2 technical repeats, with error bars representing standard deviations.

B.4 Microscopy studies for the detection of *ftsZ* silencing (40x)

We tried to detect *fts*Z gene silencing by looking for the indicative elongation phenotype using microscopy techniques. Gapmers were added to 100 µL of *E. coli* AS19 cultures at 10^5 cfu/mL to achieve a final concentration of 100 µM. The mixture was subsequently incubated at 37 °C whilst shaking. At various time points, 10 µL of the bacterial culture was transferred onto an adhesive microscope slide and visualized in brightfield mode on a Leica DMi8 inverted microscope with 20x and 40x objectives. The contrast of the images was digitally enhanced using ImageJ.[290] The images obtained with a 20x objective are shown in the main text. The images obtained with a 40x objective are provided in this section (**Figure B15 – Figure B25**).

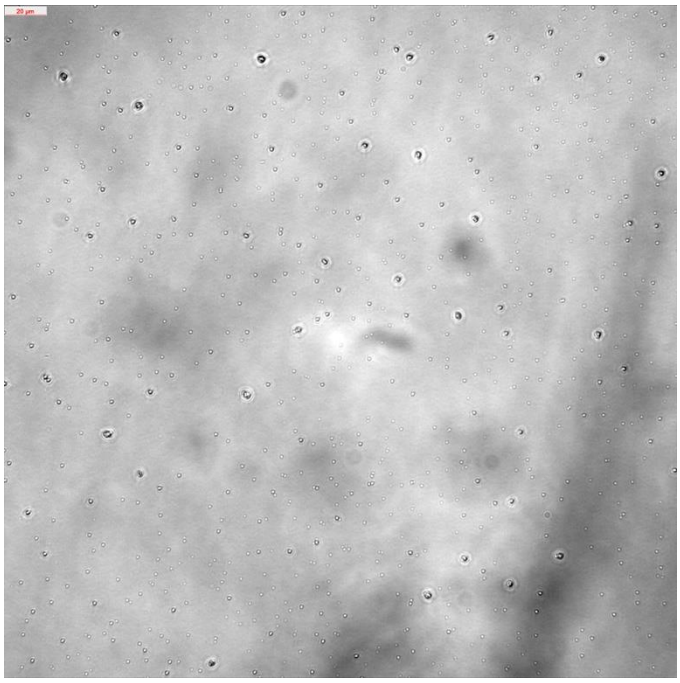

Figure B15. Brightfield images of *E. coli* AS19 incubated for 200 min at 37 °C in the absence of any gapmer. The experiment was performed as described in the main text (40x objective). The scale bar represents 20 µm.

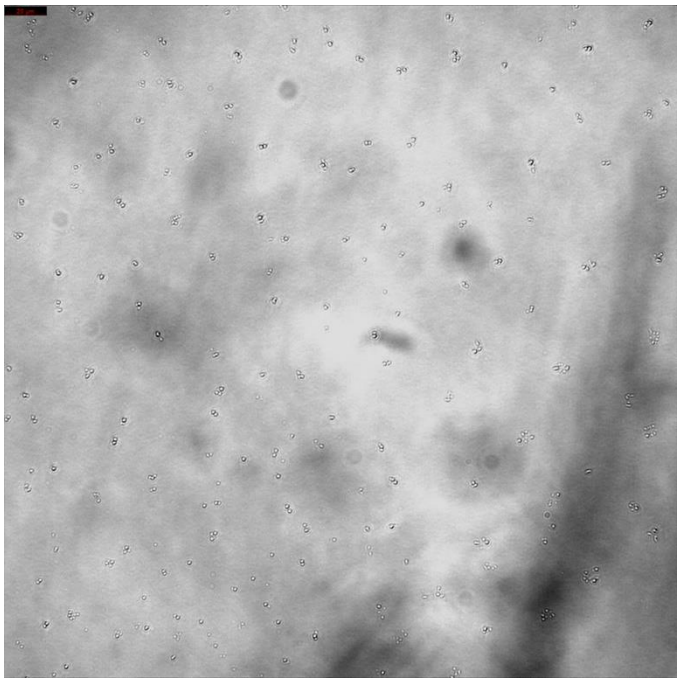

Figure B16. Brightfield images of *E. coli* AS19 incubated for 400 min at 37 °C in the absence of any gapmer. The experiment was performed as described in the main text (40x objective). The scale bar represents 20 µm.

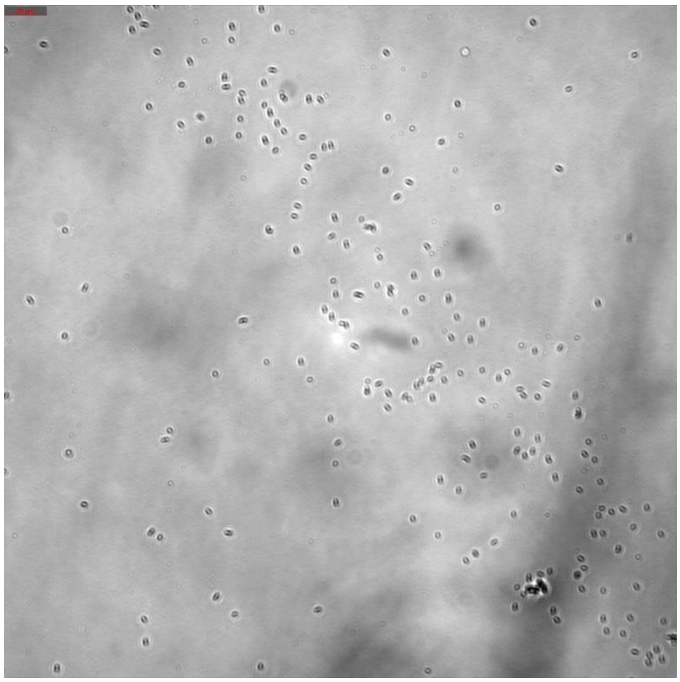

Figure B17. Brightfield images of *E. coli* AS19 incubated for 600 min at 37 °C in the absence of any gapmer. The experiment was performed as described in the main text (40x objective). The scale bar represents 20 µm.

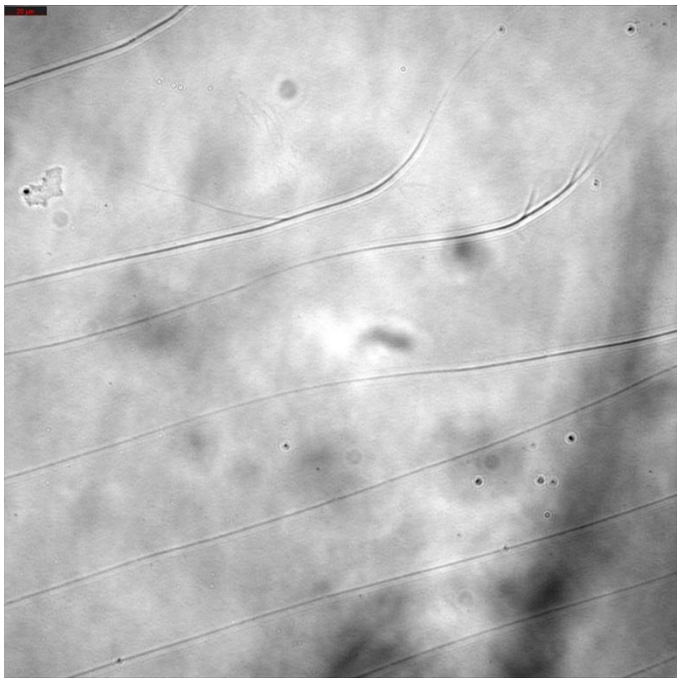

Figure B18. Brightfield images of *E. coli* AS19 incubated for 200 min at 37 °C in the presence of 100 µM Gap-1. The experiment was performed as described in the main text (40x objective). The scale bar represents 20 µm.

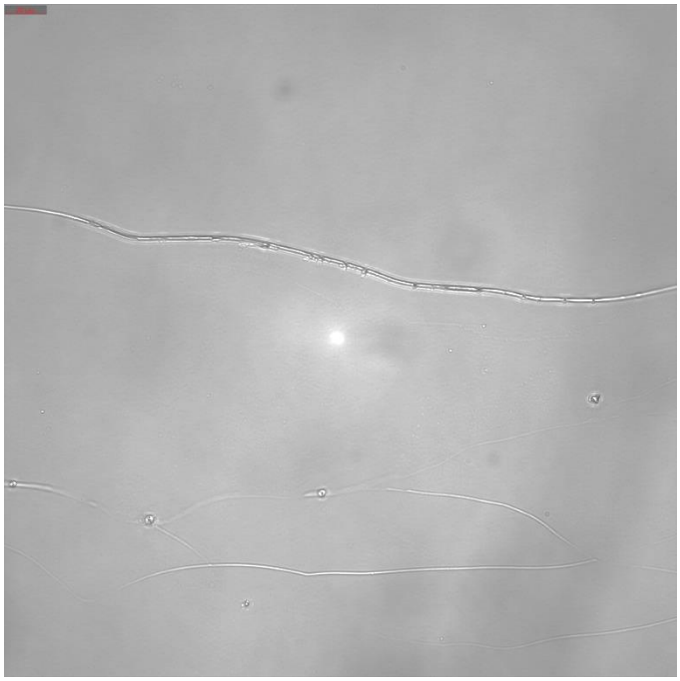

Figure B19. Brightfield images of *E. coli* AS19 incubated for 200 min at 37 °C in the presence of 100 µM Gap-2. The experiment was performed as described in the main text (40x objective). The scale bar represents 20 µm.

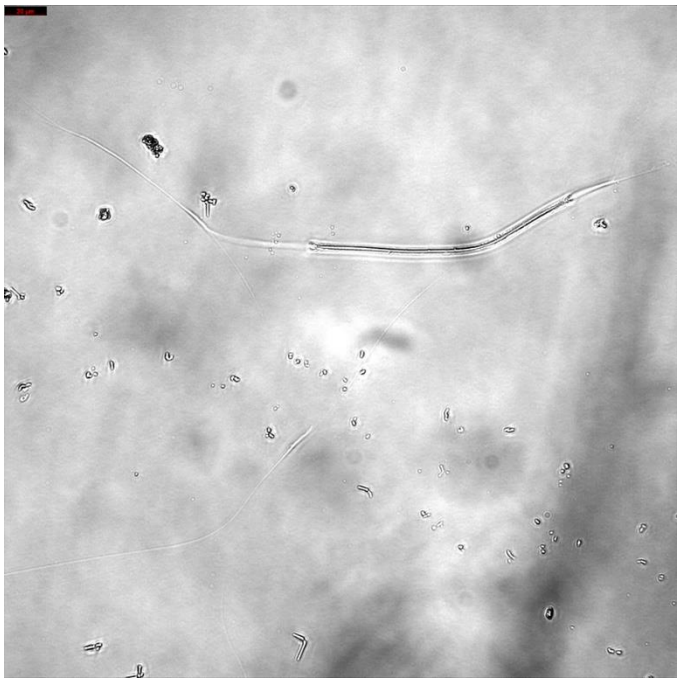

Figure B20. Brightfield images of *E. coli* AS19 incubated for 400 min at 37 °C in the presence of 100 µM Gap-2. The experiment was performed as described in the main text (40x objective). The scale bar represents 20 µm.

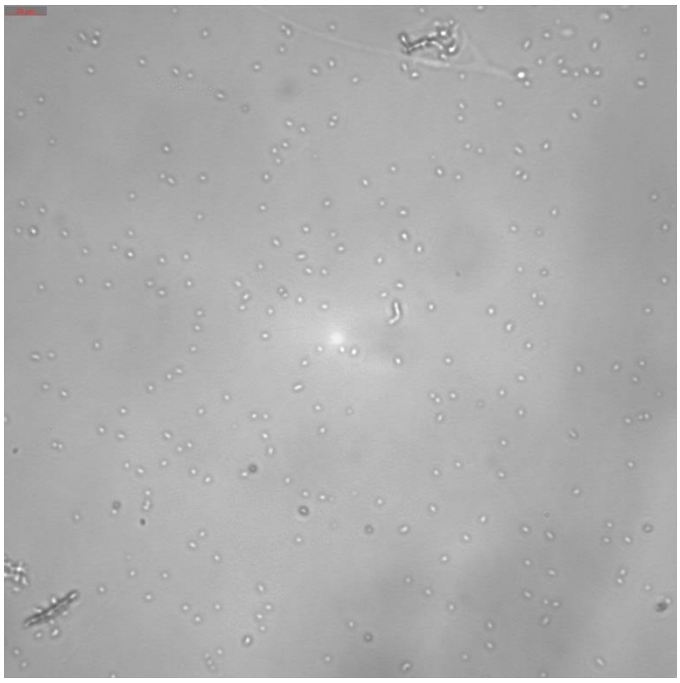

Figure B21. Brightfield images of *E. coli* AS19 incubated for 600 min at 37 °C in the presence of 100 µM Gap-2. The experiment was performed as described in the main text (40x objective). The scale bar represents 20 µm.

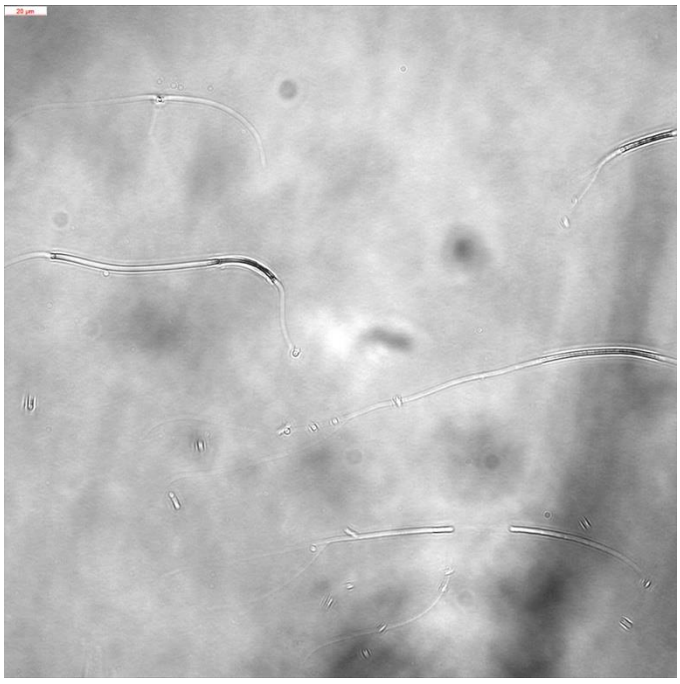

Figure B22. Brightfield images of *E. coli* AS19 incubated for 200 min at 37 °C in the presence of 100 µM Gap-3. The experiment was performed as described in the main text (40x objective). The scale bar represents 20 µm.

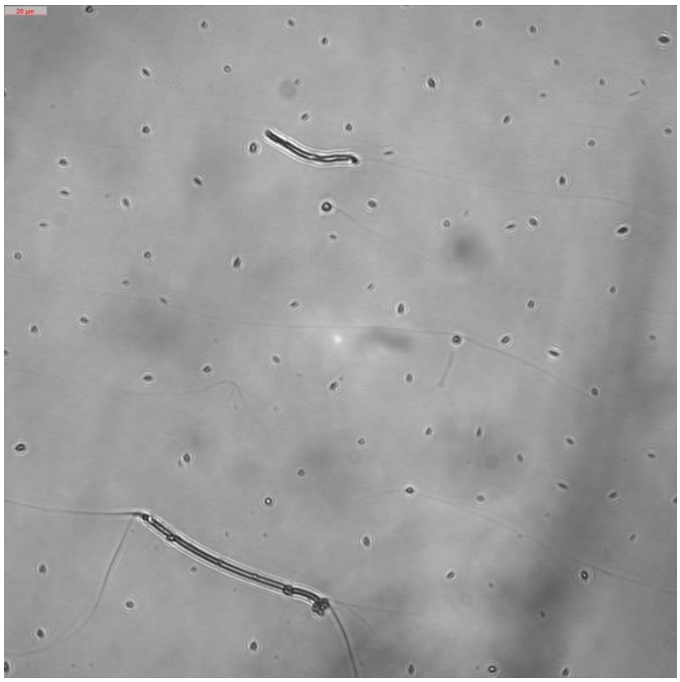

Figure B23. Brightfield images of *E. coli* AS19 incubated for 200 min at 37 °C in the presence of 100 µM Gap-4. The experiment was performed as described in the main text (40x objective). The scale bar represents 20 µm.

Figure B24. Brightfield images of *E. coli* AS19 incubated for 200 min at 37 °C in the presence of 100 µM Gap-5. The experiment was performed as described in the main text (40x objective). The scale bar represents 20 µm.

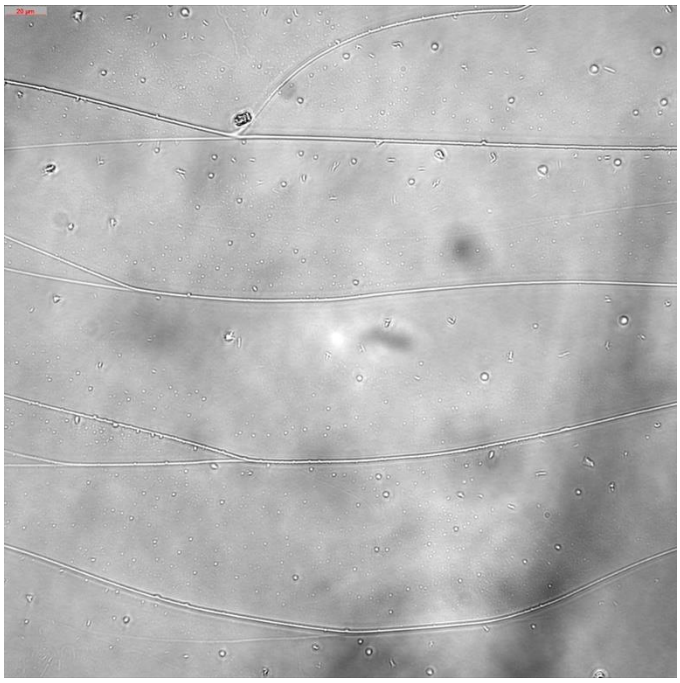

Figure B25. Brightfield images of *E. coli* AS19 incubated for 200 min at 37 °C in the presence of 100 µM Gap-2. The experiment was performed as described in the main text (40x objective). The scale bar represents 20 µm.

Appendix C Supporting Information for Chapter 4

C.1 Additional gels of the *in vitro* RNase P assay

The *in vitro* RNase P recruitment experiments were performed using 2 pmol target mRNA (ftsZ mRNA (40nt)), 8.8 pmol recruiter EGS oligonucleotide and 8.8 pmol M1RNA. After 1.5 h and 24 h incubation a 15% urea PAGE was run to determine the amount of mRNA cleavage. The gels corresponding to one repeat after 1.5 hours incubation are given in the main text. In this section, we provide the full gels of all repeats at both time points (1.5 h and 24 h) (**Figure C1- Figure C50**).

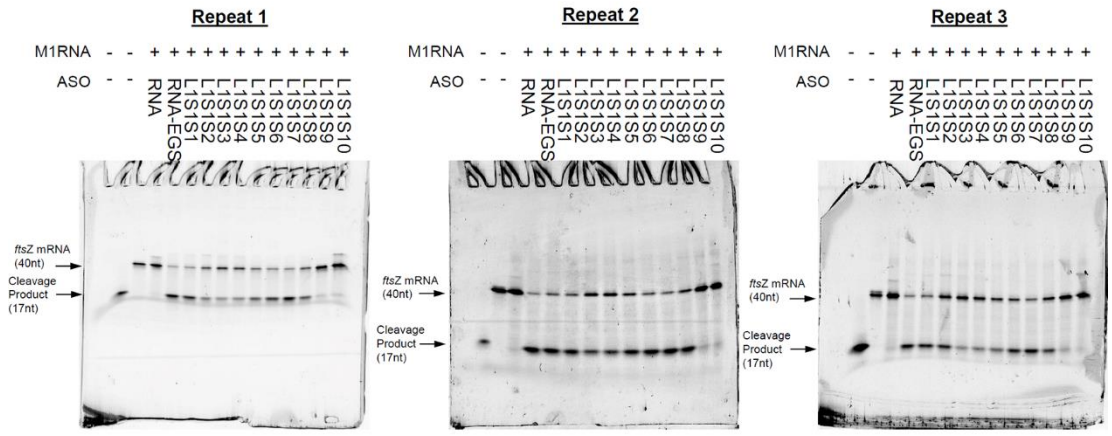

Figure C1. *In vitro* recruitment of RNase P by the oligonucleotides in Library 1 Set 1, after 1.5 hours incubation. The experiment was run as described in the main text. The first well contains a FAM labelled 17-mer and the second well contains FAM labelled target *ftsZ* mRNA (40nt) only; they are intended as a ladder.

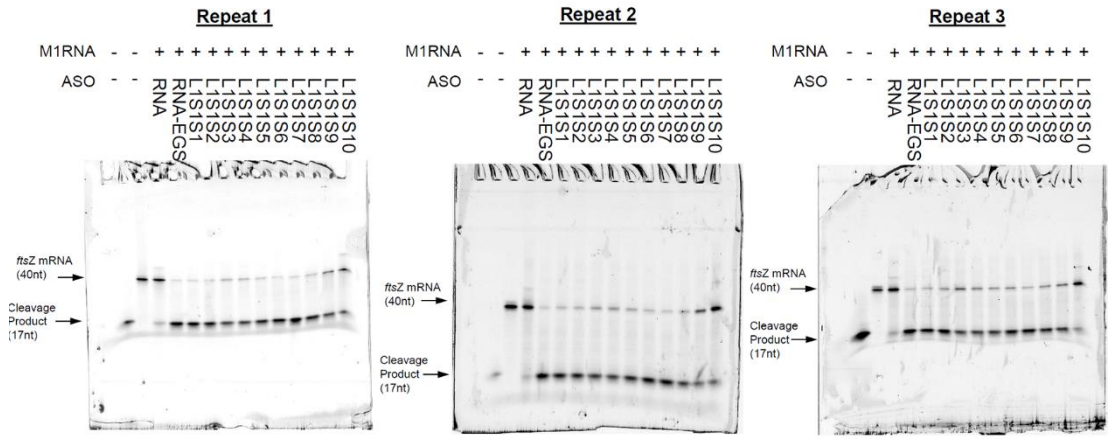

Figure C2. *In vitro* recruitment of RNase P by the oligonucleotides in Library 1 Set 1, after 24 hours incubation. The experiment was run as described in the main text. The first well contains a FAM labelled 17-mer and the second well contains FAM labelled target *ftsZ* mRNA (40nt) only; they are intended as a ladder.

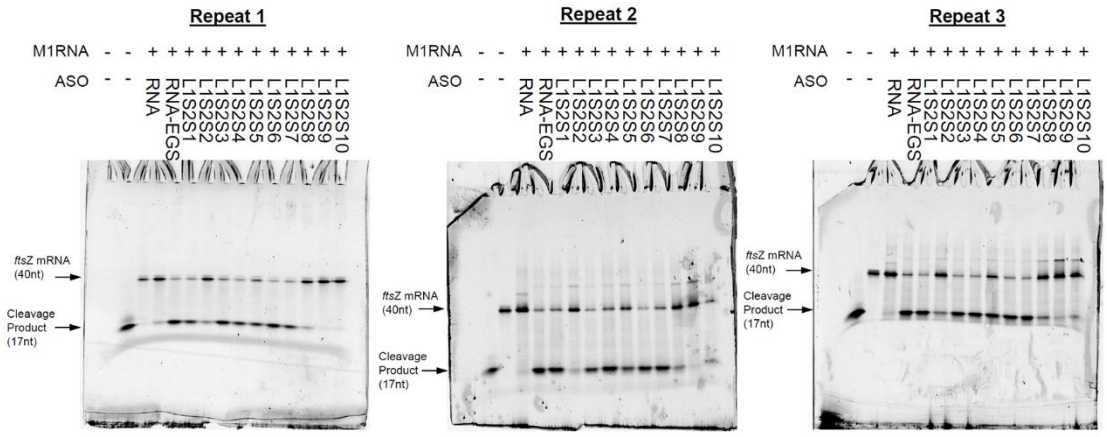

Figure C3. *In vitro* recruitment of RNase P by the oligonucleotides in Library 1 Set 2, after 1.5 hours incubation. The experiment was run as described in the main text. The first well contains a FAM labelled 17-mer and the second well contains FAM labelled target *ftsZ* mRNA (40nt) only; they are intended as a ladder.

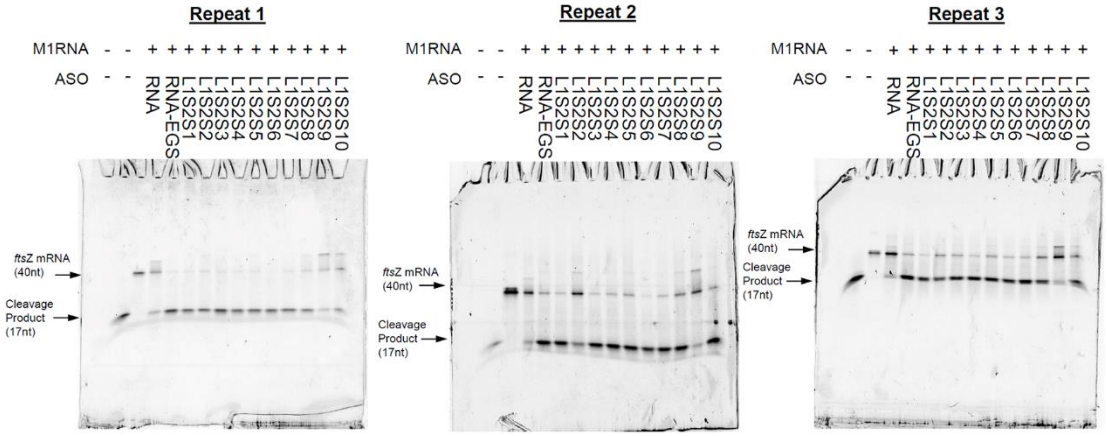

Figure C4. *In vitro* recruitment of RNase P by the oligonucleotides in Library 1 Set 2, after 24 hours incubation. The experiment was run as described in the main text. The first well contains a FAM labelled 17-mer and the second well contains FAM labelled target *ftsZ* mRNA (40nt) only; they are intended as a ladder.

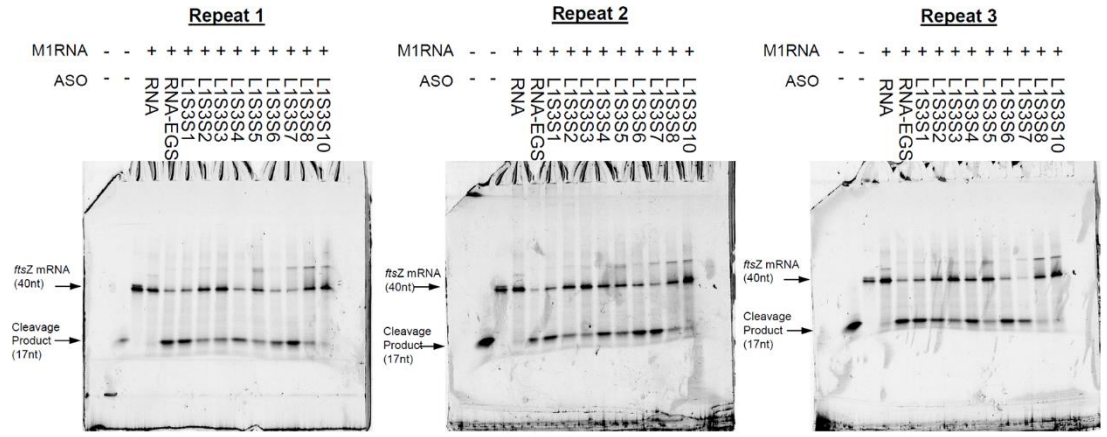

Figure C5. *In vitro* recruitment of RNase P by the oligonucleotides in Library 1 Set 3, after 1.5 hours incubation. The experiment was run as described in the main text. The first well contains a FAM labelled 17-mer and the second well contains FAM labelled target *ftsZ* mRNA (40nt) only; they are intended as a ladder.

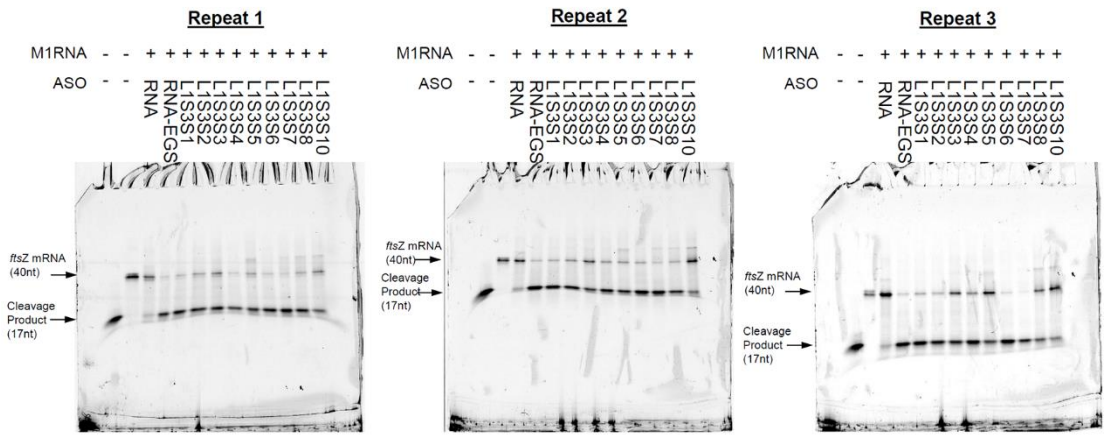

Figure C6. *In vitro* recruitment of RNase P by the oligonucleotides in Library 1 Set 3, after 24 hours incubation. The experiment was run as described in the main text. The first well contains a FAM labelled 17-mer and the second well contains FAM labelled target *ftsZ* mRNA (40nt) only; they are intended as a ladder.

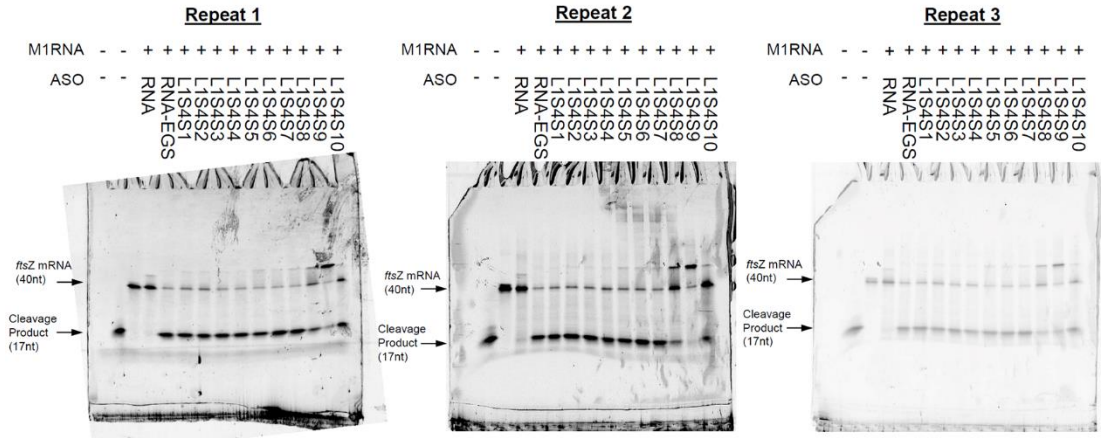

Figure C7. *In vitro* recruitment of RNase P by the oligonucleotides in Library 1 Set 4, after 1.5 hours incubation. The experiment was run as described in the main text. The first well contains a FAM labelled 17-mer and the second well contains FAM labelled target *ftsZ* mRNA (40nt) only; they are intended as a ladder.

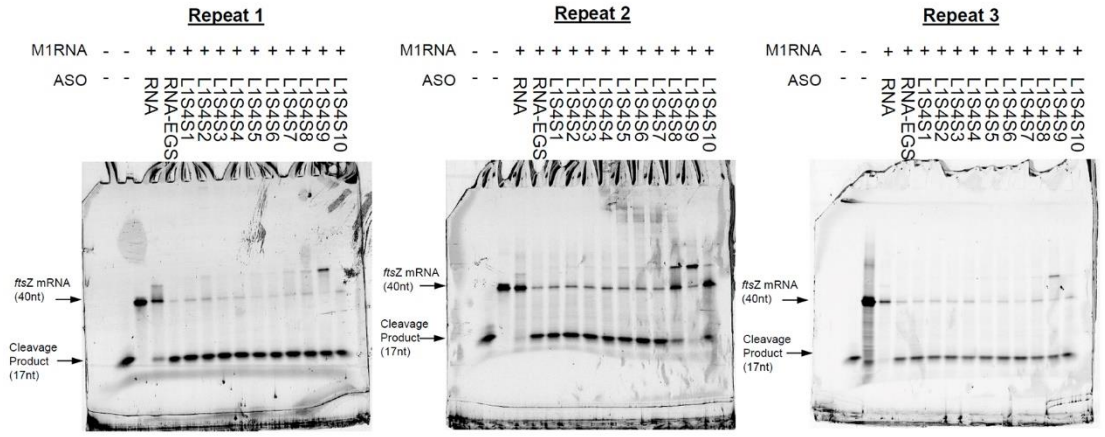

Figure C8. *In vitro* recruitment of RNase P by the oligonucleotides in Library 1 Set 4, after 24 hours incubation. The experiment was run as described in the main text. The first well contains a FAM labelled 17-mer and the second well contains FAM labelled target *ftsZ* mRNA (40nt) only; they are intended as a ladder.

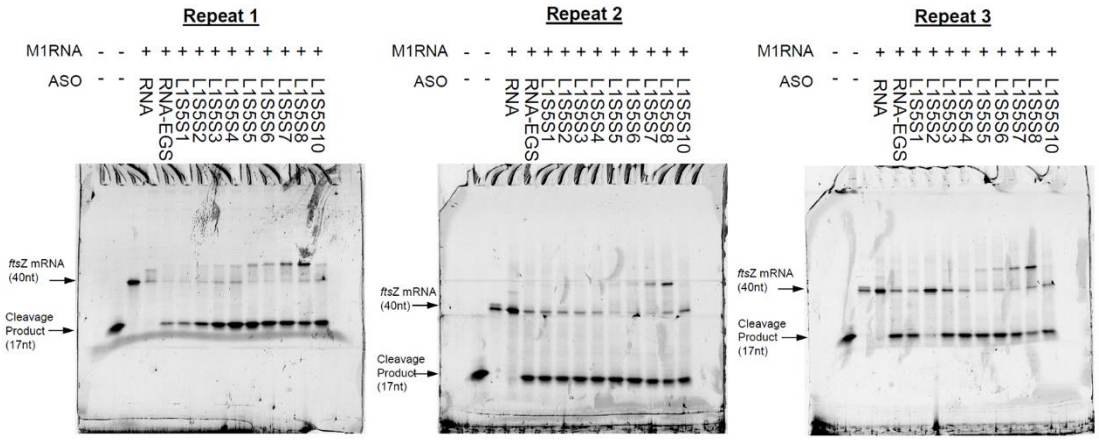

Figure C9. *In vitro* recruitment of RNase P by the oligonucleotides in Library 1 Set 5, after 1.5 hours incubation. The experiment was run as described in the main text. The first well contains a FAM labelled 17-mer and the second well contains FAM labelled target *ftsZ* mRNA (40nt) only; they are intended as a ladder.

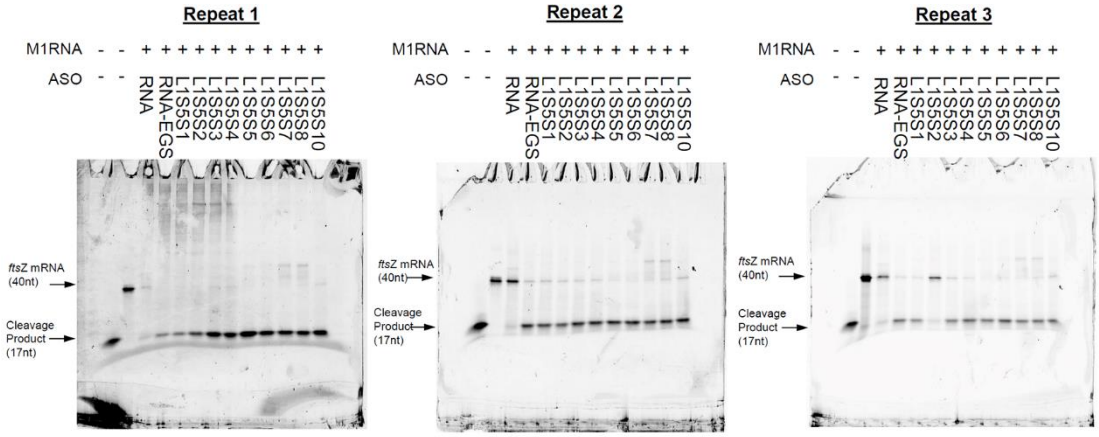

Figure C10. *In vitro* recruitment of RNase P by the oligonucleotides in Library 1 Set 5, after 24 hours incubation. The experiment was run as described in the main text. The first well contains a FAM labelled 17-mer and the second well contains FAM labelled target *ftsZ* mRNA (40nt) only; they are intended as a ladder.

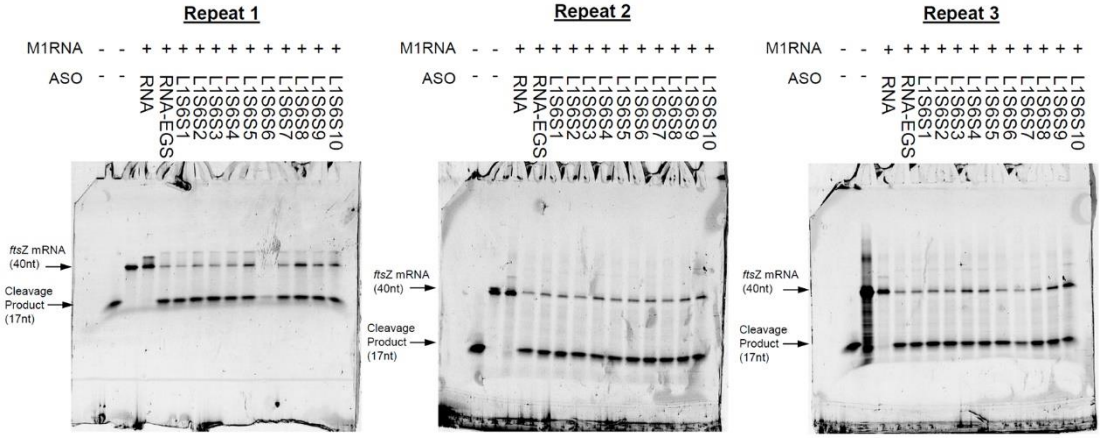

Figure C11. *In vitro* recruitment of RNase P by the oligonucleotides in Library 1 Set 6, after 1.5 hours incubation. The experiment was run as described in the main text. The first well contains a FAM labelled 17-mer and the second well contains FAM labelled target *ftsZ* mRNA (40nt) only; they are intended as a ladder.

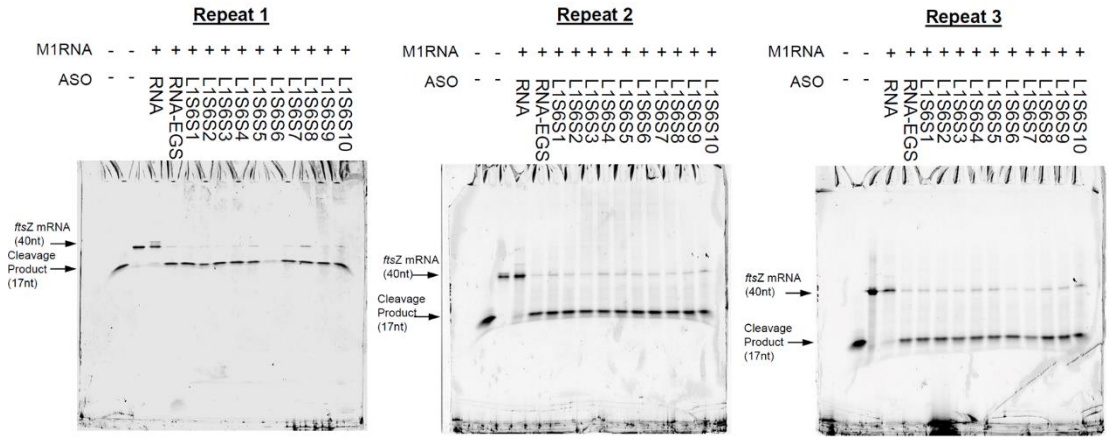

Figure C12. *In vitro* recruitment of RNase P by the oligonucleotides in Library 1 Set 6, after 24 hours incubation. The experiment was run as described in the main text. The first well contains a FAM labelled 17-mer and the second well contains FAM labelled target *ftsZ* mRNA (40nt) only; they are intended as a ladder.

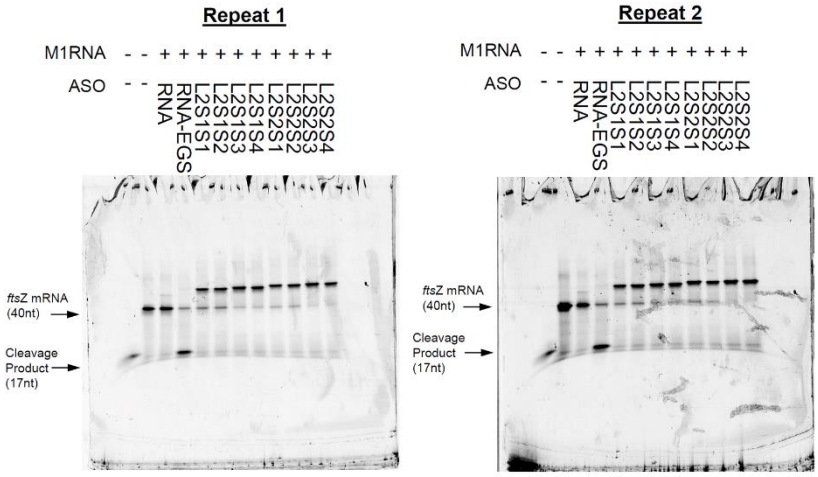

Figure C13. *In vitro* recruitment of RNase P by the oligonucleotides in Library 2 Set 1 and Set 2, after 1.5 hours incubation. The experiment was run as described in the main text. The first well contains a FAM labelled 17-mer and the second well contains FAM labelled target *ftsZ* mRNA (40nt) only; they are intended as a ladder.

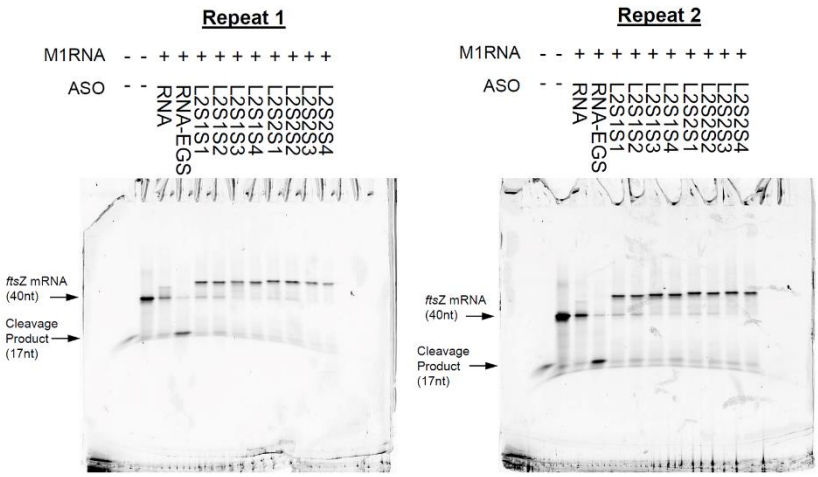

Figure C14. *In vitro* recruitment of RNase P by the oligonucleotides in Library 2 Set 1 and Set 2, after 24 hours incubation. The experiment was run as described in the main text. The first well contains a FAM labelled 17-mer and the second well contains FAM labelled target *ftsZ* mRNA (40nt) only; they are intended as a ladder.

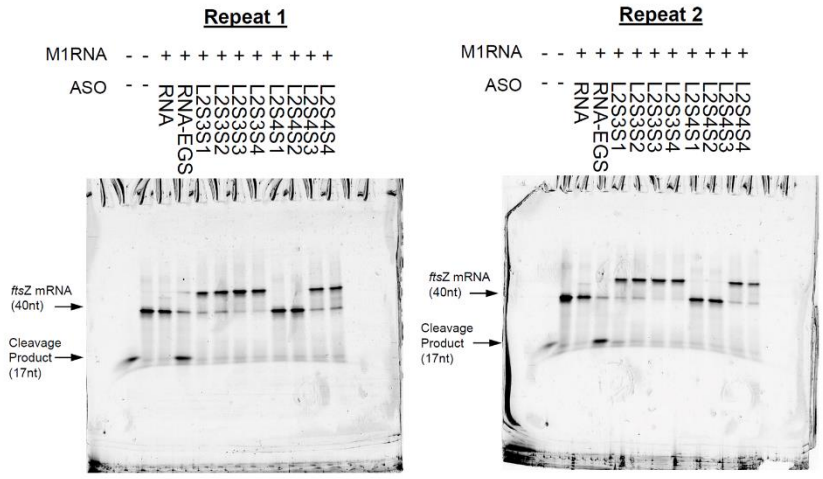

Figure C15. *In vitro* recruitment of RNase P by the oligonucleotides in Library 2 Set 3 and some of Set 4, after 1.5 hours incubation. The experiment was run as described in the main text. The first well contains a FAM labelled 17-mer and the second well contains FAM labelled target *ftsZ* mRNA (40nt) only; they are intended as a ladder.

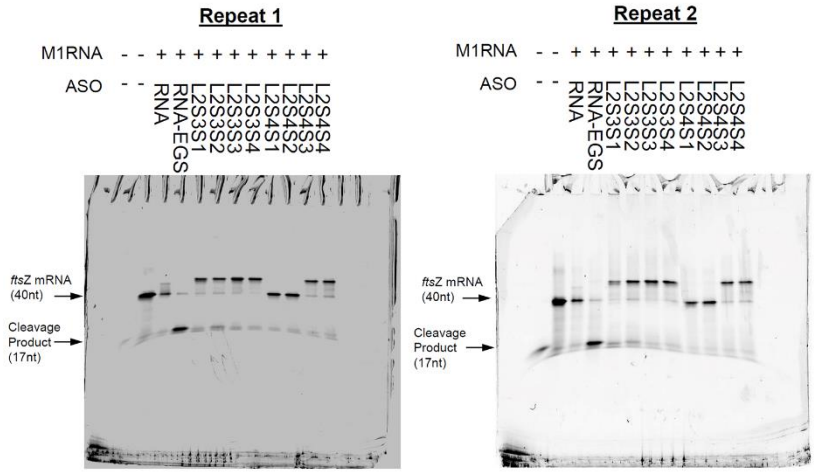

Figure C16. *In vitro* recruitment of RNase P by the oligonucleotides in Library 2 Set 3 and some of Set 4, after 24 hours incubation. The experiment was run as described in the main text. The first well contains a FAM labelled 17-mer and the second well contains FAM labelled target *ftsZ* mRNA (40nt) only; they are intended as a ladder.

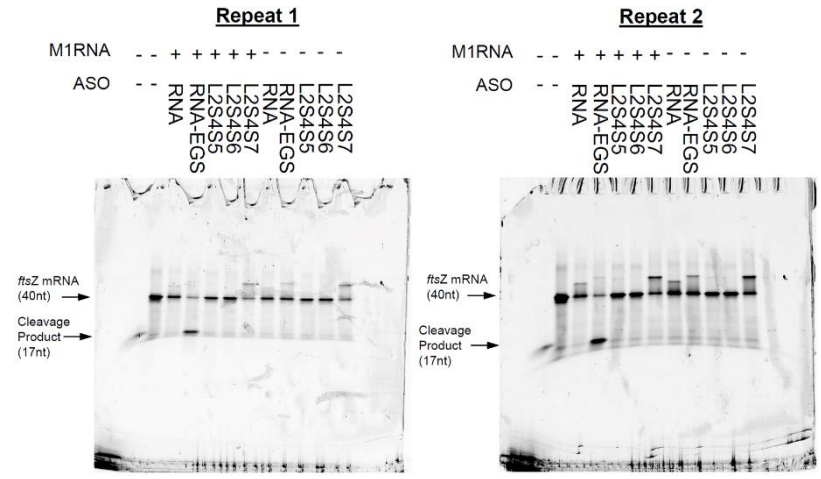

Figure C17. *In vitro* recruitment of RNase P by some of the oligonucleotides in Library 2 Set 4, after 1.5 hours incubation. The experiment was run as described in the main text. The first well contains a FAM labelled 17-mer and the second well contains FAM labelled target *ftsZ* mRNA (40nt) only; they are intended as a ladder.

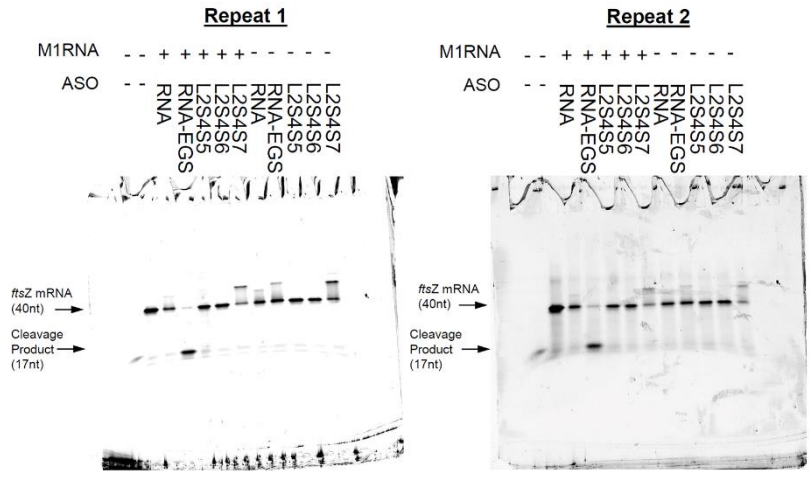

Figure C18. *In vitro* recruitment of RNase P by some of the oligonucleotides in Library 2 Set 4, after 24 hours incubation. The experiment was run as described in the main text. The first well contains a FAM labelled 17-mer and the second well contains FAM labelled target *ftsZ* mRNA (40nt) only; they are intended as a ladder.

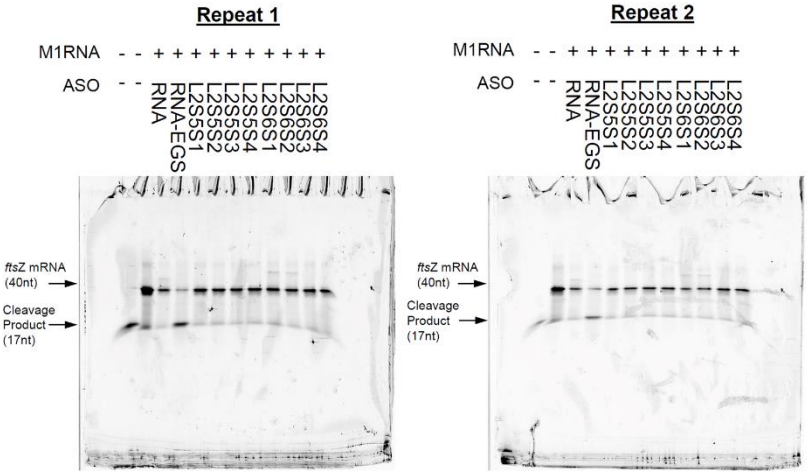

Figure C19. *In vitro* recruitment of RNase P by the oligonucleotides in Library 2 Set 5 and Set 6, after 1.5 hours incubation. The experiment was run as described in the main text. The first well contains a FAM labelled 17-mer and the second well contains FAM labelled target *ftsZ* mRNA (40nt) only; they are intended as a ladder.

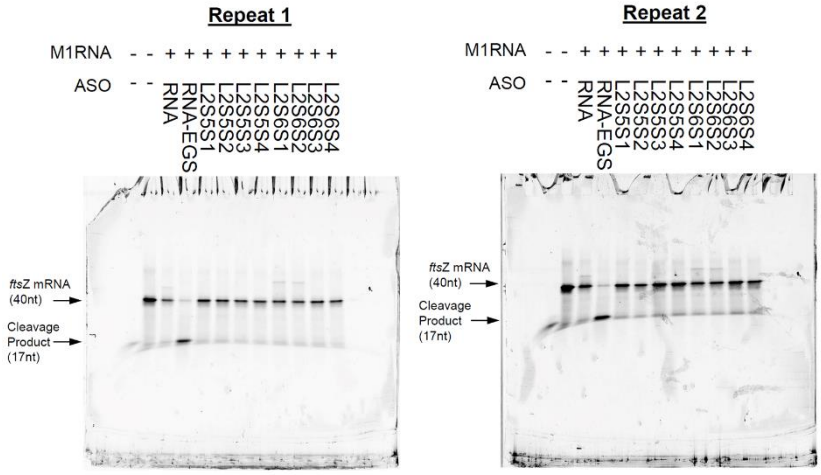

Figure C20. *In vitro* recruitment of RNase P by the oligonucleotides in Library 2 Set 5 and Set 6, after 24 hours incubation. The experiment was run as described in the main text. The first well contains a FAM labelled 17-mer and the second well contains FAM labelled target *ftsZ* mRNA (40nt) only; they are intended as a ladder.

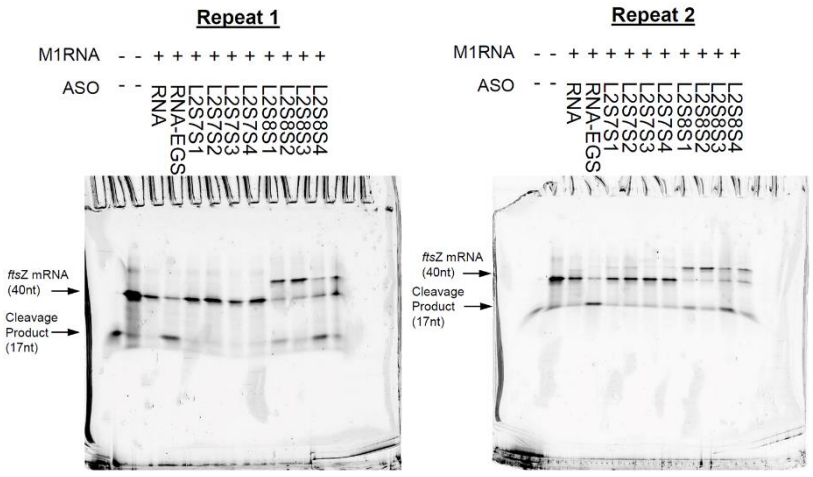

Figure C21. *In vitro* recruitment of RNase P by the oligonucleotides in Library 2 Set 7 and some of Set 8, after 1.5 hours incubation. The experiment was run as described in the main text. The first well contains a FAM labelled 17-mer and the second well contains FAM labelled target *ftsZ* mRNA (40nt) only; they are intended as a ladder.

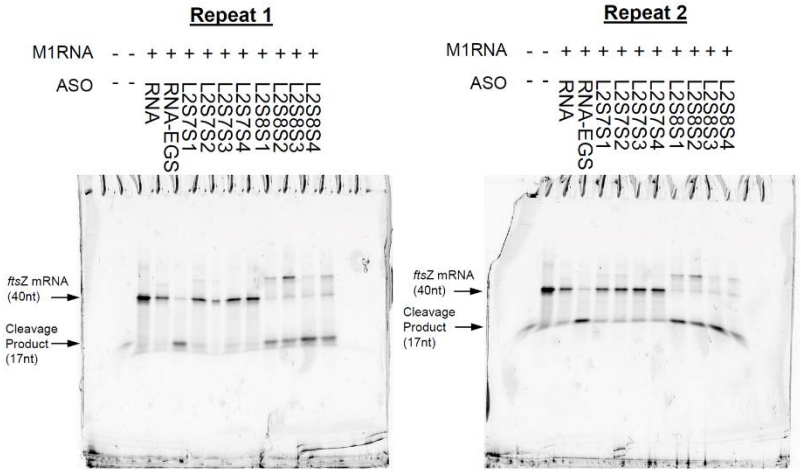

Figure C22. *In vitro* recruitment of RNase P by the oligonucleotides in Library 2 Set 7 and some of Set 8, after 24 hours incubation. The experiment was run as described in the main text. The first well contains a FAM labelled 17-mer and the second well contains FAM labelled target *ftsZ* mRNA (40nt) only; they are intended as a ladder.

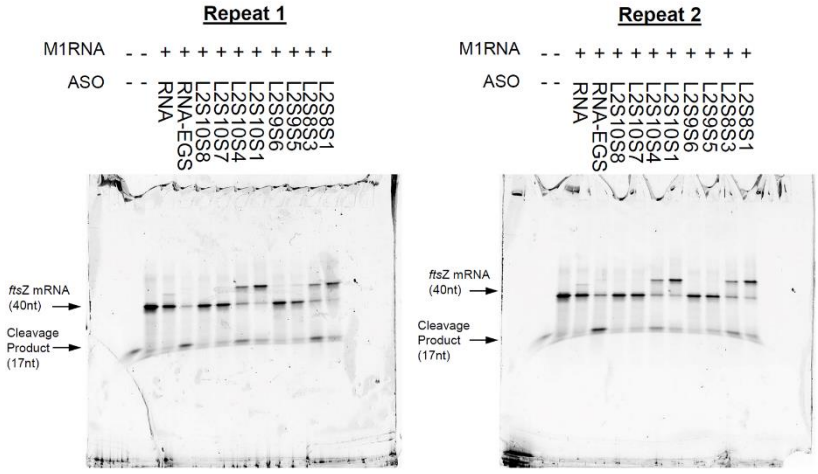

Figure C23. *In vitro* recruitment of RNase P by some of the oligonucleotides in Library 2 Set 8, Set 9 and Set 10, after 1.5 hours incubation. The experiment was run as described in the main text. The first well contains a FAM labelled 17-mer and the second well contains FAM labelled target *ftsZ* mRNA (40nt) only; they are intended as a ladder.

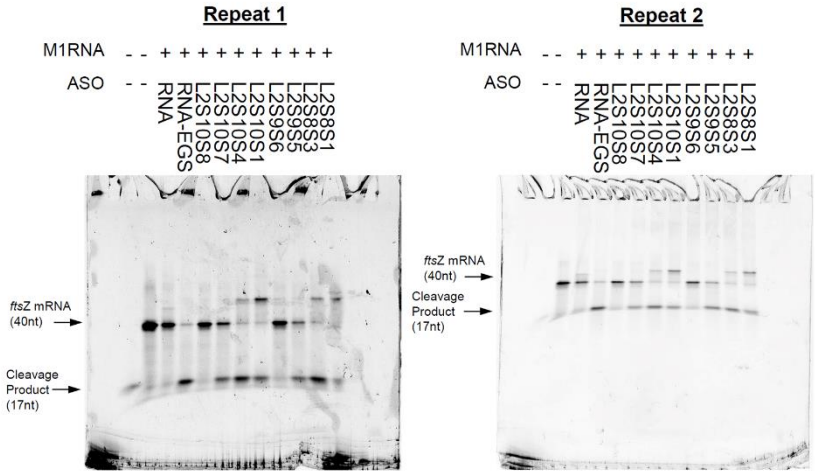

Figure C24. *In vitro* recruitment of RNase P by the oligonucleotides in Library 2 Set 8, Set 9 and Set 10, after 24 hours incubation. The experiment was run as described in the main text. The first well contains a FAM labelled 17-mer and the second well contains FAM labelled target *ftsZ* mRNA (40nt) only; they are intended as a ladder.

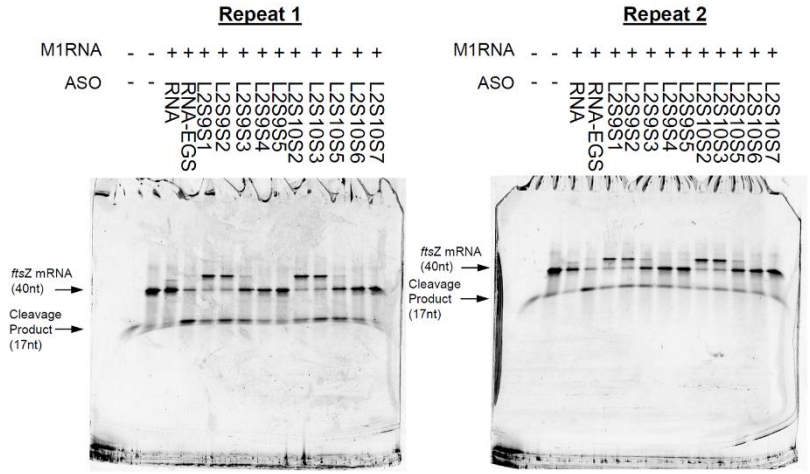

Figure C25. *In vitro* recruitment of RNase P by some of the oligonucleotides in Library 2 Set 9 and Set 10, after 1.5 hours incubation. The experiment was run as described in the main text. The first well contains a FAM labelled 17-mer and the second well contains FAM labelled target *ftsZ* mRNA (40nt) only; they are intended as a ladder.

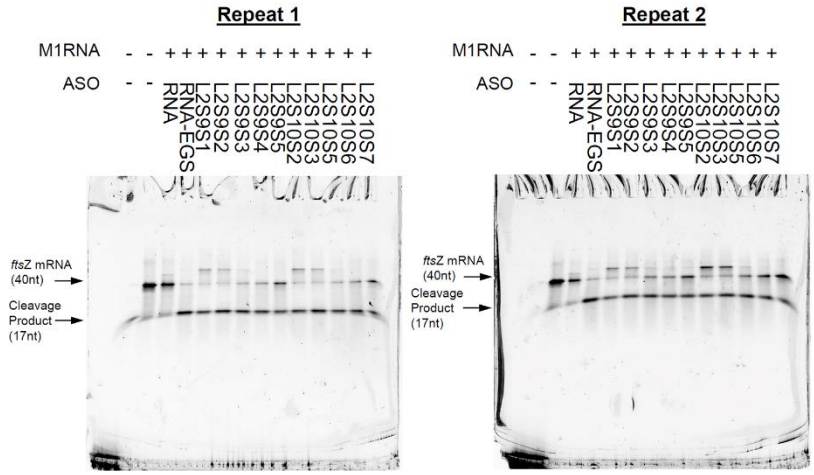

Figure C26. *In vitro* recruitment of RNase P by the oligonucleotides in Library 2 Set 9 and Set 10, after 24 hours incubation. The experiment was run as described in the main text. The first well contains a FAM labelled 17-mer and the second well contains FAM labelled target *ftsZ* mRNA (40nt) only; they are intended as a ladder.

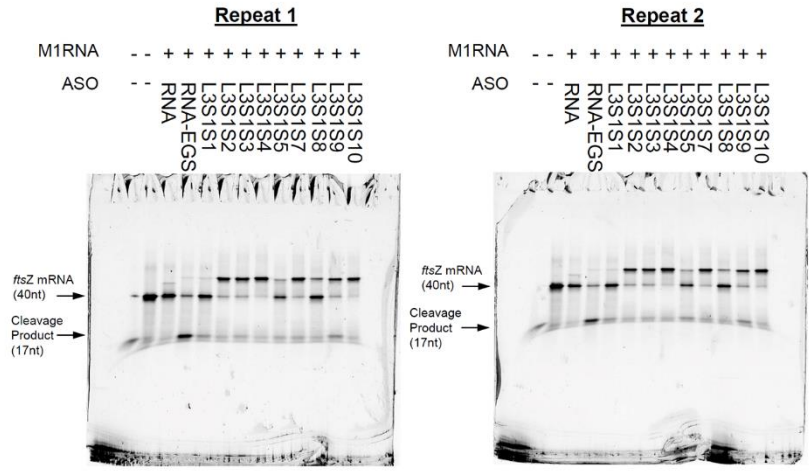

Figure C27. *In vitro* recruitment of RNase P by some of the oligonucleotides in Library 3 Set 1, after 1.5 hours incubation. The experiment was run as described in the main text. The first well contains a FAM labelled 17-mer and the second well contains FAM labelled target *ftsZ* mRNA (40nt) only; they are intended as a ladder.

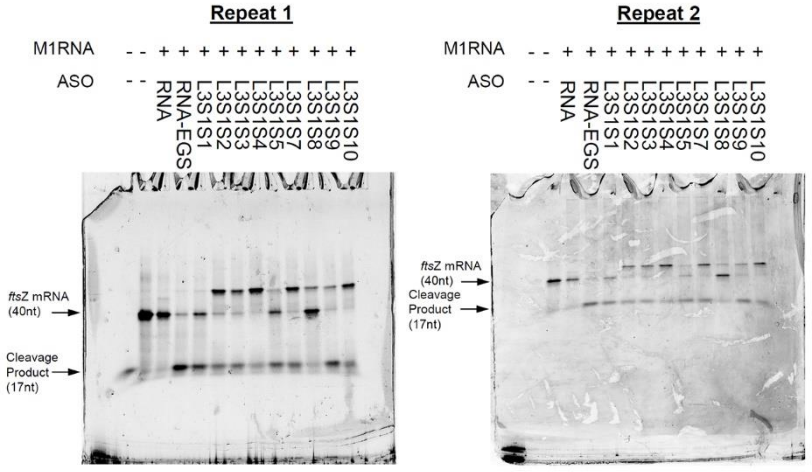

Figure C28. *In vitro* recruitment of RNase P by some of the oligonucleotides in Library 3 Set 1, after 24 hours incubation. The experiment was run as described in the main text. The first well contains a FAM labelled 17-mer and the second well contains FAM labelled target *ftsZ* mRNA (40nt) only; they are intended as a ladder.

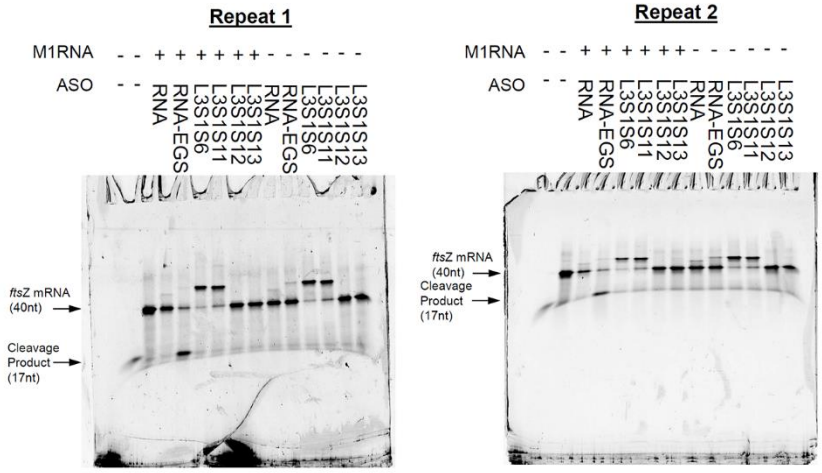

Figure C29. *In vitro* recruitment of RNase P by some of the oligonucleotides in Library 3 Set 1, after 1.5 hours incubation. The experiment was run as described in the main text. The first well contains a FAM labelled 17-mer and the second well contains FAM labelled target *ftsZ* mRNA (40nt) only; they are intended as a ladder.

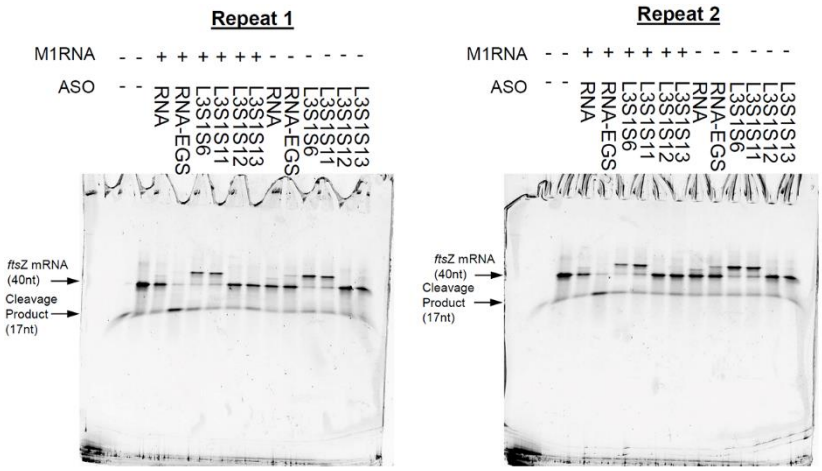

Figure C30. *In vitro* recruitment of RNase P by some of the oligonucleotides in Library 3 Set 1, after 24 hours incubation. The experiment was run as described in the main text. The first well contains a FAM labelled 17-mer and the second well contains FAM labelled target *ftsZ* mRNA (40nt) only; they are intended as a ladder.

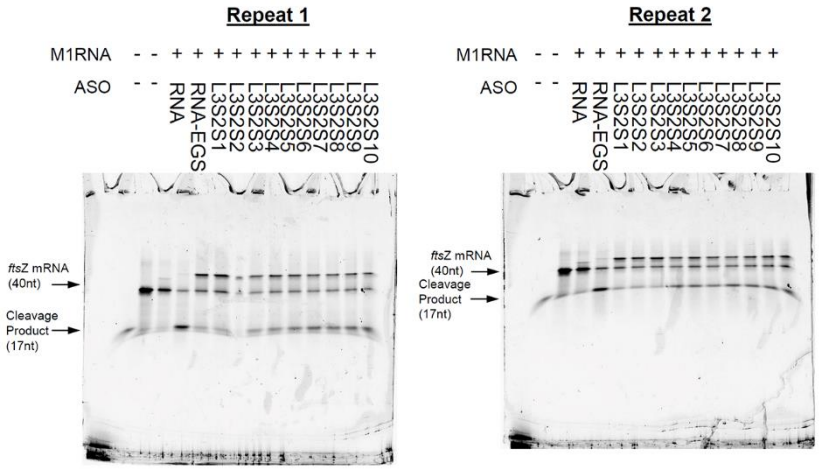

Figure C31. *In vitro* recruitment of RNase P by the oligonucleotides in Library 3 Set 2, after 1.5 hours incubation. The experiment was run as described in the main text. The first well contains a FAM labelled 17-mer and the second well contains FAM labelled target *ftsZ* mRNA (40nt) only; they are intended as a ladder.

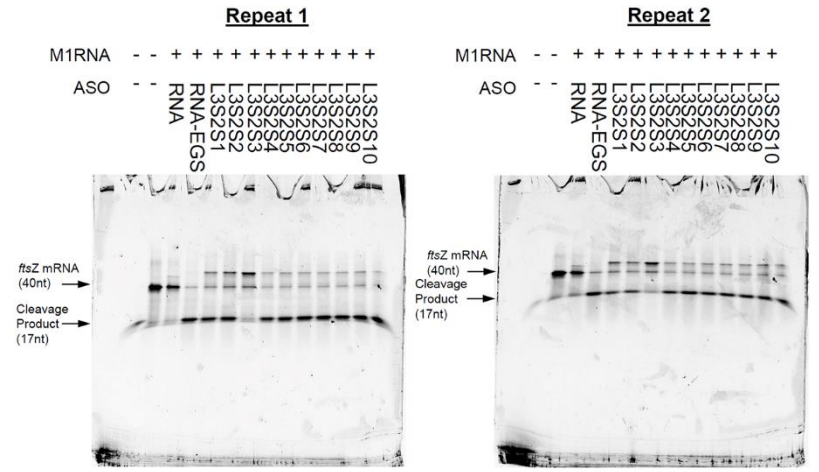

Figure C32. *In vitro* recruitment of RNase P by the oligonucleotides in Library 3 Set 2, after 24 hours incubation. The experiment was run as described in the main text. The first well contains a FAM labelled 17-mer and the second well contains FAM labelled target *ftsZ* mRNA (40nt) only; they are intended as a ladder.

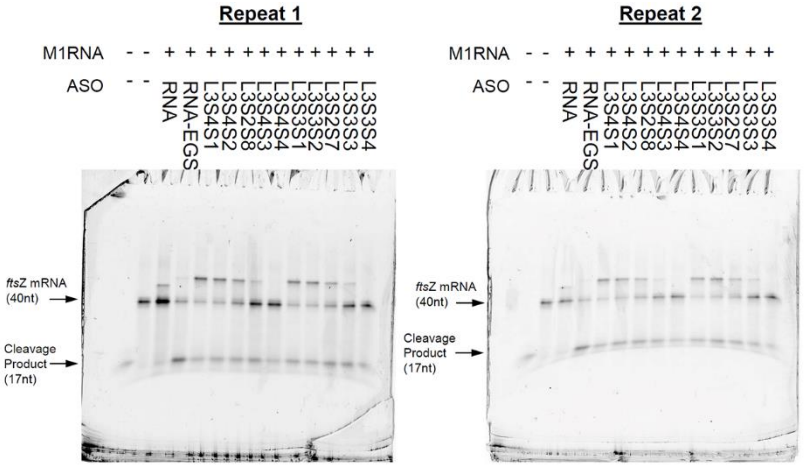

Figure C33. *In vitro* recruitment of RNase P by the oligonucleotides in Library 3 Set 3 and Set 4, after 1.5 hours incubation. The experiment was run as described in the main text. The first well contains a FAM labelled 17-mer and the second well contains FAM labelled target *ftsZ* mRNA (40nt) only; they are intended as a ladder.

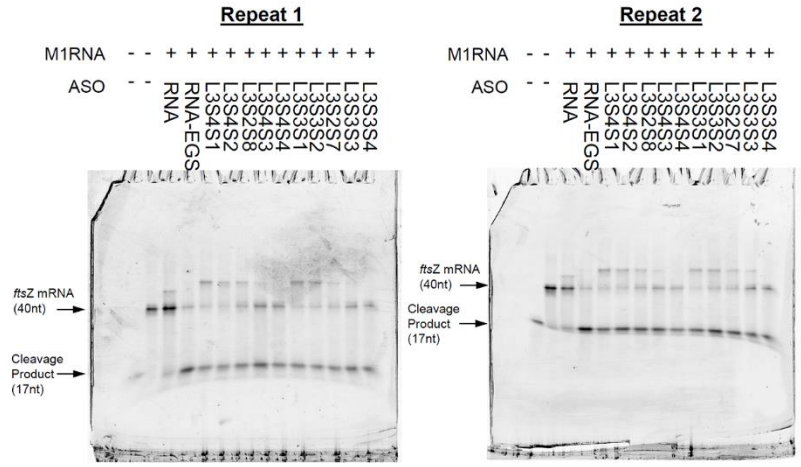

Figure C34. *In vitro* recruitment of RNase P by the oligonucleotides in Library 3 Set 3 and Set 4, after 24 hours incubation. The experiment was run as described in the main text. The first well contains a FAM labelled 17-mer and the second well contains FAM labelled target *ftsZ* mRNA (40nt) only; they are intended as a ladder.

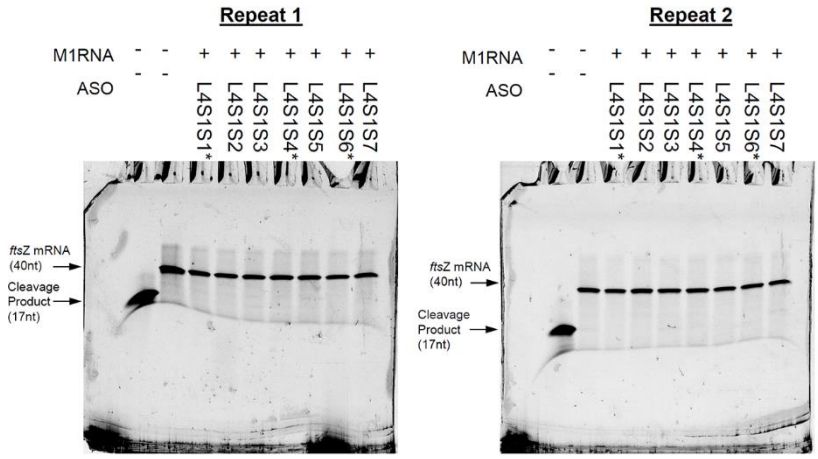

Figure C35. *In vitro* recruitment of RNase P by the oligonucleotides in Library 4 Set 1, after 1.5 hours incubation. The experiment was run as described in the main text. The first well contains a FAM labelled 17-mer and the second well contains FAM labelled target *ftsZ* mRNA (40nt) only; they are intended as a ladder. * refers to non-EGS controls.

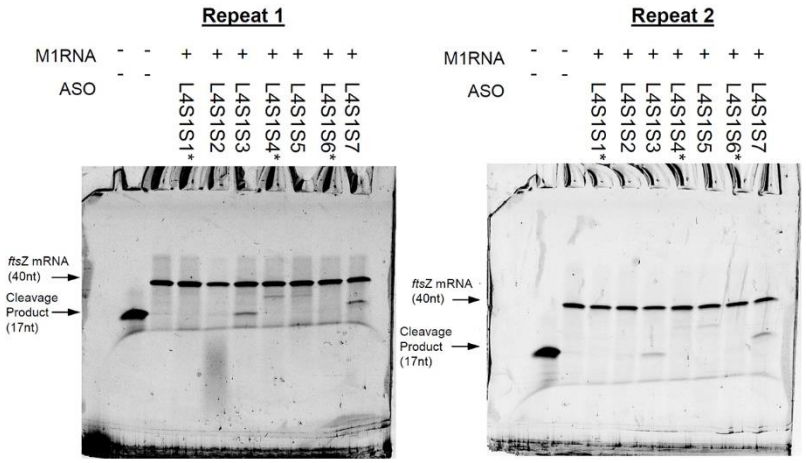

Figure C36. *In vitro* recruitment of RNase P by the oligonucleotides in Library 4 Set 1, after 24 hours incubation. The experiment was run as described in the main text. The first well contains a FAM labelled 17-mer and the second well contains FAM labelled target *ftsZ* mRNA (40nt) only; they are intended as a ladder. * refers to non-EGS controls.

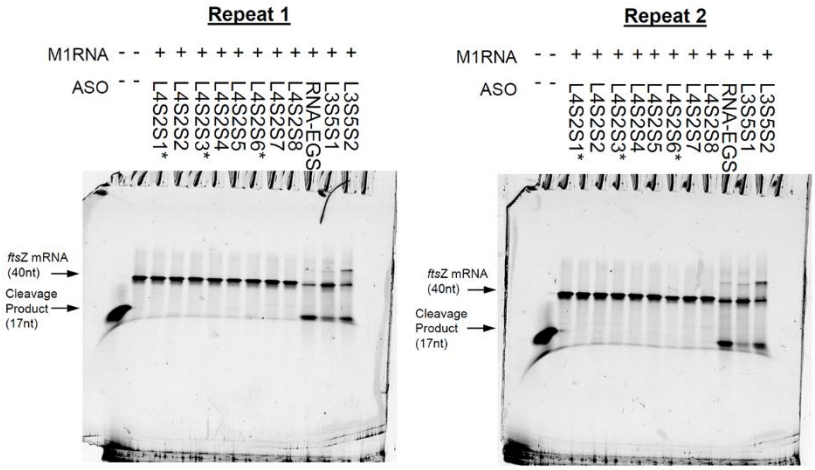

Figure C37. *In vitro* recruitment of RNase P by the oligonucleotides in Library 4 Set 2, after 1.5 hours incubation. The experiment was run as described in the main text. The first well contains a FAM labelled 17-mer and the second well contains FAM labelled target *ftsZ* mRNA (40nt) only; they are intended as a ladder. * refers to non-EGS controls.

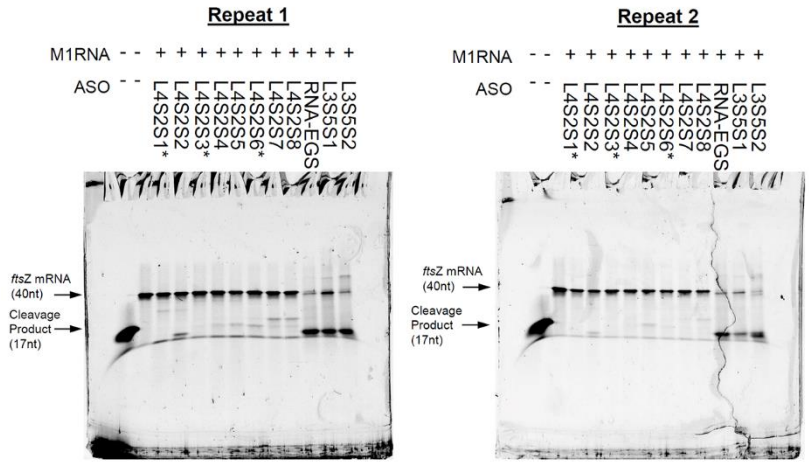

Figure C38. *In vitro* recruitment of RNase P by the oligonucleotides in Library 4 Set 2, after 24 hours incubation. The experiment was run as described in the main text. The first well contains a FAM labelled 17-mer and the second well contains FAM labelled target *ftsZ* mRNA (40nt) only; they are intended as a ladder. * refers to non-EGS controls.

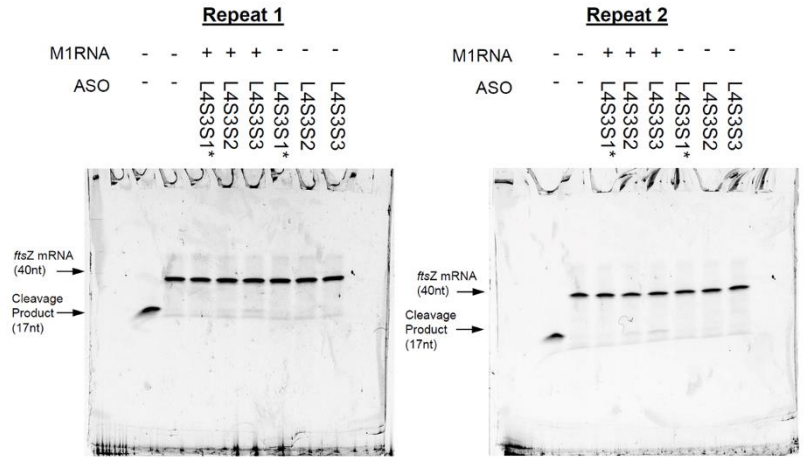

Figure C39. *In vitro* recruitment of RNase P by some oligonucleotides in Library 4 Set 3, after 1.5 hours incubation. The experiment was run as described in the main text. The first well contains a FAM labelled 17-mer and the second well contains FAM labelled target *ftsZ* mRNA (40nt) only; they are intended as a ladder. * refers to non-EGS controls.

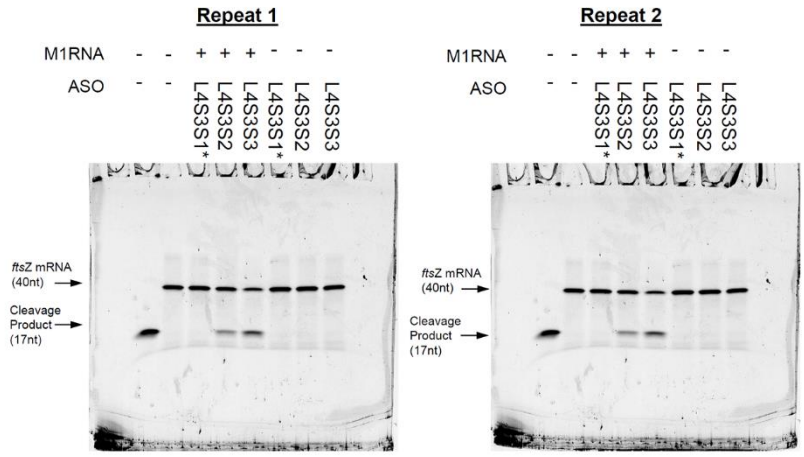

Figure C40. *In vitro* recruitment of RNase P by some oligonucleotides in Library 4 Set 3, after 24 hours incubation. The experiment was run as described in the main text. The first well contains a FAM labelled 17-mer and the second well contains FAM labelled target *ftsZ* mRNA (40nt) only; they are intended as a ladder. * refers to non-EGS controls.

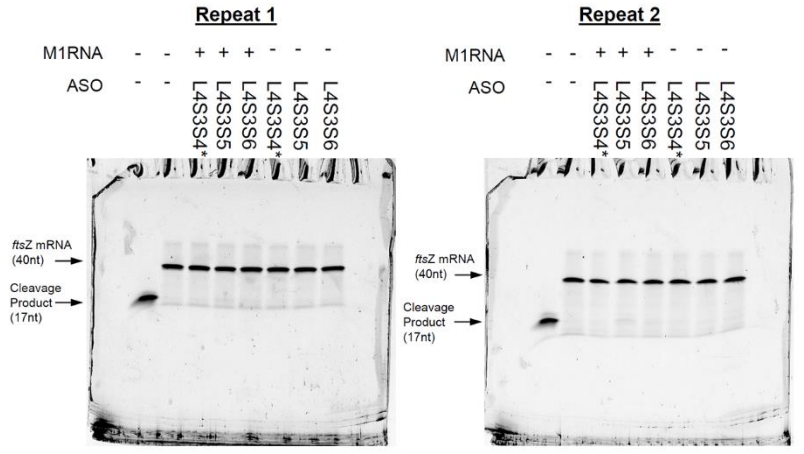

Figure C41. *In vitro* recruitment of RNase P by some oligonucleotides in Library 4 Set 3, after 1.5 hours incubation. The experiment was run as described in the main text. The first well contains a FAM labelled 17-mer and the second well contains FAM labelled target *ftsZ* mRNA (40nt) only; they are intended as a ladder. * refers to non-EGS controls.

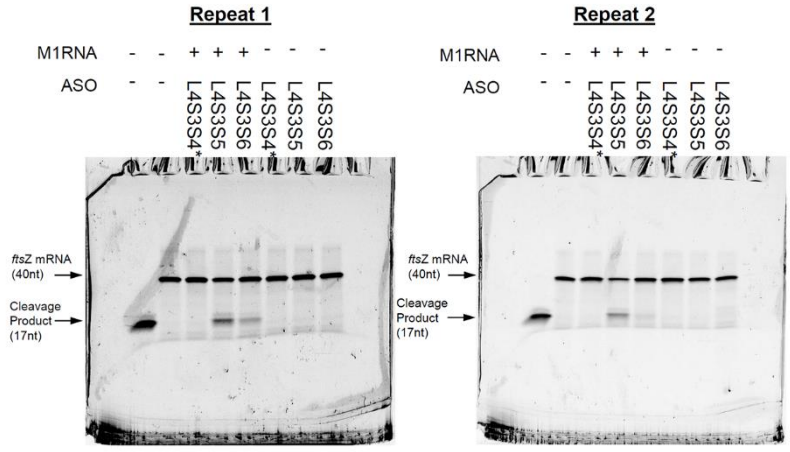

Figure C42. *In vitro* recruitment of RNase P by some oligonucleotides in Library 4 Set 3, after 24 hours incubation. The experiment was run as described in the main text. The first well contains a FAM labelled 17-mer and the second well contains FAM labelled target *ftsZ* mRNA (40nt) only; they are intended as a ladder. * refers to non-EGS controls.

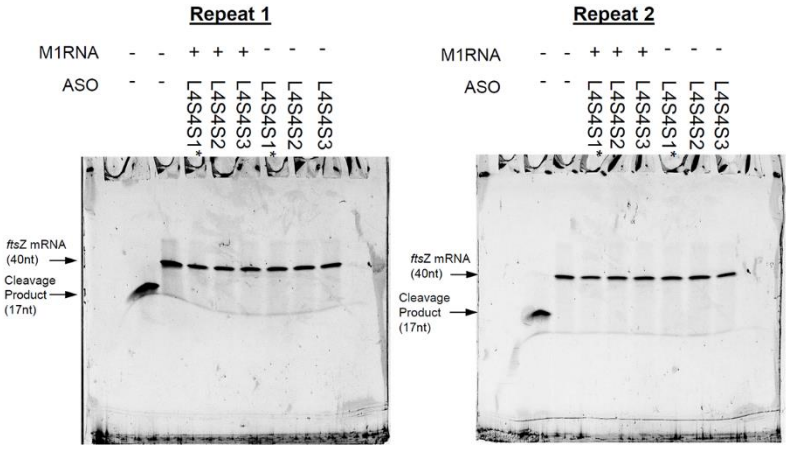

Figure C43. *In vitro* recruitment of RNase P by the oligonucleotides in Library 4 Set 4, after 1.5 hours incubation. The experiment was run as described in the main text. The first well contains a FAM labelled 17-mer and the second well contains FAM labelled target *ftsZ* mRNA (40nt) only; they are intended as a ladder. * refers to non-EGS controls.

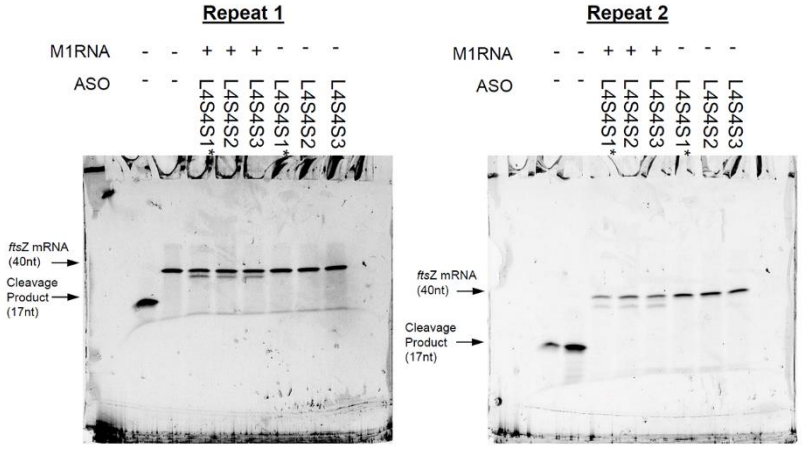

Figure C44. *In vitro* recruitment of RNase P by the oligonucleotides in Library 4 Set 4, after 24 hours incubation. The experiment was run as described in the main text. The first well contains a FAM labelled 17-mer and the second well contains FAM labelled target *ftsZ* mRNA (40nt) only; they are intended as a ladder. * refers to non-EGS controls.

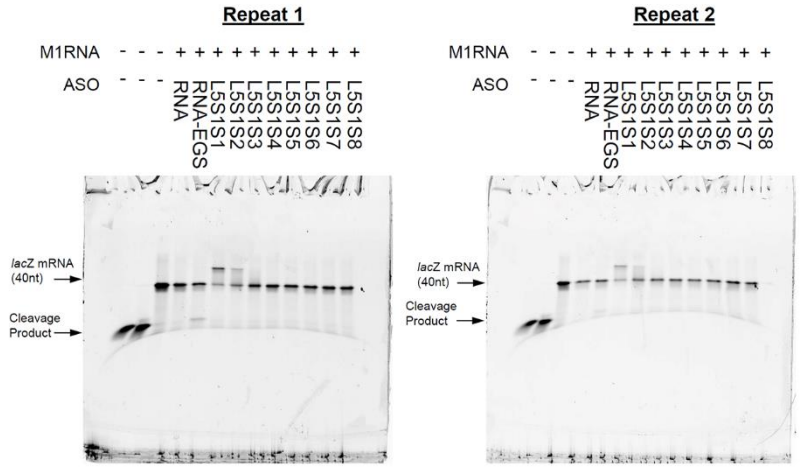

Figure C45. *In vitro* recruitment of RNase P by the oligonucleotides in Library 5 Set 1, after 1.5 hours incubation. The experiment was run as described in the main text. The first 2 wells contains a FAM labelled 17 or 15-mer and the third well contains FAM labelled target *ftsZ* mRNA (40nt) only; they are intended as a ladder.

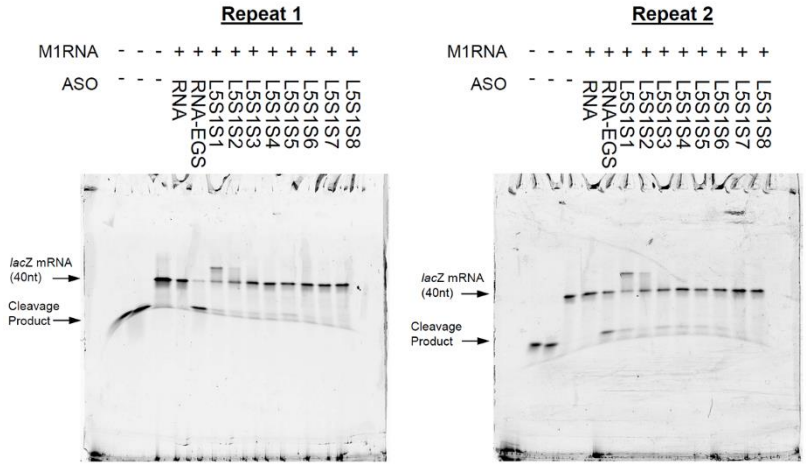

Figure C46. *In vitro* recruitment of RNase P by the oligonucleotides in Library 5 Set 1, after 24 hours incubation. The experiment was run as described in the main text. The first 2 wells contains a FAM labelled 17 or 15-mer and the third well contains FAM labelled target *ftsZ* mRNA (40nt) only; they are intended as a ladder.

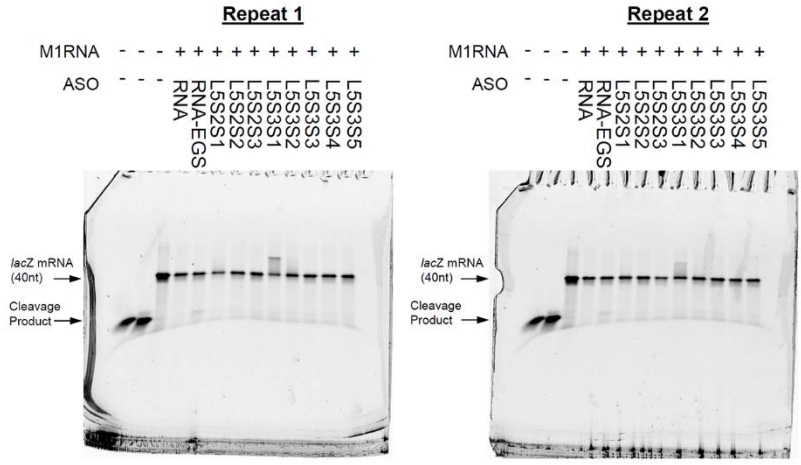

Figure C47. *In vitro* recruitment of RNase P by the oligonucleotides in Library 5 Set 2 and Set 3, after 1.5 hours incubation. The experiment was run as described in the main text. The first 2 wells contains a FAM labelled 17 or 15-mer and the third well contains FAM labelled target *ftsZ* mRNA (40nt) only; they are intended as a ladder.

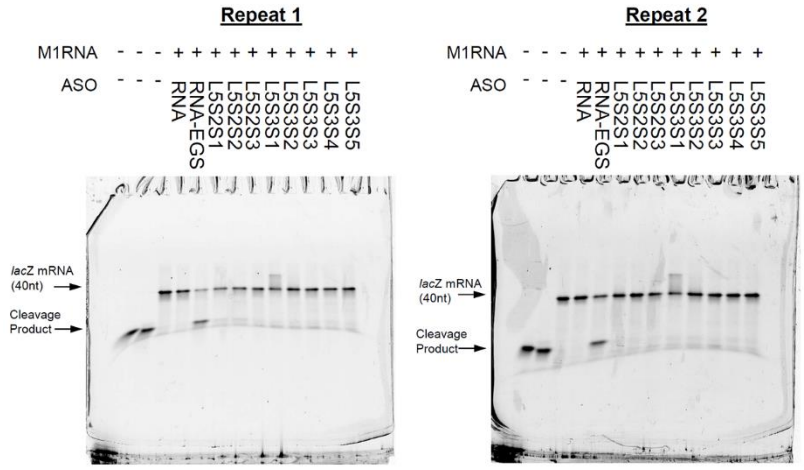

Figure C48. *In vitro* recruitment of RNase P by the oligonucleotides in Library 5 Set 2 and Set 3, after 24 hours incubation. The experiment was run as described in the main text. The first 2 wells contains a FAM labelled 17 or 15-mer and the third well contains FAM labelled target *ftsZ* mRNA (40nt) only; they are intended as a ladder.

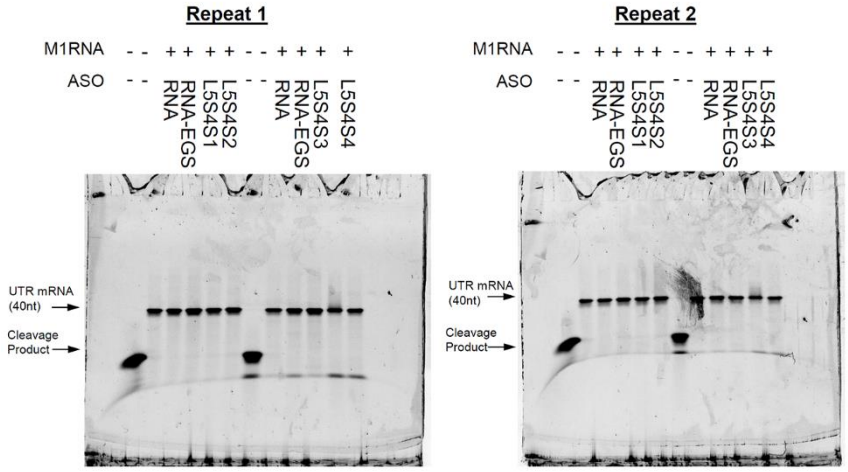

Figure C49. *In vitro* recruitment of RNase P by the oligonucleotides in Library 5 Set 4, after 1.5 hours incubation. The experiment was run as described in the main text. The first well contains a FAM labelled 17-mer and the second well contains FAM labelled target *ftsZ* mRNA (40nt) only; they are intended as a ladder.

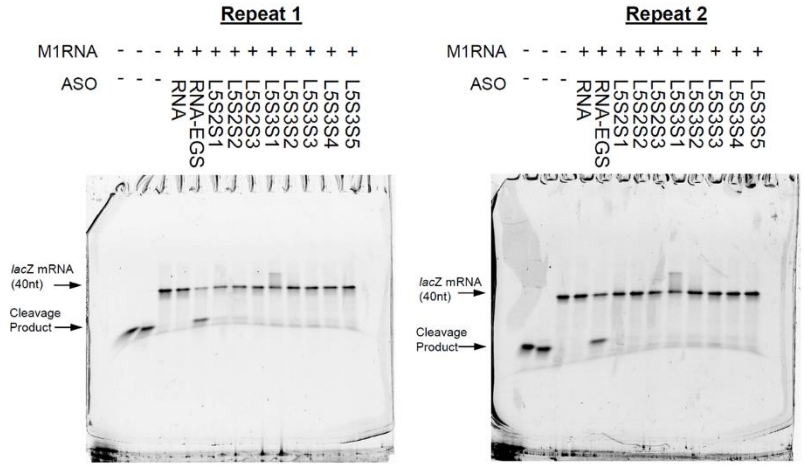

Figure C50. *In vitro* recruitment of RNase P by the oligonucleotides in Library 5 Set 4, after 24 hours incubation. The experiment was run as described in the main text. The first well contains a FAM labelled 17-mer and the second well contains FAM labelled target *ftsZ* mRNA (40nt) only; they are intended as a ladder.

C.2 Additional gels of the *in vitro* RNase H assay

The *in vitro* RNase H recruitment activity of some of the EGSs was investigated using RNase H kit EN0201, purchased from Thermo Fisher Scientific. In 30 µL reaction were mixed 4 x 10^{-3} units of RNase H, 2 pmol target mRNA, 8.8 pmol gapmer and 10x reaction buffer. The reaction was run at 37 °C for 24 hours. At two different time points (1.5 h and 24 h), a 7 µL sample was withdrawn from the reaction, and 7 µL formamide was added to stop the reaction. The samples were subsequently loaded onto a denaturing 15% urea polyacrylamide gel, run using electrophoresis and visualized on a GE Typhoon FLA 7000 biomolecular with the FAM channel at 700 pmt. All results are shown in **Figure C51-Figure C64.**

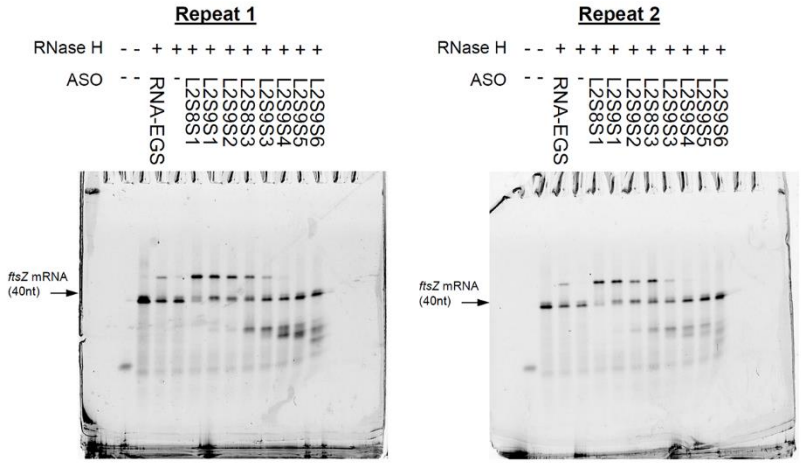

Figure C51. *In vitro* recruitment of RNase H by the oligonucleotides of Library 2 Set 9 after 1.5 h incubation. The experiment was run as described in the main text. The first well contains a FAM labelled 17-mer and the second well contains FAM labelled target *ftsZ* mRNA (40nt) only; they are intended as a ladder.

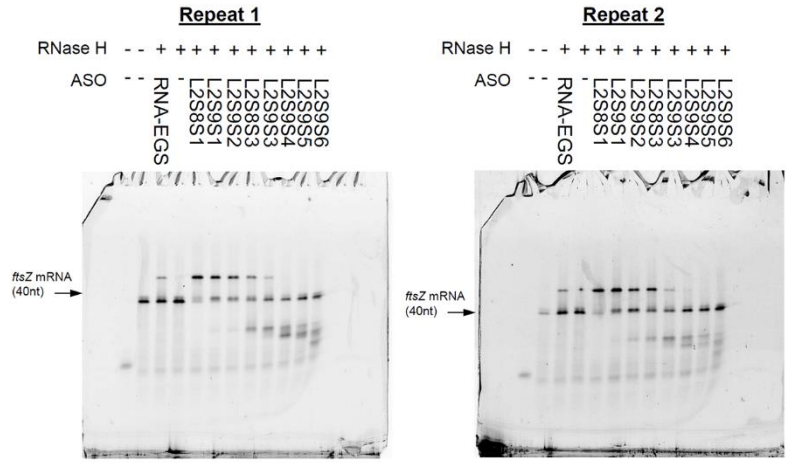

Figure C52. *In vitro* recruitment of RNase H by the oligonucleotides of Library 2 Set 9 after 24 h incubation. The experiment was run as described in the main text. The first well contains a FAM labelled 17-mer and the second well contains FAM labelled target *ftsZ* mRNA (40nt) only; they are intended as a ladder.

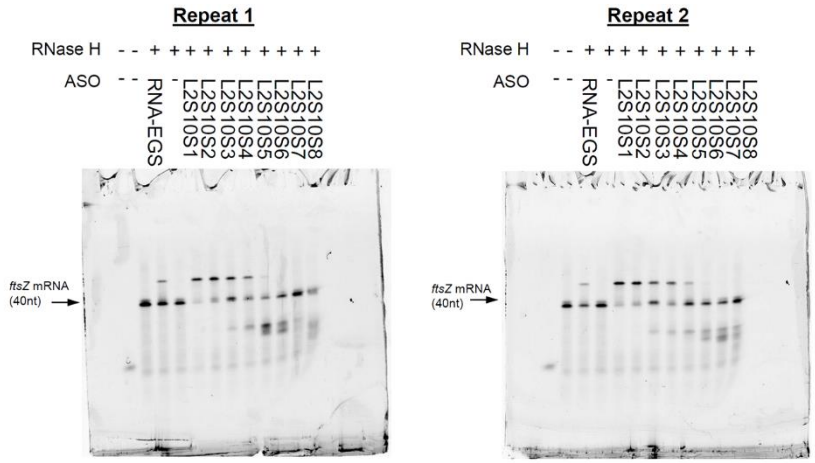

Figure C53. *In vitro* recruitment of RNase H by the oligonucleotides of Library 2 Set 10 after 1.5 h incubation. The experiment was run as described in the main text. The first well contains a FAM labelled 17-mer and the second well contains FAM labelled target *ftsZ* mRNA (40nt) only; they are intended as a ladder.

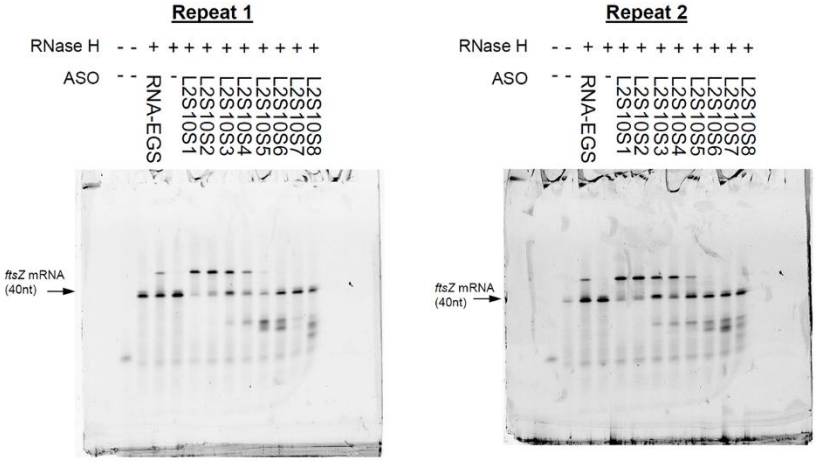

Figure C54. *In vitro* recruitment of RNase H by the oligonucleotides of Library 2 Set 10 after 24 h incubation. The experiment was run as described in the main text. The first well contains a FAM labelled 17-mer and the second well contains FAM labelled target *ftsZ* mRNA (40nt) only; they are intended as a ladder.

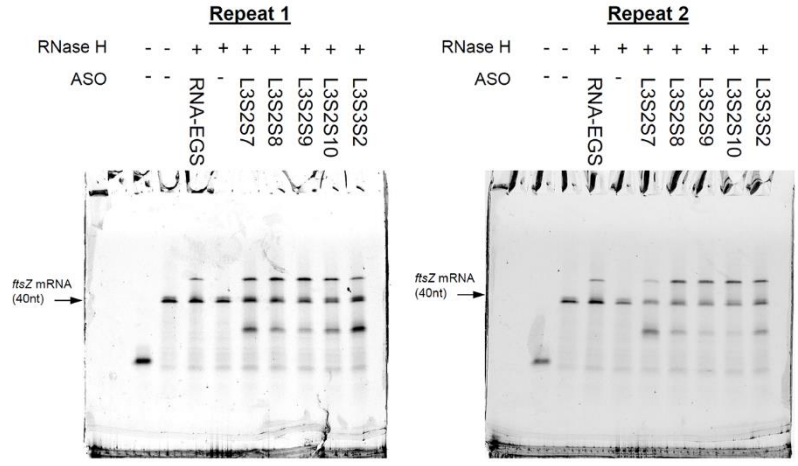

Figure C55. *In vitro* recruitment of RNase H by the oligonucleotides of Library 3 Set 2 after 1.5 h incubation. The experiment was run as described in the main text. The first well contains a FAM labelled 17-mer and the second well contains FAM labelled target *ftsZ* mRNA (40nt) only; they are intended as a ladder.

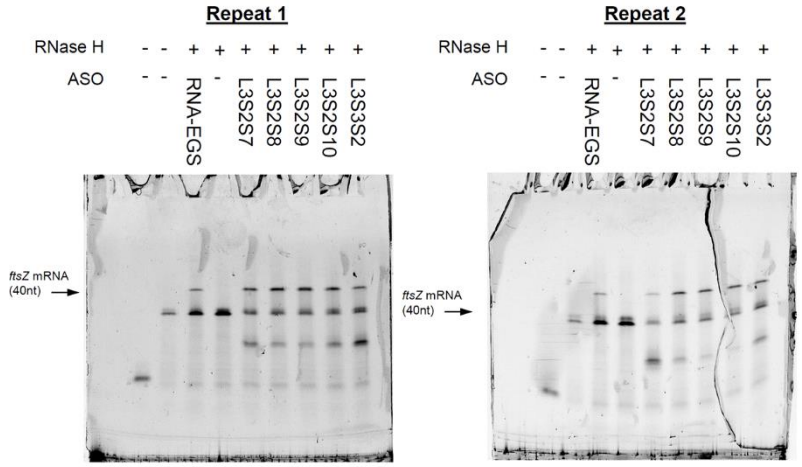

Figure C56. *In vitro* recruitment of RNase H by the oligonucleotides of Library 3 Set 2 after 24 h incubation. The experiment was run as described in the main text. The first well contains a FAM labelled 17-mer and the second well contains FAM labelled target *ftsZ* mRNA (40nt) only; they are intended as a ladder.

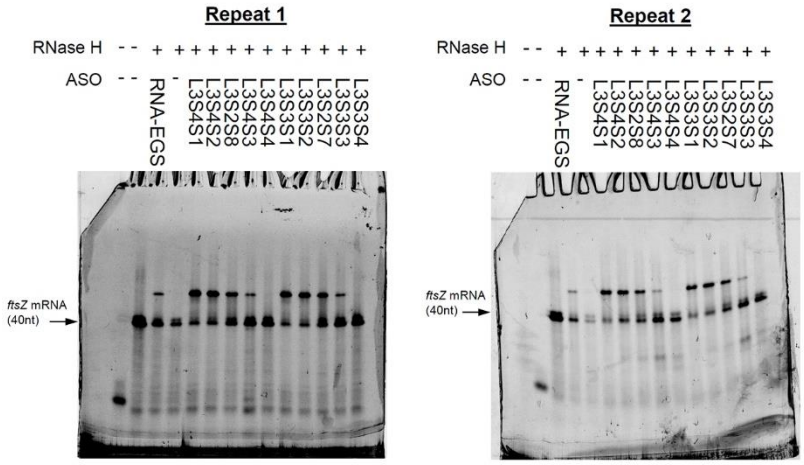

Figure C57. *In vitro* recruitment of RNase H by the oligonucleotides of Library 3 Set 3 and Set 4 after 1.5 h incubation. The experiment was run as described in the main text. The first well contains a FAM labelled 17-mer and the second well contains FAM labelled target *ftsZ* mRNA (40nt) only; they are intended as a ladder.

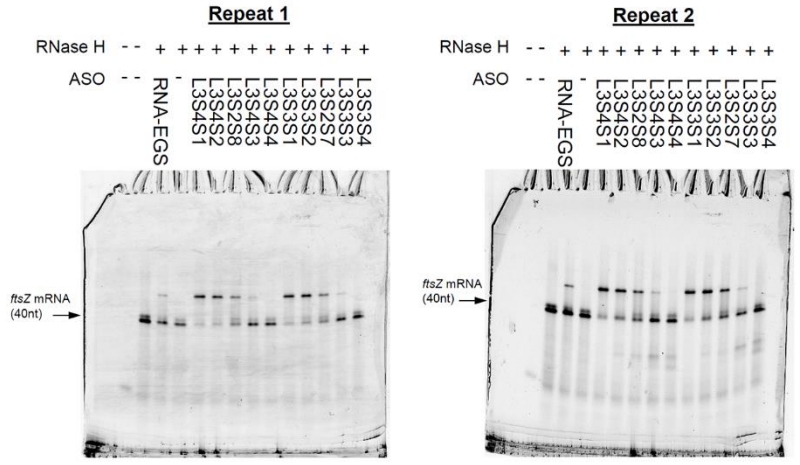

Figure C58. *In vitro* recruitment of RNase H by the oligonucleotides of Library 3 Set 3 and Set 4 after 24 h incubation. The experiment was run as described in the main text. The first well contains a FAM labelled 17-mer and the second well contains FAM labelled target *ftsZ* mRNA (40nt) only; they are intended as a ladder.

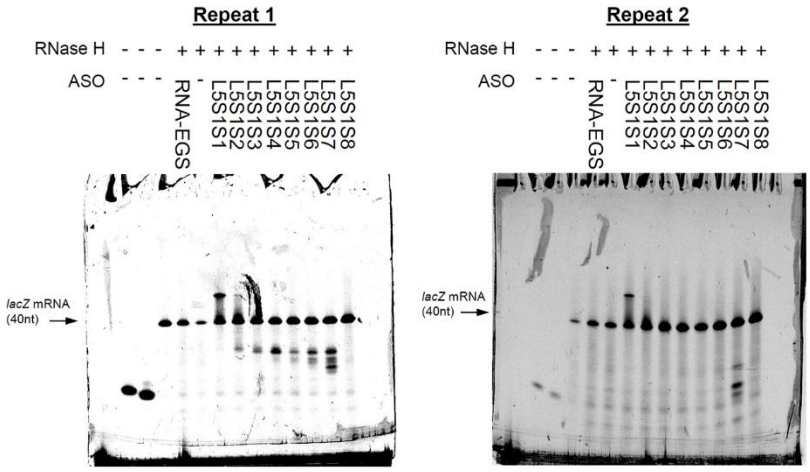

Figure C59. *In vitro* recruitment of RNase H by the oligonucleotides of Library 5 Set 1 after 1.5 h incubation. The experiment was run as described in the main text. The first 2 wells contains a FAM labelled 15- or 17-mer and the third well contains FAM labelled target *ftsZ* mRNA (40nt) only; they are intended as a ladder.

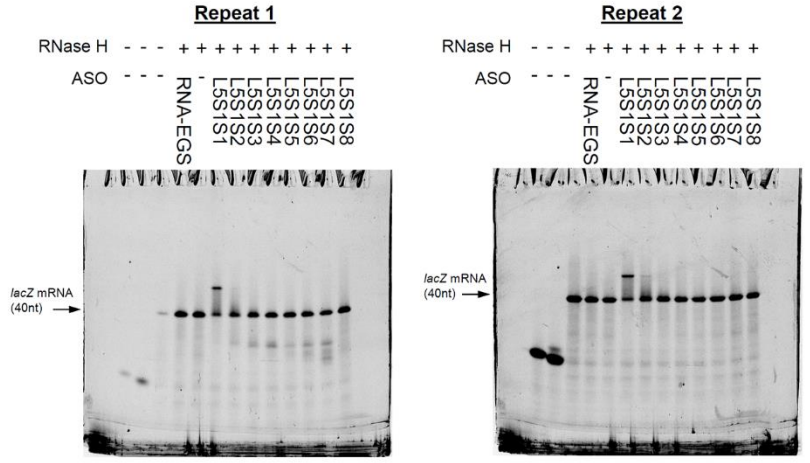

Figure C60. *In vitro* recruitment of RNase H by the oligonucleotides of Library 5 Set 1 after 24 h incubation. The experiment was run as described in the main text. The first 2 wells contains a FAM labelled 15- or 17-mer and the third well contains FAM labelled target *ftsZ* mRNA (40nt) only; they are intended as a ladder.

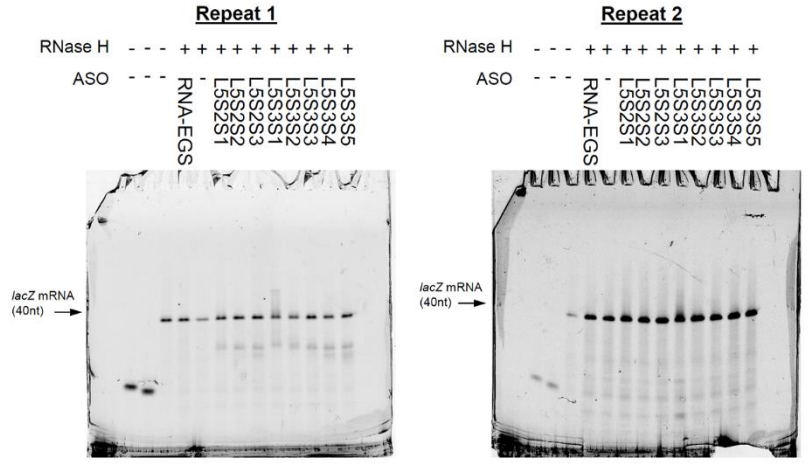

Figure C61. *In vitro* recruitment of RNase H by the oligonucleotides of Library 5 Set 2 and Set 3 after 1.5 h incubation. The experiment was run as described in the main text. The first 2 wells contains a FAM labelled 15- or 17-mer and the third well contains FAM labelled target *ftsZ* mRNA (40nt) only; they are intended as a ladder.

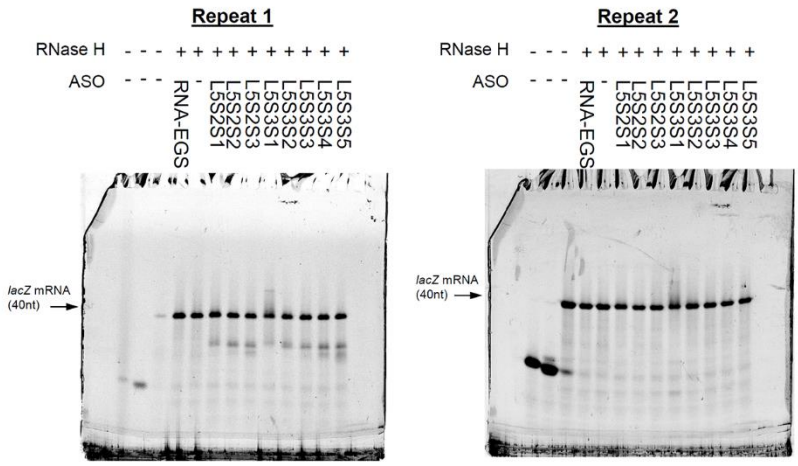

Figure C62. *In vitro* recruitment of RNase H by the oligonucleotides of Library 5 Set 2 and Set 3 after 24 h incubation. The experiment was run as described in the main text. The first 2 wells contains a FAM labelled 15- or 17-mer and the third well contains FAM labelled target *ftsZ* mRNA (40nt) only; they are intended as a ladder.

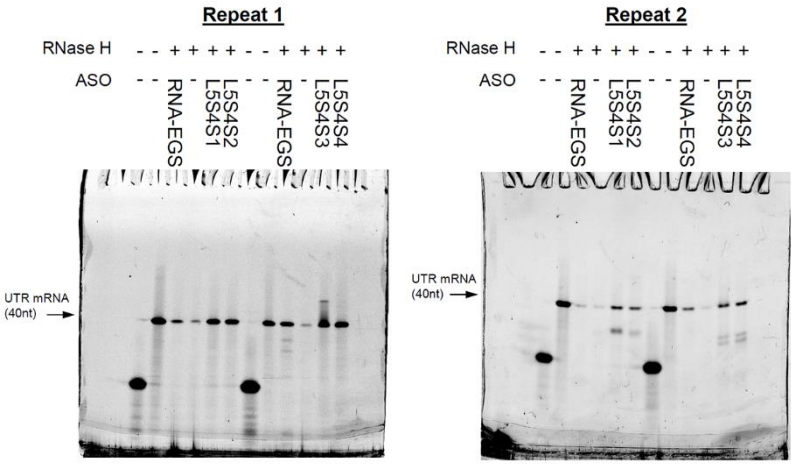

Figure C63. *In vitro* recruitment of RNase H by the oligonucleotides of Library 5 Set 4 after 1.5 h incubation. The experiment was run as described in the main text. The first well contains a FAM labelled 17-mer and the second well contains FAM labelled target *ftsZ* mRNA (40nt) only; they are intended as a ladder.

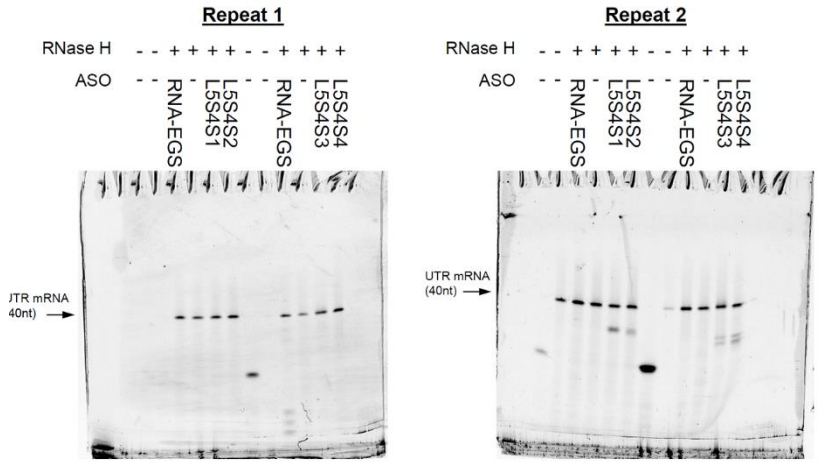

Figure C64. *In vitro* recruitment of RNase H by the oligonucleotides of Library 5 Set 4 after 24 h incubation. The experiment was run as described in the main text. The first well contains a FAM labelled 17-mer and the second well contains FAM labelled target *ftsZ* mRNA (40nt) only; they are intended as a ladder.

C.3 Identifying regions of the *lacZ* gene

The EcoCyc[256] website was used to determine the mRNA sequence of the *lacZ* gene in *E. coli* strain K-12 MG1655. The mRNA sequence was subsequently investigated using Mfold[284] to determine the single stranded sites (using the ss-count). This allowed us to identify two regions of at least 12 nucleotides long that have a high single-strand character (ss-count of 20 are higher for all residues), and complementary ASOs were designed to bind to the chosen regions (see **Figure C65**). The sequences of the ASOs designed this way are given in the main text.

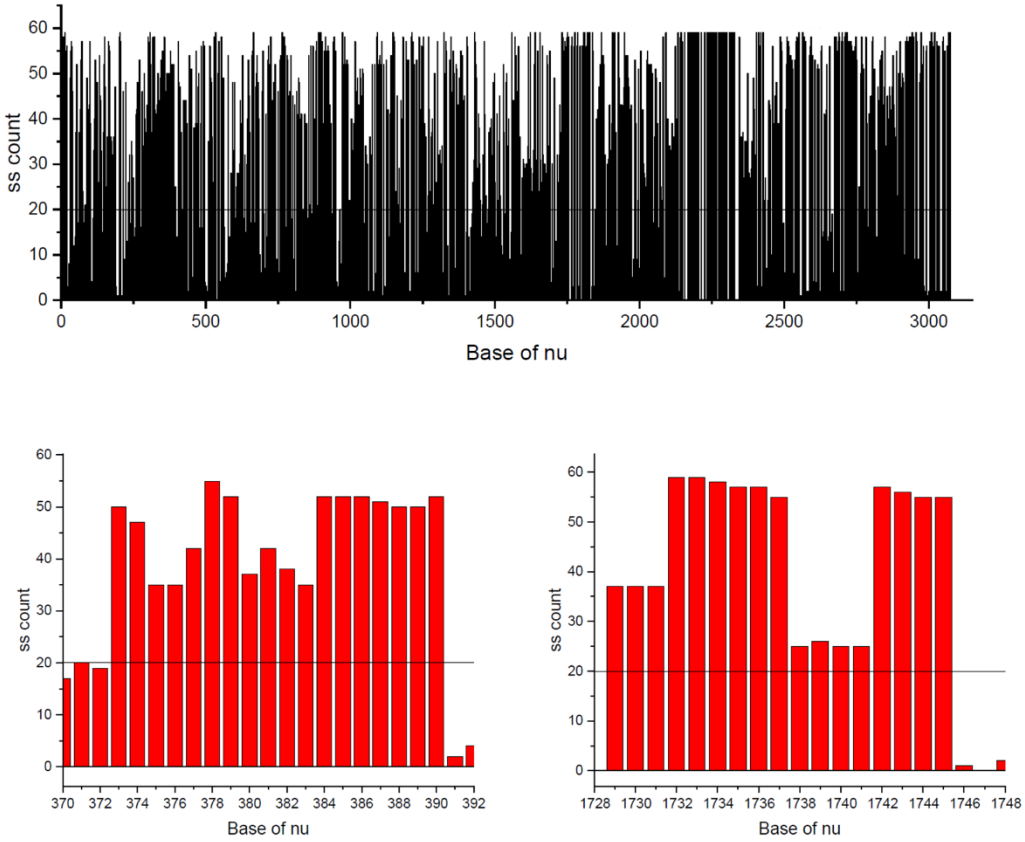

Figure C65. Ss-count for the *lacZ* mRNA calculated using Mfold, top the full length of the mRNA, and the rest are regions with at least 12 consecutive nucleotides with ss-count above 20. Based on the selected regions above we designed EGSs targeting sections in these regions.

C.4 Microscopy studies for the detection of *ftsZ* silencing (40x)

We tried to detect *fts*Z gene silencing by looking for the indicative elongation phenotype using microscopy techniques. The EGSs were added to 100 µL of *E. coli* AS19 cultures at 10^5 cfu/mL to achieve a final concentration of 100 µM. The mixture was subsequently incubated at 37 °C whilst shaking. After 200 minutes, 10 µL of the bacterial culture was transferred onto an adhesive

microscope slide and visualized in brightfield mode on a Leica DMi8 inverted microscope with 20x and 40x objectives. The contrast of the images was digitally enhanced using ImageJ.[290] The images obtained with a 20x objective are shown in the main text. The images obtained with a 40x objective are provided in this section (**Figure C66 – Figure C77**).

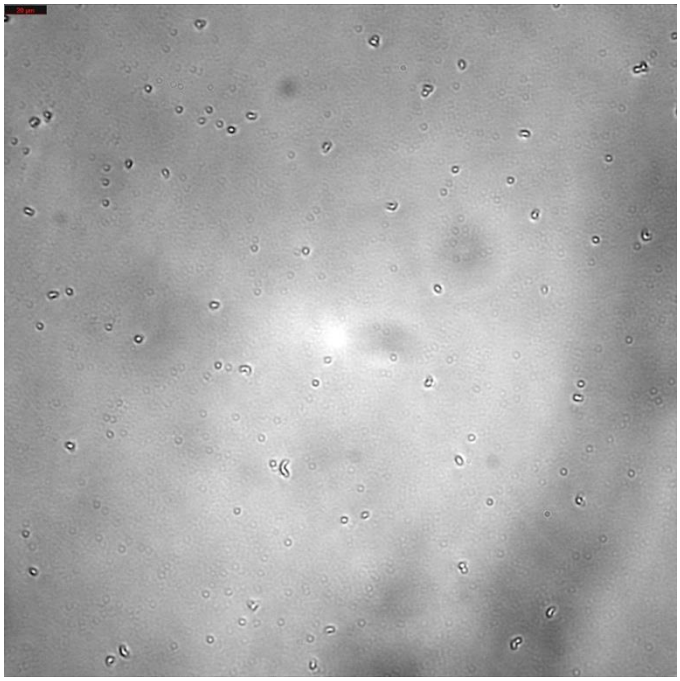

Figure C66. Brightfield images of *E. coli* AS19 incubated for 200 min at 37 °C in the absence of any oligonucleotide. The experiment was performed as described in the main text (40x objective). The scale bar represents 20 µm.

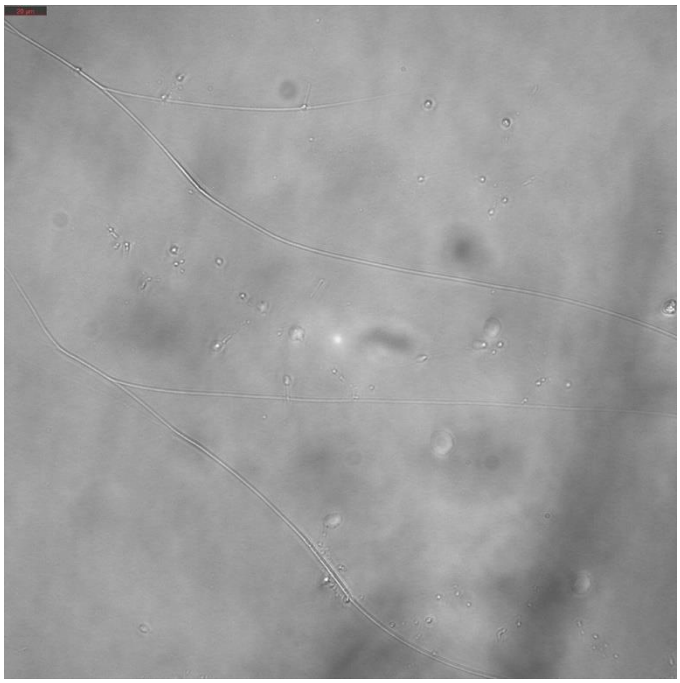

Figure C67. Brightfield images of *E. coli* AS19 incubated for 200 min at 37 °C in the presence of 100 µM L2S8S3. The experiment was performed as described in the main text (40x objective). The scale bar represents 20 µm.

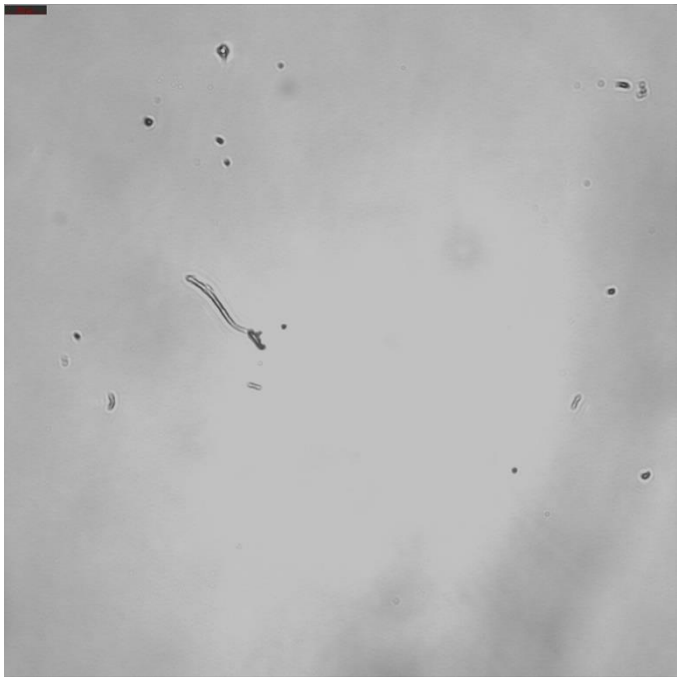

Figure C68. Brightfield images of *E. coli* AS19 incubated for 200 min at 37 °C in the presence of 100 µM L2S9S3. The experiment was performed as described in the main text (40x objective). The scale bar represents 20 µm.

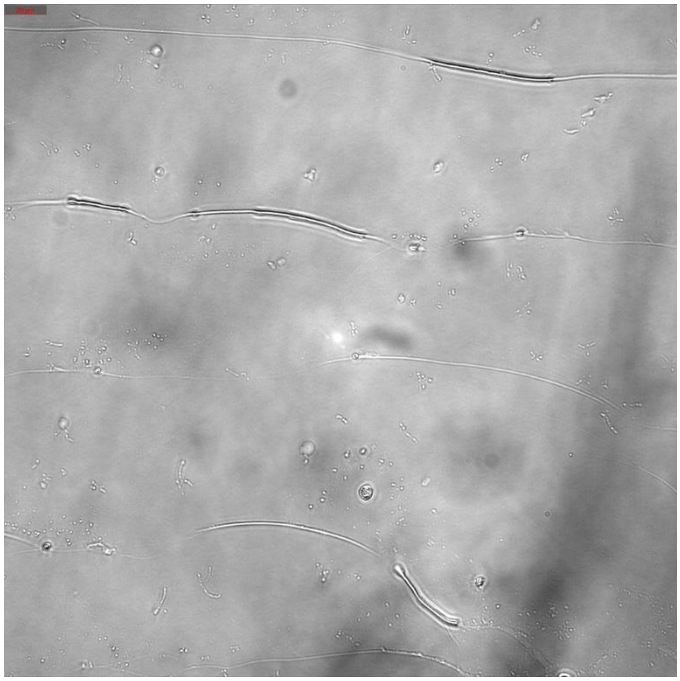

Figure C69. Brightfield images of *E. coli* AS19 incubated for 200 min at 37 °C in the presence of 100 µM L2S9S4. The experiment was performed as described in the main text (40x objective). The scale bar represents 20 µm.

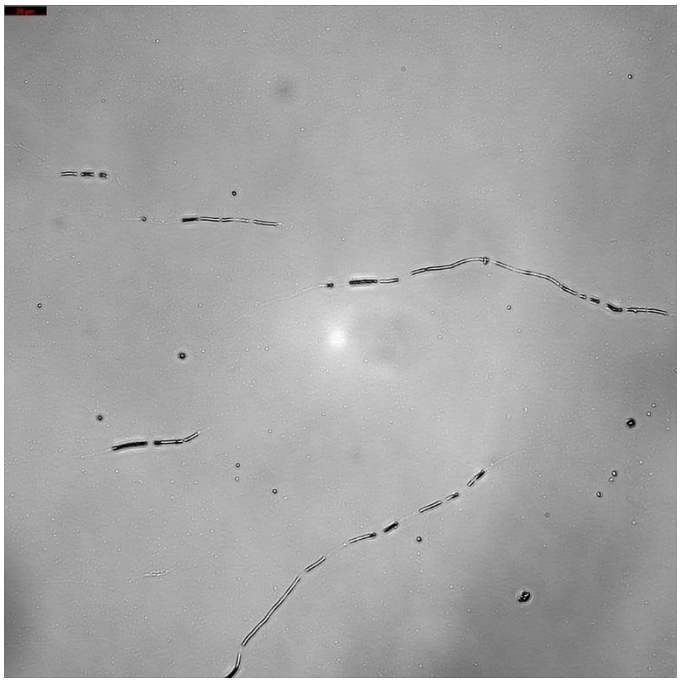

Figure C70. Brightfield images of *E. coli* AS19 incubated for 200 min at 37 °C in the presence of 100 µM L2S10S4. The experiment was performed as described in the main text (40x objective). The scale bar represents 20 µm.

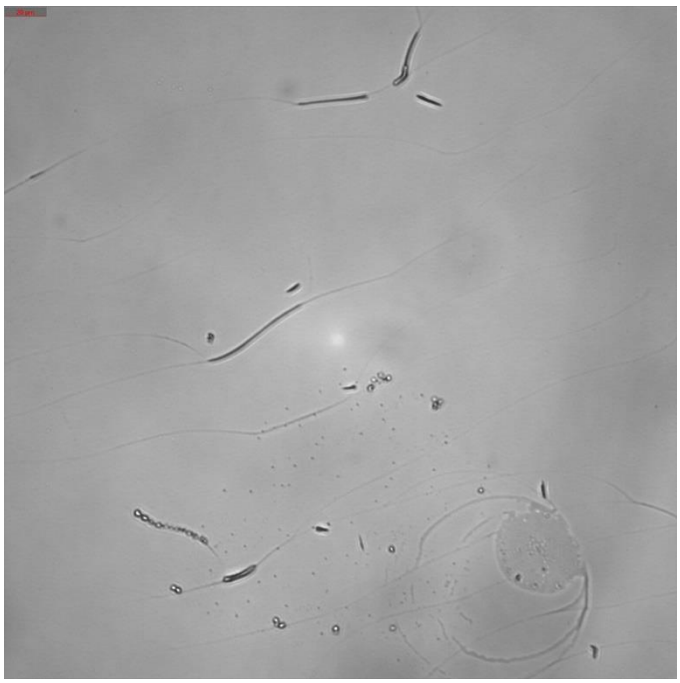

Figure C71. Brightfield images of *E. coli* AS19 incubated for 200 min at 37 °C in the presence of 100 µM L2S10S5. The experiment was performed as described in the main text (40x objective). The scale bar represents 20 µm.

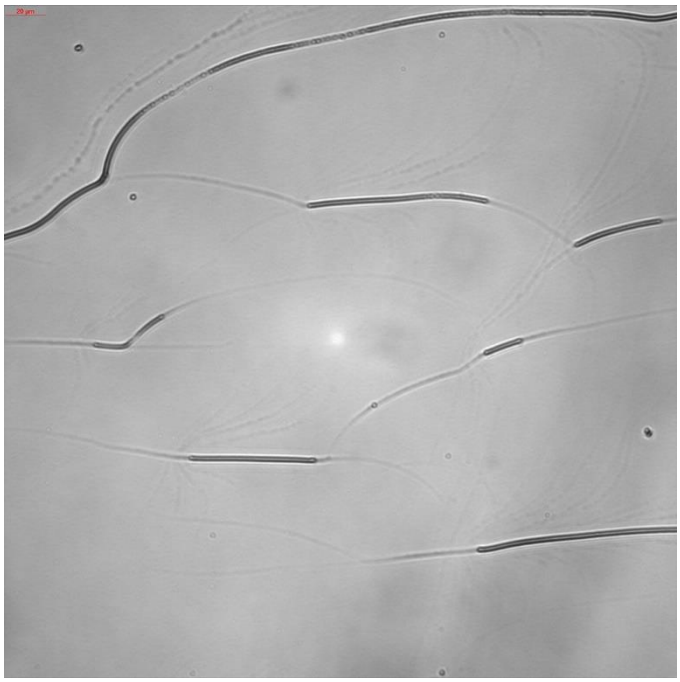

Figure C72. Brightfield images of *E. coli* AS19 incubated for 200 min at 37 °C in the presence of 100 µM L2S10S6. The experiment was performed as described in the main text (40x objective). The scale bar represents 20 µm.

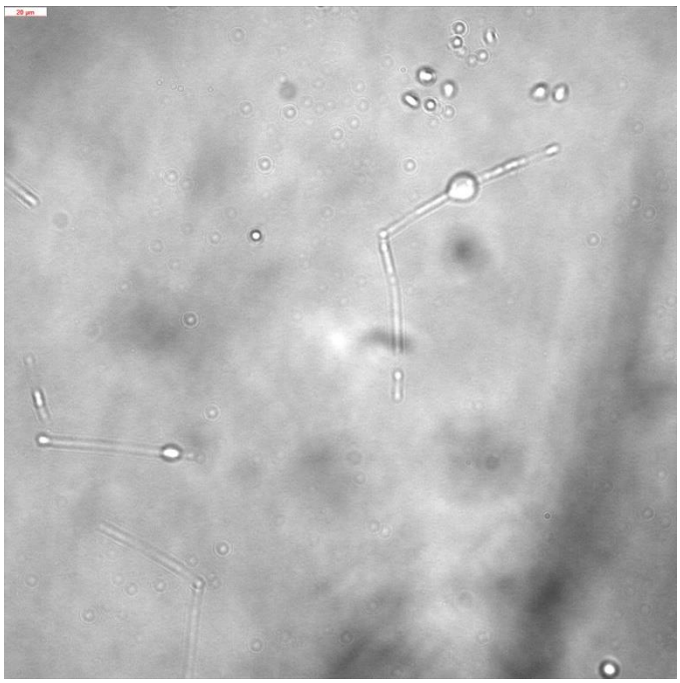

Figure C73. Brightfield images of *E. coli* AS19 incubated for 200 min at 37 °C in the presence of 100 µM L3S2S7. The experiment was performed as described in the main text (40x objective). The scale bar represents 20 µm.

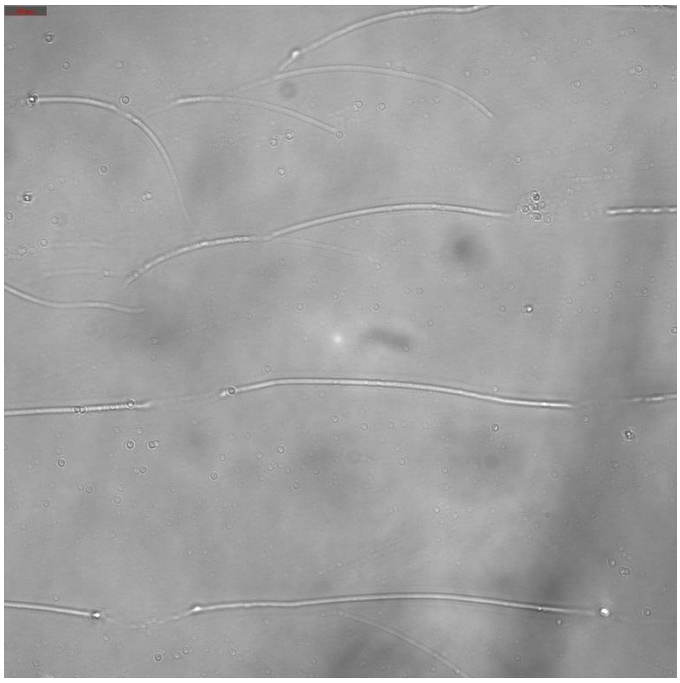

Figure C74. Brightfield images of *E. coli* AS19 incubated for 200 min at 37 °C in the presence of 100 µM L3S2S8. The experiment was performed as described in the main text (40x objective). The scale bar represents 20 µm.

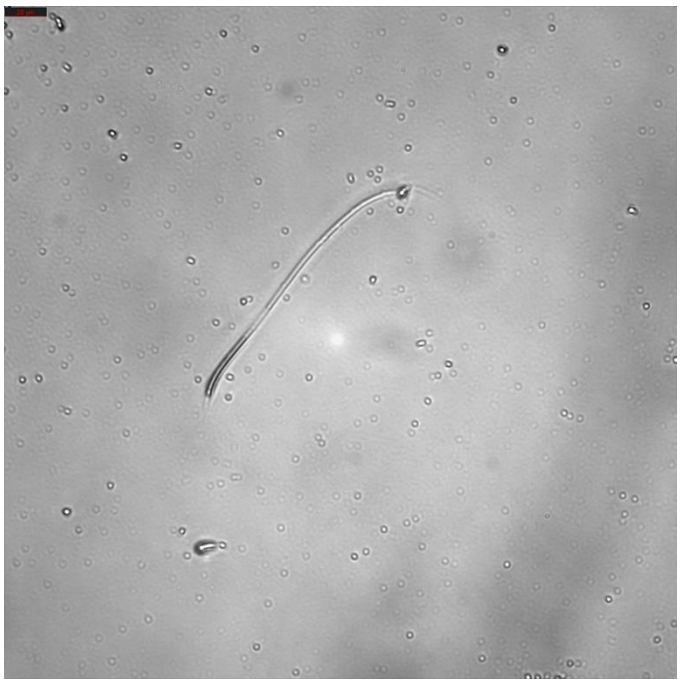

Figure C75. Brightfield images of *E. coli* AS19 incubated for 200 min at 37 °C in the presence of 100 µM L3S5S2. The experiment was performed as described in the main text (40x objective). The scale bar represents 20 µm.

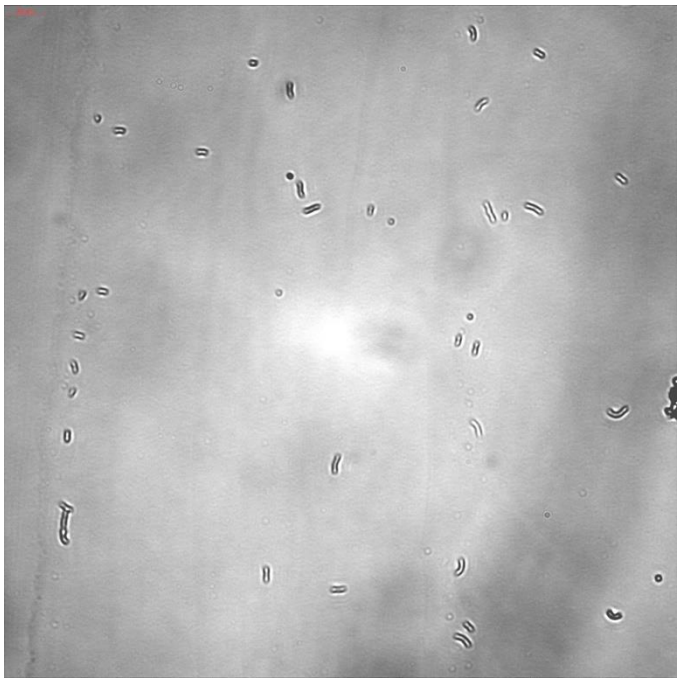

Figure C76. Brightfield images of *E. coli* AS19 incubated for 200 min at 37 °C in the presence of 100 µM L5S1S2. The experiment was performed as described in the main text (40x objective). The scale bar represents 20 µm.

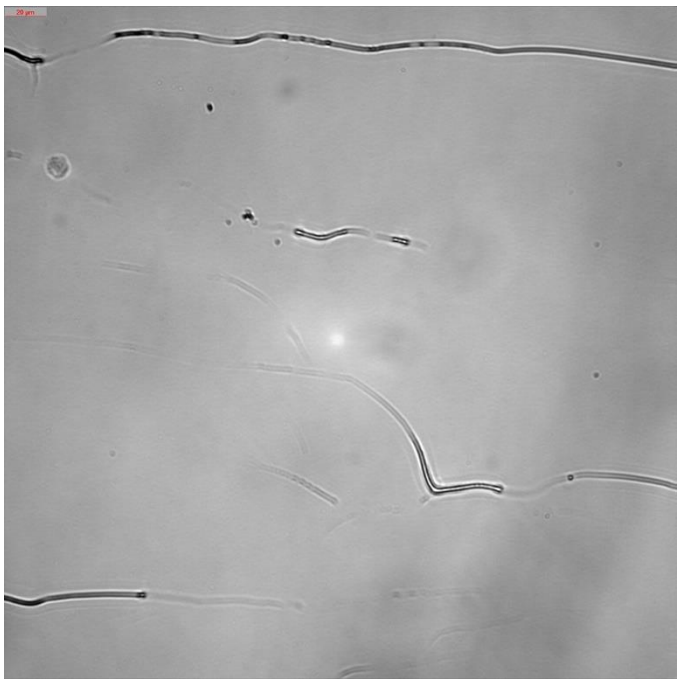

Figure C77. Brightfield images of *E. coli* AS19 incubated for 200 min at 37 °C in the presence of 100 µM L5S4S1. The experiment was performed as described in the main text (40x objective). The scale bar represents 20 µm.

List of References

1. A. Fleming, *Br. J. Exp. Pathol.*, 1929, **10**, 226.
2. S. B. Singh and J. F. Barrett, *Biochem. Pharmacol.*, 2006, **71**, 1006-1015.
3. A. Cassini, L. D. Högberg, D. Plachouras, A. Quattrocchi, A. Hoxha, G. S. Simonsen, M. Colomb-Cotinat, M. E. Kretzschmar, B. Devleesschauwer and M. Cecchini, *Lancet Infect. Dis.*, 2019, **19**, 56-66.
4. P. Ehrlich and S. Halta, *Die experimentelle chemotherapie der spirillosen*, Springer, 1910.
5. R. I. Aminov, *Front Microbiol.*, 2010, **1**, 134.
6. E. E. Hays, I. C. Wells, P. A. Katzman, C. Cain, F. A. Jacobs, S. A. Thayer, E. A. Doisy, W. Gaby, E. Roberts and R. Muir, *Biol. Chem.*, 1945, **159**, 725-750.
7. J.-F. Dubern and S. P. Diggle, *Mol. BioSyst.*, 2008, **4**, 882-888.
8. G. F. Kaufmann, R. Sartorio, S.-H. Lee, C. J. Rogers, M. M. Meijler, J. A. Moss, B. Clapham, A. P. Brogan, T. J. Dickerson and K. D. Janda, *Proc. Natl. Acad. Sci. U. S. A.*, 2005, **102**, 309-314.
9. I. Chopra, L. Hesse and A. O'Neill, *Pharmacochem. Libr.*, 2002, **32**, 213-225.
10. J. Y. Cha, A. Ishiwata and S. Mobashery, *J. Biol. Chem.*, 2004, **279**, 14917-14921.
11. E. P. Abraham and E. Chain, *Nature*, 1940, **146**, 837.
12. K. K. Kumarasamy, M. A. Toleman, T. R. Walsh, J. Bagaria, F. Butt, R. Balakrishnan, U. Chaudhary, M. Doumith, C. G. Giske, S. Irfan, P. Krishnan, A. V. Kumar, S. Maharjan, S. Mushtaq, T. Noorie, D. L. Paterson, A. Pearson, C. Perry, R. Pike, B. Rao, U. Ray, J. B. Sarma, M. Sharma, E. Sheridan, M. A. Thirunarayan, J. Turton, S. Upadhyay, M. Warner, W. Welfare, D. M. Livermore and N. Woodford, *Lancet Infect. Dis.*, 2010, **10**, 597-602.
13. C. L. Ventola, *Pharm. Ther.*, 2015, **40**, 277.
14. J. M. A. Blair, M. A. Webber, A. J. Baylay, D. O. Ogbolu and L. J. V. Piddock, *Nat. Rev. Micro*, 2015, **13**, 42-51.
15. C. P. Randall, K. R. Mariner, I. Chopra and A. J. O'Neill, *Antimicrob. Agents Chemother.*, 2013, **57**, 637-639.
16. R. F. Weaver, *Molecular biology*, McGraw-Hill Higher Education, Boston, 2012.
17. G. M. Blackburn, *Nucleic acids in chemistry and biology*, Royal Society of Chemistry, 2006.
18. E. R. Kandimalla and S. Agrawal, *Biochemistry*, 1996, **35**, 15332-15339.
19. I. Anosova, E. A. Kowal, M. R. Dunn, J. C. Chaput, W. D. Van Horn and M. Egli, *Nucleic Acids Res.*, 2015, **44**, 1007-1021.

20. Z. Luo, M. Dauter and Z. Dauter, *Acta Crystallogr. Sect. D. Biol. Crystallogr.*, 2014, **70**, 1790-1800.

21. N. Narayana and M. A. Weiss, *J. Mol. Biol.*, 2009, **385**, 469-490.

22. B. H. Mooers and A. Singh, *RNA*, 2011, **17**, 1870-1883.

23. E. Hantz, V. Larue, P. Ladam, L. Le Moyec, C. Gouyette and T. Huynh Dinh, *Int. J. Biol. Macromol.*, 2001, **28**, 273-284.

24. Y. K. Cheng and B. M. Pettitt, *J. Am. Chem. Soc.*, 1992, **114**, 4465-4474.

25. S. E. Butcher and A. M. Pyle, *Acc. Chem. Res.*, 2011, **44**, 1302-1311.

26. B. Hingerty, R. Brown and A. Jack, *J. Mol. Biol.*, 1978, **124**, 523-534.

27. F. Crick, *Nature*, 1970, **227**, 561-563.

28. D. Thieffry and S. Sarkar, *Trends Biochem. Sci*, 1998, **23**, 312-316.

29. C. Walsh, *Antibiotics: actions, origins, resistance*, American Society for Microbiology (ASM), 2003.

30. D. C. Hooper, *Drugs*, 1995, **49**, 10-15.

31. W. Wehrli, *Rev. Infect. Dis.*, 1983, **5**, S407-S411.

32. I. Chopra and M. Roberts, *Microbiol. Mol. Biol. Rev.*, 2001, **65**, 232.

33. T. Mazzei, E. Mini, A. Novelli and P. Periti, *J. Antimicrob. Chemother.*, 1993, **31**, 1-9.

34. K. W. Bayles, *Trends Microbiol.*, 2000, **8**, 274-278.

35. S. K. Straus and R. E. W. Hancock, *Biochim. Biophys. Acta, Biomembr.*, 2006, **1758**, 1215-1223.

36. A. Davydova, M. Vorobjeva, D. Pyshnyi, S. Altman, V. Vlassov and A. Venyaminova, *Crit. Rev. Microbiol.*, 2016, **42**, 847-865.

37. C. Helene, *Anti-Cancer Drug Des.*, 1991, **6**, 569-584.

38. P. S. Miller, in *Progress in Nucleic Acid Research and Molecular Biology*, eds. W. E. Cohn and K. Moldave, Academic Press, 1996, vol. 52, pp. 261-291.

39. P. C. Zamecnik and M. L. Stephenson, *Proc. Natl. Acad. Sci.*, 1978, **75**, 280-284.

40. K. Jayaraman, K. McParland, P. Miller and P. O. Ts'o, *Proc. Natl. Acad. Sci.*, 1981, **78**, 1537-1541.

41. R. S. Geary, S. P. Henry and L. R. Grillone, *Clin. Pharmacokinet.*, 2002, **41**, 255-260.

42. X.-Y. Xue, X.-G. Mao, Y. Zhou, Z. Chen, Y. Hu, Z. Hou, M.-K. Li, J.-R. Meng and X.-X. Luo, *Nanomedicine*, 2018, **14**, 745-758.

43. N. M. Dean and R. McKay, *Proc. Natl. Acad. Sci.*, 1994, **91**, 11762-11766.

44. T. Golden, N. M. Dean and R. E. Honkanen, *Microcirculation*, 2002, **9**, 51-64.

45. G. F. Deleavey and M. J. Damha, *Chem. Bio.*, 2012, **19**, 937-954.

46. J. F. Lee, G. M. Stovall and A. D. Ellington, *Curr. Opin. Chem. Biol.*, 2006, **10**, 282-289.

47. I. M. Verma, L. Naldini, T. Kafri, H. Miyoshi, M. Takahashi, U. Blömer, N. Somia, L. Wang and F. Gage, in *Genes and Resistance to Disease*, Springer, 2000, pp. 147-157.

48. E. W. Ng, D. T. Shima, P. Calias, E. T. Cunningham, D. R. Guyer and A. P. Adamis, *Nat. Rev. Drug Discovery*, 2006, **5**, 123-132.

49. R. S. Geary, B. F. Baker and S. T. Crooke, *Clin. Pharmacokinet.*, 2015, **54**, 133-146.

50. P. Sazani, K. P. V. Ness, D. L. Weller, D. W. Poage, K. Palyada and S. B. Shrewsbury, *Int. J. Toxicol.*, 2011, **30**, 313-321.

51. C. Stein, D. Castanotto, A. Krishnan and L. Nikolaenko, *Mol. Ther.-Nucleic Acids*, 2016, **5**.

52. Y. Hua, K. Sahashi, G. Hung, F. Rigo, M. A. Passini, C. F. Bennett and A. R. Krainer, *Genes Dev.*, 2010, **24**, 1634-1644.

53. A. M. Keeler and T. R. Flotte, *Annu. Rev. Virol.*, 2019, **6**.

54. J. Yang, *Expert Rev. Clin. Pharmacol.*, 2019, **12**, 95-99.

55. M. A. Gertz, M. Scheinberg, M. Waddington-Cruz, S. B. Heitner, C. Karam, B. Drachman, S. Khella, C. Whelan and L. Obici, *Expert Rev. Clin. Pharmacol.*, 2019, **12**, 701-711.

56. *Oligonucleotide-Based Therapies*, Springer, New York, 2019.

57. J. K. Watts and D. R. Corey, *J. Pathol.*, 2012, **226**, 365-379.

58. F. Eckstein, *Biochimie*, 2002, **84**, 841-848.

59. R. Geary, R. Yu and A. Levin, *Curr. Opin. Invest. Drugs (BioMed Cent.)*, 2001, **2**, 562-573.

60. L. Kibler-Herzog, G. Zon, B. Uznanski, G. Whittier and W. D. Wilson, *Nucleic Acids Res.*, 1991, **19**, 2979-2986.

61. S. M. Gryaznov, *Chem. Biodiversity*, 2010, **7**, 477-493.

62. A. H. Hall, J. Wan, E. E. Shaughnessy, B. Ramsay Shaw and K. A. Alexander, *Nucleic Acids Res.*, 2004, **32**, 5991-6000.

63. D. J. Dellinger, D. M. Sheehan, N. K. Christensen, J. G. Lindberg and M. H. Caruthers, *J. Am. Chem. Soc.*, 2003, **125**, 940-950.

64. D. Sheehan, B. Lunstad, C. M. Yamada, B. G. Stell, M. H. Caruthers and D. J. Dellinger, *Nucleic Acids Res.*, 2003, **31**, 4109-4118.

65. C. M. Yamada, D. J. Dellinger and M. H. Caruthers, *Nucleosides Nucleotides Nucleic Acids.*, 2007, **26**, 539-546.

66. T. Bentin and P. E. Nielsen, *Biochemistry*, 1996, **35**, 8863-8869.

67. S. V. Smulevitch, C. G. Simmons, J. C. Norton, T. W. Wise and D. R. Corey, *Nat. Biotech.*, 1996, **14**, 1700-1704.

68. B. R. Bill, A. M. Petzold, K. J. Clark, L. A. Schimmenti and S. C. Ekker, *Zebrafish*, 2009, **6**, 69-77.

69. D. R. Corey and J. M. Abrams, *Genome Biol.*, 2001, **2**, 1015.

70. V. V. Demidov, V. N. Potaman, M. D. Frank-Kamenetskil, M. Egholm, O. Buchard, S. H. Sönnichsen and P. E. Nlelsen, *Biochem. Pharmacol.*, 1994, **48**, 1310-1313.

71. R. M. Hudziak, E. Barofsky, D. F. Barofsky, D. L. Weller, S.-B. Huang and D. D. Weller, *Antisense Nucleic Acid Drug Dev.*, 1996, **6**, 267-272.

72. J. Summerton, *Biochim. Biophys. Acta, Gene Struct. Expression*, 1999, **1489**, 141-158.

73. L. Du and R. A. Gatti, *J. Immunol. Methods*, 2011, **365**, 1-7.

74. S. Shakeel, S. Karim and A. Ali, *J. Chem. Technol. Biotechnol.*, 2006, **81**, 892-899.

75. C. G. Simmons, A. E. Pitts, L. D. Mayfield, J. W. Shay and D. R. Corey, *Biorg. Med. Chem. Lett.*, 1997, **7**, 3001-3006.

76. H. M. Moulton, M. H. Nelson, S. A. Hatlevig, M. T. Reddy and P. L. Iversen, *Bioconjugate Chem.*, 2004, **15**, 290-299.

77. N. Sugimoto, S.-i. Nakano, M. Katoh, A. Matsumura, H. Nakamuta, T. Ohmichi, M. Yoneyama and M. Sasaki, *Biochemistry*, 1995, **34**, 11211-11216.

78. M.-Y. Chiang, H. Chan, M. A. Zounes, S. M. Freier, W. F. Lima and C. F. Bennett, *J. Biol. Chem.*, 1991, **266**, 18162-18171.

79. G. Kawai, Y. Yamamoto, T. Kamimura, T. Masegi, M. Sekine, T. Hata, T. Iimori, T. Watanabe, T. Miyazawa and S. Yokoyama, *Biochemistry*, 1992, **31**, 1040-1046.

80. T. Nishizaki, S. Iwai, E. Ohtsuka and H. Nakamura, *Biochemistry*, 1997, **36**, 2577-2585.

81. M. Majlessi, N. C. Nelson and M. M. Becker, *Nucleic Acids Res.*, 1998, **26**, 2224-2229.

82. G. R. Rettig and M. A. Behlke, *Mol. Ther.*, 2012, **20**, 483-512.

83. Y. S. Sanghvi, *Curr. Protoc. Nucleic Acid Chem.*, 2011, 4.1. 1-4.1. 22.

84. S. M. Freier and K.-H. Altmann, *Nucleic Acids Res.*, 1997, **25**, 4429-4443.

85. M. Manoharan, *Biochim. Biophys. Acta, Gene Struct. Expression*, 1999, **1489**, 117-130.

86. E. Viazovkina, M. M. Mangos, M. I. Elzagheid and M. J. Damha, *Curr. Protoc. Nucleic Acid Chem.*, 2002, 4.15. 11-14.15. 22.

87. D. M. Williams, F. Benseler and F. Eckstein, *Biochemistry*, 1991, **30**, 4001-4009.

88. A. M. Kawasaki, M. D. Casper, S. M. Freier, E. A. Lesnik, M. C. Zounes, L. L. Cummins, C. Gonzalez and P. D. Cook, *J. Med. Chem.*, 1993, **36**, 831-841.

89. B. P. Monia, E. Lesnik, C. Gonzalez, W. Lima, D. McGee, C. Guinosso, A. Kawasaki, P. D. Cook and S. Freier, *J. Biol. Chem.*, 1993, **268**, 14514-14522.

90. H. Ikeda, R. Fernandez, J. J. Barchi Jr, X. Huang, V. E. Marquez and A. Wilk, *Nucleic Acids Res.*, 1998, **26**, 2237-2244.

91. C. F. Bennett and E. E. Swayze, *Annu. Rev. Pharmacool. Toxicol.*, 2010, **50**, 259-293.

92. P. S. Pallan, E. M. Greene, P. A. Jicman, R. K. Pandey, M. Manoharan, E. Rozners and M. Egli, *Nucleic Acids Res.*, 2010, **39**, 3482-3495.

93. J.-F. Trempe, C. J. Wilds, A. Y. Denisov, R. T. Pon, M. J. Damha and K. Gehring, *J. Am. Chem. Soc.*, 2001, **123**, 4896-4903.

94. I. Berger, V. Tereshko, H. Ikeda, V. E. Marquez and M. Egli, *Nucleic Acids Res.*, 1998, **26**, 2473-2480.

95. M. Damha, C. Wilds, A. Noronha, I. Brukner, G. Borkow, D. Arion and M. Parniak, *J. Am. Chem. Soc.*, 1998, **120**, 12976-12977.

96. C. J. Wilds and M. J. Damha, *Nucleic Acids Res.*, 2000, **28**, 3625-3635.

97. A. Kalota, L. Karabon, C. Swider, E. Viazovkina, M. Elzagheid, M. Damha and A. Gewirtz, *Nucleic Acids Res.*, 2006, **34**, 451-461.

98. J. K. Watts, A. Katolik, J. Viladoms and M. J. Damha, *Org. Biomol. Chem.*, 2009, **7**, 1904-1910.

99. D. A. Braasch and D. R. Corey, *Chem. Bio.*, 2001, **8**, 1-7.

100. A. A. Koshkin, S. K. Singh, P. Nielsen, V. K. Rajwanshi, R. Kumar, M. Meldgaard, C. E. Olsen and J. Wengel, *Tetrahedron*, 1998, **54**, 3607-3630.

101. S. Obika, D. Nanbu, Y. Hari, J.-i. Andoh, K.-i. Morio, T. Doi and T. Imanishi, *Tetrahedron Lett.*, 1998, **39**, 5401-5404.

102. C. Wahlestedt, P. Salmi, L. Good, J. Kela, T. Johnsson, T. Hökfelt, C. Broberger, F. Porreca, J. Lai and K. Ren, *Proc. Natl. Acad. Sci.*, 2000, **97**, 5633-5638.

103. V. E. Marquez, M. A. Siddiqui, A. Ezzitouni, P. Russ, J. Wang, R. W. Wagner and M. D. Matteucci, *J. Med. Chem.*, 1996, **39**, 3739-3747.

104. M. Terrazas, S. M. Ocampo, J. C. Perales, V. E. Marquez and R. Eritja, *ChemBioChem*, 2011, **12**, 1056-1065.

105. C. Lopez, B. A. Arivett, L. A. Actis and M. E. Tolmasky, *Antimicrob. Agents Chemother.*, 2015, **59**, 5798-5803.

106. M. M. Mangos, K.-L. Min, E. Viazovkina, A. Galarneau, M. I. Elzagheid, M. A. Parniak and M. J. Damha, *J. Am. Chem. Soc.*, 2003, **125**, 654-661.

107. C. Leydier, L. Bellon, J.-L. Barascut, F. Morvan, B. Rayner and J.-L. Imbach, *Antisense Res. Dev.*, 1995, **5**, 167-174.

108. P. Dande, T. P. Prakash, N. Sioufi, H. Gaus, R. Jarres, A. Berdeja, E. E. Swayze, R. H. Griffey and B. Bhat, *J. Med. Chem.*, 2006, **49**, 1624-1634.

109. B. Verbeure, E. Lescrinier, J. Wang and P. Herdewijn, *Nucleic Acids Res.*, 2001, **29**, 4941-4947.

110. K. Nauwelaerts, M. Fisher, M. Froeyen, E. Lescrinier, A. Van Aerschot, D. Xu, R. DeLong, H. Kang, R. L. Juliano and P. Herdewijn, *J. Am. Chem. Soc.*, 2007, **129**, 9340-9348.

111. V. K. Sharma and J. K. Watts, *Future Med. Chem.*, 2015, **7**, 2221-2242.

112. K. Takeda and S. Akira, *Int. Immunol.*, 2005, **17**, 1-14.

113. A. Dalpke, J. Frank, M. Peter and K. Heeg, *Infect. Immun.*, 2006, **74**, 940-946.

114. S. Henry, K. Stecker, D. Brooks, D. Monteith, B. Conklin and C. F. Bennett, *J. Pharmacol. Exp. Ther.*, 2000, **292**, 468-479.

115. B. C. Froehler, S. Wadwani, T. J. Terhorst and S. R. Gerrard, *Tetrahedron Lett.*, 1992, **33**, 5307-5310.

116. R. W. Wagner, M. D. Matteucci, J. G. Lewis, A. J. Gutierrez, C. Moulds and B. C. Froehler, *Science*, 1993, **260**, 1510-1510.

117. C. Moulds, J. G. Lewis, B. C. Froehler, D. Grant, T. Huang, J. F. Milligan, M. D. Matteucci and R. W. Wagner, *Biochemistry*, 1995, **34**, 5044-5053.

118. W. M. Flanagan, R. W. Wagner, D. Grant, K.-Y. Lin and M. D. Matteucci, *Nat. Biotechnol.*, 1999, **17**, 48-52.

119. S. Gryaznov and R. G. Schultz, *Tetrahedron Lett.*, 1994, **35**, 2489-2492.

120. J. K. Watts and D. R. Corey, *J. Pathol.*, 2012, **226**, 365.

121. E. K. Sully and B. L. Geller, *Curr. Opin. Microbiol.*, 2016, **33**, 47-55.

122. H. Stein and P. Hausen, *Science*, 1969, **166**, 393-395.

123. W. F. Lima, J. B. Rose, J. G. Nichols, H. Wu, M. T. Migawa, T. K. Wyrzykiewicz, A. M. Siwkowski and S. T. Crooke, *Mol. Pharmacol.*, 2007, **71**, 83-91.

124. S. M. Cerritelli and R. J. Crouch, *FEBS J.*, 2009, **276**, 1494-1505.

125. A. Noy, A. Perez, F. Lankas, F. J. Luque and M. Orozco, *J. Mol. Biol.*, 2004, **343**, 627-638.

126. A. Noy, A. Pérez, M. Márquez, F. J. Luque and M. Orozco, *J. Am. Chem. Soc.*, 2005, **127**, 4910-4920.

127. A. Noy, F. J. Luque and M. Orozco, *J. Am. Chem. Soc.*, 2008, **130**, 3486-3496.

128. K. Klumpp, J. Q. Hang, S. Rajendran, Y. Yang, A. Derosier, P. W. K. In, H. Overton, K. E. Parkes, N. Cammack and J. A. Martin, *Nucleic Acids Res.*, 2003, **31**, 6852-6859.

129. T. Tadokoro and S. Kanaya, *FEBS J.*, 2009, **276**, 1482-1493.

130. S. Altman, *Phil. Trans. R. Soc. B.*, 2011, **366**, 2936-2941.

131. A. C. Forster and S. Altman, *Science*, 1990, **249**, 783-786.

132. K. S. Ghanta, G. A. Dokshin, A. Mir, P. M. Krishnamurthy, H. Gneid, A. Edraki, J. K. Watts, E. J. Sontheimer and C. C. Mello, *BioRxiv*, 2018, 354480.

133. A. Ray and R. Di Felice, *arXiv preprint arXiv:1904.06375*, 2019.

134. D. Rath, L. Amlinger, A. Rath and M. Lundgren, *Biochimie*, 2015, **117**, 119-128.

135. P. Mohanraju, K. S. Makarova, B. Zetsche, F. Zhang, E. V. Koonin and J. Van der Oost, *Science*, 2016, **353**, aad5147.

136. D. M. Thurtle-Schmidt and T. W. Lo, *Biochem. Mol. Biol. Educ.*, 2018, **46**, 195-205.

137. K. S. Makarova, D. H. Haft, R. Barrangou, S. J. Brouns, E. Charpentier, P. Horvath, S. Moineau, F. J. Mojica, Y. I. Wolf and A. F. Yakunin, *Nat. Rev. Microbiol.*, 2011, **9**, 467.

138. E. V. Koonin, K. S. Makarova and F. Zhang, *Curr. Opin. Microbiol.*, 2017, **37**, 67-78.

139. S. Shmakov, A. Smargon, D. Scott, D. Cox, N. Pyzocha, W. Yan, O. O. Abudayyeh, J. S. Gootenberg, K. S. Makarova and Y. I. Wolf, *Nat. Rev. Microbiol.*, 2017, **15**, 169.

140. D. C. Swarts and M. Jinek, *Wiley Interdiscip. Rev.: RNA*, 2018, **9**, e1481.

141. K. S. Makarova, Y. I. Wolf, O. S. Alkhnbashi, F. Costa, S. A. Shah, S. J. Saunders, R. Barrangou, S. J. Brouns, E. Charpentier and D. H. Haft, *Nat. Rev. Microbiol.*, 2015, **13**, 722.

142. E. Deltcheva, K. Chylinski, C. M. Sharma, K. Gonzales, Y. Chao, Z. A. Pirzada, M. R. Eckert, J. Vogel and E. Charpentier, *Nature*, 2011, **471**, 602.

143. G. Gasiunas, R. Barrangou, P. Horvath and V. Siksnys, *Proc. Natl. Acad. Sci.*, 2012, **109**, E2579-E2586.

144. Patrick D. Hsu, Eric S. Lander and F. Zhang, *Cell*, 2014, **157**, 1262-1278.

145. R. Barrangou and J. A. Doudna, *Nat. Biotechnol.*, 2016, **34**, 933.

146. F. Jiang and J. A. Doudna, *Annu. Rev. Biophys.*, 2017, **46**, 505-529.

147. A. Pickar-Oliver and C. A. Gersbach, *Nat. Rev. Mol. Cell Biol.*, 2019, 1.

148. J. R. Fagen, D. Collias, A. K. Singh and C. L. Beisel, *Curr. Opin. Biomed. Eng.*, 2017, **4**, 57-64.

149. E. Pursey, D. Sünderhauf, W. H. Gaze, E. R. Westra and S. van Houte, *PLoS pathogens*, 2018, **14**, e1006990.

150. A. A. Gomaa, H. E. Klumpe, M. L. Luo, K. Selle, R. Barrangou and C. L. Beisel, *mBio*, 2014, **5**, e00928-00913.

151. R. J. Citorik, M. Mimee and T. K. Lu, *Nat. Biotechnol.*, 2014, **32**, 1141.

152. D. Bikard, C. W. Euler, W. Jiang, P. M. Nussenzweig, G. W. Goldberg, X. Duportet, V. A. Fischetti and L. A. Marraffini, *Nat. Biotechnol.*, 2014, **32**, 1146.

153. D. Bikard and R. Barrangou, *Curr. Opin. Microbiol.*, 2017, **37**, 155-160.

154. C. A. Lipinski, F. Lombardo, B. W. Dominy and P. J. Feeney, *Adv. Drug Delivery Rev.*, 1997, **23**, 3-25.

155. R. S. Geary, D. Norris, R. Yu and C. F. Bennett, *Adv. Drug Delivery Rev.*, 2015, **87**, 46-51.

156. W. Yin and M. Rogge, *Clin. Transl. Sci.*, 2019, **12**, 98-112.

157. R. F. Epand, P. B. Savage and R. M. Epand, *Biochim. Biophys. Acta, Biomembr.*, 2007, **1768**, 2500-2509.

158. M. Berlanga, *Int. Microbiol.*, **11**, 65-66.

159. R. S. Santos, C. Figueiredo, N. F. Azevedo, K. Braeckmans and S. C. De Smedt, *Adv. Drug Delivery Rev.*, 2018, **136**, 28-48.

160. S. Cowan, T. Schirmer, G. Rummel, M. Steiert, R. Ghosh, R. Pauptit, J. Jansonius and J. Rosenbusch, *Nature*, 1992, **358**, 727.

161. S. B. Primrose and R. Twyman, *Principles of gene manipulation and genomics*, John Wiley & Sons, 2013.

162. W. J. Dower, J. F. Miller and C. W. Ragsdale, *Nucleic Acids Res.*, 1988, **16**, 6127-6145.

163. D. Hanahan, *J. Mol. Biol.*, 1983, **166**, 557-580.

164. M. Giacca and S. Zacchigna, *J. Controlled Release*, 2012, **161**, 377-388.

165. M. Imbert, G. Dias-Florencio and A. Goyenvalle, *Genes*, 2017, **8**, 51.

166. S. C. De Smedt, J. Demeester and W. E. Hennink, *Pharm. Res.*, 2000, **17**, 113-126.

167. T. V. Chirila, P. E. Rakoczy, K. L. Garrett, X. Lou and I. J. Constable, *Biomaterials*, 2002, **23**, 321-342.

168. P. L. Felgner, T. R. Gadek, M. Holm, R. Roman, H. W. Chan, M. Wenz, J. P. Northrop, G. M. Ringold and M. Danielsen, *Proc. Natl. Acad. Sci.*, 1987, **84**, 7413-7417.

169. J. H. Felgner, R. Kumar, C. N. Sridhar, C. J. Wheeler, Y. J. Tsai, R. Border, P. Ramsey, M. Martin and P. L. Felgner, *J. Biol. Chem.*, 1994, **269**, 2550-2561.

170. A. Schroeder, C. G. Levins, C. Cortez, R. Langer and D. G. Anderson, *J. Intern. Med.*, 2010, **267**, 9-21.

171. Y. Wang, L. Miao, A. Satterlee and L. Huang, *Adv. Drug Delivery Rev.*, 2015, **87**, 68-80.

172. C. Lonez, M. Vandenbranden and J.-M. Ruysschaert, *Prog. Lipid Res.*, 2008, **47**, 340-347.

173. P. Fillion, A. Desjardins, K. Sayasith and J. Lagacé, *Biochim. Biophys. Acta, Biomembr.*, 2001, **1515**, 44-54.

174. J. Meng, H. Bai, M. Jia, X. Ma, Z. Hou, X. Xue, Y. Zhou and X. Luo, *J. Antibiot*, 2012, **65**, 129.

175. F. Perche, T. L. Gall, T. Montier, C. Pichon and J.-M. Malinge, *Pharmaceuticals*, 2019, **12**, 81.

176. A. Marín-Menéndez, C. Montis, T. Díaz-Calvo, D. Carta, K. Hatzixanthis, C. J. Morris, M. McArthur and D. Berti, *Sci. Rep.*, 2017, **7**, 41242.

177. J. P. Hegarty, J. Krzeminski, A. K. Sharma, D. Guzman-Villanueva, V. Weissig and D. B. Stewart Sr, *Int. J. Nanomed.*, 2016, **11**, 3607.

178. R. L. Juliano, *Nucleic Acids Res.*, 2016, **44**, 6518-6548.

179. X. Huang, J.-C. Leroux and B. Castagner, *Bioconjugate Chem.*, 2016, **28**, 283-295.

180. R. Giannella, S. Broitman and N. Zamcheck, *J. Clin. Invest.*, 1971, **50**, 1100-1107.

181. R. Kadner, *Mol. Microbiol.*, 1990, **4**, 2027-2033.

182. M. Równicki, M. Wojciechowska, A. J. Wierzba, J. Czarnecki, D. Bartosik, D. Gryko and J. Trylska, *Sci. Rep.*, 2017, **7**, 7644.

183. P. Boisguérin, S. Deshayes, M. J. Gait, L. O'Donovan, C. Godfrey, C. A. Betts, M. J. A. Wood and B. Lebleu, *Adv. Drug Delivery Rev.*, 2015, **87**, 52-67.

184. E. Vivès, P. Brodin and B. Lebleu, *J. Biol. Chem.*, 1997, **272**, 16010-16017.

185. D. Derossi, A. H. Joliot, G. Chassaing and A. Prochiantz, *J. Biol. Chem.*, 1994, **269**, 10444-10450.

186. H. J.-P. Ryser and W.-C. Shen, *Proc. Natl. Acad. Sci.*, 1978, **75**, 3867-3870.

187. B. Allinquant, P. Hantraye, P. Mailleux, K. Moya, C. Bouillot and A. Prochiantz, *J. Cell Biol.*, 1995, **128**, 919-927.

188. J. P. Richard, K. Melikov, E. Vives, C. Ramos, B. Verbeure, M. J. Gait, L. V. Chernomordik and B. Lebleu, *J. Biol. Chem.*, 2003, **278**, 585-590.

189. W. B. Kauffman, T. Fuselier, J. He and W. C. Wimley, *Trends Biochem. Sci*, 2015, **40**, 749-764.

190. S. T. Henriques, M. N. Melo and M. A. Castanho, *Biochem. J.*, 2006, **399**, 1-7.

191. K. Konate, M. F. Lindberg, A. Vaissiere, C. Jourdan, G. Aldrian, E. Margeat, S. Deshayes and P. Boisguerin, *Int. J. Pharm.*, 2016, **509**, 71-84.

192. A. Rydström, S. Deshayes, K. Konate, L. Crombez, K. Padari, H. Boukhaddaoui, G. Aldrian, M. Pooga and G. Divita, *PloS one*, 2011, **6**, e25924.

193. A. H. van Asbeck, A. Beyerle, H. McNeill, P. H. Bovee-Geurts, S. Lindberg, W. P. Verdurmen, M. Hällbrink, U. l. Langel, O. Heidenreich and R. Brock, *ACS nano*, 2013, **7**, 3797-3807.

194. B. L. Geller, K. Marshall-Batty, F. J. Schnell, M. M. McKnight, P. L. Iversen and D. E. Greenberg, *J. Infect. Dis.*, 2013, **208**, 1553-1560.

195. S. M. Jirka, H. Heemskerk, C. L. Tanganyika-de Winter, D. Muilwijk, K. H. Pang, P. C. de Visser, A. Janson, T. G. Karnaoukh, R. Vermue and P. A. 't Hoen, *Nucleic Acid Ther.*, 2014, **24**, 25-36.

196. K. Gogoi, M. V. Mane, S. S. Kunte and V. A. Kumar, *Nucleic Acids Res.*, 2007, **35**, e139-e139.

197. L. Good, S. K. Awasthi, R. Dryselius, O. Larsson and P. E. Nielsen, *Nat. Biotechnol.*, 2001, **19**, 360-364.

198. B. Geller, J. Deere, D. Stein, A. Kroeker, H. Moulton and P. Iversen, *Antimicrob. Agents Chemother.*, 2003, **47**, 3233-3239.

199. D. Hwang and Y.-H. Lim, *Sci. Rep.*, 2015, **5**, 10029.

200. X.-X. Tan, J. K. Actor and Y. Chen, *Antimicrob. Agents Chemother.*, 2005, **49**, 3203.

201. L. D. Tilley, O. S. Hine, J. A. Kellogg, J. N. Hassinger, D. D. Weller, P. L. Iversen and B. L. Geller, *Antimicrob. Agents Chemother.*, 2006, **50**, 2789-2796.

202. M. F. N. Abushahba, H. Mohammad, S. Thangamani, A. A. A. Hussein and M. N. Seleem, *Sci. Rep.*, 2016, **6**, 20832.

203. R. A. Alajlouni and M. N. Seleem, *Nucleic Acid Ther.*, 2013, **23**, 363-367.

204. S. Goh, A. Loeffler, D. H. Lloyd, S. P. Nair and L. Good, *BMC microbiology*, 2015, **15**, 262.

205. N. Nekhotiaeva, S. K. Awasthi, P. E. Nielsen and L. Good, *Mol. Ther.*, 2004, **10**, 652-659.

206. N. Patenge, R. Pappesch, F. Krawack, C. Walda, M. A. Mraheil, A. Jacob, T. Hain and B. Kreikemeyer, *Mol. Ther.-Nucleic Acids*, 2013, **2**, e132.

207. P. Rajasekaran, J. C. Alexander, M. N. Seleem, N. Jain, N. Sriranganathan, A. R. Wattam, J. C. Setubal and S. M. Boyle, *Int. J. Antimicrob. Agents*, 2013, **41**, 358-362.

208. P. Kurupati, K. S. W. Tan, G. Kumarasinghe and C. L. Poh, *Antimicrob. Agents Chemother.*, 2007, **51**, 805-811.

209. A. Kulyté, N. Nekhotiaeva, S. K. Awasthi and L. Good, *J. Mol. Microbiol. Biotechnol.*, 2005, **9**, 101-109.

210. B. L. Mellbye, S. E. Puckett, L. D. Tilley, P. L. Iversen and B. L. Geller, *Antimicrob. Agents Chemother.*, 2009, **53**, 525-530.

211. H. Bai, Y. You, H. Yan, J. Meng, X. Xue, Z. Hou, Y. Zhou, X. Ma, G. Sang and X. Luo, *Biomaterials*, 2012, **33**, 659-667.

212. S. Liang, Y. He, Y. Xia, H. Wang, L. Wang, R. Gao and M. Zhang, *Int. J. Infect. Dis.*, 2015, **30**, 1-6.

213. H. Bai, G. Sang, Y. You, X. Xue, Y. Zhou, Z. Hou, J. Meng and X. Luo, *PloS one*, 2012, **7**, e29886.

214. A. Ghosal and P. E. Nielsen, *Nucleic Acid Ther.*, 2012, **22**, 323-334.

215. K. Maekawa, M. Azuma, Y. Okuno, T. Tsukamoto, K. Nishiguchi, K.-i. Setsukinai, H. Maki, Y. Numata, H. Takemoto and M. Rokushima, *Biorg. Med. Chem.*, 2015, **23**, 7234-7239.

216. A. M. Hansen, G. Bonke, C. J. Larsen, N. Yavari, P. E. Nielsen and H. Franzyk, *Bioconjugate Chem.*, 2016, **27**, 863-867.

217. M. F. Abushahba, H. Mohammad, S. Thangamani, A. A. Hussein and M. N. Seleem, *Sci. Rep.*, 2016, **6**.

218. J. P. Hegarty and D. B. Stewart, *Appl. Microbiol. Biotechnol.*, 2018, **102**, 1055-1065.

219. B. L. Geller, J. Deere, L. Tilley and P. L. Iversen, *J. Antimicrob. Chemother.*, 2005, **55**, 983-988.

220. L. D. Tilley, B. L. Mellbye, S. E. Puckett, P. L. Iversen and B. L. Geller, *J. Antimicrob. Chemother.*, 2006, **59**, 66-73.

221. R. G. Panchal, B. L. Geller, B. Mellbye, D. Lane, P. L. Iversen and S. Bavari, *Nucleic Acid Ther.*, 2012, **22**, 316-322.

222. A. J. Sawyer, D. Wesolowski, N. Gandotra, A. Stojadinovic, M. Izadjoo, S. Altman and T. R. Kyriakides, *Int. J. Pharm.*, 2013, **453**, 651-655.

223. J. Meng, F. Da, X. Ma, N. Wang, Y. Wang, H. Zhang, M. Li, Y. Zhou, X. Xue, Z. Hou, M. Jia and X. Luo, *Antimicrob. Agents Chemother.*, 2015, **59**, 914-922.

224. J. J. Howard, C. R. Sturge, D. A. Moustafa, S. M. Daly, K. R. Marshall-Batty, C. F. Felder, D. Zamora, M. Yabe-Gill, M. Labandeira-Rey, S. M. Bailey, M. Wong, J. B. Goldberg, B. L. Geller and D. E. Greenberg, *Antimicrob. Agents Chemother.*, 2017, **61**, e01938-01916.

225. E. Oh, Q. Zhang and B. Jeon, *J. Antimicrob. Chemother.*, 2014, **69**, 375-380.

226. J. Meng, G. He, H. Wang, M. Jia, X. Ma, F. Da, N. Wang, Z. Hou, X. Xue and M. Li, *J. Antibiot*, 2015, **68**, 158-164.

227. A. L. Bothwell, R. L. Garber and S. Altman, *J. Biol. Chem.*, 1976, **251**, 7709-7716.

228. N. Jarrous and V. Gopalan, *Nucleic Acids Res.*, 2010, **38**, 7885-7894.

229. B. C. Stark, R. Kole, E. J. Bowman and S. Altman, *Proc. Natl. Acad. Sci.*, 1978, **75**, 3717-3721.

230. C. Guerrier-Takada, K. Gardiner, T. Marsh, N. Pace and S. Altman, *Cell*, 1983, **35**, 849-857.

231. S. Altman and J. Smith, *Nature*, 1971, **233**, 35-39.

232. Y. Komine, M. Kitabatake, T. Yokogawa, K. Nishikawa and H. Inokuchi, *Proc. Natl. Acad. Sci.*, 1994, **91**, 9223-9227.

233. P. Alifano, F. Rivellini, C. Piscitelli, C. M. Arraiano, C. B. Bruni and M. S. Carlomagno, *Genes Dev.*, 1994, **8**, 3021-3031.

234. W. McClain, C. Guerrier-Takada and S. Altman, *Science*, 1987, **238**, 527-530.

235. N. J. Reiter, A. Osterman, A. Torres-Larios, K. K. Swinger, T. Pan and A. Mondragon, *Nature*, 2010, **468**, 784-789.

236. V. Gopalan, A. Vioque and S. Altman, *J. Biol. Chem.*, 2002, **277**, 6759-6762.

237. C. Guerrier-Takada, Y. Li and S. Altman, *Proc. Natl. Acad. Sci.*, 1995, **92**, 11115-11119.

238. J. McKinney, C. Guerrier-Takada, D. Wesolowski and S. Altman, *Proc. Natl. Acad. Sci.*, 2001, **98**, 6605-6610.

239. J. S. McKinney, H. Zhang, T. Kubori, J. E. Galán and S. Altman, *Nucleic Acids Res.*, 2004, **32**, 848-854.

240. A. J. S. Bistué, H. Ha, R. Sarno, M. Don, A. Zorreguieta and M. E. Tolmasky, *Antimicrob. Agents Chemother.*, 2007, **51**, 1918-1925.

241. A. J. S. Bistué, F. A. Martín, N. Vozza, H. Ha, J. C. Joaquín, A. Zorreguieta and M. E. Tolmasky, *Proc. Natl. Acad. Sci.*, 2009, **106**, 13230-13235.

242. J.-P. Perreault and S. Altman, *J. Mol. Biol.*, 1992, **226**, 399-409.

243. A. Jackson, S. Jani, C. Davies-Sala, A. J. C. Soler-Bistué, A. Zorreguieta and M. E. Tolmasky, *Biol. Methods Protoc.*, 2016, **1**.

244. J.-h. Ko, M. Izadjoo and S. Altman, *RNA*, 2008, **14**, 1656-1662.

245. E. W. Lundblad, G. Xiao, J.-h. Ko and S. Altman, *Proc. Natl. Acad. Sci.*, 2008, **105**, 2354-2357.

246. G. Xiao, E. W. Lundblad, M. Izadjoo and S. Altman, *PloS one*, 2008, **3**, e3719.

247. N. Shen, J.-h. Ko, G. Xiao, D. Wesolowski, G. Shan, B. Geller, M. Izadjoo and S. Altman, *Proc. Natl. Acad. Sci.*, 2009, **106**, 8163-8168.

248. C. D. Sala, A. J. Soler-Bistué, L. Korprapun, A. Zorreguieta and M. E. Tolmasky, *PloS one*, 2012, **7**, e47690.

249. X. Cheng, J.-H. Ko and S. Altman, *RNA*, 2011, **17**, 544-549.

250. I. Cho, S. A. Kazakov and V. Gopalan, *J. Mol. Biol.*, 2011, **405**, 1121-1127.

251. C. Davies-Sala, A. Soler-Bistué, R. A. Bonomo, A. Zorreguieta and M. E. Tolmasky, *Ann. N.Y. Acad. Sci.*, 2015, **1354**, 98-110.

252. M. Ma, L. Benimetskaya, I. Lebedeva, J. Dignam, G. Takle and C. Stein, *Nat. Biotechnol.*, 2000, **18**, 58-61.

253. J. P. Leonetti, G. Degols and B. Lebleu, *Bioconjugate Chem.*, 1990, **1**, 149-153.

254. S. Goh, J. M. Boberek, N. Nakashima, J. Stach and L. Good, *PloS one*, 2009, **4**, e6061.

255. R. Dryselius, S. K. Aswasti, G. K. Rajarao, P. E. Nielsen and L. Good, *Oligonucleotides*, 2003, **13**, 427-433.

256. I. M. Keseler, A. Mackie, M. Peralta-Gil, A. Santos-Zavaleta, S. Gama-Castro, C. Bonavides-Martínez, C. Fulcher, A. M. Huerta, A. Kothari, M. Krummenacker, M. Latendresse, L. Muñiz-Rascado, Q. Ong, S. Paley, I. Schröder, A. G. Shearer, P. Subhraveti, M. Travers, D. Weerasinghe, V. Weiss, J. Collado-Vides, R. P. Gunsalus, I. Paulsen and P. D. Karp, *Nucleic Acids Res.*, 2013, **41**, D605-D612.

257. L. Good and P. E. Nielsen, *Nat. Biotechnol.*, 1998, **16**, 355-358.

258. S. Goh, J. M. Boberek, N. Nakashima, J. Stach and L. Good, *PloS one*, 2009, **4**, e6061.

259. D. W. Hecht, D. M. Citron, M. Cox, N. Jacobus, S. Jenkins, A. Onderdonk, D. Roe-Carpenter, J. Rosenblatt and H. Wexler, *Methods for Antimicrobial Susceptibility Testing of Anaerobic Bacteria: Approved Standard*, Clinical and Laboratory Standards Institute Wayne, PA, 2007.

260. M. Vaara and M. Porro, *Antimicrob. Agents Chemother.*, 1996, **40**, 1801-1805.

261. D. H. Juers, B. W. Matthews and R. E. Huber, *Protein Sci.*, 2012, **21**, 1792-1807.

262. T. Baba, T. Ara, M. Hasegawa, Y. Takai, Y. Okumura, M. Baba, K. A. Datsenko, M. Tomita, B. L. Wanner and H. Mori, *Mol. Syst. Biol.*, 2006, **2**.

263. N. Ohtani, M. Haruki, M. Morikawa, R. J. Crouch, M. Itaya and S. Kanaya, *Biochemistry*, 1999, **38**, 605-618.

264. N. Ohtani, M. Haruki, M. Morikawa and S. Kanaya, *J. Biosci. Bioeng.*, 1999, **88**, 12-19.

265. M. Nowotny, S. A. Gaidamakov, R. J. Crouch and W. Yang, *Cell*, 2005, **121**, 1005-1016.

266. M. Nowotny and W. Yang, *EMBO J.*, 2006, **25**, 1924-1933.

267. W. Yang, J. Y. Lee and M. Nowotny, *Mol. Cell*, 2006, **22**, 5-13.

268. M. Nowotny, S. A. Gaidamakov, R. Ghirlando, S. M. Cerritelli, R. J. Crouch and W. Yang, *Mol. Cell*, 2007, **28**, 264-276.

269. F. Eckstein, *J. Am. Chem. Soc.*, 1970, **92**, 4718-4723.

270. F. Eckstein, *Tetrahedron Lett.*, 1967, **8**, 1157-1160.

271. F. Eckstein, *Antisense Nucleic Acid Drug Dev.*, 2000, **10**, 117-121.

272. S. Agrawal and E. R. Kandimalla, *Mol. Med. Today*, 2000, **6**, 72-81.

273. M. D. Sørensen, L. Kværnø, T. Bryld, A. E. Håkansson, B. Verbeure, G. Gaubert, P. Herdewijn and J. Wengel, *J. Am. Chem. Soc.*, 2002, **124**, 2164-2176.

274. R. Kole, A. R. Krainer and S. Altman, *Nat. Rev. Drug Discovery*, 2012, **11**, 125-140.

275. K. A. Lennox and M. A. Behlke, *J. Rare Dis. Res. Treat*, 2016, **1**, 66-70.

276. M. Frieden, S. M. Christensen, N. D. Mikkelsen, C. Rosenbohm, C. A. Thrue, M. Westergaard, H. F. Hansen, H. Ørum and T. Koch, *Nucleic Acids Res.*, 2003, **31**, 6365-6372.

277. T. Koch, C. Rosenbohm, H. F. Hansen, B. Hansen, E. M. Straarup and S. Kauppinen, in *Therapeutic Oligonucleotides*, ed. J. Kurreck, RSC, Cambridge, 2008, pp. 103-141.

278. S. K. Singh, A. A. Koshkin, J. Wengel and P. Nielsen, *Chem. Commun.*, 1998, 455-456.

279. E. M. Straarup, N. Fisker, M. Hedtjärn, M. W. Lindholm, C. Rosenbohm, V. Aarup, H. F. Hansen, H. Ørum, J. B. R. Hansen and T. Koch, *Nucleic Acids Res.*, 2010, **38**, 7100-7111.

280. J. Kurreck, *FEBS J.*, 2003, **270**, 1628-1644.

281. J. Kurreck, E. Wyszko, C. Gillen and V. A. Erdmann, *Nucleic Acids Res.*, 2002, **30**, 1911-1918.

282. S. T. Crooke, K. M. Lemonidis, L. Neilson, R. Griffey, E. A. Lesnik and B. P. Monia, *Biochem. J.*, 1995, **312**, 599-608.

283. P. P. Seth, A. Siwkowski, C. R. Allerson, G. Vasquez, S. Lee, T. P. Prakash, E. V. Wancewicz, D. Witchell and E. E. Swayze, *J. Med. Chem.*, 2008, **52**, 10-13.

284. M. Zuker, *Nucleic Acids Res.*, 2003, **31**, 3406-3415.

285. K. Ezzat, Y. Aoki, T. Koo, G. McClorey, L. Benner, A. Coenen-Stass, L. O'Donovan, T. Lehto, A. Garcia-Guerra, J. Nordin, A. F. Saleh, M. Behlke, J. Morris, A. Goyenvalle, B. Dugovic, C. Leumann, S. Gordon, M. J. Gait, S. El−Andaloussi and M. J. A. Wood, *Nano Lett.*, 2015, **15**, 4364-4373.

286. M. J. Gait, *CMLS, Cell. Mol. Life Sci.*, 2003, **60**, 844-853.

287. X.-X. Tan, J. K. Actor and Y. Chen, *Antimicrob. Agents Chemother.*, 2005, **49**, 3203-3207.

288. F. Wang, Y. Wang, X. Zhang, W. Zhang, S. Guo and F. Jin, *J. Controlled Release*, 2014, **174**, 126-136.

289. L. T. Nguyen, E. F. Haney and H. J. Vogel, *Trends Biotechnol.*, 2011, **29**, 464-472.

290. C. A. Schneider, W. S. Rasband and K. W. Eliceiri, *Nat. Methods*, 2012, **9**, 671-675.

291. M. R. Hassler, A. A. Turanov, J. F. Alterman, R. A. Haraszti, A. H. Coles, M. F. Osborn, D. Echeverria, M. Nikan, W. E. Salomon and L. Roux, *Nucleic Acids Res.*, 2018, **46**, 2185-2196.

292. K. A. Hurley, T. M. Santos, G. M. Nepomuceno, V. Huynh, J. T. Shaw and D. B. Weibel, *J. Med. Chem.*, 2016, **59**, 6975-6998.

293. K. D. Kusuma, M. Payne, A. T. Ung, A. L. Bottomley and E. J. Harry, *ACS Infect. Dis.*, 2019, **5**, 1279-1294.

294. J. S. Jepsen, M. D. Sørensen and J. Wengel, *Oligonucleotides*, 2004, **14**, 130-146.

295. F. Eckstein, *Nucleic Acid Ther.*, 2014, **24**, 374-387.

296. S. Karaki, C. Paris and P. Rocchi, in *Antisense Therapy*, IntechOpen, 2019.

297. A. GrÜnweiler and R. K. Hartmann, *BioDrugs*, 2007, **21**, 235-243.

298. A. Jackson, S. Jani, C. Davies-Sala, A. J. Soler-Bistué, A. Zorreguieta and M. E. Tolmasky, *Biol. Methods Protoc.*, 2016, **1**.

299. M. M. Evers, L. J. Toonen and W. M. van Roon-Mom, *Adv. Drug Delivery Rev.*, 2015, **87**, 90-103.

300. J. K. Watts, G. F. Deleavey and M. J. Damha, *Drug Discovery Today*, 2008, **13**, 842-855.

301. B. E. Gryder, M. J. Akbashev, M. K. Rood, E. D. Raftery, W. M. Meyers, P. Dillard, S. Khan and A. K. Oyelere, *ACS Chem. Biol.*, 2013, **8**, 2550-2560.

302. G. D. Fasman and H. A. Sober, *Handbook of biochemistry and molecular biology*, CRC press Cleveland, 1977.

303. Bakersfield College, *Chemistry B1A lab manual*, https://www.scribd.com/document/339866378/Hydrogen-Peroxide-Analysis-4, Accessed May 2016.

304. New England BioLabs, *Tm calculator*, https://www.neb.com/tools-and-resources, Accessed August 2017.